

Cutting Edge 2017

What a great honour it is to be writing introductory words to this issue of *Acta Chimica Slovenica*, whose editor prof. dr. Aleksander Pavko with his editorial team and prof. dr. Slavko Kaučič, president of Slovenian Chemical Society and publisher of ACSi, kindly supported our initiative to dedicate this issue to enthusiastic young researchers in the field of chemical sciences.

Students are first exposed to independent research during their bachelor and/or masters' thesis, where they are given a role in already ongoing projects within the research laboratory and are often assigned to solve minor research problems. But already after initial hours of independent work, a nostalgia for practical laboratory courses emerges, with perpetually working experiments and eternal buffer fountains. Due to these bitter realisations, minor research problems become therefore all but minor for a young researcher. However, these initial struggles are in the wider perspective just one of the impressions forming the greater picture of how a world of research in reality truly is. Although the previously mentioned technical obstacles can fast be overcome with good mentorship and guidance, presenting the research work either in form of publications or at the conferences still seems to be a privilege reserved for experienced researchers.

Driven by this observation, an idea was formed in 2014 to organize a conference for students and young researchers. Since this coincided with opening of the new premises of the Faculty of chemistry and chemical tech-

nology of University of Ljubljana (UL FCCT), we believed it would be the best venue for this occasion. The organization of the first Cutting Edge conference, which took place in September 2015, was in hands of Sara Drvarič-Talian, at that time a masters' student in chemistry and two young UL FCCT staff members, dr. Jakob Kljun from the Chair of Inorganic Chemistry and myself from the Chair of Biochemistry. To our great surprise, the conference was attended by more than 100 participants from Slovenia as well as other countries with researchers from various fields of chemistry as well as environment preservation, pharmacy, construction, materials, medicine and civil engineering. Most of them presented their work during a poster exhibition, while selected masters' and doctoral students got a chance to present their research in the form of oral presentations. An organisational frame of the conference was set, formed by three main sections: Science Behind the Living, Technologies for the Earth and Environment and Materials of the Future, which were introduced by renowned experts.

Due to the positive feedback, we decided to make this conference a biennial tradition. To our delight, two more young UL FCCT researchers joined the organisation committee: doc. dr. Aleš Ručigaj from the Chair of Materials and Polymer Engineering and a PhD student, assistant from the Chair of Biochemistry, Aljaž Gaber. Soon a decision was made to form a society, of which main commitment is to organize scientific events for young re-

searchers. Beside Cutting Edge conference, we organized a three-day event, Days of Chemical Sciences in 2016, which included a poster conference of Chemical sciences doctoral students, public popular science lectures, presentation of research activities at the UL FCCT and a Science Incubator, where personal experience of how to get a scholarship or a research starting grant were presented. An underlying concept behind all activities of the Cutting Edge society is to form a platform, enabling young scientists not only to present their research but also to meet their peers and discuss their ideas beyond the learning curriculum.

For this year's conference, we made another step further and offered our junior participants the opportunity to publish their own scientific articles. Young scientists were invited to submit an article, which had to undergo a standard reviewing process, and we are more than proud to present 10 of accepted papers in this dedicated September edition of *Acta Chimica Slovenica*. Six of them cover topics from the Science Behind the Living: Eva Jarc and Ema Guštin with the colleagues present their work on lipid droplet formation in Hela cervical cancer cells, Zorica Latinović with the colleagues explain the effect of disintegrins from the venom of *Vipera ammodytes* on breast cancer cells, Klemen Stojan with the colleagues show results of *in vitro* assessment of potential bladder papillary neoplasm treatment with functionalized polyethyleneimine coated magnetic nanoparticles, Anžej Hladnik and Jana Ferdin with their colleagues present data regarding presence of Trans-activation Response Element (TAR) RNA in the plasma of a subset of aviremic HIV-1 infected patients, Sandi Brudar with his colleagues also investigated disease induced changes in human blood plasma by use of DSC and IAC, while Tomaž Martini and his colleagues present a possible link between circadian rhythms to metabolism by interaction of PER2 with the constitutive androstane receptor. Three articles were classified into Technologies for the Earth and Environment section: Evelin Gruden with the colleagues evaluate the potential of animal bone char as a metal stabilization agent in metal contaminated soil, Žane Temova with the colleagues present a novel HPLC-UV method for simultaneous determination

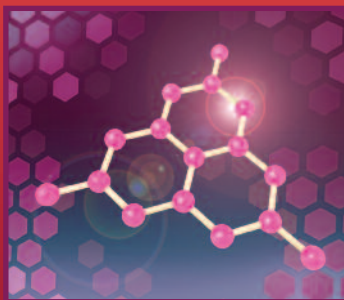
of fat-soluble vitamins and Coenzyme Q10 in medicines and supplements, while Milena Ivanović and her colleagues show an interesting chemometric characterization of Slovenian red wines. Last but not least, Miha Virant and Sara Drvarič-Talian with their colleagues present modeling of the correlation between molecular electrostatic potential and pKa on sets of carboxylic acids, phenols and anilines.

We are looking forward to hearing these presentations at the conference, since the authors were given a priority to be chosen for oral presentations together with few other ones who will be selected by scientific committee members of each section. This year we are truly grateful to prof. dr. Andreja Žgajnar Gotvajn who is responsible for the section Technologies for the Earth and Environment, prof. dr. Janez Plavec who is in charge of the Science Behind the Living section and doc. dr. Boštjan Genorio who took over the Materials of the Future section. We are thankful to them for sharing their expertise and experience with us, thus sustaining the level of the Cutting Edge conference at a high scientific level.

None of our plans could be carried out without genuine support of the Faculty leadership. We sincerely thank the Dean of UL FCCT, prof. dr. Matjaž Krajnc, whose doors were always open for us, providing much appreciated guidance and motivation to implement our ideas no matter how naïve or overoptimistic they sometimes were. Starting in 2017, prof. dr. Jurij Svete was given a mandate as the new Dean of UL FCCT. We look forward to continuing our good cooperation, since prof. Svete was the chairman of the Science Behind the Living section at Cutting Edge 2015 conference.

Stimulated by the positive responses we receive, we hope and aim to continue with activities we set to accomplish. Kindly welcome to read through selected research articles and looking forward to meeting you at the next Cutting Edge conference in 2019.

Marina Klemenčič
Cutting Edge Society
Faculty of Chemistry and Chemical Technology
University of Ljubljana

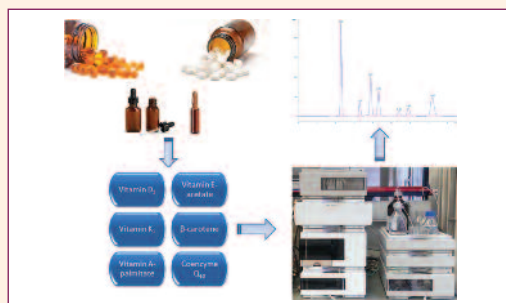


SCIENTIFIC PAPER

523–529 Analytical chemistry

Novel HPLC-UV Method for Simultaneous Determination of Fat-soluble Vitamins and Coenzyme Q10 in Medicines and Supplements

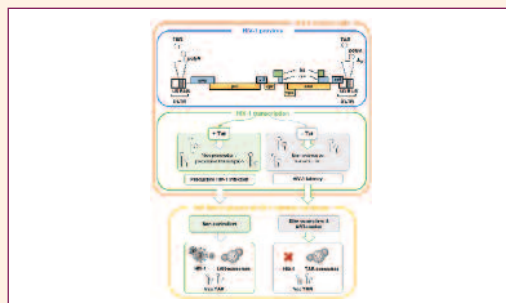
Žane Temova Rakuša, Eva Srečnik and Robert Roškar



530–536 Biomedical applications

Trans-Activation Response Element RNA is Detectable in the Plasma of a Subset of Aviremic HIV-1-Infected Patients

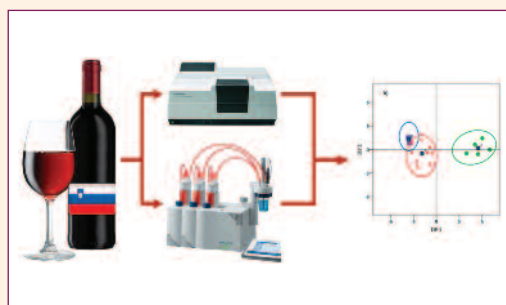
Anžej Hladnik, Jana Ferdin, Katja Goričar, Steven G. Deeks, Boris M. Peterlin, Ana Plemenitaš, Vita Dolžan and Metka Lenassi



537–542 Analytical chemistry

Chemometric Characterization of Slovenian Red Wines

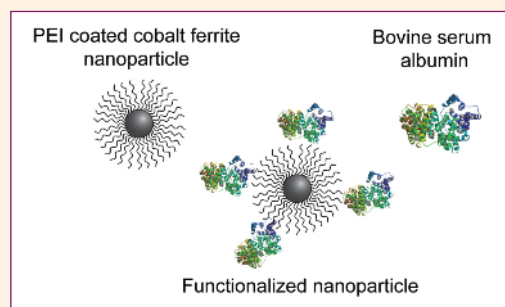
Milena Ivanović, Anja Petek, Maša Islamčević Razboršek and Mitja Kolar



543–548 Biomedical applications

***In vitro* Assessment of Potential Bladder Papillary Neoplasm Treatment with Functionalized Polyethyleneimine Coated Magnetic Nanoparticles**

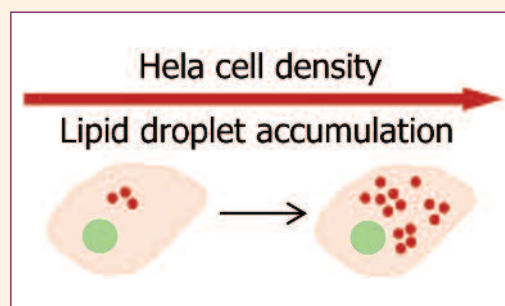
Klemen Strojan, Jasna Lojk, Vladimir Boštjan Bregar, Mateja Erdani Kreft, Jurij Svete, Peter Veranič and Mojca Pavlin



549–554 Biochemistry and molecular biology

Lipid Droplet Formation in HeLa Cervical Cancer Cells Depends on Cell Density and the Concentration of Exogenous Unsaturated Fatty Acids

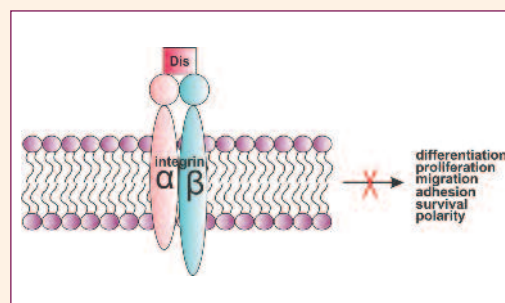
Ema Guštin, Eva Jarc, Ana Kump and Toni Petan



555–559 Biochemistry and molecular biology

Disintegrins from the Venom of *Vipera ammodytes ammodytes* Efficiently Inhibit Migration of Breast Cancer Cells

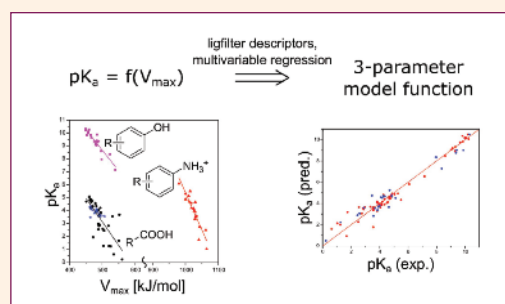
Zorica Latinović, Adrijana Leonardi, Toni Petan, Margareta Žlajpah and Igor Križaj



560–563 Physical chemistry

Modelling the Correlation Between Molecular Electrostatic Potential and pK_a on Sets of Carboxylic Acids, Phenols and Anilines

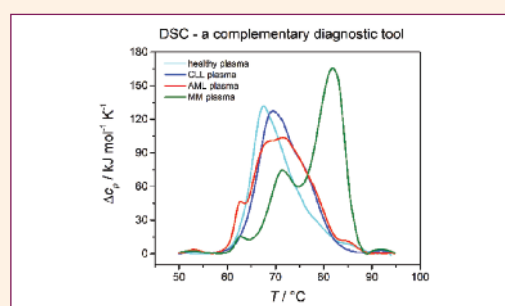
Miha Virant, Sara Drvarič Talian, Črtomir Podlipnik and Barbara Hribar-Lee



564–570 Biochemistry and molecular biology

Use of Differential Scanning Calorimetry and Immunoaffinity Chromatography to Identify Disease Induced Changes in Human Blood Plasma Proteome

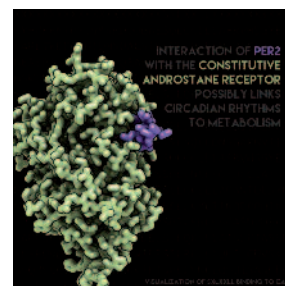
Sandi Brudar, Urh Černigoj, Helena Podgornik, Mojca Kržan and Iztok Prislan



571–576 Biochemistry and molecular biology

Interaction of PER2 with the Constitutive Androstane Receptor Possibly Links Circadian Rhythms to Metabolism

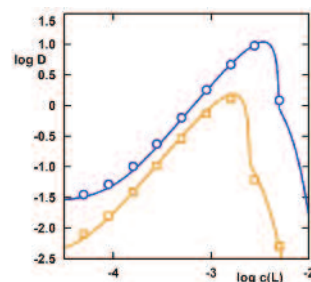
Tomaž Martini, Jurij Stojan, Damjana Rozman and Uršula Prosenč Zmrzljak



582–589 Analytical chemistry

N,N,N',N'-Tetrabutyl-1,10-phenanthroline-2,9-dicarboxamide as Very Effective Extraction Agent for Trivalent Europium and Americium

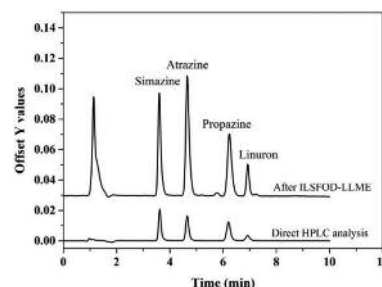
Emanuel Makrlík, Petr Vanura, Pavel Selucký, Vasily Babain, Dmitriy Dar'in and Mikhail Alyapyshev



590–597 Analytical chemistry

Ionic Liquid-Assisted Liquid–Liquid Microextraction based on the Solidification of Floating Organic Droplet in Sample Preparation for Simultaneous Determination of Herbicide Residues in Fruits

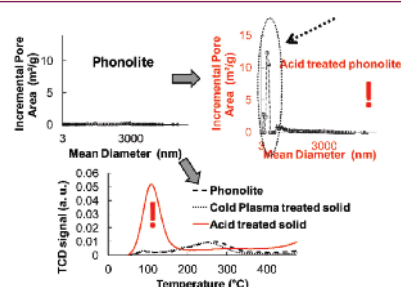
Jitlada Vichapong, Yanawath Santaladchaiyakit, Rodjana Burakham and Supalax Srijaranai



598–602 Materials science

Cold Plasma and Acid Treatment Modification Effects on Phonolite

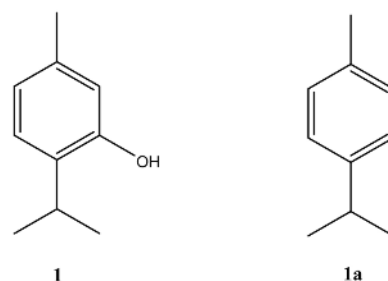
José Miguel Hidalgo-Herrador, Zdenek Tišler, Pavlína Hajková, Lenka Soukupová, Lenka Zárbynická and Karla Černá



603–612 Organic chemistry

Synthesis, Antimicrobial Activity and *in silico* Studies on Thymol Esters

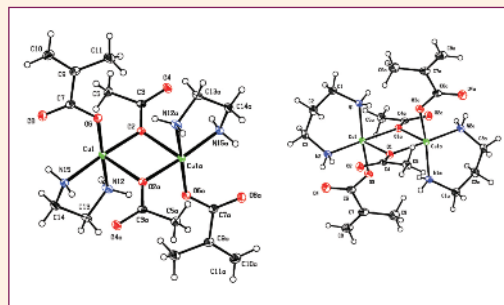
Jelena Lazarević, Ana Kolarević, Aleksandra Đorđević, Gordana Stojanović, Andrija Šmelcerović, Pierangela Ciuffreda and Enzo Santaniello



613–620 Inorganic chemistry

Synthesis, X-ray Structural Characterization, and DFT Calculations of Binuclear Mixed-ligand Copper(II) Complexes Containing Diamine, Acetate and Methacrylate Ligands

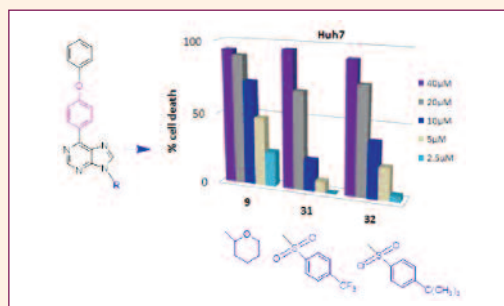
Rasoul Vafazadeh, Mansoor Namazian, Mahshad Chavoshiyan, Anthony C. Willis and Paul D. Carr



621–632 Organic chemistry

Synthesis of Some Substituted 6-Phenyl Purine Analogues and Their Biological Evaluation as Cytotoxic Agents

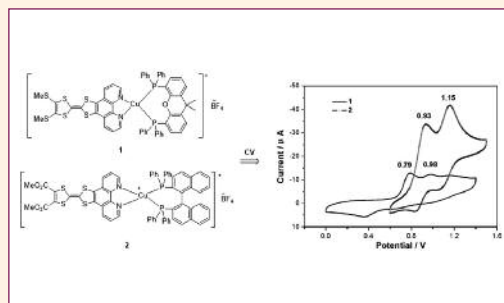
Asligul Kucukdumlu, Meral Tuncbilek, Ebru Bilget Guven and Rengul Cetin Atalay



633–637 Organic chemistry

Synthesis and Properties of two Cu^I Complexes Involving Tetrathia-fulvalene-Fused Phenanthroline Ligand

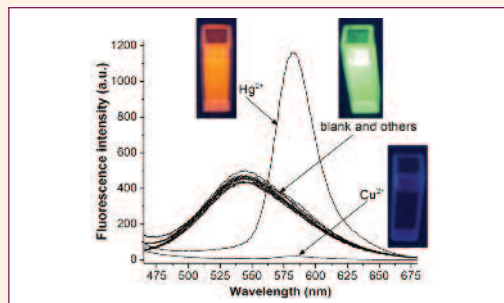
Zhi-Gang Niu, Xue-You Wang, Hao-Hua Chen, Xun Wang¹ Sun Wei, Dong-Min Wu, Guang-Ying Chen, Jie Qin and Gao-Nan Li



638–643 Analytical chemistry

A Dansyl-Rhodamine Based Fluorescent Probe for Detection of Hg²⁺ and Cu²⁺

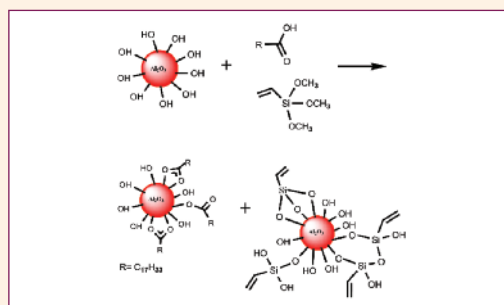
Shizhuang Yuan, Wei Su and Enju Wang



644–653 Materials science

Surface Modification of Alumina Nanoparticles: A Dispersion Study in Organic Media

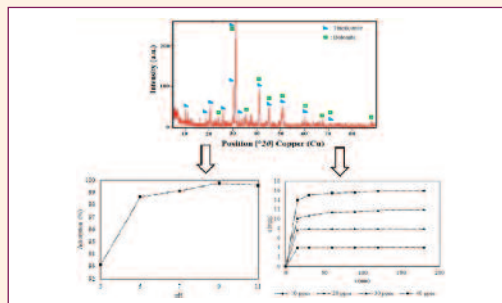
Esmail Soleimani and Narges Zamani



654–660 Chemical, biochemical and environmental engi-

Adsorption of Cr(III) from Aqueous Solution using Borax Sludge

Fatma Tugce Senberber, Meral Yildirim, Nevin Karamahmut Mermer and Emek Moroydor Derun



661–671 Chemical education

Effectiveness of Student Learning during Experimental Work in Primary School

Ana Logar, Cirila Pekljaj and Vesna Ferik Savec

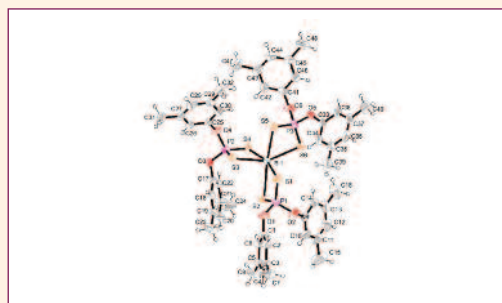
Students solving of worksheets while taking part in STUDENTS' HANDS ON EXPERIMENTAL WORK			
Teachers	Solved worksheets [%]	Correctly solved worksheets* [%]	Teacher checks the worksheet at the end of the experimental work.
Teacher D	100.0	75.8	YES
Teacher E	18.8	81.9	NO
Teacher F	100.0	82.1	YES
Teacher G	68.3	41.9	NO
Teacher K	97.5	100.0	YES
Teacher L	65.0	93.4	NO
Teacher M	100.0	100.0	YES
Teacher N	80.0	67.4	NO
Teacher P	100.0	72.9	NO
Teacher R	98.1	93.1	NO
Average value	78.8	81.0	

*Percentage of correctly solved worksheet among all the solved worksheets.

672–678 Inorganic chemistry

Bismuth(III) Complexes with Bis(dimethylphenyl) Dithiophosphates: Synthesis, Characterization and Crystal Structure of $[\{(3,5\text{-CH}_3)_2\text{C}_6\text{H}_3\text{O}\}_2\text{PS}_2]_3\text{Bi}$

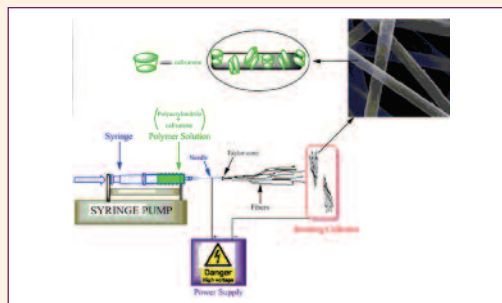
Ruchi Khajuria, Sandeep Kumar, Mandeep Kour, Atiya Syed, Geeta Hundal and Sushil K. Pandey



679–685 Materials science

Electrospun Nanofibrous Polyacrylonitrile/calixarene Mats: an Excellent Adsorbent for the Removal of Chromate Ions from Aqueous Solutions

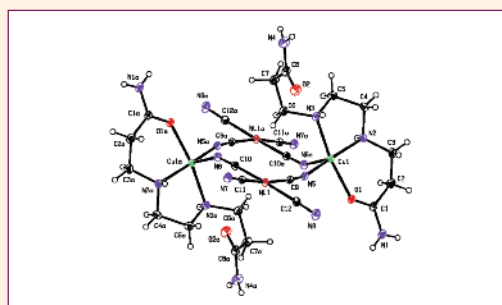
Mevlut Bayrakci, Fatih Ozcan, Bahar Yilmaz and Seref Ertul



686–691 Inorganic chemistry

Synthesis of Hetero- and Homo-multinuclear Complexes with a Tetracyanonickelate Anion: Structural Characterization $[\text{Cu}(\text{bcen})\text{Ni}(\text{CN})_4]_2$

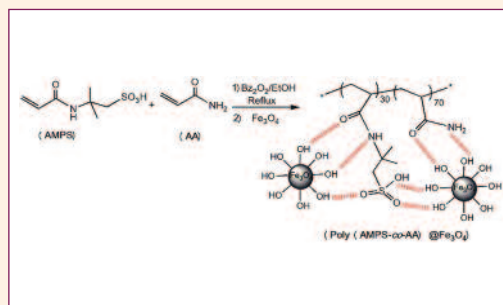
Rasoul Vafazadeh, Amin Dehghani-Firouzabadi and Anthony C. Willis



692–700 Organic chemistry

Magnetite-Containing Sulfonated Polyacrylamide as a Nanocatalyst for the Preparation of Biscoumarins

Kaveh Parvanak Boroujeni, Shahla Hadizadeh, Sodabeh Hasani, Abdulhamid Fadavi and Mansooreh Shahrokh

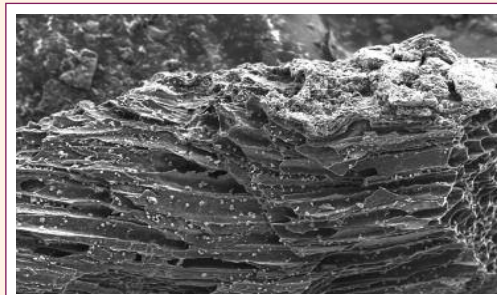


SHORT COMMUNICATION

577–581 Applied chemistry

Preliminary Evaluation of Animal Bone Char as Potential Metal Stabilization Agent in Metal Contaminated Soil

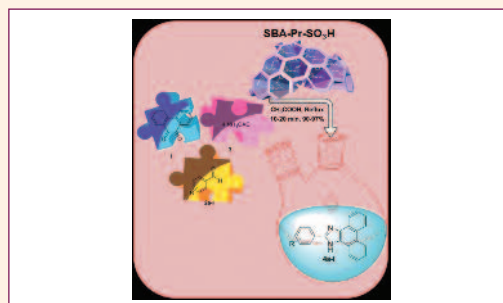
Evelin Gruden, Peter Bukovec and Marija Zupančič



701–706 Organic chemistry

Synthesis of 2,4,5-Trisubstituted Phenanthroimidazole Derivatives using SBA-Pr-SO₃H as a Nanocatalyst

Ghodsi Mohammadi Ziarani, Elham Tavaf, Vaezeh Fathi Vavsari and Alireza Badii



707–713 Organic chemistry

Design, Preparation and Characterization of MoO₃H-functionalized Fe₃O₄@SiO₂ Magnetic Nanocatalyst and Application for the One-pot Multicomponent Reactions

Mahtab Kiani, Mehrnoosh Hendijani, Mohammad Mohammadipour and Ali Zamanian



Scientific paper

Novel HPLC-UV Method for Simultaneous Determination of Fat-soluble Vitamins and Coenzyme Q10 in Medicines and Supplements

Žane Temova Rakuša, Eva Srečnik and Robert Roškar*

University of Ljubljana, Faculty of Pharmacy, Aškerčeva cesta 7, 1000 Ljubljana, Slovenia

* Corresponding author: E-mail: robert.roskar@ffa.uni-lj.si;
Tel: +386 1 4769 655, Fax: +386 1 4258 031

Received: 30-08-2016

For Cutting Edge 2017

Abstract

A precise, accurate and rapid HPLC-UV method for simultaneous determination of fat-soluble vitamins (vitamin D3, E-acetate, K1, β -carotene, A-palmitate) and coenzyme Q10 was developed and validated according to ICH guidelines. Optimal chromatographic separation of the analytes in minimal analysis time (8 min) was achieved on a Luna C18 150 \times 4.6 mm column using a mixture of acetonitrile, tetrahydrofuran and water (50:45:5, v/v/v). The described reversed phase HPLC method is the first published for quantification of these five fat-soluble vitamins and coenzyme Q10 within a single chromatographic run. The method was further applied for quantification of the analytes in selected liquid and solid dosage forms, registered as nutritional supplements and prescription medicines, which confirmed its suitability for routine analysis.

Keywords: Fat-soluble vitamins, coenzyme Q10, HPLC, nutrition supplements, pharmaceuticals

1. Introduction

Fat-soluble vitamins (FSVs) are essential for a variety of biochemical and physiological functions in human body, such as epithelial cell differentiation and vision (vitamin A), calcium and phosphate homeostasis (vitamin D), antioxidative protection in cell membranes (vitamin E) and blood coagulation (vitamin K).^{1,2} As FSV, with the exception of vitamin D3, cannot be obtained by endogenous synthesis, food or vitamin preparations are their main sources. Due to the large number of commercially available vitamin preparations and their widespread use, the quality control of these preparations is extremely important, especially because of the risk of toxicity from excessive intake of vitamins A and D.³

HPLC methods, coupled with different detection techniques: UV,^{4–12} FLD,⁶ ECD,¹³ and MS^{5,14} offer the best approach to accurate content determination of the main FSVs in foods, pharmaceuticals and nutritional supplements. The published HPLC-UV methods for quality control of preparations containing FSVs are quite limited in terms of separation and simultaneous determination of FSVs,^{4,5,7,8,11} often have run time longer than 15 min^{4–6,9,12}

and generally require complicated and time-consuming sample preparation.^{11,12,15,16} Further on, to our knowledge none of the published HPLC methods offer simultaneous determination of FSVs and also β -carotene and coenzyme Q10, which are often found along in medicines and nutritional supplements.

We aimed to develop rapid, accurate, precise and selective HPLC-UV method for simultaneous quantification of FSVs (in their most commonly used forms: A-palmitate, D3, E-acetate, K1 and A provitamin – β -carotene) and coenzyme Q10, using simple and fast extraction procedures (without alkaline saponification or solid phase extraction). The optimised HPLC method was successfully validated according to the ICH guidelines. In addition, medicines and nutritional supplements in liquid and solid dosage forms were analysed to confirm the adequacy of the method.

2. Experimental

2.1. Chemicals and Reagents

All FSVs (vitamin A-palmitate, D3, E-acetate, K1 and β -carotene), butylated hydroxytoluene (BHT), anhy-

drous ferric chloride, *n*-hexane, 85% orthophosphoric acid (H₃PO₄) and HPLC grade: acetonitrile, methanol and tetrahydrofuran (THF) were purchased from Sigma-Aldrich (Steinheim, Germany). Coenzyme Q10 (CoQ10) was obtained from Kaneka Corporation (Osaka, Japan). Ultra-pure water was obtained through a Milli-Q water purification system A10 Advantage (Millipore Corporation, Bedford, MA, USA).

2. 2. Instrumentation and Chromatographic Conditions

Chromatographic analysis was performed on an Agilent 1100/1200 series HPLC system (Agilent Technologies, Waldbronn, Germany) equipped with UV-VIS detector and ChemStation data acquisition system. Chromatographic separation was performed on a reversed-phase Luna C18 (2) 150 × 4.6 mm, 5 μm particle size column (Phenomenex, Torrance, USA) at 25 °C using acetonitrile-tetrahydrofuran-water (50:45:5, v/v/v) as a mobile phase at flow-rate of 1 mL/min. Injection volume (V_{inj}) was 20 μL for all tested samples, except for samples from Preparation 2 and 3, where it was adjusted to 3 and 5 μL, respectively. Detection was carried out at 270 nm.

2. 3. Preparation of Standard Solutions

Standard solutions of FSVs and CoQ10 were prepared fresh daily by dissolving appropriate amounts in 0.05% (*m/v*) solution of BHT in *n*-hexane. Nine calibration standards were prepared as mixtures of all tested compounds in 0.05% (*m/v*) solution of BHT in *n*-hexane in different concentration ranges for different analytes, selected considering the concentrations and proportions of the analytes in the investigated pharmaceutical formulations (Table 1). Quality control (QC) samples at three concentration levels were prepared by diluting separately prepared stock solutions with 0.05% (*m/v*) solution of BHT

in *n*-hexane (Table 1). Prepared calibration standards and QC samples were evaporated to dryness under a stream of nitrogen at 40 °C (TurboVap LV, Caliper, Hopkinton-MA, USA). Dry residues were reconstituted in 1.0 mL of 0.01% (*m/v*) solution of BHT in mobile phase.

2. 4. Method Validation

The method was validated according to ICH guidelines Q2(R1)¹⁷ in terms of selectivity, linearity, limit of quantification, precision, accuracy, recovery, sample stability and robustness.

Method selectivity was assessed by comparing chromatograms of individual standard solutions, mixture containing all standards, all used solvents and several common excipients found in commercial preparations (citric acid, sodium hydrogen phosphate, glycerol, propylene glycol, sodium benzoate, methyl- and propylparaben).

Linearity was evaluated based on nine calibration standards (Table 1). The procedure was repeated three times, using different stock solution, for three consecutive days of the validation. Injection volume during validation was 20 μL. Linearity was determined based on least-square linear regression. The acceptance criterion for determination coefficient was R² > 0.999.

Limit of quantification (LOQ) was calculated from the regression lines, using the following equations: LOQ = (10 × σ) / S, where σ is the standard deviation of the intercept, S is the average slope of the calibration curve.

Accuracy and precision were examined in terms of repeatability, precision and accuracy (intra- and inter-day) during three consecutive validation days, based on three QC samples covering low (QC_L), medium (QC_M) and high ranges (QC_H) of the calibration standards (Table 1). QC samples were prepared separately, in triplicate, each day of the validation. Injection repeatability was evaluated on three concentration levels by re-injecting the same QC sample six times. Intra- and inter-day pre-

Table 1. Concentrations of calibration standards and QC samples

		Concentration [mg/L]					
		β-carotene	A-palmitate	D3	CoQ10	E-acetate	K1
Calibration standards		60	600	50	400	2600	150
		36	360	30	240	1560	90
		12	120	10	80	520	30
		6.0	60	5.0	40	260	15
		1.2	12	1.0	8.0	52	3.0
		0.60	6.0	0.50	4.0	26	1.5
		0.30	3.0	0.25	2.0	13	0.75
		0.12	1.2	0.10	0.80	5.2	0.30
		0.06	0.60	0.05	0.40	2.6	0.15
	QC samples*	QC _H	48	480	40	320	2080
QC _M		24	240	20	160	1040	60
QC _L		3.0	30	2.5	20	130	7.5

* QC_H, QC_M and QC_L – quality control samples with high, medium and low concentrations

cision (relative standard deviation – RSD) was expected to be not more than 5% (2% for injection repeatability) and intra- and inter-day accuracy (ratio (%) between calculated concentration for the obtained QC response based on the line equation and nominal concentration, which was calculated considering the sample preparation) within $\pm 5\%$. Accuracy of the injection volume variations was evaluated by re-injecting different volumes (3, 5, 15, 25 and 30 μL) of the same QC sample three times and comparing it proportionally to the nominal value (injection volume 20 μL) and was expected to be within $\pm 5\%$.

Sample stability was evaluated at three concentration levels (QC) and additionally in samples from Preparation 6 (tablets) and Preparation 7 (capsules) at 25 °C for two days (at 0 and 24 h) and was expressed as ratio between the concentration at 24 h and the concentration at time 0. The acceptance criterion was $100 \pm 5\%$.

Method recovery was determined by spiking preparation solutions with approximately the same amount of the analytes, as contained in the preparations, in triplicate. Non-spiked preparations and standard solutions containing the added amounts were separately analysed. Average recoveries were calculated by the formula: recovery (%) = $100 \times (\text{concentration found in spiked sample} - \text{concentration found in unspiked sample}) / \text{added concentration}$.

The robustness of the method was investigated by deliberate modifications made to chromatographic conditions and sample preparation procedure. In sample preparation procedure for preparations in solid dosage form, different vortexing times (10 ± 5 min), shaking times (30 ± 10 min), sonication times (10 ± 5 min) and different drying temperature (40 ± 5 °C) were tested. To evaluate robustness in terms of chromatographic conditions, different injection volumes (20 ± 5 μL), column temperatures (25 ± 2 °C), flow rates (1.00 ± 0.05 mL/min), detection wavelengths (270 ± 5 nm) and mobile phase compositions acetonitrile-tetrahydrofuran-water (50.50:44.55:4.95 and 50:45:5 v/v/v) were tested.

2. 5. Sample Preparation of Nutritional Supplements and Medicines

The validated method was further applied to assay vitamins and CoQ10 content in commercially available pharmaceutical preparations: three solutions, three tablets and two soft-shelled capsules, registered as medicines or nutritional supplements. Each preparation was prepared and analysed in triplicate.

Liquid preparations were either directly analysed (Preparation 2 and 3) or diluted 100-fold with 0.01% (m/v) solution of BHT in mobile phase prior to analysis (Preparation 1). The extraction procedure for tablets was as follows: one tablet (whole or powdered depending on the preparation) was added to 2.0 mL of 0.1% H_3PO_4 into

a centrifuge tube and vortexed for 10 min. Organic solvent (8.0 mL of 0.05% (m/v) solution of BHT in *n*-hexane) was added to the samples, before their further sonication (10 min) and vortexing (2 min). Samples were then centrifuged for 10 min at 25 °C and 5000 rpm. Fraction of the clear supernatant (1–3 mL depending on the preparation) was evaporated to dryness under a stream of nitrogen at 40 °C and reconstituted in 1.0 mL of 0.01% (m/v) solution of BHT in mobile phase. The content of vitamins and CoQ10 in soft-shelled capsules was evaluated by cutting one capsule in half and adding organic solvent (*n*-hexane with 0.05% (m/v) BHT : THF = 95:5 (v/v)). The samples were sonicated (10 min), shaken (30 min) and centrifuged (10 min, 25 °C, 5000 rpm). The clear supernatant (0.5 mL) was evaporated to dryness under a stream of nitrogen at 40 °C and reconstituted in 1.0 mL of 0.01% (m/v) solution of BHT in mobile phase. Samples from preparations containing CoQ10 (Preparation 6 and 7) were additionally reconstituted in 1.0 mL of 0.1% (m/v) solution of Fe^{3+} in mobile phase, which acts as an oxidant and enables evaluation of total CoQ10.

3. Results and Discussion

3. 1. Optimization of Chromatographic Conditions

The main objective of the study was to obtain optimal analytical method in terms of sample preparation and chromatographic conditions for simultaneous quantification of FSVs and CoQ10 in medicines and nutritional supplements. Chromatographic conditions were optimized in order to achieve baseline separated, symmetric peaks of the target analytes in minimal analysis time. Selection of stationary phase (various C18 reversed phase analytical columns) was based on our experience and previous research. Several mixtures of acetonitrile and methanol in isocratic and gradient modes were tested and found suitable for chromatographic separation of all tested analytes except CoQ10, which eluted only after THF was added to the mobile phase. Various mixtures of acetonitrile, THF and water at flow rates 0.5–2.0 mL/min and column temperatures 25–40 °C and detection wavelengths 210–325 nm were tested to optimize the chromatographic separation of all tested vitamins as well as both reduced and oxidized form of CoQ10. Detection wavelength 270 nm was selected as optimal compromise between absorbance of the individual analytes and their concentration in the tested preparations, with particular reference to vitamins D3 and K1, which have the lowest contents in the tested multivitamin preparations. Optimized chromatographic conditions resulted in symmetric and separated peaks with a short run time (Figure 1). The obtained run time is considerably shorter in comparison to other similar published HPLC-UV methods.^{4–6,9,12}

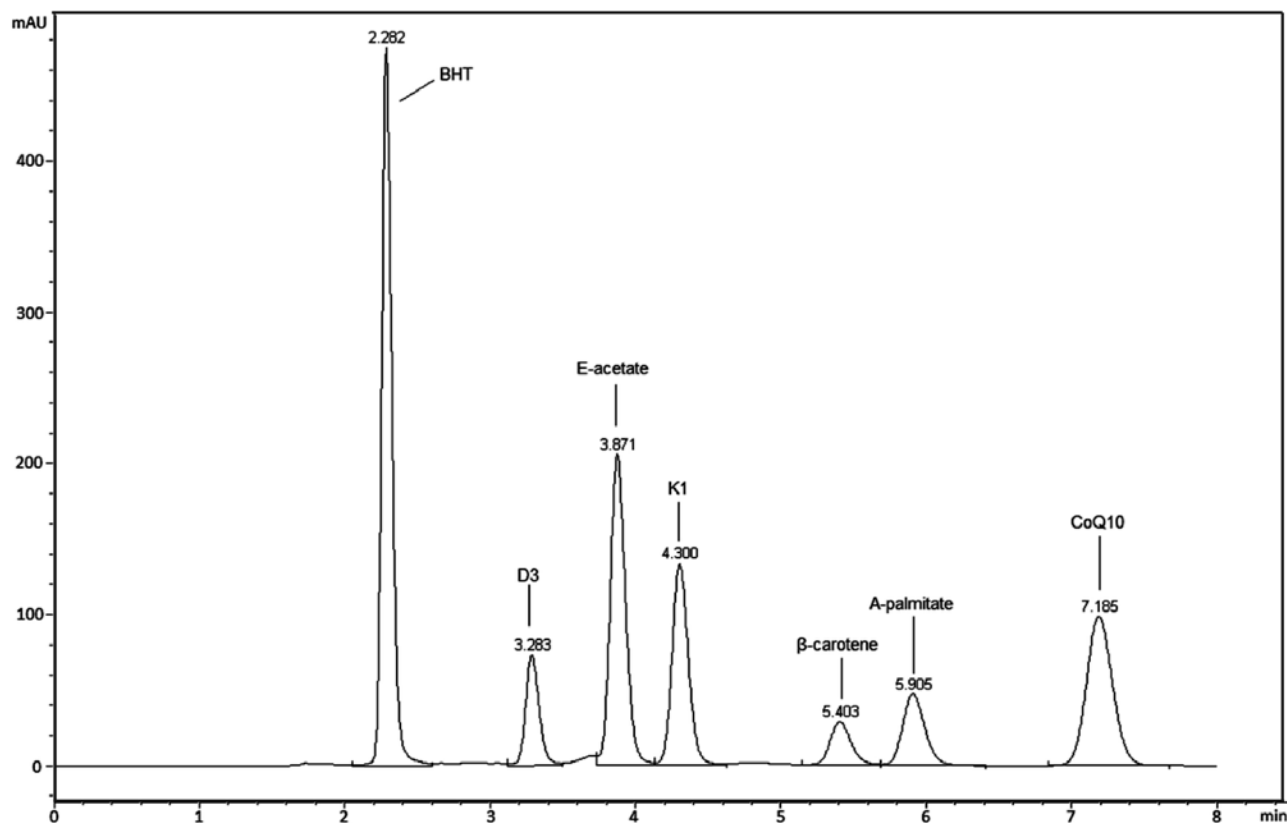


Figure 1: A chromatogram of standard mixture of fat-soluble vitamins and coenzyme Q10.

3. 2. Optimization of Sample Preparation

The optimised HPLC method was further applied to evaluate the content of FSVs and CoQ10 in commercial pharmaceuticals with particular attention to sample preparation, as a crucial step in the analysis of medicines and nutritional supplements. We aimed to develop simple and fast extraction procedure with a minimal number of steps and solvent consumption.

The extraction procedure for tablets was adjusted from Temova and Roškar's method for vitamin D3 extraction,¹⁸ which comprised of addition of 0.1% H_3PO_4 to two tablets, vortexing for 2 min, subsequent addition of methanol (8.0 mL), sonication (10 min), vortexing (2 min) and centrifugation of the samples. In order to determine the optimal method, studies were done with (2.0 mL) and without the addition of 0.1% H_3PO_4 to one powdered tablet. Hereafter, different shaking times (0, 2, 4, 5 and 15 min with vortex mixer and 30 min with rotary mixer), organic solvents (methanol, *n*-hexane and mobile phase), sonication times (0, 5, 10, 15 min), further shaking times (0, 2 and 4 min with vortex mixer and 30 min with rotary mixer) and centrifugation times (0, 10 and 15 min) at 25 °C and 5000 rpm were tested. The best extraction in terms of method recoveries was achieved with the addition of 2.0 mL of 0.1% H_3PO_4 into a centrifuge tube with one tab-

let, vortexing for 10 min and addition of 0.05% (*m/v*) solution of BHT in *n*-hexane (8.0 mL), before their further sonication (10 min) and vortexing (2 min). Samples were then centrifuged for 10 min at 25 °C and 5000 rpm.

The optimization of the extraction procedure for soft-shelled capsules started with investigation of extraction organic solvents (anhydrous ethanol, methanol, *n*-hexane, different mixtures of *n*-hexane and methanol, mobile phase, *n*-hexane:THF = 95:5 (*v/v*)), to determine the optimal solvent, which was found to be *n*-hexane with 0.05% (*m/v*) BHT : THF = 95:5 (*v/v*). THF was added to solve the issue of poor solubility of β -carotene. Further on, sonication time (0, 5, 10, 15 min), shaking time (15, 30, 45, 60 min) and reconstitution solvent (methanol, mobile phase and 0.01% (*m/v*) solution of BHT in mobile phase) were tested in order to obtain optimal recoveries of the extraction procedure. The final extraction parameters (10 min sonication, 30 min shaking and 0.01% (*m/v*) solution of BHT in mobile phase as reconstitution solvent) provided suitable recoveries and sample stability of all analytes (Table 3).

3. 3. Method Validation

Selectivity of the method was confirmed as no interfering peaks were found at retention times of the selected

analytes (Figure 1). The standard calibration curves were linear over concentration ranges as presented in Table 2. Appropriate linearity was achieved with the addition of lipophilic antioxidant – BHT, especially for vitamin A-palmitate ($R^2 = 0.9945$ without BHT) and β -carotene ($R^2 = 0.9935$ without BHT). As shown in Table 2 on the example of QC medium sample, intra-day, inter-day and accuracy of the injection volume variations was better than $\pm 5\%$ at all times, which is within the defined acceptance criteria. Similarly, intra and inter-day precision were below 3% in all cases and injection repeatability was less than 2% (Table 2). Sample stability after 24 h was assessed

in order to ensure that the obtained concentration results adequately reflect those directly after sampling. Stability of all tested analytes in QC samples and samples from Preparation 6 and 7 after 24 h in the autosampler at 25 °C was within the defined acceptance criteria $100 \pm 5\%$. Such sample stability in QC samples was obtained after the addition of BHT, especially for vitamin A-palmitate and β -carotene, which were found subject to extensive degradation without appropriate stabilization with BHT (22 and 70% after 24 h for vitamin A-palmitate and β -carotene, respectively). Method was found robust to slight changes in both chromatographic and sample preparation

Table 2. Validation data

Analyte	Range [mg/L]	LOQ [mg/L]	R^2	Accuracy			Precision		Injection repeatability
				Intra-day	Inter-day	Variation of Vinj*	Intra-day	Inter-day	
A-palmitate	1.2 – 600	1.2	0.9996	100.90	100.96	99.7–101.4	0.27	0.20	0.19
CoQ10	0.80 – 400	0.80	0.9997	100.89	100.94	100.0–101.5	0.53	0.98	0.10
D3	0.25 – 50	0.15	0.9998	100.99	101.06	99.9–100.9	0.55	2.69	0.24
E-acetate	2.6 – 2600	1.5	0.9996	99.93	99.90	99.1–103.2	0.56	2.32	0.14
K1	0.30 – 150	0.20	0.9997	101.18	101.24	100.0–101.7	0.40	0.87	0.13
β -carotene	0.12 – 60	0.12	0.9997	101.24	101.30	100.0–100.4	0.52	1.28	1.83

* different injection volumes (3, 5, 15, 25 and 30 μ L), calculated to nominal injection volume 20 μ L

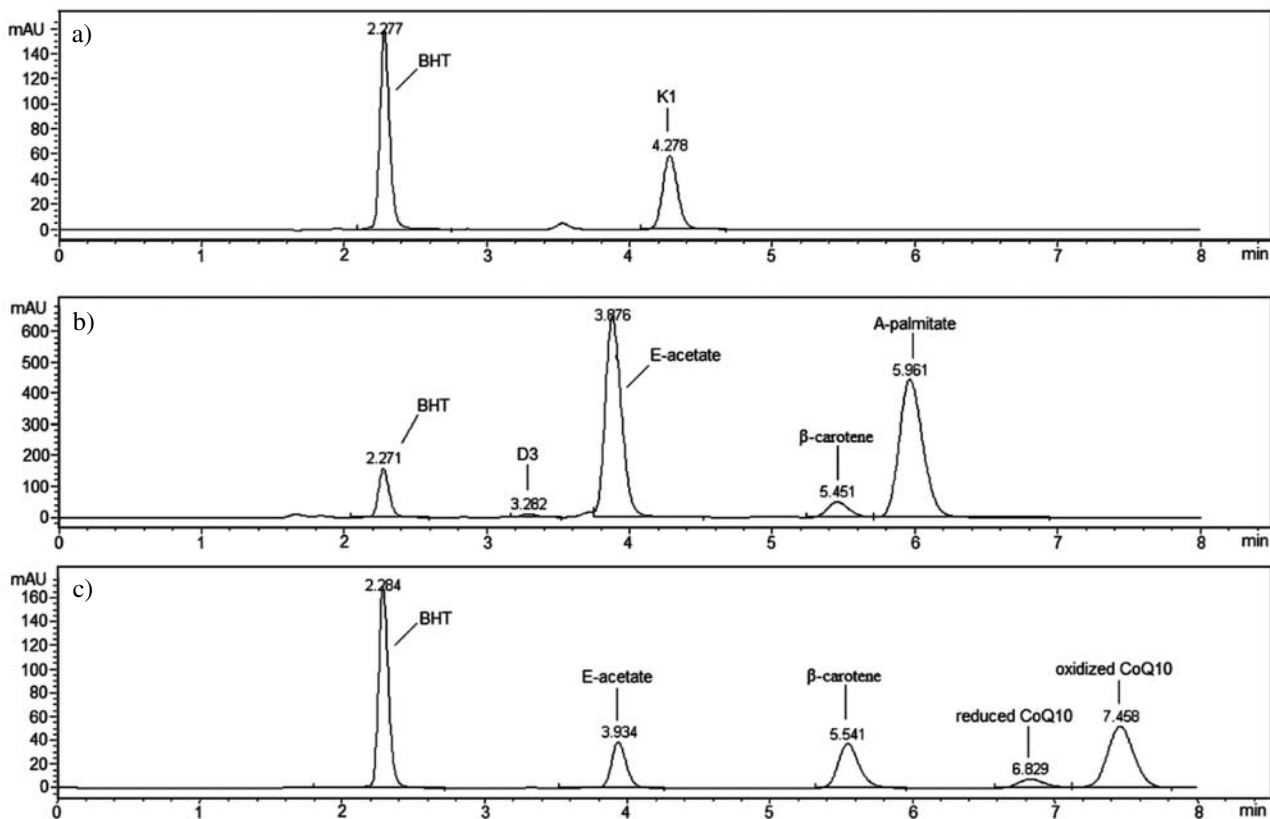


Figure 2: Representative chromatograms of a) Preparation 1 – solution, b) Preparation 5 – tablets and c) Preparation 7 – capsules, which also contains a reduced form of CoQ10 that is chromatographically separated from its general form (oxidized CoQ10).

parameters. The obtained results from samples prepared with deviations in the sample preparation procedure, were accurate ($100 \pm 5\%$) and precise ($RSD < 5\%$). In all varied chromatographic conditions the resolution between the studied compounds was not altered, demonstrating the robustness of the method.

3. 4. Assay in Nutritional Supplements and Medicines

In order to test the applicability of the developed and validated HPLC method to commercial multi-vitamin preparations, six pharmaceutical preparations, registered as medicines and two nutritional supplements in various dosage forms (solutions, tablets, soft shelled capsules) were tested to evaluate the content of the analytes in relation to the value claimed on the label. Liquid preparations were either directly analysed (Preparation 2 and 3) or diluted with 0.01% (*m/v*) solution of BHT in mobile phase prior to analysis (Preparation 1). Samples from tablets and capsules were prepared according to the optimised extraction procedure (Section 3.2) Representative chromatograms of samples from all three dosage forms are presented in Fi-

gure 2. The results for average contents and calculated method recoveries are presented in Table 3. High recoveries and low standard error values (Table 3) confirmed the suitability of the established HPLC method for quantification of the target analytes in liquid and solid preparation without any pre-treatment (Preparation 2 and 3) or after a simple and rapid pre-treatment (other preparations).

4. Conclusions

The main novelty in our approach is the developed HPLC method, which to our knowledge, is the first published method for simultaneous determination of five fat-soluble vitamins (A-palmitate, D3, E-acetate, K1 and A provitamin – β -carotene) and coenzyme Q10. Moreover, analysis time of only 8 min is favourable in comparison to other published HPLC-UV methods for determination of fewer fat-soluble vitamins. The obtained results from the assay in commercial nutrition supplements and medicines confirmed that the method is appropriate for routine analysis and quality control of multi-vitamin products in pharmaceutical and health food industries. Considering

Table 3. Average content in medicines and nutritional supplements along with method recoveries ($n = 3$)

	Analyte	Declared content	Determined content (average \pm standard error [%])	Method recovery [#] [%]	
Solutions	Medicines	K1	10 mg/mL	PREPARATION 1 9.97 \pm 0.02 mg/mL 103.8	
		A-palmitate	3300 μ g/mL	PREPARATION 2 4594 \pm 3 μ g/mL	
		D3	50 μ g/mL	62.4 \pm 0.2 μ g/mL 100.1	
		D3	100 μ g/mL	PREPARATION 3 114.7 \pm 0.3 μ g/mL 98.4	
	Tablets	Medicines	A-palmitate	330 μ g/tbl	PREPARATION 4 394 \pm 1 μ g/tbl 99.3
			D3	2 μ g/tbl	2.43 \pm 0.04 μ g/tbl 99.3
A-palmitate			2750 μ g/tbl	PREPARATION 5 3336 \pm 55 μ g/tbl 94.2	
Nutritional supplement		D3	10 μ g/tbl	12.2 \pm 0.1 μ g/tbl 95.8	
		E-acetate	15 mg/tbl	17.8 \pm 0.3 mg/tbl 96.9	
		β -carotene*	/	0.120 \pm 0.003 mg/tbl 104.2	
Capsules	Medicine	A-palmitate	800 μ g/tbl	PREPARATION 6 863 \pm 16 μ g/tbl 99.6	
		CoQ10	4.5 mg/tbl	3.92 \pm 0.17 mg/tbl 99.2	
		D3	5 μ g/tbl	7.32 \pm 0.07 μ g/tbl 104.8	
		E-acetate	12 mg/tbl	12.2 \pm 0.8 mg/tbl 97.2	
	Nutritional supplement	K1	25 μ g/tbl	18.1 \pm 0.7 μ g/tbl 97.4	
		CoQ10	30 mg/caps	PREPARATION 7 28.6 \pm 0.1 mg/caps 102.3	
		E-acetate	24 mg/caps	34.3 \pm 0.2 mg/caps 98.1	
		β -carotene*	/	3.36 \pm 0.02 mg/caps 108.0	
	E-acetate	30 mg/caps	PREPARATION 8 45.5 \pm 0.8 mg/caps 99.8		
	β -carotene	7 mg/caps	8.03 \pm 0.10 mg/caps 108.2		

* content not defined; # method recovery calculated according to the formula in section 2.4.

that most of the tested preparations had considerably higher contents than labelled (up to 150%), quality control of these preparations is of extreme importance.

5. References

1. S. Kucukkolbasi, N. Ires, H. Kara. *J. Selcuk Univ. Nat. Appl. Sci.* **2001**, 30–47.
2. O. Heudi, M. Trisconi, C. Blake. *J. Chromatogr. A* **2004**, 1022, 115–123.
<https://doi.org/10.1016/j.chroma.2003.09.062>
3. F. Granado-Lorencio, E. Rubio, I. Blanco-Navarro, B. Pérez-Sacristán, R. Rodríguez-Pena, F. J. García López. *Food Chem. Toxicol.* **2012**, 50, 2106–8.
<https://doi.org/10.1016/j.fct.2012.03.001>
4. S. N. Anuradha, S. Arunkumar. *Int. J. Pharma. Bio. Sci.* **2012**, 3, 322–327.
5. D. E. Breithaupt, S. Kraut. *Eur. Food Res. Technol.* **2006**, 643–649. <https://doi.org/10.1007/s00217-005-0195-7>
6. S. Kucukkolbasi, O. Bilber, H. Filiz Ayyildiz, H. Kara. *Quim. Nov.* **2013**, 36, 1044–1051.
7. G. Kłackow, E. L. Anuszevska. *Acta Pol. Pharm.* **2000**, 57, 167–170.
8. B. Buszewski, W. Zbanyszek. *J. Liq. Chromatogr. Relat. Technol.* **2002**, 25, 1229–1241.
<https://doi.org/10.1081/JLC-120004021>
9. L. Chen, L. Zhiyong, K. Xuejun, Z. Xiaoling, Z. Shenglan, G. Zhongze. *Procedia Environ. Sci.* **2011**, 8, 588–595.
<https://doi.org/10.1016/j.proenv.2011.10.091>
10. S. Wielinski, A. Olszanowski. *J. Liq. Chrom. Rel. Technol.* **2001**, 24, 201–213.
<https://doi.org/10.1081/JLC-100001482>
11. P. Moreno, V. Salvadó. *J. Chromatogr. A* **2000**, 870, 207–215. [https://doi.org/10.1016/S0021-9673\(99\)01021-3](https://doi.org/10.1016/S0021-9673(99)01021-3)
12. V. Kienen, W. F. Costa, J. V. Visentainer, N. E. Souza, C. C. Oliveira. *Talanta* **2008**, 75, 141–146.
<https://doi.org/10.1016/j.talanta.2007.10.043>
13. I. Acworth, P. Gamache. Thermo Fisher Scientific, Chelmsford, MA, USA.
14. C. Nimalaratne, C. Sun, J. Wu, J. M. Curtis, A. Schieber. *Food Res. Int.* **2014**, 66, 69–77.
<https://doi.org/10.1016/j.foodres.2014.08.034>
15. J. L. Luque-García, L. Castro. *J. Chromatogr. A* **2001**, 935, 3–11. [https://doi.org/10.1016/S0021-9673\(01\)01118-9](https://doi.org/10.1016/S0021-9673(01)01118-9)
16. A. Jedlička, J. Klimeš. *Chem. Pap.* **2005**, 59, 202–222.
17. International Conference on Harmonization (ICH) Guidelines, Q2(R1) Validation of analytical procedures, Commission of the European Communities, **2005**.
18. Ž. Temova, R. Roškar. *J. Chromatogr. Sci.* **2016**, 54, 1180–6.
<https://doi.org/10.1093/chromsci/bmw048>

Povzetek

Razvili in validirali smo natančno, točno in hitro HPLC-UV metodo za sočasno vrednotenje lipofilnih vitaminov (vitamin D3, E-acetat, K1, β -karoten, A-palmitat) in koencima Q10. Optimalno kromatografsko ločbo analitov v kratkem času analize (8 min) smo dosegli na koloni Luna C18 150 \times 4,6 mm z uporabo mobilne faze: acetonitril, tetrahidrofuran in voda (50: 45: 5, v/v/v). Opisana reverznofazna HPLC-UV metoda je prva objavljena analizna metoda za sočasno vrednotenje izbranih lipofilnih vitaminov in koencima Q10. Metodo smo nadalje uporabili za vrednotenje teh analitov v izbranih zdravilih in prehranskih dopolnilih, v tekočih in trdnih farmacevtskih oblikah ter tako potrdili njeno primernost za rutinsko uporabo.

Scientific paper

Trans-Activation Response Element RNA is Detectable in the Plasma of a Subset of Aviremic HIV-1–Infected Patients

Anžej Hladnik,¹ Jana Ferdin,¹ Katja Goričar,¹ Steven G. Deeks,²
Boris M. Peterlin,² Ana Plemenitaš,¹ Vita Dolžan¹ and Metka Lenassi^{1,*}

¹ Institute of Biochemistry, Faculty of Medicine, University of Ljubljana, Ljubljana, Slovenia

² Department of Medicine, University of California, San Francisco (UCSF), San Francisco, California, USA

* Corresponding author: E-mail: metka.lenassi@mf.uni-lj.si

Tel: +386-1-5437658; Fax: +386-1-5437641

Received: 31-08-2016

For Cutting Edge 2017

Abstract

Determining the HIV-1 reservoir size in infected individuals is of great importance for improvement of their treatment. Plasma trans-activation response element (TAR) RNA has been suggested as one of the possible biomarkers. TAR RNA is produced during non-processive transcription in HIV-1 productively infected and latent T cells. Here, plasma samples and paired exosome samples of 55 subjects from the observational SCOPE cohort were analysed for the presence of TAR RNA. First, a PCR-based assay was optimized, which provided 100% specificity and 100% sensitivity in differentiating HIV-1 infected non-controllers from uninfected individuals. Next, TAR RNA was detected in the plasma of 63% of aviremic HIV-1–infected patients, who were either treated with antiretroviral therapy or were elite controllers. Although TAR RNA levels did not correlate with patient gender, age, CD4 levels, CD8 levels, they tended to correlate with CD4/CD8 ratio ($P = 0.047$). This study is the first to investigate plasma TAR RNA in a relatively large cohort of HIV-1–infected patients. We additionally show that the TAR RNA molecules in the plasma of aviremic patients are not limited to exosomes.

Keywords: HIV-1, trans-activation response element, exosomes, latency, HIV-1 reservoir, miRNA

1. Introduction

HIV remains a major global public health issue, and the World Health Organisation has estimated that around 36.7 million people were infected at the end of 2015. In the majority of HIV-1–infected patients, the combination antiretroviral therapy (ART) reduces plasma HIV-1 RNA to clinically undetectable levels. However, this treatment cannot eradicate proviruses hidden in CD4 T cells and other latent reservoirs.¹ Over 90% of these proviruses are believed to be defective, such that they cannot produce intact viruses,² although they were recently shown to produce novel protein-encoding RNA species.³ These might contribute to chronic inflammation, which together with antiretroviral drug toxicity and the traditional risk factors, might promote increased risk of developing non-

AIDS–associated diseases in ART-treated adults (e.g., cardiovascular, liver, renal and bone diseases, cancers).^{4–6} Thus, determination of the size of the HIV-1 reservoir in aviremic individuals is important for the understanding of HIV pathogenesis and to adjust the therapy to improve the quality of life of the patient.

One potential biomarker of the patient HIV-1 reservoir is the transactivation-response element (TAR) RNA and its micro RNAs, hiv-1-miR-TAR-3p and hiv-1-miR-TAR-5p. The 57-nucleotide TAR hairpin structure is part of the long terminal repeat promoter of the HIV genome (Figure 1A). This acts as a binding site for the viral-encoded transactivator protein Tat, which is important for induction of transcription of full-length viral mRNAs during productive infection (i.e., processive transcription). In the absence of Tat during latency, transcription is lar-

gely non-processive, which results in the release of short RNAs that include the TAR region (Figure 1B).⁷ In infected primary T lymphocytes and latently infected cell lines, these short TAR RNAs are processed by Dicer to yield *hiv-1*-miR-TAR-3p, and to a lesser extent also *hiv-1*-miR-TAR-5p.^{8–12} HIV TAR miRNAs target and modulate the expression of several T-cell mRNAs that are involved in apoptosis resistance of HIV-1-infected cells.^{13,14} They can also repress viral gene expression through transcriptional silencing in HIV-1-infected 293 cells⁸ and human primary macrophages,¹⁵ thereby contributing to viral latency.

Importantly, TAR RNA and miR-TARs are released from HIV-1-infected cells within exosomes, which have a putative role in decreasing apoptosis and increasing sus-

ceptibility to HIV-1 infection of recipient T cells,¹⁶ and increasing release of proinflammatory cytokines from recipient macrophages.^{12,17} TAR-RNA-containing exosomes have also been detected in the serum of a small number of aviremic HIV-1-infected patients.^{12,16,17} Exosomes are nano-sized membrane vesicles that are secreted by fusion of multivesicular bodies with the plasma membrane of the cell. They are released from cells in culture *in vitro* and are found in various body fluids *in vivo*, like blood plasma, cerebrospinal fluid, urine, and others (reviewed in They et al.¹⁸). Exosomes consist of a lipid bilayer membrane that surrounds a small amount of cytosol, and they contain various typical proteins, lipids and nucleic acids, which mirror the composition of the cell of origin.¹⁹ Exo-

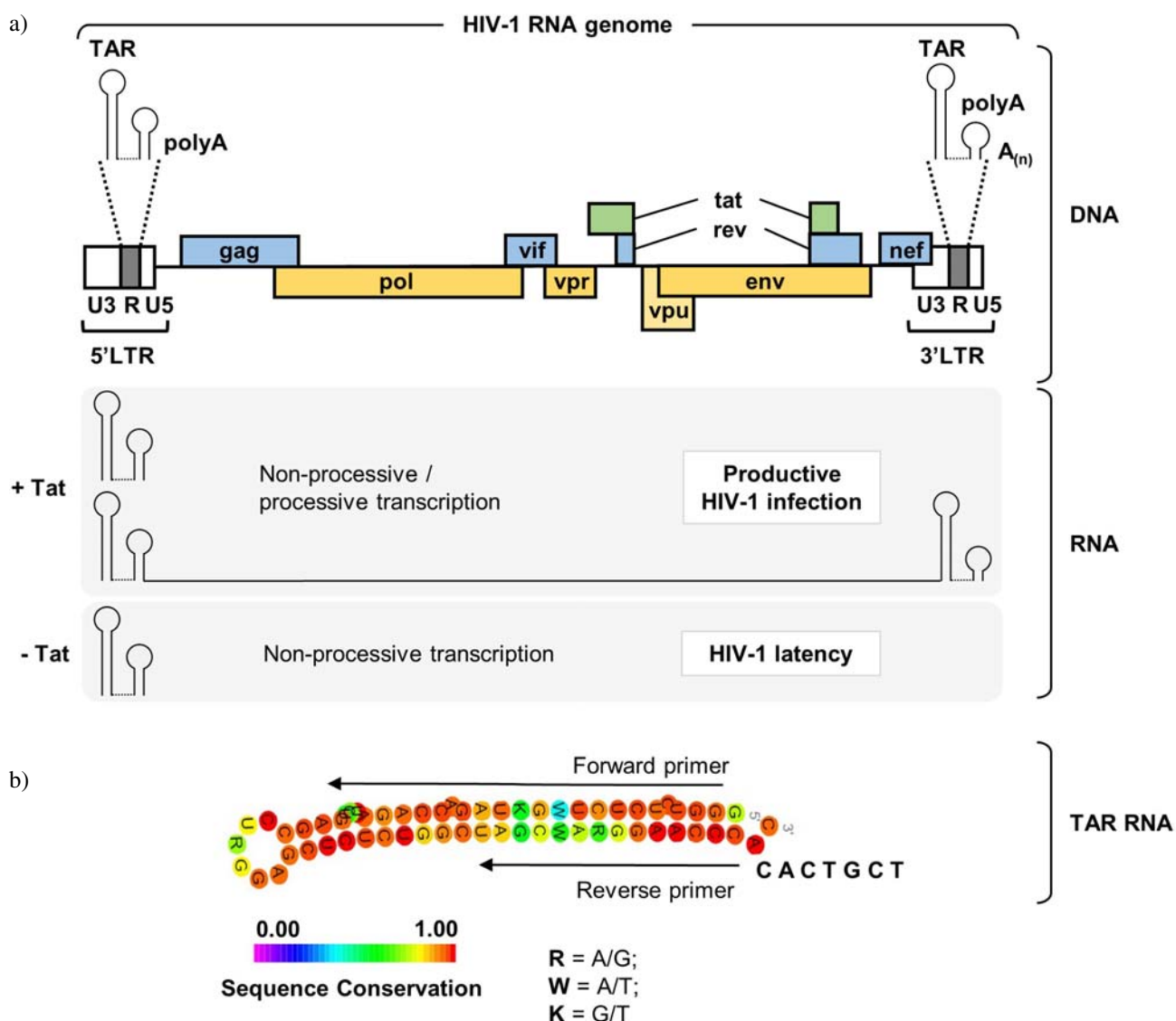


Figure 1. TAR as part of the HIV-1 provirus, HIV-1 genome, and TAR RNA. (a) Scheme of the HIV-1 genome (modified from Harwig et al.¹¹), showing the long terminal repeat (LTR) region divided into the U3, R (including TAR) and U5 domains. In the presence of Tat (+Tat), full-length viral RNA and short TAR RNA molecules are transcribed, while in the absence of Tat (-Tat), only TAR RNA is produced. (b) Structure and sequence conservation of the TAR hairpin (57 nucleotides) with the indicated oligonucleotides used for the specific amplification of TAR RNA.

somes have an important role in physiological processes and various pathological conditions,^{20–22} including HIV pathogenesis,^{23,24} and thus have promising potential for human diagnostics and therapeutic applications.²⁵

The aim of the present study was to determine whether TAR RNA can be found in the blood plasma of aviremic HIV-1-infected patients in a relatively large cohort, and to examine whether detection of TAR RNA correlates to patient clinical characteristics. To this end, a TAR-specific PCR assay was first optimised on uninfected controls and viral non-controllers, with determination of its specificity and sensitivity. Next, plasma TAR-RNA levels were determined in a cross-sectional study of ART-suppressed patients and elite controllers.

2. Experimental

2.1. Subjects

This study was based on 55 plasma samples from the Observational Study of the Consequences of the Protease Inhibitor Era (SCOPE) cohort, which were collected from well-characterised HIV-infected volunteers of diverse demographic and clinical status at the HIV/AIDS clinic of the San Francisco General Hospital, following protocols approved by the University of California, San Francisco, Committee on Human Research. All of the subjects provided written informed consent.

In brief, whole blood samples were collected in commercially available EDTA-treated tubes and processed by low-speed centrifugation (2000× *g*, 15 min) within 2 h, with the supernatants aliquoted, frozen, and stored at –70 °C. The study subjects were stratified into four groups: (i) HIV-1 uninfected subjects ('HIV negative'; *n* = 9); (ii) 'non-controllers' (*n* = 8), as HIV-1-infected patients who had never been treated with ART; (iii) ART-treated virologic controllers ('ART-suppressed'; *n* = 19), as HIV-1-infected patients with undetectable plasma HIV RNA levels for at least 6 months while treated with ART; and (iv) spontaneous virologic controllers ('elite controllers'; *n* = 19), as untreated HIV-infected patients who had shown at least three documented plasma HIV RNA levels <75 copies/mL over at least a 12-month period. The clinical characteristics of these patients are given in Table 1.

2.2. RNA Extraction from Plasma and Plasma Exosomes

Initially, the plasma samples (1 mL) were slowly defrosted on ice (i.e., approximately 1 h at 4 °C) and centrifuged (2000× *g*, 30 min) to remove precipitated lipids and any remaining white blood cells and platelets. The TRIzol nucleic acid extraction reagent (Invitrogen) was added to an aliquot (200 µL) of each plasma sample, which were then mixed well and stored at –70 °C until further proces-

sing. The rest of the plasma of each sample was filtered through a 0.45-µm membrane (Millipore), diluted threefold with Dulbecco's phosphate-buffered saline, and centrifuged (110,000× *g*, 2 h; SW-41 Ti rotor) on a 20% sucrose cushion, to purify the exosomes. The pelleted exosomes, and in the case of the non-controllers also the viruses, were resuspended in Dulbecco's phosphate-buffered saline, after which TRIzol nucleic acid extraction reagent was added, and the samples were stored at –70 °C until further processing.

For the extraction of small non-coding RNA from these processed samples, a combination of TRIzol RNA extraction and spin column miRNA enrichment was used, as described previously by Valadi et al.²⁶ First, the RNA extraction with TRIzol (Invitrogen) was carried out following the manufacturer guidelines, until the phase separation by chloroform, after which the upper aqueous phase of each sample was transferred to RNeasy spin columns (miRNeasy mini kits; Qiagen), and the manufacturer instructions were followed. In the last step, the enriched small non-coding RNA was eluted from the columns with 50 µL RNase-free water with centrifugation at 15,000× *g* for 2 min.

2.3. TAR-RNA-specific Reverse-transcription

Gene-specific cDNA for TAR RNA was generated using SuperScript IV Reverse Transcriptase kits (Invitrogen) and the TAR-specific reverse primer (TAR-R [+42 - +62]: 5'- AGC AGT GGG TTC CCT AGT TAG - 3'; Figure 1B), following the manufacturer instructions. In brief, each single 10 µL reverse transcription reaction started with 0.5 µL 10 mM dNTP mix, 1 µL 2 µM TAR-R [+42 - +62] primer, 2.5 µL RNase free H₂O, and 2 µL plasma / exosomes RNA, combined as a volume of 6 µL. This RNA-primer mix was heated at 65 °C for 5 min, and then incubated on ice for at least 1 min. Next, the following additions were made to the RNA-primer mixture: 2 µL 5× SSIV Buffer, 0.5 µL 100 mM 1,4-dithiothreitol, 1 µL ribonuclease inhibitor (RNaseOUT, 40 U/µL; Invitrogen) and 0.5 µL SuperScript IV Reverse Transcriptase (200 U/µL; Invitrogen). This total mixture of 10 µL was then incubated at 55 °C for 10 min, heat inactivated at 80 °C for 10 min, and stored at –20 °C.

2.4. TAR-specific PCR Detection

PCR analysis was performed using two different polymerase systems: ExiLent SYBR Green master mix (Exiqon), and GoTaq Green master mix (Promega). The PCR reaction mixture of 25 µL contained: 5 µL TAR-specific cDNA (diluted 5-fold in DNase free H₂O), 12.5 µL 2× PCR master mix, 5 µL DNase-free H₂O, and 2.5 µL 10 µM TAR-primer mix (TAR-R [+42 - +62]: 5'- AGCAGTGGGTTCCCTAGTTAG - 3'; TAR-F:

5'-GGTCTCTCTGGTTAGACC-3'). The PCR amplification started with denaturation at 95 °C for 2 min, followed by 40 amplification cycles of 30 s at 95 °C, 30 s at 60 °C, and 30 s at 72 °C. After amplification, the PCR-products were resolved in 5% agarose gels containing ethidium bromide, which were run at 110 V in TBE buffer. Finally, the TAR-specific PCR-product was documented by Mini-Bis (DNR BioImaging Systems, Biosciences). For samples, where TAR-specific PCR-product was not detected, the PCR was repeated on undiluted TAR-specific cDNA (2.5 µL per 25 µL reaction).

2. 5. Statistical Analysis

Median and interquartile ranges or frequencies were used to describe continuous or categorical variables. Mann-Whitney tests or Fisher's exact tests were used to compare clinical characteristics among groups with differing TAR expression. Statistical analysis was performed using IBM SPSS Statistics, version 19.0 (IBM Corporation, Armonk, USA). The level of statistical significance was set at $P < 0.05$.

3. Results and Discussion

Determination of the HIV-1 reservoir size in infected individuals is of great importance for the improvement of their treatment, and plasma TAR RNA might serve as one such biomarker. TAR RNA was previously detected in two sera and sera-exosome-enriched samples from avire-

mic ART-suppressed patients and elite controllers,¹⁶ and in an additional four sera exosome-enriched samples from aviremic ART-suppressed patients.¹⁷ However, to date, plasma TAR-RNA levels have never been tested on a larger cohort of HIV-1-infected patients. In the present study, plasma samples and paired exosome samples of 55 subjects from the SCOPE cohort were analysed for the presence of TAR RNA. The clinical characteristics of these patients are given in Table 1.

First, the TAR-specific PCR-based assay was optimised using the samples from the uninfected controls ($n = 9$) and the viral non-controllers ($n = 8$), which were expected to test negative and positive for TAR RNA, respectively. In our hands, the previously used method for TAR RNA detection with quantitative PCR has not worked correctly,¹⁷ with non-specific products identified using melting curve analysis. Therefore, traditional PCR amplification was performed using TAR-specific oligonucleotides binding to TAR-specific reverse transcribed cDNA, and the ExiLENT SYBR Green or GoTaq Green master mixes (Figure 1B). To improve resolution, the PCR products were separated on 5% agarose gels and revealed by ethidium bromide. For the non-controllers, both of these master mixes typically amplified a 64-bp-long TAR-specific PCR product, plus one or more smaller unspecific PCR products, which probably represented oligonucleotide dimers (Supplementary Figure 1). The identity of the TAR-specific product was confirmed by DNA sequencing (data not shown). An individual was declared TAR RNA positive if one of the DNA polymerase PCR assays (i.e., with ExiLENT or GoTaq) amplified a specific TAR product from

Table 1: Clinical characteristics of the study participants.

Clinical characteristic	Patient group			
	HIV negative	Non-controllers	ART-suppressed	Elite controllers
Gender [n (%)]	9 (100)	8 (100)	19 (100)	19 (100)
Male	8 (88.9)	6 (75.0)	15 (78.9)	12 (63.1)
Female	1 (11.1)	0 (0.0)	4 (21.1)	5 (26.3)
Intersex*	0 (0.0)	1 (12.5)	0 (0.0)	0 (0.0)
Male to female transgender	0 (0.0)	1 (12.5)	0 (0.0)	2 (10.5)
Age (years)	52.0	49.5	57.0	50.0
[median (25%–75%)]	(35.0–59.0)	(40.0–53.8)	(49.0–60.0)	(40.0–55.0)
CD4 (cells/mm ³)	738	401	649	1047
[median (25%–75%)]	(397.5–1317.0)	(254.5–690.8)	(461.0–721.0)	(955.0–1301.0)
CD8 (cells/mm ³)	443	1662	761	734
[median (25%–75%)]	(261.5–623.5)	(1048.8–1850.8)	(587.0–920.0)	(490.0–964.0)
CD4/CD8 ratio	2.28	0.25	0.68	1.51
[median (25%–75%)]	(1.47–3.03)	(0.21–0.37)	(0.56–0.97)	(1.24–1.99)
Viral load (copies/mL)	/	24146	<75	<75
[median (25%–75%)]		(19751–36450)		
TAR [n (%)]				
Negative	9 (100.0)	0 (12.5)	10 (52.6)	4 (21.1)
Positive	0 (0.0)	8 (100.0)	9 (47.4)	15 (78.9)

* Individuals with a reproductive or sexual anatomy that is distinct from that of the typical male or female.

cDNA from one of the two sample types (i.e., plasma or plasma exosomes) (Table 1, Supplementary Table 1).

Comparison of the HIV-1–negative patients and the non-controllers showed that TAR RNA was detected in 0/9 HIV-negative patients and 8/8 non-controller patients, providing 100% specificity and 100% sensitivity. Narayanan et al.¹⁶ previously showed that TAR RNA is part of the exosomes, not only the viruses, in supernatants of HIV-1–infected primary CD4 T-cell cultures. Furthermore, the present analysis was performed on RNA that was enriched for small molecules, like miRNAs. It can therefore be speculated that at least some of the detected TAR molecules in the non-controllers were the TAR RNAs produced by non-processive transcription during their HIV-1 productive infection and latency (Figure 1A),¹¹ although the presence of TAR-containing full-length HIV RNA transcripts cannot be excluded.

Next, the detection of TAR RNA in the plasma of HIV-1–infected patients was tested, in terms of those with suppressed plasma HIV-1 RNA levels with the use of ART (i.e., ART-suppressed) or without (elite controllers). The likely source of HIV-1 RNA in these patients would be latently infected cells.¹¹ Nine out of 19 ART-suppressed patients and 15/19 elite controllers were positive for TAR RNA (Table 1). In contrast, all of the aviremic HIV-1–infected patients in two previous studies were positive for TAR RNA,^{16,17} although only up to four samples were tested, along with pooled blood sera from six patients, which might well have overridden their true TAR-RNA status. On the other hand, the absence of the TAR-RNA

signal in some of the aviremic HIV-1–infected patients studied here might also be due to lower sensitivity of the traditional PCR used in the present study compared to the quantitative PCR used in these previous studies.^{16,17} Among all of the TAR-positive aviremic HIV-1–infected patients ($n = 24$; Supplementary Table 1), TAR RNA of exosomal origin was detected in only nine, which implies that TAR RNA was also present outside of exosomes, in the plasma, which is contrary to previous reports.¹⁷ Alternatively, the freezing and thawing might have impacted on the structural integrity of the exosomes to cause release of TAR RNA into the plasma, although some recent studies reported no or limited effects of plasma freeze-thawing on exosome or exosomal RNA recovery.^{27,28}

To better understand which clinical characteristics might be associated with the presence of TAR RNA in the plasma of aviremic HIV-1–infected patients, TAR-negative and TAR-positive patients were compared using Mann-Whitney and Fisher's exact tests. The presence of TAR RNA in the plasma of these patients did not correlate with patient gender, age, CD4 levels, CD8 levels, but tended to correlate with CD4/CD8 ratio ($P = 0.047$, Table 2). CD4 T cells are the primary target of HIV-1, whereby this infection promotes their depletion, although their levels partially recover in patients receiving ART.²⁹ The anti-HIV-1–specific CD8 T cells are activated by the CD4 T cells, and they are crucial in the control of viremia, whereby they increase in response to ongoing viral replication.²⁹ Interestingly, the CD4 T-cell nadir (i.e., the lowest point to which the CD4 cell count dropped), the CD4/CD8 ratio,

Table 2: Comparison of distribution of clinical characteristics among TAR-negative and TAR-positive aviremic HIV-1–infected patients.

Clinical characteristic	TAR		P value
	Negative	Positive	
Gender [n (%)]	14 (100)	24 (100)	
Male	11 (78.6)	16 (66.7)	0.508 ^a
Female	2 (14.3)	7 (29.2)	
Male to female transgender	1 (7.1)	1 (4.2)	
Age (years)	57.5	52.0	0.135 ^b
[median (25%–75%)]	(44.0–61.3)	(42.3–57.5)	
CD4 (cells/mm ³)	625.5	967.5	0.067 ^b
[median (25%–75%)]	(486.5–904.0)	(660.0–1090.0)	
CD8 (cells/mm ³)	869	645	0.330 ^b
[median (25%–75%)]	(644.5–953.5)	(516.5–905.3)	
CD4/CD8 ratio	0.71	1.26	0.047 ^b
[median (25%–75%)]	(0.54–1.49)	(0.86–1.77)	
Treatment with protease inhibitor [n (%)] ^c			
No	5 (50.0)	4 (44.4)	1.000 ^a
Yes	5 (50.0)	5 (55.6)	
Treatment with non-nucleoside reverse transcriptase inhibitors [n (%)] ^c			
No	6 (60.0)	7 (77.8)	0.628 ^a
Yes	4 (40.0)	2 (22.2)	

^a calculated using Fisher exact tests; ^b calculated using Mann-Whitney tests; ^c only ART-suppressed patients.

and the CD4 T-cell counts were previously shown to be inversely associated with HIV-1 proviral DNA levels, as one of the measures of the reservoir size.^{30,31}

Previous studies have shown that some protease inhibitor treatments can allow low-level viral replication to occur.^{6,32} We therefore compared TAR-RNA levels in patients treated with different ART regimes (Table 2). No differences were observed among the patients who received protease inhibitors compared to patients who did not receive protease inhibitors. On the other hand, in patients who received treatment based on non-nucleoside reverse transcriptase inhibitors, TAR RNA was detected less often, compared to patients who did not receive non-nucleoside reverse transcriptase inhibitors; however this difference did not reach statistical significance (Table 2).

As this study was performed on a limited sample size, further larger studies with better power and with further information on additional clinical characteristics (e.g., inflammatory and reservoir data) are needed to test for correlation of TAR-RNA with CD4/CD8 ratio in HIV-1-suppressed patients, and to provide an explanation of the differences in the TAR-RNA levels and the role of ART regimen in these patients. Any influence of genetic polymorphisms that affect ART efficacy³³ on the plasma TAR levels also needs to be examined.

4. Conclusions

In the present study, a PCR-based assay for detection of plasma TAR RNA was initially established. TAR RNA was detected in the plasma samples of 63% of the aviremic HIV-1-infected patients (i.e., ART-suppressed plus elite controllers), with its source likely to be from non-processive transcription in the HIV-1 latently infected cells, such as the CD4 T cells. The presence of TAR RNA in the plasma tended to correlate only with CD4/CD8 ratio out of the available clinical characteristics of these patients. In addition, this study shows that the TAR RNA molecules in the plasma of aviremic patients are not limited to the exosomes. These findings should be further validated in a study with larger sample size and more detailed patient information.

CONFLICT OF INTEREST: The authors declare that they have no conflicts of interest with the contents of this article.

FUNDING: This study was supported by the Slovenian National Research Agency grants J3-5499, Z3-7198 and P1-0170.

ETHICAL APPROVAL: Written informed consent was obtained from all of the SCOPE cohort participants, and the study was approved by the University of California,

San Francisco, Committee on Human Research, following Federal Guidelines.

5. References

1. N. K. Saksena, S. J. Potter, *AIDS Rev.* **2003**, *5*, 3–18.
2. K. M. Bruner, A. J. Murray, R. A. Pollack, M. G. Soliman, S. B. Laskey, A. A. Capoferri, et al., *Nat. Med.* **2016**, *22*, 1043–1049. <https://doi.org/10.1038/nm.4156>
3. H. Imamichi, R. L. Dewar, J. W. Adelsberger, C. A. Rehm, U. O'Doherty, E. E. Paxinos, et al., *Proc. Natl. Acad. Sci. U S A.* **2016**, *113*, 8783–8788. <https://doi.org/10.1073/pnas.1609057113>
4. A. N. Phillips, J. Neaton, J. D. Lundgren, *AIDS* **2008**, *22*, 2409–2418. <https://doi.org/10.1097/QAD.0b013e3283174636>
5. S. G. Deeks, A. N. Phillips, *Br. Med. J.* **2009**, *338*, a3172. <https://doi.org/10.1136/bmj.a3172>
6. H. Hatano, M. C. Strain, R. Scherzer, P. Bacchetti, D. Wentworth, R. Hoh, et al., *J. Infect. Dis.* **2013**, *208*, 1436–1442. <https://doi.org/10.1093/infdis/jit453>
7. M. S. Weinberg, K. V. Morris, *DNA Cell Biol.* **2006**, *25*, 223–231. <https://doi.org/10.1089/dna.2006.25.223>
8. Z. Klase, P. Kale, R. Winograd, M. V. Gupta, M. Heydarian, R. Berro, et al., *BMC Mol. Biol.* **2007**, *8*, 63. <https://doi.org/10.1186/1471-2199-8-63>
9. D. L. Ouellet, I. Plante, P. Landry, C. Barat, M. E. Janelle, L. Flamand, et al., *Nucleic Acids Res.* **2008**, *36*, 2353–2365. <https://doi.org/10.1093/nar/gkn076>
10. N. C. Schopman, M. Willemsen, Y. P. Liu, T. Bradley, A. van Kampen, F. Baas, et al., *Nucleic Acids Res.* **2012**, *40*, 414–427. <https://doi.org/10.1093/nar/gkr719>
11. A. Harwig, A. Jongejan, A. H. van Kampen, B. Berkhout, A. T. Das, *Nucleic Acids Res.* **2016**, *44*, 4340–4353. <https://doi.org/10.1093/nar/gkw167>
12. M. A. Bernard, H. Zhao, S. C. Yue, A. Anandaiah, H. Koziel, S. D. Tachado, *PLoS One.* **2014**, *9*, e106006. <https://doi.org/10.1371/journal.pone.0106006>
13. D. L. Ouellet, J. Vigneault-Edwards, K. Letourneau, L. A. Gobeil, I. Plante, J. C. Burnett, et al., *Retrovirology.* **2013**, *10*, 86. <https://doi.org/10.1186/1742-4690-10-86>
14. Z. Klase, R. Winograd, J. Davis, L. Carpio, R. Hildreth, M. Heydarian, et al., *Retrovirology.* **2009**, *6*, 18. <https://doi.org/10.1186/1742-4690-6-18>
15. L. Li, H. Feng, Q. Da, H. Jiang, L. Chen, L. Xie, et al., *Arch. Virol.* **2016**, *161*, 1115–1123. <https://doi.org/10.1007/s00705-016-2755-5>
16. A. Narayanan, S. Iordanskiy, R. Das, R. Van Duyn, S. Santos, E. Jaworski, et al., *J. Biol. Chem.* **2013**, *288*, 20014–20033. <https://doi.org/10.1074/jbc.M112.438895>
17. G. C. Sampey, M. Saifuddin, A. Schwab, R. Barclay, S. Punya, M. C. Chung, et al., *J. Biol. Chem.* **2016**, *291*, 1251–1266. <https://doi.org/10.1074/jbc.M115.662171>
18. C. Thery, S. Amigorena, G. Raposo, A. Clayton, *Curr. Protoc. Cell Biol.* **2006**, *Chapter 3*, Unit 3 22.

19. M. P. Zaborowski, L. Balaj, X. O. Breakefield, C. P. Lai, *Bioscience* **2015**, *65*, 783–797. <https://doi.org/10.1093/biosci/biv084>
20. E. I. Buzas, B. Gyorgy, G. Nagy, A. Falus, S. Gay, *Nat. Rev. Rheumatol.* **2014**, *10*, 356–364. <https://doi.org/10.1038/nrrheum.2014.19>
21. B. Gyorgy, T. G. Szabo, M. Pasztoi, Z. Pal, P. Misjak, B. Aradi, et al., *Cell. Mol. Life Sci.* **2011**, *68*, 2667–2688. <https://doi.org/10.1007/s00018-011-0689-3>
22. J. S. Schorey, S. Bhatnagar, *Traffic* **2008**, *9*, 871–881. <https://doi.org/10.1111/j.1600-0854.2008.00734.x>
23. M. Lenassi, G. Cagney, M. Liao, T. Vautotic, K. Bartholomeussen, Y. Cheng, et al., *Traffic* **2010**, *11*, 110–122. <https://doi.org/10.1111/j.1600-0854.2009.01006.x>
24. A. D. Raymond, P. Diaz, S. Chevelon, M. Agudelo, A. Yndart-Arias, H. Ding, et al., *J. Neurovirol.* **2016**, *22*, 129–139. <https://doi.org/10.1007/s13365-015-0397-0>
25. B. Gyorgy, M. E. Hung, X. O. Breakefield, J. N. Leonard, *Annu. Rev. Pharmacol. Toxicol.* **2015**, *55*, 439–464. <https://doi.org/10.1146/annurev-pharmtox-010814-124630>
26. H. Valadi, K. Ekstrom, A. Bossios, M. Sjostrand, J. J. Lee, J. O. Lotvall, *Nat. Cell Biol.* **2007**, *9*, 654–659. <https://doi.org/10.1038/ncb1596>
27. M. Jayachandran, V. M. Miller, J. A. Heit, W. G. Owen, *J. Immunol. Methods* **2012**, *375*, 207–214. <https://doi.org/10.1016/j.jim.2011.10.012>
28. Q. Ge, Y. Zhou, J. Lu, Y. Bai, X. Xie, Z. Lu, *Molecules* **2014**, *19*, 1568–1575. <https://doi.org/10.3390/molecules19021568>
29. S. E. Langford, J. Ananworanich, D. A. Cooper, *AIDS Res. Ther.* **2007**, *4*, 11. <https://doi.org/10.1186/1742-6405-4-11>
30. T. W. Chun, J. S. Justement, P. Pandya, C. W. Hallahan, M. McLaughlin, S. Liu, et al., *J. Infect. Dis.* **2002**, *185*, 1672–1676. <https://doi.org/10.1086/340521>
31. M. R. Boulassel, N. Chomont, N. P. Pai, N. Gilmore, R. P. Sekaly, J. P. Routy, *J. Clin. Virol.* **2012**, *53*, 29–32. <https://doi.org/10.1016/j.jcv.2011.09.018>
32. M. J. Buzon, M. Massanella, J. M. Llibre, A. Esteve, V. Dahl, M. C. Puertas, et al., *Nat. Med.* **2010**, *16*, 460–465. <https://doi.org/10.1038/nm.2111>
33. A. V. Coelho, S. P. Silva, L. C. de Alencar, G. Stocco, S. Crovella, L. A. Brandao, et al., *J. Clin. Pharmacol.* **2013**, *53*, 1286–1293. <https://doi.org/10.1002/jcph.165>

Povzetek

Določitev velikosti rezervoarjev HIV-1 v okuženih posameznikih, lahko pomembno prispeva k izboljšanju njihovega zdravljenja. Eden izmed potencialnih bioznačevalcev za prisotnost rezervoarjev je v plazmi prisoten TAR (angl. *trans-activation response element*) RNA. TAR RNA nastane med ne-procesivnim genskim prepisovanjem v celicah, ki so produktivno ali latentno okužene z virusom HIV-1. V okviru študije smo prisotnost TAR RNA preučevali v vzorcih krvne plazme ter iz nje izoliranih eksosomov 55 oseb iz kohorte SCOPE. Vzpostavili smo metodo detekcije TAR RNA, ki temelji na reakciji PCR, ter z njo s 100 % specifičnostjo ter občutljivostjo ločili nezdravljene viremične bolnike, okužene s HIV-1, od zdravih posameznikov. TAR RNA smo dokazali v plazmi 63 % aviremičnih bolnikov, okuženih s HIV-1, kot so elitni kontrolerji in posamezniki zdravljeni z ART (angl. *antiretroviral therapy*). Kljub temu, da prisotnost TAR RNA ni povezana s starostjo, spolom, številom CD4 in CD8 celic, je analiza nakazala na korelacijo z razmerjem celic CD4/CD8 ($P = 0,047$). To je prva študija analize prisotnosti plazemske TAR RNA na razmeroma velikem številu bolnikov, okuženih s HIV-1. Poleg tega smo pokazali, da molekule TAR RNA v plazmi aviremičnih bolnikov niso prisotne zgolj v eksosomih.

Scientific paper

Chemometric Characterization of Slovenian Red Wines

Milena Ivanović,¹ Anja Petek,¹ Maša Islamčević Razboršek¹ and Mitja Kolar²¹ University of Maribor, Faculty of Chemistry and Chemical Engineering, Smetanova ulica 17, 2000 Maribor² University of Ljubljana, Faculty of Chemistry and Chemical Engineering, Večna pot 113, 1000 Ljubljana

* Corresponding author: E-mail: mitja.kolar@fkkt.uni-lj.si

Tel.: (+386)-1-4798-694

Received: 31-08-2016

For Cutting Edge 2017

Abstract

Total phenolic (TPC), flavonoid (TFC) and tannin (TTC) contents, total SO₂, total acids, pH, and reducing sugars were measured in twenty five Slovenian red wines from three key wine producing regions, Podravje, Posavje and Primorska. The results were chemometrically analysed and the wines were classified according to wine growing region and vine variety. Principal component analysis proved that TPC, TFC and TTC contents were primarily responsible for variation in the wines. Additionally, linear discriminant analysis (LDA) was performed and resulted in the satisfactory classification of samples by both vine variety and region.

Keywords: Slovenian red wines, quality parameters of wine, polyphenols, chemometric analysis.

1. Introduction

Slovenia is a small European country with a long history of wine production in three key wine growing regions, Podravje in the east, Primorska in the west and Posavje just south of the center. In Slovenia there are more than 28,000 wineries, producing between 80 and 90 million annually, of which 25% is red wine. Most of the red wine is produced in Primorska from two well-known vine varieties, Refošk and Merlot.

Wine is a complex matrix and its major components are water (81%), ethanol (between 11% and 15%) and sugars. Additionally, it contains a wide range of organic and inorganic compounds, including polyphenols, different organic acids and nitrogenous compounds.¹ The concentration levels of these compounds are influenced by several oenological factors such as origin, vine variety, wine-making practices, ageing and vintage. Their quantitative determination in wines is of considerable importance, since it is known that they are responsible for the wine's taste (polyphenols), colour (anthocyanins), and for beneficial health effects including antioxidant and anti-inflammatory activities.^{2,3} Wine classification is a very important

topic in order to detect possible frauds and to establish wine authenticity, which is an important consideration in international markets.⁴ This process consists of building mathematical-statistical models based on quantitative and qualitative information about the natural constituents, such as content of trace elements,⁵ organic wine constituents such as volatile compounds,⁶ sugars,⁷ polyphenols,⁸ anthocyanins,⁹ etc.

Slovenian wine legislation¹⁰ prescribes that all wines should be submitted to chemical and sensoric-organoleptic analysis before being released to the market. After wines pass the tests, they are assigned a quality level according to the *Zaščiteno geografsko poreklo* (ZGP), which is similar to the European Union's QWP-SR system (Quality Wines Produced in Specified Regions.) Several articles about different analytical techniques, including high-performance liquid chromatography (HPLC), high-performance ion chromatography exclusion (HPICE), inductively coupled plasma emission spectroscopy (ICP-OES), isotope ratio mass spectrometry (IRMS), site-specific natural isotopic fractionation nuclear magnetic resonance (SNIF-NMR) and inductively coupled plasma mass spectrometry

(ICP-MS) for the determination of different compounds and chemometric classification of Slovenian wines based on these results have been published.^{11–13} In our previous paper,¹⁴ Slovenian red wines were characterized according to the phenolic acids content, and classified according to vine variety and Slovenian wine growing regions. In the present study, several more variables were taken into account, total polyphenol content (TPC), condensed tannins content (TTC), flavonoids content (TFC), total reducing sugars, total acids content and total SO₂ content were determined in twenty-five Slovenian red wines. Additionally, the results obtained were used to build chemometric models for the classification of Slovenian red wines of different vine varieties from the three wine growing regions.

2. Experimental

2.1. Chemicals and Wine Samples

Rutin, vanillin, gallic acid, Folin-Ciocalteu reagent and NaOH were supplied by Merck (Germany). Na₂CO₃, I₂ and KI were purchased from Sigma-Aldrich (Germany). AlCl₃ and H₂SO₄ were purchased from Fluka (USA) and methanol (MeOH) from JT Baker (Germany). CH₃COONa and HCl were supplied by Carlo Erba (Italy), CuSO₄ and KNaC₄H₄O₆ were purchased from Kemika (Croatia).

Twenty-five red wines from different Slovenian wineries and different varieties (Table 1) were purchased from local supermarkets. All the wine samples tested originated from four vintages (2011–2015). The wines were stored in a refrigerator at +4°C until analysed.

2.2. Instrumentation

Spectrophotometric measurements were carried out using a Cary 100 Varian UV/VIS spectrophotometer (USA). All titration determinations were performed on a Mettler Toledo T50 automatic titration system, using a DGi111-SC glass electrode and DMi140-SC platinum ring electrode. All samples were analysed in triplicate.

2.3. Analytical Methods

2.3.1. Total Polyphenols Content (TPC)

Total polyphenol content (TPC) was determined according to the slightly modified standard spectrophotometric method described by Dewanto et al.¹⁵ The TPC was expressed as grams of gallic acid equivalents per litre (g GAE L⁻¹).

2.3.2. Total Flavonoids Content (TFC)

As with TPC, the total flavonoids content (TFC) was measured by UV-VIS spectrophotometer against blank at 415 nm.¹⁵ The TFC was expressed as grams of rutin per litre (g RUT L⁻¹).

2.3.3. Total Condensed Tannins Content (TTC)

Condensed tannins were determined according to the methods described by Sun et al.¹⁶ The absorbance was measured at 500 nm against methanol as blank. The TTC was expressed as grams of catechin per litre (g CAT L⁻¹).

2.3.4. Chemical Parameters Determined Using an Automatic Titration System

For all other chemical parameters, a Mettler Toledo T50 automatic titration system was used. Total SO₂ was determined according to the M564 method. 5 mL of 5 M NaOH were added to 50 mL of each wine sample, then left to stand for 15 min; after that, 7 mL of 25% H₂SO₄ and 10 mL of 10% KI were added and the sample was titrated with I₂. Total acids content was determined according to the M561 method, where to 10 mL of the wine sample, 40 mL of deionised water was added and the sample was titrated with 0.1 M NaOH. For determination of reducing sugars, M566/567 and M568 methods were used, where Fehling solutions (I and II) and titrant solution were prepared initially. To an aliquot of the wine sample (1–3 mL), 5 mL of Fehling I, 5 mL of Fehling II solutions and 40 mL of water were added. The sample

Table 1. Number of samples per wine variety and per wine growing region.

Wine growing region	No. of samples	Vine variety	No. of samples
Primorska	13	Cabernet Sauvignon	5
		Merlot	2
		Modri Pinot	1
		Refošk	5
Podravje	5	Cabernet Sauvignon	1
		Modri Pinot	2
		Modra Frankinja	2
Posavje	7	Cabernet Sauvignon	1
		Modra Frankinja	4
		Portugalka	2

was boiled for exactly 2 minutes and then cooled to room temperature. Then 10 mL of 10% H₂SO₄ and 10 mL 10% KI were added and the mixture was titrated with 0.1 M Na₂S₂O₃. pH was measured according to the M390 method.¹⁷

2. 4. Statistical Analysis

Microsoft Excel was used for the data preparation and result outputs. Statistical data treatment was performed using SPSS Statistics (IBM Corp. Released 2013. IBM SPSS Statistics for Windows, Version 22.0. Armonk, NY: IBM Corp.).

3. Results and Discussion

The results of all analyses performed on selected Slovenian red wines are listed in the supplementary material (Table 2). The TPC determined by the Folin-Ciocalteu method ranged from 1.24 to 4.01 g GAE L⁻¹. These values are in general accordance with results determined for Croatian, Italian, Slovakian, Austrian and Romanian red wines.^{18–23} In the literature, there is relatively little information about TFC in red wines.^{23,24} When our results are compared with the literature data, it is clear that Slovenian red wines are a very rich source of flavonoids; by applying colorimetric method using rutin as a standard, TFC was determined in the range of 0.05 to 0.38 g RUT L⁻¹. TTC were determined in the concentration range of 0.37–1.92 g CAT L⁻¹, where the lowest average TTC was determined in the Modra Frankinja variety. These results are comparable with the literature.²⁵ The highest concentration was determined in the Modri Pinot variety from the Primorska wine growing region. For comparison, red wines from Romania can contain 0.63–2.34 g of tannins L⁻¹.²³

Wines can be classified according to sugar content as dry (up to 9 g L⁻¹), semi-dry (up to 12 g L⁻¹), semi-sweet (up to 50 g L⁻¹) and sweet (above 50 g L⁻¹) wines.¹⁰ From these categories we concluded that all of the wines tested belong to the group of dry wines, as they contain from 2 to 8 g L⁻¹ of reducing sugars. The total acid content in red wines can be from 3.5 to 10 g L⁻¹,¹⁰ and all our results are in this range. According to the literature,¹⁰ total SO₂ must not exceed 160 mg L⁻¹ for a wine with reducing sugars content below 5 g L⁻¹, and must not exceed 210 mg L⁻¹ for red wines with reducing sugars content above 5 g L⁻¹. Measured SO₂ contents were between 5 and 287 mg L⁻¹ for all twenty-five samples. Increased contents of total SO₂ were found in just two samples belonging to the Modri Pinot and Modra Frankinja varieties, respectively. pH values were not significantly different from wine to wine, as they were in the range of 3.37 to 3.98 and are comparable with results reported by other authors.²⁶

3. 1. Statistical Analysis

Exploratory data analysis was performed using the SPSS program. In the first step of the statistical evaluation, the Kolmogorov-Smirnov test (with a significance level of 0.05) was used. According to the results obtained (Table 3), that total SO₂ values were not normally distributed, and a logarithmically transformed data form was created in order to achieve correct results in the deviating case. In this way prepared data were used for further analyses. The parametric Pearson correlation test (with significance levels 0.01 and 0.05) was used to determine any inter-relation between selected variables (Table 4). Statistically significant positive correlations at the confidence level 0.01 were found between the following parameters: TPC and TFC (0.721), TPC and TTC (0.897), TPC and reducing sugars (0.617) and TTC and reducing sugars (0.580). Positive correlations at the confidence level 0.05 were found between TFC and TTC (0.494) and between TFC and reducing sugars (0.489). Negative correlation at the confidence level of 0.05 was found between pH and total acids (–0.401): higher acid contents lead to lower pH values.

For testing the significance of differences between different groups of wine samples (classified according to the Slovenian wine growing regions) box plot analyses were performed. Outliers were detected in data sets of TFC (two samples-one sample from Primorska and another from the Posavje Slovenian wine growing region), pH (two samples-one sample from Primorska and another from the Podravje wine growing region) and total acids (two samples-Podravje and Posavje).

3. 3. 1. Principal Component Analysis (PCA)

For the obtained Factor Analysis results, for the creation of a PCA model based on wine growing regions only three statistically important variables were taken into account: TPC, TFC and TTC. Outliers (two samples from the TFC) were discarded from further analysis. To confirm the significance of differences between wine groups regarding the content of the aforementioned statistically important variables, ANOVA tests were performed. According to the results obtained, all of the descriptors were found to be statistically significant at the $p < 0.05$ in the ANOVA outputs. The p values for TPC, TFC and TTC were 0.03, 0.024 and 2.66×10^{-4} , respectively. As can be seen in the plot of scores in Figure 1, PC1 is well discriminated between Primorska (group 1) and Podravje (group 2) wines. The wines from the Posavje region (group 3) were positioned in the middle; some samples were dispersed into group 2. The first two PCs explained 96% of the total variance between wine growing regions of the samples analysed. The highest percentage of phenolic compounds (TPC, TFC and TTC) was found in wine samples from the Primorska region (Figure 1).

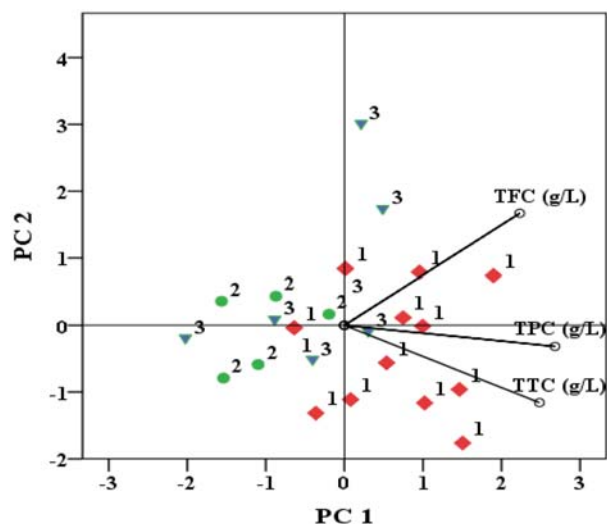


Figure 1. PCA bi-plot in the plane PC2 vs. PC1. The objects are labelled by Slovenian wine growing regions. The first principal component (PC1) explained 78% of the variation between the samples, and the second (PC2) explained 18% of the variation. PC1 and PC2 values separate samples according to TPC and TFC, respectively (\diamond Primorska wine growing region; \triangle Podravje wine growing region and \square Posavje wine growing region)

3.3.2. Linear Discriminant Analysis (LDA)

For LDA classification of the samples from three wine growing regions, TPC and TTC were selected as parameters. The graphic output of classification is shown in Figure 2. The classification rates for the categories mentioned were acceptably good; overall correct classification

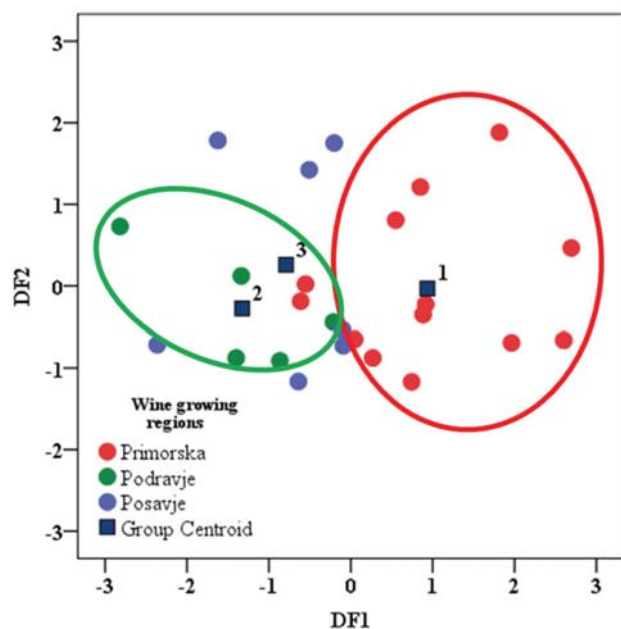


Figure 2. Graphic output of LDA in the plane of the first two discriminant functions. Classification according to Slovenian wine growing regions

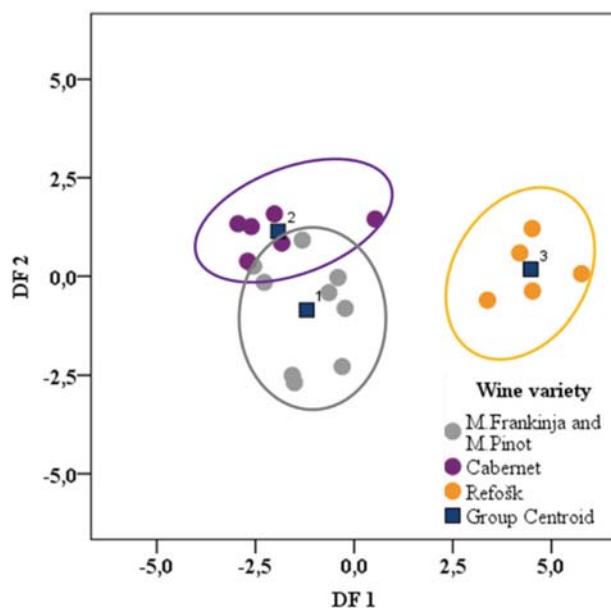


Figure 3. Graphic output of LDA in the plane of the first two discriminant functions. Classification according to varieties.

ratio was 80% for the training set and almost 70% for the validation set.

LDA was also used to categorize wine samples for the Cabernet, Refošk, Modra Frankinja and Modri Pinot varieties employing optimally selected variables: TFC, TTC and total acids content; the results are presented in Figure 3. Classification ratio was 90% for the training set, and 80% for the validation set. Using the aforementioned descriptors, the Refošk variety is distinguished from the other classes, and formed a group in the positive part of DF 1. This analysis showed a strong similarity between the Modri Pinot and Modra Frankinja vine varieties, and together they form a group in the negative part of DF 1. The similarity between these two varieties, according to some other parameters, was also shown.²⁷ LDA analysis resulted in classification of samples according to both regions and varieties.

4. Conclusions

This paper is one of a few studies on systematic chemical characterization of the most well-known Slovenian red wines. Twenty five wine samples were analysed and 7 selected chemical descriptors (variables) were used for wine characterization. The results show that Slovenian red wines are a very rich source of health beneficial compounds, especially flavonoids. Additionally, the results obtained were chemometrically processed. For this purpose, PCA and LDA were used as the main chemometrical tools. Taking into account TPC, TFC and TTC as the selected descriptors, satisfactory classification of wines was achieved with respect to (a) wine gro-

wing regions and (b) variety. This study demonstrates the usefulness of variable selection and also suggests the application of a developed model which could be used for wine classification according to several other parameters such as vintage, winemaking practices and alcohol content.

5. Acknowledgments

The authors would like to thank dr. Roman Kranvogel for his helpful comments regarding chemometric interpretation.

This work has been supported by the Erasmus Mundus Join-EU-SEE Penta project.

6. References

1. S. Moncayo, J. D. Rosales, R. Izquierdo-Hornillos, J. Anzano, J. O. Caceres, *Talanta* **2016**, *158*, 185–191. <https://doi.org/10.1016/j.talanta.2016.05.059>
2. F. Mattivi, C. Zulian, G. Nicolini, L. Valenti, *Ann. N. Y. Acad. Sci.* **2002**, *957*, 37–56. <https://doi.org/10.1111/j.1749-6632.2002.tb02904.x>
3. D. Serrano-Lourido, J. Saurina, S. Hernández-Cassou, A. Checa, *Food Chem.* **2012**, *135*, 1425–1431. <https://doi.org/10.1016/j.foodchem.2012.06.010>
4. R. Garrido-Delgado, L. Arce, A.V. Guamán, A. Pardo, S. Marco, M. Valcárcel, *Talanta*. **2011**, *84*, 471–479. <https://doi.org/10.1016/j.talanta.2011.01.044>
5. I. Geana, A. Iordache, R. Ionete, A. Marinescu, A. Ranca, M. Culea, *Food Chem.* **2013**, *138*, 1125–1134. <https://doi.org/10.1016/j.foodchem.2012.11.104>
6. B. T. Weldegergis, A. de Villiers, A. M. Crouch, *Food Chem.* **2011**, *128*, 1100–1109. <https://doi.org/10.1016/j.foodchem.2010.09.100>
7. A. Caligiani, D. Acquotti, G. Palla, V. Bocchi, *Anal. Chim. Acta.* **2007**, *585*, 110–119. <https://doi.org/10.1016/j.aca.2006.12.016>
8. L. Jaitz, K. Siegl, R. Eder, G. Rak, L. Abranko, G. Koellensperger, S. Hann, *Food Chem.* **2010**, *122*, 366–372. <https://doi.org/10.1016/j.foodchem.2010.02.053>
9. A. de De Villiers, G. Vanhoenacker, P. Majek, P. Sandra, *J. Chromatogr. A.* **2004**, *1054*, 195–204. [https://doi.org/10.1016/S0021-9673\(04\)01291-9](https://doi.org/10.1016/S0021-9673(04)01291-9)
10. Zakon o vinu (Slovenian wine laws), *Uradni list Republike Slovenije.* **2006**. <https://www.uradni-list.si/1/content?id=75822>
11. M. A. Brescia, I. J. Košir, V. Caldarella, J. Kidrič, A. Sacco, *J. Agric. Food Chem.* **2003**, *51*, 21–26. <https://doi.org/10.1021/jf0206015>
12. N. Ogrinc, I. J. Košir, M. Kocjančič, J. Kidrič, *J. Agric. Food Chem.* **2001**, *49*, 1432–1440. <https://doi.org/10.1021/jf000911s>
13. V. S. Šelih, M. Šala, V. Drgan, *Food Chem.* **2014**, *153*, 414–423. <https://doi.org/10.1016/j.foodchem.2013.12.081>
14. M. Ivanović, M. I. Razboršek, M. Kolar, *Acta Chim. Slo.* **2016**, *63*, 661–669. <https://doi.org/10.17344/acsi.2016.2534>
15. X. Dewanto, K. Wu, K. Adom, R. H. Liu, *J. Agric. Food Chem.* **2002**, *50*, 3010–3014. <https://doi.org/10.1021/jf0115589>
16. B. Sun, J. M. Richardo-Da-Silva, I. Spranger, *J. Agric. Food Chem.* **1998**, *46*, 4267–4274. <https://doi.org/10.1021/jf980366j>
17. http://www.mt.com/es/en/home/applications/Application_Browse_Laboratory_Analytics/Application_fam_browse_main.html
18. M. Šeruga, I. Novak, L. Jakobek, *Food Chem.* **2011**, *124*, 1208–12016. <https://doi.org/10.1016/j.foodchem.2010.07.047>
19. V. Katalinić, M. Miloš, D. Modun, I. Musić, M. Boban, *Food Chem.* **2004**, *86*, 593–600. <https://doi.org/10.1016/j.foodchem.2003.10.007>
20. J. Piljac, S. Martinez, T. Stipčević, Z. Petrović, M. Metikoš-Huković, *Am. J. Enol. Vitic.* **2004**, *55*, 417–422.
21. D. Di Majo, M. La Guardia, S. Giammanco, L. La Neve, M. Giammanco, *Food Chem.* **2008**, *111*, 45–49. <https://doi.org/10.1016/j.foodchem.2008.03.037>
22. A. Staško, V. Brezova, M. Mazur, M. Čertik, M. Kalinak, G. Gescheidt, *LWT- Food Sci. Technol.* **2008**, *41*, 2126–2135.
23. A. Hosu, V. M. Cristea, C. Cimpoi, *Food Chem.* **2014**, *150*, 113–118. <https://doi.org/10.1016/j.foodchem.2013.10.153>
24. L. M. Magalhaes, M. Ines, G. S. Almedia, L. Barreiros, S. Reis, M. A. Segundo, *Food Anal. Meth.* **2012**, *5*, 530–539. <https://doi.org/10.1007/s12161-011-9278-1>
25. J. F. Harbertson, R. E. Hodgins, L. N. Thurston, L. J. Schaffer, M. S. Reid, J. L. Landon, C. F. Ross, D. O. Adams, *Am J Enol Vitic.* **2008**, *59*, 210–214.
26. E. Buyuktuncel, E. Porgah, C. Colak, *Food and Nut. Sci.* **2014**, *5*, 1660–1667. <https://doi.org/10.4236/fns.2014.517179>
27. Projekt »Modra frankinja – žametno vino Posavja« http://www.modra-frankinja.com/upload/urejevalnik/datoteke/2014_11_27_Strategija-trzenja-vina-modra-frankinja_FINAL.pdf

Povzetek

Vsebnost skupnih fenolov (TPC), flavonoidov (TFC) in taninov (TTC), kakor tudi skupni SO_2 , skupne kisline, pH, reducirajoči sladkorji so bili določeni v petindvajsetih slovenskih rdečih vinih iz treh ključnih vinorodnih območij: Podravja, Posavja in Primorske. Rezultati so bili kemometrično ovrednoteni, vina pa razvrščena glede na vinorodno območje in sorto vinske trte. Metoda glavnih osi je pokazala, da so vsebnosti TPC, TFC in TTC v prvi vrsti odgovorne za razliko med vini. Z rezultati linearne diskriminantne analize (LDA) pa smo ugotovili, da so analizirani parametri odvisni tako od sorte vinske trte kot tudi od vinorodnega območja.

Scientific paper

In vitro Assessment of Potential Bladder Papillary Neoplasm Treatment with Functionalized Polyethyleneimine Coated Magnetic Nanoparticles

Klemen Strojan,¹ Jasna Lojk,^{1,2} Vladimir Boštjan Bregar,¹ Mateja Erdani Kreft,² Jurij Svete,³ Peter Veranič^{2,*} and Mojca Pavlin^{1,4*}

¹ Group for nano and biotechnological applications, University of Ljubljana, Faculty of Electrical Engineering, Tržaška cesta 25, Ljubljana, Slovenia

² Institute of Cell biology, University of Ljubljana, Faculty of Medicine, Vrazov trg 2, Ljubljana, Slovenia

³ Faculty of Chemistry and Chemical Technology, Večna Pot 113, Ljubljana, Slovenia

⁴ Institute of Biophysics, University of Ljubljana, Faculty of Medicine, Vrazov trg 2, Ljubljana, Slovenia

* Corresponding author: E-mail: mojca.pavlin@fe.uni-lj.si; peter.veranic@mf.uni-lj.si

Received: 01-09-2016

For Cutting Edge 2017

Abstract

Normal porcine urothelial cells have been shown to have a much lower rate of endocytosis than urothelial papillary neoplasm cells. This could be used as a mechanism for selective delivery of toxic compounds, such as polyethyleneimine coated nanoparticles (NPs). However, these NPs induce nonselective toxicity through direct membrane disruption. This toxicity can be reduced by functionalization of NPs with L-glutathione reduced or bovine serum albumin by reducing their surface charge. Functionalization was confirmed with Fourier Transform Infrared Spectroscopy, Dynamic Light Scattering and zeta potential measurements. Viability assays showed that bovine serum albumin coating reduced NPs cytotoxicity immediately after 3 h exposure and that such NPs were more toxic to urothelial papillary neoplasm cells compared to normal porcine urothelial cells at 50 µg/ml NPs concentration. However, 24 h after exposure, bovine serum albumin functionalized NPs had similar effect on viability of both cell lines. NPs showed some selective toxicity towards urothelial papillary neoplasm cells compared to normal cells after 3 h, however this was not confirmed after 24 h.

Keywords: polyethyleneimine, urothelial cell models, magnetic nanoparticles, toxicity, urothelial papillary neoplasm

1. Introduction

Urothelial papillary neoplasms are a group of non-invasive urinary bladder cancers that have a high recurrence rate and can progress to an invasive form of bladder cancer.^{1,2} The treatment typically involves transurethral resection followed by intravesical therapy, where chemotherapeutic agents are administered directly into the bladder.³ Despite obvious advantages of local delivery, intravesical therapy has its limitations and is thus an important area for further development,⁴ in which nanoparticles (NPs) proved to be a promising strategy for improvement.⁵

Several different types of NPs have already been designed for treatment of bladder cancer, mostly to deliver chemotherapeutic drugs and other therapeutic and imaging molecules.^{6–11} For targeted delivery to bladder cancer cells, different ligands have been used, such as lectins^{12,13} or transferrin.¹⁴ Also, magnetic targeting has been applied for delivery of magnetic NPs with encapsulated doxorubicin.¹⁵ *In vivo* studies demonstrated that complexation or encapsulation of cytotoxic agents into different NPs (liposomes, polymeric NPs) can improve the efficiency of intravesical therapy.^{6–11,16} Moreover, some NP formulations are already in preclinical and clinical studies.¹⁷

Furthermore, in a recent study we have shown enhanced uptake of anionic polyacrylic acid (PAA) coated

cobalt ferrite NPs by urothelial papillary neoplasm cell model (RT4) compared to differentiated normal porcine urothelial cell model (NPU). Similar selective uptake was also shown for cationic chitosan coated poly- ϵ -caprolactone NPs by mouse bladder carcinoma cells compared to normal mouse urinary bladder cells.¹⁸ The highly localized intravesical treatment in combination with the significant difference in endocytic activity between normal and cancerous cells thus represents a unique opportunity for selective delivery of anti-cancer therapeutics, such as NPs.

In this paper we analyse potential applicability of polyethyleneimine (PEI) coated NPs for selective treatment of urothelial papillary cells. PEI is a cationic polymer with one of the highest cationic charge-density potentials,¹⁹ that is mostly used as a transfection agent.^{20,21} PEI has been already successfully applied as a delivery vehicle on bladder cancer models^{22,23} and researchers have also used PEI in a clinical study for the treatment of bladder cancer (NCT00595088). However, cationic properties of PEI are also responsible for its toxicity^{24–28} either through direct membrane damage (i.e. extracellular toxicity) or through damage to the endosomes, lysosomes and mitochondria (i.e. intracellular toxicity).^{25,26,29,30} So to achieve selective cytotoxicity of NPs for cancer cells compared to normal cells based on the selective NPs uptake into cancer cells, the extracellular toxicity of PEI NPs had to be reduced first.

The aim of the study was to design modified PEI NPs coated with the additional layer in order to obtain selective toxicity against cancer cells, and to test their effectiveness. We tested two coatings: L-glutathione reduced (GSH)³¹ and bovine serum albumin (BSA)^{32,33} for which we hypothesized that would reduce extracellular toxicity (membrane toxicity) while retaining intracellular toxicity.

2. Experimental

2.1. Nanoparticle Synthesis and Characterization

PEI coated cobalt ferrite (CoFe_2O_4) NPs were prepared as described previously.^{20,31,34} PEI NPs were additionally functionalized with L-glutathione reduced (GSH; Sigma-Aldrich, St. Luis, Missouri, USA) at 0.25 to 1 mass ratio (PEI_GSH NPs), or with bovine serum albumin (BSA; Sigma-Aldrich) at 0.5 to 1 mass ratio (PEI_BSA NPs) immediately prior to use. NPs were dialyzed against distilled water and sterilized by filtration. IR spectra of dry samples were recorded on a Bruker FTIR (Fourier Transform Infrared Spectroscopy) Alpha Platinum ATR spectrophotometer (Bruker, Billerica, Massachusetts, USA). Dynamic light scattering and zeta potential were measured using Malvern Zetasizer NanoZS (Malvern Industries, Malvern, UK).

2.2. Cell Culturing

Cells were maintained at 37 °C in a humidified 5% CO_2 atmosphere. Human bladder papillary neoplasm (RT4) cells were grown in A-DMEM/F12 (Gibco, Gaitersburg, Maryland, USA), 5% fetal bovine serum (FBS; Gibco), 4 mM glutamax (Gibco), 100 U/ml penicillin, and 100 $\mu\text{g}/\text{ml}$ streptomycin. Cultures of primary normal porcine urothelial cells (NPU) were established from porcine urinary bladder as described previously.³⁵ For the establishment of the highly differentiated normal porcine urothelial (NPU) cell model, which represents a biomimetic model of a normal differentiated urothelium *in vivo*, cells were grown in UroM medium without FBS and with physiological 2.5 mM calcium concentration for 3 weeks before experiments.

The experiments with NPU cells were approved by the Veterinary Administration of the Slovenian Ministry of Agriculture and Forestry in compliance with the Animal Health Protection Act and the Instructions for Granting Permits for Animal Experimentation for Scientific Purposes.

2.3. Viability Testing

Cell viability was determined with Trypan blue viability assay. Cells were incubated with PEI, PEI_GSH or PEI_BSA NPs (50, 100, 150 $\mu\text{g}/\text{ml}$) for 3 h in A-DMEM cell culture medium without FBS and washed to remove the NPs. Cells were trypsinized immediately after the 3 h incubation or after additional 24 h culturing in the complete medium (A-DMEM for RT4 cells and UroM for NPU cells) without NPs. Trypsinized cells were stained with Trypan Blue stain (Life Technologies, Eugene, Oregon, USA) and counted using CountessTM Automated Cell Counter (Invitrogen, Carlsbad, California, USA). The number of dead cells was subtracted from the total number of cells to obtain the number of viable cells. The percentage of viable cells (*Viability*) in a given sample was determined as the ratio between the number of viable cells in each sample (N_s) and the number of all cells in the control sample (N_0):

$$\text{Viability} = 100 \times N_s/N_0. \quad (1)$$

2.4. Transmission Electron Microscopy

Transmission electron microscopy was performed as described in Bregar *et al.*³⁴ following 3 h incubation with 50 $\mu\text{g}/\text{ml}$ PEI and PEI_BSA NPs.

2.5. Data Analysis

Data analysis was performed in R software environment (version 3.2.2.). Results are shown as mean and standard error of the mean for three independent experiments.

3. Results and Discussion

In our previous study, we showed that the uptake of PAA coated NPs is higher in the urothelial tumour cell models (RT4, T24) compared to NPU cells due to lower endocytic activity of healthy urothelial cells. Due to cell-type dependent nature of such selective uptake, this principle could be applied also to other NP types, including PEI NPs. PEI NPs have so far been used for delivery of other toxic molecules,^{22,23} however PEI itself can also cause toxicity through membrane damage, ROS induction and lysosomal damage.³⁶ We wanted to exploit PEI intrinsic toxicity as a mechanism to induce selective toxicity, but in order to limit PEI toxicity to NPU cells, PEI's ability to damage outer cell membranes (non-selective toxicity) had to be reduced. The aim of the study was to modify PEI NPs with the negatively charged GSH and BSA molecules to decrease PEI NPs highly positive surface charge and thus to obtain selective toxicity. GSH was chosen for its antioxidant properties and excess of negative charge, in order to reduce the zeta potential of the modified (PEI_GSH NPs). This strategy proved to be efficient for reducing cytotoxicity of PEI_NPs towards CHO cells.³¹ BSA was used as a protein pre-coating, a strategy described in Mirshafie *et al.*³²

The successful modifications were confirmed with physicochemical characterization of NPs through the differences in FTIR spectra (Figure 1), changes in DLS (Figure 2a) and zeta potential measurements (Figure 2B). DLS measurements showed that functionalization with GSH reduced the hydrodynamic diameter of PEI NPs (122 ± 19 nm) to 93 ± 32 nm, indicating additional stabilization of NPs by GSH in distilled water (Figure 2a). This effects was most probably due to steric repulsion of GSH molecules on PEI NP surface, which impeded the formation of NP aggregates.³⁷ On the other hand, BSA coating increased the hydrodynamic diameter to 179 ± 6 nm. Upon additional functionalization, the highly positive zeta potential of PEI NPs (56 ± 1 mV) was reduced to 44 ± 5 mV and 50 ± 4 mV for GSH and BSA, respectively (Figure 2B). This was due to interaction of anionic GSH or BSA molecules with cationic PEI NPs, which neutralized some of the functional groups on the surface of PEI NPs.

We postulated that reduction of the highly positive charge of PEI NPs would decrease their binding to the plasma membrane and thus reduce the membrane damage and increasing their selective toxicity. Moreover, we assumed that the exposure to acidic pH and proteolytic enzymes in the lysosomes would damage the GSH and BSA layers, thus exposing again the highly cationic surface of PEI NPs and enabling intracellular cytotoxic action of PEI. It is important to note that if the incubation of NPs would be performed in a standard culture medium with serum, this could modify internalization and the cytotoxicity, since protein corona importantly determines biological response of the cells to NPs.³⁸

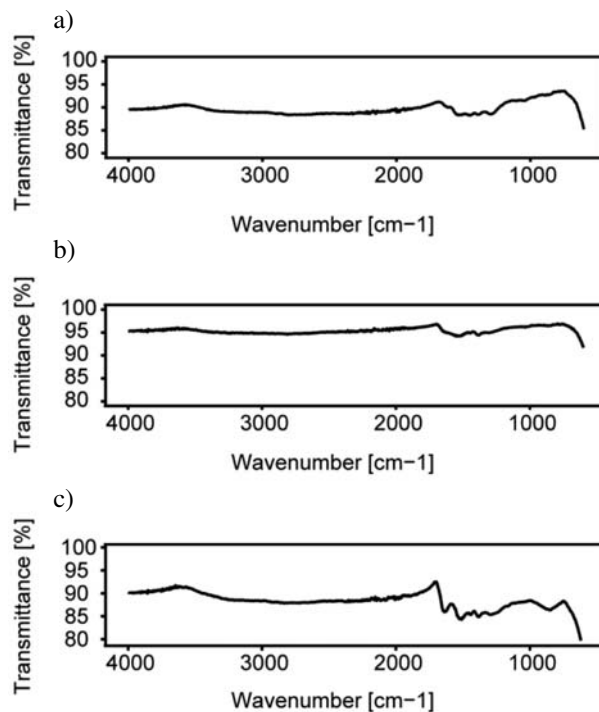


Figure 1: FTIR spectra of PEI (a), PEI_GSH (b) and PEI_BSA (c) NPs.

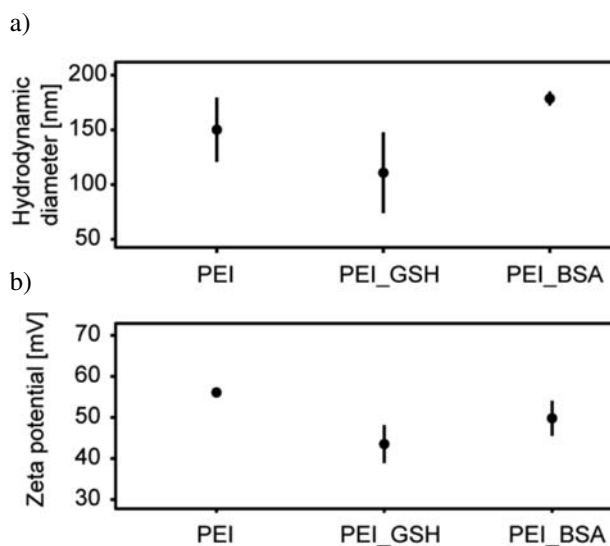


Figure 2: Physical characterization of NPs. Hydrodynamic diameter of PEI, PEI_GSH and PEI_BSA NPs dispersed in water (a). Zeta potential of PEI, PEI_GSH and PEI_BSA NPs dispersed in water (b). Means with standard errors of the mean from three independent experiments are shown.

To simulate potential intravesical therapy, normal (NPU) and papillary neoplasm (RT4) urothelial cell models were exposed to increasing concentrations of the three types of NPs for 3 h and viability was determined with Trypan blue viability assay (Figure 3). Experiments were performed in the media without FBS, as this was

more relevant for potential *in vivo* application. Immediately after the incubation, a significant proportion of dead cells was observed in all treated samples, among which PEI NPs predictably induced the highest toxicity. BSA coating (PEI_BSA NPs) showed the highest reduction of PEI NPs toxicity, resulting in increased NPU cell viability at concentrations 50 and 100 $\mu\text{g/ml}$ (Figure 3A). The hig-

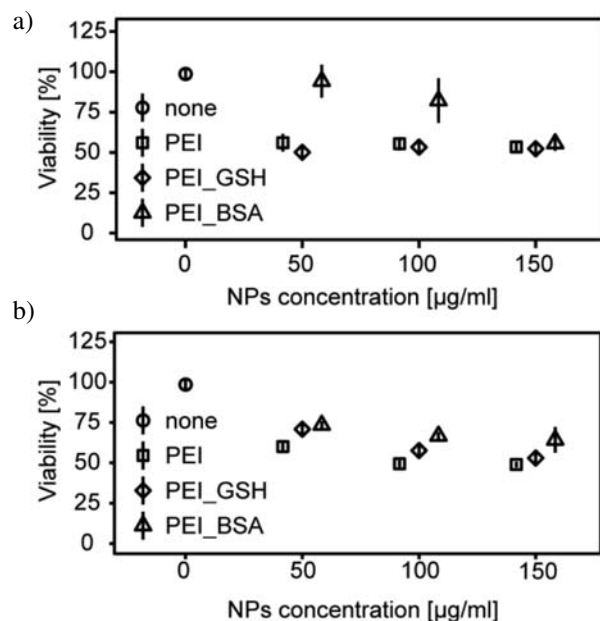


Figure 3: Viability of NPU (a) and RT4 (b) cells immediately after 3 h exposure to increasing concentrations of PEI, PEI_BSA and PEI_GSH NPs. Viability was determined by Trypan Blue viability assay. Means with standard errors of the mean from three independent experiments are shown.

hest selective toxicity was obtained with 50 $\mu\text{g/ml}$ PEI_BSA NPs, where the obtained viability was 90% and 75% for NPU and RT4 cells, respectively. On the other hand, PEI and PEI_GSH NPs induced no selective toxicity to RT4 compared to NPU cells (Figure 3). Interestingly, the overall cytotoxicity of NPs was greater in NPU cells than in RT4 cells, which is most probably due to a higher number of cell layers in RT4 cell model, but could also be due to the different molecular composition of cell membrane in RT4 and NPU cells.³⁹

Interestingly, the increasing NP concentration had only a small effect on cell viability. This can be explained by short exposure time, which limited the sedimentation and internalization of NPs. Moreover, cells in these cell models grow in confluent layers, thus limiting the exposure to NPs only to the uppermost layer. All used NP concentrations were enough to damage the first layer and the remaining cell debris protected the lower laying cells. This was confirmed with TEM analysis, where following 3 h incubation, NPs were observed in contact only with the uppermost cell layer of RT4 in membrane structures which could represent macropinocytotic uptake (Figure 4) and possibly lead to internalization of NPs. No NPs were observed associated with NPU cells (Figure 4).

To determine, if these NPs can cause delayed selective toxicity, cell models were cultured for additional 24 h after the initial 3 h NP exposure (Figure 5). PEI and PEI_BSA NPs caused additional cytotoxicity to RT4 cells after 24 h compared to cytotoxicity determined immediately after 3 h exposure, partially due to intracellular toxicity, and also partially due to delayed effect of the 3 h exposure to NPs. The later effect was confirmed on NPU

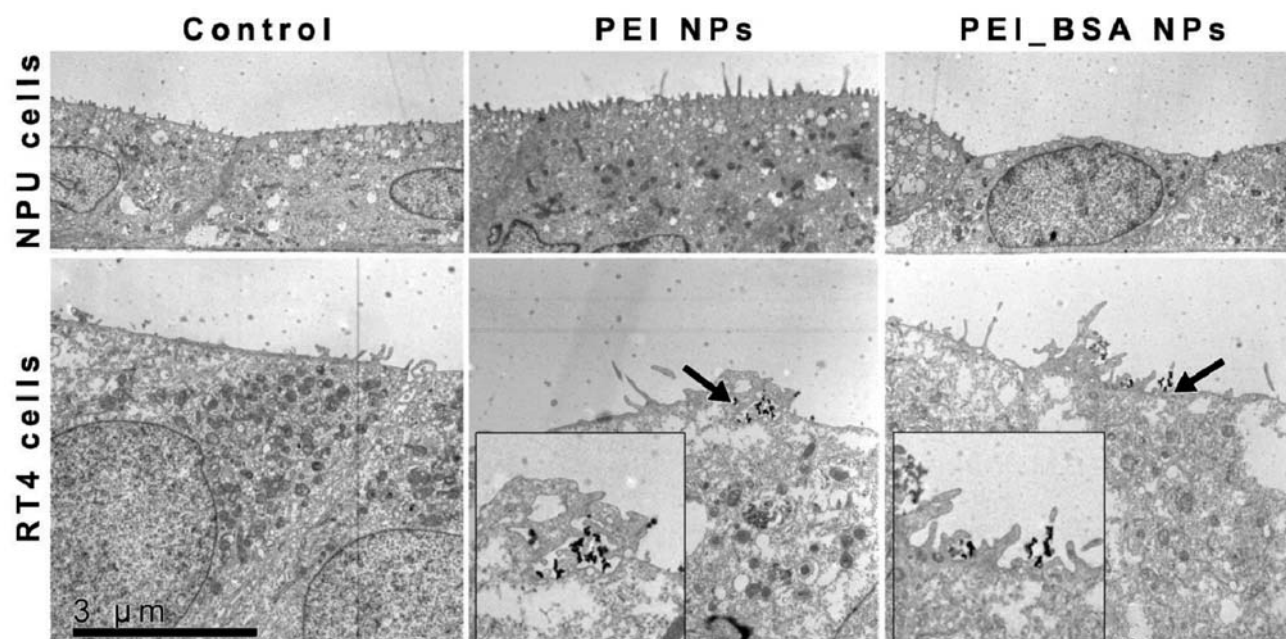


Figure 4: TEM micrographs of NPU and RT4 cells without NPs (control), with 50 $\mu\text{g/ml}$ PEI NPs or 50 $\mu\text{g/ml}$ PEI_BSA NPs after 3 h incubation. Arrows denote NPs.

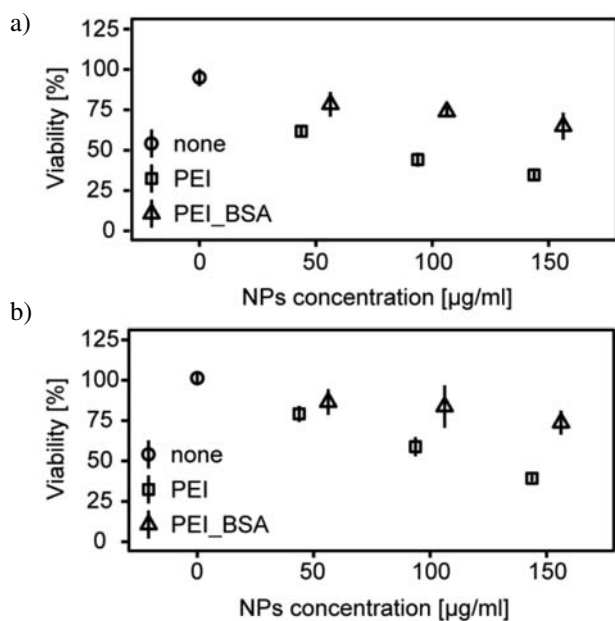


Figure 5: Viability of NPU (a) and RT4 (b) cells 24h after the 3h exposure to increasing concentrations of PEI and PEI_BSA NPs. Viability was determined 24h after the removal of NPs, by Trypan blue viability assay. Means with standard errors of the mean from three independent experiments are shown.

cells, since a reduced viability was observed for both PEI and PEI_BSA NPs. For both cell lines, this reduction in viability could be caused by NPs that remained on the surface of cell models after the washing step. Again, PEI_BSA NPs proved to be less toxic to NPU and RT4 cells compared to PEI NPs at equal concentrations. Also, only a negligible number of dead cells were observed (results not shown), indicating that the damaged cells were washed away, and leaving only healthy cells to regenerate the urothelium. Thus, analysis after 24 h showed that developed NP formulations exhibit no selective toxicity for cancer RT4 cells.

Unfortunately, despite the promising results on the reduction of PEI NP toxicity, the additional BSA coating did not induce selective toxicity towards cancer cells. This is partially caused by the still high extracellular toxicity of modified NPs at the concentrations used, but could also be due to the short incubation time, which significantly limited the interactions between NPs and cell membranes and thus also the amount of internalized NPs in RT4 cells. Additional strategies to more effectively reduce the extracellular toxicity of PEI NPs should thus be explored.

4. Conclusions

PEI NPs were successfully coated with GSH or BSA and the functionalization was confirmed with FTIR, DLS and zeta potential measurements. Reduced extracellular toxicity of PEI NPs with additional functionalization

proved to be a promising method for achieving selective toxicity to urothelial cells after 3 h of exposure, as indicated by the reduced cytotoxicity of BSA modified PEI NPs towards NPU cells compared to RT4 cells. However, viability experiments performed 24 h after the initial exposure to NPs indicated that further optimisation is needed in order to decrease nonspecific membrane toxicity of NPs and thus obtain therapeutic window with specific cytotoxicity to RT4 cancer cells.

5. Acknowledgements

We express gratitude to Urša Tomažin, Sanja Čabraja, Linda Štrus, Nada Pavlica Dubarič, and Sabina Železnik for their technical assistance. The study was supported by the Slovenian Research Agency (Grants No. J7-7424, J3-6794, J2-6758, P1-0055, J3-7494, P3-0108, and Young Researchers Program).

6. References

1. J. I. Epstein, *Int. J. Surg. Pathol.* **2010**, *18*, 106S–111S. <https://doi.org/10.1177/1066896910370471>
2. J. K. McKenney, M. B. Amin, R. H. Young, *Mod. Pathol.* **2003**, *16*, 623–629. <https://doi.org/10.1097/01.MP.0000073973.74228.1E>
3. S. Holmang, H. Hedelin, C. Anderstrom, E. Holmberg, C. Busch, S. L. Johansson, *J. Urol.* **1999**, *162*, 702–707. <https://doi.org/10.1097/00005392-199909010-00019>
4. J. Nirmal, Y.-C. Chuang, P. Tyagi, M. B. Chancellor, *Urol. Sci.* **2012**, *23*, 70–77. <https://doi.org/10.1016/j.urols.2012.07.005>
5. L. Neutsch, M. Wambacher, E.-M. Wirth, S. Spijker, H. Kählig, M. Wirth, F. Gabor, *Int. J. Pharm.* **2013**, *450*, 163–176. <https://doi.org/10.1016/j.ijpharm.2013.04.058>
6. G. Chen, Y. He, X. Wu, Y. Zhang, C. Luo, P. Jing, *Braz. J. Med. Biol. Res.* **2012**, *45*, 771–776. <https://doi.org/10.1590/S0100-879X2012007500111>
7. N. Erdoğar, A. B. Iskit, H. Eroğlu, M. F. Sargon, N. A. Mungan, E. Bilensoy, *J. Nanosci. Nanotechnol.* **2015**, *15*, 10156–10164. <https://doi.org/10.1166/jnn.2015.11690>
8. M. R. Kang, G. Yang, R. F. Place, K. Charisse, H. Epstein-Barash, M. Manoharan, L.-C. Li, *Cancer Res.* **2012**, *72*, 5069–5079. <https://doi.org/10.1158/0008-5472.CAN-12-1871>
9. J.-H. Kim, Y.-S. Kim, K. Park, S. Lee, H. Y. Nam, K. H. Min, H. G. Jo, J. H. Park, K. Choi, S. Y. Jeong, R.-W. Park, I.-S. Kim, K. Kim, I. C. Kwon, *J. Control. Release Off. J. Control. Release Soc.* **2008**, *127*, 41–49. <https://doi.org/10.1016/j.jconrel.2007.12.014>
10. D. T. Martin, C. J. Hoimes, H. Z. Kaimakliotis, C. J. Cheng, K. Zhang, J. Liu, M. A. Wheeler, W. K. Kelly, G. N. Tew, W. M. Saltzman, R. M. Weiss, *Nanomedicine Nanotechnol. Biol. Med.* **2013**, *9*, 1124–1134. <https://doi.org/10.1016/j.nano.2013.05.017>

11. C. Mugabe, Y. Matsui, A. I. So, M. E. Gleave, J. H. E. Baker, A. I. Minchinton, I. Manisali, R. Liggins, D. E. Brooks, H. M. Burt, *Clin. Cancer Res. Off. J. Am. Assoc. Cancer Res.* **2011**, *17*, 2788–2798. <https://doi.org/10.1158/1078-0432.CCR-10-2981>
12. L. Neutsch, E.-M. Wirth, S. Spijker, C. Pichl, H. Kählig, F. Gabor, M. Wirth, *J. Control. Release Off. J. Control. Release Soc.* **2013**, *169*, 62–72. <https://doi.org/10.1016/j.jconrel.2013.04.004>
13. L. Neutsch, M. Wambacher, E.-M. Wirth, S. Spijker, H. Kählig, M. Wirth, F. Gabor, *Int. J. Pharm.* **2013**, *450*, 163–176. <https://doi.org/10.1016/j.ijpharm.2013.04.058>
14. A. S. L. Derycke, A. Kamuhabwa, A. Gijssens, T. Roskams, D. De Vos, A. Kasran, J. Huwyler, L. Missiaen, P. A. M. de Witte, *J. Natl. Cancer Inst.* **2004**, *96*, 1620–1630. <https://doi.org/10.1093/jnci/djh314>
15. T. Leakakos, C. Ji, G. Lawson, C. Peterson, S. Goodwin, *Cancer Chemother. Pharmacol.* **2003**, *51*, 445–450.
16. Z. Lu, T.-K. Yeh, J. Wang, L. Chen, G. Lyness, Y. Xin, M. G. Wientjes, V. Bergdall, G. Couto, F. Alvarez-Berger, C. E. Kosarek, J. L.-S. Au, *J. Urol.* **2011**, *185*, 1478–1483. <https://doi.org/10.1016/j.juro.2010.11.091>
17. T. Sun, Y. S. Zhang, B. Pang, D. C. Hyun, M. Yang, Y. Xia, *Angew. Chem. Int. Ed.* **2014**, *53*, 12320–12364.
18. E. Bilensoy, C. Sarisozen, G. Esendağlı, A. L. Doğan, Y. Aktaş, M. Şen, N. A. Mungan, *Int. J. Pharm.* **2009**, *371*, 170–176. <https://doi.org/10.1016/j.ijpharm.2008.12.015>
19. O. Boussif, F. Lezoualc'h, M. Antoniet, Zanta, M. D. Mergny, D. Scherman, B. Demeneix, J.-P. Behr, *Proc. Natl. Acad. Sci.* **1995**, *92*, 7297–7301. <https://doi.org/10.1073/pnas.92.16.7297>
20. S. Prijic, L. Prosen, M. Cemazar, J. Scancar, R. Romih, J. Lavrencak, V. B. Bregar, A. Coer, M. Krzan, A. Znidarsic, G. Sersa, *Biomaterials* **2012**, *33*, 4379–4391. <https://doi.org/10.1016/j.biomaterials.2012.02.061>
21. F. Scherer, M. Anton, U. Schillinger, J. Henkel, C. Bergemann, A. Kruger, B. Gansbacher, C. Plank, *Gene Ther.* **2002**, *9*, 102–109. <https://doi.org/10.1038/sj.gt.3301624>
22. C. Mugabe, B. A. Hadaschik, R. K. Kainthan, D. E. Brooks, A. I. So, M. E. Gleave, H. M. Burt, *BJU Int.* **2009**, *103*, 978–986. <https://doi.org/10.1111/j.1464-410X.2008.08132.x>
23. P. Sweeney, T. Karashima, H. Ishikura, S. Wiehle, M. Yamashita, W. F. Benedict, R. J. Cristiano, C. P. N. Dinney, *Cancer Res.* **2003**, *63*, 4017–4020.
24. T.-L. Hwang, I. A. Aljuffali, C.-F. Lin, Y.-T. Chang, J.-Y. Fang, *Int. J. Nanomedicine* **2015**, *10*, 371–385.
25. S. Moghimi, P. Symonds, J. Murray, A. Hunter, G. Debska, A. Szewczyk, *Mol. Ther.* **2005**, *11*, 990–995. <https://doi.org/10.1016/j.ymthe.2005.02.010>
26. C. Hoskins, A. Cuschieri, L. Wang, *J Nanobiotechnol* **2012**, *10*, 15.
27. D. Fischer, Y. Li, B. Ahlemeyer, J. Kriegelstein, T. Kissel, *Biomaterials* **2003**, *24*, 1121–1131. [https://doi.org/10.1016/S0142-9612\(02\)00445-3](https://doi.org/10.1016/S0142-9612(02)00445-3)
28. E. Fröhlich, *Int. J. Nanomedicine* **2012**, 5577. <https://doi.org/10.2147/IJN.S36111>
29. L. Parhamifar, A. K. Larsen, A. C. Hunter, T. L. Andresen, S. M. Moghimi, *Soft Matter* **2010**, *6*, 4001. <https://doi.org/10.1039/c000190b>
30. R. V. Benjaminsen, M. A. Matthebjerg, J. R. Henriksen, S. M. Moghimi, T. L. Andresen, *Mol. Ther.* **2012**, *21*, 149–157. <https://doi.org/10.1038/mt.2012.185>
31. K. Strojjan, J. Lojk, V. B. Bregar, P. Veranič, M. Pavlin, *Toxicol. In Vitro* **2017**, DOI 10.1016/j.tiv.2017.02.007.
32. V. Mirshafiee, R. Kim, S. Park, M. Mahmoudi, M. L. Kraft, *Biomaterials* **2016**, *75*, 295–304. <https://doi.org/10.1016/j.biomaterials.2015.10.019>
33. A. O. Elzoghby, W. M. Samy, N. A. Elgindy, *J. Controlled Release* **2012**, *157*, 168–182. <https://doi.org/10.1016/j.jconrel.2011.07.031>
34. V. B. Bregar, J. Lojk, V. Šuštar, P. Veranič, M. Pavlin, *Int. J. Nanomedicine* **2013**, *8*, 919–931.
35. T. Višnjar, P. Kocbek, M. E. Kreft, *Histochem. Cell Biol.* **2012**, *137*, 177–186. <https://doi.org/10.1007/s00418-011-0893-0>
36. H. Lv, S. Zhang, B. Wang, S. Cui, J. Yan, *J. Controlled Release* **2006**, *114*, 100–109. <https://doi.org/10.1016/j.jconrel.2006.04.014>
37. H. Li, Z. Cui, C. Han, *Sens. Actuators B Chem.* **2009**, *143*, 87–92. <https://doi.org/10.1016/j.snb.2009.09.013>
38. A. Lesniak, F. Fenaroli, M. P. Monopoli, C. Åberg, K. A. Dawson, A. Salvati, *ACS Nano* **2012**, *6*, 5845–5857. <https://doi.org/10.1021/nn300223w>
39. N. Resnik, U. Repnik, M. E. Kreft, K. Sepčić, P. Maček, B. Turk, P. Veranič, *PLOS ONE* **2015**, *10*, e0137878. <https://doi.org/10.1371/journal.pone.0137878>

Povzetek

Normalne prašičje urotelijske celice imajo nižjo stopnjo endocitoze kot urotelijske celice papilarne neoplazme. To lahko izkoristimo kot mehanizem za selektivno dostavo nanodelcev oplaščenih s polietileniminom. Nanodelci pa lahko delujejo toksično tudi preko interakcije s celično membrano. Tej toksičnosti se lahko izognemo z dodatno plastjo nasprotno nabitih molekul na površini nanodelcev. V našem primeru smo to želeli doseči z dodatno plastjo glutationa oziroma govejega serumskega albumina. Test viabilnosti je pokazal, da dodatna plast govejega serumskega albumina uspešno zmanjša neselektivno citotoksičnost nanodelcev takoj po 3 h izpostavitvi. Taisti nanodelci so izkazali višjo citotoksičnost na urotelijskih celicah papilarne neoplazme v primerjavi z normalnimi prašičjimi urotelijskimi celicami pri koncentraciji 50 µg/ml. 24 h po izpostavitvi je učinek nanodelcev enak na obeh celičnih linijah.

Scientific paper

Lipid Droplet Formation in HeLa Cervical Cancer Cells Depends on Cell Density and the Concentration of Exogenous Unsaturated Fatty Acids

Emma Guštin,^{1,#} Eva Jarc,^{1,2,#} Ana Kump^{1,2} and Toni Petan^{1,*}¹ *Department of Molecular and Biomedical Sciences, Jožef Stefan Institute, Ljubljana, Slovenia*² *Jožef Stefan International Postgraduate School, Ljubljana, Slovenia*# *These authors contributed equally to this work.** *Corresponding author: E-mail: toni.petan@ijs.si*
*Phone: + 386 1 477 3713**Received: 12-09-2016****For Cutting Edge 2017***

Abstract

Cytosolic lipid droplets (LDs) store excess fatty acids (FAs) in the form of neutral lipids and prevent starvation-induced cancer cell death. Here we studied the ability of mono- and polyunsaturated FAs to affect LD formation and survival in HeLa cervical cancer cells. We found that the LD content in HeLa cells increases with cell density, but it decreases in MDA-MB-231 breast cancer cells. Exogenously-added unsaturated FAs, including oleic (OA), linoleic (LA), arachidonic (AA), eicosapentaenoic (EPA) and docosahexaenoic acid (DHA) displayed a similar ability to alter LD formation in HeLa cells. There was a dual, concentration-dependent effect on neutral lipid accumulation: low micromolar concentrations of LA, AA and DHA reduced, while all FAs induced LD formation at higher concentrations. In serum starved HeLa cells, OA stimulated LD formation, but, contrary to expectations, it promoted cell death. Our results reveal a link between cell population density and LD formation in HeLa cells and show that unsaturated FAs may both suppress or stimulate LD formation. This dynamic regulation of LD content must be accounted for when studying the effects of lipids and lipid metabolism-targeting drugs on LD metabolism in HeLa cells.

Keywords: lipid droplets, lipid metabolism, cell density, HeLa cervical cancer cells, unsaturated fatty acids, apoptosis

1. Introduction

Tumours have developed different molecular mechanisms that enable their uncontrolled proliferation.¹ Oncogene activation and loss of tumour suppressors lead to both proliferative and metabolic reprogramming of cancer cells. The most common metabolic adaptations in cancer are increased glucose uptake, high rate of anaerobic glycolysis and increased glutamine consumption, but recent studies have revealed a dependence on elevated *de novo* lipid synthesis, internalization of exogenous lipids, mitochondrial fatty acid (FA) oxidation and lipid mediator-induced proliferative signalling.^{1–4} Lipids and their metabolites are currently under intense investigation in cancer-related studies, where new aspects of their role in

cancer signalling, survival and apoptosis are beginning to emerge.

Lipid droplets (LDs) are now widely recognized as dynamic cytosolic organelles, present in all eukaryotic cells, with prominent roles reaching beyond that of inert energy storage depots.⁵ LDs are composed of a tightly packed core of neutral lipids, triacylglycerol (TAG) and sterol esters, surrounded by a phospholipid monolayer embedded with proteins and enzymes. At the cellular level, besides providing energy and building blocks for biosyntheses, they have important roles in protein quality control, viral replication and cell signalling, and are implicated in physiological processes ranging from immunity to neural development.⁶ Strong evidence suggests that LDs also control the synthesis of an array of lipid signal-

ling molecules and that changes in LD metabolism influence the risk of developing metabolic diseases and cancer.^{7,8}

Increased accumulation of LDs has been observed in cancer cells *in vivo* and *in vitro* and LDs have been proposed as markers of cancer aggressiveness.^{2,4,9–12} The mechanisms of their involvement in cancer are currently under intense investigation. LDs are primary cellular sources of FAs for mitochondrial β -oxidation, which has been shown to enable cancer cell survival during various stress conditions.^{13–15} We have previously shown that secreted phospholipase A₂-induced release of unsaturated FAs induces TAG synthesis and LD formation in aggressive breast cancer cells, thus stimulating proliferation and preventing cell death during serum starvation.^{16,17} The protective effects of LDs are associated with upregulation of β -oxidation enzymes and may be abolished with etomoxir, a potent inhibitor of β -oxidation. Intriguingly, LD formation is also induced during complete cell starvation, i.e. in the absence of glucose, amino acids and exogenous sources of lipid, when LDs become critical for providing FAs for β -oxidation that enables the survival of different cells, including HeLa cervical cancer cells.^{18,19}

The role of different unsaturated FA species in supporting LD accumulation and cell survival in different cancer cell types in different environmental conditions is not clear. In general, LDs prevent FA lipotoxicity by acting as transient buffers for excess endogenous and exogenous FAs. Saturated FAs are particularly toxic to the cell and induce ER-stress and apoptosis, while monounsaturated FAs, such as oleic acid (OA; 18:1, ω -9), are generally regarded as cytoprotective.²⁰ The supplementation of unsaturated FAs may even avert lipotoxicity by syphoning saturated FAs to inert TAGs stored in LDs.²¹ A number of studies have demonstrated that polyunsaturated FAs (PUFAs) have distinct and contrasting effects in cancer, with ω -6 PUFAs, such as arachidonic acid (AA; 20:4, ω -6), mostly displaying pro-tumorigenic effects and ω -3 PUFAs, such as eicosapentaenoic (EPA; 20:5, ω -3) and docosahexaenoic acid (DHA; 22:6, ω -3), showing anti-tumorigenic, anti-inflammatory and pro-apoptotic effects in cancer cells.^{22,23} However, the association between LD metabolism and individual FA species in the context of cancer cell survival and metabolism is unknown. Here we studied the ability of different exogenous unsaturated FAs, namely OA, linoleic acid (LA; 18:2, ω -6), AA, EPA and DHA to induce LD formation and affect cell death in HeLa cervical cancer cells.

2. Experimental

2. 1. Materials

HeLa cervical adenocarcinoma cells (HeLa H2 clone) were obtained from John V. Moran, Howard Hughes Medical Institute, USA. MDA-MB-231 breast adenocar-

cinoma cells and RPMI-1640 culture medium were from ATCC (USA). DMEM, foetal bovine serum (FBS) and Dulbecco's phosphate buffered saline (DPBS) were from Gibco, USA. Nile Red, tetramethylrhodamine, methyl ester (TMRM), LA, EPA, DHA, AA, fatty acid-free bovine serum albumin (FAF-BSA) were from Sigma-Aldrich (USA), YO-PRO-1 iodide, TrypLE Select were from Life Technologies (USA), while OA and DMSO were from Merck (Germany).

2. 2. Cell Lines and Culture Conditions

HeLa and MDA-MB-231 cells were cultured in DMEM and RPMI-1640 medium, respectively, supplemented with 10% FBS. In experiments with serum-deprived cells, FBS was replaced by 0.02% FAF-BSA to render cells quiescent. Exogenously added FAs were complexed with 0.5% FAF-BSA or 10% FBS in culture medium for 1 h at room temperature before addition to cell culture.

2. 3. Flow Cytometry Analysis of Cellular LD Content

LD analysis was performed as described previously.¹⁶ Briefly, cells were seeded in complete medium in 24-well culture plates, left to attach for 24 h, and treated with different concentrations of FAs for 48 h. Prior to treatment, FAs were complexed as described above. Cells were harvested, the pellet resuspended in 500 μ l of 1 μ g/ml Nile Red solution in DPBS, incubated in the dark for 10 min and analysed by flow cytometry on a BD FACSCalibur system (BD Biosciences, USA). Logarithmic fluorescence signals were collected using the FL1 filter (530/30) from at least 2×10^4 events per sample.

2. 4. TMRM/YO-PRO-1 Apoptosis Assay

Cell death was determined by measuring mitochondrial and plasma membrane integrity using the TMRM/YO-PRO-1 assay and flow cytometry as described previously.¹⁷ Cells were seeded in complete medium in 24-well plates at a concentration of 3×10^4 cells/well. 24 h later, the medium was replaced by serum-free DMEM containing 0.02% FAF-BSA and the cells pre-starved for 24 h. Medium was replaced, cells treated with different concentrations of FAs (pre-complexed with DMEM containing 0.5% FAF-BSA) and incubated for 168 h. Cells were harvested, the pellet resuspended in 100 μ l of 150 nM TMRM in DPBS and incubated in the dark for 15 min. Finally, 1 μ l of 20 μ M YO-PRO-1 in DMSO was added and cells incubated for additional 10 min. TMRM and YO-PRO-1 signals from 5×10^4 cells per sample were measured by flow cytometry using the FL1 (530/30) and FL3 (650LP) filters. TMRM negative and YO-PRO-1 positive cells were considered apoptotic.

2. 5. Statistical Analysis

Data are presented as means \pm SEM. Graphpad Prism (GraphPad Software, USA) was used for statistical analysis, using one-way ANOVA with Bonferroni adjustment for multiple comparisons. P values lower than 0.05 were considered statistically significant.

3. Results and Discussion

In the course of our flow cytometry assay optimization for the detection of LDs in HeLa cells, we observed significant changes in their LD content depending on the number of cells seeded. In order to determine whether cell density affects LD accumulation, HeLa cells were seeded at different densities, grown for 48 h in complete medium and the average LD amount in the cell population was determined by flow cytometry. We found that the LD content in HeLa cells increased proportionally with cell density (Fig. 1a). On the contrary, the average LD amount in MDA-MB-231 breast cancer cells, a cell line with high propensity for LD formation from exogenous FAs,¹⁶ decreased with cell density (Fig. 1b). Namely, rapidly proliferating cancer cells grown in complete medium are highly metabolically active and they take up and metabolize glucose and amino acids to support biosynthesis, cell growth and proliferation.¹ Lipids may be synthesized *de novo* or are taken up from exogenous sources, and are necessary for the maintenance and synthesis of cell membranes and thus a prerequisite for cell proliferation.⁴ Therefore, we expected that LD content will decrease with increasing cell density, since there is an increasing number of cells competing for the fixed supply of exogenous lipids found in serum. The increase in LD

amount in HeLa cells suggests that with increasing cell density, and in the absence of contact inhibition, HeLa cells either gradually increase the rate of exogenous lipid uptake or significantly upregulate *de novo* lipid synthesis. In both cases, LDs may be necessary for supporting cell growth and proliferation processes characteristic of HeLa cells. In support of our finding, a similar relationship between LD amount and cell density has been reported for C6 rat glioma cells in culture,²⁴ and, interestingly, an increase in the amount and size of LDs is characteristic of adipogenic differentiation, which may occur also in cancer cells, including cancer stem cell subpopulations of HeLa cells.^{25,26} Although the role of LDs in cell growth and proliferation is not clear, it may be easily envisaged that LDs act as master regulators of cellular lipid homeostasis, finely tuning the balance between lipid requirements and supply during cell growth. Additionally, LDs may be necessary to alleviate ER-stress that occurs in cancer cells undergoing oncogene-driven, uncontrolled proliferation.^{27,28}

We next asked whether different exogenous unsaturated FA species vary in their abilities to induce LD accumulation in HeLa cells. We found that all tested FAs displayed a similar ability to modulate LD accumulation in HeLa cells (Fig. 2a–e). As expected, high micromolar concentrations of FAs, which are regularly used to induce LD formation in various cell types, stimulated LD accumulation in HeLa cells. This is in accordance with the conserved mechanism of prevention of FA lipotoxicity by their incorporation into TAG and LD formation.^{20,21} Surprisingly, a slight decrease in neutral lipid levels was observed when cells were exposed to low concentrations of FAs (10 μ M and below; Fig. 2a–e). A statistically significant reduction for LA, AA and DHA, which reduced LD amounts by 20, 15 and 19%, respectively, was indeed confirmed in a separate experiment using

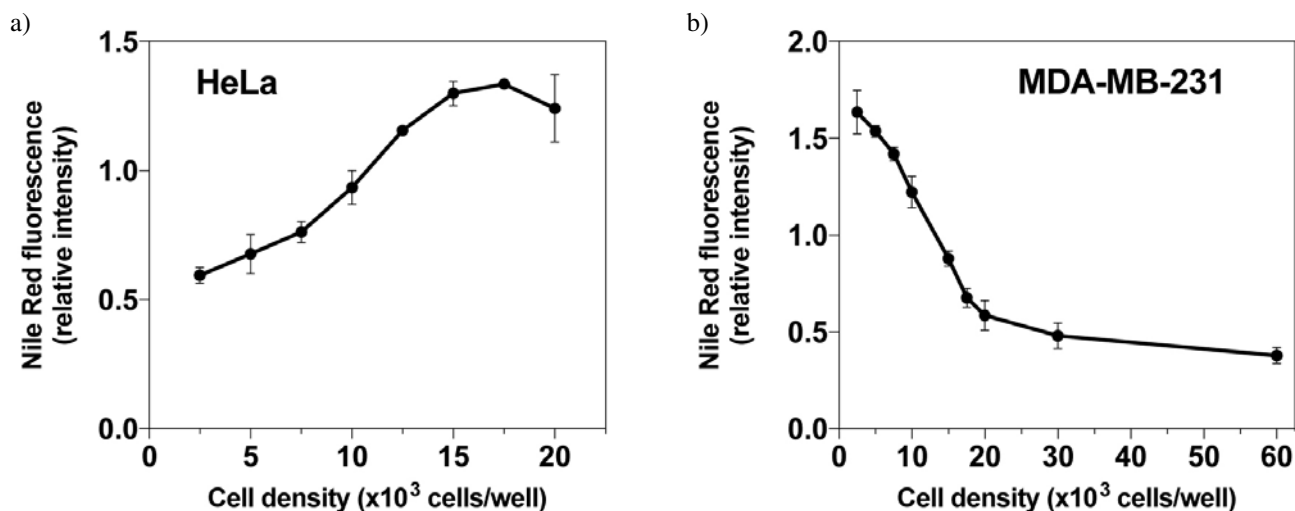


Figure 1. LD content in HeLa cells increases with cell density. (a) HeLa and (b) MDA-MB-231 cells were seeded in 24-well plates at the stated cell densities in complete medium. After 24 h the medium was replaced and cells were cultivated for another 48 h in complete medium. Cells were collected, stained with Nile Red and LD content was determined by flow cytometry. The resulting values are means \pm SEM of at least two experiments performed in duplicate.

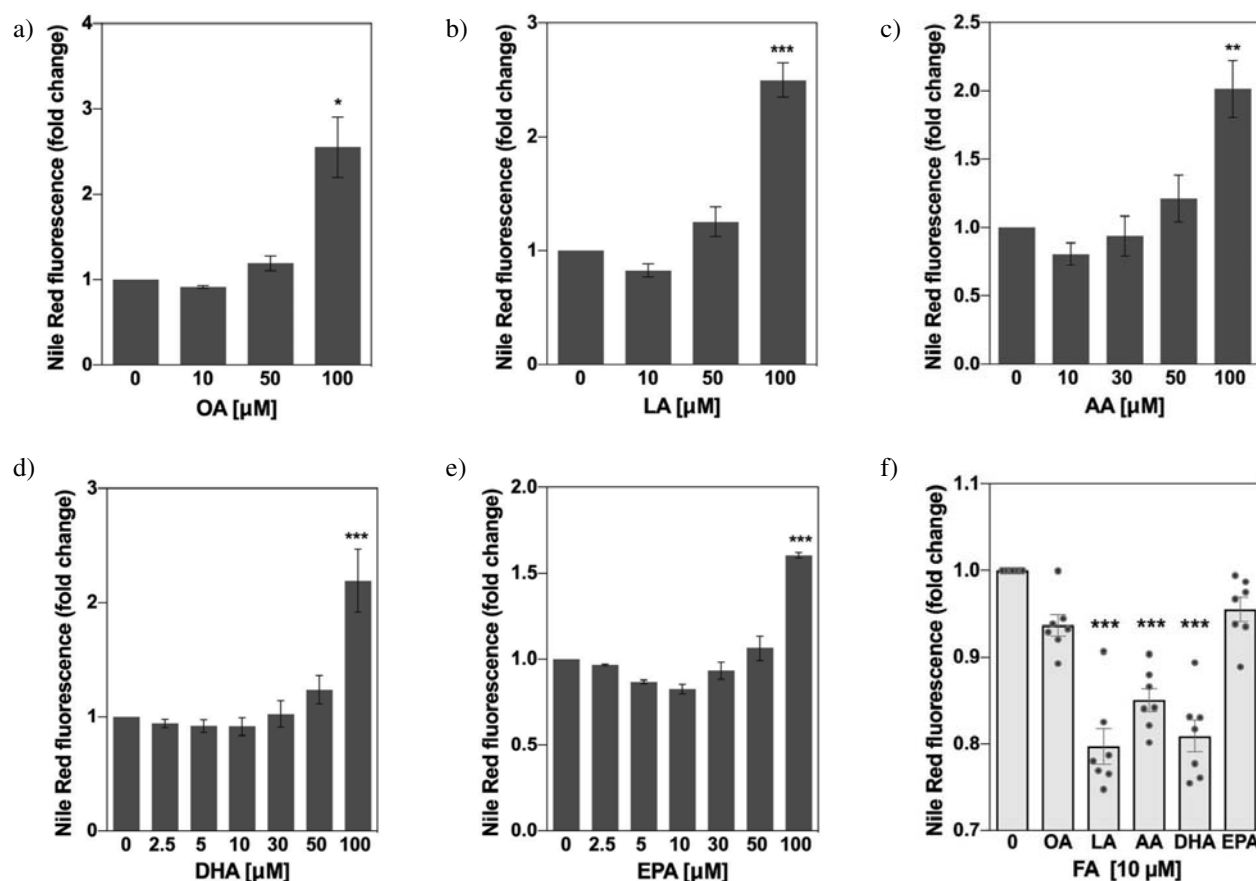


Figure 2. Unsaturated FAs have dual effects on LD accumulation in HeLa cells. (a) HeLa cells were grown for 48 h in complete media in the presence of a range of concentrations of OA (a), LA (b), AA (c), DHA (d) and EPA (e) or in the presence of 10 μM of each FA (f). LD content was determined by flow cytometry. The resulting values are means \pm SEM of at least two (Fig. 2a–e) or seven (Fig. 2f) experiments performed in duplicate. Results that are statistically significant over control samples are indicated (*, $P < 0.05$; **, $P < 0.01$; ***, $P < 0.001$; one-way ANOVA with Bonferroni adjustment).

only 10 μM FAs (Fig. 2f). The negative effect on LD accumulation may be a consequence of stimulated LD breakdown or suppressed LD formation, and is reminiscent to the anti-adipogenic effect of unsaturated FAs, in particular ω -3 PUFAs, in differentiating adipocytes.²⁹ The relevance of this finding for cancer cell biology remains to be established.

We have shown recently that OA induces LD formation in MDA-MB-231, MCF-7 and T-47D breast cancer cells, but it suppresses starvation-induced cell death only in MDA-MB-231 cells.¹⁶ To find out whether OA promotes LD accumulation and suppresses the death of HeLa cells, we treated starving HeLa cells with a range of concentrations of OA. Interestingly, we observed that OA induced significant LD accumulation only at the highest concentration used and it did not reduce, but it rather promoted cell death at higher concentrations (Fig. 3). Thus, in contrast to the highly invasive MDA-MB-231 cells,¹⁶ and despite the well-known cytoprotective effect of OA,²⁰ our results suggest that serum-deprived HeLa cells cannot use exogenous OA to support cell survival. It is possible that starved HeLa cells are either not efficient in packa-

ging exogenous OA into TAGs for transient storage in LDs or their LD breakdown pathways are overly active, thus leading to lipotoxicity of the unesterified OA.^{3,31}

4. Conclusions

We show that LD content in HeLa cells is proportional with cell culture density, that unsaturated FAs have differential effects on LD accumulation, and that OA cannot support the survival of starved HeLa cells. These interesting novel features of LD metabolism in HeLa cells may be useful for future studies providing fresh insights into cancer LD metabolism, in particular the relationship between cancer cell proliferation and lipid metabolism.

5. Acknowledgements

We are grateful to John V. Moran for providing the HeLa cell line. This work was supported by the 1000-15-

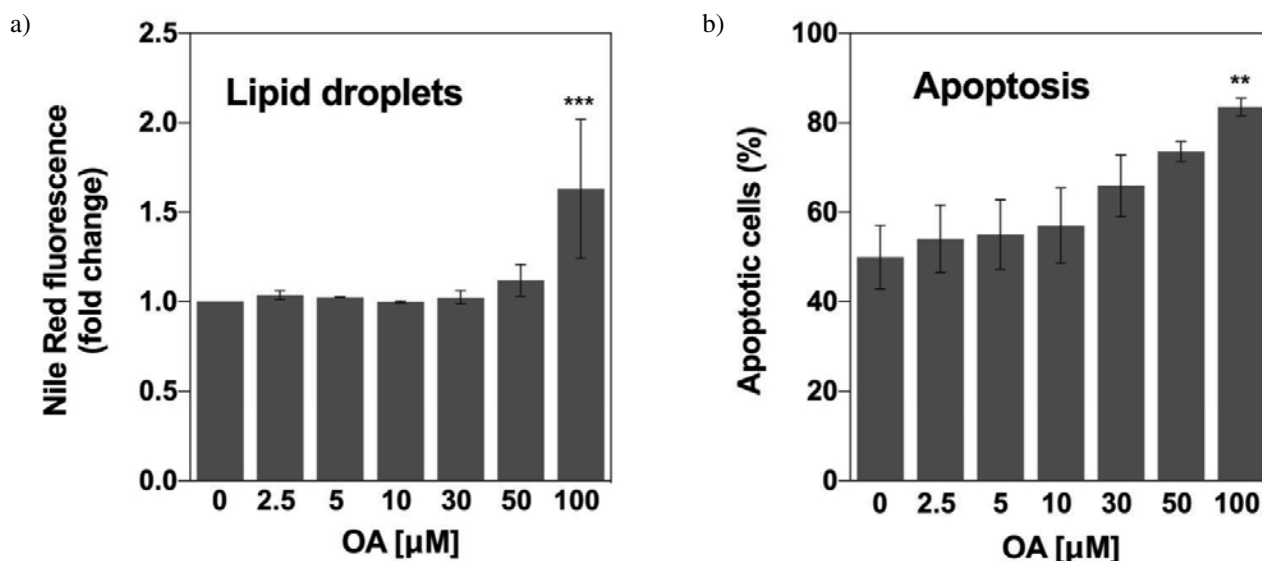


Figure 3. OA-induced LD accumulation does not provide a survival advantage for serum-deprived HeLa cells. HeLa cells were seeded in complete medium, left to attach for 24 h and pre-starved for 24 h in serum-deprived medium. Cells were then incubated with different concentrations of FAs for 168 h in serum-deprived medium. (a) LD content and (b) apoptosis were determined by flow cytometry. The resulting values are means \pm SEM of at least two experiments performed in duplicate. Results that are statistically significant over control samples are indicated (*, $P < 0.05$; **, $P < 0.01$; ***, $P < 0.001$; one-way ANOVA with Bonferroni adjustment).

106 Young Researcher grant to E.J. and the P1-0207 Research Programme grant from the Slovenian Research Agency.

Conflicts of interest

None of the authors declare any conflict of interest.

6. References

- N. N. Pavlova, C. B. Thompson, *Cell Metab.* **2016**, *23*, 27–47. <https://doi.org/10.1016/j.cmet.2015.12.006>
- S. Beloribi-Djefaflija, S. Vasseur, F. Guillaumond, *Oncogenesis* **2016**, *5*, 189. <https://doi.org/10.1038/oncsis.2015.49>
- E. Currie, A. Schulze, R. Zechner, T. C. Walther, R. V. Jr. Farese, *Cell Metab.* **2013**, *18*, 153–61. <https://doi.org/10.1016/j.cmet.2013.05.017>
- C. R. Santos, A. Schulze, *FEBS J.* **2012**, *279*, 2610–23. <https://doi.org/10.1111/j.1742-4658.2012.08644.x>
- R. V. Farese, T. C. Walther, *Cell* **2009**, *139*, 855–60. <https://doi.org/10.1016/j.cell.2009.11.005>
- Y. Ohsaki, M. Suzuki, T. Fujimoto, *Chem. Biol.* **2014**, *21*, 86–96. <https://doi.org/10.1016/j.chembiol.2013.08.009>
- A. Dichlberger, S. Schlager, K. Maaninka, W. J. Schneider, P. T. Kovanen, *J. Lipid Res.* **2014**, *55*, 2471–8. <https://doi.org/10.1194/jlr.M048553>
- G. Haemmerle, T. Moustafa, G. Woelkart et al., *Nat. Med.* **2011**, 1076–85. <https://doi.org/10.1038/nm.2439>
- A. S. Greenberg, R. A. Coleman, F. B. Kraemer et al., *J. Clin. Invest.* **2011**, *121*, 2102–10. <https://doi.org/10.1172/JCI46069>
- L. Tirinato, C. Liberale, S. F. Di et al., *Stem Cells* **2015**, *33*, 35–44. <https://doi.org/10.1002/stem.1837>
- T. M. Accioly, P. Pacheco, C. M. Monteiro-Maya et al., *Cancer Res.* **2008**, *68*, 1732–40. <https://doi.org/10.1158/0008-5472.CAN-07-1999>
- P. T. Bozza, J. P. Viola, *Prostaglandins Leukot. Essent. Fatty Acids* **2010**, *82*, 243–50. <https://doi.org/10.1016/j.plefa.2010.02.005>
- S. M. Jeon, N. S. Chandel, N. Hay, *Nature* **2012**, *485*, 661–5. <https://doi.org/10.1038/nature11066>
- L. S. Pike, A. L. Smift, N. J. Croteau, D. A. Ferrick, M. Wu, *Biochim. Biophys. Acta* **2011**, *1807*, 726–34.
- A. Carracedo, L. C. Cantley, P. P. Pandolfi, *Nat. Rev. Cancer* **2013**, *13*, 227–32. <https://doi.org/10.1038/nrc3483>
- A. Pucer, V. Brglez, C. Payré, J. Pungercar, G. Lambeau, T. Petan, *Mol. Cancer* **2013**, *12*, 111. <https://doi.org/10.1186/1476-4598-12-111>
- V. Brglez, G. Lambeau, T. Petan, *Biochimie* **2014**, Pt A: 114–23.
- A. S. Rambold, S. Cohen, J. Lippincott-Schwartz, *Dev. Cell* **2015**, *32*, 678–92. <https://doi.org/10.1016/j.devcel.2015.01.029>
- A. G. Cabodevilla, L. Caballero-Sánchez, E. Nintou et al., *J. Biol. Chem.* **2013**, *288*, 27777–88. <https://doi.org/10.1074/jbc.M113.466656>
- C. J. Nolan, C. Z. Larter, *J. Gastroenterol. Hepatol.* **2009**, *24*, 703–6. <https://doi.org/10.1111/j.1440-1746.2009.05823.x>
- L. L. Listenberger, X. Han, S. E. Lewis et al., *Proc. Natl. Acad. Sci. U. S. A.* **2003**, *100*, 3077–82. <https://doi.org/10.1073/pnas.0630588100>

22. D. D'Eliseo, F. Velotti, *J. Clin. Med.* **2016**, *5*, 15.
<https://doi.org/10.3390/jcm5020015>
23. B. Chénais, V. Blanckaert, *Int. J. Breast Cancer* **2012**, *2012*, 712536.
24. I. Barba, M. E. Cabañas, C. Arús, *Cancer Res.* **1999**, *59*, 1861–8.
25. J. Trullols-Carcel, C. Gallardo-Aguilar, F. Alcalde-Garcia et al., *Springerplus* **2012**, *1*, 44.
<https://doi.org/10.1186/2193-1801-1-44>
26. L. Wang, H. Guo, C. Lin, L. Yang, X. Wang, *Mol. Med. Rep.* **2014**, *9*, 2117–23.
27. I. Hapala, E. Marza, T. Ferreira, *Biol. Cell* **2011**, *103*, 271–85. <https://doi.org/10.1042/BC20100144>
28. R. M. Young, D. Ackerman, Z. L. Quinn et al., *Genes Dev.* **2013**, *27*, 115–31.
29. H. K. Kim, M. Fera-Della, J. Lin, C. A. Baile, *J. Nutr.* **2006**, *136*, 2965–9.
30. E. Przybytkowski, E. Joly, C. J. Nolan et al., *Biochem. Cell Biol.* **2007**, *85*, 301–10.
<https://doi.org/10.1139/O07-001>
31. M. Bosma, D. H. Dapito et al., *Biochim. Biophys. Acta* **2014**, *1841*, 1648–55.

Povzetek

Citosolne lipidne kapljice shranjujejo presežne maščobne kisline (MK) v obliki nevtralnih lipidov in preprečujejo smrt rakavih celic tekom stradanja. V tem delu smo preučili vplive mono- in polinenasičenih MK na tvorbo lipidnih kapljic in preživetje celic raka materničnega vratu HeLa. Pokazali smo, da vsebnost lipidnih kapljic v celicah HeLa narašča z gostoto celične kulture, v celicah raka dojke MDA-MB-231 pa pada. Eksogeno dodane nenasičene MK, oleinska (OK), linolna (LK), arahidonska (AK), eikozapentaenojska (EPK) in dokozaheksaenojska kislina (DHK) so imele podobne vplive na tvorbo lipidnih kapljic v celicah HeLa. Opazili smo dvojni, od koncentracije odvisen učinek na kopičenje nevtralnih lipidov: nizke mikromolarne koncentracije LK, AK in DHK so znižale količino lipidnih kapljic, medtem ko so pri višjih mikromolarnih koncentracijah vse MK inducirale njihovo tvorbo. OK je spodbudila tvorbo lipidnih kapljic v stradanih celicah HeLa, a je, nasprotno od pričakovanj, spodbudila tudi celično smrt. Naši rezultati razkrivajo povezavo med gostoto celic v populaciji in tvorbo lipidnih kapljic pri celicah HeLa in kažejo, da lahko nenasičene MK tako zavirajo kot tudi stimulirajo tvorbo lipidnih kapljic. To dinamično regulacijo vsebnosti lipidnih kapljic je potrebno upoštevati pri študijah učinkov lipidov in učinkovin, ki ciljajo lipidni metabolizem, na metabolizem lipidnih kapljic v celicah HeLa.

Scientific paper

Disintegrins from the Venom of *Vipera ammodytes ammodytes* Efficiently Inhibit Migration of Breast Cancer Cells

Zorica Latinović,^{1,2} Adrijana Leonardi,¹ Toni Petan,¹ Margareta Žlajpah¹ and Igor Krizaj*

¹ Department of Molecular and Biomedical Sciences, Jožef Stefan Institute, Jamova cesta 39, Ljubljana, Slovenia

² Jožef Stefan International Postgraduate School, Jamova cesta 39, Ljubljana, Slovenia

* Corresponding author: E-mail: igor.krizaj@ijs.si

Phone: +386 1 477 3626. Fax: +386 1 477 3984.

Received: 15-09-2016

For Cutting Edge 2017

Abstract

Integrins are plasma membrane proteins, whose dysfunction frequently results in cancer pathology, and therefore they represent important targets of anti-tumour therapy. Snake venoms are a rich source of disintegrins (Dis), proteins that specifically bind integrins and thus interfere with their functions. In an attempt to discover new molecules for treatment of breast cancer, the major type of cancer in women, we isolated a dimeric Dis (*Vaa*-Dis) from the venom of the nose-horned viper. By cell viability testing we demonstrated that 50 nM and higher concentrations of *Vaa*-Dis were toxic to highly invasive human breast adenocarcinoma cell line MDA-MB-231. Wound-healing assay revealed that already at one order of magnitude lower concentrations *Vaa*-Dis efficiently inhibited MDA-MB-231 cell migration. This exposed a promising anti-metastatic potential of *Vaa*-Dis and a good perspective of these natural snake venom proteins for further research and development towards the application in breast cancer treatment.

Keywords: snake venom, disintegrin, integrin, cancer, metastasis, drug

1. Introduction

Cancer, one of the deadliest diseases worldwide, is caused by inherited or acquired mutations of the genetic material. The main characteristics of cancer include sustaining proliferative signalling, evading growth suppressors, resisting cell death, enabling replicative immortality, inducing angiogenesis, and activating invasion and metastasis. Such properties enable cancer cells an unlimited growth and spreading, invasion through the organism and finally causing its death.¹ Prevention of metastatic growth is an efficient therapy in cancer control. The key roles in the process of migration and cell viability are played by transmembrane proteins called integrins.^{1,2}

Integrins are cell adhesion receptors on the cells' surface that bind components of the extracellular matrix (ECM), various biological ligands and receptors on adjacent cells. They are heterodimeric proteins consisting of

one α - and one β -subunit. 18 different α -subunits and 8 β -subunits are known, which have been found to appear in 24 different α - β combinations, each of them possessing unique binding specificity.² Recent studies have exposed integrins as important factors in tumour cell survival, tumour growth and metastasis by establishing and breaking bonds between malignant cells and molecules in their surroundings. For this reason, integrins have become important targets of anti-tumour therapy.² Despite the fact that several therapeutics, integrin antagonists, have already been developed, a search for more efficient integrin-binding substances continues.²⁻⁴

Snake venom (SV) proteins are broadly investigated as substances that can be used in diagnosis and treatment of human diseases. Among them, disintegrins (Dis) have been found to inhibit various cell functions by their interaction with different integrins, for example platelet aggregation, angiogenesis, tumour growth and metastasis.⁵

Dis are non-enzymatic cysteine-rich polypeptides. Their molecular mass ranges between 4 kDa and 15 kDa. They can be directly synthesized or formed by proteolysis of the P-II class metalloproteinases (MPs). SV Dis can be monomeric or dimeric, hetero- or homodimeric. In dimeric Dis, individual subunits are interconnected by disulfide bonds, which is crucial for stability and maintenance of a distinct globular structure. Dimerization also defines the configuration of the so called inhibitory loop, essential for the interaction with integrin receptor and, consequently, the biological activity.^{6,7}

In this work we focused on Dis from the venom of *Vipera ammodytes ammodytes* (Vaa-Dis). They were purified and biochemically characterized. We investigated their influence on cell viability and *in vitro* migration in a model of highly invasive triple-negative breast cancer and found that Vaa-Dis potentially inhibited the migration of cancer cells.

2. Material and Methods

2. 1. Purification of Vaa-Dis

Raw Vaa venom was obtained from the Institute of Immunology, Zagreb, Croatia. Lyophilized venom was stored at -20°C and before use dissolved in 50 mM Tris, 2 mM CaCl_2 , 300 mM NaCl, pH 7.0 (buffer A). 250 μL of the raw Vaa venom solution (16.67 mg) was applied on a Superdex 75 column 10/300 (GE Healthcare BioSciences AB, Sweden), equilibrated in buffer A and attached on a FPLC ÄKTA system (Amersham Biosciences, UK). Gel chromatography was performed at a constant flow rate of 0.5 ml/min. Concentration of proteins in the mobile phase was followed by measuring the absorbance at 280 nm (A_{280}). The B2 fraction was dialysed against 20 mM MES, 2 mM CaCl_2 , pH 6.5 (buffer B) and further fractionated on a SP Sepharose Fast Flow column (GE Healthcare BioSciences AB, Sweden). Bound material was eluted by addition of 500 mM NaCl in buffer B. The material not retained by the cation-exchanger was collected and separated by reverse phase-high performance liquid chromatography (RP-HPLC) on a PLRP-S column (4.6 mm \times 150 mm; 2.7 μm ; 120 \AA , Agilent Technologies, USA), equilibrated with 0.1% (v/v) trifluoroacetic acid (TFA) in water (solvent A), at a flow rate of 1 ml/min. The proteins were eluted from the column with a gradient of solvent B (90% (v/v) acetonitrile in 0.1% (v/v) TFA in water) as follows: 0–45% in 13 min and 45–55% in 10 min. A_{215} was monitored to locate proteins in fractions, which were collected manually. Samples were dried using a vacuum concentrator SpeedVac (Savant, USA).

2. 2. SDS-PAGE Analysis

Venom samples were analysed using 15% (m/v) polyacrylamide gels in the presence of SDS (SDS-PAGE) un-

der non-reducing and reducing conditions according to Laemmli.⁸ Proteins in gels were visualized by Page-BlueTM (Thermo Scientific, USA) as instructed by the manufacturer. Molecular mass standards were from Fermentas (Lithuania).

2. 3. N-terminal Amino Acid Sequence Analysis

Proteins were N-terminally sequenced by automated Edman degradation on a Procise 492A protein sequencing system (Applied Biosystems, USA).

2. 4. Culturing of MDA-MB-231 Cells

To carry out the migration assays the highly invasive breast cancer cell line MDA-MB-231 (ATCC, USA) was used. Cells were grown in RPMI-1640 medium (Invitrogen, USA) supplemented with 10% (v/v) fetal bovine serum (FBS) at 37°C in an atmosphere of 5% (v/v) CO_2 . Adherent cell monolayers were routinely cultured in T25 and T75 tissue culture flasks (Corning, USA) and passaged in ratios of 1 : 3 to 1 : 4.

2. 5. Cell Viability Testing

The *in vitro* cytotoxic potency of Vaa-Dis was evaluated using the PrestoBlueTM viability assay (Invitrogen, USA) essentially as described previously.⁹ Cells were trypsinized and counted by Trypan blue (Thermo Scientific, USA) exclusion assay¹⁰ using a hemocytometer (Fortuna, Germany). Cells were seeded in 96-well plates (TPP, Switzerland) at a density of 5000 cells/well in 100 μL RPMI-1640 medium and left to attach overnight. Cells were then treated with different concentrations of Vaa-Dis (0.005; 0.05; 0.5; 5; 50; 500 nM) for 0, 24, 48, and 72 h. After the treatment, 10 μL of PrestoBlueTM was added to each well, and the plates were incubated for 30 min at 37°C . Cell supernatants were transferred to black microtiter plates (Corning, USA) and fluorescence was measured at an excitation of 560 nm and emission of 590 nm on an Infinite M1000 microplate reader (Tecan, Switzerland) to determine metabolic activity of the cells. Wells containing only the cell culturing medium and PrestoBlueTM were used as blank reference standards. Experiments were performed in triplicate. The normalization of cell viability was calculated as the ratio of sample absorbance to control absorbance (cells in media without Vaa-Dis).

2. 6. Wound-healing Assay

The wound-healing assay (WHA) was used to estimate the potency of Vaa-Dis to inhibit cell migration (anti-migratory potency). MDA-MB-231 cells were trypsinized, counted as specified above and plated in 48-well cell culture dishes (TPP, Switzerland) at a density of 2×10^5

cells/well. Wounds (millimetre gaps) were then scratched in each cell monolayer using a pipette tip. Dead cells were removed by washing with D-PBS buffer and solutions of *Vaa*-Dis in RPMI-1640/10% FBS at different concentrations (2.5, 5.0, 7.5 and 15.0 nM) were added. Control samples contained only media. The influence of *Vaa*-Dis on cell migration was determined by observing the width of the gap under a CKX41 inverted microscope equipped with an E-450 camera (Olympus, Japan) after 1 h, 6 h, 12 h and 24 h of incubation. The gap was analysed using the ImageJ software (Softonic International S.A., Spain). The width of the gap was measured as specified (Suppl. Fig. 1) in three different wells for each concentration and incubation time.

2. 7. Statistical Analysis

Each experiment was performed in at least three independent repeats. If not stated otherwise, data are presented as a mean percent difference from control with cor-

responding standard error of the mean. Statistical tests were run by GraphPad Prism 6 (GraphPad Software Inc., La Jolla, CA, USA) using two-way ANOVA followed by Dunett's multiple comparisons test. Statistical significance is as follows: not significant for $p > 0.05$ (no mark in Fig. 2); significant for $p \leq 0.05$ (* in Fig. 2), $p \leq 0.001$ (** in Fig. 2) and $p \leq 0.0001$ (***) in Fig. 2).

3. Results and Discussion

Using gel-filtration chromatography we separated in the first step the raw venom of *Vaa* into seven fractions (A–F in Fig. 1a). The efficient inhibition of platelet aggregation induced by ADP or collagen by the gel filtration fraction B2 has been suggested to be due to the presence of Dis, which may obstruct this process by binding to $\alpha_{IIb}\beta_3$ fibrinogen receptor.¹¹ For this reason, we decided to analyse the fraction B2 further and split it on a strong cation exchanger into a fraction retained by the exchanger

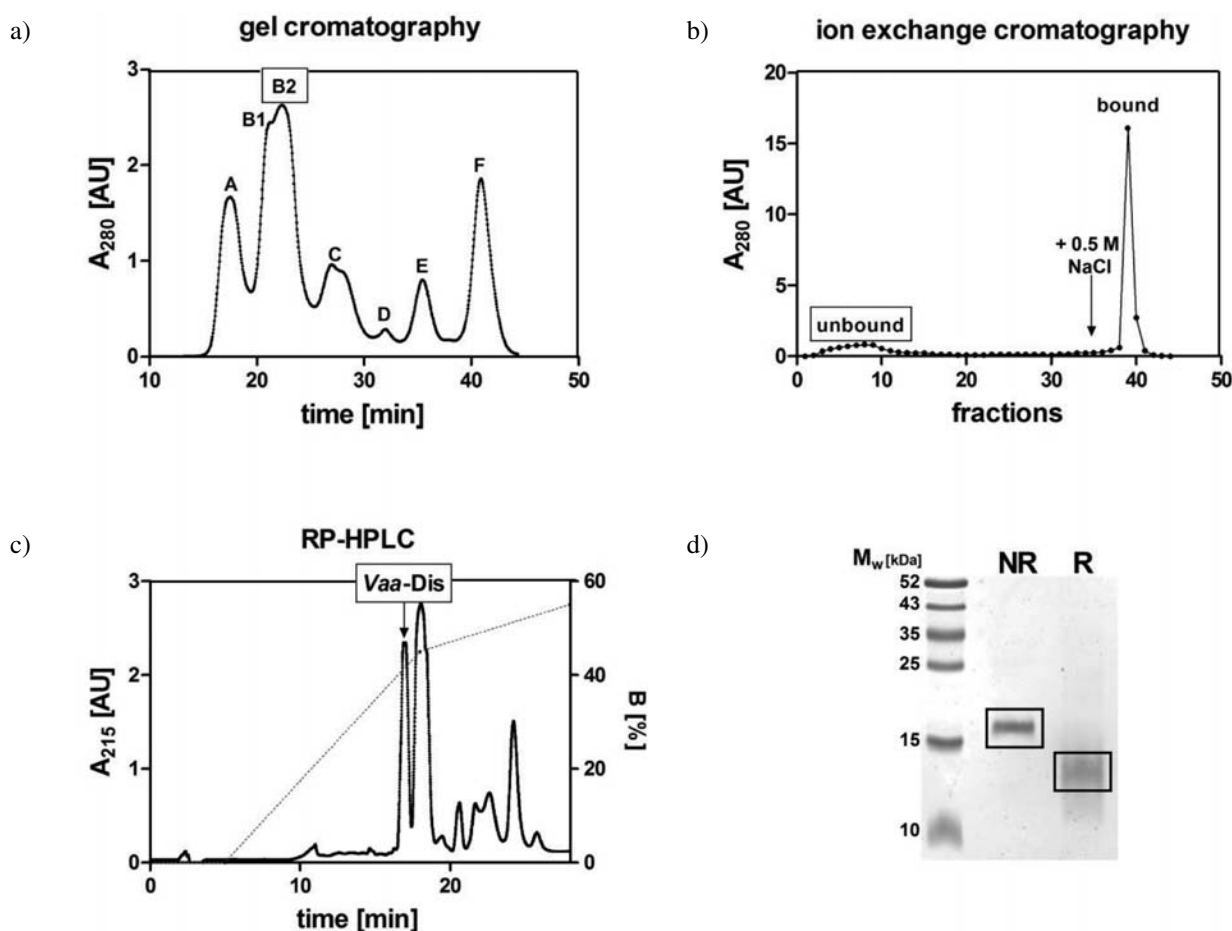


Figure 1: Purification of Dis from the *Vaa* venom. (a) Using gel filtration on Superdex 75, the raw venom of *Vaa* was split to seven fractions. Presence of Dis in fraction B2 was indicated by its strong inhibition of platelet aggregation.¹⁰ (b) Separation of the gel filtration fraction B2 on the SP Sepharose Fast Flow column to column-bound and unbound part. (c) RP-HPLC analysis of the proteins not retained by the SP Sepharose on the PLPR-S column. *Vaa*-Dis eluted from the column at 40% of solvent B (90% (v/v) acetonitrile in 0.1% (v/v) TFA in water). Dotted line designates the gradient, while full line the absorbance. (d). SDS-PAGE analysis of *Vaa*-Dis under non-reducing (NR) or reducing (R) conditions revealed the presence of only one protein band. The gel was stained by PageBlue™.

(bound) and a flow-through fraction (unbound) (Fig. 1b). The latter was chromatographed on an RP-HPLC column. *Vaa*-Dis was found in a sharp peak eluting at 40% of solvent B (Fig. 1c). SDS-PAGE analysis of this peak under non-reducing conditions revealed only one protein band of about 17 kDa. Under reducing conditions the protein displayed a lower apparent molecular mass of about 13 kDa (Fig. 1d). This was expected as the usual structure of *Viperidae* Dis is a cystine-crosslinked dimer,^{6,8} which dissociates to monomers in the presence of reducing agents. The homogeneity of *Vaa*-Dis sample was inspected by N-terminal amino acid sequencing using Edman degradation. Two N-terminal sequences, NSANP and NSGNP, were obtained, both characteristic for Dis.¹² Considering also the SDS-PAGE analysis, this means that the *Vaa*-Dis sample did not contain any non-Dis protein. The heterogeneous N-terminal sequence of the sample indicates that *Vaa*-Dis is either a heterodimer or a mixture of two homodimeric Dis proteins. Calvete et al. reported about VA6, a homodimeric Dis from the venom of *Vipera ammodytes* with the N-terminal sequence NSANP identical to one of the sequences that we have found in our sample.¹² This is a hint that our sample may consist of two homodimeric rather than one heterodimeric Dis. VA6 is an RGD motif-containing Dis.^{5,10} It has been demonstrated that such Dis efficiently bind to $\alpha_{IIb}\beta_3$ receptor on platelets and in this way inhibit platelet aggregation.¹² The observed inhibition of ADP- and collagen-induced platelet aggregation by the *Vaa* venom gel filtration fraction B2¹¹ thus also suggests the same interpretation of our results.

Some RGD-containing Dis have been demonstrated to inhibit $\alpha_v\beta_3$ (vitronectin receptor)-mediated migration of endothelial and cancer cells – two examples of such SV Dis are triflavin and DisBa-01.¹³ As one of our main research topics is discovering new substances to oppose breast cancer, the major cause of death in women population worldwide,¹⁴ the possibility that *Vaa*-Dis also affects the migration of cancer cells directed our subsequent experiments. To this end, resolving the question of whether *Vaa*-Dis is a heterodimeric Dis or a mixture of two homodimeric Dis was secondary so we did not go further to answer it. We study metastatic breast cancer on a model cell line, highly invasive human breast adenocarcinoma MDA-MB-231 cells. We found that *Vaa*-Dis is not cytotoxic to these cells at concentrations lower than 50 nM (Fig. 2a). At 50 nM and higher concentrations, *Vaa*-Dis induced a significant drop in cell viability, possibly by effecting proliferation and/or dying of the cells. Both processes are namely regulated *via* integrins,^{2,4} which are present in higher amounts in cancer cells than in the healthy cells.⁵ The level of expression of integrins $\alpha_v\beta_3$, $\alpha_v\beta_5$, $\alpha_5\beta_1$, $\alpha_6\beta_4$, $\alpha_4\beta_1$ and $\alpha_v\beta_6$ has been found in positive correlation with the ability of cells to migrate.¹³ In MDA-MB-231 cells the integrin $\alpha_v\beta_5$ and $\alpha_v\beta_3$ are particularly highly expressed.¹³ Drugs should not be toxic to healthy cells therefore the effect of *Vaa*-Dis on migration of cancer cell was evaluated

at sub-cytotoxic concentrations of *Vaa*-Dis. As evident from the WHA results presented in Suppl. Fig. 1 and Fig. 2b, *Vaa*-Dis significantly slowed down the *in vitro* migration of MDA-MB-231 cells already at the concentration of 2.5 nM, well below concentrations at which cytotoxic effects were detected (Fig. 2a) and in the same concentration range as rhodostomin, triflavin and trigramin, all SV Dis.¹⁵

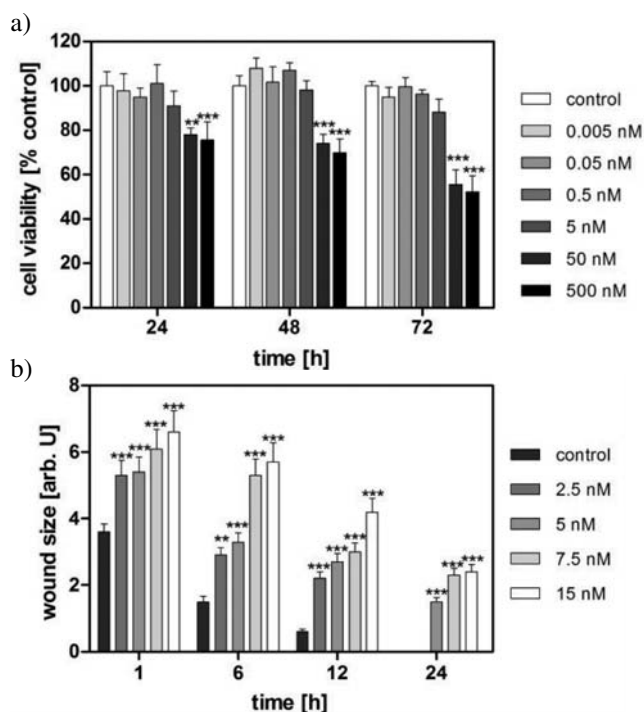


Figure 2: Effects of *Vaa*-Dis on breast cancer cells. (a) As established by PrestoBlue™ cell viability testing, the cytotoxicity of *Vaa*-Dis for MDA-MB-231 cells is evident at 50 nM and higher concentrations. Each result is an average of three independent experiments. (b) The wound-healing assay on MDA-MB-231 cells was performed in the presence of *Vaa*-Dis at concentrations, which did not affect cell viability. Each result is an average of three independent experiments. Units are arbitrary (arb. U). Statistical significance is displayed as follows: no mark for $p > 0.05$ (not significant), * for $p \leq 0.05$, ** for $p \leq 0.001$ and *** for $p \leq 0.0001$.

4. Conclusions

We have described the isolation and characterisation of novel Dis from the venom of *Vaa*. Due to a potent cancer cell anti-migratory activity, *Vaa*-Dis sample is promising for further research and development towards the use in breast cancer therapy.

5. Acknowledgements

This work was supported by the grant from the Slovenian Research Agency (P1-0207). We are grateful to Klemen Strojani (M.Sc., Faculty of Electrical Engineering,

University of Ljubljana) for the help with the statistical analysis of cell culture data and Petra Malavašič (M.Sc., Department of Molecular and Biomedical Sciences, Jožef Stefan Institute) for the help with cell culture experiments.

6. References

1. D. Hanahan, R. A. Weinberg, *Cell*. **2011**, *144*, 646–674. <https://doi.org/10.1016/j.cell.2011.02.013>
2. L. Seguin, J. S. Desgrosellier, S. M. Weis, D. A. Cheresh, *Trends Cell Biol.* **2015**, *25*, 234–40. <https://doi.org/10.1016/j.tcb.2014.12.006>
3. A. M. Alizadeh, S. Shiri, S. Farsinejad, *Tumour Biol.* **2014**, *35*, 8483–8523. <https://doi.org/10.1007/s13277-014-2421-z>
4. J. S. Desgrosellier, D. A. Cheresh, *Nat. Rev. Cancer* **2010**, *10*, 9–22. <https://doi.org/10.1038/nrc2748>
5. J. K. Arruda Macêdo, J. W. Fox, M. de Souza Castro, *Curr. Protein Pept. Sci.* **2015**, *16*, 532–548. <https://doi.org/10.2174/1389203716666150515125002>
6. J. J. Calvete, *Toxicon* **2013**, *62*, 40–49. <https://doi.org/10.1016/j.toxicon.2012.09.005>
7. J. J. Calvete, L. Sanz, P. Cid, P. de la Torre, M. Flores-Díaz, M. C. Dos Santos, A. Borges, A. Bremono, Y. Angulo, B. Lomonte, A. Alape-Girón, J. M. Gutiérrez, *J. Proteome Res.* **2010**, *9*, 528–544. <https://doi.org/10.1021/pr9008749>
8. U. K. Laemmli, *Nature* **1970**, *227*, 680–685. <https://doi.org/10.1038/227680a0>
9. A. Pucer, V. Brglez, C. Payré, J. Pungerčar, G. Lambeau, T. Petan, *Mol. Cancer*. **2013**, *12*, 111. <https://doi.org/10.1186/1476-4598-12-111>
10. W. Strober, *Curr. Protoc. Immunol.* **2001**, *Appendix 3*, Appendix 3B.
11. T. Sajevec, A. Leonardi, I. Križaj, *Toxin Rev.* **2014**, *33*, 33–36. <https://doi.org/10.3109/15569543.2013.835827>
12. J. J. Calvete, M. P. Moreno-Murciano, R. D. G. Theakston, D. G. Kisiel, C. Marcinkiewicz, *Biochem. J.* **2003**, *372*, 725–734. <https://doi.org/10.1042/bj20021739>
13. H. S. Selistre-de-Araujo, C. L. S. Pontes, C. F. Montenegro, A. C. B. M. Martin, *Toxins (Basel)*, **2010**, *2*, 2606–2621. <https://doi.org/10.3390/toxins2112606>
14. R. D. Baird, C. Caldas, *BMC Med.* **2013**, *11*, 151. <https://doi.org/10.1186/1741-7015-11-151>
15. R. S. Yang, H. S. Chiang, C. H. Tang, C. S. Yeh, T. F. Huang, *Toxicon* **2005**, *46*, 387–393. <https://doi.org/10.1016/j.toxicon.2005.05.002>

Povzetek

Integrini so proteini v plazemski membrani celic. Nepravilno delovanje teh proteinov lahko vodi v nastanek tumorjev, zato so pomembna tarča protitumorskih terapij. Disintegrini (Dis) so proteini iz kačjega strupa, ki se specifično vežejo na integrin in s tem ovirajo njihovo normalno delovanje. Z namenom odkrivanja novih molekul za terapijo raka dojke, najbolj razširjene vrste raka pri ženskah, smo iz strupa modrasa izolirali dimerni Dis (*Vaa*-Dis). Izmerili smo vpliv *Vaa*-Dis na viabilnost celic celične linije visoko invazivnega adenokarcinoma dojke MDA-MB-231 in ugotovili, da je bil *Vaa*-Dis v koncentracijah, višjih od 50 mM, za celice toksičen. Test celjenja celične rane, s katerim smo preverili vpliv *Vaa*-Dis na migracijo celic, pa je pokazal, da je *Vaa*-Dis učinkovito upočasnijo migracijo rakavih celic že pri koncentracijah, ki so bile za en velikostni red nižje. Dobljeni rezultati potrjujejo antimetastatski potencial *Vaa*-Dis in predstavljajo dober obet za nadaljnji razvoj teh molekul iz kačjega strupa v smeri priprave novih učinkovin za zdravljenje raka dojke.

Scientific paper

Modelling the Correlation Between Molecular Electrostatic Potential and pK_a on Sets of Carboxylic Acids, Phenols and Anilines

Miha Virant,^{1,*} Sara Drvarič Talian,^{2,*} Črtomir Podlipnik¹
and Barbara Hribar-Lee¹

¹ Faculty of Chemistry and Chemical Technology, University of Ljubljana, Večna pot 113, SI-1000 Ljubljana, Slovenia

² National Institute of Chemistry, Hajdrihova 19, SI-1000 Ljubljana, Slovenia

* Corresponding author: E-mail: miha.virant@fkkt.uni-lj.si; sara.drvarictalian@ki.si

Received: 04-10-2016

For Cutting Edge 2017

Abstract

Calculations of molecular electrostatic potential were correlated with experimental pK_a values for different sets of acidic molecules (carboxylic acids, phenols, and anilines) to obtain linear relationships of variable quality. A single tri-parameter model function was constructed to describe the pK_a dependence on MEP maxima together with two automatically generated molecular descriptors, namely the counts of carboxylic acid and amine functional groups.

Keywords: molecular electrostatic potential, pK_a, quantum mechanical calculations, multivariable linear regression

1. Introduction

Any distribution of the electrical charge in a molecule creates an electrostatic potential $V(\mathbf{r})$ at each point of the surrounding space \mathbf{r} :¹

$$V(\mathbf{r}) = \sum_A \frac{z_A}{|\mathbf{R}_A - \mathbf{r}|} - \int \frac{\rho(\mathbf{r}') d\mathbf{r}'}{|\mathbf{r}' - \mathbf{r}|} \quad (1)$$

where z_A is the charge of the nucleus A located at \mathbf{R}_A , and $\rho(\mathbf{r})$ is the electronic density function of the molecule, that can be determined either computationally, or experimentally by diffraction methods.² This so-called molecular electrostatic potential (MEP) is a well-established tool for interpreting and predicting molecular reactivity.^{2–5}

One of the physico-chemical properties that have recently been shown to be correlated with the MEP is pK_a value which describes the acid strength of certain organic acids.^{6–7} The background of the correlation is due to the fact that MEP is a quantum-mechanical descriptor influenced by electronic or stereoelectronic properties of the groups in close vicinity to a particular acidic atom. Similarly, NAO (the sum of valence p natural atomic orbitals) has also been used for such calculations and it has been

proven that this descriptor is equivalent to MEP.⁸ Other examples of descriptors in QSAR models that have already been successfully used for determining pK_a values are topological⁹, atom type descriptors¹⁰, and group philicity¹¹.

The correlation was established by comparing the calculated MEP values via different theoretical methods with the experimentally determined pK_a values for the same sets of compounds. The success of the method consequently depends on the training set used in the program learning process, and the similarity of the studied compounds.⁷

A relatively good correlation between the maximum in MEP and the pK_a value was found for amines, anilines, carboxylic acids, alcohols, sulfonic acids, and tioles.¹² Furthermore, a good correlation was established recently between pK_a and the most positive value of the MEP of benzoic acids and phenols, and between the most negative value of MEP and the local ionization energies of these compounds.¹³ Nevertheless, all the published work has studied only one set of similar compounds and to the best of our knowledge, a model that could be applied to the wider array of differently functionalized molecules has not yet been presented.

Since the knowledge of the pK_a values is vital for predicting the reactivity of the compounds in question and is therefore of broad interest in drug design, toxicology studies, chemical synthesis etc., it is desirable to extend the current knowledge to other compounds.

This paper describes the correlation between pK_a values and MEP for certain tested carboxylic acids, phenols, and anilines and additional physico-chemical descriptors, which are introduced in a regression model to improve the correlation.

2. Methods

Calculations of molecular electrostatic potential maxima (V_{max}) were executed using Spartan '14 (v. 1.1.4) software. Energy minimizations of equilibrium geometries were performed on sets of 39 aliphatic carboxylic acids, 17 monosubstituted benzoic acids, 19 mono-substituted anilines, and 19 phenols (Given in Supporting Information, Table S1).

The starting molecular conformations were formed using the Merck molecular force field (MMFF) optimization.¹⁴ Further, semi-empirical methods AM1, and PM6, ab initio Hartree-Fock method HF 6-31G*, and a density functional theory method B3LYP 6-31G* were used to calculate the MEP.¹⁵

Several isoelectronic densities (0.2, 0.02, 0.002, and 0.0002) were examined for a linear correlation between the maximum in MEP, V_{max} , and pK_a values obtained from the literature.^{16,17} The best correlation was obtained for the isoelectronic value of 0.02, which was used in the further calculations.

To improve the correlation between pK_a and calculated descriptors from MEP, CANVAS's ligfilter descriptors were included into the calculation of multiple linear regression analysis with CANVAS software from Schrödinger 2015 Suite. These descriptors denote the presence/absence of certain functional groups, which are important for the stability of the molecules studied. The model was constructed using V_{max} and two best suited ligfilter descriptors, which count the number of certain functional groups.

For the validation of the model, a group of 87 compounds was divided into two sets. The first set of compounds (named training set) was composed of 70% randomly selected compounds, which were used for building a model. The second one (testing set) contained the remaining 30% of compounds used for the validation of the prediction capacity of the model.

The best subset of descriptors for the construction of the model was selected with CANVAS's simulated annealing¹⁹ algorithm with performing maximum of 1000 MC steps, initial and final temperature which corresponds to standard deviation of y being 0.5 and 0.05 respectively.

3. Results and Discussion

The results for the correlation between V_{max} in MEP for the isoelectronic density 0.02 and pK_a for phenols (a), anilines (b), aliphatic (c), and benzoic acids (d) are given below. Multivariable analysis of the compounds studied is presented in subsection (e).

a) The correlation between V_{max} and pK_a for the chosen set of monosubstituted phenols is shown in Figure 1. The results obtained with different methods are shown with different symbols/colours.

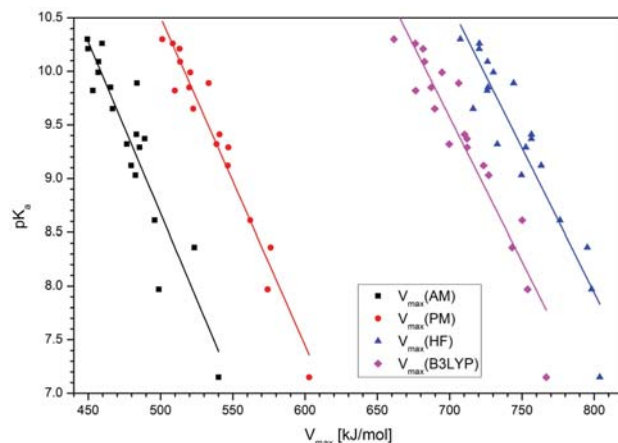


Figure 1. The correlation between the V_{max} calculated using different methods at IsoValue 0.02, and pK_a values^{16,17} of phenols.

Regardless of the used method for calculating the MEP, the correlation coefficient, R^2 , is around 0.8. If we disregard the values for nitrophenols calculated via PM6 method, the slopes of the fitted curves are approximately the same, indicating that the results are not dependent on the method of calculation.

b) The results for the anilines are shown in Figure 2. For the determination of the correlation for the set of anilines, we modelled the V_{max} on protonated molecules (ani-

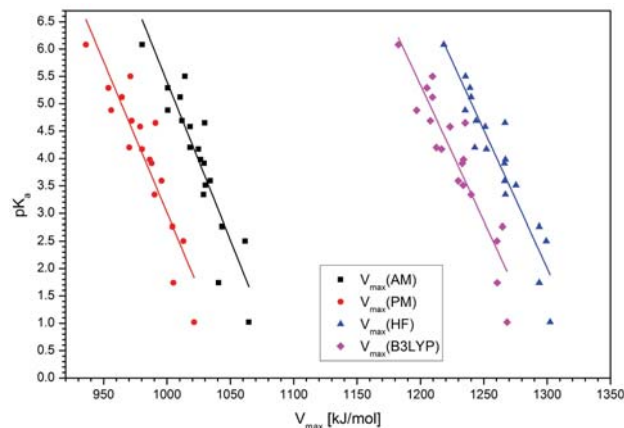


Figure 2. The correlation between the V_{max} calculated using different methods at IsoValue 0.02, and pK_a values^{16,17} of anilines.

linium cations). As with the set of phenols, the value of R^2 being higher than 0.8 shows good correlation between calculated and experimental properties.

c) In the case of aliphatic acids, a poor correlation between V_{\max} and pK_a was obtained (Figure 3). The correlation coefficient R^2 ranged from 0.395 to 0.588, depending on the method of calculation, the semi-empirical PM6 method having the lowest score. Poor correlations could be the consequence of structural diversity of the test set, and its larger pK_a range span.¹⁵ However, to indisputably prove this speculation, further calculations on a larger set of systematically substituted aliphatic acids would be required.

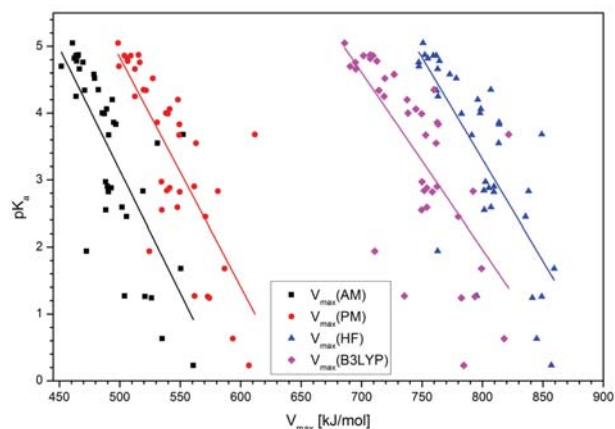


Figure 3. The correlation between the V_{\max} calculated using different methods at IsoValue 0.02, and pK_a values^{16,17} of aliphatic acids.

d) The results for the correlation between V_{\max} and pK_a for the benzoic acids studied is shown in Figure 4. As seen, the values of V_{\max} and pK_a for the set of mono-substituted benzoic acids are poorly correlated. We speculate that the solvent effect, which was not specifically accounted for in the calculations, could be the reason. An evident deviation from linearity can be observed in values for *p*-methoxybenzoic, which could be due to the stronger reso-

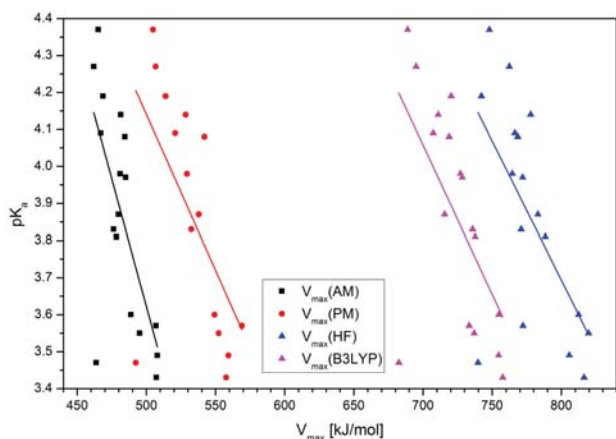


Figure 4. The correlation between the V_{\max} calculated using different methods at IsoValue 0.02, and pK_a values^{16,17} of benzoic acids.

nance effect from substituent in *para* position influencing the MEP in a non-linear fashion corresponding to pK_a . The relatively large scatter in the studied pK_a range, therefore, suggests a non-linear response of the V_{\max} to the electronic effects of some substituents.

As evident from the Figure 5, the obtained linear correlations for the applied molecules can be classified into three groups. By incorporating additional parameters, it should be possible to construct a single model to predict pK_a values for all four molecule sets.

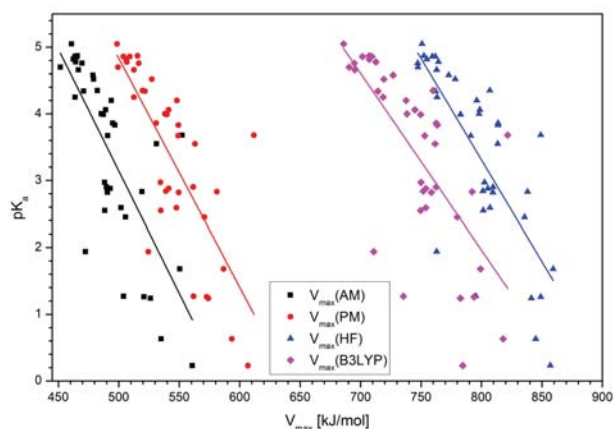


Figure 5. Experimental pK_a values^{16,17} as a function of V_{\max} (AM1) for all molecule sets.

e) To improve the obtained correlations we made an attempt to include some software-generated descriptors into the multivariable analysis. Using CANVAS, we determined ligfilter descriptors to be the parameters of choice. The inclusion of a number of carboxylic acids or carboxylates (N_{COO}) and a number of quaternary ammonium groups ($N_{\text{NH4+}}$) together with calculated V_{\max} provides the possibility of unifying the correlation between chemical descriptors and pK_a for different types of molecules (Figure 6).

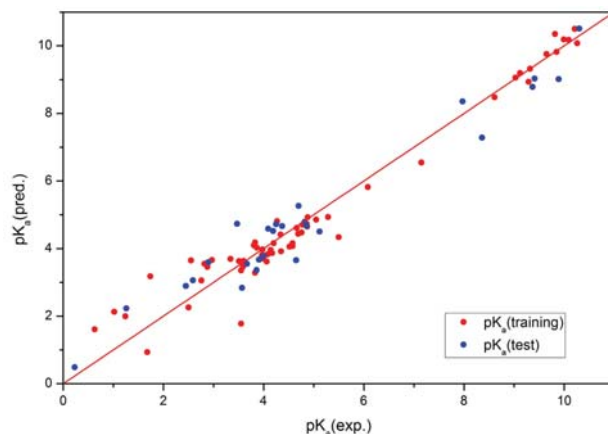


Figure 6. Predicted versus experimental pK_a values^{16,17} for training and testing sets of molecules.

Some deviations are present in the case of dicarboxylic aliphatic acids. As a result, they were excluded from the set for model construction. Using a more complicated calculation method does not notably improve the correlation. R^2 has the same value (0.96) for the models with V_{\max} from AM1, HF or B3LYP methods. A slight distinction between models can be seen from the quality of prediction for a test set of molecules. The Q^2 parameter for the models with V_{\max} from AM1, HF or B3LYP methods has the values 0.95, 0.92 and 0.92, respectively. Calculated parameters and the equation of the model for the simplest computational method are given in Table 1. The data for models obtained via B3LYP, and HF method is presented in Table S2 (see Supporting Information) for comparison. The implemented descriptors were used as a correction factor to enable the construction of a single model for different sets of compounds.

Table 1. Coefficients of the model for pK_a prediction with V_{\max} (AM1) and its statistical parameters.

Model	Coefficient	Standard deviation
N_0	30.2	± 1.5
V_{\max} (AM1)	-0.0438	± 0.0032
N_{COO}	-5.16	± 0.18
$N_{\text{NH}_4^+}$	6.18	± 0.59

$$pK_{a(\text{pred.})} = -0.0438 V_{\max} - 5.16 N_{\text{COO}} + 6.18 N_{\text{NH}_4^+} + 30.2$$

Set of compounds	Validation parameter
training	$R^2 = 0.96$
testing	$Q^2 = 0.95$

4. Conclusions

Good correlations were obtained between the maxima of molecular electrostatic potential and pK_a values for anilines and phenols. With the inclusion of certain physico-chemical descriptors, it was possible to unify the correlation between chemical descriptors and pK_a for different types of molecules with a single model function. The correlation is satisfying even with the simplest quantum mechanical calculation methods (semi-empirical method AM1).

Povzetek

V članku smo predstavili linearno zvezo med izračunanimi vrednostmi molekulskega elektrostatskega potenciala (MEP) in eksperimentalnimi pK_a vrednostmi. Obravnavali smo sete različnih molekul (karboksilne kisline, fenole in aniline), za katere smo dobili dobre linearne korelacije z maksimumi MEP. Z uvedbo avtomatično generiranih molekularskih deskriptorjev, natančneje števila karboksilnih skupin in števila amino skupin, smo uspeli sestaviti enoten triparametrski model za izračun pK_a , ki je zajemal vse obravnavane molekule.

5. References

- J. S. Murray, K. Sen (Eds.): Molecular electrostatic potentials: concepts and applications, Elsevier, Amsterdam, Netherlands, **1996**.
- P. Politzer, D. G. Truhlar (Eds.): Chemical application of atomic and molecular electrostatic potentials, Plenum, New York, **1981**.
- E. Scrocco, J. Tomasi, *Adv. Quantum Chem.* **1978**, *11*, 115–193. [https://doi.org/10.1016/S0065-3276\(08\)60236-1](https://doi.org/10.1016/S0065-3276(08)60236-1)
- P. Sjöberg, P. Politzer, *J. Phys. Chem.* **1990**, *94*, 3959–3961. <https://doi.org/10.1021/j100373a017>
- P. Politzer, P. R. Laurence, K. Jayasuriya, *Environ. Health Persp.* **1985**, *61*, 191–202. <https://doi.org/10.1289/ehp.8561191>
- U. A. Chaudry, P. L. A. Popelier, *J. Org. Chem.* **2004**, *69*, 233–241. <https://doi.org/10.1021/jo0347415>
- J. Cerar, Č. Podlipnik, *Acta Chim. Slov.* **2008**, *55*, 999–1008. <https://doi.org/10.1063/1.3251124>
- Liu, S.; Schauer, C. K.; Pedersen, L.G. *J. Chem. Phys.* **2009**, *131*, 164107.
- Milletti, F.; Storchi, L.; Sforza, G.; Cruciani, G. *J. Chem. Inf. Model.* **2007**, *47*, 2172–2181. <https://doi.org/10.1021/ci700018y>
- Xing, Li.; Glen, R. C. *J. Chem. Inf. Comput. Sci.* **2002**, *42*, 796–805. <https://doi.org/10.1021/ci010315d>
- Parthasarathi, R.; Padmanabhan, J.; Elango, M.; Chitra, K.; Subramanian, V.; Chattaraj, P. K. *J. Phys. Chem. A* **2006**, *110*, 6540–6544. <https://doi.org/10.1021/jp055849m>
- S. Liu, L. G. Pedersen, *J. Phys. Chem. A* **2009**, *113*, 3648–3655. <https://doi.org/10.1021/jp811250r>
- Y. Ma, K. C. Gross, C. A. Hollingsworth–239.
- T. A. Halgren, *J. Comp. Chem.* **1996**, *17*, 490–519. [https://doi.org/10.1002/\(SICI\)1096-987X\(199604\)17:5/6<490::AID-JCC1>3.0.CO;2-P](https://doi.org/10.1002/(SICI)1096-987X(199604)17:5/6<490::AID-JCC1>3.0.CO;2-P)
- A. R. Leach: Molecular Modelling, principles and applications; Pearson Education Limited, Essex, United Kingdom, **2001**.
- A. Albert, E. P. Serjeant: Ionization constants of acids and bases, Methuen, London, United Kingdom, **1962**.
- D. D. Perrin, (Ed.): Dissociation constants of organic bases in aqueous solution, Butterworths, London, United Kingdom, **1965**.
- W. H. Press, S. A. Teukolsky, W. T. Vetterling, B. P. Flannery: Numerical recipes in C, Cambridge University Press, Cambridge, United Kingdom, **1992**, pp 680–706.
- P. J. M. van Laarhoven, E. H. L. Aarts (Eds.): Simulated annealing: theory and application, Springer Science and Business Media. Dordrecht, Netherlands. **1987**.

Scientific paper

Use of Differential Scanning Calorimetry and Immunoaffinity Chromatography to Identify Disease Induced Changes in Human Blood Plasma Proteome

Sandi Brudar,¹ Urh Černigoj,² Helena Podgornik,³ Mojca Kržan⁴
and Iztok Prislan^{5,*}

¹ University of Ljubljana, Faculty of Chemistry and Chemical Technology, 1000 Ljubljana, Slovenia

² BIA Separations, 5270 Ajdovščina, Slovenia

³ University Medical Centre Ljubljana, Department of Haematology, 1000 Ljubljana, Slovenia

⁴ University of Ljubljana, Faculty of Medicine, 1000 Ljubljana, Slovenia

⁵ University of Ljubljana, Biotechnical Faculty, 1000 Ljubljana, Slovenia

* Corresponding author: E-mail: iztok.prislan@bf.uni-lj.si

Received: 05-10-2016

For Cutting Edge 2017

Abstract

Differential scanning calorimetry provides unique signatures of blood plasma samples. Plasma samples from diseased individuals yield specific thermograms, which differ from each other and from plasma samples of healthy individuals. Thermograms from individuals suffering from chronic lymphocytic leukemia, multiple myeloma and acute myeloid leukemia were measured with DSC. To obtain additional information about thermal behaviour of plasma proteins immunoaffinity chromatography was introduced. An immunoextraction of HSA using a chromatographic column with immobilized anti-HSA was carried out in order to enrich less abundant plasma proteins, which could provide a further insight into disease development. Efficiency of HSA depletion and protein composition of fractionated plasma was validated by SDS-PAGE.

Keywords: DSC, IAC, blood plasma, immunoextraction, diagnostic tool

1. Introduction

Despite of rapid development of medicine and other sciences, timely and reliable diagnosis of diseases is sometimes still a pretentious task. In addition when it comes to ascertaining the health status of an individual some diagnostic procedures are very invasive. A solution to such difficulties could lie in new methods for human plasma analysis. Human plasma serves as an important source of information about human health. Various diseases are often associated with biomarkers, which have been defined by Hulka et al. as biochemical, molecular or cellular changes that are measureable in human fluids, tissues and cells.¹ The human plasma proteome consists of more than

3000 proteins and peptides, therefore the search for potential disease biomarkers, and their identification in the plasma proteome is a very complicated procedure.² Only ten proteins make up 90% of the mass of plasma proteins and albumin (HSA) and immunoglobulins (Ig) represent 75% out of these ten proteins. Majority of biomarkers in blood plasma are often scarce and small in size. Consequently, their detection can be limited by the presence of more abundant and larger proteins such as HSA or IgG². Because of the complexity of plasma no single technique can fully exploit the information plasma has to offer. Until now mass spectrometry and 2D-electrophoresis have been routinely used for detection and characterization of specific biomarkers.³ Chaires et al. have discovered the poten-

tial use of differential scanning calorimetry (DSC) for plasma analysis.² Using a DSC to analyze plasma yields a thermogram that is sensitive to differences in thermodynamic properties of the most abundant plasma proteins. Chaires et al. have shown that thermograms of plasma from diseased individuals differ significantly from thermograms of plasma from healthy individuals.^{2,4} Another tool to facilitate the search for biomarkers is liquid chromatography, in particular affinity chromatography and ion-exchange chromatography. Several researchers have demonstrated that depletion of most abundant plasma proteins amplifies the contribution of least abundant plasma proteins, thus creating the opportunity to uncover and study specific proteins/peptides.^{5,6} Polymethacrylate chromatographic monoliths afford flow rate independent binding capacity and resolution for large biomolecules due to the convective nature of the flow, which allows relatively short analysis times compared to traditional chromatographic supports.⁷ Having these advantages in mind we decided to partially deplete human serum albumin from plasma sample using chromatographic monoliths bearing immunoaffinity ligand. The purpose of our research was to develop and optimize procedures for combined use of DSC and immunoaffinity chromatography (IAC) for the investigation of different plasma samples from diseased individuals.

2. Experimental

2.1. Plasma Samples

We investigated plasma samples from three individuals with three different haematological diseases, namely chronic lymphocytic leukemia (CLL), multiple myeloma (MM) and acute myeloid leukemia (AML). Individuals diagnosed with MM and AML were females and the one with CLL was a male. Due to ethical issues further information about these individuals cannot be revealed. Chaires et al.⁸ have shown that the main shape of plasma thermograms is unbiased by age, gender and ethnicity, however small deviations in HSA unfolding signal amplitudes can be observed due to higher HSA concentrations in male plasma samples. For the control sample blood plasma from a healthy child was used. At the University Medical Centre Ljubljana (UMCL) the peripheral blood samples were withdrawn in tubes with EDTA and centrifuged at 2500 RPM for 10 minutes to obtain plasma. The use of plasma was approved by National Medical Ethics Committee (Approval number: MZ 0120-299/2016-2, KME 83/05/16)

Because only 3 plasma samples were investigated we have to emphasize that this is only a preliminary study in which our main aim was to identify the effectiveness of our approach and not to generalize differences for the three investigated diseases. It should be clear that for validation of our method more plasma samples should be

analyzed. Even though only one set of measurements was performed for CLL and AML samples, the robustness and reproducibility of our method was tested with other plasma samples (data not shown) and two separate fractionations of MM sample (Figure S1).

2.2. Sample Preparation

The buffer solutions used in our experiments consisted of 20 mM disodium phosphate and 300 mM NaCl. HCl was added to disodium phosphate to reach pH of 7.4. All buffers were filtered before use. Samples were first diluted 5- to 7-fold and then extensively dialyzed against the buffer at 4 °C (three changes of buffer solution in 24 h) using a dialysis tube Float-A-Lyzer with a 3500 Da cut-off. Total protein concentration of plasma samples was determined spectrophotometrically according to the bicinchoninic acid method procedure (Sigma-Aldrich).⁹

2.3. IAC Protocol

Separations were performed using a Knauer high-performance liquid chromatography (HPLC) workstation, consisting of two pumps, an autosampler injection system with a sample loop volume of 100 µL and a UV-detector at a wavelength of 280 nm. Samples were loaded by using a mobile phase consisting of 20 mM disodium phosphate and 300 mM NaCl, pH = 7.4 at a flow rate of 1 mL/min. For experimental data acquisition, Eurochrom 2000 software was used. The hydrazide-modified monolithic chromatographic column (CIM[®] HIDA) with 1 mL bed volume and 6 µm pore size was provided by BIA Separations d.o.o. The immobilization of polyclonal anti-HSA was performed according to the procedure described by Tarasova et al.¹⁰ and the determined dynamic binding capacity at 50% breakthrough of prepared CIM αHSA column for pure HSA in phosphate buffered saline was 0.35 mg/mL. Before injection, diluted and dialyzed plasma samples were filtered through 0.45 µm membrane filters (Sartorius) and diluted with dialysate to a total protein concentration of approximately 4 to 5 mg/mL. 100 µL loop was used to load the sample and flow-through and bound fractions of plasma were collected. Succeeding collection of flow-through fraction the bound fraction was eluted using 0.1 M HCOOH, pH = 2.5, followed by immediate neutralization by 200 mM disodium phosphate, 300 mM NaCl, pH = 8.5. Both fractions were transferred to Vivaspin sample concentrators with MWCO of 3500 Da and centrifuged to final volume of 1 to 1.5 mL at 5000 RPM. This was repeated 18 times.

2.4. DSC Protocol

DSC thermograms were obtained using nano DSC II (CSC). Dialyzed plasma samples were diluted 3- to 4-fold with dialysate and degassed for 15 min. DSC scans were

recorded from 20 °C to 100 °C at 2 °C/min. Corresponding buffer scans were also recorded. Raw data was analyzed with NanoAnalyze software and Microsoft Excel. The corresponding baseline (buffer–buffer) scans were subtracted from the plasma scans and normalized to total protein concentration to obtain partial heat capacity as a function of temperature.

2. 5. SDS-PAGE

Fractions were examined using sodium dodecyl sulfate polyacrylamide gel electrophoresis (SDS-PAGE). Plasma fractions from IAC were diluted to a final concentration between 0.5 and 1.0 mg/mL. Separation of proteins was performed on 12% resolving gel and 4% stacking gel. Electrophoresis was carried out under reducing conditions according to the basic Laemmli SDS-PAGE procedure.¹¹ Gels were run at 200 V and 15 °C for 75 min. Visualization of protein bands was done by silver staining.¹² Gel images were altered to achieve more efficient interpretation of result (color was changed to black&white and positions of lanes on the same gel were shuffled). Unaltered images can be seen in Figure S2.

3. Results and Discussion

3. 1. Comparison of Blood Plasma Thermograms

Figure 1 shows that plasma thermograms belonging to diseased individuals differ significantly from one another and from “healthy” plasma thermograms. The thermo-

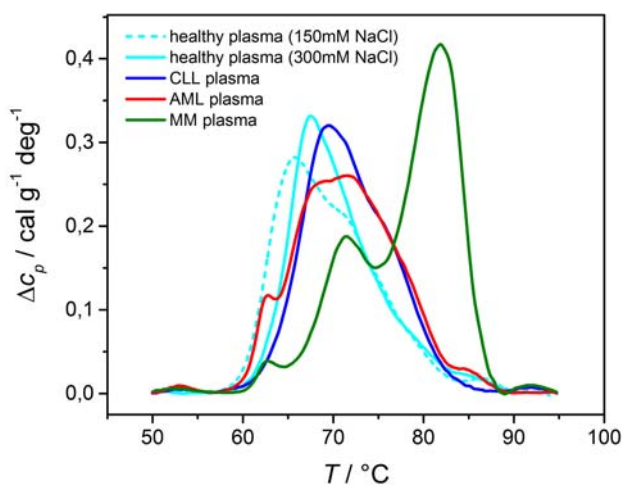


Figure 1. Comparison of thermograms of blood plasma from diseased individuals dissolved in 20 mM phosphate buffer and 300 mM NaCl and with a thermogram of blood plasma from healthy individual dissolved in 10 mM phosphate buffer and 150 mM NaCl (dashed cyan line) and 20 mM phosphate buffer and 300 mM NaCl (full cyan line).

grams of plasma display multiple peaks that can be associated to the melting temperatures (T_m) characteristic of main plasma proteins.

Chaires et al. have performed thermal denaturation of “healthy” blood plasma at heating rate of 1 °C/min and in 10 mM phosphate buffer with 150 mM NaCl to mimic physiological conditions. Several peaks were identified corresponding to transition temperatures of fibrinogen ($T_m \sim 51$ °C), HSA ($T_m \sim 63$ °C), IgG ($T_m \sim 70$ °C) and transferrin ($T_m \sim 85$ °C).² Thermograms in our research were recorded at heating rate of 2 °C/min to increase the number of processed samples and 20 mM phosphate buffer with 300 mM NaCl was used to avoid non-specific plasma-column interactions. Higher heating rate and salt concentration shifted the melting temperatures of majority of plasma proteins to higher values (Figure 1). Thus T_m of fibrinogen shifts to ~ 53 °C, T_m of HSA to ~ 67 °C, T_m of IgG to ~ 72 °C and T_m of transferrin to ~ 86 °C. Melting temperatures are not the only obtainable data from thermograms. The integration of area under the thermograms of plasma yields the enthalpy of plasma proteins denaturation (Table 1).

Table 1. Denaturation enthalpies of plasma from healthy individual and from blood plasma of diseased individuals. NF–non-fractionated plasma; F1–flow-through plasma fraction. Experimental error due to baseline correction is $\pm 5\%$.¹³

Sample	Unfolding enthalpy [cal/g]
Healthy plasma	3.64 ± 0.18
CLL plasma NF	3.80 ± 0.19
CLL plasma F1	2.94 ± 0.15
AML plasma NF	3.96 ± 0.20
AML plasma F1	2.89 ± 0.14
MM plasma NF	4.57 ± 0.23
MM plasma F1	4.27 ± 0.21

Figure 1 shows that thermograms obtained from thermal denaturation of blood plasma from diseased individuals are shifted to higher temperatures. The shift in unfolding temperatures is in agreement with previously reported results for other diseases.^{2,14,15,16} Proteins in plasma from diseased individuals seem to unfold at higher temperatures for a yet undefined reason. Chaires et al. had hypothesized that such stabilization of proteins occurs due to interactions between major plasma proteins and specific disease biomarkers.² Thermal denaturation of plasma from an individual with CLL yields a thermogram, where at least four transitions could be identified. These could correspond to denaturation of fibrinogen ($T_m \sim 53$ °C), HSA ($T_m \sim 68$ °C), IgG ($T_m \sim 72$ °C) and transferrin ($T_m \sim 91$ °C). The transitions are shifted from 0 to 5 °C towards higher temperatures when compared to thermogram of “healthy” plasma. For instance, T_m of fibrinogen does not change, but T_m of transferrin is shifted for approximately

5 °C. The denaturation enthalpy of non-fractionated CLL plasma is 3.80 ± 0.19 cal/g. This value is approximately the same as the denaturation enthalpy of plasma proteins from healthy individuals. Figure 1 shows that DSC thermograms of CLL and AML plasma are distinct even though both diseases are characterized by prominent changes in blood leukocytes not in plasma protein composition. In the thermogram of plasma from an individual with AML an additional endothermic peak can be observed at 62 °C. We hypothesize this peak is present due to thermal denaturation of haptoglobin, as it is supposed to unfold in the same temperature region as HSA.² T_m values of fibrinogen and transferrin from AML plasma denaturation seem to be at approximately the same position as T_m values from “healthy” plasma denaturation. The denaturation enthalpy of non-fractionated blood plasma from an individual with AML is 3.96 ± 0.20 cal/g, which is comparable to denaturation enthalpy of CLL and “healthy” plasma. Lastly Figure 1 shows a specific thermogram of plasma from an individual with MM. Three main transition peaks for most abundant plasma proteins can be characterized. A similar thermogram for this disease was obtained by Todinova et al.¹⁷ Thermally induced peaks are shifted to higher temperatures to an even greater extent than those characteristic for proteins from CLL and AML plasma samples. Also in contrast to AML and CLL samples protein concentration in MM plasma was increased above reference range (94 g/L) due to monoclonal IgG fraction (M spike) typical for MM. Thermogram exhibits three distinct peaks ($T_{m1} \sim 62$ °C, $T_{m2} \sim 71$ °C and $T_{m3} \sim 82$ °C) and is dramatically different from other thermograms. The determined enthalpy of denaturation for non-fractionated MM plasma was 4.57 ± 0.23 cal/g, which is approximately 20% higher from denaturation enthalpies of other samples. These results suggest that the amount of unfolding enthalpy is not a determining factor for disease conditions. We believe that only the shape of plasma thermograms can serve as a diagnostic tool for disease determination.

3. 2. Fractionation and Characterization of Proteins in Blood Plasma

To gain further insight into thermal behavior of different blood plasma samples, fractionation of plasma samples and thermal denaturation of obtained fractions were carried out. The thermogram of the flow-through fraction of plasma from an individual with CLL in Figure 2 shows a distinct drop in signal intensity in the region characteristic of HSA, as a result of HSA depletion by a CIM α HSA column. As a result, transition peaks for other proteins are more pronounced. Along with enrichment of less abundant proteins we can observe an entirely new peak at approximately 65 °C, which seems to have been previously masked by HSA. We hypothesize that this peak is a result of haptoglobin denaturation.

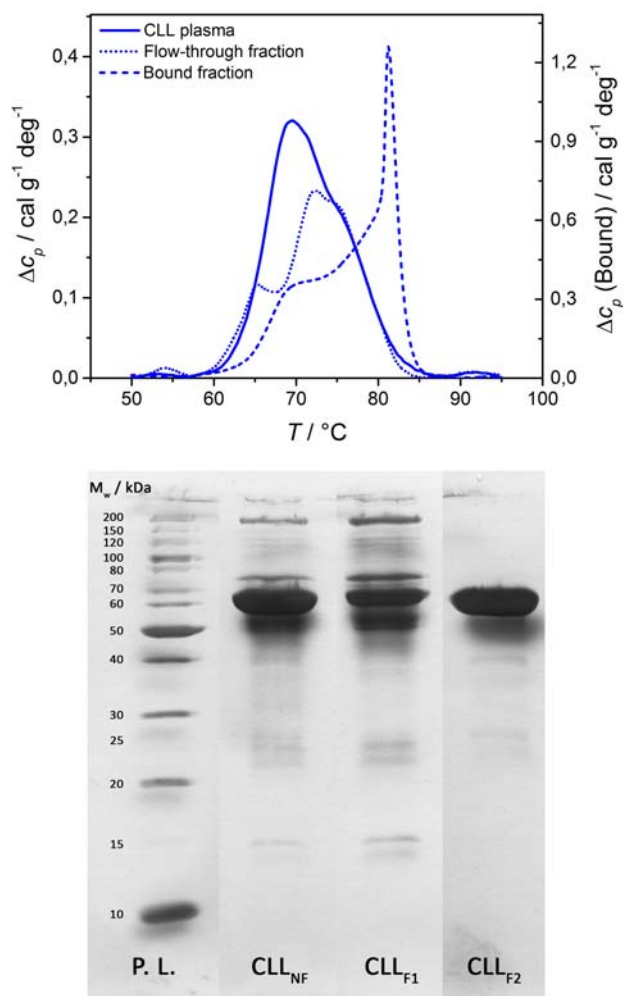


Figure 2. Thermograms of blood plasma from an individual with CLL (top). DSC thermogram of a non-fractionated blood plasma sample (full line) is compared to thermograms of flow-through (dotted line) and bound fraction (dashed line) obtained from HPLC fractionation. The right ΔC_p axis corresponds to the bound fraction. SDS-PAGE of blood plasma from an individual with CLL (bottom); P. L. – protein library, CLL_{NF} – non-fractionated blood plasma (1 mg/mL), CLL_{F1} – flow-through fraction (1 mg/mL), CLL_{F2} – bound fraction (0.8 mg/mL).

The obtained unfolding enthalpy of the flow-through fraction of CLL plasma was 2.94 ± 0.15 cal/g (Table 1), which is 22% lower than that of non-fractionated plasma. The thermogram of the bound fraction in Figure 2 shows a major exothermic effect above 82 °C due to protein aggregation. We hypothesize that this phenomenon is due to elution of HSA with HCOOH, even though this fraction was intercepted by high capacity buffer to neutralize acid. Very acidic conditions are non-physiological for HSA and can change its structure in a way that favors aggregation. Similar behavior of bound fractions was observed in all plasma samples and reported by other researchers^{18,19} and will not be discussed any further. Together with the thermogram of the flow-

through fraction, results of SDS-PAGE (Figure 2) show that only partial HSA depletion was achieved even though the applied concentration was below theoretical binding capacity. This was most likely due to complexity of plasma samples and overuse of our CIM α HSA column. Even though HSA is still present in the flow-through fraction, the corresponding thermogram seems to be missing peak assigned to HSA denaturation. We have to assume that HSA unfolding is masked by the unfolding of other plasma proteins. CLL_{F2} lane (bound fraction) displays an intensive band at 66 kDa, characteristic of HSA, no slower migrating bands and some low intensity bands in lower MW region that could correspond to heavy (~50 kDa) and light (~25 kDa) IgG chains. Results of flow-through fraction PAGE can be seen in CLL_{F1} la-

ne. An intensive band at ~180 kDa, representing a subunit of α_2 -macroglobulin, is present in the high MW γ -region. Below in the β -region lies a distinct band at 80 kDa, characteristic of transferrin. HSA band is less intensive but still present because in order to reduce the number of fractionations, high concentration of plasma with HSA concentration on the limit of binding capacity was injected on CIM α HSA column. Beneath the band representing HSA there is a broader band consisting of B β -fibrinogen at ~56 kDa, transthyretin at ~55 kDa and heavy IgG chains at ~50 kDa. The band at ~15 kDa could not be identified.²⁰ It is clear that intensities of all bands, which were weaker in the whole plasma sample are noticeably increased in the CLL_{F1} lane, suggesting that enrichment of less abundant proteins was successful.

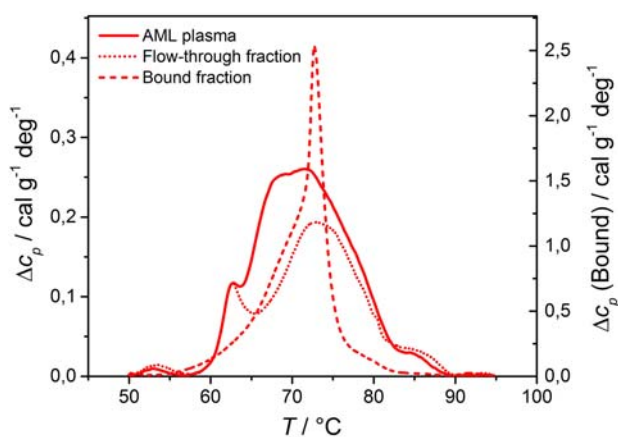


Figure 3. Thermograms of blood plasma from an individual with AML (top). DSC thermogram of a non-fractionated blood plasma sample (full line) is compared to thermograms of flow-through (dotted line) and bound fraction (dashed line) obtained from HPLC fractionation. The right ΔC_p axis corresponds to the bound fraction. SDS-PAGE of blood plasma from an individual with AML (bottom); P. L. – protein library, AML_{NF} – non-fractionated blood plasma (1 mg/mL), AML_{F1} – flow-through fraction (1 mg/mL), AML_{F2} – bound fraction (0.7 mg/mL).

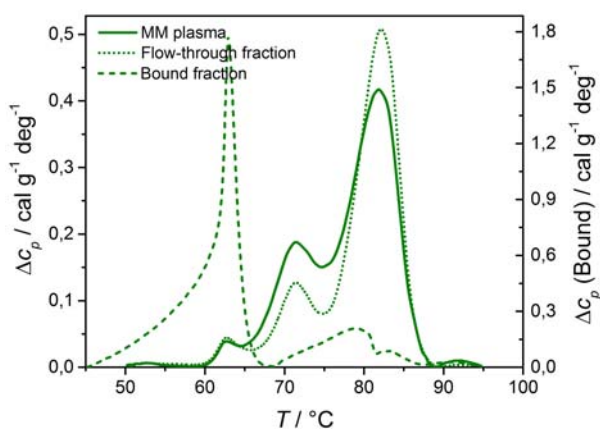


Figure 4. Thermograms of blood plasma from an individual with MM (top). DSC thermogram of a non-fractionated blood plasma sample (full line) is compared to thermograms of flow-through (dotted line) and bound fraction (dashed line) obtained from HPLC fractionation. The right ΔC_p axis corresponds to the bound fraction. SDS-PAGE of blood plasma from an individual with MM (bottom); P. L. – protein library, MM_{NF} – non-fractionated blood plasma (1 mg/mL), MM_{F1} – flow-through fraction (1 mg/mL), MM_{F2} – bound fraction (0.5 mg/mL).

The thermogram of the flow-through fraction of AML plasma (Figure 3) shows that depletion of HSA from blood plasma resulted in well-defined peak at 62 °C which in our opinion is a result of haptoglobin denaturation. Signals for other plasma proteins, such as fibrinogen at 53 °C and transferrin at 86 °C are also slightly enriched. The remaining peak at 72 °C can be attributed to IgG denaturation. The obtained unfolding enthalpy for the flow-through fraction was 2.89 ± 0.14 cal/g (Table 1), which is approximately 27% lower than for non-fractionated AML plasma. Thermogram obtained from thermal denaturation of the bound fraction of AML plasma (Figure 3) displays an intensive endothermic peak, followed by a steep exothermic effect characteristic of protein aggregation. Results of SDS-PAGE of AML plasma (Figure 3) show an intensive HSA band in AML_{F2} lane, suggesting that we have successfully depleted the majority of HSA from the AML plasma. Some faster migrating bands corresponding to heavy (~50 kDa) and light (~25 kDa) IgG chains can also be seen in AML_{F2} lane. AML_{F1} lane corresponds to the flow-through fraction and contains a band at 66 kDa showing that not all of HSA was removed. The intensities of other bands are increased, proving that we have succeeded in increasing the relative concentration of other proteins.

When comparing thermograms of non-fractionated sample and flow-through fraction of the MM plasma (Figure 4), a distinct drop in signal intensity at temperature of 71 °C and increase in signal intensity at temperature of 82 °C are observed. The denaturation enthalpy of the flow-through fraction was 4.27 ± 0.21 cal/g, which is only 7% lower than for non-fractionated MM plasma. SDS-PAGE of MM flow-through fraction, MM_{F1}, shows decreased intensity of HSA band at 66 kDa and increased intensities of other bands (Figure 4). On the other hand SDS-PAGE of MM bound fraction, MM_{F2}, shows strong band, characteristic of HSA along with weaker bands representing heavy and light IgG chains. SDS-PAGE results suggest that almost all of the HSA is removed from flow through fraction which could be associated to drop in DSC signal intensity at temperature of 71 °C. Thermograms of MM plasma show that HSA and IgG unfolding have shifted to higher temperature, perhaps due to interactions with drugs²¹ or interactions with monoclonal immunoglobulin.²² About 25 % drop in DSC signal intensity at temperature of 71 °C does not correspond to drop in band intensity observed in SDS-PAGE which means that HSA is unfolding in the same region as other proteins. Comparison of lanes with bound fractions in Figures 2, 3 and 4 reveals that the intensities faster migrating bands are strongest in the case of MM plasma. This could be a result of HSA-IgG complex formation, non-specific interactions or column degradation and should be further investigated. The stained gel (Figure 4) gives information not only about the effectiveness of MM plasma fractionation, but also of multiple myeloma signs. This is especially evident

from several protein bands in MM_{NF} lane. A weak band, characteristic of HSA and abnormally intensive bands, characteristic of heavy and light IgG chains can be observed. Both phenomena are typical of multiple myeloma²⁰ and it should be emphasized that MM plasma was obtained from patient with IgG clonality and light chain kappa restriction.

4. Conclusions

DSC provides a unique signature of the three examined diseases (chronic lymphocytic leukemia, multiple myeloma and acute myeloid leukemia), thus showing potential for plasma proteome investigation. Because only 3 plasma samples were investigated we have to emphasize that obtained results may not be used to generalize differences for the three investigated diseases. IAC with the use of a CIM α HSA column enables enrichment of less abundant plasma proteins, thus providing the tool to enhance the relative presence and/or influence of potential disease biomarkers. Enrichment of plasma proteins in flow-through fractions was verified with SDS-PAGE and analyzed with DSC. The obtained results suggest that combination of DSC and IAC could be introduced as a possible novel and non-invasive diagnostic tool, although further research in this field is required.

5. Acknowledgements

We acknowledge the financial support of the Slovenian Research Agency through Program Groups P1-0201, P4-0121 and P4-0369. We are also grateful to Iva Hafner Bratkovič for contributing important knowledge on making and staining SDS-PAGE gels. This work was partially supported by the European Commission FP7 projects Prot-HiSPRA (grant number 282506) and HTP-GlycoMet (grant number 324400).

6. References

1. R. Mayeux, *Neurotherapeutics*, **2004**, *1*, 182–188. <http://dx.doi.org/10.1602/neurorx.1.2.182>
2. N. C. Garbett, J. J. Miller, A. B. Jensen, J. B. Chaires, *Biophys. J.*, **2008**, *94*, 1377–1383. <http://dx.doi.org/10.1529/biophysj.107.119453>
3. P. Maurya, P. Meleady, P. Dowling, M. Clynes, *Anticancer Res.*, **2007**, *27*, 1247–1256. <http://ar.iiarjournals.org/content/27/3A/1247.long>
4. N. C. Garbett, M. L. Merchant, C. W. Helm, A. B. Jensen, J. B. Klein, J. B. Chaires, *PLoS One*, **2014**, *9*, e84710, 1–12. <http://dx.doi.org/10.1371/journal.pone.0084710>
5. T. Čerk Petrič, P. Brne, B. Gabor, L. Govednik, M. Barut, A. Štrancar, L. Zupančič Kralj, *J. Pharm. Biomed. Anal.*, **2007**,

- 43, 243–249. <http://dx.doi.org/10.1016/j.jpba.2006.06.019>
6. C. Wu, J. Duan, T. Liu, R. D. Smith, W.-J. Qian, *J. Chromatogr. B Analyt. Technol. Biomed. Life Sci.*, **2016**, *1021*, 57–68. <http://dx.doi.org/10.1016/j.jchromb.2016.01.015>
7. U. Černigoj, U. Vidic, B. Nemeč, J. Gašperšič, J. Vidič, N. Lendero Krajnc, A. Štrancar, A. Podgornik, *J. Chromatogr. A*, **2016**, *1464*, 72–78. <http://dx.doi.org/10.1016/j.chroma.2016.08.014>
8. N. C. Garbett, C. S. Mekmaysy, C. W. Helm, A. B. Jenson, J. B. Chaires, *Exp. Mol. Pathol.* **2009**, *86*, 186–191. <http://dx.doi.org/10.1016/j.yexmp.2008.12.001>
9. C. M. Stoscheck, *Methods in Enzymol.*, **1990**, *182*, 50–69. [http://dx.doi.org/10.1016/0076-6879\(90\)82008-P](http://dx.doi.org/10.1016/0076-6879(90)82008-P)
10. I. A. Tarasova, A. A. Lobas, U. Černigoj, E. M. Solovyeva, B. Mahlberg, M. V. Ivanov, T. Panić-Janković, Z. Nagy, M. L. Pridatchenko, A. Pungor, B. Nemeč, U. Vidic, J. Gašperšič, N. Lendero Krajnc, J. Vidič, M. V. Gorshkov, G. Mitulović, *Electrophoresis*, **2016**, *37*, 2322–2327. <http://dx.doi.org/10.1002/elps.201500489>
11. U. K. Laemmli, *Nature*, **1970**, *227*, 680–685. <http://dx.doi.org/10.1038/227680a0>
12. M. Chevillet, S. Luche, T. Rabilloud, *Nat. Protoc.*, **2006**, *1*, 1852–1858. <http://dx.doi.org/10.1038/nprot.2006.288>
13. C. M. Olsen, H.-T. Lee, L. A. Marky, *J. Phys. Chem. B*, **2009**, *113*, 2587–2595. <http://dx.doi.org/10.1021/jp806853n>
14. N. C. Garbett, M. L. Merchant, J. B. Chaires, J. B. Klein, *Biochim. Biophys. Acta*, **2013**, *1830*, 4675–4680. <http://dx.doi.org/10.1016/j.bbagen.2013.05.007>
15. A. Michnik, Z. Drzazga, K. Michalik, A. Barczyk, I. Santura, E. Sozańska, W. Pierzchała, *J. Therm. Anal. Calorim.*, **2010**, *102*, 57–60. <http://dx.doi.org/10.1007/s10973-009-0602-6>
16. L. Kikalishvili, M. Ramishvili, G. Nemsadze, T. Lezhava, P. Khorava, M. Gorgoshidze, M. Kiladze, J. Monaselidze, *J. Therm. Anal. Calorim.*, **2015**, *120*, 501–505. <http://dx.doi.org/10.1007/s10973-015-4426-2>
17. S. Todinova, S. Krumova, L. Gartcheva, C. Robeerst, S. G. Taneva, *Anal. Chem.*, **2011**, *83*, 7992–7998. <http://dx.doi.org/10.1021/ac202055m>
18. G. A. Picó, *Int. J. Biol. Macromol.*, **1997**, *20*, 63–73. [http://dx.doi.org/10.1016/S0141-8130\(96\)01153-1](http://dx.doi.org/10.1016/S0141-8130(96)01153-1)
19. A. Kumar Shaw, S. Kumar Pal, *J. Photoch. Photobio. B.*, **2008**, *90*, 69–77. <http://dx.doi.org/10.1016/j.jphotobiol.2007.11.003>
20. D. F. Keren: Protein Electrophoresis in Clinical Diagnosis, Hodder Arnold, London, Great Britain, **2003**, pp. 63–108 and 151–168. http://www.aun.edu.eg/molecular_biology/Protein%20workshop/&%20Protein%20Electrophoresis_clinical%20diagnosis.pdf
21. R. Thakur, A. Das, V. Sharma, C. Adhikari, K. S. Ghosh, A. Chakraborty, *Phys. Chem. Chem. Phys.*, **2015**, *17*, 16937–16946. <http://dx.doi.org/10.1039/c4cp05734a>
22. F. Barcelo, J. J. Cerda, A. Gutierrez, T. Jimenez-Marco, M. A. Duran, A. Novo, T. Ros, A. Sampol, J. Portugal, *PLoS ONE*, **2015**, *10*, 1–15. <http://dx.doi.org/10.1371/journal.pone.0120316>

Povzetek

Diferenčna dinamična kalorimetrija (DSC) nam nudi svojevrsten vpogled v lastnosti proteoma krvne plazme. Termogrami krvne plazme bolnih posameznikov so specifični in se razlikujejo med seboj, kakor tudi od krvne plazme zdravih posameznikov. Z DSC smo izmerili termograme krvne plazme posameznikov s kronično limfatično levkemijo, plazmocitomom in akutno mieloično levkemijo ter jih med seboj primerjali. Da bi pridobili dodatne informacije o termično inducirani denaturaciji plazemskih proteinov, smo uporabili imunoafinitetno kromatografijo. S kromatografsko kolono z imobiliziranimi anti-HSA protitelesi smo izvedli imunoekstrakcijo HSA in s tem povečali delež manj pogostih proteinov v krvni plazmi. To nam je omogočilo snemanje termogramov frakcij z različno proteinsko sestavo in s tem boljše razumevanje interakcij med proteini, ki sestavljajo krvno plazmo. Učinkovitost odstranitve HSA in sestavo frakcionirane krvne plazme smo preverili z uporabo SDS-PAGE.

Scientific paper

Interaction of PER2 with the Constitutive Androstane Receptor Possibly Links Circadian Rhythms to Metabolism

Tomaž Martini,¹ Jurij Stojan,² Damjana Rozman¹
and Uršula Prošenc Zmrzljak^{1,*}

¹ Center for Functional Genomics and Bio-chips, Institute of Biochemistry, Faculty of Medicine, University of Ljubljana, Zaloška cesta 4, Ljubljana, Slovenia

² Institute of Biochemistry, Faculty of Medicine, University of Ljubljana, Vrazov trg 2, Ljubljana, Slovenia

* Corresponding author: E-mail: ursula.prosenc@mf.uni-lj.si
Tel: +386 1 543 75 92 fax: +386 1 543 75 88

Received: 06-11-2016

For Cutting Edge 2017

Abstract

Period 2 (PER2) is an important factor in daily oscillations called circadian rhythms, which are emerging as one of the most important regulatory networks, responsible for homeostasis and transcriptional regulation of a number of genes. Our work shows that PER2 could act as a co-activator of the constitutive androstane receptor (CAR), a key nuclear receptor (NR) that regulates the metabolism of endobiotics and xenobiotics. Bioinformatic analysis shows that PER2 and CAR possess structural elements that could enable them to interact which was confirmed experimentally by CoIP experiment. Co-transfection of mouse hepatocarcinoma cells with plasmids overexpressing *Per2* and *Car* increases expression of *Bmal1*, a potential CAR target gene, more than transfections with *Car* only. This is the first report indicating the interaction of PER2 and CAR.

Keywords: circadian rhythms, metabolism, period 2, constitutive androstane receptor, co-activator

1. Introduction

Circadian rhythms are daily oscillations in most cells and organisms. They are governed by autonomous molecular circadian oscillators that are synchronized by external cues, such as light and food. The circadian machinery is composed of positive and negative transcriptional and translational feedback loops. The major positive loop comprises of transcriptional activators BMAL1 and CLOCK that can heterodimerize and drive their own transcription as well as that of elements of the negative loop, such as *Period* (PER) homologues, *Cryptochromes* and *Rev-erb α* . The transcriptional repression of *Bmal1* due to REV-ERB α can be counter-balanced by ROR α and PPAR α .^{1–3}

PER2 is involved in the negative feedback loop where it directly interacts with the transactivation complex of BMAL1-CLOCK and represses its transcriptional activation capability. It also acts in the positive loop where

it drives *Bmal1* expression by acting as a co-activator of NRs, eg PPAR α .¹ PER2 in metabolic and mental disorders, cancer and other pathologies is currently being intensively studied.^{4–8} Due to its two LXXLL structural motifs, which can interact with a hydrophobic pocket of NRs, it has been studied as a nuclear receptor co-activator.⁹ Perhaps one of the most important transcriptional regulator of metabolism is CAR, a NR regulator of primary and secondary metabolism. CAR can be directly or indirectly activated by various endogenous ligands, eg bilirubin, and xenobiotics, eg barbiturates.^{10–18} After activation and nuclear localization it interacts with co-activators and heterodimerization factors, most often the retinoid X receptor (RXR). The final protein complex can transactivate enzymes of the cytochrome P450 (CYP), glucuronosyltransferase (UGT) and multi drug resistance protein (MRP) families.^{3,13,15,19–21}

The interaction between nuclear receptors and their co-activators is a well-documented interaction that is

highly conserved among species.^{9,22} Nuclear receptors have high levels of similarity in their ligand binding domains, especially in the region of helices 3, 4 and 5. These helices form a hydrophobic cleft which interacts with leucines of the co-activators' LXXLL motifs. The two residues between the three leucines have little or no importance to binding of LXXLL motifs as they are in direct contact with the surrounding aqueous solution. Charged residues of the helices 3–5 form interactions with amino acids surrounding the LXXLL motifs which are crucial for the specificity of interactions and recognition of appropriate co-activators. The most important factor for specificity of co-activators are the two residues just before the first leucine of the LXXLL motif, usually referred as –2 and –1. Of most interest to this study was the class 3 of LXXLL motifs, according to Savkur and Burris, which encompasses motifs SXLXXLL.^{9,23}

Here it was shown that CAR and PER2 interact with, and activate *Bmal1* transcription. The initial prediction was made on the basis of homology of LXXLL motifs of PER2 and several known CAR co-activators and was confirmed experimentally. Our data presents the first report of communication between drug metabolism and the circadian rhythm at the level of direct interaction between PER2 and CAR.

2. Results

Bioinformatic analysis of the transcription factor binding sites using MatInspector, Matrix Library 9.4 and User-defined IUPAC strings revealed potential binding sites for CAR on the *Bmal1* promoter, eg for CAR/RXR at 414-438 (positive strand) of GXP_5050588 (*Bmal1 Mus musculus*).^{24–26} This provided a sufficient basis for the transfection experiments that showed induced expression of a *Bmal1 luc* reporter when Hepa 1-6 cells were transfected with *Car* ($P < 0.01$). The induction was further enhanced when co-transfection with *Car* and *Per2* was performed ($P < 0.01$) which suggests an either direct or indirect influence of PER2 on CAR transactivation of *Bmal1* (Figure 1). Surprisingly, the transactivation of *Bmal1* with vectors overexpressing CAR and PER2 was not significantly different than transactivation with positive control overexpressing PPAR α and PER2 (Figure 1) that co-immunoprecipitate at *Bmal1* regulatory sites.¹ The lack of a statistically significant difference might suggest a similar mechanism of transactivation which may lead to the exploration of structural properties of both PER2 and CAR to evaluate if a direct interaction between the proteins is plausible.

Bioinformatic analysis showed that PGC1 α (PPAR γ C1A), a known CAR and PPAR γ co-activator, may interact with CAR via its motif SLLKKLL (*Mus musculus*), which is homologous to both SXLXXLL motifs of PER2 (Figure 2), namely SGLLNLL (*Mus muscu-*

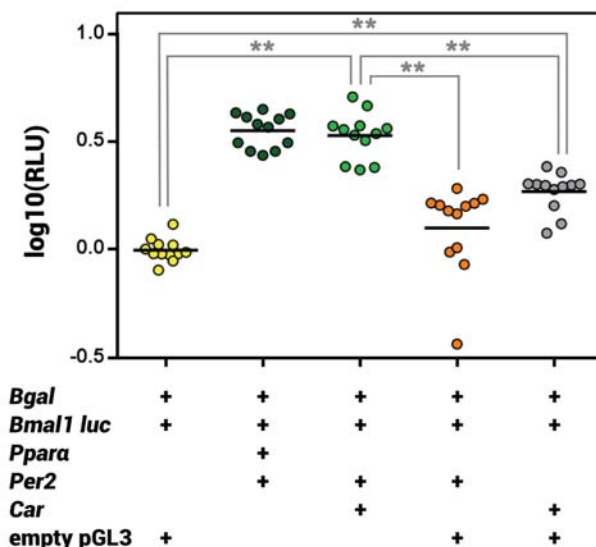


Figure 1. Co-transfection of Hepa 1-6 cells with CAR and PER2 overexpression plasmids induces promoter activity of *Bmal1 luc* reporter. This induction is similar to the one observed when performing co-transfections with Ppara α and Per2 ($P < 0.0001$) and different to the one observed when performing transfections with *Car* only ($P < 0.0001$). The log10 relative luciferase units of individual wells for the specific transfection mix are shown. ** - $P < 0.01$

lus) and SDLLNLL (*Mus musculus*).^{27–29} A further co-activator of CAR and PPAR γ , PGC1 β , which has three LXXLL motifs, all with a serine at a 1 or -2 position, also exists. A similar arrangement with a serine residue in front of a LXXLL motif can also be observed in NCoA6, another CAR co-activator.^{28,30}

As both PER2 and PGC1 α are co-activators of PPAR γ , a NR involved in lipid and carbohydrate metabolism, attention was focused on the homology of the nuclear receptor. Most receptor residues that are in contact with LXXLL motifs have no charge pointing towards the co-activator motifs, besides two very distinct lysins at both the CAR and PPAR γ at homologous positions. The receptors also seem to have high 3D similarity of the hydrophobic cleft as helices 3, 4, 5 are positioned in a similar manner. Both receptors seem to bind LXXLL motifs at the »end of helix 5« to the »end of helix 3«, which coincides with the lysine positioning.^{31–35} Even though this could be projected onto many nuclear receptors, the position of the lysine at helix 5 could additionally explain the favouring of co-activators with a serine before LXXLL.^{9,29,36}

The hypothesis that PER2 and CAR interact directly was confirmed with co-immunoprecipitation (Figure 3). For this, *Car-Flag* and *Per2-V5* co-transfection was performed. Initial release of proteins from Sepharose beads was performed at 70 °C and revealed the V5 reactive protein at an approximate size of 40 kDa. After additional heating of Sepharose at 95 °C for 2 min, a 135

hPER2/1st	O15055	KSHENEIRYHPFRMTPYLKVKVRDQQGAE SQ LCCLL LAERVHSGYEAPRIPPEKRI
hPER2/2nd	O15055	TSRDQPKAPLTRDEPSDTQNSDALST SG LLNLL LNEDLCSASGSAASESLGSG
hPGC1α/2nd	Q9UBK2	DGDVTTDNEASPSSMPDGTTPPQEAEE SL LKLL LAPANTQLSYNECSGLSTQN
hPGC1α/3rd	Q9UBK2	PAIVKTENSWSNKAKSICQQQKQRRP CE LLKY LTNDPPHTKPTENRNSSRD
hPGC1β/1st	Q86YN6	SASPAPSSAPPSPAPEKPSAPAPEVDEL SL LQKLL LATSYPSTSSDTQKEGTAWR
hPGC1β/2nd	Q86YN6	PKACSNPSQQVRSRPSWRHHSKASWAE FI LRELL LQDVLCDVSKPYRLATPVYA
hNCoA6/1st	Q14686	PFSGAPNGNQMSCGQNPGFVNKDVT LT SPL LVNLL LQSDISAGHFGVNNKQNTN
hNCoA6/2nd	Q14686	DGQPSDPNKLPSVEENKLVSPAMREAP TS LSQLL DNSGAPNVTIKPPGLTDLEV
mPER2/1st	O54943	KHHENEIRYQPFMRTPYLKVKVQEQGAE SQ LCCLL LAERVHSGYEAPRIPPEKRI
mPER2/2nd	O54943	TSRDRQPKAPPTCNEPSDTQNSDAIST SD LLNLL LGEDLCSATGSALSRSYGASA
mPGC1α/2nd	O70343	DGAVTTDNEASPSSMPDGTTPPQEAEE SL LKLL LAPANTQLSYNECSGLSTQN
mPGC1α/3rd	O70343	PAIVKTENSWSNKAKSICQQQKQRRP CE LLKY LTNDPPHTKPTENRNSSRD
mPGC1β/1st	Q8VHJ7	GLAAFPELDEGDTSPCTPASAPLSAPP SPT LERLL SPASDVDELSLLQKLLLAT
mPGC1β/2nd	Q8VHJ7	PASPAPLSAPPSPPTLERLLSPASDVDEL SL LQKLL LATSPTASSDALKDGTWS
mPGC1β/3rd	Q8VHJ7	PIPQACSSLSRQVQPRSRHPPKAFWTE FI LRELL LQDILCDVSKPYRLAIPVYA
mNCoA6/1st	Q9JL19	PFGGAPNGSQMSCGQNPGFVNKDVT LT SPL LVNLL LQSDISAGHFGVNNKQNTN
mNCoA6/2nd	Q9JL19	DGQPLDPNKLPSVEENKLVSPAMREAP TS LSQLL DNSGAPNVTIKPPGLTDLEV

Figure 2. Alignment showing similarity between PER2 and known co-activator LXXLL motifs of CAR, namely PGC1alpha, NCoA6 and PGC1beta.^{28,30} The letters h and m before the protein name designate species *Homo sapiens* and *Mus musculus*, with the sequential number of the noted LXXLL and UniProt/Swiss-Prot entry number following the protein name. The predicted LXXLL motifs with residues marked as 1-5 are shown in red, as are serines located just before LXXLL. Of note is a negatively charged side-chain, or a hydroxyl group containing residues (E, S, T) just in front of the -2 serine.²⁹

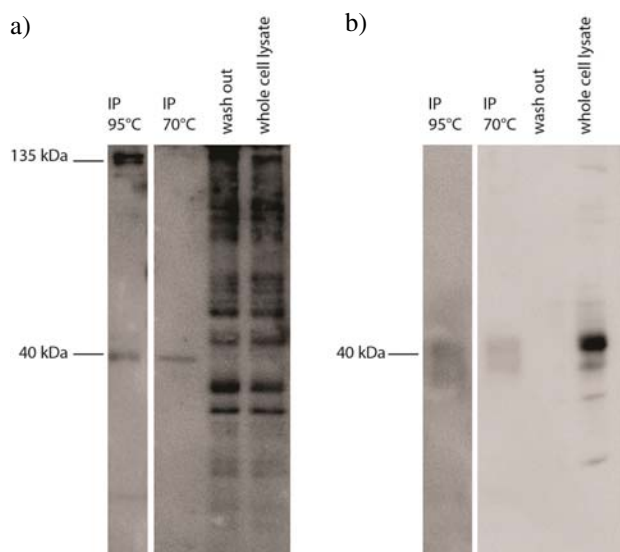


Figure 3. Co-immunoprecipitation with FLAG Ab conjugated Sepharose of *Car-Flag* and *Per2-V5*. A: Western blot with V5 Ab – PER2 shows two bands, at 40 and 135 kDa. After the final incubation of Sepharose beads at 70 °C, only the 40 kDa form was visible on the blot. The 135 kDa isoform was visible after additional incubation at 95 °C. B: Western blot with FLAG Ab – the signal of CAR is in the range of expected protein size (40 kDa).

kDa protein was released (Figure 3A), corresponding to the expected size of PER2.²⁹ The FLAG reactive protein was detected very faintly, irrespective of temperature, at 40 kDa (Figure 3B). This could correspond to CAR.²⁹ This corroborates the prediction that the two proteins could interact in a co-activator and nuclear receptor manner.

3. Materials and Methods

3. 1. Plasmids

Bmal1 luc, having a *Bmal1* promoter cloned into a pGL3 luciferase reporter vector, *Per2*, coding for a V5-tagged PER2, and *Pparα* constructs were kindly provided by J. Ripperger and U. Albrecht (Department of Biology, Faculty of Science, University of Fribourg, Switzerland) and have been previously described in more detail.¹

The *Car* expression construct was kindly provided by JeanMarc Pascussi (Institut de genomique fonctionnelle, Montpellier, France) and it was constructed by Negishi Masahiko (NIH, North Carolina, USA) and has previously been described in more detail.³⁷

The *Car-Flag* plasmid was kindly provided by Negishi Masahiko (NIH, North Carolina, USA) and has previously been described in more detail.³⁸

An empty pGL3 basic vector (Promega) was used to perform transfections with equal amounts of DNA. All wells were transfected with 50 ng *Bgal* – pSV-β-Galactosidase Control Vector (Promega), for normalization. All constructs besides the commercial pGL3 basic and *Bgal* represent *Mus musculus*.

3. 2. Transfections

Transfections were performed on Hepa 1-6 cells available from the European Collection of Authenticated Cell Cultures. The cells were held at 5% CO₂ and 37 °C and transferred to 96-well microplates 24 hours prior to transfections with 5 × 10⁶ cells in DMEM and 10% FBS. For transfections X-tremeGENE HP DNA (Roche) was

used according to manufacturer's instructions. Total plasmid mass was equal to 200 ng per well, with each construct of interest at 50 ng and total mass added to 200 ng with the pGL3 basic vector. The negative control represents transfections with *Bgal*, *Bmal1 luc* and pGL3 basic vector, a positive control of *Bgal*, *Bmal1 luc*, *Ppar α* and *Per2* was used.

3. 3. Luciferase assay and statistical analysis of results

Cells were lysed using Passive Lysis Buffer (Promega). Luciferase assay was performed using the ONE-Glo Luciferase (Promega) according to manufacturer's instructions and measurements were performed on Synergy H4 (BioTek). Results were normalized using analysis of β -galactosidase activity and additional normalization to positive control using luciferase activity was performed for microplate comparison. Analysis of variance was performed and results were logarithmized to achieve variance homogeneity. The t-test analysis was performed with GraphPad Prism 6.0 software. In cases where significance is very high, the software returns p values in the form $p > 0.0001$.

3. 4. Co-immunoprecipitation (Co-IP)

HeLa cells were seeded on 6-well plates and co-transfected with *Car-Flag* and V5-tagged *Per2* using Lipofectamine 2000 (Thermo Fisher Scientific). Cells were harvested 2 days after transfection using 200 microliters of the lysis buffer: 50 mM Tris · HCl at pH 7.5, 150 mM NaCl, 0.5% (w/v) NP-40 and complemented with protease inhibitors (Roche). The cell lysate was agitated for 10 min at 4 °C and centrifuged at 14000 g 20 min at 4 °C. Supernatant was transferred to a tube containing FLAG-coupled Sepharose beads (Sigma-Aldrich) and rotated for 2 h at 4 °C. After the centrifugation at 10000 g for 5 min at 4 °C the supernatant was then collected and stored as a whole cell lysate sample. Sepharose was washed 3 times with additional 200 microliters of lysis buffer and the first wash-out was collected as wash out sample. 50 microliters of Laemmli buffer was added to the Sepharose, followed by heating for 10 min at 70 °C and again for 2 min at 95 °C. Western blot was performed with 3 different samples: whole cell lysate, wash out and immunoprecipitate (IP) in two parallel conditions, one with anti-FLAG Ab A8592 (Sigma-Aldrich) and the other with anti-V5 Ab V8137 (Sigma-Aldrich).

3. 5. Discussion

The comparable transactivation of *Bmal1* following co-transfections with *Car/Per2*, or *Ppar α /Per2* may suggest a similar mechanism of transcriptional activation of *Bmal1*. If this is the case then, in conjunction with ChIP

experiments revealing binding of PER2 and PPAR α at regulatory regions of *Bmal1*,¹ this could further support the proposal that PER2 could potentially act as CAR's co-activator and that the pair can form transactivation complexes either alone or with other partners. This is further supported by finding CAR binding sites at the *Bmal1* promoter. The discovery is interesting as both proteins are important for cell homeostasis. However, PER2 is not the only co-activator of these nuclear receptors and PER2 is expressed at certain times of the day. To confidently state how important is the effect of different *Bmal1* transcriptional activity, this should be tested on reporter cell lines. We can speculate that additive effects of xenobiotic ingestion, social jet lag and nutrition overload can affect circadian clock driven endogenous liver metabolism. This can result in liver abnormalities, such as non-alcoholic fatty liver disease that could terminate in HCC.

Since some of the predictions of this study were based on homology, it is worth noting that according to Savkur and Burris the amino acid at -1 of their class 3 LXXLL motifs should be a non-polar amino acid.⁹ However, since human and mouse 2nd PER2 LXXLL have G or D at -1, with high conservation of the rest of the sequence, motifs that do not follow this strict consensus of an unpolar -1 residue are shown in our alignment.²⁹ As well as this, the residue at -1 most probably points outwards from the hydrophobic pocket and therefore does not directly interact with helices 3-5 of NRs.³⁹ It would be worth exploring if it could interact with the charge clamp of NRs.^{9,31,40-42}

Another interesting observation is the presence of a band at approximately 40 kDa at the western blot with anti-V5 Ab. Similar sized bands have been observed in our previous work, where a >40 kDa band was detected with western blot from mouse liver samples, with the use of a different Ab (Abcam ab467). Unfortunately this could not be verified using our CoIP samples with these Ab, as Abcam does not provide this specific Ab any more. Work from other researchers has shown the existence of a shorter PER2S isoform in *Homo sapiens* with the size of 45 kDa and co-IP at 55 kDa.⁴³ If a similar truncated form of PER2 was observed, it could be speculated that PER2 can interact with CAR with its first LXXLL. However, this does not exclude an interaction of PER2 with CAR with its second LXXLL.¹ It may be possible that a co-activator interacts with an NR with multiple LXXLL motifs, but with a different affinity. Although a cocktail of protease inhibitors were used with the lysis buffer, it is still possible that the >40kDa band is a product of protein degradation.

It is interesting to note that *Car* shows both diurnal expression patterns in liver, with *Car* mRNA levels oscillating in phase with *Bmal1*, and the possibility to be activated by ligands. The induction could very well be dependent on the phase or time of induction.^{44,45} If this is the case, such findings should be considered in the pharmacoki-

netics of drug active ingredients, especially as CAR regulates the expression of several CYPs.^{18,21,46} This work may therefore provide an important new link in understanding the connection between internal clock machinery, metabolism and pharmacokinetics.

As CAR can be activated by xenobiotics, such as flavonoids, catechins and similar polyphenols, and also active ingredients of drugs, eg. barbiturates, paracetamol and some compounds with a steroid-like structure, it would also be interesting to see if such activation has any physiological effect on transcription of genes involved in circadian rhythms.^{13,16,19,46} It would be possible that high levels of CAR could affect the molecular clock in the periphery, but CAR also binds other co-activators. We cannot exclude that the robust molecular clock could be affected, which would mean that different CAR activators (eg. xenobiotics) could have an effect on liver circadian regulation of various metabolic pathways.

This work also suggests that period homologues should be considered as possible NR co-activators, not only of NRs that have an established role in circadian rhythms. Perhaps such mechanisms of multiple co-activators being able to activate a single NR could provide a compensatory mechanism in case of co-activator deregulation. On the other hand, different co-activators are expressed differentially in tissues with different phases of expression, which could in fact define a NR's tissue and time specific function.

In conclusion, we show that CAR and PER2 can form an interaction which has implications for circadian aspects of drug metabolism.

3. 6. Authors' contributions

T. M. performed transfections, the luciferase assay and bioinformatical and structural analyses. The bioinformatical and structural analyses were performed under expert supervision and guidance of J.S.. U.P.Z. first noticed the possibility of an interaction between CAR and PER2 during her preliminary screenings for interactions of PER2 with nuclear receptors. She also performed co-IP. Experiment planning and protocol preparation was performed by U.P.Z. and D. R. The manuscript draft was prepared by T. M. and finalised by all authors. All authors read and approved the final manuscript.

3. 7. Acknowledgements

We would kindly like to thank J. Ripperger and U. Albrecht for providing *Bmal1 luc*, *Per2* and *Ppar α* constructs, JM. Pascussi for the *Car* expression construct and M. Nagishi for the *Car-Flag*. The view of J. Ačimovič on statistical analysis of transfection results is highly appreciated. A sincere thank you to M. Hafner, Ni. and Nu. Trošt and Ž. Urlep for their advice. We would also like to thank I. Mlinarič Raščan for a critical overview. The work

described here contains part of the master thesis work of T. M. and was supported by the Slovenian Research Agency program grants P1-0104 and P1-0390.

4. References

1. I. Schmutz et al., *Genes Dev.* **2010**, *24* (4), 345–357. <https://doi.org/10.1101/gad.564110>
2. R. Chavan et al., *Nat. Commun.* **2016**, *7*.
3. U. P. Zmrzljak, D. Rozman, *Chem. Res. Toxicol.* **2012**, *25* (4), 811–824. <https://doi.org/10.1021/tx200538r>
4. M. Zeman et al., *Mol. Med. Rep.* **2008**, *1* (4), 599–603.
5. T. Okabe et al., *PLoS ONE* **2014**, *9* (10), e109693. <https://doi.org/10.1371/journal.pone.0109693>
6. S.-T. Chen et al., .
7. B. Grimaldi et al., *Cell Metab.* **2010**, *12* (5), 509–520. <https://doi.org/10.1016/j.cmet.2010.10.005>
8. G. Hampp et al., *Curr. Biol.* **2008**, *18*, 678–683. <https://doi.org/10.1016/j.cub.2008.04.012>
9. R. S. Savkur, T. P. Burris, *J. Pept. Res. Off. J. Am. Pept. Soc.* **2004**, *63* (3), 207–212. <https://doi.org/10.1111/j.1399-3011.2004.00126.x>
10. M. Hafner et al., *Curr. Drug Metab.* **2011**, *12* (2), 173–185. <https://doi.org/10.2174/138920011795016890>
11. W. Huang et al., *Proc. Natl. Acad. Sci. U. S. A.* **2003**, *100* (7), 4156–4161. <https://doi.org/10.1073/pnas.0630614100>
12. H. R. Kast et al., *J. Biol. Chem.* **2002**, *277* (4), 2908–2915. <https://doi.org/10.1074/jbc.M109326200>
13. T. Kawamoto et al., *Mol. Cell. Biol.* **1999**, *19* (9), 6318–6322. <https://doi.org/10.1128/MCB.19.9.6318>
14. K. Kobayashi et al., *Arch. Toxicol.* **2015**, *89* (7), 1045–1055. <https://doi.org/10.1007/s00204-015-1522-9>
15. J. M. Maglich et al., *J. Biol. Chem.* **2004**, *279* (19), 19832–19838. <https://doi.org/10.1074/jbc.M313601200>
16. J.-M. Pascussi et al., *Mol. Pharmacol.* **2000**, *58* (6), 1441–1450.
17. T. Rezen, *Expert Opin. Drug Metab. Toxicol.* **2011**, *7* (4), 387–398. <https://doi.org/10.1517/17425255.2011.558083>
18. J. Zhang et al., *Science* **2002**, *298* (5592), 422–424. <https://doi.org/10.1126/science.1073502>
19. R. Yao et al., *J. Agric. Food Chem.* **2010**, *58* (4), 2168–2173. <https://doi.org/10.1021/jf903711q>
20. H. Yang, H. Wang, *Protein Cell* **2014**, *5* (2), 113–123. <https://doi.org/10.1007/s13238-013-0013-0>
21. K. Monostory, Z. Dvorak, *Curr. Drug Metab.* **2011**, *12* (2), 154–172. <https://doi.org/10.2174/138920011795016854>
22. A. Brenna et al., *Mol. Biol. Cell* **2012**, *23* (19), 3863–3872. <https://doi.org/10.1091/mbc.E12-02-0142>
23. K. Suino et al., *Mol. Cell* **2004**, *16* (6), 893–905.
24. K. Cartharius et al., *Bioinformatics* **2005**, *21* (13), 2933–2942. <https://doi.org/10.1093/bioinformatics/bti473>
25. C. Frank et al., *J. Biol. Chem.* **2003**, *278* (44), 43299–43310. <https://doi.org/10.1074/jbc.M305186200>

26. K. A. Arnold et al., *Nucl. Recept.* **2004**, 2 (1), 1. <https://doi.org/10.1186/1478-1336-2-1>
27. G. B. Rha et al., *J. Biol. Chem.* **2009**, 284 (50), 35165–35176. <https://doi.org/10.1074/jbc.M109.052506>
28. T. Shiraki et al., *J. Biol. Chem.* **2003**, 278 (13), 11344–11350. <https://doi.org/10.1074/jbc.M212859200>
29. A. Bateman et al., *Nucleic Acids Res.* **2015**, 43 (D1), D204–D212. <https://doi.org/10.1093/nar/gku989>
30. S. Surapureddi et al., *Mol. Pharmacol.* **2008**, 74 (3), 913–923. <https://doi.org/10.1124/mol.108.048983>
31. K. Suino et al., *Mol. Cell* **2004**, 16 (6), 893–905.
32. K. Wakabayashi et al., *Biol. Pharm. Bull.* **2011**, 34 (7), 1094–1104. <https://doi.org/10.1248/bpb.34.1094>
33. Y. Li et al., *J. Biol. Chem.* **2008**, 283 (27), 19132–19139. <https://doi.org/10.1074/jbc.M802040200>
34. L. Shan et al., *Mol. Cell* **2004**, 16 (6), 907–917.
35. S. Hennig et al., *PLoS Biol.* **2009**, 7 (4), e94. <https://doi.org/10.1371/journal.pbio.1000094>
36. H. M. Berman et al., *Nucleic Acids Res.* **2000**, 28 (1), 235–242. <https://doi.org/10.1093/nar/28.1.235>
37. P. Honkakoski et al., *Mol. Cell. Biol.* **1998**, 18 (10), 5652–5658. <https://doi.org/10.1128/MCB.18.10.5652>
38. Y. E. Timsit, M. Negishi, *PLoS ONE* **2014**, 9 (5). <https://doi.org/10.1371/journal.pone.0096092>
39. R. A. Sayle, E. J. Milner-White, *Trends Biochem. Sci.* **1995**, 20 (9), 374. [https://doi.org/10.1016/S0968-0004\(00\)89080-5](https://doi.org/10.1016/S0968-0004(00)89080-5)
40. M. V. Milburn et al., *Nature* **1998**, 395 (6698), 137–143. <https://doi.org/10.1038/25931>
41. C. y Chang et al., *Mol. Cell. Biol.* **1999**, 19 (12), 8226–8239. <https://doi.org/10.1128/MCB.19.12.8226>
42. I. Dussault et al., *Mol. Cell. Biol.* **2002**, 22 (15), 5270–5280. <https://doi.org/10.1128/MCB.22.15.5270-5280.2002>
43. D. Avitabile et al., *Cell. Mol. Life Sci.* **2014**, 71 (13), 2547–2559. <https://doi.org/10.1007/s00018-013-1503-1>
44. Y. Kanno et al., *Nucl. Recept.* **2004**, 2 (1), 6. <https://doi.org/10.1186/1478-1336-2-6>
45. X. Yang et al., *Cell* **2006**, 126 (4), 801–810. <https://doi.org/10.1016/j.cell.2006.06.050>
46. L. M. Slosky et al., *Mol. Pharmacol.* **2013**, 84 (5), 774–786. <https://doi.org/10.1124/mol.113.086298>
47. R. A. Sayle, E. J. Milner-White, *Trends Biochem. Sci.* **1995**, 20 (9), 374. [https://doi.org/10.1016/S0968-0004\(00\)89080-5](https://doi.org/10.1016/S0968-0004(00)89080-5)
48. V. Ritchie, D. W., Venkatraman, **2010**.
49. P. M. C. Guex, N., *Electrophoresis* **1997**, 18, 2714–2723. <https://doi.org/10.1002/elps.1150181505>
50. M. Tarini et al., *IEEE Trans. Vis. Comput. Graph.* **2006**, 12 (5). <https://doi.org/10.1109/TVCG.2006.115>

Povzetek

Period 2 (PER2) je pomemben faktor pri dnevni oscilacijah, imenovanih cirkadiani ritmi. Ti so eni najpomembnejših regulatornih zank, ki so pomembne za uravnavanje homeostaze in uravnavanja prepisa velikega števila genov. Dokazali smo, da lahko PER2 deluje kot ko-aktivator konstitutivnega androstanskega receptorja (CAR), ključnega jedrnega receptorja pri uravnavanju metabolizma endobiotikov in ksenobiotikov. Bioinformatična analiza je pokazala, da PER2 in CAR vsebujeta strukturne elemente, ki omogočajo njuno interakcijo. To je bilo eksperimentalno potrjeno s CoIP poskusom. KO-transfekcija mišjih hepatokarcinomskih celic s plazmidi, ki omogočajo povečano izražanje *Per2* in *Car*, poveča izražanje *Bmall*, potencialni tarčni gen CAR. Povečano izražanje *Bmall* v celicah je višje, kot če so tranficirane le s *Car* plazmidom. To je prvo poročilo o interakciji PER2 in CAR.

Short communication

Preliminary Evaluation of Animal Bone Char as Potential Metal Stabilization Agent in Metal Contaminated Soil

Evelin Gruden, Peter Bukovec and Marija Zupančič*

Faculty of Chemistry and Chemical Technology, University of Ljubljana, Večna pot 113, SI 1000 Ljubljana, Slovenia

* Corresponding author: E-mail: marija.zupancic@fkk.uni-lj.si,

Phone: +386 1 4798 531

Received: 04-09-2016

For Cutting Edge 2017

Abstract

The aim of this study was to evaluate the potential effect of animal bone char (ABC) addition on metal mobility in mine tailings. The mobility of metals after addition of ABC to tailings at four different application rates (0.6 g, 1.2 g, 1.8 g and 3.6 g ABC per 100 g of tailings) was evaluated by Toxicity Characteristic Leaching Procedure (TCLP) one step extraction. The obtained results indicated that the mobility of Pb, Cr and Cd gradually decreased with increasing quantity of added ABC. According to the TCLP, mobile concentrations of Pb in tailings exceeded threshold values for almost eight times. After ABC addition, Pb TCLP-extractable concentrations decreased from 39 mg L⁻¹ in tailings to lower than the TCLP limit values of 5 mg L⁻¹ at all ABC application rates, except in mixtures with the lowest addition of ABC. We concluded that ABC could be a successful metal stabilization agent for multi-metal contaminated soil, although attention should be paid at highly As contaminated soil.

Keywords: Animal bone char, metal stabilization, phosphate, mine tailings

1. Introduction

The contamination of soil with Pb is an important ecological problem worldwide whereas mining is among the main sources of Pb contamination in mine areas.¹ Contaminated mine sites are poorly developed soils, depleted of organic matter and nutrients and are characterized by their excessive metal contents.² In the past, large amounts of mine wastes were dumped near the sites where they were produced and dispersed into nearby soils, crops and ecosystem.³⁻⁴ The accumulation of metals in soil may have serious consequences for animal and human health through the food chain, groundwater, plant growth and microorganism diversity.⁴⁻⁵

In situ chemical immobilization is a promising green and cost effective soil remediation technique where mobile metal chemical species are transformed into less mobile ones by adding different amendments.⁵⁻⁶ Phosphate amendments have been shown to be highly effective to reduce metal mobility and bioavailability. Many metals (Pb, Zn, Cd, Cu and others) can precipitate with phosphate sources as relatively insoluble metal phosphate species.

Pb can be mainly converted into insoluble forms, such as pyromorphite (Pb₅(PO₄)₃OH).^{1,7-8}

Animal bone char (ABC) is a granular material, rich of phosphates, that is produced by animal bone pyrolysis.⁹⁻¹⁰ It mainly contains about 70–76 % of biological, relatively crystalline calcium hydroxyapatite (Ca₅(PO₄)₃(OH)), 9–11 % of organic carbon and 7–9 % of CaCO₃.¹¹⁻¹² Few previous studies highlighted the potential use of ABC as a green and low-cost P-amendment for Pb and Zn immobilisation in contaminated soil.^{9,13} However the use of ABC as a metal stabilization agents in multi-metal contaminated soil has rarely been reported.

In this research we investigated the use of ABC as metal immobilization agents and potential remediation solution for degraded metal contaminated area as mine tailings.

2. Experimental

In this study the mine tailings from Sasa zinc and lead mine in Macedonia were used as an example of metal

contaminated poorly developed mine area soil. The tailings were previously air dried and analyzed for their physical and chemical properties. The tailings had a loamy sand (LS) texture (74.9% sand, 17.4% silt and 7.7% clay). The principal crystalline tailings mineral phases were pyrite (FeS_2), quartz (SiO_2), epidote ($\text{Ca}_2\text{Al}_2\text{FeSi}_3\text{O}_{13}\text{H}$), clinocllore ($\text{Mg}_{3.75}\text{Fe}_{1.25}^{2+}\text{Si}_3\text{Al}_2\text{O}_{10}(\text{OH})_8$), cordierite ($\text{Na}_{0.47}(\text{Mg}_{0.76}\text{Fe}_{1.1}\text{Li}_{0.14})(\text{Al}_{3.6}\text{Be}_{0.4})\text{Si}_5\text{O}_{18}(\text{H}_2\text{O})_{0.8}$), calcite (CaCO_3) and mica ($\text{K}(\text{Mg}_{2.665}\text{Li}_{0.225}\text{Na}_{0.110})(\text{Si}_{3.312}\text{Fe}_{0.688}\text{O}_{10})\text{F}_2$). The total element concentration in tailings was determined as the content of elements soluble in aqua regia according to SIST ISO 11466:1996. The mobility of elements was evaluated according to the SIST EN 12457–4 one-stage batch test (water extraction, S/L = 1:10) and Toxicity Characteristic Leaching Procedure – TCLP.¹⁴ To classify and quantify the metal fractionation in tailings, the modified BCR sequential extraction procedure was conducted.¹⁵ *Exchangeable fraction* was evaluated on 1 g of tailings by extraction with 40 mL of 0.11 mol L⁻¹ acetic acid solution, *reducible fraction* with 40 mL of 0.5 mol L⁻¹ $\text{NH}_2\text{OH} \cdot \text{HCl}$, *oxidizable fraction* with 10 mL of 30 % H_2O_2 and *residual fraction* with 6 mL of HCl, 2 mL of HNO_3 and 2 mL of HF.

The animal bone char (ABC) was air dried and powdered by planetary mill. The physicochemical properties of tailings and ABC are outlined in Table 1.

To immobilize metals in contaminated soil sample, mixtures of tailings with ABC were prepared. ABC was added to tailings at four different application rates: 0.59 g,

1.19 g, 1.82 g and 3.64 g ABC per 100 g of tailings. To achieve sufficient homogenization, the mixtures were prepared as water suspensions, shaken by a mechanical shaker for 1 h and slowly air dried. All of the experiments were carried out in triplicate.

The Toxicity Characteristic Leaching Procedure (TCLP) was carried out to evaluate the metal stabilization efficiency of the ABC.¹⁴ 20 mL of 0.11 M acetic acid (pH = 2.83) were added to 1.000 ± 0.001 g of air-dried samples in 30 mL polypropylene centrifugation tubes. The samples were shaken by a mechanical shaker for 20 hours at 150 rpm. The extractants were separated from the solid residues by centrifugation at 2800 rpm for 15 min and filtered through a cellulose nitrate filter of 0.45 μm pore size (Sartorius, Germany).

The mobility of P in mixtures was evaluated by sodium hydrogen carbonate extraction of mixtures following by spectrometric determination of P according to SIST ISO 11263:1996. The absorbance measurements were carried out at 880 nm.

3. Results and Discussion

Total metal concentration, acetic acid and water extractable metal concentrations in tailings and the corresponding legislative limits are presented in Table 2.

The total concentrations of Cu, Zn, As and Pb in tailings exceeded the critical limits of dangerous substances

Table 1: Physicochemical properties of the mine tailings and ABC.

Tailings sample (T)		ABC sample	
pH value (CaCl_2)	7.46 ± 0.02	pH value (CaCl_2)	7.53 ± 0.04
Cation exchange capacity (cmol kg^{-1})	6.8	Available P content (mg kg^{-1})	600 ± 15
Reduction potential (mV)	392	Total P content (%)	15.5 ± 0.3
Total C content (%)	0.78	Total C content (%)	9.51
Organic C content (%)	0.19	Total N content (%)	0.64
Inorganic C content (%)	0.59	Total H content (%)	0.94

Table 2: Total metal concentration (mg kg^{-1}), TCLP (mg L^{-1}) and water extractable (mg L^{-1}) metal concentrations in tailings with the corresponding legislative limits.

	Cr	Co	Ni	Cu	Zn	As	Cd	Pb
Total metal concentration								
Conc. (mg kg^{-1})	37	15	33	212	2423	93	12	3316
^a Critical level (mg kg^{-1})	380	240	210	300	720	55	12	530
TCLP								
Conc. (mg L^{-1})	0.007	0.010	0.043	0.08	7	0.030	0.046	39
Regulatory levels (mg L^{-1})	5.0	–	–	–	250	5.0	1.0	5.0
Water extracts (S/L = 1:10)								
Conc. (mg L^{-1})	< 0.002	< 0.002	< 0.002	< 0.002	< 0.02	< 0.002	< 0.002	0.031
^b Limit value (mg L^{-1})	0.3	–	0.6	0.6	18	0.3	0.03	0.3

^a The critical legislative limits of dangerous substances in soil.¹⁶ ^b The legislative limits for soil burdening with waste spreading.¹⁷

in the soil stated in Slovenian legislation,¹⁶ whereas the concentrations of metals in water extracts were far below the legal limits.¹⁷ The mobility of metals, evaluated by TCLP, was also quite low, except for Pb which acetic acid extractable concentrations exceed the TCLP regulatory limits by a factor of almost eight.

The partitioning of metals in tailings determined by modified BCR procedure is presented in Figure 1. Pb in tailings was mainly partitioned between exchangeable (29.7 %), residual (27.0 %) and oxidizable fraction (26.4 %). The highest proportion of Cr and As were found in the residual fraction, additionally Co, Ni, Cu, Zn and Cd were mainly partitioned in the residual and oxidizable fraction. Small amounts of metals in exchangeable form indicate that the mobility of metals was quite low, except for Pb, which is in agreement with our TCLP results.

The change in pH values of soil is normally an important mechanism for metal stabilization.¹³ In this study the pH value of ABC was just slightly higher than the pH value of tailings. Therefore, the addition of ABC to tailings did not significantly change the pH of the mixtures (values between 7.44 and 7.56) and therefore have negligible influence on metal bioavailability reduction.

The stabilisation of specific elements in mixtures was estimated by comparing TCLP metal concentrations of mixtures to TCLP metal concentrations of tailings (Fig. 2).

The most efficient stabilization of metals was achieved for Pb. The addition of ABC at application rates of 0.6 %, 1.2 %, 1.8 % and 3.6 % decreased the mobility of Pb to

45 %, 12 %, 5 % and 3 % of the Pb mobility in tailings, respectively. Application of ABC at higher application rates was very effective in reducing the TCLP concentration of Pb to values lower than the USEPA toxic regulatory level (5 mg L^{-1}).¹⁴ Pb mobility reduction could be due to the formation of Pb hydroxyapatite-like minerals ($\text{Pb}_{10}(\text{PO}_4)_6(\text{OH})_2$) by precipitation of Pb and P released from calcium hydroxyapatite.¹³ As shown in Fig. 2, the mobility of P gradually increases with respect to increasing application rate of ABC to tailing, but still remained at environmentally acceptable levels.

High metal stabilization efficiencies were also observed for Cr and Cd, respectively. Their mobility decreased down to 8 % (Cr) and 63 % (Cd) of original mobility in tailings. For both elements the increase in ABC addition resulted in increased stabilization efficiency. On the other hand, the effect of ABC on Zn mobility was quite small. A significant stabilization effect was observed only at the highest ABC application rates (80 % of Zn mobility in tailings), whereas at low application rates, the effect was even slightly destabilizing. As mentioned in literature, a possible removal mechanism for these three elements, besides metal phosphates precipitation, could be due to sorption mechanisms, like surface complexation and ion exchange.^{1,9,18}

Unlike other elements, the mobility of As increased 0.9, 1.3, 1.5 and 2.3 times in mixtures T-ABC(0.6), T-ABC(1.2), T-ABC(1.8) and T-ABC(3.6), respectively. The highest TCLP concentrations of As was 0.069 mg L^{-1} (1.39 mg kg^{-1}) and still remained well below the TCLP re-

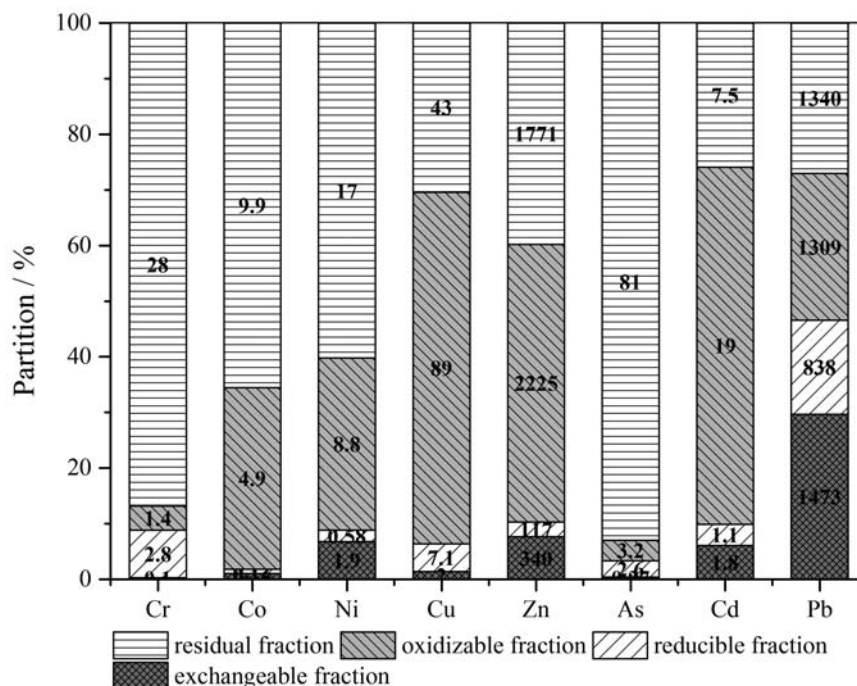


Fig. 1. Partitioning of metals in tailings, determined by modified BCR procedure (with corresponding concentration values in mg of metal per kg of tailings).

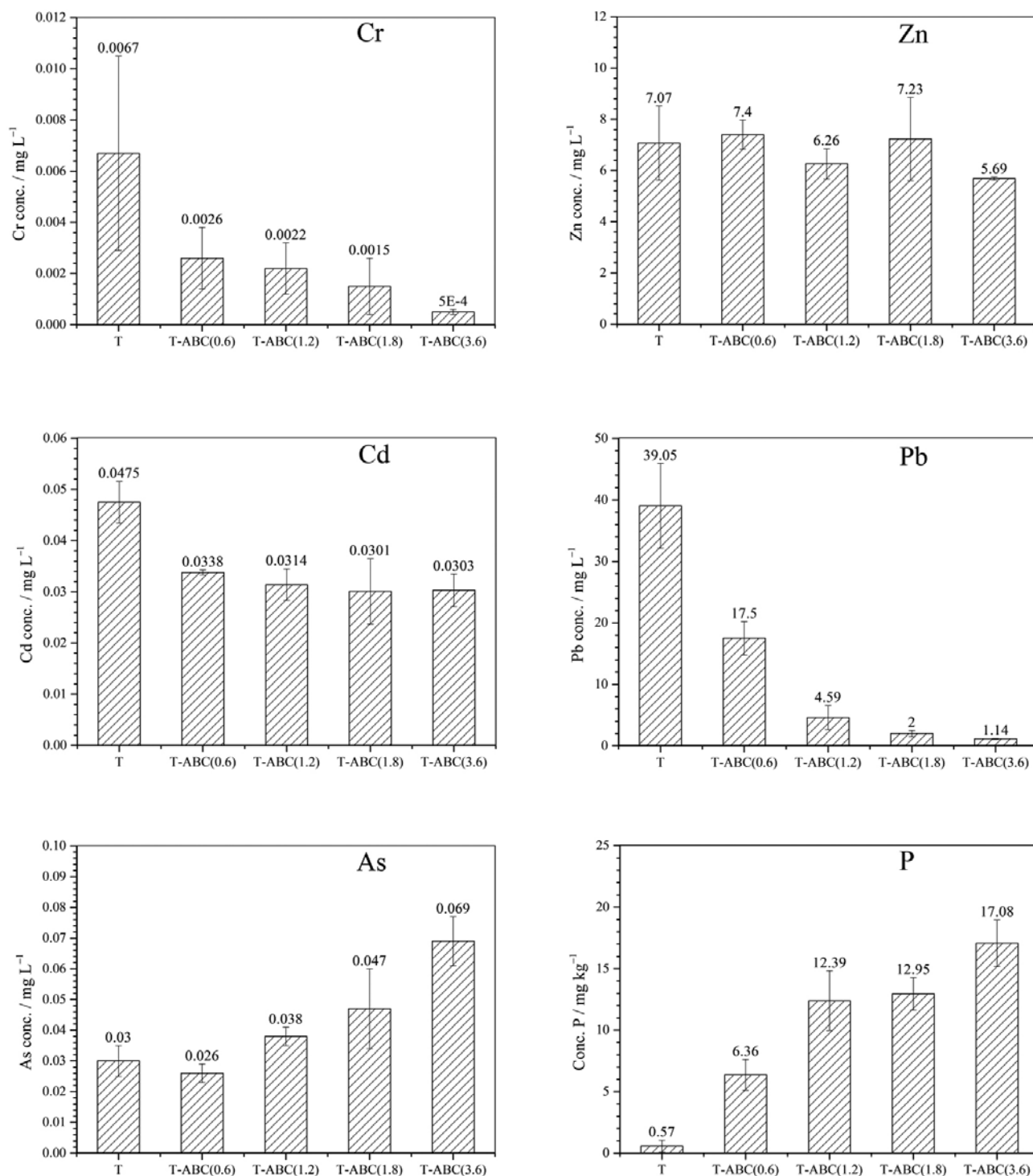


Fig. 2. TCLP concentrations of metals (in mg L⁻¹) and the mobility of P (in mg kg⁻¹) of the tailings and mixtures. Results are presented as the average of three replicates with standard deviations as the error bars.

gulatory value of 5 mg L⁻¹. As(V) species at moderately acidic and neutral pH can be present as arsenate(V) oxyanions.¹⁹ Since the arsenate(V) is very similar to phosphate(V), competitive adsorption could occur and result as increased leaching of As.⁶

4. Conclusions

The addition of ABC to the studied multi-element contaminated mine tailings resulted in a considerable reduction of TCLP-extractable Pb, Cr and Cd in mixtures up

to 3 %, 8 % and 63 % of concentrations in extracts of tailings, respectively. After the treatment, the concentration of acetic acid extractable Pb decreased below the regulatory level stated by TCLP. The addition of ABC gradually induced the desorption of the retained As in tailings and the increased concentration of mobile P in mixtures, but concentrations of As still remained far below TCLP threshold.

In summary, ABC amendments show promising results as metal-stabilization agents, especially for Pb immobilization. However, attention should be paid upon ABC amendments to highly mobile arsenic-metal polluted soil.

5. Acknowledgements

This research study was funded by financial support provided by the Ministry of Higher Education, Science and Technology (P1-0134) of the Republic of Slovenia.

6. References

1. I. R. Sneddon, M. Orueetxebarria, M. E. Hodson, P. F. Schofield, E. Valsami-Jones, *Environ. Pollut.* **2006**, *144*, 816–825. <https://doi.org/10.1016/j.envpol.2006.02.008>
2. L. Beesley, O. S. Inneh, G. J. Norton, E. Moreno-Jimenez, T. Pardo, R. Clemente, J. J. C. Dawson, *Environ. Pollut.* **2014**, *186*, 195–202. <https://doi.org/10.1016/j.envpol.2013.11.026>
3. G. Fellet, M. Marmiroli, L. Marchiol, *Sci. Total Environ.* **2014**, *468-469*, 598–608. <https://doi.org/10.1016/j.scitotenv.2013.08.072>
4. J. Pérez-Esteban, C. Escolástico, A. Masaguer, C. Vargas, A. Moliner, *Chemosphere* **2014**, *103*, 164–171. <https://doi.org/10.1016/j.chemosphere.2013.11.055>
5. D. Houben, L. Evrard, P. Sonnet, *Chemosphere* **2013**, *92*, 1450–1457. <https://doi.org/10.1016/j.chemosphere.2013.03.055>
6. M. Zupančič, S. Lavrič, P. Bukovec, *J. Environ. Monit.* **2012**, *14*, 704–710. <https://doi.org/10.1039/c2em10798h>
7. I. R. Sneddon, M. Orueetxebarria, M. E. Hodson, P. F. Schofield, E. Valsami-Jones, *Appl. Geochem.* **2008**, *23*, 2414–2424. <https://doi.org/10.1016/j.apgeochem.2008.02.028>
8. Z. Y. Huang, J. Li, Y. L. Cao, C. Cai, Z. Zhang, *Geoderma* **2016**, *264*, 126–131. <https://doi.org/10.1016/j.geoderma.2015.10.013>
9. X. W. Hao, Y. Z. Huang, Y. S. Cui, *Acta Ecol. Sin.* **2010**, *30*, 118–122. <https://doi.org/10.1016/j.chnaes.2010.03.012>
10. M. J. Zwetsloot, J. Lehmann, T. Bauerle, S. Vanek, R. Hestrin, A. Nigussie, *Plant Soil* **2016**, *408*, 95–105. <https://doi.org/10.1007/s11104-016-2905-2>
11. U. Iriarte-Velasco, J. L. Ayastuy, L. Zudaire, I. Sierra, *Chem. Eng. J.* **2014**, *251*, 217–227. <https://doi.org/10.1016/j.cej.2014.04.048>
12. J. C. Moreno-Piraján, R. Gómez-Cruz, V. S. García-Cuello, L. Giraldo, *J. Anal. Appl. Pyrol.* **2010**, *89*, 122–128. <https://doi.org/10.1016/j.jaap.2010.06.007>
13. S. B. Chen, Y. G. Zhu, Y. B. Ma, G. McKay, *Environ. Pollut.* **2006**, *139*, 433–439. <https://doi.org/10.1016/j.envpol.2005.06.007>
14. USEPA, SW-846: Test Methods for Evaluating Solid Waste, Physical/Chemical Methods, Analytical Method 1311: Toxicity Characteristic Leaching Procedure, Washington, DC, **2008**.
15. G. Rauret, J. F. Lopez-Sanchez, A. Sahuquillo, R. Rubio, C. Davidson, A. Ure, Ph. Quevauviller, *J. Environ. Monit.* **1999**, *1*, 57–61. <https://doi.org/10.1039/a807854h>
16. Official Gazette of RS, Decree on the limit, warning and critical levels of hazardous substances in the soil, Nos. 68/96 and 41/04 - ZVO-1, **1996**.
17. Official Gazette of RS, Decree on burdening the soil by waste, Nos. 34/08 and 61/11, **2008**.
18. A. H. M. G. Hyder, S. A. Begum, N. O. Egiebor, *J. Environ. Chem. Eng.* **2015**, *3*, 1329–1336. <https://doi.org/10.1016/j.jece.2014.12.005>
19. H. Jin, S. Capareda, Z. Chang, J. Gao, Y. Xu, J. Zhang, *Bioresour. Technol.* **2014**, *169*, 622–629. <https://doi.org/10.1016/j.biortech.2014.06.103>

Povzetek

Namen našega raziskovalnega dela je bil proučiti vpliv dodatka biooglja, pripravljenega iz živalskih kosti (ABC), na mobilnost kovin v jalovinskem materialu. Jalovinskemu materialu smo dodali štiri različne deleže ABC (0,6 g, 1,2 g, 1,8 g in 3,6 g ABC na 100 g jalovine) in določili mobilnost kovin s pomočjo enostopenjske ekstrakcije z 0,11 M očetno kislino (TCLP Toxicity Characteristic Leaching Procedure). Rezultati so pokazali, da se mobilnost Pb, Cr in Cd postopoma zmanjšuje z naraščajočo količino dodanega ABC. Pb je s stališča mejnih vrednosti, določenih s strani TCLP, predstavljal edini problematični element v vzorcu. Koncentracija Pb v očetnokislinskih ekstraktih se je pri treh višjih dodatkih ABC zmanjšala z 39 mg L⁻¹ na vrednosti, ki so bile pod mejno vrednostjo TCLP testa (5 mg L⁻¹). Rezultati so pokazali uporabnost ABC kot učinkovitega stabilizacijskega sredstva za s kovinami onesnažena tla.

Scientific paper

N,N,N',N'-Tetrabutyl-1,10-phenanthroline-2,9-dicarboxamide as Very Effective Extraction Agent for Trivalent Europium and Americium

Emanuel Makrlík,^{1,*} Petr Vaňura,² Pavel Selucký,³ Vasily Babain,^{4,5}
Dmitriy Dar'in⁶ and Mikhail Alyapyshev^{5,7}

¹ Faculty of Environmental Sciences, Czech University of Life Sciences, Prague, Kamýcká 129,
165 21 Prague 6 - Suchbát, Czech Republic

² Department of Analytical Chemistry, University of Chemistry and Technology, Prague, Technická 5,
166 28 Prague 6, Czech Republic

³ Nuclear Research Institute, 250 68 Řež, Czech Republic

⁴ ThreeArc Mining Ltd., 5, Stary Tolmachevskiy per., 115184, Moscow, Russia

⁵ ITMO University, 49, Kronverksky pr., 197101, St. Petersburg, Russia

⁶ Institute of Chemistry, St. Petersburg State University, 7–9, Universitetskaya nab., 199034, St. Petersburg, Russia

⁷ Polymetal International, Narodnogo Opolcheniya 2, 198216, St. Petersburg, Russia

* Corresponding author: E-mail: makrlík@centrum.cz

Phone: +420 376 594 672

Received: 17-02-2017

Abstract

Solvent extraction of microamounts of Eu^{3+} and Am^{3+} from water into nitrobenzene by means of a mixture of hydrogen dicarbollylcobaltate (H^+B^-) and *N,N,N',N'*-tetrabutyl-1,10-phenanthroline-2,9-dicarboxamide (L) was studied. The equilibrium data were explained assuming that the species HL^+ , H_2L^{2+} , HL_2^+ , ML_2^{3+} , and ML_3^{3+} ($\text{M}^{3+} = \text{Eu}^{3+}$, Am^{3+} ; L = *N,N,N',N'*-tetrabutyl-1,10-phenanthroline-2,9-dicarboxamide) are extracted into the nitrobenzene phase. Extraction and stability constants of the cationic complex species in nitrobenzene saturated with water were determined and discussed. From the experimental results it is evident that this effective *N,N,N',N'*-tetrabutyl-1,10-phenanthroline-2,9-dicarboxamide receptor for the Eu^{3+} and Am^{3+} cations could be considered as a potential extraction agent for nuclear waste treatment.

Keywords: Europium and americium; *N,N,N',N'*-Tetrabutyl-1,10-phenanthroline-2,9-dicarboxamide; Extraction and stability constants; Water–nitrobenzene system; Solvent extraction.

1. Introduction

Removal of heavy metals from wastes and soils is a very urgent environmental and technological problem. Solvent extraction is one of the most popular methods for separation of hazardous metals and for radioactive waste processing. One of the most challenging tasks in high-level waste (HLW) processing is the separation of

americium and curium from lanthanides. High selectivity of actinides/lanthanides separation has been achieved when polynitrogen extractants were employed.^{1–9} However, in spite of very high separation factors for americium/europium separation, some ligands proposed so far have demonstrated some disadvantages (e. g., low chemical stability, slow kinetics, and limited solubility in diluents).

Dicarboxylic acid diamides are a subject of active research as potential extractants of actinides (in particular of minor actinides) from radioactive wastes. Important information, concerning substituted malonic diamides has been reported.^{10,11} Lately, interest has shifted to the properties of tetraalkyl-diglycolamides,^{12–15} with emphasis on tetraoctyl-diglycolamide (TODGA), suggested as an extractant of Pu(IV), Np(IV), Am(III), and Cm(III) in solutions with hydrocarbon diluents.^{12–14} The ability of TODGA to extract many other metals has been discussed^{15,16} and the very high extractive capacity of this agent was shown to allow its application as a solid extractant.¹⁷ Complexation of trivalent lanthanides and actinides with several novel diglycolamide-functionalized calixarenes has been studied recently.^{18–20} Besides, some of these functionalized calixarenes have been applied for the isolation of carrier-free ⁹⁰Y from ⁹⁰Sr.²¹

The dicarbollylcobaltate anion²² and some of its halogen derivatives have been employed often for the solvent extraction of various metal cations (e. g., Cs⁺, Sr²⁺, Ba²⁺, Eu³⁺, and Am³⁺) from aqueous solutions into a polar organic phase, both under laboratory conditions for theoretical or analytical purposes,^{23–27} and on the technological scale for the separation of some high-activity isotopes in the reprocessing of spent nuclear fuel and acidic radioactive waste.^{28,29} Furthermore, a process involving chlorinated cobalt dicarbollide, polyethylene glycol, and diphenyl-*N,N*-dibutylcarbamoylmethyl phosphine oxide, also called UNEX, has been suggested for the simultaneous recovery of cesium, strontium, lanthanides, and actinides from highly acidic media into phenyltrifluoromethyl sulfone (abbrev. FS-13).^{28,29} It is necessary to emphasize that the FS-13 diluent was developed for the UNEX process as an alternative organic diluent to the highly polar nitrobenzene. Finally, FS-13 has the advantage of low viscosity and good solubility of metal solvates as well as the UNEX extractants.²⁹ However, in Russia, nitrobenzene derivatives (e.g., 3-nitro- α,α,α -trifluorotoluene, also denoted by F-3) have been successfully utilized as diluents for cobalt dicarbollide processes.²⁸

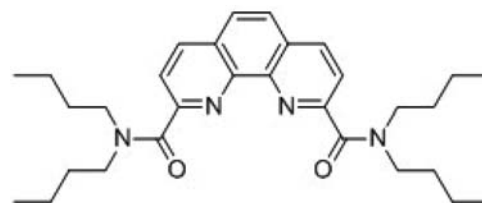
Recently, diamides of 1,10-phenanthroline-2,9-dicarboxylic acid have been proposed as selective extractants for trivalent americium and curium. The mixture of *N,N,N',N'*-tetraoctyl-1,10-phenanthroline-2,9-dicarboxamide and Br-cosan effectively extracts americium with a separation factor ($SF_{Am/Eu}$) over forty.³⁰ High $SF_{Am/Eu}$ values (up to 51) have been also demonstrated for metal extraction by 1,10-phenanthroline-2,9-dicarboxamides from perchloric media.³¹

In the current work, the solvent extraction of microamounts of trivalent europium and americium into nitrobenzene by using hydrogen dicarbollylcobaltate (H^+B^-)²² and *N,N,N',N'*-tetraabutyl-1,10-phenanthroline-2,9-dicarboxamide (abbrev. L; see Scheme 1) was investigated. In this context we must add that the solvent extraction of these trivalent cations into nitrobenzene by means

of the mentioned electroneutral *N,N,N',N'*-tetraabutyl-1,10-phenanthroline-2,9-dicarboxamide ligand (L) is nearly negligible; therefore, the mixture of H^+B^- and L was employed. Moreover, we intended to find the composition of the species in the organic phase of the water–nitrobenzene extraction system and to determine the corresponding equilibrium constants.

2. Experimental

N,N,N',N'-Tetraabutyl-1,10-phenanthroline-2,9-dicarboxamide (puriss., $\geq 99\%$; abbrev. L; see Scheme 1) was supplied by St. Petersburg State University, Russia, and it was employed as received. Cesium dicarbollylcobaltate, Cs^+B^- , was synthesized by the method published by Hawthorne et al.³² Other chemicals used (Lachema, Brno, Czech Republic) were of reagent grade purity. A nitrobenzene solution of hydrogen dicarbollylcobaltate (H^+B^-)²² was prepared from Cs^+B^- by the procedure described elsewhere.³³ The carrier-free radionuclides ^{152,154}Eu³⁺ and ²⁴¹Am³⁺ were obtained from Polatom, Poland; their radionuclidic purities were 99.9%.



Scheme 1. Structural formula of *N,N,N',N'*-tetraabutyl-1,10-phenanthroline-2,9-dicarboxamide (abbrev. L).

The extraction experiments in the two-phase systems water– HNO_3 –^{152,154}Eu³⁺ (ca. 20 kBq)–nitrobenzene – L (*N,N,N',N'*-tetraabutyl-1,10-phenanthroline-2,9-dicarboxamide) – H^+B^- and water– HNO_3 –²⁴¹Am³⁺ (ca. 20 kBq)–nitrobenzene – L (*N,N,N',N'*-tetraabutyl-1,10-phenanthroline-2,9-dicarboxamide) – H^+B^- were performed in 10 mL polypropylene test-tubes with polypropylene stoppers, using 2 mL of each phase. In these extraction systems, the respective initial aqueous phases additionally contained 2×10^{-6} mol/L of $Eu(NO_3)_3$. The test-tubes filled with the solutions were shaken for 30 min at 25 ± 1 °C, using a laboratory shaker. However, under these conditions, the equilibria in the systems under study were established after approximately 5 min of shaking. Then the phases were separated by centrifugation. Finally, 1 mL samples were taken from each phase and their γ -activities were measured by means of a well-type NaI(Tl) scintillation detector connected to a γ -analyzer Triathler (Hidex, Turku, Finland).

The equilibrium distribution ratios of europium and americium, *D*, were determined as the ratios of the corres-

ponding measured radioactivities of $^{152,154}\text{Eu}^{3+}$ and $^{241}\text{Am}^{3+}$ in the nitrobenzene and aqueous samples (the uncertainties of these distribution ratios were always lower than 3%).

3. Results and Discussion

The dependences of the logarithm of the europium and americium distribution ratios ($\log D$) on the logarithm of the numerical value of the total (analytical) concentration of the N,N,N',N' -tetrabutyl-1,10-phenanthroline-2,9-dicarboxamide ligand in the initial nitrobenzene phase, $\log c(L)$, are presented in Figures 1 and 2, as well as in Tables 1 and 2, respectively. The initial concentrations of hydrogen dicarbollycobaltate (H^+B^-) in the organic phase, $c_B = 0.0025$ and 0.005 mol/L, as well as the initial concentration of HNO_3 in the aqueous phase, $c(\text{HNO}_3) = 0.05$ mol/L, are always related to the volume of one phase. The occurrence of the characteristic maxima on these dependences can be explained qualitatively in terms of the competition between the charged trivalent complexes $\text{ML}_{n,\text{org}}^{3+}$ ($\text{M}^{3+} = \text{Eu}^{3+}, \text{Am}^{3+}$) and the protonized ligand L (i.e., HL_{org}^+ , $\text{H}_2\text{L}_{\text{org}}^{2+}$, and $\text{HL}_{2,\text{org}}^+$; in detail, see the text below) during the balancing of the dicarbollycobaltate electrostatic charge in the organic phase, analogously as in our previous work.³⁴

Regarding the results of our previous papers,^{22,25–27,35} the considered water– HNO_3 – M^{3+} (microamounts; $\text{M}^{3+} = \text{Eu}^{3+}, \text{Am}^{3+}$)–nitrobenzene– N,N,N',N' -tetrabutyl-1,10-

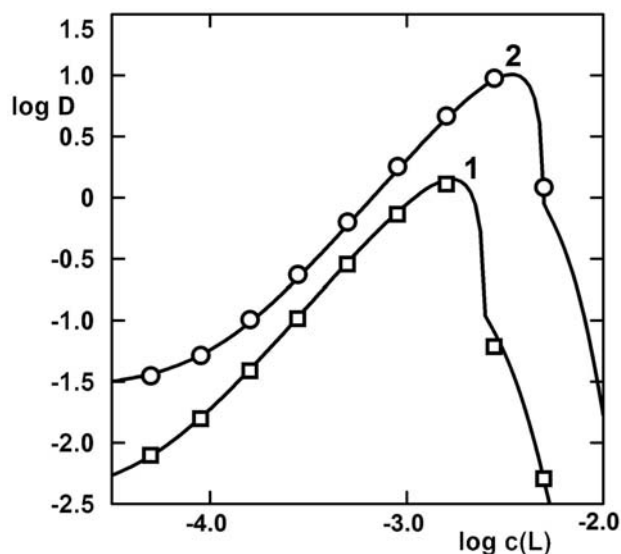


Figure 1. $\log D$ as a function of $\log c(L)$, where $L = N,N,N',N'$ -tetrabutyl-1,10-phenanthroline-2,9-dicarboxamide, for the system water – HNO_3 – Eu^{3+} (microamounts)–nitrobenzene– N,N,N',N' -tetrabutyl-1,10-phenanthroline-2,9-dicarboxamide (L)– H^+B^- ; **1** $c(\text{HNO}_3) = 0.05$ mol/L, $c_B = 0.0025$ mol/L; **2** $c(\text{HNO}_3) = 0.05$ mol/L, $c_B = 0.005$ mol/L. The curves were calculated using the constants given in Table 5.

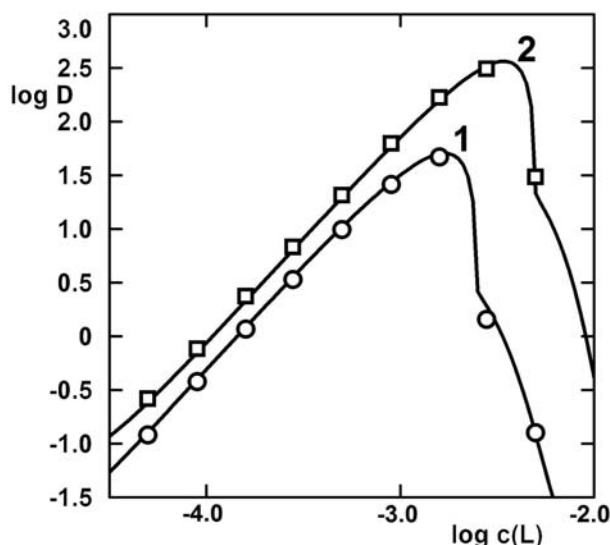


Figure 2. $\log D$ as a function of $\log c(L)$, where $L = N,N,N',N'$ -tetrabutyl-1,10-phenanthroline-2,9-dicarboxamide, for the system water – HNO_3 – Am^{3+} (microamounts)–nitrobenzene– N,N,N',N' -tetrabutyl-1,10-phenanthroline-2,9-dicarboxamide (L)– H^+B^- ; **1** $c(\text{HNO}_3) = 0.05$ mol/L, $c_B = 0.0025$ mol/L; **2** $c(\text{HNO}_3) = 0.05$ mol/L, $c_B = 0.005$ mol/L. The curves were calculated using the constants given in Table 6.

Table 1. Logarithm of the europium distribution ratio ($\log D$) as a function of logarithm of the numerical value of the analytical concentration of the N,N,N',N' -tetrabutyl-1,10-phenanthroline-2,9-dicarboxamide ligand in the initial nitrobenzene phase ($\log c(L)$); the values of $\log c(L)$ and $\log D$ are given for all experimental points.

$c(\text{HNO}_3) = 0.05$ mol/L, $c_B = 0.0025$ mol/L
 –4.301, –2.105; –4.046–1.805; –3.796, –1.413; –3.553, –0.987;
 –3.301, –0.545; –3.046 –0.140; –2.796, 0.109; –2.553, –1.215;
 –2.301 –2.297

$c(\text{HNO}_3) = 0.05$ mol/L, $c_B = 0.005$ mol/L
 –4.301, –1.455; –4.046, –1.288; –3.796, –0.994; –3.553, –0.630;
 –3.301, –0.201; –3.046, 0.252; –2.796, 0.666; –2.553, 0.977;
 –2.301, 0.084

Table 2. Logarithm of the americium distribution ratio ($\log D$) as a function of logarithm of the numerical value of the analytical concentration of the N,N,N',N' -tetrabutyl-1,10-phenanthroline-2,9-dicarboxamide ligand in the initial nitrobenzene phase ($\log c(L)$); the values of $\log c(L)$ and $\log D$ are given for all experimental points.

$c(\text{HNO}_3) = 0.05$ mol/L, $c_B = 0.0025$ mol/L
 –4.301, –0.921; –4.046, –0.422; –3.796, 0.065; –3.553, 0.526;
 –3.301, 0.992; –3.046, 1.414; –2.796, 1.669; –2.553, 0.156;
 –2.301, –0.901

$c(\text{HNO}_3) = 0.05$ mol/L, $c_B = 0.005$ mol/L
 –4.301, –0.584; –4.046, –0.117; –3.796, 0.372; –3.553, 0.831;
 –3.301, 1.313; –3.046, 1.796; –2.796, 2.223; –2.553, 2.491;
 –2.301, 1.482

phenanthroline-2,9-dicarboxamide (L)–H⁺B[−] systems can be described by the set of reactions:



to which the following equilibrium constants correspond:

$$K_D = \frac{[L_{\text{org}}]}{[L_{\text{aq}}]} \quad (7)$$

$$\beta(HL^+_{\text{org}}) = \frac{[HL^+_{\text{org}}]}{[H^+_{\text{org}}][L_{\text{org}}]} \quad (8)$$

$$\beta(H_2L^{2+}_{\text{org}}) = \frac{[H_2L^{2+}_{\text{org}}]}{[H^+_{\text{org}}]^2[L_{\text{org}}]} \quad (9)$$

$$\beta(HL^+_{2,\text{org}}) = \frac{[HL^+_{2,\text{org}}]}{[H^+_{\text{org}}][L_{\text{org}}]^2} \quad (10)$$

$$K_{\text{ex}}(M^{3+}_{\text{org}}) = \frac{[M^{3+}_{\text{org}}][H^+_{\text{aq}}]^3}{[M^{3+}_{\text{aq}}][H^+_{\text{org}}]^3} \quad (11)$$

$$K_{\text{ex}}(ML^{3+}_{n,\text{org}}) = \frac{[ML^{3+}_{n,\text{org}}][H^+_{\text{aq}}]^3}{[M^{3+}_{\text{aq}}][L_{\text{org}}]^n[H^+_{\text{org}}]^3} \quad (12)$$

The subscripts “aq” and “org” denote the aqueous and organic phases, respectively. At this point we must add that Eq. (5) characterizes the investigated two-phase systems for $[L_{\text{org}}] \rightarrow 0$.

A subroutine UBBE, based on the relations given above, the mass balance of the *N,N,N',N'*-tetrabutyl-1,10-phenanthroline-2,9-dicarboxamide (L) ligand and the electroneutrality conditions in both phases of the system under consideration, was formulated^{36,37} and introduced into a more general least-squares minimizing program LETAGROP³⁸ used for determination of the “best” values of the extraction constants $K_{\text{ex}}(ML^{3+}_{n,\text{org}})$ ($M^{3+} = \text{Eu}^{3+}$, Am^{3+} ; $L = N,N,N',N'$ -tetrabutyl-1,10-phenanthroline-2,9-dicarboxamide). The minimum of the sum of uncertainties in log D, i.e., the minimum of the expression

$$U = \sum(\log D_{\text{calc}} - \log D_{\text{exp}})^2 \quad (13)$$

was sought.

The values $\log K_D = 2.2$ (see Table 5, footnote a), $\log\beta(HL^+_{\text{org}}) = 9.4$ (Table 5, footnote b), $\log\beta(H_2L^{2+}_{\text{org}}) = 11.0$ (Table 5, footnote b), $\log\beta(HL^+_{2,\text{org}}) = 12.7$ (Table 5, footnote b), $\log K_{\text{ex}}(\text{Eu}^{3+}_{\text{org}}) = 1.3$ (inferred from Ref. 40), and $K_{\text{ex}}(\text{Am}^{3+}_{\text{org}}) = 1.5$ (inferred from Ref. 40) were used for the respective calculations. The results are listed in Tables 3 and 4. From these tables it is evident that the extraction data can be best explained assuming the complexes ML^{3+}_2 and ML^{3+}_3 ($M^{3+} = \text{Eu}^{3+}$, Am^{3+} ; $L = N,N,N',N'$ -tetrabutyl-1,10-phenanthroline-2,9-dicarboxamide) to be extracted into the nitrobenzene phase.

Table 3. Comparison of various models of europium extraction from aqueous solution of HNO₃ by nitrobenzene solution of H⁺B[−] in the presence of *N,N,N',N'*-tetrabutyl-1,10-phenanthroline-2,9-dicarboxamide (L).

Europium complexes in the organic phase	logK _{ex} ^a	U ^b
EuL ₂ ³⁺	24.31 (24.79)	23.50
EuL ₃ ³⁺	32.84 (33.39)	17.60
EuL ₂ ³⁺ , EuL ₃ ³⁺	23.76 ± 0.21, 31.12(31.41)	0.03

^a The values of the extraction constants are given for each complex. The reliability interval of the constants is given as 3σ(K), where σ(K) is the standard deviation of the constant K.³⁸ These values are given in the logarithmic scale using the approximate expression $\log K \pm \{\log [K+1.5\sigma(K)] - \log [K-1.5\sigma(K)]\}$. For σ(K) > 0.2 K, the previous expression is not valid and then only the upper limit is given in the parentheses in the form of log K (log [K + 3σ(K)]).³⁸

^b The error-square sum $U = \sum(\log D_{\text{calc}} - \log D_{\text{exp}})^2$.

Table 4. Comparison of various models of americium extraction from aqueous solution of HNO₃ by nitrobenzene solution of H⁺B[−] in the presence of *N,N,N',N'*-tetrabutyl-1,10-phenanthroline-2,9-dicarboxamide (L).

Americium complexes in the organic phase	logK _{ex} ^a	U ^b
AmL ₂ ³⁺	25.92 (26.59)	20.14
AmL ₃ ³⁺	34.46 (35.17)	16.98
AmL ₂ ³⁺ , AmL ₃ ³⁺	25.15 ± 0.22, 32.24(32.52)	0.02

^a See Table 3, footnote a. ^b See Table 3, footnote b.

Knowing the values $K_{\text{ex}}(\text{Eu}^{3+}_{\text{org}}) = 1.3$ and $\log K_{\text{ex}}(\text{Am}^{3+}_{\text{org}})$, which were inferred from Ref. 40, as well as the extraction constants $\log K_{\text{ex}}(\text{EuL}^{3+}_{2,\text{org}}) = 23.76$, $\log K_{\text{ex}}(\text{EuL}^{3+}_{3,\text{org}}) = 31.12$, $\log K_{\text{ex}}(\text{AmL}^{3+}_{2,\text{org}}) = 25.15$, and $\log K_{\text{ex}}(\text{AmL}^{3+}_{3,\text{org}}) = 32.24$ (Tables 5 and 6), the stability constants of the complexes ML^{3+}_2 and ML^{3+}_3 ($M^{3+} = \text{Eu}^{3+}$, Am^{3+} ; $L = N,N,N',N'$ -tetrabutyl-1,10-phenanthroline-2,9-dicarboxamide) in the nitrobenzene phase defined as

$$\beta(ML^{3+}_{2,\text{org}}) = \frac{[ML^{3+}_{2,\text{org}}]}{[M^{3+}_{\text{org}}][L_{\text{org}}]^2} \quad (14)$$

$$\beta(ML^{3+}_{3,\text{org}}) = \frac{[ML^{3+}_{3,\text{org}}]}{[M^{3+}_{\text{org}}][L_{\text{org}}]^3} \quad (15)$$

can be calculated employing the following simple relations:

$$\log \beta(\text{ML}_{2,\text{org}}^{3+}) = \log K_{\text{ex}}(\text{ML}_{2,\text{org}}^{3+}) - \log K_{\text{ex}}(\text{M}_{\text{org}}^{3+}) \quad (16)$$

$$\log \beta(\text{ML}_{3,\text{org}}^{3+}) = \log K_{\text{ex}}(\text{ML}_{3,\text{org}}^{3+}) - \log K_{\text{ex}}(\text{M}_{\text{org}}^{3+}) \quad (17)$$

The respective equilibrium constants are summarized in Tables 5 and 6. It should be noted that the stability constants of the cationic complex species $\text{ML}_{2,\text{org}}^{3+}$ and $\text{ML}_{3,\text{org}}^{3+}$ ($\text{M}^{3+} = \text{Eu}^{3+}, \text{Am}^{3+}$; $\text{L} = N,N,N',N'$ -tetrabutyl-1,10-phenanthroline-2,9-dicarboxamide) in water-saturated nitrobenzene are $\log\beta(\text{EuL}_{2,\text{org}}^{3+}) = 22.46$, $\log\beta(\text{AmL}_{2,\text{org}}^{3+}) = 23.65$, $\log\beta(\text{EuL}_{3,\text{org}}^{3+}) = 29.82$, and $\log\beta(\text{AmL}_{3,\text{org}}^{3+}) = 30.74$, as given in Tables 5 and 6. This means that in the mentioned nitrobenzene medium, the stability constants of the complexes $\text{AmL}_{2,\text{org}}^{3+}$ and $\text{AmL}_{3,\text{org}}^{3+}$ are somewhat higher than those of the corresponding cationic complex species $\text{EuL}_{2,\text{org}}^{3+}$ and $\text{EuL}_{3,\text{org}}^{3+}$.

Moreover, Figure 3 presents the contributions of the species $\text{H}_{\text{org}}^{+}$, $\text{HL}_{\text{org}}^{+}$, $\text{H}_2\text{L}_{\text{org}}^{2+}$, and HL_2^{+} to the total hydro-

Table 5. Equilibrium constants in the water– HNO_3 – Eu^{3+} (microamounts)–nitrobenzene– N,N,N',N' -tetrabutyl-1,10-phenanthroline-2,9-dicarboxamide (L)– H^+B^- system.

Equilibrium	log K
$\text{L}_{\text{aq}} \rightleftharpoons \text{L}_{\text{org}}$	2.2 ^a
$\text{H}_{\text{org}}^{+} + \text{L}_{\text{org}} \rightleftharpoons \text{HL}_{\text{org}}^{+}$	9.4 ^b
$2\text{H}_{\text{org}}^{+} + \text{L}_{\text{org}} \rightleftharpoons \text{H}_2\text{L}_{\text{org}}^{2+}$	11.0 ^b
$\text{H}_{\text{org}}^{+} + 2\text{L}_{\text{org}} \rightleftharpoons \text{HL}_2^{+}$	12.7 ^b
$\text{Eu}_{\text{aq}}^{3+} + 3\text{H}_{\text{org}}^{+} \rightleftharpoons \text{Eu}_{\text{org}}^{3+} + 3\text{H}_{\text{aq}}^{+}$	1.3 ^c
$\text{Eu}_{\text{aq}}^{3+} + 2\text{L}_{\text{org}} + 3\text{H}_{\text{org}}^{+} \rightleftharpoons \text{EuL}_{2,\text{org}}^{3+} + 3\text{H}_{\text{aq}}^{+}$	23.76
$\text{Eu}_{\text{aq}}^{3+} + 3\text{L}_{\text{org}} + 3\text{H}_{\text{org}}^{+} \rightleftharpoons \text{EuL}_{3,\text{org}}^{3+} + 3\text{H}_{\text{aq}}^{+}$	31.12
$\text{Eu}_{\text{org}}^{3+} + 2\text{L}_{\text{org}} \rightleftharpoons \text{EuL}_{2,\text{org}}^{3+}$	22.46
$\text{Eu}_{\text{org}}^{3+} + 3\text{L}_{\text{org}} \rightleftharpoons \text{EuL}_{3,\text{org}}^{3+}$	29.82

^a Determined by the method of the concentration dependent distribution.³⁹ ^b Determined by the method described in Ref. 34. ^c Inferred from Ref. 40.

Table 6. Equilibrium constants in the water– HCl – Am^{3+} (microamounts)–nitrobenzene– N,N,N',N' -tetrabutyl-1,10-phenanthroline-2,9-dicarboxamide (L)– H^+B^- system.

Equilibrium	log K
$\text{L}_{\text{aq}} \rightleftharpoons \text{L}_{\text{org}}$	2.2 ^a
$\text{H}_{\text{org}}^{+} + \text{L}_{\text{org}} \rightleftharpoons \text{HL}_{\text{org}}^{+}$	9.4 ^b
$2\text{H}_{\text{org}}^{+} + \text{L}_{\text{org}} \rightleftharpoons \text{H}_2\text{L}_{\text{org}}^{2+}$	11.0 ^b
$\text{H}_{\text{org}}^{+} + 2\text{L}_{\text{org}} \rightleftharpoons \text{HL}_2^{+}$	12.7 ^b
$\text{Am}_{\text{aq}}^{3+} + 3\text{H}_{\text{org}}^{+} \rightleftharpoons \text{Am}_{\text{org}}^{3+} + 3\text{H}_{\text{aq}}^{+}$	1.5 ^c
$\text{Am}_{\text{aq}}^{3+} + 2\text{L}_{\text{org}} + 3\text{H}_{\text{org}}^{+} \rightleftharpoons \text{AmL}_{2,\text{org}}^{3+} + 3\text{H}_{\text{aq}}^{+}$	25.15
$\text{Am}_{\text{aq}}^{3+} + 3\text{L}_{\text{org}} + 3\text{H}_{\text{org}}^{+} \rightleftharpoons \text{AmL}_{3,\text{org}}^{3+} + 3\text{H}_{\text{aq}}^{+}$	32.24
$\text{Am}_{\text{org}}^{3+} + 2\text{L}_{\text{org}} \rightleftharpoons \text{AmL}_{2,\text{org}}^{3+}$	23.65
$\text{Am}_{\text{org}}^{3+} + 3\text{L}_{\text{org}} \rightleftharpoons \text{AmL}_{3,\text{org}}^{3+}$	30.74

^a Determined by the method of the concentration dependent distribution.³⁹ ^b Determined by the method described in Ref. 34. ^c Inferred from Ref. 40.

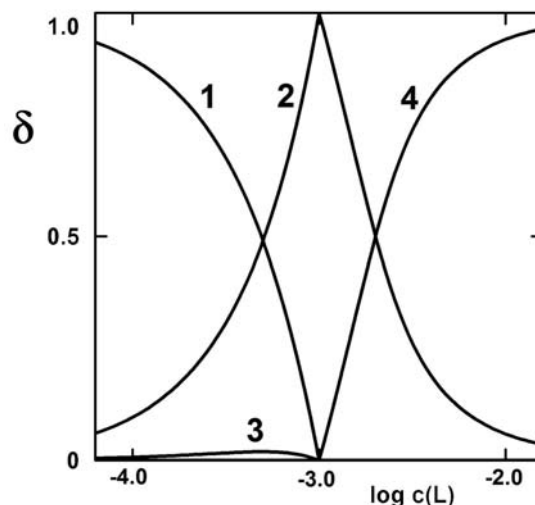


Figure 3. Distribution diagram of hydrogen cation in the equilibrium nitrobenzene phase of the water– HNO_3 – Eu^{3+} (microamounts)–nitrobenzene– N,N,N',N' -tetrabutyl-1,10-phenanthroline-2,9-dicarboxamide (L)– H^+B^- extraction system in the forms of H^+ , H_2L^{2+} , and HL_2^+ ; $c(\text{HNO}_3) = 0.05$ mol/L, $c_{\text{B}} = 0.0025$ mol/L. 1 $\delta(\text{H}^+) = [\text{H}_{\text{org}}^+]/c(\text{H}^+)_{\text{org}}$, 2 $\delta(\text{HL}^+) = [\text{HL}_{\text{org}}^+]/c(\text{H}^+)_{\text{org}}$, 3 $\delta(\text{H}_2\text{L}^{2+}) = 2[\text{H}_2\text{L}_{\text{org}}^{2+}]/c(\text{H}^+)_{\text{org}}$, 4 $\delta(\text{HL}_2^+) = [\text{HL}_2^+]/c(\text{H}^+)_{\text{org}}$, where $c(\text{H}^+)_{\text{org}} = [\text{H}_{\text{org}}^+] + [\text{HL}_{\text{org}}^+] + 2[\text{H}_2\text{L}_{\text{org}}^{2+}] + [\text{HL}_2^+]$. The distribution curves were calculated using the constants given in Table 5.

gen cation concentration in the equilibrium nitrobenzene phase, whereas Figures 4 and 5 show the contributions of the cations $\text{M}_{\text{org}}^{3+}$, $\text{ML}_{2,\text{org}}^{3+}$, and $\text{ML}_{3,\text{org}}^{3+}$ ($\text{M}^{3+} = \text{Eu}^{3+}, \text{Am}^{3+}$; $\text{L} = N,N,N',N'$ -tetrabutyl-1,10-phenanthroline-2,9-dicar-

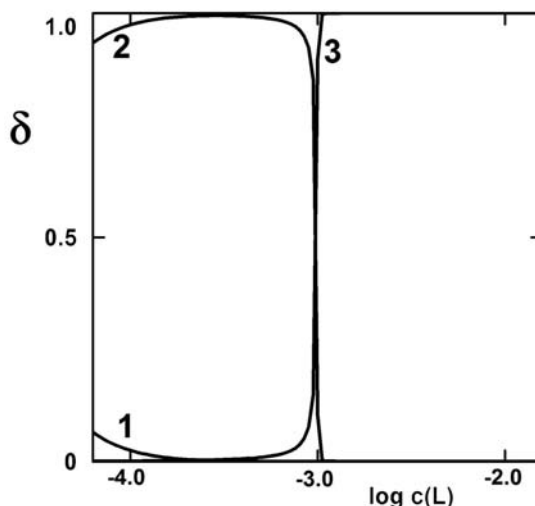


Figure 4. Distribution diagram of europium in the equilibrium nitrobenzene phase of the water– HNO_3 – Eu^{3+} (microamounts)–nitrobenzene– N,N,N',N' -tetrabutyl-1,10-phenanthroline-2,9-dicarboxamide (L)– H^+B^- extraction system in the forms of Eu^{3+} , $\text{EuL}_{2,\text{org}}^{3+}$, and $\text{EuL}_{3,\text{org}}^{3+}$; $c(\text{HNO}_3) = 0.05$ mol/L, $c_{\text{B}} = 0.0025$ mol/L. 1 $\delta(\text{Eu}^{3+}) = [\text{Eu}_{\text{org}}^{3+}]/c(\text{Eu}^{3+})_{\text{org}}$, 2 $\delta(\text{EuL}_{2,\text{org}}^{3+}) = [\text{EuL}_{2,\text{org}}^{3+}]/c(\text{Eu}^{3+})_{\text{org}}$, 3 $\delta(\text{EuL}_{3,\text{org}}^{3+}) = [\text{EuL}_{3,\text{org}}^{3+}]/c(\text{Eu}^{3+})_{\text{org}}$, where $c(\text{Eu}^{3+})_{\text{org}} = [\text{Eu}_{\text{org}}^{3+}] + [\text{EuL}_{2,\text{org}}^{3+}] + [\text{EuL}_{3,\text{org}}^{3+}]$. The distribution curves were calculated using the constants given in Table 5.

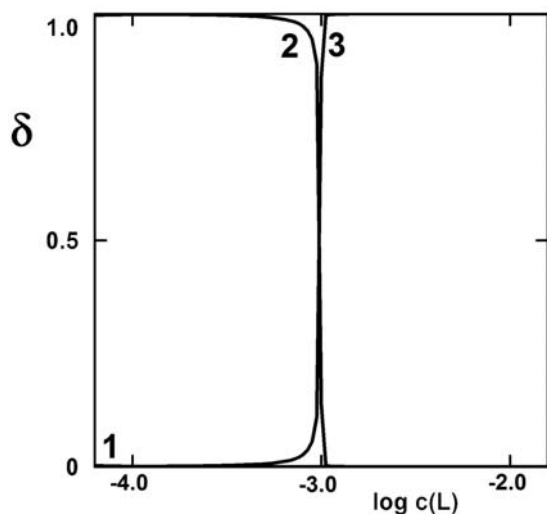
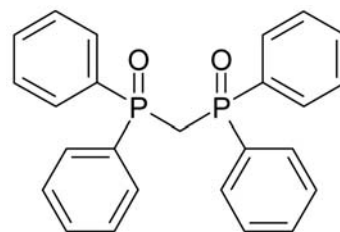


Figure 5. Distribution diagram of americium in the equilibrium nitrobenzene phase of the water–HNO₃–Am³⁺ (microamounts)–nitrobenzene–*N,N,N',N'*-tetrabutyl-1,10-phenanthroline-2,9-dicarboxamide (L)–H⁺B⁻ extraction system in the forms of Am³⁺, AmL₂³⁺, and AmL₃³⁺; c(HNO₃) = 0.05 mol/L, c_B = 0.0025 mol/L. **1** $\delta(\text{Am}^{3+}) = [\text{Am}_{\text{org}}^{3+}]/c(\text{Am}^{3+})_{\text{org}}$, **2** $\delta(\text{Am}_2^{3+}) = [\text{AmL}_{2,\text{org}}^{3+}]/c(\text{Am}^{3+})_{\text{org}}$, **3** $\delta(\text{AmL}_3^{3+}) = [\text{AmL}_{3,\text{org}}^{3+}]/c(\text{Am}^{3+})_{\text{org}}$, where $c(\text{Am}^{3+})_{\text{org}} = [\text{Am}_{\text{org}}^{3+}] + [\text{AmL}_{2,\text{org}}^{3+}] + [\text{AmL}_{3,\text{org}}^{3+}]$. The distribution curves were calculated using the constants given in Table 6.

boxamide) to the total trivalent metal cation concentrations in the corresponding equilibrium organic phase. From Figures 3, 4, and 5 it follows that the species HL_{2,org}⁺, EuL_{3,org}³⁺, and AmL_{3,org}³⁺ are present in significant concentrations only at relatively high amounts of the *N,N,N',N'*-tetrabutyl-1,10-phenanthroline-2,9-dicarboxamide (L) ligand in the systems under consideration. On the other hand, the contributions of the cations H₂L_{org}²⁺, Eu_{org}³⁺, and Am_{org}³⁺ are very small, as also follows from Figures 3, 4, and 5.

Finally, Table 7 summarizes the stability constants of the complex species ML₂³⁺ and ML₃³⁺ (M³⁺ = Eu³⁺, Am³⁺) with two electroneutral ligands L (L = *N,N,N',N'*-tetrabutyl-1,10-phenanthroline-2,9-dicarboxamide, bis(diphenylphosphino)methane dioxide (DPPMDO) – see Scheme 2) in water-saturated nitrobenzene. From the data re-



Scheme 2. Structural formula of bis(diphenylphosphino)methane dioxide (abbrev. DPPMDO).

viewed in this table it is apparent that in the considered nitrobenzene medium, the stabilities of the complexes ML_{2,org}³⁺ and ML_{3,org}³⁺ (M³⁺ = Eu³⁺, Am³⁺) containing *N,N,N',N'*-tetrabutyl-1,10-phenanthroline-2,9-dicarboxamide ligand are essentially higher than those of respective cationic complexes ML_{2,org}³⁺ and ML_{3,org}³⁺ (M³⁺ = Eu³⁺, Am³⁺) with the ligand DPPMDO. It means that complexation ability towards Eu³⁺ and Am³⁺ of the *N,N,N',N'*-tetrabutyl-1,10-phenanthroline-2,9-dicarboxamide ligand under study is also substantially higher than that of the DPPMDO ligand.

In conclusion, we must state that the separation factors SF_{Am/Eu}, reached in the studied two-phase water–nitrobenzene extraction system, defined by means of the corresponding equilibrium distribution ratios, D(Am³⁺) / D(Eu³⁺), are in the range from 12 to 38. This fact follows from the results presented in Figures 1 and 2 or in Tables 1 and 2, respectively.

4. Conclusions

In the present work, the solvent extraction of trivalent europium and americium from acidic aqueous solutions into nitrobenzene was investigated by means of a mixture of hydrogen dicarbollyl cobaltate (H⁺B⁻) and *N,N,N',N'*-tetrabutyl-1,10-phenanthroline-2,9-dicarboxamide (L). It was proven that the cationic species HL₂⁺, H₂L_{org}²⁺, HL₂⁺, ML₂³⁺ and ML₃³⁺ (M³⁺ = Eu³⁺, Am³⁺; L = *N,N,N',N'*-tetrabutyl-1,10-phenanthroline-2,9-dicarboxamide) are extracted into the organic phase of the water–ni-

Table 7. Stability constants of the complexes ML₂³⁺ and ML₃³⁺ (M³⁺ = Eu³⁺, Am³⁺; L = *N,N,N',N'*-tetrabutyl-1,10-phenanthroline-2,9-dicarboxamide, bis(diphenylphosphino)methane dioxide (DPPMDO) – see Scheme 2) in nitrobenzene saturated with water at 25 °C.

Quantity	L	
	DPPMDO ^a	<i>N,N,N',N'</i> -tetrabutyl-1,10-phenanthroline-2,9-dicarboxamide ^b
log β(EuL _{2,org} ³⁺)	17.76	22.46
log β(EuL _{3,org} ³⁺)	24.59	29.82
log β(AmL _{2,org} ³⁺)	17.73	23.65
log β(AmL _{3,org} ³⁺)	24.72	30.74

^a Ref. 27. ^b This work.

trobenzene system. It was found that in nitrobenzene saturated with water, the stability constants of the complexes $\text{AmL}_{2,\text{org}}^{3+}$ and $\text{AmL}_{3,\text{org}}^{3+}$ are somewhat higher than those of the corresponding cationic species $\text{EuL}_{2,\text{org}}^{3+}$ and $\text{EuL}_{3,\text{org}}^{3+}$. Finally, it was evidenced experimentally that the N,N,N',N' -tetrabutyl-1,10-phenanthroline-2,9-dicarboxamide ligand can be considered in the nitrobenzene medium as the very strong receptor for the Eu^{3+} and Am^{3+} cations. On the basis of the previous facts it is obvious that this investigated electroneutral ligand L could be also considered as a potential extraction agent for nuclear waste treatment.

5. Acknowledgements

This work was supported by the Grant Agency of Faculty of Environmental Sciences, Czech University of Life Sciences, Prague, Project No.: 42900/1312/3114 entitled “Environmental Aspects of Sustainable Development of Society,” by the Czech Ministry of Education, Youth, and Sports, Project MSM No.: 20/2015, and finally, by the Government of Russian Federation, Grant No.: 074-001.

6. References

1. T. Retegan, L. Berthon, C. Ekberg, A. Fermvik, G. Skarnermark, N. Zorz, *Solvent Extr. Ion Exch.* **2009**, *27*, 663–682. <http://dx.doi.org/10.1080/07366290903113991>
2. A. Fermvik, C. Ekberg, S. Englund, M. R. S. J. Foreman, G. Modolo, T. Retegan, G. Skarnermark, *Radiochim. Acta* **2009**, *97*, 319–324. <http://dx.doi.org/10.1524/ract.2009.1615>
3. D. Magnusson, B. Christiansen, R. Malmbeck, J.-P. Glatz, *Radiochim. Acta* **2009**, *97*, 497–502. <http://dx.doi.org/10.1524/ract.2009.1647>
4. D. Magnusson, B. Christiansen, M. R. S. Foreman, A. Geist, J.-P. Glatz, R. Malmbeck, G. Modolo, D. Serrano-Purroy, C. Sorel, *Solvent Extr. Ion Exch.* **2009**, *27*, 97–106. <http://dx.doi.org/10.1080/07366290802672204>
5. F. W. Lewis, L. M. Harwood, M. J. Hudson, M. G. B. Drew, J. F. Desreux, G. Vidick, N. Bouslimani, G. Modolo, A. Wilden, M. Sypula, T.-H. Vu, J.-P. Simonin, *J. Am. Chem. Soc.* **2011**, *133*, 13093–13102. <http://dx.doi.org/10.1021/ja203378m>
6. M. J. Hudson, L. M. Harwood, D. M. Laventine, F. W. Lewis, *Inorg. Chem.* **2013**, *52*, 3414–3428. <http://dx.doi.org/10.1021/ic3008848>
7. A. Bremer, D. M. Whittaker, C. A. Sharrad, A. Geist, P. J. Panak, *Dalton Trans.* **2014**, *43*, 2684–2694. <http://dx.doi.org/10.1039/C3DT52204K>
8. F. W. Lewis, M. J. Hudson, L. M. Harwood, *Synlett* **2011**, *18*, 2609–2632. <http://dx.doi.org/10.1055/s-0030-1289557>
9. P. J. Panak, A. Geist, *Chem. Rev.* **2013**, *113*, 1199–1236. <http://dx.doi.org/10.1021/cr3003399>
10. C. Cuillerdier, C. Musikas, P. Hoel, L. Nigond, X. Vitart, *Separ. Sci. Technol.* **1991**, *26*, 1229–1244. <http://dx.doi.org/10.1080/01496399108050526>
11. V. K. Manchanda, P. N. Pathak, *Separ. Pur. Technol.* **2004**, *35*, 85–103. <http://dx.doi.org/10.1016/j.seppur.2003.09.005>
12. Y. Sasaki, G. R. Choppin, *Anal. Sci.* **1996**, *12*, 225–230. <http://dx.doi.org/10.2116/analsci.12.225>
13. Y. Sasaki, Y. Sugo, S. Suzuki, S. Tachimori, *Solvent Extr. Ion Exch.* **2001**, *19*, 91–103.
14. Y. Sasaki, S. Tachimori, *Solvent Extr. Ion Exch.* **2002**, *20*, 21–34. <http://dx.doi.org/10.1081/SEI-100108822>
15. Y. Sasaki, Y. Sugo, S. Suzuki, T. Kimura, *Anal. Chim. Acta* **2005**, *543*, 31–37. <http://dx.doi.org/10.1016/j.aca.2005.04.061>
16. S. A. Ansari, P. N. Pathak, V. K. Manchanda, M. Husain, A. K. Prasad, V. S. Parmar, *Solvent Extr. Ion Exch.* **2005**, *23*, 463–479. <http://dx.doi.org/10.1081/SEI-200066296>
17. E. P. Horwitz, D. R. McAlister, A. H. Bond, R. E. Barrans, Jr., *Solvent Extr. Ion Exch.* **2005**, *23*, 319–344. <http://dx.doi.org/10.1081/SEI-200049898>
18. M. Iqbal, P. K. Mohapatra, S. A. Ansari, J. Huskens, W. Verboom, *Tetrahedron* **2012**, *68*, 7840–7847. <http://dx.doi.org/10.1016/j.tet.2012.07.036>
19. P. K. Mohapatra, M. Iqbal, D. R. Raut, W. Verboom, J. Huskens, S. V. Godbole, *Dalton Trans.* **2012**, *41*, 360–363. <http://dx.doi.org/10.1039/c1dt11561h>
20. D. R. Raut, P. K. Mohapatra, S. A. Ansari, S. V. Godbole, M. Iqbal, D. Manna, T. K. Ghanty, J. Huskens, W. Verboom, *RSC Advances* **2013**, *3*, 9296–9303. <http://dx.doi.org/10.1039/c3ra40241j>
21. P. K. Mohapatra, D. R. Raut, M. Iqbal, J. Huskens, W. Verboom, *Appl. Radiat. Isot.* **2014**, *85*, 133–138. <http://dx.doi.org/10.1016/j.apradiso.2013.12.010>
22. E. Makrlík, P. Vaňura, *Talanta* **1985**, *32*, 423–429. [http://dx.doi.org/10.1016/0039-9140\(85\)80110-7](http://dx.doi.org/10.1016/0039-9140(85)80110-7)
23. E. Makrlík, P. Vaňura, P. Selucký, *J. Solut. Chem.* **2009**, *38*, 1129–1138. <http://dx.doi.org/10.1007/s10953-009-9434-z>
24. E. Makrlík, P. Vaňura, P. Selucký, *J. Solut. Chem.* **2010**, *39*, 692–700. <http://dx.doi.org/10.1007/s10953-010-9525-x>
25. E. Makrlík, P. Vaňura, P. Selucký, V. A. Babain, I. V. Smirnov, *Acta Chim. Slov.* **2009**, *56*, 718–722.
26. E. Makrlík, P. Vaňura, Z. Sedláková, *J. Radioanal. Nucl. Chem.* **2010**, *283*, 157–161. <http://dx.doi.org/10.1007/s10967-009-0134-3>
27. E. Makrlík, Z. Spíchal, P. Vaňura, P. Selucký, *J. Radioanal. Nucl. Chem.* **2013**, *295*, 2135–2140. <http://dx.doi.org/10.1007/s10967-012-2227-7>
28. V. N. Romanovskiy, I. V. Smirnov, V. A. Babain, T. A. Todd, R. S. Herbst, J. D. Law, K. N. Brewer, *Solvent Extr. Ion Exch.* **2001**, *19*, 1–21. <http://dx.doi.org/10.1081/SEI-100001370>
29. J. D. Law, R. S. Herbst, T. A. Todd, V. N. Romanovskiy, V. A. Babain, V. M. Esimantovskiy, I. V. Smirnov, B. N. Zaitsev, *Solvent Extr. Ion Exch.* **2001**, *19*, 23–36. <http://dx.doi.org/10.1081/SEI-100001371>

30. M. Galletta, S. Scaravaggi, E. Macerata, A. Famulari, A. Mele, W. Panzeri, F. Sansone, A. Casnati, M. Mariani, *Dalton Trans.* **2013**, 42, 16930–16938. <http://dx.doi.org/10.1039/c3dt52104d>
31. D. Manna, S. Mula, A. Bhattacharyya, S. Chattopadhyay, T. K. Ghanty, *Dalton Trans.* **2015**, 44, 1332–1340. <http://dx.doi.org/10.1039/c4dt02402h>
32. M. F. Hawthorne, D. C. Young, T. D. Andrews, D. V. Howe, R. L. Pilling, A. D. Pitts, M. Reintjes, L. F. Warren, P. A. Wegner, *J. Am. Chem. Soc.* **1968**, 90, 879–896. <http://dx.doi.org/10.1021/ja01006a008>
33. E. Makrlík, *Collect. Czech. Chem. Commun.* **1992**, 57, 289–295. <https://doi.org/10.1135/cccc19920289>
34. P. Vaňura, J. Rais, P. Selucký, M. Kyrš, *Collect. Czech. Chem. Commun.* **1979**, 44, 157–166. <https://doi.org/10.1135/cccc19790157>
35. E. Makrlík, P. Vaňura, Z. Spíchal, P. Selucký, *J. Radioanal. Nucl. Chem.* **2013**, 298, 243–248. <http://dx.doi.org/10.1007/s10967-013-2517-8>
36. P. Vaňura, E. Makrlík, J. Rais, M. Kyrš, *Collect. Czech. Chem. Commun.* **1982**, 47, 1444–1464. <https://doi.org/10.1135/cccc19821444>
37. P. Vaňura, E. Makrlík, *Collect. Czech. Chem. Commun.* **1993**, 58, 1324–1336. <https://doi.org/10.1135/cccc19931324>
38. L. G. Sillén, B. Warnqvist, *Arkiv Kemi* **1969**, 31, 315–339.
39. J. Rais, E. Šebestová, P. Selucký, M. Kyrš, *J. Inorg. Nucl. Chem.* **1976**, 38, 1742–1744. [http://dx.doi.org/10.1016/0022-1902\(76\)80673-2](http://dx.doi.org/10.1016/0022-1902(76)80673-2)
40. J. Rais, S. Tachimori, *Separ. Sci. Technol.* **1994**, 29, 1347–1365. <http://dx.doi.org/10.1080/01496399408006945>

Povzetek

Proučevali smo ekstrakcijo mikrokoličin Eu^{3+} in Am^{3+} iz vode v nitrobenzen s pomočjo mešanice hidrogen dikarbollkobaltata (H^+B^-) in *N,N,N',N'*-tetrabutyl-1,10-fenantrolin-2,9-dikarboksamida (L). Ravnotežje smo obravnavali s predpostavko, da se kompleksi HL^+ , H_2L^{2+} , HL_2^+ , ML_2^{3+} , in ML_3^{3+} ($\text{M}^{3+} = \text{Eu}^{3+}, \text{Am}^{3+}$) ekstrahirajo v fazo nitrobenzena. Določili smo konstante ekstrakcije in stabilnosti kationskih kompleksov v nitrobenzenu, nasičenem z vodo. Iz dobljenih eksperimentalnih podatkov je razvidno, da *N,N,N',N'*-tetrabutyl-1,10-fenantrolin-2,9-dikarboksamid sodeluje kot receptor za Eu^{3+} in Am^{3+} ter bi ga torej lahko uporabljali pri ravnanju z z jedrskimi odpadki.

Scientific paper

Ionic Liquid-Assisted Liquid–Liquid Microextraction based on the Solidification of Floating Organic Droplet in Sample Preparation for Simultaneous Determination of Herbicide Residues in Fruits

Jitlada Vichapong,^{1,*} Yanawath Santaladchaiyakit,² Rodjana Burakham³
and Supalax Srijarana³

¹ Creative Chemistry and Innovation Research Unit, Department of Chemistry and Center of Excellence for Innovation in Chemistry, Faculty of Science, Maharakham University, Maharakham 44150, Thailand

² Department of Chemistry, Faculty of Engineering, Rajamangala University of Technology Isan, Khon Kaen Campus, Khon Kaen 40000, Thailand

³ Materials Chemistry Research Center, Department of Chemistry and Center of Excellence for Innovation in Chemistry, Faculty of Science, Khon Kaen University, Khon Kaen 40002, Thailand

* Corresponding author: E-mail: jitlada.v@msu.ac.th, jitlada_v@yahoo.com
Tel. +66 43 75 4246; fax: +66 43

Received: 06-03-2017

Abstract

An ionic liquid-assisted liquid–liquid microextraction based on the solidification of floating organic droplet (ILSFOD-LLME) was investigated for analysis of four herbicide residues (i.e. simazine, atrazine, propazine, and linuron) by high performance liquid chromatography. For ILSFOD-LLME, the optimal extraction conditions were 5% w/v Na₂SO₄, 30 μ L [C₄MIM][PF₆]RTIL, 100 μ L of 1-octanol, ultrasonication time 30 s and centrifugation at 5000 rpm for 5 min. Under the optimal conditions, linearity was obtained within the range of 0.1–1000 μ g kg⁻¹, with the correlation coefficients greater than 0.999. The high enrichment factors of the target analytes were in the range of 64.5–139.9 and low limit of detection could be obtained. A modified QuEChERS was applied for fruit sample preparation before analysis. Matrix effects were also investigated using matrix matched standards for construction of the calibration graph. The proposed method has been successfully applied for extraction and preconcentration of herbicide residues in fruit samples, and good recoveries in the range of 87.32% to 99.93% were obtained.

Keywords: QuEChERS; ILSFOD-LLME; ionic liquid; extraction; HPLC; herbicides

1. Introduction

Triazines and phenylureas are widely used in agriculture around the world as selective pre- and post-emergence herbicides for the control of broadleaf and grassy weeds.¹ The intensive application of herbicides has resulted in the contamination of the atmosphere, ground and wastewaters, agricultural products and, consequently, in the direct and indirect pollution of food and food products.² The European Union (EU) legislation harmonizes a maximum residue limits (MRLs) of the pesticides and

fixes default value of MRLs at 0.01 mg kg⁻¹ for human food and animal feeding stuffs.³ Because of these restrictions, it is important to develop simple, rapid, environmentally friendly and sensitive analytical methods for monitoring of trace level of triazine and phenylurea herbicides.

Almost all of the analytical methods for herbicide residues are based on separation techniques, i.e. gas chromatography (GC), high-performance liquid chromatography (HPLC), and capillary electrochromatography. High-performance liquid chromatography (HPLC)^{4,5} with

UV and PDA detection has been adopted as an effective and reliable technique for the determination of selected herbicides. Due to the low concentration of these compounds and matrix complexity of real sample, an effective sample preparation and preconcentration can be used. Sample pretreatment is an important step in chemical step, especially in the analysis of trace analytes in environmental samples,⁶ and compensates for the drawbacks of UV detector. The quick, easy, cheap, effective, rugged and safe (QuEChERS) method has been presented for the analysis of pesticide residues in fruits and vegetables.⁷ It is based on the acetonitrile extraction, addition of salts to induce partition and then clean-up by dispersive solid-phase extraction (DSPE) with sorbents, such as C18, primary secondary amine (PSA) and graphitized carbon black (GCB).⁸ It provides some advantages including high recovery for wide polarity and volatility range of pesticides and the use of small amounts of organic solvent. However, one of the main drawbacks of QuEChERS methodology is that there is no pesticide concentration step in the final extract.⁹

Dispersive liquid-liquid microextraction (DLLME) has been investigated to resolve this problem. However, one of the main drawbacks of DLLME methodology is that there is toxic organic solvent as extraction solvent such as chlorobenzene, chloroform and carbon tetrachloride. Therefore, the development of sample preparation methods based on green analytical chemistry is highly interesting to investigate.¹⁰ Ionic liquids (ILs) consist of organic cations and organic or inorganic anion with some special characteristics, such as negligible vapor pressure, good chemical and thermal stability, good ability to dissolve both organic and inorganic compounds, as well as adjustable miscibility and polarity.^{11,12} At least part of the current interest is due to the favorable environmental properties of ILs, which support their use as green solvents in sample preparation processes.¹³ In 2011, ILs have been used as extraction solvents in dispersive liquid-liquid microextraction (DLLME),^{14,15} microwave assisted ionic-liquid microextraction (MAILME),¹⁶ ionic liquid-salt aqueous two-phase floatation (ILATPF),¹⁷ and single drop microextraction (SDME).¹⁸

The first application by ionic-liquid foaming-based solvent floatation was reported in 2012 by Li et al.¹⁹ for trace level determination of triazine and phenylurea herbicides in yoghurt. In this work a strong and active oxidizing agent such as perchloric acid was used. In this study, a simple extraction procedure using acetonitrile, namely modified QuEChERS, followed by preconcentration with ionic liquid-assisted liquid-liquid microextraction based on the solidification of floating organic droplet (ILSFOD-LLME) was investigated for determination of some herbicides, including simazine, atrazine, propazine, and linuron. The experimental parameters affecting the extraction efficiency and enrichment factor were investigated and the proposed method was applied to analyze surface water

and fruit samples. The satisfactory recovery was achieved. Compared to DLLME method, the proposed method offers advantage of extraction and preconcentration in a simple and sensitive extraction step.

2. Experimental

2. 1. Chemicals and Reagents

All reagents were of at least analytical reagent grade. All herbicide standards of herbicides including simazine, atrazine, propazine, and linuron were obtained from Fluka (Germany). The stock solutions of each herbicide were prepared at 1000 mg L⁻¹ by dissolving each herbicide standard in methanol. Working standard solutions were prepared by diluting the stock solution with water. Methanol (MeOH), acetonitrile (ACN) and 1-octanol of HPLC grade were obtained from Merck (Germany). Sodium chloride (NaCl) and anhydrous sodium sulphate (Na₂SO₄) were obtained from Ajax Finechem (New Zealand), sodium acetate (CH₃COONa) and sodium carbonate (Na₂CO₃) were obtained from Carlo Erba (France). 1-butyl-3-methylimidazolium hexafluorophosphate [C₄MIM][PF₆] RTIL was provided by Merck (Germany). Aqueous solutions were prepared with deionized water from RiOs™ Type I Simplicity 185 (Millipore Waters, USA) with the resistivity of 18.2 MΩ.cm⁻¹.

2. 2. Instrumentation

Chromatographic separation was performed on a Waters 1525 binary HPLC pump (USA), a Rheodyne injector with a sample loop of 20 μL and a Waters 2489 UV/Visible detector. The Empower software was used for data acquisition. A LiChroCART RP-8 endcapped (4.6 × 150 mm, 5.0 μm) column (Merck, Germany) was used. A centrifuge (Centurion, England) was used for complete phase separation. An ultrasonic bath (Dksh, Germany) and a vortex mixer (Fisher Scientific, USA) were also used.

2. 3. Ionic Liquid-Assisted Liquid-Liquid Microextraction based on the Solidification of Floating Organic Droplet Procedure

A volume of 10.00 mL of the standard solution (or sample solution) and 5% w/v of Na₂SO₄ was placed in a conical bottom tube. The solution was then vortexed before adding 30 μL of [C₄MIM][PF₆] RTIL. Then, 100 μL of 1-octanol was rapidly injected into the solution through the 1-mL syringe and the tube was ultrasonicated for 30 s to obtain the mass transfer and provide high extraction efficiency. In order to complete the phase separation, the tube was centrifuged at 5000 rpm for 5 min and the reconstituted solution was floated on the top of the solution. The

upper phase (~100 to 150 μL) was directly injected into HPLC. The concentrations of the reagents used in this work were optimized (see Optimization of ILSFOD-LLME).

2. 4. Chromatographic Separation Conditions

After extraction procedure, four herbicides were separated using isocratic elution of 52% (v/v) methanol in water at a flow rate of 1.0 mL min^{-1} . The separation column was at room temperature. The detection was at 220 nm. Four herbicides were separated within 7 min with the elution order of simazine, atrazine, propazine, and linuron. The retention time (t_R) and resolution (Rs) are shown in Table 1.

Table 1. The retention time (t_R) and resolution (Rs) of the studied compounds after HPLC analysis

Analyte	Retention time (t_R , min)	Resolution (Rs)
Simazine	1.48	–
Atrazine	4.65	3.72
Propazine	6.20	4.44
Linuron	6.93	2.16

2. 5. Sample Preparation

Fruit samples including orange, guava, apple and grape were randomly purchased from local markets at Mahasarakham province in Northeast Thailand. The edible parts of fruit samples (500 g) were cut and blended using a commercial food mixer. A modified QuEChERS method²⁰ was applied for sample preparation of the studied fruit samples. Briefly the procedure was as follows: 10 g of sample was placed in a 50-mL centrifugation tube and mixed with 25 mL of 1% (v/v) acetic acid in acetonitrile, and the mixture was vortexed for 1 min. After that, sodium acetate and anhydrous magnesium sulphate (15 g) were added and the mixture was immediately shaken manually. The solution was then centrifuged at 3500 rpm for 10 min. The supernatant was subsequently evaporated to dryness using a rotary evaporator (40 °C water bath). The resulting residue was re-dissolved with 10.00 mL of water before extraction by ionic liquid-assisted liquid–liquid microextraction based on the solidification of floating organic droplet and analysis using HPLC.

Matrix-match calibration standards were prepared by adding known amounts of selected herbicides from 0.01–0.50 $\mu\text{g g}^{-1}$ to the real sample extracts. In order to confirm the accuracy of the proposed method, recovery was tested. For recovery determinations, samples of blended fruit were spiked with the standard solution at three levels of concentration, 10, 50 and 100 $\mu\text{g kg}^{-1}$, for each of herbicide. The spiked samples were allowed to stand for

10 min before extraction to allow the spiked solution to penetrate the test materials.

3. Results and Discussion

3. 1. Optimization of Conditions for ILSFOD-LLME

Several extraction parameters for ILSFOD-LLME such as salt addition, type and volume of RTIL, type and volume of extraction solvent, vortex, ultrasonication and centrifugation time, were investigated and the optimum conditions have been established. All the experiments were performed in triplicate by spiking 10 mL of water with 50 $\mu\text{g kg}^{-1}$ of each herbicide and the mean of the results was used for optimization of the extraction efficiency of the method.

Generally, the addition of salt could increase the ionic strength of the aqueous medium with an electrolyte, reduce the solubility of both analytes and the RTIL in the aqueous sample solution and promote analyte transfer into the organic phase.²¹ To investigate the effect of salt addition on the extraction efficiency, various kinds of salts including NaCl, Na_2SO_4 , Na_2CO_3 , CH_3COONa were studied with the concentration of each salt being kept constant at 1% (w/v), and the results were compared with those obtained from the process without salt addition. As shown in Figure 1a, it was found that the addition of Na_2SO_4 provided higher extraction efficiency in terms of peak area of target herbicides. Therefore, Na_2SO_4 was selected for further study.

The effect of salt addition on the extraction efficiency in terms of peak area was investigated by the addition of different concentrations of Na_2SO_4 from 1 to 10% (w/v) into aqueous sample solution while keeping other experimental parameters constant. As shown in Figure 1b, the results of this study indicated that peak areas of selected herbicides increased with the increase in Na_2SO_4 up to 5% (w/v). Beyond this point, the extraction efficiency decreased because higher amounts caused an increase of the solubility of the RTIL in aqueous phase at high ionic strength, therefore reducing the volume of the sediment (RTIL) phase.²² Consequently, Na_2SO_4 5% (w/v) was used for further studies.

Selection of the appropriate RTIL, is an important parameter in order to obtain satisfactory extraction performance of the target analytes. RTIL could accelerate the emulsification of extraction solvent into the aqueous sample solution under ultrasound, resulting in increasing the extraction recovery. To work as an alternative solvent, an RTIL must meet certain requirements, such as being insoluble in water, having a low volatility and high extraction capability.²² Based on these consideration, 1-butyl-3-methylimidazolium hexafluorophosphate [C_4MIM][PF_6] RTIL was used in this study owing to its low viscosity and

compatibility to chromatographic system, compared with $[C_6MIM][PF_6]$ and $[C_8MIM][PF_6]$.²³ The effect of the RTIL volume was studied in the range of 5–50 μL (data not shown). It was found that symmetrical peaks, good baseline and high sensitivity was observed when $[C_4MIM][PF_6]$ 30 μL was added. Thus, RTIL 30 μL was chosen as disperser solvent.

The selection of suitable extraction solvent is of a great importance for the extraction of selected herbicides. The extraction solvent is dispersed as fine droplets in the sample solution, which is convenient for the mass transfer of the target analytes from the aqueous phase into the organic phase. 1-octanol (density, 0.8240 g mL^{-1}), 1-dodecanol (density, 0.8309 g mL^{-1}) and 2-dodecanol (density, 0.8290 g mL^{-1}) were investigated as an extraction solvent (data not shown). It was observed that 1-octanol provided high extraction efficiency because 1-octanol has a lower density than the other extraction solvents and the solubility of 1-octanol in the common dispersive solvent was low. Therefore, 1-octanol was considered as an appropriate extraction solvent for the microextraction step.

The volume of the extraction solvent in microextraction step has a direct influence on the volume of the floated phase and substantial enrichment factor for the final concentration.²⁶ Different volumes of 1-octanol (50, 100, 150, 200, 250, and 300 μL) were investigated with the other experimental parameters being kept constant. It was found that if the extraction solvent volume is 50 μL , the solution cannot complete phase separation. Moreover, the extraction solvent volume more than 100 μL decreased the peak areas of target herbicides, which may be due to the increased extract volume with the analyte signal decreased accordingly. As can be seen from Figure 1c, the highest extraction efficiency was obtained using 100 μL of 1-octanol. Therefore, 100 μL of 1-octanol was selected for further studies.

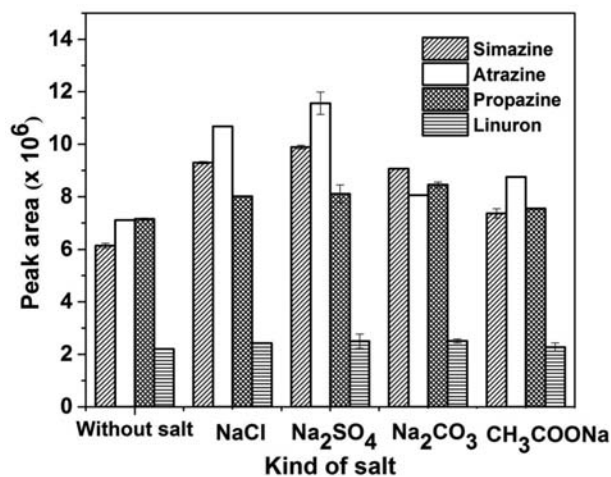


Figure 1a. Effect of salt addition on the extraction of selected herbicides

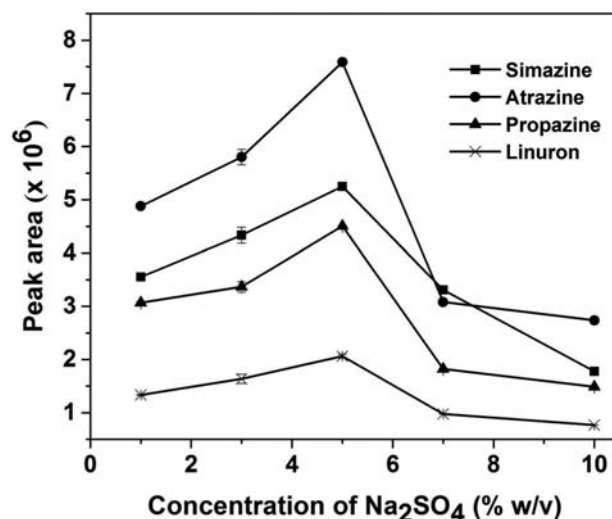


Figure 1b. Effect of concentration of salt on the extraction of selected herbicides

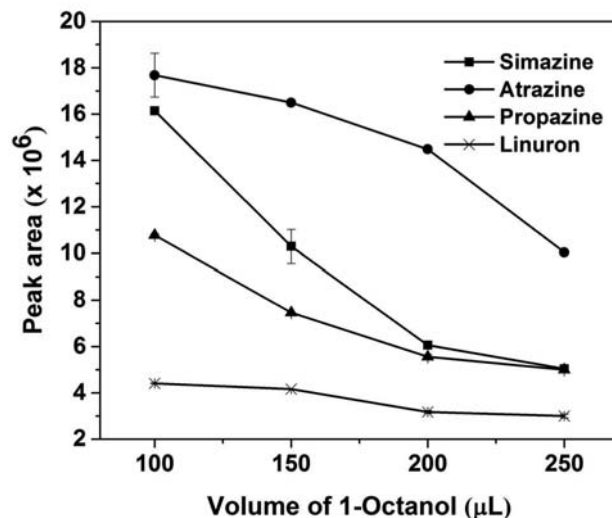


Figure 1c. Effect of volume of 1-octanol on the extraction of selected herbicides

Generally, the dispersion of the extraction solvent into the aqueous sample could depend on the rotational speed, vortex and ultrasonication time.²⁵ Both rapid dispersion and mass transfer processes are the most important parameters in the extraction process, which is regarded as the interval time between the formation of cloudy solution and before centrifuging. The effect of the ultrasonication time affects the mass transfer between two phases in the extraction procedure, and the influence of ultrasonication time on the peak area was studied in the range of 30–150 s, under the optimal experimental conditions (data not shown). Results revealed that there was no significant effect on the extraction efficiencies at different extraction times. In the experiment, 30 s was chosen as extraction time.

In extraction process, centrifugation time affects the size of the settled phase and the concentration of analyte in the extract phase. The effect of centrifugation time on the extraction efficiency of the proposed method was investigated by varying the centrifugation time from 2–10 min, at the speed of 3500 rpm (data not shown). It was observed that the peak areas of the analyte slightly increased up to 5 min, and then stayed constant. Thus, centrifugation time 5 min was selected for further experiments.

3. 2. Analytical Performances

Quantitative parameters of the proposed method such as linear ranges, linear equation, coefficient of determination (R^2), precision, limit of detection (LOD), limit of quantitation (LOQ) and enrichment factor (EF) were evaluated under the optimal conditions (Table 2). Before extraction using the proposed method, the selected herbicides show linearity in the range from 10 to 5000 $\mu\text{g kg}^{-1}$ with correlation coefficient (R^2) greater than 0.98. Limits of detection (LODs) of the analytes were determined based on the signal to noise (S/N) ratio of 3 and found to be 10 $\mu\text{g kg}^{-1}$ for all compounds. The limit of quantitation (LOQ) (S/N = 10) was found to be 30 $\mu\text{g kg}^{-1}$. After extraction using the proposed method, the selected herbicides exhibit good linearity in the range from 0.1 to 1000 $\mu\text{g kg}^{-1}$ with correlation coefficient (R^2) of 0.9991–0.9997. Limits of detection (LODs) of the analytes were determined based on the signal to noise (S/N) ratio of 3 and found in the range of 0.01–0.10 $\mu\text{g kg}^{-1}$. The limit of quantitation (LOQ) (S/N = 10) was found in the range of 0.03–0.30 $\mu\text{g kg}^{-1}$. In order to test the reproducibility of the proposed method, precision in terms of intra-day and inter-days were studied by replicate injection of the stan-

dard mixture of 0.01 $\mu\text{g kg}^{-1}$ each in a day ($n = 5$) and several days ($n = 3 \times 5$). The relative standard deviations (RSDs) were less than 2.88% and 6.38% for retention time (t_r) and peak area, respectively. The enrichment factor (EF), defined as the concentration ratio of the analytes in the settled phase (C_{set}) and in the aqueous sample (C_o), were in the range of 64.5–139.9. The chromatograms obtained for the separation of selected herbicides by direct HPLC injection (Figure 2a) and ILSFOD-LLME combined with HPLC (Figure 2b) were compared. Using the proposed ILSFOD-LLME, the chromatographic signals of selected herbicides were increased.

3. 3. Application to Real Samples

To test the applicability of the method for selected herbicides determination in fruit samples, four fruits were collected and examined. Matrix effects are known to be problematic in pesticide residue analysis, which can result in either decreased detection response or increased analytical signal.⁸ The extent of matrix effects can be calculated as the percent differences in slopes of the calibration graphs from matrix-matching vs. those from standards in solvent-only.²⁶ In this work, matrix-matched calibration was used for quantitation of the selected herbicides in fruit samples. The working linear range was 0.1–50 $\mu\text{g kg}^{-1}$. The slope of the matrix-matched calibration graph is dependent on the sample matrix, however, the correlation coefficients (R^2) of greater than 0.999 were obtained for all compounds (as shown in Table 3). From the analytical results, all target herbicides frequently appeared in studied samples. The results are summarized in Table 4. The concentration ranges of residues were 2.0–4.0 $\mu\text{g kg}^{-1}$ for simazine, 3.0–7.0 $\mu\text{g kg}^{-1}$ for atrazine, 0.5–4.0 $\mu\text{g kg}^{-1}$ for propazine, and 0.2–4.0 $\mu\text{g kg}^{-1}$

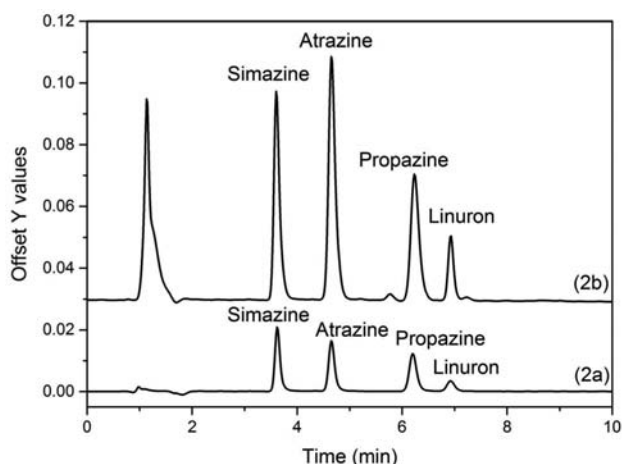


Figure 2. Chromatogram obtained for the separation of selected herbicides by (a) direct HPLC injection and (b) after preconcentration using ILSFOD-LLME combined with HPLC: concentration of all standard herbicides was 500 $\mu\text{g kg}^{-1}$.

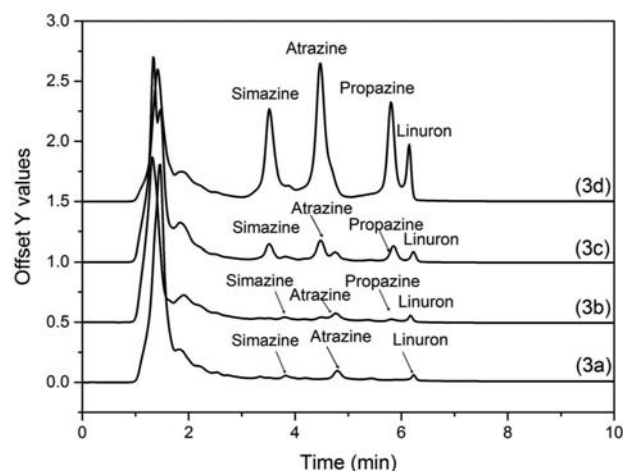


Figure 3. Chromatogram of (a) orange sample, (b) orange sample spiked at 10 $\mu\text{g kg}^{-1}$ of each herbicide, (c) orange sample spiked at 50 $\mu\text{g kg}^{-1}$ of each herbicide, and (d) orange sample spiked at 100 $\mu\text{g kg}^{-1}$ of each herbicide

Table 2. Analytical performance of ionic liquid-assisted dispersive liquid–liquid microextraction method compared to direct HPLC method for determination of selected herbicides

Analyte	Linear range ($\mu\text{g kg}^{-1}$)	Linear equation	R^2	EF	LOD ($\mu\text{g kg}^{-1}$)	LOQ ($\mu\text{g kg}^{-1}$)	Intra-day ^{a)} (n = 5) t_R	Area	Inter-day (n = 3 × 5) t_R	Area
Simazine	0.1–1000 (10–5000) ^{b)}	$y = (2 \times 10^7x) + 12922$ ($y = 309890x - 2939.7$)	0.9996 (0.9896)	64.5	0.1 (10)	0.3 (30)	0.18 (0.24)	2.18 (2.20)	0.79 (0.50)	7.72 (7.44)
Atrazine	0.1–1000 (10–5000)	$y = (4 \times 10^7x) - 141252$ ($y = 285914x - 6568$)	0.9997 (0.9989)	139.9	0.1 (10)	0.3 (30)	0.24 (0.20)	2.58 (2.41)	0.37 (0.40)	5.68 (6.25)
Propazine	0.1–1000 (10–5000)	$y = (2 \times 10^7x) + 80699$ ($y = 237118x - 9871.2$)	0.9991 (0.9726)	84.3	0.01 (10)	0.03 (30)	0.20 (0.16)	4.55 (2.03)	0.33 (0.28)	6.51 (5.05)
Linuron	0.1–1000 (10–5000)	$y = (6 \times 10^6x) + 227967$ ($y = 80665x - 2610.6$)	0.9993 (0.9992)	74.4	0.01 (10)	0.03 (30)	0.32 (0.16)	4.89 (1.51)	0.48 (0.44)	7.22 (8.12)

^{a)} Precision was investigated at the concentration of $100 \mu\text{g kg}^{-1}$. ^{b)} The values in parentheses are obtained from direct HPLC method.

Table 3. Matrix-matched calibrations of selected herbicides in fruit juice samples (n = 3)

Analyte	Simazine		Atrazine		Propazine		Linuron	
	Linear equation	R^2	Linear equation	R^2	Linear equation	R^2	Linear equation	R^2
Orange (n = 3)	$y = 2009890x + 12922$	0.9996	$y = 4061210x - 14231$	0.9997	$y = 2231237x - 22415$	0.9991	$y = 6000929x + 32715$	0.9998
Guava (n = 3)	$y = 2554631x + 12543$	0.9998	$y = 4778145x - 19911$	0.9998	$y = 2384111x - 24110$	0.9997	$y = 6277880x + 23612$	0.9998
Apple (n = 3)	$y = 2164434x + 28812$	0.9994	$y = 4431631x - 22114$	0.9990	$y = 2174632x - 22110$	0.9993	$y = 6154680x + 23625$	0.9994
Grape (n = 3)	$y = 2182608x + 18116$	0.9995	$y = 4412534x - 12310$	0.9992	$y = 2545602x - 22313$	0.9992	$y = 6666124x + 32310$	0.9997

kg^{-1} for linuron. However, the amount of some herbicides found in fruit sample was lower than the MRLs established by EU (simazine, 0.01 mg kg^{-1} in orange, apple, and guava; atrazine and linuron, 0.05 mg kg^{-1} in orange, apple, grape, and guava).

In order to validate the accuracy of the presented extraction method, different amounts of target analytes were spiked to fruit samples at concentration levels of 10, 50, and $100 \mu\text{g kg}^{-1}$. The spiked samples were analyzed and the results are shown in Table 5. Recoveries were between 87.32% and 99.93%, and RSD values ranged from 1.15% to 6.57%. The results demonstrated that the matrix effects caused by the fruit samples had a negligible effect on the efficiency and sensitivity of the proposed method. Figure 3 shows chromatograms corresponding to real sample and real sample spiked with selected herbicides.

4. Conclusions

A method of ILSFOD-LLME coupled to HPLC has been investigated for sensitive and robust determination of selected herbicides in fruit samples. The effective sample preparation using modified QuEChERS method was used. The target compounds were simply extracted by 1-octanol with ionic liquid $[\text{C}_4\text{MIM}][\text{PF}_6]$ as green disperser solvent, which is less toxic than the solvent normally used in the typical conventional DLLME. The matrix-matched calibration provided good recoveries in real sample determination at trace levels of herbicides. The proposed method shows good analytical features providing low limit of detection at the levels of $0.1 \mu\text{g kg}^{-1}$ which are below the acceptable MRLs established by EU. A high preconcentration factor in the range of 64.5 to 139.9, good recoveries and high reproducibility were also obtained. The proposed method offers the advantages of simplicity and sensitivity.

5. Acknowledgements

The authors gratefully acknowledge financial supports for this research from Center of Excellence for Innovation in Chemistry (PERCH-CIC), Maharakham University, National Research Council of Thailand (NRCT), The Thailand Research Fund (TRF) and the Commission on Higher Education (CHE).

Table 4. Analysis of selected herbicides in fruit juice samples

Samples	Amount found \pm SD, $\mu\text{g kg}^{-1}$ (n = 3)			
	Simazine	Atrazine	Propazine	Linuron
Orange (n = 3)	4.0 \pm 0.02	7.0 \pm 0.10	–	0.2 \pm 0.01
Guava (n = 3)	–	3.0 \pm 0.20	0.5 \pm 0.01	4.0 \pm 0.01
Apple (n = 3)	–	4.0 \pm 0.01	4.0 \pm 0.01	–
Grape (n = 3)	2.0 \pm 0.10	–	–	–

–; not detected

Table 5. Recovery obtained from the determination of target herbicides in fruit juice samples (n = 3)

Analytes	Spiked ($\mu\text{g kg}^{-1}$)	Orange (n = 3)		Guava (n = 3)		Apple (n = 3)		Grape (n = 3)	
		RR (%)	RSD (%)	RR (%)	RSD (%)	RR (%)	RSD (%)	RR (%)	RSD (%)
Simazine	10	93.55	1.80	97.27	1.23	97.78	4.63	98.65	1.56
	50	97.13	2.30	95.83	2.64	92.37	1.54	91.72	1.78
	100	94.63	1.02	96.56	2.59	95.33	2.65	96.57	1.58
Atrazine	10	92.63	2.32	87.32	2.33	95.87	2.73	87.75	2.27
	50	93.23	3.05	93.62	2.61	97.39	3.54	90.23	3.23
	100	97.69	3.04	92.18	2.27	93.43	1.41	92.17	3.57
Propazine	10	92.87	1.15	92.17	2.83	89.82	4.54	92.83	2.76
	50	93.53	2.22	98.78	3.37	99.58	3.58	91.57	6.57
	100	92.12	2.35	92.23	2.63	91.27	4.53	89.84	5.38
Linuron	10	99.78	3.43	99.67	2.78	98.67	4.73	99.93	2.23
	50	91.63	2.33	91.23	1.15	92.25	4.23	92.25	2.37
	100	94.32	2.78	90.43	3.75	93.57	4.41	91.58	2.48

RR: Relative recovery RSD: Relative standard deviation

6. References

- R. Fang, G. Chen, L. Yi, Y. Shao, L. Zhang, Q. Cai, J. Xiao, *Food Chem.* **2014**, *145*, 41–48. <https://doi.org/10.1016/j.foodchem.2013.08.028>
- X. Yang, R. Yu, S. Zhang, B. Cao, Z. Liu, L. Lei, N. Li, Z. Wang, L. Zhang, H. Zhang, Y. Chen, *J. Chromatogr. B* **2014**, *972*, 111–116. <https://doi.org/10.1016/j.jchromb.2014.10.001>
- Pesticide EUMRLs Database **2008**
- H. R. Sobhi, Y. Yamini, R. H. Hosseini, B. Abadi, *J. Pharmaceut. Biomed.* **2007**, *45*, 769–774. <https://doi.org/10.1016/j.jpba.2007.09.026>
- E. Bichon, M. Dupuis, B. L. Bizec, F. André, *J. Chromatogr. B* **2006**, *838*, 96–106. <https://doi.org/10.1016/j.jchromb.2006.04.019>
- G. Zhao, S. Song, C. Wang, Q. Wu, Z. Wang, *Anal. Chim. Acta* **2011**, *708*, 155–159. <https://doi.org/10.1016/j.aca.2011.10.006>
- J. Vichapong, R. Burakham, S. Srijaranai, K. Grudpan, *Talanta* **2011**, *84*, 1253–1258. <https://doi.org/10.1016/j.talanta.2011.01.002>
- N. Wongsu, R. Burakham, *Food Anal. Methods* **2012**, *5*, 849–855. <https://doi.org/10.1007/s12161-011-9317-y>
- Y. Santaladchayakit, S. Srijaranai, *J. Sep. Sci.* **2014**, *37*, 3354–3361. <https://doi.org/10.1002/jssc.201400699>
- M. Yang, P. Zhang, L. Hu, R. Lu, W. Zhou, S. Zhang, H. Gao, *J. Chromatogr. A* **2014**, *1360*, 47–56. <https://doi.org/10.1016/j.chroma.2014.07.076>
- A. Martín-Calero, V. Pino, J. H. Ayala, V. González, A. M. Afonso, *Talanta* **2009**, *79*, 590–597. <https://doi.org/10.1016/j.talanta.2009.04.032>
- C. F. Poole, N. Lenca, *Trends Anal. Chem.* **2015**, *71*, 144–156. <https://doi.org/10.1016/j.trac.2014.08.018>
- Y. Wang, J. You, R. Ren, Y. Xiao, S. Gao, H. Zhang, A. Yu, *J. Chromatogr. A* **2010**, *1217*, 4241–4246. <https://doi.org/10.1016/j.chroma.2010.03.031>
- T. D. Nguyen, J. E. Yu, D. M. Lee, G.-H. Lee, *Food Chem.* **2008**, *110*, 207–213. <https://doi.org/10.1016/j.foodchem.2008.01.036>
- M. Asensio-Ramos, J. Hernández-Borges, T. M. Borges-Miquel, M. Á. Rodríguez-Delgado, *J. Chromatogr. A* **2011**, *1218*, 4808–4816. <https://doi.org/10.1016/j.chroma.2010.11.030>
- S. Gao, J. You, X. Zheng, Y. Wang, R. Ren, R. Zhang, Y. Bai, H. Zhang, *Talanta* **2010**, *82*, 1371–1377. <https://doi.org/10.1016/j.talanta.2010.07.002>
- J. Han, Y. Wang, C. Yu, C. Li, Y. Yan, Y. Liu, L. Wang, *Anal. Chim. Acta* **2011**, *685*, 138–145. <https://doi.org/10.1016/j.aca.2010.11.033>
- X. Wen, Q. Deng, J. Guo, *Spectrochim. Acta A* **2011**, *79*, 1941–1945. <https://doi.org/10.1016/j.saa.2011.05.095>

19. N. Li, R. Zhang, L. Nian, R. Ren, Y. Wang, H. Zhang, A. Yu, *J. Chromatogr. A* **2012**, *1222*, 22–28.
<https://doi.org/10.1016/j.chroma.2011.12.019>
20. R. Romero-González, A. Garrido Frenich, J.L. Martínez Vidal, *Talanta* **2008**, *76*, 211–225.
<https://doi.org/10.1016/j.talanta.2008.02.041>
21. J. Xue, X. Chen, W. Jiang, F. Liu, H. Li, *J. Chromatogr. B* **2015**, *975*, 9–17.
<https://doi.org/10.1016/j.jchromb.2014.10.029>
22. M. Yang, X. Xi, X. Wu, R. Lu, S. Zhang, H. Gao, *J. Chromatogr. A* **2015**, *1381*, 37–47.
<https://doi.org/10.1016/j.chroma.2015.01.016>
23. C. F. Poole, S. K. Poole, *J. Chromatogr. A* **2010**, *1217*, 2268–2286. <https://doi.org/10.1016/j.chroma.2009.09.011>
24. X. Xu, R. Su, X. Zhao, Z. Liu, Y. Zhang, D. Li, X. Li, H. Zhang, Z. Wang, *Anal. Chim. Acta* **2011**, *707*, 92–99.
<https://doi.org/10.1016/j.aca.2011.09.018>
25. Z.-H. Yang, Y.-L. Lu, Y. Liu, T. Wu, Z.-Q. Zhou, D.-H. Liu, *J. Chromatogr. A* **2011**, *1218*, 7071–7077.
<https://doi.org/10.1016/j.chroma.2011.08.029>
26. S. J. Lehotay, K. A. Son, H. Kwon, U. Koesukwiwat, W. Fu, K. Mastovska, E. Hoh, N. Leepipatpiboon, *J. Chromatogr. A* **2010**, *1217*, 2548–2560.
<https://doi.org/10.1016/j.chroma.2010.01.044>

Povzetek

Preučevali smo mikroekstrakcijo z ionsko tekočino, osnovano na strjeni plavajoči organski kapljici (ILSFOD-LLME) za analizo štirih preostankov herbicidov (simazin, atrazin, propazin in linuron) z visoko zmogljivo tekočinsko kromatografijo. Za ILSFOD-LLME so bili optimalni ekstrakcijski pogoji 5% w/v Na₂SO₄, 30 µL [C₄MIM][PF₆]RTIL, 100 µL 1-oktanol, čas ultrazvoka 5 min in centrifugiranje pri 5000 rpm 30 s. Pri optimalnih pogojih je bila linearnost v območju 0,1–1000 µg kg⁻¹, korelacijski koeficienti pa večji kot 0,999. Visoki obogatitveni faktorji za analite so bili v območju 64,5–139,9, dobili smo tudi nizko mejo zaznave. Za pripravo vzorcev sadja pred analizo smo uporabili modificirano QuEChERS metodo. Raziskali smo tudi matrične učinke, tako da smo standarde v ustrezni matrici uporabili za pripravo umeritvene krivulje. Predlagano metodo smo uspešno uporabili za ekstrakcijo in predkoncentracijo ostankov herbicidov v vzorcih sadja. Dobili smo dobre izkoristke v območju 87,32% do 99,93%.

Scientific paper

Cold Plasma and Acid Treatment Modification Effects on Phonolite

José Miguel Hidalgo-Herrador,* Zdeněk Tišler, Pavlína Hajková,
Lenka Soukupová, Lenka Zárýbnická and Karla Černá

Unipetrol Centre for Research and Education / UNICRE, Areál Chempark, 436 70, Litvínov-Záluží I, Czech Republic.

* Corresponding author: E-mail: jose.hidalgo@unicre.cz

Received: 06-03-2017

Abstract

A sample of phonolite was treated by cold plasma and hydrochloric acid diluted in water to study the change of its structure and acid properties. The phonolite and treated samples were analysed by XRD, elemental analysis XRF, specific surface area BET, TPD-NH₃ and FT-IR spectroscopy. They were also tested in the adsorption of Ca, K, Mg, P and Na impurities present in waste cooking oil. Plasma treated sample presented almost the same structure with some surface differences respect to the original phonolite. However, acid treated sample presented bigger total surface compared to the other samples, different structure, composition and acid properties.

Keywords: phonolite, cold plasma, acid treatment, structure modification, adsorption

1. Introduction

Phonolite is an igneous rock formed composed mainly by alkali feldspar and other compounds.¹ Many works were published about phonolite but they were based mainly in geology, geochemistry or mineralogy. Nevertheless, a lower number of publications were found about the experimental modification of the structure of phonolite. However, some experiments were carried out with the aim of studying the structure modifications of new solids obtained at high temperature and pressure.^{2–5} Acid treatment of solids has been extensively studied for many applications such as catalysis, agriculture, membranes, etc. This treatment could be an effective tool to modify the structure and composition of the phonolite.¹ Acid treatment could be an advantage increasing the porosity of the material for using it as adsorbent or catalyst as described for other type of materials.⁶ Also, it could be a disadvantage as K⁺ donor material for being used as fertilizer.⁷ Nevertheless, no previous publications were found about the acid treatment effects on phonolite structure. Another treatment for the modification of solids is the plasma application which has been used for modifying the adsorbent surfaces.^{8–10} Plasma is classified as cold plasma when the temperature used is lower than 500 °C. The advantages of this treatment are clean reaction and a short processing time without affect-

ing the bulk structure.^{11,12} However, this treatment could also be a disadvantage for changing its bulk structure. Some studies using cold plasma were published.^{11–15} Nevertheless, no studies have been reported on the modification of phonolite using this methodology. This paper is the first study on the modification of phonolite using cold plasma and acid treatment. The aim of this work was to study the modification of the phonolite by using two separate processes (surface modification by cold plasma and structure change by acid treatment).

2. Experimental

The phonolite (Ph) was supplied in powder form by the company Keramost a. s.¹⁶ Ph sample (20 g) was dried at 120 °C overnight. Then, it was leached by 3M HCl solution (80 °C for 4 h). The phonolite:acid (g:ml) ratio was 1:10. After the leaching process, the product was filtered, washed (by several times with hot demineralised water) and dried overnight at 120 °C. Finally, the dried samples were calcined at 500 °C during 6 h (gradient 1 °C/min from room temperature) in air obtaining the acid treated phonolite (A-Ph). The plasma treated phonolite (CP-Ph) was synthesized by nonthermal DBD plasma which was conducted in ambient air (humidity 32%) at atmospheric

pressure and the discharges were operated in filamentary mode (they were constituted by a high amount of tiny micro discharges randomly distributed over the entire area of the electrodes). The plasma reactor consisted of two plane parallel electrodes covered with a 1 mm layer of dielectric. The upper electrode (105 × 20 × 12 mm) was covered with corundum and the bottom electrode (120 × 60 × 20 mm) with a mobile rubber providing transport of the material at the same time. The distance between the electrodes was 4 mm. Plasma treatment conditions and parameters were: AC source voltage 20 kV, frequency 3 kHz, nominal power 120 W, modification time periods 5 s. XRF, XRD, specific surface area BET and NH₃ temperature programmed desorption (TPD-NH₃) were carried out using the same methodology described in the literature.¹⁷ Mercury porosimetry measurements were performed on a Micromeritics AutoPore IV 9510 mercury porosimeter. All samples were dried before the analysis in a glass-cell at 110 °C under vacuum for 16 hours. Attenuated total reflectance technique (ATR) using an instrument Nicolet iS 10-Thermo Scientific (crystal diamond; number of scans = 64; resolution 4 cm⁻¹) was used for the FT-IR measurements. The scanning electron microscopy (SEM) was carried out using a Zeiss ULTRA Plus microscope equipped with Oxford detector for energy-dispersive analysis (EDX). Finally, the samples were tested in the adsorption of Ca, Mg, K, P and Na in waste cooking oil (WCO). The adsorption procedure was carried out using 20 g of filtered WCO which was previously heated at 95 °C. Then, 2 g of sorbent (phonolite) were added. The mixture was stirred during 1 hour at room temperature and filtered. Finally, the liquid product was analyzed by the instrument ICP-OES/Agilent 725. The WCO elemental composition was 78 %wt. of carbon, 11.9 %wt. of hydrogen, 0.387 mg kg⁻¹ of Ca, 0.104 mg kg⁻¹ of Mg, 1.02 mg kg⁻¹ of K, 2.04 mg kg⁻¹ of P, 1.82 mg kg⁻¹ of Na, 4.13 mg kg⁻¹ of sulfur and 64.2 mg kg⁻¹ of nitrogen content. The supplied WCO presented a total acid number of 2 mg KOH g⁻¹.

3. Results and Discussion

As shown in XRF results, practically no changes were found for samples Ph and CP-Ph (Table 1). Sample A-Ph presented higher Si and lower Al, Na and K contents respect to the Ph sample. The acid treatment implied an increment in the total porosity as consequence of the removing of Al, Na and K. Also, the content of Fe and Ca decreased for A-Ph respect to the Ph sample.

Almost identical Hg porosimetry results were found for Ph and CP-Ph samples with a low total porosity. No mesopores and a minimum number of micropores were detected in these samples. Acid treatment supposed an increment in the total porosity. The increment of the porosity in the 3–30 nm range (mesopores) was an interesting result taking in account possibly future applications of this material as catalyst or absorbent for large molecules. Nevertheless, BET specific surface showed a bigger specific surface compared than the total pore area by Hg porosimetry (table 1) indicating the presence of a high number of micropores. The acid treatment also implied an increment in the total intrusion volume of the sample mainly due to the macropores volume.

XRD results informed about a similar content of analcime 25.2%, nepheline 42.9% and sanidine 31.9% in samples Ph and CP-Ph. However, a change in the structure-composition was found for the A-Ph sample with 41.7%, 14.9%, 1.2% and 42.3% of sanidine, nepheline, analcime and albite respectively. Surely, these changes were produced mainly by the removing of Al, Na during the acid treatment process of the original phonolite as reflected in the elemental composition.

For FT-IR results, some bands were identified between 1200 and 650 cm⁻¹ which were related to bond stretchings of Si–O–Si or Si–O–Al, due to the presence of silicon and aluminium oxides. The treatment of each sample at 100 °C removed the possible content of water

Table 1. Elemental XRF Composition and surface area.

Material	Ph	CP-Ph	A-Ph
Specific Surface BET (m ² g ⁻¹)	4.9	8	167
Hg porosimetry / Total pore area (m ² g ⁻¹)	1.7	2.3	34
Composition	(%wt.)	(%wt.)	(%wt.)
Si	26.5	26.5	38.6
Al	11.8	11.9	4.5
Na	7.9	7.9	1.7
K	5.1	5.1	4.3
Fe	1.4	1.3	0.6
Ca	0.7	0.7	0.1
Cl	0.3	0.4	0.1
Ti	0.2	0.2	0.1
¹ Calculated sum	99.4	99.4	99.6

¹Total sum of theoretically present SiO₂, Al₂O₃, Na₂O, K₂O, Fe₂O₃, CaO, Cl and TiO₂.

in the samples. Thus, no representative bands between 3650 and 3200 cm^{-1} related to the vibration stretching of OH bond were found.^{5,18} However, the OH vibration stretching also could be due to the OH present in minerals. So, a low content of hydroxides is expected for the surface of these solids. The cold plasma treatment could modified slightly the surface of the phonolite as shown in a more intensive band at 850–1150 cm^{-1} for sample Ph compared to CP-Ph. The biggest change was found for the A-Ph sample. The lost of intensity in the bands range of 650–1300 cm^{-1} was surely due to a lower amount of Si-O-Si and/or Si-O-Al bonds type. A-Ph sample contained less Al than the other samples so it could be reason of the lowest intensity band. The difference between samples Ph and CP-Ph could be explained by the change of Si-O-Al to other type of bonds which could affect the acidity of the sample.

For the TPD- NH_3 characterization (Fig. 1), all materials showed a broad NH_3 desorption peak stretched in a wide range from 175 to 350 °C corresponding to the intermediate and stronger acid sites. The characteristics and the amount of acid sites varied when the phonolite was treated. CP-Ph presented slightly lower intensity in the signal related to the intermediate and strong acid sites and the same intensity than Ph for the weak acid sites. A-Ph

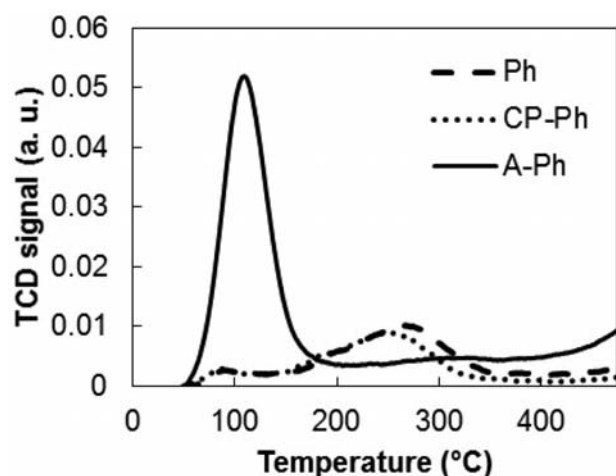


Fig. 1. TPD- NH_3 for Ph, CP-Ph and A-Ph samples. 100 mg of sample was pre-treated in He at 500 °C, cooled to 180 °C and finally saturated with ammonia. Then, the temperature was increased to 500 °C with a rate of 15 °C/min.

sample presented the highest number of weak acid sites (peak at 100 °C) as consequence of the removing of Al instead of a higher % of Si present in the surface of the solid. Thus, the acid treatment implied an increment in the total number of weak acid sites and the cold plasma treatment slight decrease in the number of intermediate and stronger acid sites.

WCO adsorption test results (Table 2) were different depending on the type of adsorbent used. When the oil was treated with Ph, the filtered product presented higher Ca, K and Na contents. However, the content of P was a half from the original WCO content, for the oil treated with Ph. CP-Ph oil treatment supposed a clear increment of K and Na in the final oil. Only the treatment using A-Ph solid supposed a decrease in Ca, Mg, K, P and Na in the oil. CP-Ph oil treatment test results informed about a bigger increment of K and Na compounds in the oil respect to the results from the treated oil with Ph. These different results could be attributed only to the different surface of Ph and CP-Ph because the two solids presented similar elemental composition and XRD results. Thus, A-Ph was the only solid, which actuated as absorber and not as donor of Ca, Mg, K, P and Na in these tests.

SEM images (Fig. 2) of Ph and CP-Ph showed particles of approximately 5–20 μm size ratio in diameter with different forms. For sample A-Ph, the particle size was in the 5–40 μm range. The differences are not clear between the Ph and CP-Ph samples. Nevertheless, sample A-Ph presented a clear difference in its surface respect to the original phonolite.

The same sample of phonolite was treated three times (acid and plasma treatments) and the resultant XRF, XRD and Hg porosimetry measurements presented almost the same results (XRF elemental composition with a percentage error lower than 0.5%). The adsorption procedure was repeated three times presenting similar results for the elemental analyses with a percentage error lower than 1% (Ca, Na, sulphur, Mg, K and nitrogen contents).

4. Conclusions

The phonolite was modified by acid and cold plasma treatments. Then, it was tested in a WCO absorption test. The cold plasma treatment supposed a modification of the

Table 2. Ca, Mg, K, P and Na contents in WCO treated samples with Ph, CP-Ph and A-Ph.

Parametr	Oil-Feedstock	Oil/Ph	Oil/CP-Ph	Oil/A-Ph
Ca [mg kg^{-1}]	0.39	1.07	1.56	0.25
Mg [mg kg^{-1}]	0.10	0.09	0.23	0.04
K [mg kg^{-1}]	1.02	2.14	7.53	1.00
P [mg kg^{-1}]	2.04	1.33	1.5	1.07
Na [mg kg^{-1}]	1.82	3.56	5.15	1.25

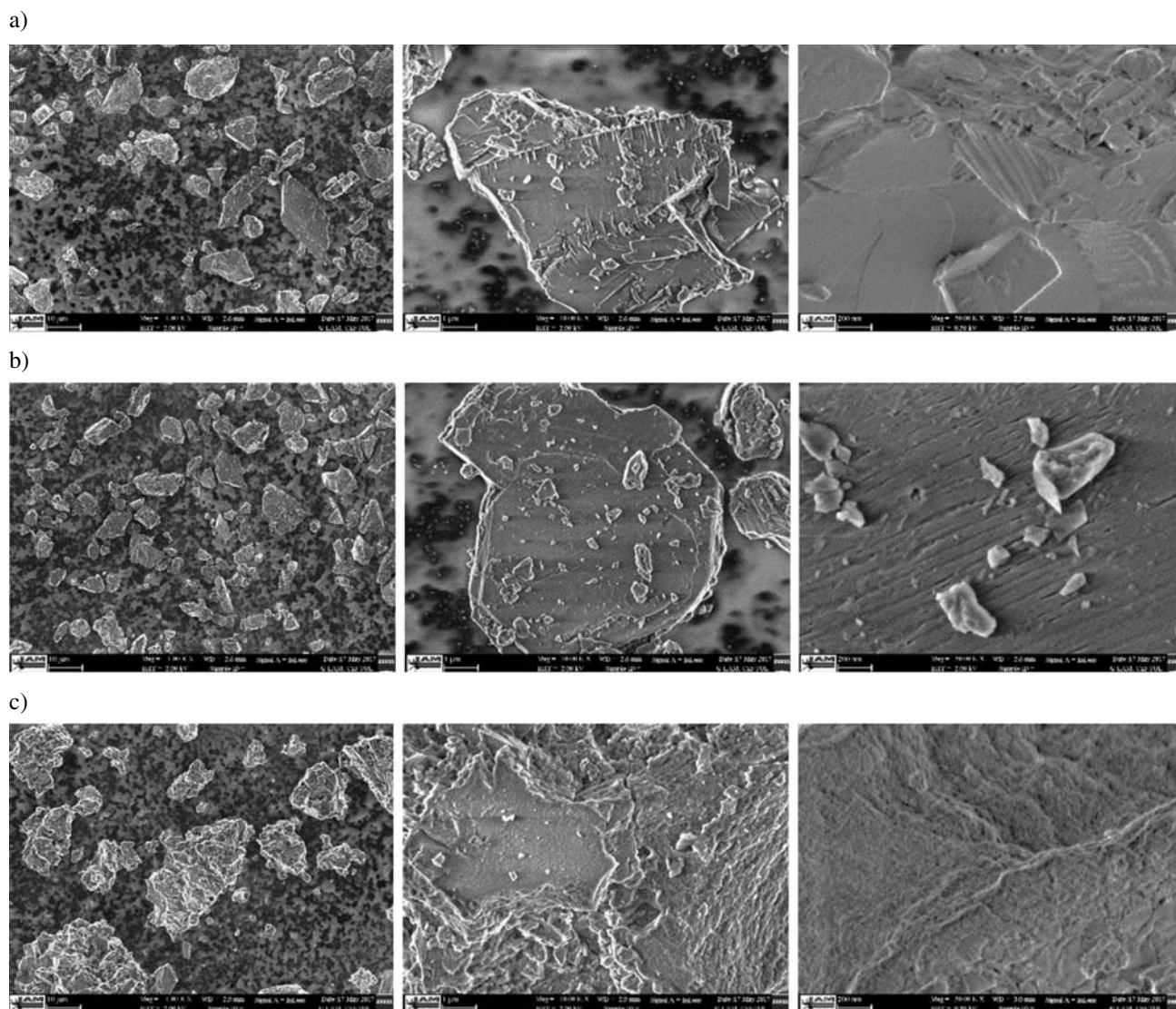


Fig. 2. SEM images. (a) Ph (x1,000, x10,000 and x50,000); (b) CP-Ph (x1,000, x10,000 and x50,000); (c) A-Ph (x1,000, x10,000 and x50,000).

original Ph surface and the acid treatment supposed a change in the original Ph structure and composition changing dramatically its total surface and acid properties. For the WCO tests, A-Ph sample absorbed the biggest amount of Ca, Mg, K, P and Na. This work could be the beginning of another new generation of materials, which could be used in many current applications.

5. Acknowledgements

The publication/presentation is a result of the Project Development of the UniCRE Centre (Project Code LO1606) which was financially supported by the Ministry of Education, Youth and Sports of the Czech Republic under the National Programme for Sustainability I.

5. Supplementary Material

The document contains the XRD, Hg isotherms, FT-IR figures and some more detailed information about TPD-NH₃ and SEM experimental procedures.

7. References

1. Imperial College Rock Library, Glossary: Phonolite. Imperial College London, South Kensington Campus, London SW7 2AZ. Web link accessed on 02/14/2017. Web link: <https://wwwf.imperial.ac.uk/earthscienceandengineering/rocklibrary/viewglossrecord.php?Term=phonolite>
2. Y. Moussallam, C. Oppenheimer, P. Scaillet, R. Kyle, *J Petrology* **2013**, *54*, 1285–1307. <https://doi.org/10.1093/petrology/egt012>

3. V. A. Kutolin, V. A. Shirokih, Tailings and mine waste reprocessing for production of the foamed glass, *5th Annual International Conference on Tailings and Mine Waste*, Colorado State Univ., Ft. Collins, Civil Engineering, Geotech Engineering Program, Tailings and mine waste 98, (Jan 26–28, 1998) 909–916. Edited by J.D. Nelson.
4. J. L. Capitaneo, F. T. Silva, C. M. F. Vieira, *Silic. Ind.* **2005**, 70, 161–165.
5. A. M. S. Teixeira, F. M. S. Garrido, M. E. Medeiros, J. A. Sampaio, *Int. J. Miner. Process.* **2015**, 145, 57–65. <https://doi.org/10.1016/j.minpro.2015.07.002>
6. S. Morin, A. Berreghis, P. Ayrault, N. S. Gnep, M. Guisnet, *J. Chem. Soc. Faraday Trans.* **1997**, 93, 3269–3275. <https://doi.org/10.1039/a702538f>
7. K. von Wilpert, M. Lukes, *Nutr. Cycl. Agroecosys.* **2003**, 65, 115–127. <https://doi.org/10.1023/A:1022103325310>
8. N. Celini, F. Poncin-Epaillard, F. Bergaya, *Polymer* **2007**, 48, 58–67. <https://doi.org/10.1016/j.polymer.2006.11.018>
9. G. Le Du, N. Celini, F. Poncin-Epaillard, F. Bergaya, *Surf. Coat. Technol.* **2006**, 201, 5815–5821. <https://doi.org/10.1016/j.surfcoat.2006.10.025>
10. C. Saka, O. Şahin, *Color. Technol.* **2011**, 127, 246–255. <https://doi.org/10.1111/j.1478-4408.2011.00306.x>
11. K. F. Grythe, F. K. Hansen, *Langmuir* **2006**, 22, 6109–6124. <https://doi.org/10.1021/la053471d>
12. M. Lehocky, H. Drnovska, B. Lapcikova, A. M. Barros-Timmons, T. Trindade, M. Zembala, L. Jr. Lapcik, *Colloids Surf. A* **2003**, 222, 125–131.
13. Ö. Şahin, M. Kaya, C. Saka, *Appl. Clay Sci.* **2015**, 116, 46–53. <https://doi.org/10.1016/j.clay.2015.08.015>
14. M. Kaya, M. F. Dilekoğlu, Ö Şahin, C. Saka, *Plasma Chem. Plasma Process.* **2016**, 36, 1417–1430. <https://doi.org/10.1007/s11090-016-9745-y>
15. O. Yavuz, C. Saka, *Appl. Clay Sci.* **2013**, 85, 96–102. <https://doi.org/10.1016/j.clay.2013.09.011>
16. Phonolite supplied by the company Keramost. Web link accessed on 05/31/2017. Web link: <http://www.keramost.cz/en/products/-/phonolite>
17. J.M. Hidalgo, Z. Tišler, D. Kubička, K. Raabova, R. Bulaňek, *J. Mol. Catal. A Chem.* **2016**, 420, 178–189. <https://doi.org/10.1016/j.molcata.2016.04.024>
18. R. L. Frost, A. López, F. L. Theiss, A. W. Romano, R. Scholz, *Spectrochim. Acta A Mol. Biomol. Spectrosc.* **2014**, 133, 521–525. <https://doi.org/10.1016/j.saa.2014.06.034>

Povzetek

Vzorci fonolita smo obdelovali v hladni plazmi in razredčeni klorovodikovi kislini ter preučevali vpliv postopkov na strukturo in kislinske lastnosti. Analizirali smo jih z naslednjimi metodami: rentgensko praškovo difrakcijo (XRD), elementno analizo (rentgensko fluorescenčno spektrometrijo XRF), meritvami specifične površine (BET), temperaturno programirano desorpcijo NH₃ (TPD – NH₃) in infrardečo spektroskopijo (FT-IR). Preizkušali smo tudi primernost vzorcev za adsorpcijo nečistoč Ca, K, Mg, P in Na iz odpadnega jedilnega olja. Vzorci, ki smo jih obdelali v plazmi, so imeli glede na začetno stanje skoraj enako strukturo z nekaj razlikami na površini. Večji vpliv je imelo obdelovanje s kislino. V tem primeru se je povečala površina vzorca, spremenila njegova struktura in sestava ter kislinske lastnosti.

Scientific paper

Synthesis, Antimicrobial Activity and *in silico* Studies on Thymol Esters

Jelena Lazarević,^{1*} Ana Kolarević,² Aleksandra Đorđević,³ Gordana Stojanović,³ Andrija Šmelcerović,^{1,2} Pierangela Ciuffreda⁴ and Enzo Santaniello⁵

¹ Department of Chemistry, Faculty of Medicine, University of Niš, Bul. dr Zorana Đinđića 81, 18000 Niš (Serbia)

² Department of Pharmacy, Faculty of Medicine, University of Niš, Bul. dr Zorana Đinđića 81, 18000 Niš (Serbia)

³ Department of Chemistry, Faculty of Science and Mathematics, University of Niš, Višegradska 33, 18000 Niš (Serbia)

⁴ Dipartimento di Scienze Biomediche e Cliniche »L. Sacco«, Università degli Studi di Milano, Via G. B. Grassi 74, 20157 Milano, Italy

⁵ Department of Biomedical Sciences, Humanitas University, Via Manzoni 113, 20089 Rozzano - Milano, Italy

* Corresponding author: E-mail: jelena217@yahoo.com

Received: 11-03-2017

Abstract

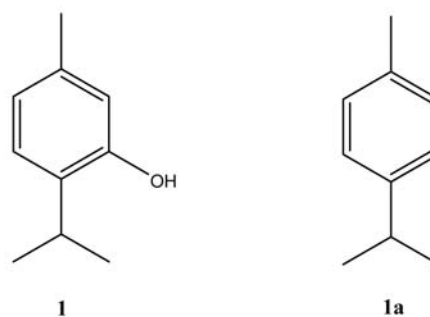
Derivatisation of parent structure in terpenoids often results in enhancement of biological activity of newly obtained compounds. Thymol, a naturally occurring phenol biosynthesized through the terpene pathway, is a well known biocide with strong antimicrobial attributes and diverse therapeutic activities. We have aimed our study on a single modification of phenolic functionality in thymol in order to obtain a small focused library of twenty thymyl esters, ten of which were new compounds. All compounds were involved in *in vitro* antimicrobial testing. Another important aspect of current study was implementation of *in silico* calculation of physico-chemical, pharmacokinetic and toxicological properties, which could be helpful by giving an additional guidance in further research.

Keywords: chemical synthesis, thymyl esters, *in vitro* antimicrobial activity, *in silico* calculation

1. Introduction

Terpenoids constitute an abundant and potent group of natural products, which play an important role in the enzyme systems of plants and reflect conspicuous biological activity against various pests. Their biological activity is believed to be related to the nature and the position of functional groups or substituents.¹ Chemical modification of natural monoterpenoids has been reported to result in enhancement of biological activities when compared to parent compounds.^{2–5} Thymol (**1**), a monoterpene biosynthetically directly related to *para*-cymene (**1a**)⁶ and a naturally occurring phenol, is a well known biocide and most dominant constituent of the oils of thyme (*Thymus vulgaris* L.) and oregano (*Origanum vulgare* L.).

Numerous studies have demonstrated the antimicrobial effect of thymol, ranging from inducing antibiotic



Scheme 1. Chemical structures of thymol (**1**) and *para*-cymene (**1a**).

susceptibility in drug-resistant pathogens through a synergistic effect, to a powerful antioxidant properties.⁷ Thymol has been shown to be an effective fungicide, particularly against fluconazole-resistant strains⁸ and was demonstrated to have strong antimutagenic effect.⁹ In addi-

tion, there is evidence that thymol has antitumor properties.¹⁰

The primary mode of antibacterial action of thymol is not fully known, but is believed to involve outer- and inner membrane disruption, and interaction with membrane proteins and intracellular targets.^{11–16} The mode of action of thymol against yeast and fungi has been sparsely investigated, though certain studies point to interactions with the cell envelope and intracellular targets.^{16–19}

Thymyl derivatives are well represented in Asteraceae plants, particularly within tribes Senecioneae, Eupatorieae, Inuleae and Helenieae. In some *Inula*, *Doronicum* and *Pulicaria* species, thymyl derivatives rather than sesquiterpenoids are the major root constituents.^{20–23} A review by Talavera-Aleman and collaborators²⁴ estimated that only 10% of known functionalized thymyl derivatives have been employed in biological testing, showing vast array of diverse activities, such as antimicrobial^{4,5,22,25–27} (several papers reporting inhibitory activity against plants' pathogenic fungi^{22,26}), antioxidant,²⁸ antinociceptive,²⁹ anti-parasitic (antileishmanial),^{30,31} antiprotozoal,³² insecticidal³³ and piscicidal³⁴ activity. The usefulness of thymyl derivatives as transdermal drug delivery enhancers has also been reported.³⁵

There are several papers reporting isolation, synthesis^{4,23,29,33,36} and biological activity^{4,5,22,25,28–30,33} of thymyl esters. Grodnitzky and Coats³³ have tested insecticidal activity of thymyl esters of acetic, dichloroacetic, trichloroacetic, chlorodifluoroacetic, pivalic and chloropivalic acid on *Musca domestica*. Mathela and collaborators⁴ evaluated antibacterial activity of thymyl esters of acetic, propanoic, 2-methylpropanoic, 3-methylbutanoic, but-2-enoic, benzoic and 2-phenylacetic acids and reported the enhancement in the activity of derivatives in comparison to thymol. Kumbhar and Dewang⁵ tested antifungal activity and observed structure-activity relationship, stating that thymyl ethers showed better antifungal potency over esters (thymyl acetate, benzoate, cinnamate, dithymyl malonate, succinate and glutarate) and that the addition of a methylene group or a carbon, an olefinic bond or an aromatic moiety in side chain led to compounds with improved potency over the parent compound (thymol).⁵ Angeles-Lopez et al.²⁹ have undertaken a study to establish the potential acute toxicity and the antinociceptive activity in animal models of thymyl esters of C₂–C₆ straight chain, C₄–C₆ acids positional isomers, diastereoisomers of 2-pentenoic, and of benzoic acid, reporting several esters with antinociceptive effect at a dose of 1 mg/kg.

Keeping in view diverse pharmacological activities of thymol^{7–19} and preliminary results on bioactivity of thymyl derivatives^{4,5,22,25,28–30,33} we have set the aim of our study. By making a single modification of a phenolic functionality in thymol we have obtained a series of ester compounds (**3a–t**), performed their structural characterization, *in vitro* antimicrobial testing and *in silico* calcula-

tion of physico-chemical, pharmacokinetic and toxicological properties. The most important contribution of this study is the synthesis of ten new compounds (**3i**, **3k–s**) followed by results obtained in antimicrobial assay and *in silico* calculations, which all together could be an important aspect and an additional guidance in further research.

2. Materials and Methods

2.1. Chemicals Used

All of the reagents, standards and solvents used were of analytical reagent grade. Unless specified otherwise, all chemicals were purchased from Merck (Darmstadt, Germany).

2.2. General Synthetic Procedures

Acetyl, benzoyl and palmitoyl chloride were purchased from Sigma-Aldrich. The conversion of the other carboxylic acids to acyl chlorides^{37,38} and the preparation of thymyl esters utilized methods from the literature.^{39,40} Scheme 1 presents the synthesis of thymyl esters.

2.2.1. General Procedures for Synthesis of Acid Chlorides

(a) An old procedure developed by Brown³⁷ was used for the preparation of volatile acid chlorides. This procedure involves the action of a relatively slightly volatile benzoyl chloride upon an organic acid. Following this protocol, the synthesis of chlorides up to 10 carbons, as well as 2-chloroacetyl chloride was achieved. In a round-bottom flask equipped by a fractionating column 0.25 mol of the acid and 0.375 mol of benzoyl chloride were placed. The mixture was heated until the boiling point was reached, and then the acid chloride was distilled from the reaction mixture. The material so obtained was used directly in the synthesis.

(b) For the preparation of chlorides higher than 10 C atoms the corresponding acid was refluxed for 2 h with thionyl chloride in CCl₄.³⁸ The solvent and the excess of thionyl chloride were removed with the aid of the water pump vacuum.

The products obtained in either way were used directly in the synthesis.

2.2.2. General Procedure for the Synthesis of Thymyl Esters **3a–t**

Series of thymyl esters were made following the procedure described by Paolini et al.³⁹ A solution of acid chloride (4.5 mmol) in CH₂Cl₂ (15 mL) was added drop by drop to a cooled mixture (0 °C) of thymol (3.3 mmol) and Et₃N (4.5 mmol) in CH₂Cl₂ (20 mL). The mixture was stirred at room temperature and then refluxed for 3 h. The

organic layer was washed with water (3 × 200 mL), dried over anhydrous Na₂SO₄ and concentrated under vacuum. The esters were purified by column chromatography, stationary phase Silica Gel 60 (70–230 mesh), mobile phase (hexane/diethyl ether, gradient 9:1 to 8:2). For yields, see supplementary data.

Thymyl Acetate (3a)

Chromatographic purification gave colorless oil. C₁₂H₁₆O₂ (*M* = 192.25); yield 85%; MS (EI): *m/z* (%) 192 (M⁺) (11.3), 151 (4.8), 150 (42.6), 151 (4.8), 135 (100), 136 (11.0), 115 (7.3), 105 (4.7), 77 (5.1), 43 (4.1); RI (HP5-MS): 1367; ¹H NMR (500.13 MHz, CDCl₃): δ (ppm) 7.22 (1H, d, *J* = 8 Hz, Ar-H), 7.05 (1H, d, *J* = 8 Hz, Ar-H), 6.84 (1H, s, Ar-H), 3.00 (1H, spt, *J* = 7 Hz, CH), 2.34 (6H, s, CH₃), 1.22 (6H, d, *J* = 7 Hz, CH₃); ¹³C NMR (125.76 MHz, CDCl₃): δ (ppm) 169.77 (C=O), 147.84 (C_{Ar}), 136.95 (C_{Ar}), 136.52 (C_{Ar}), 127.52 (C_{Ar}), 126.78 (C_{Ar}), 123.23 (C_{Ar}), 26.89 (CH), 26.57 (CO-CH₃), 22.99 (2 × CH₃), 21.21 (CH₃).

Thymyl 2-Chloroacetate (3b)

Chromatographic purification gave colorless oil. C₁₂H₁₅O₂Cl (*M* = 226.70); yield 85%; MS (EI): *m/z* (%) 226 (M⁺) (10.1), 150 (30.4), 149 (19.4), 136 (9.4), 133 (11.1), 115 (6.5), 105 (8.1), 91 (14.6), 77 (11.4); RI (HP5-MS): 1572; ¹H NMR (500.13 MHz, CDCl₃): δ (ppm) 7.24 (1H, d, *J* = 8 Hz, Ar-H), 7.08 (1H, d, *J* = 7.6 Hz, Ar-H), 6.87 (1H, s, Ar-H), 4.33 (2H, s, CH₂), 3.00 (1H, spt, *J* = 6.90 Hz, CH), 2.34 (3H, s, CH₃), 1.22 (6H, d, *J* = 6.90 Hz, CH₃). ¹³C NMR (125.76 MHz, CDCl₃): δ (ppm) 166.11 (C=O), 147.45 (C_{Ar}), 136.81 (C_{Ar}), 136.79 (C_{Ar}), 127.64 (C_{Ar}), 126.60 (C_{Ar}), 122.20 (C_{Ar}), 40.74 (CH₂), 27.01 (CH), 22.98 (2 × CH₃), 20.77 (CH₃-Ar).

Thymyl Propanoate (3c)

Chromatographic purification gave colorless oil. C₁₃H₁₈O₂ (*M* = 206.28); yield 82%; MS (EI): *m/z* (%) 206 (M⁺) (9.5), 151 (4.5), 150 (42.1), 135 (100), 136 (9.5), 115 (5.7), 105 (5.4), 91 (11.0), 77 (5.1), 57 (12.6); RI (HP5-MS): 1455; ¹H NMR (500.13 MHz, CDCl₃): δ (ppm) 7.21 (1H, d, *J* = 8 Hz, Ar-H), 7.04 (1H, d, *J* = 8 Hz, Ar-H), 6.83 (1H, s, Ar-H), 2.99 (1H, spt, *J* = 14 Hz, CH), 2.63 (2H, q, *J* = 8 Hz, CH₂), 2.33 (3H, s, CH₃), 1.32 (3H, m, CH₃), 1.21 (6H, d, *J* = 7 Hz, CH₃); ¹³C NMR (125.76 MHz, CDCl₃): δ (ppm) 173.16 (C=O), 147.93 (C_{Ar}), 136.96 (C_{Ar}), 136.5 (C_{Ar}), 126.69 (C_{Ar}), 123.24 (C_{Ar}), 122.77 (C_{Ar}), 27.73 (CH), 26.91 (CH₂), 22.90 (CH₃), 23.03 (2 × CH₃), 9.31 (CH₃).

Thymyl Butanoate (3d)

Chromatographic purification gave yellowish oil. C₁₄H₂₀O₂ (*M* = 220.31); yield 84%; MS (EI): *m/z* (%) 220 (M⁺) (9.7), 151 (6.1), 150 (55.5), 136 (9.5), 135 (100), 115 (5.4), 105 (5.7), 91 (10.4), 71 (9.3), 43 (7.1); RI (HP5-MS): 1544; ¹H NMR (500.13 MHz, CDCl₃): δ

(ppm) 7.21 (1H, d, *J* = 8 Hz, Ar-H), 7.04 (1H, d, *J* = 8 Hz, Ar-H), 6.82 (1H, s, Ar-H), 2.99 (1H, spt, *J* = 7 Hz, CH), 2.58 (2H, t, *J* = 7 Hz, CH₂), 2.33 (3H, s, CH₃), 1.84 (2H, sxt, *J* = 7 Hz, CH₂), 2.1 (6H, d, *J* = 7 Hz, CH₃), 1.08 (3H, t, *J* = 7 Hz, CH₃); ¹³C NMR (125.76 MHz, CDCl₃): δ (ppm) 172.34 (C=O), 147.88 (C_{Ar}), 136.98 (C_{Ar}), 136.49 (C_{Ar}), 126.66 (C_{Ar}), 125.99 (C_{Ar}), 123.24 (C_{Ar}), 36.24 (CH₂), 26.90 (CH), 23.07 (2 × CH₃), 18.55 (CH₂), 13.78 (CH₃).

Thymyl 2-Methylpropanoate (3e)

Chromatographic purification gave colorless oil. C₁₄H₂₀O₂ (*M* = 220.31); yield 75%; MS (EI): *m/z* (%) 220 (M⁺) (11.4), 150 (59.6), 136 (9.4), 135 (100), 115 (7.3), 105 (8.0), 91 (15.1), 77 (6.8), 71 (18.8), 43 (21.9); RI (HP5-MS): 1495; ¹H NMR (500.13 MHz, CDCl₃): δ (ppm) 7.21 (1H, d, *J* = 8 Hz, Ar-H), 7.03 (1H, d, *J* = 7.6 Hz, Ar-H), 6.81 (1H, s, Ar-H), 2.99 (1H, spt, *J* = 6.9 Hz, CH), 2.85 (1H, spt, *J* = 7 Hz, CH), 2.33 (3H, s, CH₃) 1.36 (6H, d, *J* = 7.3 Hz, 2 × CH₃), 1.21 (6H, d, *J* = 6.9 Hz, 2 × CH₃). ¹³C NMR (125.76 MHz, CDCl₃): δ (ppm) 175.71 (C=O), 147.99 (C_{Ar}), 136.97 (C_{Ar}), 136.47 (C_{Ar}), 126.62 (C_{Ar}), 126.56 (C_{Ar}), 122.14 (C_{Ar}), 33.95 (CH), 26.78 (CH), 22.99 (2 × CH₃), 19.20 (CH₃), 19.05 (2 × CH₃).

Thymyl Pentanoate (3f)

Chromatographic purification gave colorless oil. C₁₅H₂₂O₂ (*M* = 234.33); yield 87%; MS (EI): *m/z* (%) 234 (M⁺) (8.1), 151 (7.4), 150 (67.6), 135 (100), 136 (9.3), 115 (5.5), 105 (6.1), 91 (10.7), 85 (8.0), 57 (16.4); RI (HP5-MS): 1640; ¹H NMR (500.13 MHz, CDCl₃): δ (ppm) 7.21 (1H, d, *J* = 8 Hz, Ar-H), 7.04 (1H, d, *J* = 8 Hz, Ar-H), 6.82 (1H, s, Ar-H), 2.99 (1H, spt, *J* = 14 Hz, CH), 2.6 (2H, t, *J* = 7.6 Hz, CH₂), 2.33 (3H, s, CH₃), 1.79 (2H, quin, *J* = 7.5 Hz, CH₂), 1.49 (2H, sxt, *J* = 15 Hz, CH₂), 1.21 (6H, d, *J* = 6.9 Hz, 2 × CH₃), 1.01 (3H, t, *J* = 7.5 Hz, CH₃); ¹³C NMR (125.76 MHz, CDCl₃): δ (ppm) 172.45 (C=O), 147.90 (C_{Ar}), 136.95 (C_{Ar}), 136.45 (C_{Ar}), 126.96 (C_{Ar}), 126.3 (C_{Ar}), 122.7 (C_{Ar}), 34.06 (CH₂), 27.06 (CH₂), 27.02 (CH), 22.28 (CH₂), 22.96 (2 × CH₃), 20.76 (CH₃-Ar), 18.55 (CH₂), 13.8 (CH₃).

Thymyl 3-Methylbutanoate (3g)

Chromatographic purification gave colorless oil. C₁₅H₂₂O₂ (*M* = 234.33); yield 81%; MS (EI): *m/z* (%) 234 (M⁺) (8.9), 151 (8.3), 150 (71.4), 135 (100), 136 (9.3), 115 (5.4), 105 (6.8), 91 (11.0), 85 (9.3), 52 (21.5); RI (HP5-MS): 1590; ¹H NMR (500.13 MHz, CDCl₃): δ (ppm) 7.21 (1H, d, *J* = 8 Hz, Ar-H), 7.04 (1H, d, *J* = 7.6 Hz, Ar-H), 6.81 (1H, s, Ar-H), 3.00 (1H, spt, *J* = 6.9 Hz, CH), 2.48 (2H, d, *J* = 6.9 Hz, CH₂), 2.33 (3H, s, CH₃), 2.28 (1H, m, CH), 1.49 (2H, sxt, *J* = 15 Hz, CH₂), 1.20 (6H, d, *J* = 6.9 Hz, 2 × CH₃), 1.09 (6H, d, *J* = 6.6 Hz, 2 × CH₃); ¹³C NMR (125.76 MHz, CDCl₃): δ (ppm) 171.74 (C=O), 147.87 (C_{Ar}), 136.99 (C_{Ar}), 136.45 (C_{Ar}), 126.99 (C_{Ar}), 126.32 (C_{Ar}), 122.70 (C_{Ar}), 43.34 (CH₂), 26.98

(CH₂), 25.98 (CH), 23.01 (2 × CH₃), 22.44 (2 × CH₃), 20.78 (CH₃-Ar).

Thymyl Hexanoate (3h)

Chromatographic purification gave colorless oil, C₁₆H₂₄O₂ (*M* = 248.36); yield 79%; MS (EI): *m/z* (%) 248 (M⁺) (7.3), 151 (8.9), 150 (79.2), 136 (9.4), 135 (100), 105 (6.7), 99 (6.6), 91 (10.5), 71 (9.7), 43 (9.3); RI (HP5-MS): 1738; ¹H NMR (500.13 MHz, CDCl₃): δ (ppm) 7.20 (1H, d, *J* = 8 Hz, Ar-H), 7.03 (1H, d, *J* = 7.6 Hz, Ar-H), 6.81 (1H, s, Ar-H), 2.98 (1H, spt, *J* = 6.9 Hz, CH), 2.58 (2H, t, *J* = 7.6 Hz, CH₂), 2.32 (3H, s, CH₃), 1.79 (2H, quin, *J* = 7.5 Hz, CH₂), 1.41 (4H, m, CH₂), 1.20 (6H, d, *J* = 6.9 Hz, CH₃), 0.95 (3H, m, CH₃); ¹³C NMR (125.76 MHz, CDCl₃): δ (ppm) 172.50 (C=O), 147.90 (C_{Ar}), 137.00 (C_{Ar}), 136.50 (C_{Ar}), 127.00 (C_{Ar}), 126.3 (C_{Ar}), 122.7 (C_{Ar}), 34.38 (CH₂), 31.36 (CH₂), 27.08 (CH), 24.76 (CH₂), 23.03 (2 × CH₃), 22.36 (CH₂), 20.83 (CH₃), 13.94 (CH₃).

Thymyl Heptanoate (3i)

Chromatographic purification gave colorless oil, C₁₇H₂₆O₂ (*M* = 262.39); yield 84%; MS (EI): *m/z* (%) 262 (M⁺) (7.6), 151 (10.8), 150 (95.6), 149 (5.3), 136 (9.4), 135 (100), 113 (5.6), 105 (6.4), 91 (9.8), 43 (9.4); RI (HP5-MS): 1840; ¹H NMR (500.13 MHz, CDCl₃): δ (ppm) 7.21 (1H, d, *J* = 8 Hz, Ar-H), 7.03 (1H, d, *J* = 8 Hz, Ar-H), 6.81 (1H, s, Ar-H), 2.99 (1H, spt, *J* = 14 Hz, CH), 2.59 (2H, t, *J* = 8 Hz, CH₂), 2.33 (3H, s, CH₃), 1.79 (2H, m, CH₂), 1.45 (2H, m, CH₂), 1.36 (4H, m, CH₂), 1.22 (6H, m, CH₃), 0.92 (3H, m, CH₃); ¹³C NMR (125.76 MHz, CDCl₃): δ (ppm) 172.53 (C=O), 147.91 (C_{Ar}), 136.99 (C_{Ar}), 136.49 (C_{Ar}), 126.99 (C_{Ar}), 126.33 (C_{Ar}), 122.73 (C_{Ar}), 34.39 (CH₂), 31.44 (CH₂), 28.84 (CH₂), 27.03 (CH), 25.0 (CH₂), 23.0 (2 × CH₃), 22.49 (CH₂), 20.8 (CH₃-Ar), 14.01 (CH₃).

Thymyl Octanoate (3j)

Chromatographic purification gave colorless oil, C₁₈H₂₈O₂ (*M* = 276.41); yield 85%; MS (EI): *m/z* (%) 276 (M⁺) 151 (11.3), 150 (100), 136 (9.3), 135 (98.3), 109 (6.4), 105 (7.2), 91 (10.9), 57 (27.2), 55 (9.4), 43 (6.3); RI (HP5-MS): 1938; ¹H NMR (500.13 MHz, CDCl₃): δ (ppm) 7.21 (1H, d, *J* = 7.9 Hz, Ar-H), 7.03 (1H, d, *J* = 7.9 Hz, Ar-H), 6.81 (1H, s, Ar-H), 2.99 (1H, spt, *J* = 6.9 Hz, CH), 2.59 (2H, t, *J* = 7.5 Hz, CH₂), 2.33 (3H, s, CH₃), 1.79 (2H, quin, *J* = 7.5 Hz, CH₂), 1.47–1.29 (8H, m, CH₂), 1.21 (6H, bd, CH₃), 0.92 (3H, t, *J* = 6.8 Hz, CH₃); ¹³C NMR (125.76 MHz, CDCl₃): δ (ppm) 174.20 (C=O), 148.00 (C_{Ar}), 136.80 (C_{Ar}), 136.09 (C_{Ar}), 127.00 (C_{Ar}), 126.30 (C_{Ar}), 122.80 (C_{Ar}), 36.10 (CH₂), 34.00 (CH₂), 32.04 (CH₂), 29.00 (CH₂), 28.00 (CH), 26.00 (CH₂), 23.0 (2 × CH₃), 22.10 (CH₂), 20.5 (CH₃-Ar), 14.00 (CH₃).

Thymyl Nonanoate (3k)

Chromatographic purification gave colorless oil, C₁₉H₃₀O₂ (*M* = 290.44); yield 79.80%; MS (EI): *m/z* (%)

290 (M⁺) (5.7), 151 (12.0), 150 (100), 141 (3.2), 136 (7.7), 135 (79.0), 121 (3.4), 117 (2.0), 115 (2.3), 91 (3.3); RI (HP5-MS): 2044; ¹H NMR (500.13 MHz, CDCl₃): δ (ppm) 7.24–7.19 (1H, m, Ar-H), 7.06–7.01 (1H, bd, Ar-H), 6.84–6.79 (1H, bs, Ar-H), 3.04–2.93 (1H, bm, CH), 2.63–2.56 (2H, bm, CH₂), 2.36–2.31 (3H, s, CH₃), 1.84–1.75 (2H, bm, CH₂), 1.49–1.26 (10H, bm, CH₂), 1.24–1.18 (6H, bt, CH₃), 0.95–0.87 (3H, bm, CH₃); ¹³C NMR (125.76 MHz, CDCl₃): δ (ppm) 172.53 (C=O), 147.91 (C_{Ar}), 136.99 (C_{Ar}), 136.49 (C_{Ar}), 126.99 (C_{Ar}), 126.33 (C_{Ar}), 122.73 (C_{Ar}), 36.10 (CH₂), 34.20 (CH₂), 32.00 (CH₂), 28.80 (2 × CH₂), 27.60 (CH), 25.60 (CH₂), 23.0 (2 × CH₃), 22.50 (CH₂), 20.8 (CH₃-Ar), 14.01 (CH₃).

Thymyl Decanoate (3l)

Chromatographic purification gave colorless oil, C₂₀H₃₂O₂ (*M* = 304.47); yield 75.50%; MS (EI): *m/z* (%) 304 (M⁺) (4.6), 151 (12.3), 150 (100), 136 (6.7), 135 (71.9), 109 (5.3), 91 (5.7), 71 (4.8), 57 (4.8), 55 (5.5); RI (HP5-MS): 2147; ¹H NMR (500.13 MHz, CDCl₃): δ (ppm) 7.21 (1H, d, *J* = 8 Hz, Ar-H), 7.03 (1H, d, *J* = 7.6 Hz, Ar-H), 6.82 (1H, s, Ar-H), 2.99 (1H, spt, *J* = 6.9 Hz, CH), 2.59 (2H, t, *J* = 7.5 Hz, CH₂), 2.33 (3H, s, CH₃), 1.8 (2H, quin, *J* = 7.5 Hz, CH₂), 1.49–1.25 (12H, bm, CH₂), 1.21 (6H, d, *J* = 6.9 Hz, CH₃), 0.91 (3H, t, *J* = 6.2 Hz, CH₃); ¹³C NMR (125.76 MHz, CDCl₃): δ (ppm) 172.52 (C=O), 147.91 (C_{Ar}), 136.99 (C_{Ar}), 136.48 (C_{Ar}), 126.99 (C_{Ar}), 126.33 (C_{Ar}), 122.73 (C_{Ar}), 34.39 (CH₂), 31.85 (CH₂), 29.43 (CH₂), 29.25 (2 × CH₂), 29.17 (CH₂), 27.04 (CH), 25.05 (CH₂), 23.0 (2 × CH₃), 22.67 (CH₂), 20.8 (CH₃-Ar), 14.09 (CH₃).

Thymyl Undecanoate (3m)

Chromatographic purification gave colorless oil, C₂₁H₃₄O₂ (*M* = 318.49); yield 82.00%; MS (EI): *m/z* (%) 318 (M⁺) 151 (7.9), 150 (100), 149 (7.4), 135 (80.1), 134 (6.8), 105 (7.0), 91 (13.3), 57 (18.4), 55 (20.2), 43 (12.1); RI (HP5-MS): 2245; ¹H NMR (500.13 MHz, CDCl₃): δ (ppm) 7.21 (1H, d, *J* = 8 Hz, Ar-H), 7.03 (1H, d, *J* = 7.6 Hz, Ar-H), 6.82 (1H, s, Ar-H), 2.99 (1H, spt, *J* = 13.9 Hz, CH), 2.59 (2H, t, *J* = 7.46 Hz, CH₂), 2.33 (3H, s, CH₃), 1.79 (2H, quin, *J* = 7.54 Hz, CH₂), 1.41–1.48 (2H, m, CH₂), 1.26–1.39 (12H, m, CH₂), 1.21 (6H, d, *J* = 6.94 Hz, CH₃), 0.91 (3H, t, *J* = 6.76 Hz, CH₃); ¹³C NMR (125.76 MHz, CDCl₃): δ (ppm) 172.52 (C=O), 147.91 (C_{Ar}), 136.99 (C_{Ar}), 136.48 (C_{Ar}), 126.99 (C_{Ar}), 126.33 (C_{Ar}), 122.73 (C_{Ar}), 34.39 (CH₂), 31.88 (CH₂), 29.54 (CH₂), 29.47 (CH₂), 29.30 (CH₂), 29.26 (CH₂), 29.17 (CH₂), 27.04 (CH), 25.05 (CH₂), 23.0 (2 × CH₃), 22.67 (CH₂), 20.8 (CH₃-Ar), 14.10 (CH₃).

Thymyl Dodecanoate (3n)

Chromatographic purification gave colorless oil, C₂₂H₃₆O₂ (*M* = 332.52); yield 76.30%; MS (EI): *m/z* (%) 332 (M⁺) (4.4), 151 (15.2), 150 (100), 136 (6.7), 135 (67.8), 109 (7.3), 91 (4.6), 57 (6.4), 55 (5.6), 43 (3.6); RI

(HP5-MS): 2355; ^1H NMR (500.13 MHz, CDCl_3): δ (ppm) 7.21 (1H, d, $J = 8$ Hz, Ar-H), 7.03 (1H, d, $J = 8$ Hz, Ar-H), 6.81 (1H, s, Ar-H), 2.98 (1H, spt, $J = 6.9$ Hz, CH), 2.59 (2H, t, $J = 7.6$ Hz, CH_2), 2.33 (3H, s, CH_3), 1.79 (2H, quin, $J = 7.5$ Hz, CH_2), 1.48–1.40 (14H, m, CH_2), 1.20 (6H, d, $J = 6.9$ Hz, CH_3), 0.90 (3H, t, $J = 6.8$ Hz, CH_3); ^{13}C NMR (125.76 MHz, CDCl_3): δ (ppm) 172.55 (C=O), 147.91 (C_{Ar}), 136.99 (C_{Ar}), 136.49 (C_{Ar}), 126.99 (C_{Ar}), 126.33 (C_{Ar}), 122.73 (C_{Ar}), 34.40 (CH_2), 31.90 (CH_2), 29.60 ($2 \times \text{CH}_2$), 29.47 (CH_2), 29.33 (CH_2), 29.18 (CH_2), 29.17 (CH_2), 27.04 (CH), 25.06 (CH_2), 23.01 ($2 \times \text{CH}_3$), 22.68 (CH_2), 20.81 (CH_3 -Ar), 14.10 (CH_3).

Thymyl Tridecanoate (3o)

Chromatographic purification gave colorless oil, $\text{C}_{23}\text{H}_{38}\text{O}_2$ ($M = 346.55$); yield 85.1%; MS (EI): m/z (%) 346 (M^+) (2.4), 347 (0.6), 197 (0.9), 152 (0.9), 151 (12.9), 150 (100), 137 (0.4), 136 (5.0), 135 (54.2), 119 (0.5); RI (HP5-MS): 2453; ^1H NMR (500.13 MHz, CDCl_3): δ (ppm) 7.21 (1H, d, $J = 7.98$ Hz, Ar-H), 7.03 (1H, d, $J = 7.98$ Hz, Ar-H), 6.81 (1H, s, Ar-H), 2.98 (1H, spt, $J = 13.9$ Hz, CH), 2.59 (2H, t, $J = 7.63$ Hz, CH_2), 2.33 (3H, s, CH_3), 1.79 (2H, quin, $J = 7.54$ Hz, CH_2), 1.26–1.48 (16H, m, CH_2), 1.20 (6H, d, $J = 6.94$ Hz, CH_3), 0.90 (3H, t, $J = 6.76$ Hz, CH_3); ^{13}C NMR (125.76 MHz, CDCl_3): δ (ppm) 172.5 (C=O), 147.9 (C_{Ar}), 137 (C_{Ar}), 136.5 (C_{Ar}), 127.0 (C_{Ar}), 126.3 (C_{Ar}), 122.7 (C_{Ar}), 34.43 (CH_2), 31.94 (CH_2), 29.67 ($2 \times \text{CH}_2$), 29.51 (CH_2), 29.38 (CH_2), 29.3 (CH_2), 29.22 (CH_2), 27.08 (CH), 25.09 (CH_2), 23.04 ($2 \times \text{CH}_3$), 22.71 (CH_2), 20.83 (CH_3 -Ar), 14.13 (CH_3).

Thymyl Tetradecanoate (3p)

Chromatographic purification gave colorless oil, $\text{C}_{24}\text{H}_{40}\text{O}_2$ ($M = 360.57$); yield 72.05%; MS (EI): m/z (%) 360 (M^+) (1.9), 152 (0.9), 151 (12.7), 150 (100), 135 (50.7), 134 (4.8), 121 (1.3), 117 (0.7), 115 (1.9), 109 (5.1); RI (HP5-MS): 2555; ^1H NMR (500.13 MHz, CDCl_3): δ (ppm) 7.21 (1H, d, $J = 8$ Hz, Ar-H), 7.03 (1H, d, $J = 7.6$ Hz, Ar-H), 6.81 (1H, s, Ar-H), 2.99 (1H, spt, $J = 6.9$ Hz, CH), 2.59 (2H, t, $J = 7.6$ Hz, CH_2), 2.33 (3H, s, CH_3), 1.79 (2H, quin, $J = 7.5$ Hz, CH_2), 1.49–1.25 (20H, m, CH_2), 1.21 (6H, d, $J = 6.9$ Hz, CH_3), 0.91 (3H, t, $J = 6.9$ Hz, CH_3); ^{13}C NMR (125.76 MHz, CDCl_3): δ (ppm) 172.53 (C=O), 147.93 (C_{Ar}), 136.99 (C_{Ar}), 136.48 (C_{Ar}), 126.99 (C_{Ar}), 126.33 (C_{Ar}), 122.73 (C_{Ar}), 34.39 (CH_2), 31.92 (CH_2), 29.67 (CH_2), 29.65 ($2 \times \text{CH}_2$), 29.60 (CH_2), 29.48 (CH_2), 29.35 (CH_2), 29.27 (CH_2), 29.19 (CH_2), 27.04 (CH), 25.06 (CH_2), 23.00 ($2 \times \text{CH}_3$), 22.68 (CH_2), 20.80 (CH_3 -Ar), 14.10 (CH_3).

Thymyl Pentadecanoate (3q)

Chromatographic purification gave colorless oil, $\text{C}_{25}\text{H}_{42}\text{O}_2$ ($M = 374.60$); yield 68.90%; MS (EI): m/z (%) 374 (M^+) (5.3), 151 (23.9), 150 (100), 149 (7.5), 136 (8.3), 135 (76.4), 109 (11.9), 71 (4.4), 57 (7.0), 55 (6.2); RI (HP5-MS): 2669; ^1H NMR (500.13 MHz, CDCl_3): δ

(ppm) 7.21 (1H, d, $J = 8$ Hz, Ar-H), 7.03 (1H, d, $J = 8$ Hz, Ar-H), 6.81 (1H, s, Ar-H), 2.99 (1H, spt, $J = 6.90$ Hz, CH), 2.59 (2H, t, $J = 7.6$, CH_2), 2.33 (3H, s, CH_3), 1.79 (2H, quin, $J = 7.5$ Hz, CH_2), 1.48–1.24 (22H, bm, CH_2), 1.21 (6H, d, $J = 6.90$ Hz, CH_3), 0.9 (3H, t, $J = 6.90$ Hz, CH_3); ^{13}C NMR (125.76 MHz, CDCl_3): δ (ppm) 172.54 (C=O), 147.92 (C_{Ar}), 136.99 (C_{Ar}), 136.49 (C_{Ar}), 126.99 (C_{Ar}), 126.33 (C_{Ar}), 122.73 (C_{Ar}), 34.40 (CH_2), 31.92 (CH_2), 29.67 ($2 \times \text{CH}_2$), 29.65 ($2 \times \text{CH}_2$), 29.60 (CH_2), 29.48 (CH_2), 29.35 (CH_2), 29.27 (CH_2), 29.18 (CH_2), 27.04 (CH), 25.06 (CH_2), 23.01 ($2 \times \text{CH}_3$), 22.68 (CH_2), 20.81 (CH_3 -Ar), 14.10 (CH_3).

Thymyl Hexadecanoate (3r)

Chromatographic purification gave colorless oil, $\text{C}_{26}\text{H}_{44}\text{O}_2$ ($M = 388.63$); yield 95.06%; MS (EI): m/z (%) 388 (M^+) (5.8), 150 (100), 135 (65.4), 121 (4.3), 108 (3.4), 105 (4.0), 97 (3.3), 69 (5.6), 55 (6.1), 43 (4.3); RI (HP5-MS): 2772; ^1H NMR (500.13 MHz, CDCl_3): δ (ppm) 7.20 (1H, d, $J = 8$ Hz, Ar-H), 7.03 (1H, d, $J = 8$ Hz, Ar-H), 6.81 (1H, s, Ar-H), 2.98 (1H, spt, $J = 6.90$ Hz, CH), 2.58 (2H, t, $J = 7.5$, CH_2), 2.33 (3H, s, CH_3), 1.78 (2H, quin, $J = 7.5$ Hz, CH_2), 1.51–1.28 (24H, bm, CH_2), 1.21 (6H, d, $J = 6.90$ Hz, CH_3), 0.9 (3H, t, $J = 6.90$ Hz, CH_3); ^{13}C NMR (125.76 MHz, CDCl_3): δ (ppm) 172.50 (C=O), 147.94 (C_{Ar}), 136.99 (C_{Ar}), 136.49 (C_{Ar}), 126.99 (C_{Ar}), 126.33 (CH_{Ar}), 122.73 (C_{Ar}), 34.40 (CH_2), 31.92 (CH_2), 29.68 ($2 \times \text{CH}_2$), 29.65 ($2 \times \text{CH}_2$), 29.60 (CH_2), 29.47 (CH_2), 29.35 (CH_2), 29.27 (CH_2), 29.19 (CH_2), 25.06 (CH_2), 23.01 ($2 \times \text{CH}_3$), 22.68 (CH_2), 20.81 (CH_3 -Ar), 14.10 (CH_3).

Thymyl Heptadecanoate (3s)

Chromatographic purification gave colorless oil, $\text{C}_{27}\text{H}_{46}\text{O}_2$ ($M = 402.65$); yield 72.50%; MS (EI): m/z (%) 402 (M^+), 151 (19.6), 150 (100), 136 (5.4), 135 (55.2), 109 (9.2), 71 (3.3), 69 (3.0), 57 (5.5), 55 (5.0), 43 (3.0); RI (HP5-MS): 2870; ^1H NMR (500.13 MHz, CDCl_3): δ (ppm) 7.21 (1H, d, $J = 7.9$ Hz, Ar-H), 7.03 (1H, d, $J = 7.9$ Hz, Ar-H), 6.82 (1H, s, Ar-H), 2.99 (1H, spt, $J = 6.80$ Hz, CH), 2.59 (2H, t, $J = 7.5$, CH_2), 2.33 (3H, s, CH_3), 1.8 (2H, quin, $J = 7.5$ Hz, CH_2), 1.48–1.25 (26H, bm, CH_2), 1.21 (6H, d, $J = 6.80$ Hz, CH_3), 0.91 (3H, t, $J = 6.90$ Hz, CH_3); ^{13}C NMR (125.76 MHz, CDCl_3): δ (ppm) 172.50 (C=O), 147.9 (C_{Ar}), 137.0 (C_{Ar}), 136.5 (C_{Ar}), 127.0 (C_{Ar}), 126.30 (CH_{Ar}), 122.70 (C_{Ar}), 34.43 (CH_2), 31.96 (CH_2), 29.72 ($2 \times \text{CH}_2$), 29.52 ($2 \times \text{CH}_2$), 29.40 (CH_2), 29.31 (CH_2), 29.22 (CH_2), 26.54 (CH_2), 25.09 (CH_2), 23.05 ($2 \times \text{CH}_3$), 22.72 (CH_2), 20.84 (CH_3 -Ar), 14.15 (CH_3).

Thymyl Benzoate (3t)

Chromatographic purification gave white solid, $\text{C}_{17}\text{H}_{18}\text{O}_2$ ($M = 254.32$); yield 95%; MS (EI): m/z (%) 254 (M^+), (9.7), 150 (2.7), 149 (25.0), 133 (2.3), 106 (9.4), 105 (100), 91 (5.1), 78 (3.1), 77 (34.5), 51 (4.1); RI (HP5-MS): 1955; ^1H NMR (500.13 MHz, CDCl_3): δ (ppm) 8.26

(2H, d, $J = 7.3$ Hz, Ar-H), 7.68 (1H, t, Ar-H), 7.56 (2H, t, Ar-H), 7.28 (1H, d, $J = 8$ Hz, Ar-H), 7.11 (1H, d, $J = 8$ Hz, Ar-H), 6.98 (1H, s, Ar-H), 3.10 (1H, spt, $J = 6.90$ Hz, CH), 2.38 (3H, s, CH₃), 1.25 (6H, d, $J = 6.90$ Hz, CH₃); ¹³C NMR (125.76 MHz, CDCl₃): δ (ppm) 165.33 (C=O), 148.11 (C_{Ar}), 137.16 (C_{Ar}), 136.62 (C_{Ar}), 133.50 (C_{Ar}), 130.12 (2 × CH_{Ar}), 129.63 (CH_{Ar}), 128.60 (2 × CH_{Ar}), 127.15 (CH_{Ar}), 126.45 (CH_{Ar}), 122.84 (CH_{Ar}), 27.24 (CH), 23.03 (2 × CH₃), 20.85 (CH₃-Ar).

2. 3. Identification of Synthesized Compounds

2. 3. 1. GC-MS Analysis

MS spectra of samples of the synthesized compounds were recorded on a 7890/7000B GC/MS/MS triple quadrupole system (Agilent Technologies, USA, equipped with a Combi PAL auto sampler). The fused silica capillary column HP-5MS (5% phenylmethylsiloxane, 30 m × 0.25 mm, film thickness 0.25 μ m, Agilent Technologies, Palo Alto, CA, USA) was used. The injector, source and interface operated at 250, 230 and 300 °C, respectively. The temperature program: from 60 for 5 min isothermal to 300 °C at a heating rate of 8 °C/min and on 300 °C for 5 min isothermal. The solutions in hexane were injected in split ratio 10:1. The carrier gas was helium with a flow of 1.0 mL/min. Post run: back flash for 1.89 min, at 280 °C, with helium at 50 psi. MS conditions were as follows: ionization voltage of 70 eV, acquisition mass range 50–650, scan time 0.32 s. Semi-quantitative analysis was carried out directly from peak areas in the GC profile.

Linear retention indices (RI) were determined based on the retention times of C₈–C₄₀ alkanes run on HP-5MS column using the above mentioned temperature programme.⁴¹

2. 3. 2. NMR Analysis

¹H NMR spectra were recorded in CDCl₃ (isotopic enrichment 99.95%) solutions at 25 °C using a Bruker AVANCE 500 instrument (500.13 MHz for ¹H, 125.76 MHz for ¹³C) using 5 mm inverse detection broadband probes and deuterium lock.

2. 4. Antimicrobial Activity

2. 4. 1. Microbial Strains

The *in vitro* antimicrobial activity of the synthesized compounds was tested against a panel of laboratory control strains belonging to the American Type Culture Collection Maryland, USA. Gram-positive: *Bacillus subtilis* ATCC 6633 and *Staphylococcus aureus* ATCC 6538; Gram-negative: *Escherichia coli* ATCC 8739, *Pseudomonas aeruginosa* ATCC 9027; fungal organisms: *Aspergil-*

lus niger ATCC 16404 and *Candida albicans* ATCC 10231. The Gram-negative bacteria *Salmonella abony* NCTC 6017 and *Salmonella typhimurium* ATCC 14028 were obtained from the National Collection of Type Cultures. All microorganisms were maintained at –20 °C under appropriate conditions and regenerated twice before use in the manipulations.

2. 4. 2. Screening of Antimicrobial Activity

The minimal inhibitory concentration (MIC) of esters was determined based on a broth microdilution method in 96-well microtitre plates.⁴² The inocula of the bacterial strains were prepared from overnight broth cultures and suspensions were adjusted to 0.5 McFarland standard turbidity. Dimethyl sulphoxide (10% aqueous solution) was used to dissolve and to dilute samples to the highest concentration to be tested (stock concentrations 1 mg/mL). A serial doubling dilution of the samples was prepared in a 96-well microtiter plate, using the method of Sarker et al.⁴³ with slight modifications. The minimal bactericidal/fungicidal concentration (MBC/MFC) was evaluated as the lowest concentration of tested samples at which inoculated microorganisms were 99.9% killed. Tests were carried out in triplicate.

2. 5. *In silico* Physico-chemical, Pharmacokinetic and Toxicological Properties of the Synthesized Compounds

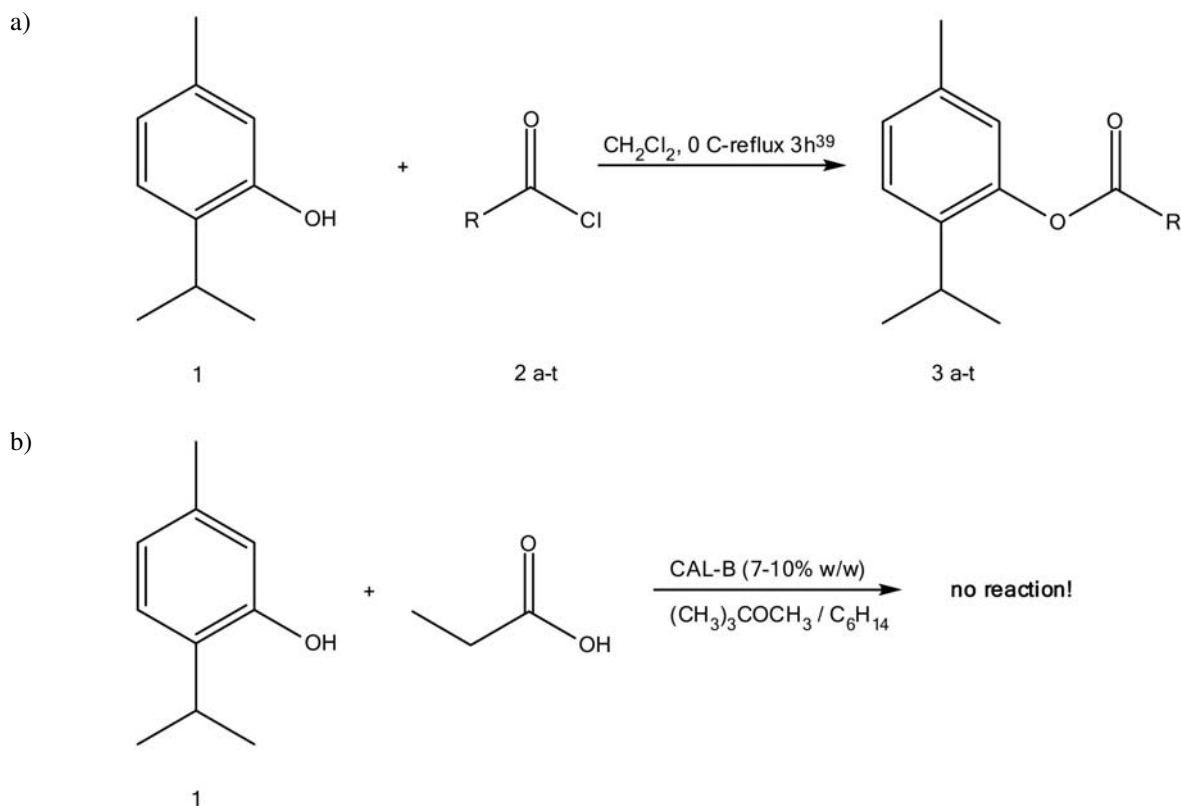
In order to obtain a complete picture of the synthesized compounds **3a–t** an *in silico* study was performed. Physico-chemical, pharmacokinetic and toxicological properties of compounds were calculated using the Molinspiration,⁴⁴ admetSAR,⁴⁵ DataWarrior⁴⁶ and Toxtree prediction tools.⁴⁷

3. Results and Discussion

3. 1. Chemical Synthesis

A small focused library of twenty thymyl esters was synthesized. To the best of our knowledge ten of twenty compounds are new (i.e. **3i**, **3k–s**; Scheme 1).

Although enzyme-catalyzed esterification of alcohols of different structures is a well-established approach,⁴⁸ the enzymatic esterification of phenols is not frequently reported.⁴⁹ Since a biocatalytic approach appeared especially appealing to us, we have tried to repeat the experimental protocol reported for the esterification of functionalized phenols with *Candida antarctica* lipase (CAL-B)⁴⁹ using thymol and propanoic acid as substrates and *tert*-butyl methyl ether and hexane as solvents. However, although no reaction occurred in our hands, the biocatalytic approach deserves further investigation within the recent trends of green chemistry methodologies.



Scheme 2. Synthesis of thymyl esters: (a) chemical synthesis approach; (b) enzyme-catalyzed approach.

Table 1. Thymyl esters: chemical entity, yields (%) and entry

R	Yield (%)	Product Name and Number
CH ₃	85.00	Thymyl Acetate 3a
CH ₂ Cl	85.00	Thymyl 2-Chloroacetate 3b
CH ₂ CH ₃	82.00	Thymyl Propanoate 3c
CH ₂ CH ₂ CH ₃	84.00	Thymyl Butanoate 3d
CH(CH ₃) ₂	75.00	Thymyl 2-Methylpropanoate 3e
CH ₂ (CH ₂) ₂ CH ₃	87.00	Thymyl Pentanoate 3f
CH ₂ CH(CH ₃) ₂	81.00	Thymyl 3-Methylbutanoate 3g
CH ₂ (CH ₂) ₃ CH ₃	79.00	Thymyl Hexanoate 3h
CH ₂ (CH ₂) ₄ CH ₃	84.00	Thymyl Heptanoate 3i
CH ₂ (CH ₂) ₅ CH ₃	85.00	Thymyl Octanoate 3j
CH ₂ (CH ₂) ₆ CH ₃	79.80	Thymyl Nonanoate 3k
CH ₂ (CH ₂) ₇ CH ₃	75.50	Thymyl Decanoate 3l
CH ₂ (CH ₂) ₈ CH ₃	82.00	Thymyl Undecanoate 3m
CH ₂ (CH ₂) ₉ CH ₃	76.30	Thymyl Dodecanoate 3n
CH ₂ (CH ₂) ₁₀ CH ₃	85.10	Thymyl Tridecanoate 3o
CH ₂ (CH ₂) ₁₁ CH ₃	72.05	Thymyl Tetradecanoate 3p
CH ₂ (CH ₂) ₁₂ CH ₃	68.90	Thymyl Pentadecanoate 3q
CH ₂ (CH ₂) ₁₃ CH ₃	95.06	Thymyl Hexadecanoate 3r
CH ₂ (CH ₂) ₁₄ CH ₃	72.50	Thymyl Heptadecanoate 3s
Ph	95.00	Thymyl Benzoate 3t

3. 2. Antimicrobial Activity

The results obtained in broth microdilution assay are presented in Supplementary data, Table S1. The assayed

samples were less effective than antibiotic/antimycotic used as reference standard and if noted, activity was never greater than the values obtained for the parent compound **1** (MIC/MBC/MFC never exceeded 0.5 mg/mL, Supplementary data, Table S1). The results are indicating selective susceptibility of the microorganisms, with *S. aureus* (**3a,b,e**), *P. aeruginosa* (**3b,j,k,p**) and *C. albicans* (**3a–e,g,n,p**) being the most sensitive strains to synthesized derivatives. On the other hand, five microorganisms (*B. subtilis*, *E. coli*, *S. abony*, *S. typhimurium* and *A. niger*) were completely resistant to synthesized compounds tested (initial concentration 1 mg/mL).

Five of our samples (**3a,c,e,g,t**) are matching the samples tested by Mathela and collaborators,⁴ who were making evaluation of antibacterial activity on *Streptococcus mutans* (MTCC 890), *S. aureus* (MTCC 96), *B. subtilis* (MTCC 121), *Staphylococcus epidermidis* (MTCC 435) and *E. coli* (MTCC 723), and who reported the enhancement of the activity for esters in comparison to thymol. For all other synthesized compounds antimicrobial results are reported for the first time. An interesting fact is that MIC values by Mathela⁴ were three- (2-methylpropanoate **3c** and 3-methylbutanoate **3e**) to even ten- (acetate **3a**) times lower for *B. subtilis* than for thymol. Having in best case comparable, but never greater MIC values than for thymol itself, in our *in vitro* experiment we could not confirm such results.⁴ The importance of free hydroxyl group in the phenolic structure was confirmed in terms of

activity when carvacrol was compared to its methyl ether,⁵⁰ however results presented by Mathela⁴ are contrary to the above-mentioned fact and to our results (Supplementary data, Table S1).

3. 3. *In silico* Study

3. 3. 1. Physico-chemical Properties of the Thymyl Esters 3a–t

Lipinski's rule of 5 gives evaluation to drug-likeness and determines if a substance with certain pharmacological or biological activity has properties that would make it a likely orally active drug in humans.⁵¹ Calculations of important molecular parameters stated by Lipinski such as fragment based contributions and correction factors ($m_i \text{Log P}$), topological polar surface area (TPSA) and drug-likeness were obtained by Molinspiration software.⁴⁴ Drug-likeness score of compounds 3a–t is given in Supplementary data, Table S2.

Seven compounds (3a–g) had $m_i \text{LogP}$ values below 5 and thus were predicted to have sufficient oral bioavailability. The rest of the compounds were estimated as lipophilic. All of the tested compounds (3a–t) had TPSA below 60 \AA^2 , and thus were predicted to have both good intestinal absorption and good BBB penetration. All of the tested compounds (3a–t) had less than 10 H-bond acceptors (n_{ON}) and less than 5 H-bond donors (n_{OHNH}). The conformational flexibility, described by the number of rotatable bonds (n_{rotb}), for 12 compounds (3a–k,t) was between 0 and 10, which warrants good oral bioavailability. Finally, all compounds (3a–t) had both molecular weight (MW) and molecular volume below 500.

Calculated physico-chemical properties showed that seven thymyl esters (3a–g) were predicted to have good oral bioavailability, with values for fragment based contributions and correction factors $m_i \text{LogP} < 5$, $\text{TPSA} < 140$, $\text{MW} < 500$, $n_{\text{ON}} < 10$, $n_{\text{OHNH}} < 5$ and $n_{\text{rotb}} < 10$.

3. 3. 2. Pharmacokinetic Properties of the Thymyl Esters 3a–t

Absorption properties of compounds 3a–t were predicted by admetSAR⁴⁵ (Supplementary data, Table S3). The results suggested that all of the tested compounds (3a–t) might be able to pass through blood-brain barrier (BBB) and penetrate into the CNS, might be capable of being absorbed by intestine, and were supposed to have positive Caco-2 permeability. Moreover, compounds 3a–t were predicted as non-substrates for P-glycoprotein, non-inhibitors of P-glycoprotein, and as non-inhibitors against renal organic cation transporter (ROCT).

Metabolic properties of the thymyl esters 3a–t were predicted by admetSAR⁴⁵ (Supplementary data, Table S4). None of the compounds was predicted as CYP450 2C9 and 2D6 substrate, while 16 compounds (3b,d,f,h–t) were predicted as CYP450 3A4 substrates. All of the te-

sted compounds were predicted as CYP450 1A2 inhibitors, but none of them was predicted as CYP450 2D6 and 3A4 inhibitors. Moreover, 15 compounds (3b,d,h–t) might be able to inhibit CYP450 2C19 enzyme, while only compound 3t was predicted as CYP450 2C9 inhibitor. Almost all thymyl esters (3a–s) were predicted to have low CYP inhibitory promiscuity, except compound 3t.

3. 3. 3. Toxicological Properties of the Thymyl Esters 3a–t

The structural alerts for DNA and protein binding for compounds 3a–t were predicted using Toxtree prediction tool based on decision tree approach.⁴⁷ Compounds 3a–t showed structural alerts for DNA binding as they were predicted as compounds able to undergo Michael addition. Moreover, compounds 3a–t showed structural alerts for protein binding due to their predicted ability to undergo Michael addition, ability to participate in acyl transfer and ability to undergo $\text{S}_{\text{N}}2$ reactions (results given in Supplementary data, Table S5).

Toxicological properties of compounds 3a–t predicted by admetSAR⁴⁵ have characterized compounds 3a–t as weak HERG (human Ether-à-go-go-Related Gene) inhibitors, non-AMES toxic and non-carcinogens, but highly toxic for fish, *Tetrahymena pyriformis* and honey bee. Ready biodegradable were supposed to be six compounds (3a,c–g). Depending on the risk for acute oral toxicity, only compound 3b was predicted as Category II, or compound with LD_{50} value greater than 50 mg/kg but less than 500 mg/kg, while the rest of the tested compounds (3a,c–t) were predicted as Category III, or compounds with LD_{50} values greater than 500 mg/kg but less than 5000 mg/kg. According to the TD_{50} values, compounds 3a–t were predicted as »non-required« or non-carcinogenic chemicals (Supplementary data, Table S6).

Only one study involving thymyl esters was undertaken to establish the potential acute toxicity in animal models.²⁹ The esters shown no acute toxicity to mice at doses higher than 5000 mg/kg which represents good congruence and indicate the usefulness of data obtained in our *in silico* study.

Toxicological properties of thymyl esters 3a–t predicted by DataWarrior⁴⁶ have shown that only compound 3b has a high risk for all mutagenic, tumorigenic, reproductive and irritant effects. Compound 3h was predicted to have high risk for tumorigenic and irritant effects. However, all compounds were predicted to have high risk for irritant effects (Supplementary data, Table S7).

4. Conclusion

We synthesized twenty esters of thymol, of which ten represent new compounds. All of the compounds were employed in antimicrobial bioassay and was found that

lower representatives of the synthesized homologous series of esters are antimicrobials comparable to thymol and can be considered as activity key holders, too. Results of our *in silico* study predicted that seven esters (lower representatives and short-chain fatty acids esters **3a–g**) obey Lipinski's rule of five, showing drug-likeness. The rest of the compounds were estimated as lipophilic. All compounds, except thymyl 2-chloroacetate (**3b**) and thymyl hexanoate (**3h**), were predicted as non-mutagenic, non-tumorigenic, non-AMES toxic and non-carcinogenic, but highly toxic for fish, *T. pyriformis* and honey bee. They are likely to be absorbed by intestine and were predicted as ready biodegradable, weak HERG inhibitors, Category III of risk for acute toxicity, with no risk for reproductive effects, but with high risk for irritant effects. Taking in consideration predicted *in silico* properties and estimated drug likeness score, pharmacological and toxicological profile, thymyl esters might be used as prodrugs. Among the chemical bonds used to link parental drug and carrier, esters have already proven to be promising due to their amenability to hydrolysis *in vivo* and are most frequently used in order to enhance the lipophilicity⁵² and passive membrane transport.

5. Acknowledgement

The authors acknowledge the Ministry of Science and Technological Development of Serbia for financial support (project 451-03-821/2012-14 and 172044) as well as internal project of Faculty of Medicine, University of Niš (project no. 4).

6. References

1. E. Breitmaier, Terpenes: flavors, fragrances, pharmaca, pheromones, Wiley-VCH Verlag GmbH & Co. KGaA, Weinheim, Germany, **2006**.
2. J. R. Coats, L. L. Karr, C. D. Drewas, in: *Naturally occurring pest bioregulators*; P. H. Hedin, Ed.; ACS Symposium Series 449; American Chemical Society: Washington, DC, **1991**, pp. 305.
3. R. Tsao, S. Lee, P. J. Rice, C. Jensen, J. R. Coats, in *Synthesis and Chemistry of Agrochemicals IV*; D. R. Baker, J. G. Fenyes, G. S. Basarab, Eds; ACS Symposium Series 584; American Chemical Society: Washington, DC, **1995**, p. 312.
4. C. S. Mathela, K. Singh, V. K. Gupta, *Acta Pol. Pharm.* **2010**, *67*, 375–380.
5. P. P. Kumbhar, P. M. Dewang, *J. Sci. Ind. Res.* **2001**, *60*, 645–648.
6. A. J. Polouse, R. Croteau, *Arch. Biochem. Biophys.* **1978**, *187*, 307–314.
[https://doi.org/10.1016/0003-9861\(78\)90039-5](https://doi.org/10.1016/0003-9861(78)90039-5)
7. K. Palaniappan, R. A. Holley, *Int. J. Food Microbiol.* **2010**, *140*, 164–168.
<https://doi.org/10.1016/j.ijfoodmicro.2010.04.001>
8. A. Aijaz, K. Amber, Y. Snowber, A. K. Luqman, *Fitoterapia*, **2010**, *81*, 1157–1162.
<https://doi.org/10.1016/j.fitote.2010.07.020>
9. N. Mezzoug, A. Elhadri, A. Dallouh, S. Amkiss, N. S. Skali, J. Abrini, A. Zhiri, D. Baudoux, B. Diallo, M. El Jaziri, M. Idaomar, *Res.-Gen. Tox. En. Mutat.* **2007**, *629*, 100–110.
<https://doi.org/10.1016/j.mrgentox.2007.01.011>
10. A. Andersen, *Int. J. Toxicol.* **2006**, *25*, 29–127.
<https://doi.org/10.1080/10915810600716653>
11. J. Sikkema, J. A. M. DeBont, B. Poolman, *Microbiol. Rev.* **1995**, *59*, 201–222.
12. I. M. Helander, H. L. Alakomi, K. Latva-Kala, T. Mattila-Sandholm, I. Pol, E. J. Smid, L. G. M. Gorris, A. Von Wright, *J. Agric. Food Chem.* **1998**, *46*, 3590–3595.
<https://doi.org/10.1021/jf980154m>
13. R. J. W. Lambert, P. N. Skandamis, P. J. Coote, G. J. E. Nychas, *J. Appl. Microbiol.* **2001**, *91*, 453–462.
<https://doi.org/10.1046/j.1365-2672.2001.01428.x>
14. S. E. Walsh, J. Y. Maillard, A. D. Russell, C. E. Catrenich, D. L. Charbonneau, R. G. Bartolo, *J. Appl. Microbiol.* **2003**, *94*, 240–247.
<https://doi.org/10.1046/j.1365-2672.2003.01825.x>
15. J. Xu, F. Zhou, B. P. Ji, R. S. Pei, N. Xu, *Lett. Appl. Microbiol.* **2008**, *47*, 174–179.
<https://doi.org/10.1111/j.1472-765X.2008.02407.x>
16. M. Hyldgaard, T. Mygind, R. L. Meyer, *Front. Microbiol.* **2012**, *3*, 1–24.
<https://doi.org/10.3389/fmicb.2012.00012>
17. M. A. Ghannoum, L. B. Rice, *Clin. Microbiol. Rev.* **1999**, *12*, 501–517.
18. M. D. Cristani, M. Arrigo, G. Mandalari, F. Castelli, M. G. Sarpietro, D. Micieli, V. Venuti, G. Bisignano, A. Saija, D. Trombetta, *J. Agric. Food Chem.* **2007**, *55*, 6300–6308.
<https://doi.org/10.1021/jf070094x>
19. A. Ahmad, A. Khan, F. Akhtar, S. Yousuf, I. Xess, L. Khan, N. Manzoor, *Eur. J. Clin. Microbiol. Infect. Dis.* **2012**, *30*, 41–50. <https://doi.org/10.1007/s10096-010-1050-8>
20. F. Bohlmann, P. K. Mahanta, J. Jakupovic, R. C. Rastogi, A. A. Natu, *Phytochemistry* **1978**, *17*, 1165–1172.
[https://doi.org/10.1016/S0031-9422\(00\)94308-5](https://doi.org/10.1016/S0031-9422(00)94308-5)
21. F. Bohlmann, C. Zdero, *Phytochemistry* **1977**, *16*, 1243–1245. [https://doi.org/10.1016/S0031-9422\(00\)94366-8](https://doi.org/10.1016/S0031-9422(00)94366-8)
22. J. Zhao, Y. Li, Q. Lui, K. Gao, *Food Chem.* **2010**, *120*, 512–516.
<https://doi.org/10.1016/j.foodchem.2009.10.045>
23. T. Xu, M. Gherib, C. Bekhechi, F. Atik-Bekkara, H. Casabianca, F. Tomi, J. Casanova, A. Bighellia, *Flavour Fragr. J.* **2015**, *30*, 83–90. <https://doi.org/10.1002/ffj.3223>
24. A. Talavera-Aleman, G. Rodriguez-Garcia, Y. Lopez, H. A. Garcia-Gutierrez, J. M. Torres-Valencia, R. E. del Rio, C. M. Cerda-Garcia-Rojas, P. Joseph-Nathan, M. A. Gomez-Hurtao, *Phytochem. Rev.* **2016**, *15*, 251–277.
<https://doi.org/10.1007/s11101-015-9412-6>
25. A. Stojakowska, B. Kedzia, W. Kisiel, *Fitoterapia* **2005**, *76*, 687–690. <https://doi.org/10.1016/j.fitote.2005.05.003>

26. S. Tawata, S. Taira, N. Kobamoto, M. Ishihara, S. Toyama, *J. Pestic. Sci.* **1996**, *21*, 141–146.
<https://doi.org/10.1584/jpestics.21.141>
27. H. Liang, F. Bao, X. Dong, R. Tan, C. Zhang, Q. Lu, Y. Cheng, *Molecules*, **2007**, *12*, 1606–1613.
<https://doi.org/10.3390/12081606>
28. J. Mastelić, I. Jerković, I. Blažević, M. Poljak-Blaži, S. Borovici, I. Ivančić-Baće, V. Smrečki, N. Zarković, K. Brčić-Kostić, D. Vikić-Topić, N. Muller, *J. Agric. Food Chem.* **2008**, *56*, 3989–3996.
29. G. Angeles-Lopez, A. Perez-Vasquez, F. Hernandez-Luis, M. Deciga-Campos, R. Bye, E. Linares, R. Mata, *J. Ethnopharmacol.* **2010**, *131*, 425–432.
<https://doi.org/10.1016/j.jep.2010.07.009>
30. S. M. de Morais, N. S. Vila-Nova, C. M. Leal Bevilaqua, F. C. Rondon, C. H. Lobo, A. de Alencar Araripe Noronha Moura, A. D. Sales, A. P. Ribeiro Rodrigues, J. R. de Figueiredo, C. C. Campello, M. E. Wilson, H. F. de Andrade Jr, *Bioorg. Med. Chem.* **2014**, *22*, 6250–6255.
<https://doi.org/10.1016/j.bmc.2014.08.020>
31. S. Robledo, E. Osorio, D. Munoz, L. M. Jaramillo, A. Restrepo, G. Arango, I. Velez, *Antimicrob. Agents Chemother.* **2005**, *49*, 1652–1655.
<https://doi.org/10.1128/AAC.49.4.1652-1655.2005>
32. C. Bustos-Brito, M. Sanchez-Castellanos, B. Esquivel, J. S. Calderon, F. Calzada, L. Yopez-Mulia, A. Hernandez-Barragan, P. Joseph-Nathan, G. Cuevas, L. Quijano, *J. Nat. Prod.* **2014**, *77*, 358–363.
<https://doi.org/10.1021/np400964w>
33. J. Grodnitzky, J. R. Coats, *J. Agric. Food Chem.* **2002**, *50*, 4576–4580. <https://doi.org/10.1021/jf0201475>
34. T. Yoshida, K. Mori, G. He, *Heterocycles* **1995**, *41*, 1923–1926. <https://doi.org/10.3987/COM-95-7148>
35. S. Wagner, A. Suter, I. Merfort, *Planta Med.* **2004**, *70*, 897–903. <https://doi.org/10.1055/s-2004-832613>
36. D. H. More, N. S. Pawar, P. M. Dewang, S. L. Patil, P. P. Mahulikar, *Russ. J. Gen. Chem.* **2004**, *74*, 217–218.
<https://doi.org/10.1023/B:RUGC.0000025504.59745.09>
37. H. C. Brown, *J. Am. Chem. Soc.* **1938**, *60*, 1325–1328.
<https://doi.org/10.1021/ja01273a014>
38. W. G. Rose, *J. Am. Chem. Soc.* **1947**, *69*, 1384–1387.
<https://doi.org/10.1021/ja01198a043>
39. J. Paolini, A. Muselli, A. F. Bernardini, A. Bighelli, J. Casanova, J. Costa, *Flavour Fragr. J.* **2007**, *22*, 479–487.
<https://doi.org/10.1002/ffj.1824>
40. D. Pavlović, B. Modec, D. Dolenc, *Acta Chim. Slov.* **2015**, *62*, 362–370.
<https://doi.org/10.17344/acsi.2014.1306>
41. H. Van Den Dool, P. D. Kratz, *J. Chromatogr. A* **1963**, *11*, 463–471.
[https://doi.org/10.1016/S0021-9673\(01\)80947-X](https://doi.org/10.1016/S0021-9673(01)80947-X) Et
42. NCCLS, Performance Standards for Antimicrobial Susceptibility Testing: Eleventh Informational Supplement, M100-S11. **2003**, National Committee for Clinical Laboratory Standards, Wayne, PA.
43. S. A. Sarker, L. Nahar Y. Kumarasamy, *Methods* **2007**, *42*, 321–324.
<https://doi.org/10.1016/j.ymeth.2007.01.006>
44. Molinspiration Home Page. <http://www.molinspiration.com/> (Accessed January 2017).
45. admetSAR Home Page. <http://lmmed.ecust.edu.cn:8000/predict/> (Accessed January 2017).
46. DataWarrior Home Page. (Accessed January 2017).
47. G. Patlewicz, N. Jeliazkova, R. J. Safford, A. P. Worth, B. Aleksiev, *Environ. Res.* **2008**, *19*, 495–524.
48. E. Santaniello, P. Ferraboschi, P. Grisenti, *Enzyme Microb. Technol.* **1993**, *15*, 367–382.
[https://doi.org/10.1016/0141-0229\(93\)90123-J](https://doi.org/10.1016/0141-0229(93)90123-J)
49. G. J. H. Buisman, C. T. W. van Helteren, G. F. H. Kramer, J. W. Veldsink, J. T. P. Derksen and F. P. Cuperus, *Biotechnol. Lett.* **1998**, *20*, 131–136.
<https://doi.org/10.1023/A:1005368222340>
50. H. J. D. Dorman, S. G. Deans, *J. Appl. Microbiol.* **2000**, *80*, 308–316.
<https://doi.org/10.1046/j.1365-2672.2000.00969.x>
51. C. A. Lipinski, F. Lombardo, B. W. Dominy, P. J. Feeney, *Adv. Drug. Deliv. Rev.* **2012**, *64*, 4–17.
<https://doi.org/10.1016/j.addr.2012.09.019>
52. D. Yancheva, E. Cherneva, M. Quick, B. Mikhova, B. Shvachev, R. Nikolova, A. Djordjevic, M. Untergehrer, G. Jürgenliemk, B. Kraus, A. Smelcerovic, *Acta Chim. Slov.* **2015**, *62*, 689–699.
<https://doi.org/10.17344/acsi.2015.1418>

Povzetek

Z derivatizacijo izhodnih struktur terpenoidov lahko pogosto pripravimo nove spojine, ki imajo izboljšane biološke aktivnosti. Naravni fenolov derivat timol, ki biosintezno nastane po terpenski poti, predstavlja dobro znan biocid z močnim protimikrobnim delovanjem in različnimi drugimi terapevtskimi aktivnostmi. Namen naše študije je bil pripraviti majhno, fokusirano knjižnico dvajsetih timolnih estrov s pomočjo ene same modifikacije fenolne funkcionalne skupine v timolu. Deset izmed pripravljenih spojin je novih. Vsem sintetiziranim spojinam smo *in vitro* določili protimikrobne lastnosti. Drug pomemben aspekt naše študije pa je bila uporaba *in silico* računskih metod za določitev fizikalno-kemijskih, farmakokinetičnih in toksikoloških lastnosti spojin, kar je omogočilo dodaten vpogled v njihove aktivnosti in daje nove usmeritve za nadaljnje raziskave.

Scientific paper

Synthesis, X-ray Structural Characterization, and DFT Calculations of Binuclear Mixed-ligand Copper(II) Complexes Containing Diamine, Acetate and Methacrylate Ligands

Rasoul Vafazadeh,^{1,*} Mansoor Namazian,¹ Mahshad Chavoshiyan,¹
Anthony C. Willis² and Paul D. Carr²

¹ Department of Chemistry, Faculty of Science, Yazd University, Yazd, Iran.

² Research School of Chemistry, Australian National University, Canberra, ACT 2601, Australia.

* Corresponding author: E-mail: rvafazadeh@yazd.ac.ir
Tel: +98 3538214778; Fax: +98 3537250110

Received: 28-03-2017

Abstract

The dinuclear Cu(II) complexes [Cu(en)(MAA)(μ -CH₃COO)]₂ (**1**) and [Cu(pn)(MAA)(μ -CH₃COO)]₂ (**2**) where MAA, en and pn are methacrylate, ethylenediamine and 1,3-propylenediamine, respectively, have been synthesized and characterized by elemental analysis, FT-IR and UV-Vis spectroscopy. The structures of the complexes have been determined by single-crystal X-ray diffraction analyses. In the dinuclear complexes **1** and **2** the two copper centers are five-coordinated and exhibit distorted square pyramidal geometries. The theoretical geometries of the studied compounds have been calculated by means of density functional theory (DFT) at the B3LYP/6-311+G(d,p)/LanL2DZ level considering effective core potential (ECP).

Keyword: Copper complex; Dinuclear; Methacrylate; Diamine; DFT

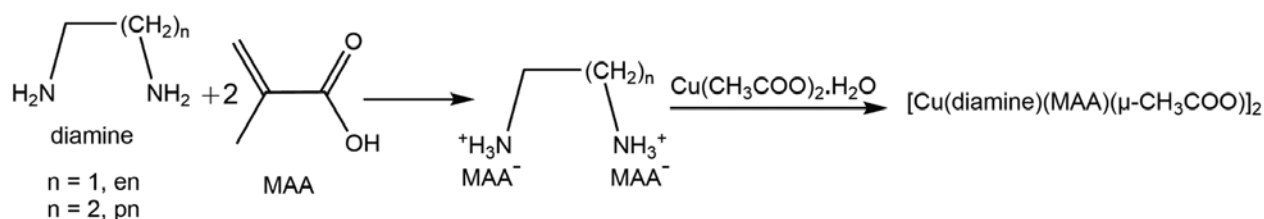
1. Introduction

Recently, specific attention have been paid to the synthesis of multinuclear complexes because of their importance in the fields of bioinorganic chemistry,^{1–4} molecular magnetic materials,^{5,6} catalysts,^{7,8} and their interesting chemical structures.^{2,8–13} One strategy for synthesis of di- and multi-nuclear compounds includes the use of bridging ligands and so metal centers are forced by the molecular topology to stay close to each other.^{10–14} The carboxylates and their derivatives exhibit various possible bonding modes when coordinating to metal ions such as monodentate and bidentate either by forming bridges or chelation. Nevertheless, carboxylate ligands commonly act as bidentate ligand in the transition metal complexes. Generally, each of the two oxygen atoms of the carboxylate group are coordinated to a different metal ion as bridging ligands.^{15–17} However, metal complexes with these ligands could adopt different coordination modes, depending on the nature of metal ion and the presence of other ligands.^{17–19}

Copper is an essential element to biological functions. The exchangeable portion of copper in blood plasma occurs mainly as a result of mixed-ligand formation involving copper–nitrogen interactions. Cu(II) mixed-ligand antineoplastic agents, containing diamine ligands exhibit cytotoxicity, genotoxicity, and antitumor effects.^{20,21}

In the present work, we report the synthesis, spectroscopic characterization, structural aspects and density functional theory (DFT) calculations for two new mixed-ligand Cu(II) complexes containing diamine, acetate and methacrylate ligands. The complexes are synthesized by reaction of diamine-methacrylic acid salt (diamine are ethylenediamine, en, and 1,3-propylenediamine, pn) with Cu(II) acetate (Scheme 1).

Here, the carboxylate ligands (acetate from the initial metal acetate input and methacrylate from diamine-methacrylic acid salt) are of particular interest, since the carboxylate can coordinate to metals in different modes. The carboxylate ligands are coordinated to the copper(II)



Scheme 1. Synthesis of the complexes **1** and **2**

ion in both monodentate and bidentate modes, and binuclear copper complexes can be formed.

2. Experimental

2.1. Materials and Methods

All chemicals were of analytical reagent grade and were used without further purification. Infrared spectra were taken with an Equinox 55 Bruker FT-IR spectrometer using KBr pellets in the 400–4000 cm^{-1} range. Absorption spectra were determined in the solvent of methanol using GBC UV-Visible Cintra 101 spectrophotometer with 1 cm quartz in the range of 200–800 nm. Elemental analyses (C, H, N) were performed by using a CHNS-O 2400 II PERKIN-ELMER elemental analyzer.

2.2. X-ray Crystallography

Diffraction images **1** and **2** were measured at 150 K on Agilent Xcalibur and SuperNova diffractometers using Mo $\text{K}\alpha$ ($\lambda = 0.71073 \text{ \AA}$) and Cu $\text{K}\alpha$ ($\lambda = 1.54180 \text{ \AA}$) radiation, respectively. Data were extracted using the CrysAlis PRO package.²² The structures were solved by direct methods with the use of SIR92.²³ The structures were refined on F^2 by full-matrix least-squares techniques using the CRYSTALS program package.²⁴ The H atoms were initially refined with soft restraints on the bond lengths and angles to regularize their geometry (C–H in the range 0.93–0.98, N–H = 0.87, O–H = 0.82 \AA) and with $U_{\text{iso}}(\text{H})$ in the range 1.2–1.5 times U_{eq} of the parent atom, after which the positions were refined with riding constraints for those bonded to C and without constraints for those bonded to N or O. Atomic coordinates, bond lengths and angles and displacement parameters have been deposited at the Cambridge Crystallographic Data Centre. Crystallographic data and refinement details for the complexes are given in Table 1. Details of the refinement procedures for the structures are given in the Supplementary Information.

2.3. Theoretical Calculations

All computations were performed by means of standard DFT method using the Gaussian09 (G09) pro-

Table 1. Crystallographic data and structural refinement for complexes **1–2**

Compound	1	2
Empirical formula	$\text{C}_{16}\text{H}_{32}\text{Cu}_2\text{N}_4\text{O}_8$	$\text{C}_{18}\text{H}_{36}\text{Cu}_2\text{N}_4\text{O}_8$
Formula weight	535.54	563.60
Crystal system	Triclinic	Triclinic
Space group	$\text{P}\bar{1}$	$\text{P}\bar{1}$
T (K)	150	150
a / \AA	6.8324 (3)	6.8283 (3)
b / \AA	8.6113 (3)	9.3019 (3)
c / \AA	10.4862 (3)	10.6562 (3)
α / $^\circ$	68.132 (4)	70.211 (6)
β / $^\circ$	88.717 (3)	80.563 (7)
γ / $^\circ$	72.239 (4)	76.054 (6)
V / \AA^3	542.37 (4)	615.58 (8)
Z	1	1
$F(000)$	278	294
D_{calc} (g cm^{-3})	1.640	1.520
μ (mm^{-1})	2.01	2.55
Measured reflections	12128	9439
Independent reflections	2724	2424
R_{int}	0.032	0.023
Observed reflections	2412	2360
$R[F^2 > 2\sigma(F^2)]$	0.028	0.024
$wR(F^2)$ (all data)	0.058*	0.061**

$$*w = 1/[\sigma^2(F^2) + (0.01P)^2 + 0.69P], \text{ where } P = (\max(F_o^2, 0) + 2F_c^2)/3$$

$$**w = 1/[\sigma^2(F^2) + (0.03P)^2 + 0.52P], \text{ where } P = (\max(F_o^2, 0) + 2F_c^2)/3$$

gram package.^{25,26} The geometries of the studied complexes have been optimized at the B3LYP level of theory.²⁷ The basis set of 6-31G(2df,p) was used for the C, H, N, and O atoms as recommended by Curtiss and his co-workers, while the basis set of LanL2DZ was employed for Cu atom considering the size of complexes and hardware limitations.^{28–30} Special care was taken to select the (global) minimum energy conformation via systematic conformational searching at this level. The nature of each stationary point was established by frequency calculations at the same level of B3LYP/6-31G(2df,p)/LanL2DZ. The geometry optimizations have been completed in the absence of solvent molecules and other impurities, and the optimized structures were compared with the crystalline structures. Charges on atoms have been calculated using Natural Bond Orbital (NBO) theory at the higher level of B3LYP/6-311+G(2df,p)/LanL2TZf.^{31,32}

2. 4. Syntheses

Synthesis of **1**, 2-di(λ^4 -azanyl)ethane dimethacrylate, **L**¹ and 1,3-di(λ^4 -azanyl)propane dimethacrylate, **L**².

The diaminium-methacrylic acid salts **L**¹ and **L**², were prepared by reaction between two equivalents of methacrylic acid (20 mmol, 1.70 mL) and one equivalent of related diamine, 1,2-ethylenediamine (10 mmol, 0.67 mL) and 1,3-propanediamine (10 mmol, 0.84 mL) in methanol medium (40 mL), respectively. The resulting bright yellow solution was heated to reflux for two hours. After two days, solid yellow powder obtained was filtered, washed with acetone and acetonitrile, and dried in air.

L¹, Yield: 1.76 g (76%), m.p. 148 °C. Anal. Calc. for C₁₀H₂₀N₂O₄ (232.28): C, 51.71; H, 8.68; N, 12.06%. Found: C, 51.79; H, 8.69; N, 12.36%. IR (KBr, ν_{\max} /cm⁻¹) bands: 3500, 1650, 1530, 1455, 1380 and 1230. UV-Vis, λ_{\max} (CH₃OH)/nm: 226 (log ϵ , 4.50).

L², Yield: 1.50 g (61%), m.p. 123 °C. Anal. Calc. for C₁₁H₂₂N₂O₄ (246.31): C, 53.64; H, 9.00; N, 11.37%. Found: C, 53.36; H, 8.97; N, 11.65%. IR (KBr, ν_{\max} /cm⁻¹) bands: 3393, 1646, 1543, 1455, 1386 and 1234. UV-Vis, λ_{\max} (CH₃OH)/nm: 216 (log ϵ , 3.73).

2. 4. 1. Synthesis of Copper(II) Complexes

Cu(CH₃COO)₂·H₂O (2.00 mmol, 0.399 g) was slowly added to a methanol solution (40 mL) of the related ligand (**L**¹, 2.00 mmol, 0.464 g and **L**², 2.00 mmol, 0.492 g) and the resulting solution was stirred for two hours at room temperature. The color of solution turned to blue and after two days solid blue powder was obtained.

[Cu(en)(MAA)(μ -CH₃COO)]₂, **1**

Yield: 0.99 g (93%). The blue solid product was recrystallized from acetonitrile/toluene (3:1 v/v). Blue crystals appeared at the bottom of the vessel upon slow evaporation of the solvents, which were filtered and dried in air. Anal. Calc. for C₁₆H₃₂Cu₂N₄O₈ (534.54): C, 35.88; H, 6.02; N, 10.46%. Found: C, 35.62; H, 6.18; N, 10.36%. IR (KBr, cm⁻¹): 3254, 3154, 1630, 1592, 1559, 1454 and 1382. Electronic spectra for CH₃OH: d-d, λ_{\max} (log ϵ) 332 nm (4.03), 633 nm (1.83).

[Cu(pn)(MAA)(μ -CH₃COO)]₂, **2**

Yield: 0.48 g (43%). The blue solid product was recrystallized from dichloromethane/n-hexane/toluene (5:1:1 v/v). Blue crystals were obtained upon slow evaporation of the solvents, which were filtered and dried in air. Anal. Calc. for C₁₈H₃₆Cu₂N₄O₈ (563.60): C, 38.36; H, 6.44; N, 9.94%. Found: C, 38.53; H, 6.53; N, 9.63%. IR (KBr, cm⁻¹): 3235, 3138, 1644, 1591, 1558, 1454 and 1384. Electronic spectra for CH₃OH: d-d, λ_{\max} (log ϵ) 255 nm (4.38), 643 nm (2.07).

3. Results and Discussion

3. 1. Syntheses and Characterization of the Complexes

The diaminium-methacrylic acid salt ligands was obtained by reaction of related diamine (ethylenediamine, en, and 1,3-propylenediamine, pn) and methacrylic acid in methanol under reflux. Copper(II) complexes **1** and **2** were obtained from the reaction mixture of the related ligand with the corresponding Cu(CH₃COO)₂·H₂O salt in equimolar ratio in methanol as a solvent at room temperature. The reaction of copper(II) acetate with **L**¹ and **L**² ligands leads to the formation of dinuclear complexes **1** and **2**.

The most significant IR bands for ligands and complexes are given in the experimental section. The IR spectra of the free ligands, **L**¹ and **L**², shows ν (N–H) bands at 3500 and 3393, ν (C=C) bands at 1530 and 1543, respectively. The two strong bands at 1650 and 1455 cm⁻¹ (for **L**¹) and 1646 and 1455 cm⁻¹ (for **L**²) corresponding to stretching frequencies of the carboxylate group: asymmetric ν_{asym} (COO⁻) and symmetric ν_{sym} (COO⁻), respectively.

In IR spectra of complexes **1** and **2**, the N–H stretches (NH₂) were observed at 3254 and 3154 cm⁻¹ (for **1**), 3235 and 3138 cm⁻¹ (for **2**). Complex **1**, [Cu(en)(MAA)(μ -CH₃COO)]₂, shows strong bands at 1630 and 1420 cm⁻¹ (for methacrylate ion, MAA), 1601 and 1454 cm⁻¹ (for acetate ion) corresponding to stretching frequencies of the carboxylate groups: asymmetric ν_{asym} (COO⁻) and symmetric ν_{sym} (COO⁻), respectively. For the acetate ion the difference between asymmetric and symmetric frequencies $\Delta[\nu_{\text{asym}}(\text{COO}^-) - \nu_{\text{sym}}(\text{COO}^-)] < 200$ cm⁻¹ indicates a bridging coordination mode.^{17,33,34} The infrared spectrum of complex **2** is quite similar with the complex **1**. The bands for the asymmetric and symmetric stretching vibrations, due to the carboxylate groups appear at 1644 and 1402 cm⁻¹ (for methacrylate ion, MAA), 1591 and 1454 cm⁻¹ (for acetate ion).

The absorption spectra of the free ligands **L**¹ and **L**² in methanol solution show band n- π^* transition at 226 and 216 nm, respectively. The electronic spectra of the copper complexes **1** and **2** in methanol solution show a broad band at 633 and 643 nm and a sharper signal at 255 and 246 nm, which arise from a spin-allowed d-d transition of the copper(II) ion (d⁹ electronic configuration) and a charge transfer transition, respectively.^{35,36}

3. 2. Description of X-ray Crystal Structures **1** and **2**

The molecular structures of **1** and **2** are shown in Fig. 1. Both complexes **1** and **2** have dimeric structure. Compounds crystallize in triclinic space group P $\bar{1}$ and there is one molecule in the unit cell (Z = 1). The single crystal X-ray diffraction data for compounds **1** and **2** are li-

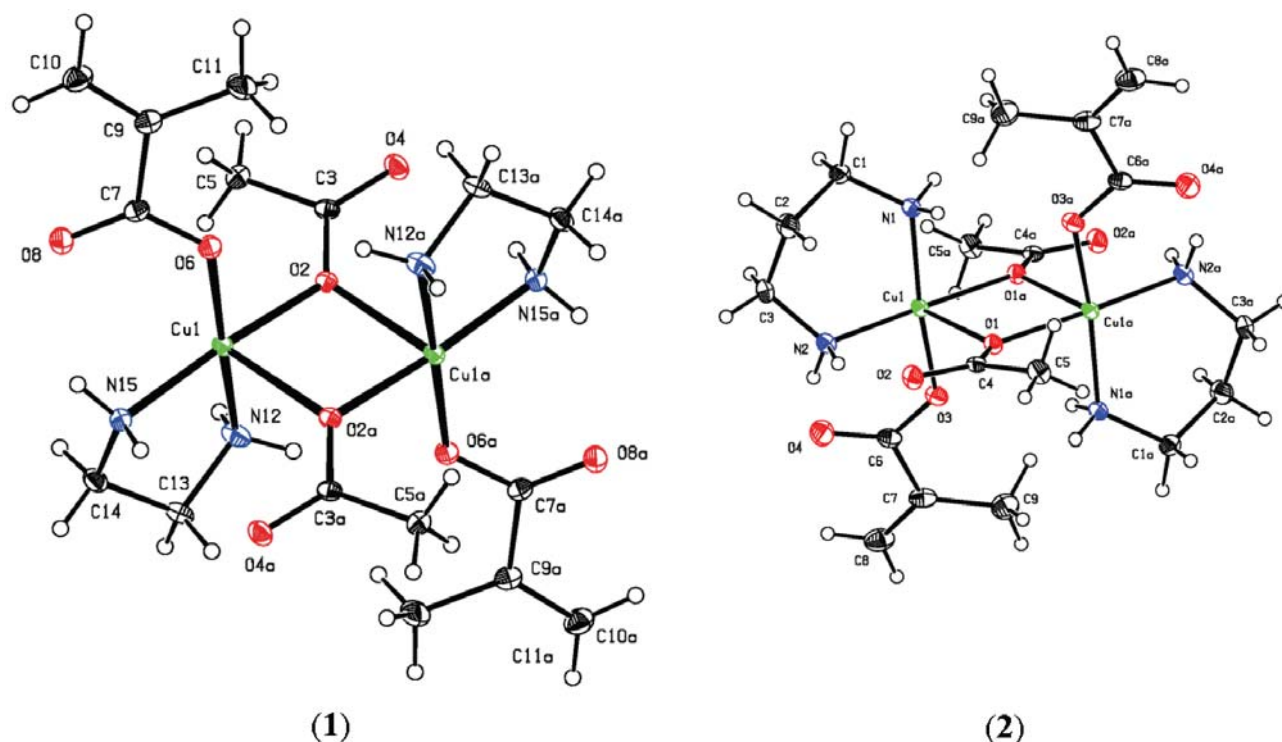


Fig. 1. The ORTEP view of complexes **1** and **2** showing 30% probability thermal ellipsoids. Symmetry codes: $-x, -y + 2, -z + 1$ for **1** and $x + 1, -y + 1, -z + 1$ for **2**.

sted in Table 1. Selected bond lengths and angles as well as interatomic distances are summarized in Table 2.

In the dimeric structures of **1** and **2**, the two copper centers are five-coordinate with distorted square pyramidal geometry. Coordination geometry about each copper ion complexes **1** and **2**, are close to square pyramidal with the Addison parameters $\tau = 0.015$ and 0.121 . The parameter of τ is defined as $\tau = (\alpha - \beta)/60$, ($\alpha > \beta$), where α and β are two largest angles around the Cu center; $\tau = 1$ for a regular trigonal bipyramid and $\tau = 0$ for a regular square pyramid.³⁷ According to the bond lengths between the copper and the coordinating atoms, the square base consists of two nitrogen atoms of the ethylenediamine (for **1**) and 1,3-propanediamine (for **2**) ligand, the oxygen atom of the methacrylate ion and the bridging acetate oxygen atom, and the apical position is occupied by the oxygen atom of the bridging acetate which has the longer Cu–O distance (i.e., the square base position consists of four short bond lengths of 1.9507(14)–2.0015(17) Å (for **1**); 1.9689(12)–2.0104(14) Å (for **2**), along the apical position with longer bond lengths of 2.2837(13) Å and 2.3069(11) Å, for **1** and **2**, respectively). The copper ion in complexes **1** and **2** is displaced from the basal plane of N_2O_2 by 0.046 and 0.024 Å towards the apical oxygen atom, respectively. The deviations from orthogonality of the *cis* bond angles (80.29(4)–98.98(6)°) and from linearity of the *trans* bond angles (168.70(5)–175.96(6)°) shows distortions from ideal square pyramidal geometry around the Cu centers.

Table 2. Selected bond lengths (Å) and angles (°) in Cu(II) complexes

bond lengths (Å)		bond angles (°)	
Complex 1			
Cu1–O2	1.9742(13)	O2–Cu1–O2 ^a	82.87(5)
Cu1–O2 ^a	2.2837(13)	O2–Cu1–O6	87.26(5)
Cu1–O6	1.9507(14)	N15–Cu1–O2	173.75(6)
Cu1–N12	2.0015(17)	N12–Cu1–O6	172.83(7)
Cu1–N15	1.9879(16)	N12–Cu1–O2	88.13(6)
C3–O2	1.282(2)	N15–Cu1–O6	98.98(6)
C3–O4	1.237(2)	O6–C7–O8	125.53(18)
Cu1...Cu1 ^a	3.1987(5)	Cu1–O2–Cu1 ^a	97.13(5)
Complex 2			
Cu1–O1	2.3069(11)	O1–Cu1–O1 ^a	80.29(4)
Cu1–O1 ^a	1.9850(11)	O3–Cu1–O1	95.73(5)
Cu1–O3	1.9689(12)	N1–Cu1–O3	168.70(5)
Cu1–N1	2.0101(14)	N2–Cu1–O1 ^a	175.96(6)
Cu1–N2	1.9825(14)	N1–Cu1–O1	89.72(5)
C4–O1	1.2867(19)	N1–Cu1–N2	94.08(6)
C4–O2	1.235(2)	O3–C6–O4	125.39(16)
Cu1...Cu1 ^a	3.2874(3)	Cu1–O1–Cu1 ^a	99.71(4)

Symmetry codes: $-x, -y + 2, -z + 1$ for **1** and $x + 1, -y + 1, -z + 1$ for **2**.

The Cu...Cu distance within the dinuclear **1** is 3.1987(5) Å which is slightly shorter than in dinuclear **2** (3.2874(3) Å). The bond lengths Cu–O and Cu–N are in the range of 1.9507(14)–2.3837(13) Å and 1.9825(14)–

2.0104(14) Å, see Table 2), respectively, which have good agreement with analogous square pyramidal Cu(II) complexes previously reported.^{9,17,38–40}

In **1**, the Cu1–(μ-O)–Cu1^a (symmetry code a: $-x, -y + 2, -z + 1$) bond angle is 97.13(5)°, which is similar to that in **2** (99.71(4)°, symmetry code a: $x + 1, -y + 1, -z + 1$, Table 2) and are in good agreement with analogous Cu(II) complexes observed in the literature.^{2,9,17,41} In complexes **1** and **2**, the C–O bond lengths of carboxylate groups in methacrylate and acetate ions are very similar (see Table 2).

The oxygen atoms of carboxylate groups (acetate and methacrylate ions) and the NH₂ amine groups of the

diamine ligand (ethylenediamine for **1** and 1,3-propylenediamine for **2**) play a significant role in intramolecular and intermolecular hydrogen-bonding interactions (Figs. 2 and 3). In **1**, the hydrogen atoms of the coordinated ethylenediamine molecule are involved in an intermolecular hydrogen-bonding interaction with the oxygen atoms of a neighboring coordinated methacrylate ion and the oxygen atoms of uncoordinated methacrylate and acetate ions. Also, there is an intramolecular hydrogen bonding between the hydrogen atom H151 of the NH of the ethylenediamine molecule with the oxygen atom O8 of uncoordinated methacrylate ion. In **2**, there are intermolecular hydrogen bonding interaction between the hydrogen

Table 3. Hydrogen bonding (Å) and angles (°) in complexes **1** and **2**

	D–H...A	D–H	H...A	D...A	D–H...A	Symmetry code
1	N15–H152...O4	0.88(3)	2.33(3)	3.084(3)	144(1)	$-x, -y + 2, -z + 1$
	N15–H152...O8	0.88(3)	2.58(3)	3.156(3)	128(1)	$-x + 1, -y + 1, -z + 1$
	N15–H151...O8	0.87(3)	2.24(3)	2.948(3)	138(1)	x, y, z
	N12–H122...O6	0.89(3)	2.40(3)	3.229(3)	155(1)	$-x, -y + 2, -z + 1$
	N12–H121...O4	0.86(3)	2.24(3)	2.997(3)	148(1)	$-x + 1, -y + 2, -z + 1$
2	N1–H1...O3	0.81(2)	2.58(2)	3.257(3)	143(2)	$-x + 1, -y + 1, -z + 1$
	N1–H2...O2	0.84(2)	2.12(2)	2.930(3)	161(2)	$x - 1, y, z$
	N2–H3...O2	0.86(2)	2.25(2)	3.028(3)	152(2)	x, y, z
	N2–H4...O4	0.82(2)	2.13(2)	2.862(3)	149(2)	x, y, z

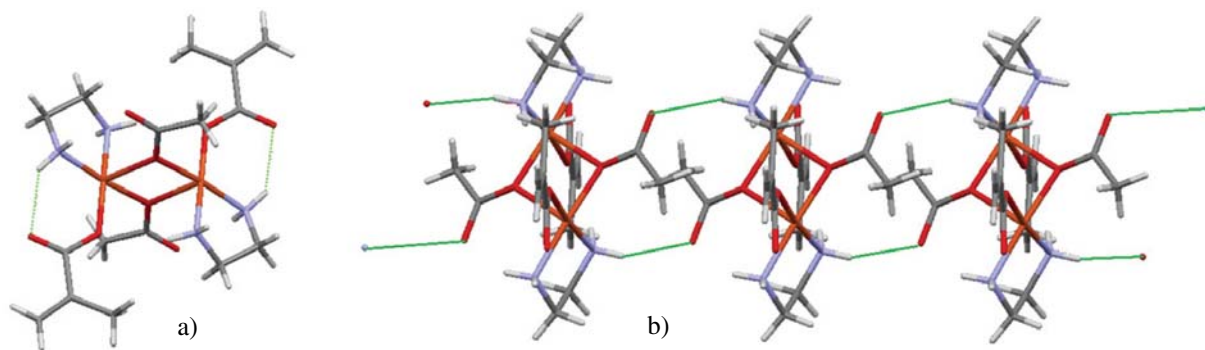


Fig. 2. Various hydrogen bonding interactions in complex **1** (a) intramolecular (b), intermolecular.

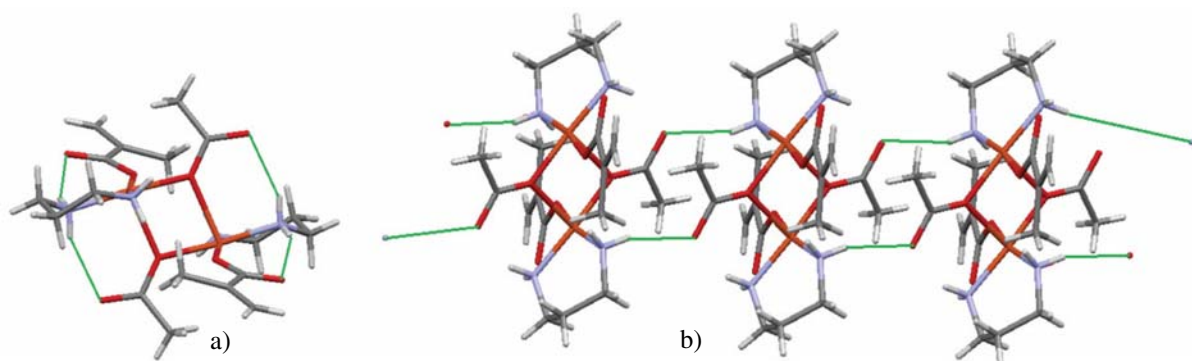


Fig. 3. Various hydrogen bonding interactions in complex **2** (a) intramolecular (b), intermolecular.

atoms of the coordinated 1,3-propylenediamine molecule with the uncoordinated oxygen atom O2 of the bridging acetate ligand and coordinated oxygen atom O3 of the methacrylate ion. Also, there are intramolecular hydrogen bonding between the hydrogen atom of the NH of the 1,3-propylenediamine molecule with the uncoordinated oxygen atoms O2 and O4 of acetate and methacrylate ions, respectively. Full details of the hydrogen bonding are given in Table 3.

3. 3. DFT Optimized Geometries

The geometry optimization of copper complexes were carried out in their singlet and triplet spin states. The optimized geometric parameters at their most stable, triplet states, is shown in Fig. 4.

As shown in Table 4, the calculated bond lengths for the studied complexes agree well with the X-ray experimental data. For example, the calculated Cu1–N12, Cu1–N15, Cu–O6 and Cu–O2 bond lengths for the dinuclear complex **1** are 2.00, 2.05, 1.96 and 2.00 Å, and they correlate nicely with the experimental values of 2.00, 1.99, 1.95 and 1.97 Å, respectively.

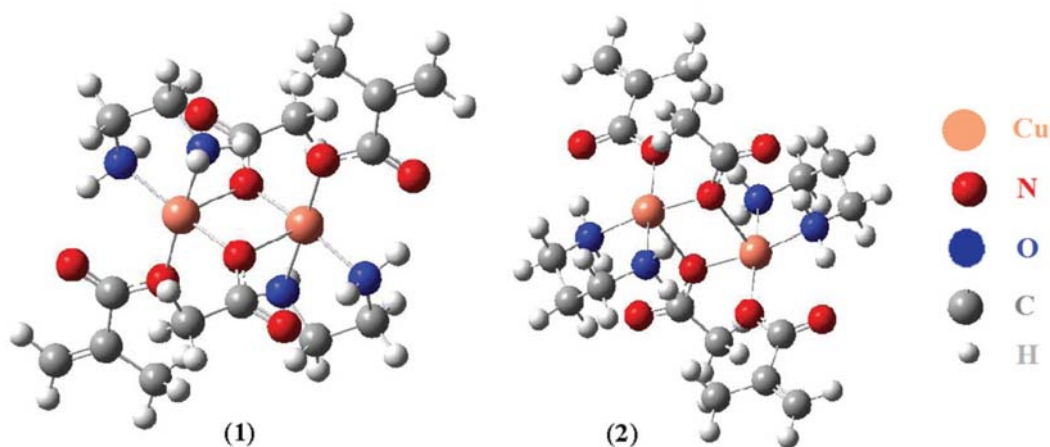


Fig. 4. The optimized structures of the complexes **1** and **2**.

Table 4. Selected geometric parameters from X-ray and DFT-B3LYP calculations

	Bond length (Å)	Expt.	Calc.	\Delta L	Bond angle (°)	Expt.	Calc.	\Delta L\theta
1	Cu1...Cu1 ^a	3.20	3.09	0.11	O2–Cu1–O6	87.3	91.1	3.8
	Cu1–O2	1.97	2.00	0.03	N12–Cu1–O2	88.1	85.3	3.0
	Cu1–O6	1.95	1.96	0.01	N15–Cu1–N12	85.4	82.6	3.0
	Cu1–N12	2.00	2.00	0.08	N15–Cu1–O6	99.0	100.9	1.9
	C3–O2	1.28	1.29	0.02	Cu1–O2–Cu1 ^a	97.1	94.4	2.7
2	Cu1...Cu1 ^a	3.29	3.26	0.03	O3–Cu1–O1	95.7	97.7	2.0
	Cu1–O3	1.97	2.00	0.03	N1–Cu1–O3	168.7	165.19	3.5
	Cu1–N2	1.98	2.01	0.03	N1–Cu1–N2	94.1	95.5	1.4
	C4–O1	1.29	1.30	0.01	N2–Cu1–O3	95.2	97.8	2.6
					Cu1–O1–Cu1 ^a	99.7	97.0	2.7

Symmetry codes: $-x, -y + 2, -z + 1$ for **1** and $x + 1, -y + 1, -z + 1$ for **2**.

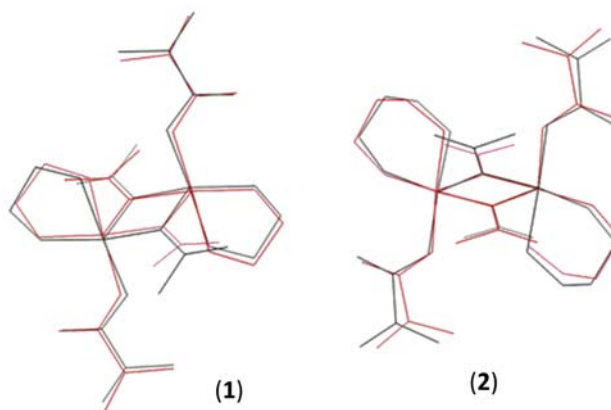


Fig. 5. Atom-by-atom superimposition of the calculated structures (black) over the X-ray structure (red); hydrogen atoms have been removed for clarity.

The differences between optimized geometrical parameters and experiment are less than 0.05 Å (bond distances) and 2° (bond angles) in most cases (see also Fig. 5).

In general, the predicted bond lengths are slightly longer in comparison with the values based upon the X-ray crystal structure data. The geometrical differences might

be a result of crystal packing forces which have an influence on the molecules as expected for the experimental ones (solid state), but the calculated geometries are in the gas phase.^{40,42} The crystal packing forces, which have an influence on the molecules, as expected for the experimental parameters (solid state), are a reason for the difference of calculated bond lengths in the gas phase and solid phase.

The calculated charges on the metal centers in complexes **1** and **2** are +0.875 and +0.873 respectively, and these values are greatly lower than the formal charge of +2. These differences are a result of charge donation from the donor atoms of ligands.

4. Conclusion

The reaction of copper(II) acetate with L¹ and L² ligands led to the formation of dinuclear copper(II) complexes **1** and **2**. The crystal structures were determined for two studied complexes. An acetate oxygen bridge, a relatively rare bridging mode of the carboxylate group, has been found in dinuclear complexes **1** and **2**. Coordination geometry for each copper ion was square pyramid. The optimized structure of complexes have been studied using the B3LYP/6-31G(d)/LanL2DZ level of theory. The calculated molecular geometries are in a very good agreement with the experimental data. It has been revealed that the triplet state for copper complexes **1** and **2** are more stable than their singlet state.

5. Supplementary Material

The deposition numbers of the studied complexes **1** and **2** are CCDC 1481551 and 1481552, respectively. These data can be obtained free-of-charge via www.ccdc.cam.ac.uk/data_request/cif, by emailing data_request@ccdc.cam.ac.uk, or by contacting The Cambridge Crystallographic Data Centre, 12 Union Road, Cambridge CB2 1EZ, UK; fax +44 1223 336033.

6. Acknowledgement

MN is thankful to Prof. Michelle L. Coote and Research School of Chemistry, The Australian National University for the offer of campus visiting position and for the Gaussian calculations. MC is grateful to the graduate school of Yazd University for the post-graduate scholarships. MN and RV are also grateful to Yazd University and the Australian National University for their valuable support.

7. References

1. F. Yu, V. M. Cangelosi, M. L. Zastrow, M. Tegoni, J. S. Ple-garia, A. G. Tebo, C. S. Mocny, L. Ruckthong, H. Qayyum, V. L. Pecoraro, *Chem. Rev.* **2014**, *114*, 3495–3578. <https://doi.org/10.1021/cr400458x>
2. R. Vafazadeh, F. Jafari, M. M. Heidari, A. C. Willis, *J. Coord. Chem.* **2016**, *69*, 1313–1325. <https://doi.org/10.1080/00958972.2016.1163547>
3. Q. R. Cheng, F. Q. Zhang, H. Zhou, Z. Q. Pan, G. Y. Liao, *J. Coord. Chem.* **2015**, *68*, 1997–2005. <https://doi.org/10.1080/00958972.2015.1032272>
4. R. Vafazadeh, A. C. Willis, *J. Coord. Chem.* **2015**, *68*, 2240–2252. <https://doi.org/10.1080/00958972.2015.1048688>
5. M. Lukyanov, E. Goreschnik, V. Kinzhybalo, M. Myskiv, *Acta Chim. Slov.* **2017**, *64*, 215–220.
6. D. Zhang, L. Kong, H. Zhang, *Acta Chim. Slov.* **2015**, *62*, 219–224.
7. S. Shit, U. Yadava, D. Saha, R. Fröhlich, *J. Coord. Chem.* **2013**, *66*, 66–76. <https://doi.org/10.1080/00958972.2012.747088>
8. S. Hazra, A. Karmakar, M. de Fátima C. Guedes da Silva, L. Dlhán, R. Boča, A. J. L. Pombeiro, *New J. Chem.* **2015**, *39*, 3424–3434. <https://doi.org/10.1039/C5NJ00330J>
9. R. Vafazadeh, R. Esteghamat-Panaha, A. C. Willis, A. F. Hill, *Polyhedron* **2012**, *48*, 51–57. <https://doi.org/10.1016/j.poly.2012.08.057>
10. R. Vafazadeh, N. Hasanzade, M. M. Heidari, A. C. Willis, *Acta Chim. Slov.* **2015**, *62*, 122–129. <https://doi.org/10.17344/acsi.2014.797>
11. R. Vafazadeh, A. C. Willis, *Acta Chim. Slov.* **2016**, *63*, 186–192. <https://doi.org/10.17344/acsi.2016.2263>
12. Z. Yolcu, S. Demir, Ö. Andaç, O. Büyükgüngör, *Acta Chim. Slov.* **2016**, *63*, 646–653. <https://doi.org/10.17344/acsi.2016.2475>
13. X. J. Li, K. Zheng., Y. T. Li, C. W. Yan, Z. Y. Wu, S. Y. Xuan, *J. Coord. Chem.* **2015**, *68*, 928–948. <https://doi.org/10.1080/00958972.2015.1009452>
14. X. Z. Zhang, Y. Gu, Y. Li, A. Liu, F. Liu, Z. You, H. L. Zhu, *Acta Chim. Slov.* **2016**, *63*, 721–725. <https://doi.org/10.17344/acsi.2016.2421>
15. C. J. Lina, J. L. Qia, Y. Q. Zheng, J. L. Lina, *J. Coord. Chem.* **2013**, *66*, 3877–3890. <https://doi.org/10.1080/00958972.2013.853053>
16. S. Singh, D. Saini, S. K. Mehta, D. Choquesillo-Lazarte, *J. Coord. Chem.* **2011**, *64*, 1544–1553. <https://doi.org/10.1080/00958972.2011.575133>
17. R. Vafazadeh, Z. Moghadas, A. C. Willis, *J. Coord. Chem.* **2015**, *68*, 4255–4271. <https://doi.org/10.1080/00958972.2015.1096349>
18. G. T. Musie, X. Li, D. R. Powell, *Inorg. Chim. Acta* **2006**, *359*, 1989–1996. <https://doi.org/10.1016/j.ica.2005.12.075>
19. P. A. Vigato, S. Tamburini, *Coord. Chem. Rev.* **2004**, *248*, 1717–2128. <https://doi.org/10.1016/j.cct.2003.09.003>
20. M. E. Bravo-Gómez, J. C. García-Ramos, I. Gracia-Mora, L. Ruiz-Azuara, *J. Inorg. Biochem.* **2009**, *103*, 299–309. <https://doi.org/10.1016/j.jinorgbio.2008.10.006>
21. A. D. Vizcaya-Ruiz, A. Rivero-Muller, L. Ruiz-Ramirez, G. E. N. Kass, L. R. Kelland, R. M. Orr, M. Dobrota, *Toxicol. In Vitro* **2001**, *14*, 1–5.

- [https://doi.org/10.1016/S0887-2333\(99\)00082-X](https://doi.org/10.1016/S0887-2333(99)00082-X)
22. Z. Otwinowski, W. Minor. *Methods in Enzymology*, Vol. 276, edited by C. W. Carter Jr & R. M.W. Sweet, New York: Academic Press, 1997, 307–326.
 23. A. Altomare, G. Cascarano, G. Giacovazzo, A. Guagliardi, M. C. Burla, G. Polidori, M. Camalli, *J. Appl. Cryst.*, **1994**, 27, 435–436.
 24. P. W. Betteridge, J. R. Carruthers, R. I. Cooper, K. Prout, D. J. Watkin, *J. Appl. Cryst.*, **2003**, 36, 1487–1487. <https://doi.org/10.1107/S0021889803021800>
 25. W. J. Hehre, L. Radom, P. V. R. Schleyer, J. A. Pople, *Ab initio Molecular Orbital Theory*, Wiley, New York, 1986.
 26. Gaussian 09, Revision D.01, M. J. Frisch, G. W. Trucks, H. B. Schlegel, G. E. Scuseria, M. A. Robb, J. R. Cheeseman, G. Scalmani, V. Barone, B. Mennucci, G. A. Petersson, H. Nakatsuji, M. Caricato, X. Li, H. P. Hratchian, A. F. Izmaylov, J. Bloino, G. Zheng, J. L. Sonnenberg, M. Hada, M. Ehara, K. Toyota, R. Fukuda, J. Hasegawa, M. Ishida, T. Nakajima, Y. Honda, O. Kitao, H. Nakai, T. Vreven, J. A. Montgomery Jr., J. E. Peralta, F. Ogliaro, M. Bearpark, J. J. Heyd, E. Brothers, K. N. Kudin, V. N. Staroverov, T. Keith, R. Kobayashi, J. Normand, K. Raghavachari, A. Rendell, J. C. Burant, S. S. Iyengar, J. Tomasi, M. Cossi, N. Rega, J. M. Millam, M. Klene, J. E. Knox, J. B. Cross, V. Bakken, C. Adamo, J. Jaramillo, R. Gomperts, R. E. Stratmann, O. Yazyev, A. J. Austin, R. Cammi, C. Pomelli, J. W. Ochterski, R. L. Martin, K. Morokuma, V. G. Zakrzewski, G. A. Voth, P. Salvador, J. J. Dannenberg, S. Dapprich, A. D. Daniels, O. Farkas, J. B. Foresman, J. V. Ortiz, J. Cioslowski, D. J. Fox, Gaussian Inc., Wallingford CT, 2010.
 27. A. D. Becke, *J. Chem. Phys.* **1993**, 98, 5648–5652. <https://doi.org/10.1063/1.464913>
 28. (a) L. A. Curtiss, P. C. Redfern, K. Raghavachari, *J. Chem. Phys.* **2007**, 126, 084108–084120. (b) J. B. Foresman, A. E. Frisch, *Exploring Chemistry with Electronic Structure Methods*, Gaussian Inc., Pittsburgh, PA, 1998. <https://doi.org/10.1063/1.2436888>
 29. P. J. Hay, W. R. Wadt, *J. Chem. Phys.* **1985**, 82, 270–283. <https://doi.org/10.1063/1.448799>
 30. P. J. Hay, W. R. Wadt, *J. Chem. Phys.* **1985**, 82, 284–298. <https://doi.org/10.1063/1.448800>
 31. P. J. Hay, W. R. Wadt, *J. Chem. Phys.* **1985**, 82, 299–310. <https://doi.org/10.1063/1.448975>
 32. J. P. Foster, F. Weinhold, *J. Am. Chem. Soc.* **1980**, 102, 7211–7218. <https://doi.org/10.1021/ja00544a007>
 33. Y. Thio, X. Yang, J. J. Vittal, *Dalton Trans.* **2014**, 43, 3545–3556. <https://doi.org/10.1039/c3dt52829d>
 34. K. Nakamoto, *Infrared and Raman Spectra of Inorganic and Coordination Compounds*, 4th ed., Wiley, New York, 1986.
 35. B. Shaabani, A. A. Khandar, M. Dusek, M. Pojarova, F. Mahmoudi, A. Feher, M. Kajnakova, *J. Coord. Chem.* **2013**, 66, 748–762. <https://doi.org/10.1080/00958972.2013.764413>
 36. N. K. Singh, M. K. Bharty, R. Dulare, R. J. Butcher, *Polyhedron* **2009**, 28, 2443–2449. <https://doi.org/10.1016/j.poly.2009.04.030>
 37. A. W. Addison, N. Rao, J. Reedijk, J. V. Rijn, G. C. Verschoor, *J. Chem. Soc. Dalton Trans.* **1984**, 1349–1356. <https://doi.org/10.1039/DT9840001349>
 38. S. Shit, C. Marschner, S. Mitra, *Acta Chim. Slov.* **2016**, 63, 129–137. <https://doi.org/10.17344/acs.2015.2024>
 39. R. Vafazadeh, B. Khaledi, A. C. Willis, *Acta Chim. Slov.* **2012**, 59, 954–958.
 40. R. Vafazadeh, B. Khaledi, A. C. Willis, M. Namazian, *Polyhedron* **2011**, 30, 1815–1819. <https://doi.org/10.1016/j.poly.2011.04.026>
 41. R. Vafazadeh, M. Alinaghi, A. C. Willis, A. Benvidi, *Acta Chim. Slov.* **2014**, 61, 121–125.
 42. G. Alpaslan, M. Macit, *Spectrochim. Acta A*, **2014**, 121, 372–380. <https://doi.org/10.1016/j.saa.2013.10.111>

Povzetek

Sintetizirali smo dva dvojedrna Cu(II) kompleksa [Cu(en)(MAA)(μ-CH₃COO)]₂ (**1**) in [Cu(pn)(MAA)(SSTimes-CH₃COO)]₂ (**2**), kjer so MAA, en in pn metacrilat, etilendiamin in 1,3-propilendiamin, ter jih okarakterizirali z elementno analizo, FT-IR in UV-Vis spektroskopijo. Strukturi kompleksov sta bili določeni z monokristalno rentgensko difrakcijo. V dvojedrnih kompleksih **1** in **2** imajo bakrovi centri koordinacijsko število pet s popačeno kvadratno piramidarno geometrijo. Izračunane geometrije proučevanih spojin so bile določene s pomočjo teorije gostotnostnega funkcionala (DFT) na B3LYP/6-311+G(d,p)/LanL2DZ nivoju z uporabo ECP.

Scientific paper

Synthesis of Some Substituted 6-Phenyl Purine Analogues and Their Biological Evaluation as Cytotoxic Agents

Asligul Kucukdumlu,¹ Meral Tuncbilek,^{1,*} Ebru Bilget Guven²
and Rengul Cetin Atalay³

¹ Department of Pharmaceutical Chemistry, Faculty of Pharmacy, Ankara University, 06100 Ankara, Turkey

² Department of Molecular Biology and Genetics, Bilkent University, 06800 Ankara, Turkey

³ Department of Bioinformatics, Graduate School of Informatics, Middle East Technical University, 06800 Ankara, Turkey

* Corresponding author: E-mail: tuncbile@pharmacy.ankara.edu.tr

Received: 06-04-2017

Abstract

A series of 6-(4-substituted phenyl)-9-(tetrahydropyran-2-yl)purines **3–9**, 6-(4-substituted phenyl)purines **10–16**, 9-((4-substituted phenyl)sulfonyl)-6-(4-substituted phenyl)purines **17–32** were prepared and screened initially for their *in vitro* anticancer activity against selected human cancer cells (liver Huh7, colon HCT116, breast MCF7). 6-(4-Phenoxyphenyl)purine analogues **9**, **16**, **30–32**, had potent cytotoxic activities. The most active purine derivatives **5–9**, **14**, **16**, **18**, **28–32** were further screened for their cytotoxic activity in hepatocellular cancer cells. 6-(4-Phenoxyphenyl)-9-(tetrahydropyran-2-yl)-9H-purine (**9**) had better cytotoxic activity (IC₅₀ 5.4 μM) than the well-known nucleobase analogue 5-FU and known nucleoside drug fludarabine on Huh7 cells. The structure–activity relationship studies reported that the substitution at C-6 positions in purine nucleus with the 4-phenoxyphenyl group is responsible for the anti-cancer activity.

Keywords: Antitumor agents; Hepatocellular carcinoma; Heterocycles; Purine derivatives; Structure-activity relationships

1. Introduction

Cancer is a major human health problem and one of the principal reasons of death in both developing and industrialized countries. Purine and purine nucleoside analogues are important anti-cancer drugs used for the treatment of both hematological malignancies and solid tumors in chemotherapy. In 1953 and 1966, among the first anti-cancer drugs 6-mercaptopurine and 6-thioguanine (Fig. 1) were used as an inhibitor of nucleic acid metabolism in childhood acute lymphoblastic leukemia, respectively.^{1–4}

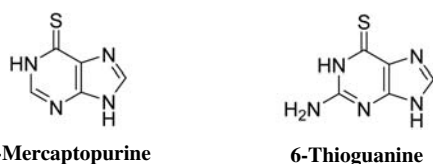


Figure 1. Structures of 6-mercaptopurine and 6-thioguanine

Potent purine-based cyclin-dependent kinase inhibitors olomoucine,⁵ roscovitine,⁶ purvalanol A, B, amino-purvalanol⁷ (Fig. 2) and heterocyclic analogues of these compounds imidazo-pyrazines,⁸ pyrazolo-pyrida-

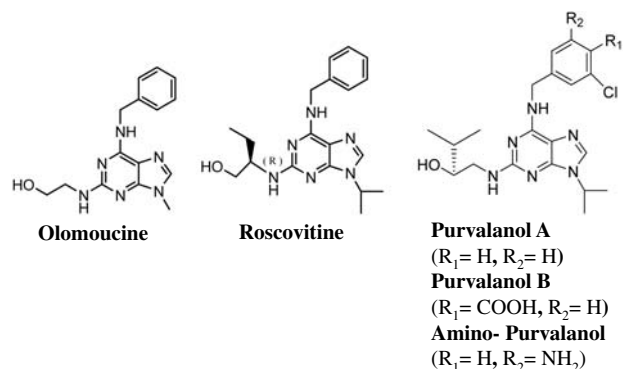


Figure 2. Structures of olomoucine, roscovitine, purvalanol A, B and amino-purvalanol

zines,⁹ imidazo-pyridines,^{10,11} thieno-pyridines,¹² pyrrolo-pyrimidines,¹³ pyrazolo-pyrimidines^{14,15} and triazolo-pyrimidines^{16,17} have been investigated as anticancer agents.

Furthermore, purine nucleosides such as fludarabine, cladribine, and pentostatine (Fig. 3) were approved in FDA for the therapy of hematologic disorders between 1991 and 1992.^{18,19}

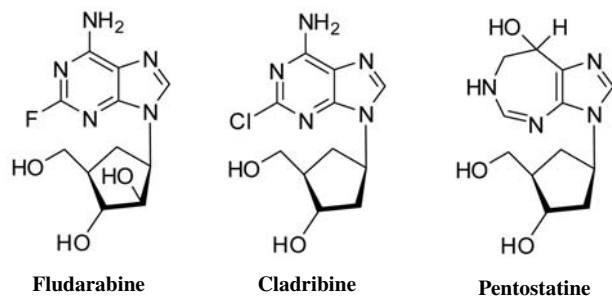


Figure 3. Structures of fludarabine, cladribine and pentostatine

Hepatocellular carcinoma (HCC) is one of the deadly cancers and affects most of the world population. It is also the fifth most common cancer in men and seventh in women, accounting for 7% of all cancer cases, and the third most common reason of cancer-connected death worldwide, with around 700,000 new cases each year.^{20–21}

Chronic liver damage is due to viral diseases, chemical exposure, environmental toxins or autoimmune diseases that are the risk factors for HCC. These conditions cause an acquired tolerance to genotoxic stress, but finally result in a cancerous case that does not respond to the mechanism of cell death.²³

The diagnosis of HCC patients is usually very poor and HCC tumors are resistant to chemotherapeutic agents. Lately, a multikinase inhibitor Sorafenib, was approved by the FDA and the EU for the treatment of hepatocellular carcinoma.²⁴ Sorafenib HCC Assessment Randomised Protocol (SHARP) indicated significantly improved overall survival and the time to progression by almost three months in cases with advanced HCC upon treatment with the antiangiogenic and antiproliferative agent Sorafenib.^{25–27} Therefore, it is essential to discover new liver-cancer-specific drugs for hepatocellular carcinoma treatment.

As a result of our ongoing investigations of purine and purine nucleoside derivatives, which have displayed promising cytotoxic activity,^{28,29} herein, we synthesized new series of substituted purines (**3–9**, **10–16**, **17–32**) and screened their anticancer activities on selected human cancer cells (liver Huh7, colon HCT116, breast MCF7); and the most potent purine derivatives (**5–9**, **14**, **16**, **18**, and **28–32**) were further tested on a panel of hepatocellular cancer cell.

2. Experimental

2. 1. Chemistry

Melting points were recorded with a capillary melting point apparatus (Electrothermal 9100) and are uncorrected. NMR spectra were recorded on a VARIAN Mercury 400 FT-NMR spectrometer (400 for ¹H, 100.6 MHz for ¹³C). TMS was used as internal standard for the ¹H and ¹³C NMR spectra; values are given in δ (ppm) and J values are in Hz. Mass spectra were taken on Waters Micro-mass ZQ by using ESI+ ionization method. Elemental analyses (C, H, N) were determined on a Leco CHNS 932 instrument and gave values within $\pm 0.4\%$ of the theoretical values. Column chromatography was accomplished on silica gel 60 (40–63 mm particle size). The chemical reagents used in synthesis were purchased from Merck, Fluka, Sigma and Aldrich.

2. 1. 1. 6-Chloro-9-(tetrahydro-2H-pyran-2-yl)-9H-purine (**2**)³⁰

p-TSA (0.01 g) was added to a solution of 6-chloropurine (0.15 g, 1 mmol) in dry THF at reflux. After 3,4-dihydro-2H-pyran (0.098 g, 1.18 mmol) was added and the mixture refluxed for 15 h. After cooling to ambient temperature the reaction mixture was treated with 1 mL 25% NH₄OH and stirred for 5 min. The solution was evaporated in vacuo and treated with 25 mL EtOAc, washed with brine and water. The organic phase was dried over Na₂SO₄, the solvent was evaporated in vacuo, and recrystallized from hexane petroleum ether to yield **2** (220 mg; 95%): mp 69–71 °C (67–69 °C³⁰). ¹H NMR (CDCl₃) δ 1.64–1.88 (m, 3H, H-pyran), 2.02–2.21 (m, 3H, H-pyran), 3.80 (td, $J_1 = 2.8$ Hz, $J_2 = 12$ Hz, 1H, H-5'a in pyran), 4.20 (d, 1H, H-5'b in pyran), 5.80 (dd, $J_1 = 10.8$ Hz, $J_2 = 2.4$ Hz, 1H, H-1' in pyran), 8.35 (s, 1H, H-8 in purine), 8.76 (s, 1H, H-2 in purine). MS (ESI+) m/z : 239.70 (10%) (M+H).

2. 1. 2. General Procedure for the Synthesis of 6-(4-Substituted Phenyl)-9-(tetrahydropyran-2-yl)-9H-purines **3–9**

6-Chloro-9-(tetrahydropyran-2-yl)-9H-purine (**2**) was dissolved in 5 mL toluene, then K₂CO₃ (1.5 mmol), 4-substituted phenylboronic acid (1.5 mmol) and Pd(Ph₃)₄ (0.05 mmol) were added. The mixture was refluxed for 12 h. The reaction mixture was concentrated in vacuo. The residue was dissolved in CH₂Cl₂ and purified by column chromatography (EtOAc–hexane, 1:3 to 1:6).

6-Phenyl-9-(tetrahydro-2H-pyran-2-yl)-9H-purine (**3**)³¹

Yield 60 mg (55%), mp 189–191 °C. ¹H NMR (CDCl₃) δ 1.67–1.86 (m, 3H, H-pyran), 2.01–2.21 (m, 3H, H-pyran), 3.83 (td, $J_1 = 11.6$ Hz, $J_2 = 2.8$ Hz, 1H, H-5'a in pyran), 4.21 (d, 1H, H-5'b in pyran), 5.86 (dd, J_1

= 10 Hz, $J_2 = 2.8$ Hz, 1H, H-1' in pyran), 7.53 (t, $J = 7.6$ Hz, 2H, H-3,5 in phenyl), 7.60 (t, $J = 7.6$ Hz, 1H, H-4 in phenyl), 8.35 (s, 1H, H-8 in purine), 8.77 (d, $J = 6.4$ Hz, 2H, H-2,6 in phenyl), 9.03 (s, 1H, H-2 in purine). MS (ESI+) m/z : 197.52 (100%) (M+H–THP), 281.71 (77%) (M+H).

6-(4-Fluorophenyl)-9-(tetrahydro-2H-pyran-2-yl)-9H-purine (4)³¹

Yield 190 mg (63%), mp 161–163 °C. ¹H NMR (DMSO-*d*₆) δ 1.57–1.65 (m, 2H, H-pyran), 1.70–1.82 (m, 1H, H-pyran), 1.97–2.03 (m, 2H, H-pyran), 2.29–2.40 (m, 1H, H-pyran), 3.72 (td, $J_1 = 3.2$ Hz, $J_2 = 11.2$ Hz, 1H, H-5'a in pyran), 4.03 (d, 1H, H-5'b in pyran), 5.81 (dd, $J_1 = 2$ Hz, $J_2 = 10.8$ Hz, 1H, H-1' in pyran), 7.43 (t, $J = 8.8$ Hz, 2H, H-3,5 in phenyl), 8.87–8.91 (m, 3H, H-2,6 in phenyl, H-8 in purine), 8.98 (s, 1H, H-2 in purine) (Ref. [31] 1.6–1.9 and 2.0–2.2 (2 \times m, 6H, CH₂), 3.81 (dt, 1H, $J_1 = 2.2$ Hz, $J_2 = 11.5$, H-5'a), 4.20 (brd, 1H, $J = 11.5$ Hz, H-5'b), 5.84 (dd, 1H, $J_1 = 10.3$ Hz, $J_2 = 2.3$ Hz, H-1'), 7.22 (t, 2H, $J = 8.7$ Hz, H-o-Ar), 8.31 (s, 1H, H-8), 8.84 (dd, 2H, $J_1 = 8.7$ Hz, $J_2 = 5.7$ Hz, H-m-Ar), 8.99 (s, 1H, H-2)). MS (ESI+) m/z : 215.5 (100%) (M+H–THP), 299.7 (100%) (M+H).

6-(4-Chlorophenyl)-9-(tetrahydro-2H-pyran-2-yl)-9H-purine (5)

Yield 240 mg (77%), mp 173–175 °C. ¹H NMR (CDCl₃) δ 1.65–1.86 (m, 3H, H-pyran), 2.02–2.18 (m, 3H, H-pyran), 3.80 (td, $J_1 = 2.8$ Hz, $J_2 = 11.6$ Hz, 1H, H-5'a in pyran), 4.19 (d, 1H, H-5'b in pyran), 5.83 (dd, $J_1 = 2.8$ Hz, $J_2 = 10.8$ Hz, 1H, H-1' in pyran), 7.51 (d, $J = 8.4$ Hz, 2H, H-3,5 in phenyl), 8.32 (s, 1H, H-8 in purine), 8.76 (d, $J = 8.4$ Hz, 2H, H-2,6 in phenyl), 8.99 (s, 1H, H-2 in purine). MS (ESI+) m/z : 231.5 (100%) (M+H–THP), 315.7 (100%) (M+H). Anal. Calcd for C₁₆H₁₅ClN₄O · 0.2EtOAc · 0.2H₂O: C, 60.05; H, 5.09; N, 16.67. Found C, 59.82; H, 4.69; N, 16.32.

6-(4-Bromophenyl)-9-(tetrahydro-2H-pyran-2-yl)-9H-purine (6)

Yield 250 mg (70%), mp 160–162 °C. ¹H NMR (CDCl₃) δ 1.64–1.87 (m, 3H, H-pyran), 2.02–2.20 (m, 3H, H-pyran), 3.81 (td, $J_1 = 2.8$ Hz, $J_2 = 11.2$ Hz, 1H, H-5'a in pyran), 4.19 (d, 1H, H-5'b in pyran), 5.84 (dd, $J_1 = 2.4$ Hz, $J_2 = 10$ Hz, 1H, H-1' in pyran), 7.67 (d, $J = 8.4$ Hz, 2H, H-3,5 in phenyl), 8.33 (s, 1H, H-8 in purine), 8.69 (d, $J = 8.8$ Hz, 2H, H-2,6 in phenyl), 8.99 (s, 1H, H-2 in purine). MS (ESI+) m/z : 275.6 (100%) (M–THP), 359.7 (78%) (M). Anal. Calcd for C₁₆H₁₅BrN₄O: C, 53.50; H, 4.21; N, 15.60. Found C, 53.29; H, 4.30; N, 15.99.

6-(4-Trifluoromethylphenyl)-9-(tetrahydro-2H-pyran-2-yl)-9H-purine (7)

Yield 250 mg (73%), mp 164–165 °C. ¹H NMR (CDCl₃) δ 1.67–1.88 (m, 3H, H-pyran), 2.05–2.21 (m, 3H,

H-pyran), 3.82 (td, $J_1 = 2.4$ Hz, $J_2 = 11.6$ Hz, 1H, H-5'a in pyran), 4.21 (d, 1H, H-5'b in pyran), 5.86 (dd, $J_1 = 2.8$ Hz, $J_2 = 10.8$ Hz, 1H, H-1' in pyran), 7.80 (d, $J = 8$ Hz, 2H, H-2,6 in phenyl), 8.37 (s, 1H, H-8 in purine), 8.91 (d, $J = 8$ Hz, 2H, H-3,5 in phenyl), 9.05 (s, 1H, H-2 in purine). MS (ESI+) m/z : 265.6 (100%) (M+H–THP), 349.8 (75%) (M+H). Anal. Calcd for C₁₇H₁₅F₃N₄O · 0.04CH₂Cl₂ · 0.15EtOAc: C, 58.05; H, 4.49; N, 15.35. Found C, 58.44; H, 4.09; N, 14.95.

6-(4-tert-Butylphenyl)-9-(tetrahydro-2H-pyran-2-yl)-9H-purine (8)

Yield 230 mg (67%), mp 161–162 °C. ¹H NMR (CDCl₃) δ 1.37 (s, 9H, CH₃), 1.66–1.84 (m, 3H, H-pyran), 2.04–2.20 (m, 3H, H-pyran), 3.81 (td, $J_1 = 2.8$ Hz, $J_2 = 11.6$ Hz, 1H, H-5'a in pyran), 4.20 (d, 1H, H-5'b in pyran), 5.84 (dd, $J_1 = 2.8$ Hz, $J_2 = 10.4$ Hz, 1H, H-1' in pyran), 7.58 (d, $J = 8.4$ Hz, 2H, H-3,5 in phenyl), 8.31 (s, 1H, H-8 in purine), 8.67 (d, $J = 8$ Hz, 2H, H-2,6 in phenyl), 9.0 (s, 1H, H-2 in purine). MS (ESI+) m/z : 253.7 (100%) (M+H–THP), 337.8 (100%) (M+H). Anal. Calcd for C₂₀H₂₄N₄O: C, 71.40; H, 7.19; N, 16.65. Found C, 71.0; H, 7.34; N, 16.78.

6-(4-Phenoxyphenyl)-9-(tetrahydro-2H-pyran-2-yl)-9H-purine (9)

Yield 220 mg (60%), mp 147–149 °C. ¹H NMR (CDCl₃) δ 1.64–1.85 (m, 3H, H-pyran), 2.02–2.18 (m, 3H, H-pyran), 3.80 (td, $J_1 = 2.4$ Hz, $J_2 = 11.6$ Hz, 1H, H-5'a in pyran), 4.19 (d, 1H, H-5'b in pyran), 5.83 (dd, $J_1 = 2.8$ Hz, $J_2 = 10.4$ Hz, 1H, H-1' in pyran), 7.08 (d, $J = 8.8$ Hz, 2H, H-2,6 in O-phenyl), 7.13–7.16 (m, 3H, H-3,5, H-4' in phenyl), 7.36 (t, $J = 8$ Hz, 2H, H-3,5 in O-phenyl), 8.30 (s, 1H, H-8 in purine), 8.78 (d, $J = 8.8$ Hz, 2H, H-2,6 in phenyl), 8.98 (s, 1H, H-2 in purine). MS (ESI+) m/z : 289.7 (88%) (M+H–THP), 373.8 (100%) (M+H). Anal. Calcd for C₂₂H₂₀N₄O₂: C, 70.95; H, 5.41; N, 15.04. Found C, 71.23; H, 5.44; N, 15.30.

2. 1. 3. General Procedure for the Synthesis of 6-(4-Substituted Phenyl)-9H-purines 10–16

A mixture of 6-(4-substituted phenyl)-9-(tetrahydro-pyran-2-yl)-9H-purines (1 mmol) **3–9**, Dowex 50 \times 8 (H⁺) (700 mg), MeOH (10 mL) and H₂O (1 mL) was refluxed. Then the reaction mixture was filtered and washed with saturated methanolic NH₃ and MeOH. The filtrate was evaporated in vacuo, and recrystallized from EtOAc–hexane.

6-Phenyl-9H-purine (10)³¹

Yield 160 mg (80%), mp 279–281 °C (280–282 °C³¹). ¹H NMR (DMSO-*d*₆) δ 7.28–7.40 (m, 3H, H-3,4,5 in phenyl), 7.76 (d, $J = 6.4$ Hz, 2H, H-2,6 in phenyl), 8.01 (s, 1H, H-8 in purine), 8.81 (s, 1H, H-2 in purine). MS (ESI+) m/z : 197.6 (100%) (M+H).

6-(4-Fluorophenyl)-9H-purine (11)³¹

Yield 190 mg (87%), mp 295–298 °C (299–302 °C³¹). ¹H NMR (DMSO-*d*₆) δ 7.41 (t, *J* = 8.8 Hz, 2H, H-3,5 in phenyl), 8.63 (s, 1H, H-8 in purine), 8.86–8.91 (m, 2H, H-2,6 in phenyl), 8.92 (s, 1H, H-2 in purine). MS (ESI+) *m/z*: 215.6 (100%) (M+H).

6-(4-Chlorophenyl)-9H-purine (12)

Yield 190 mg (83%), mp 290–292 °C. ¹H NMR (DMSO-*d*₆) δ 7.68 (d, *J* = 8.8 Hz, 2H, H-3,5 in phenyl), 8.68 (s, 1H, H-8 in purine), 8.87 (d, *J* = 8.8 Hz, 2H, H-2,6 in phenyl), 8.97 (s, 1H, H-2 in purine). MS (ESI+) *m/z*: 231.4 (100%) (M+H). Anal. Calcd for C₁₁H₇ClN₄: C, 57.28; H, 3.06; N, 24.29. Found C, 57.08; H, 3.05; N, 24.32.

6-(4-Bromophenyl)-9H-purine (13)

Yield 150 mg (55%), mp 310–311 °C. ¹H NMR (DMSO-*d*₆) δ 7.82 (d, *J* = 8.4 Hz, 2H, H-3,5 in phenyl), 8.69 (s, 1H, H-8 in purine), 8.80 (d, *J* = 8.4 Hz, 2H, H-2,6 in phenyl), 8.97 (s, 1H, H-2 in purine). MS (ESI+) *m/z*: 275.6 (100%) (M), 277.7 (M+2) (90%). Anal. Calcd for C₁₁H₇BrN₄ · 1.0H₂O: C, 45.07; H, 3.09; N, 19.11. Found C, 45.44; H, 2.97; N, 19.52.

6-(4-Trifluoromethylphenyl)-9H-purine (14)

Yield 210 mg (80%), mp 221–223 °C. ¹H NMR (DMSO-*d*₆) δ 7.66 (d, *J* = 8 Hz, 2H, H-2,6 in phenyl), 7.95 (d, *J* = 7.6 Hz, 2H, H-3,5 in phenyl), 8.33 (s, 2H, H-2,8 in purine). MS (ESI+) *m/z*: 265.6 (100%) (M+H). Anal. Calcd for C₁₂H₇F₃N₄: C, 54.54; H, 2.65; N, 21.21. Found C, 54.37; H, 2.46; N, 21.39.

6-(4-*tert*-Butylphenyl)-9H-purine (15)

Yield 220 mg (88%), mp 291–293 °C. ¹H NMR (CDCl₃) δ 1.37 (s, 9H, CH₃), 7.61 (d, *J* = 8.8 Hz, 2H, H-3,5 in phenyl), 8.34 (s, 1H, H-8 in purine), 8.71 (d, *J* = 8.4 Hz, 2H, H-2,6 in phenyl), 9.10 (s, 1H, H-2 in purine). MS (ESI+) *m/z*: 253.7 (100%) (M+H). Anal. Calcd for C₁₅H₁₆N₄ · 0.1H₂O: C, 70.89; H, 6.42; N, 22.04. Found C, 71.23; H, 6.65; N, 21.66.

6-(4-Phenoxyphenyl)-9H-purine (16)

Yield 260 mg (90%), mp 240–241 °C. ¹H NMR (DMSO-*d*₆) δ 7.14–7.25 (m, 5H, H-3,5 in phenyl, H-2,4,6 in O-phenyl), 7.46 (t, *J* = 7.6 Hz, 2H, H-3,5 in O-phenyl), 8.63 (s, 1H, H-8 in purine), 8.88 (d, *J* = 7.6 Hz, 2H, H-2,6 in phenyl), 8.92 (s, 1H, H-2 in purine). MS (ESI+) *m/z*: 289.7 (100%) (M+H). Anal. Calcd for C₁₇H₁₂N₄O · 0.22EtOAc: C, 69.79; H, 4.50; N, 18.20. Found C, 70.08; H, 4.47; N, 17.81.

2. 1. 4. General Procedure for the Sulfonylation of 6-(4-Substituted Phenyl)-9H-purines (Preparation of Compounds 17–32)

A solution of (substituted phenyl)sulfonyl chloride (2 mmol) in 5 mL CH₂Cl₂ was slowly added to a solution

of 6-(4-substituted phenyl)-9H-purines **10–16** (1 mmol) in 1 mL pyridine. The reaction mixture was stirred for 40–48 h in an ice bath. The reaction mixture was treated with 1N HCl (5 mL) and extracted with CH₂Cl₂. The extract was dried over Na₂SO₄, the solvent was evaporated in vacuo, and the residue was purified by column chromatography (hexane:CH₂Cl₂, 1:1).

9-(4-Fluorophenylsulfonyl)-6-phenyl-9H-purine (17)

Yield 71 mg (20%), mp 255–256 °C. ¹H NMR (CDCl₃) δ 7.29 (d, 2H, H-2,6 in phenyl), 7.55 (t, 3H, H-3,4,5 in phenyl), 8.39 (dd, *J*₁ = 4.8 Hz, *J*₂ = 8.8 Hz, 2H, H-2',6' in phenyl), 8.56 (s, 1H, H-8 in purine), 8.69 (dd, 2H, H-3',5' in phenyl), 9.09 (s, 1H, H-2 in purine). MS (ESI+) *m/z*: 355.7 (100%) (M+H). Anal. Calcd for C₁₇H₁₁FN₄O₂S: C, 57.62; H, 3.13; N, 15.81; S, 9.05. Found C, 57.96; H, 3.27; N, 15.59; S 9.09.

9-(4-Trifluoromethylphenylsulfonyl)-6-phenyl-9H-purine (18)

Yield 190 mg (48%), mp 222–224 °C. ¹H NMR (CDCl₃) δ 7.55 (t, 3H, H-3,4,5 in phenyl), 7.87 (d, 2H, *J* = 8.8 Hz, H-2,6 in phenyl), 8.50 (d, *J* = 8.4 Hz, 2H, H-2',6' in phenyl), 8.56 (s, 1H, H-8 in purine), 8.67–8.70 (m, 2H, H-3',5' in phenyl), 9.10 (s, 1H, H-2 in purine). ¹³C NMR (CDCl₃) δ 127.02 (q) (CF₃), 129.04, 129.62, 130.13, 131.51, 132.02, 134.78, 137.0, 137.34 (C in phenyl), 140.32 (C-5), 141.06 (C-8), 151.21 (C-6), 154.33 (C-2), 156.73 (C-4). MS (ESI+) *m/z*: 405.7 (100%) (M+H). Anal. Calcd for C₁₈H₁₁F₃N₄O₂S: C, 53.46; H, 2.74; N, 13.86; S, 7.93. Found C, 53.69; H, 2.81; N, 13.59; S 7.97.

9-(4-*tert*-Butylphenylsulfonyl)-6-phenyl-9H-purine (19)

Yield 160 mg (40%), mp 236–237 °C. ¹H NMR (CDCl₃) δ 1.30 (s, 9H, CH₃), 7.52–7.55 (m, 3H, H-3,4,5 in phenyl), 7.59 (d, *J* = 8.8 Hz, 2H, H-2,6 in phenyl), 8.23 (d, *J* = 9.2 Hz, 2H, H-3',5' in phenyl), 8.56 (s, 1H, H-8 in purine), 8.67–8.69 (m, 2H, H-2',6' in phenyl), 9.11 (s, 1H, H-2 in purine). ¹³C NMR (CDCl₃) δ 31.12 (CH₃), 35.74 (C in *tert*-butyl), 126.93, 128.76, 128.99, 130.07, 131.58, 131.79, 133.86, 135.01 (C in phenyl), 141.62 (C-5), 151.34 (C-8), 154.19 (C-6), 156.33 (C-2), 160.08 (C-4). MS (ESI+) *m/z*: 393.9 (100%) (M+H). Anal. Calcd for: C₂₁H₂₀N₄O₂S: C, 64.27; H, 5.14; N, 14.28; S, 8.17. Found C, 63.88; H, 5.19; N, 13.97; S 8.11.

9-(4-Fluorophenylsulfonyl)-6-(4-fluorophenyl)-9H-purine (20)

Yield 130 mg (35%), mp 265–267 °C. ¹H NMR (CDCl₃) δ 7.19–7.29 (m, 4H, H-3,5, H-3',5' in phenyl), 8.37 (dd, *J*₁ = 4.4 Hz, *J*₂ = 8.4 Hz, 2H, H-2',6' in phenyl), 8.54 (s, 1H, H-8 in purine), 8.77 (dd, *J*₁ = 5.6 Hz, *J*₂ = 8.4 Hz, 2H, H-2,6 in phenyl), 9.10 (s, 1H, H-2 in purine). MS (ESI+) *m/z*: 373.8 (100%) (M+H). Anal. Calcd for: C₁₇H₁₀F₂N₄O₂S · 0.5H₂O: C, 53.54; H, 2.90;

N, 14.69; S, 8.40. Found C, 53.14; H, 2.70; N, 14.45; S 8.47.

9-(4-Trifluoromethylphenylsulfonyl)-6-(4-fluorophenyl)-9H-purine (21)

Yield 140 mg (32%), mp 214–216 °C. ¹H NMR (CDCl₃) δ 7.22 (t, *J* = 8.8 Hz, 2H, H-3,5 in phenyl), 7.87 (d, *J* = 8.8 Hz, 2H, H-2',6' in phenyl), 8.49 (d, *J* = 8.4 Hz, 2H, H-3',5' in phenyl), 8.55 (s, 1H, H-8 in purine), 8.77 (dd, *J*₁ = 5.6 Hz, *J*₂ = 9.2 Hz, 2H, H-2,6 in phenyl), 9.07 (s, 1H, H-2 in purine). ¹³C NMR (CDCl₃) δ 115.88, 116.09, 125.84 (C in phenyl), 126.82 (q) (CF₃), 129.42, 130.81, 131.0, 132.22, 132.31 (C in phenyl), 140.25 (C-5), 140.87 (C-8), 151.0 (C-6), 154.08 (C-2), 155.25 (C-4). MS (ESI+) *m/z*: 423.8 (100%) (M+H). Anal. Calcd for: C₁₈H₁₀F₄N₄O₂S · 0.4CH₂Cl₂: C, 48.42; H, 2.38; N, 12.27; S, 7.02. Found C, 48.21; H, 2.48; N, 12.00; S 7.26.

9-(4-tert-Butylphenylsulfonyl)-6-(4-fluorophenyl)-9H-purine (22)

Yield 80 mg (20%), mp 226–227 °C. ¹H NMR (CDCl₃) δ 1.30 (s, 9H, CH₃), 7.21 (t, *J* = 8.8 Hz, 2H, H-3,5 in phenyl), 7.59 (d, *J* = 8.8 Hz, 2H, H-3',5' in phenyl), 8.23 (d, *J* = 8.4 Hz, 2H, H-2',6' in phenyl), 8.55 (s, 1H, H-8 in purine), 8.77 (dd, *J*₁ = 5.6 Hz, *J*₂ = 9.2 Hz, 2H, H-2,6 in phenyl), 9.09 (s, 1H, H-2 in purine). MS (ESI+) *m/z*: 411.9 (100%) (M+H). Anal. Calcd for: C₂₁H₁₉FN₄O₂S: C, 61.45; H, 4.67; N, 13.65; S, 7.81. Found C, 61.83; H, 4.78; N, 13.25; S 8.02.

9-(4-Fluorophenylsulfonyl)-6-(4-chlorophenyl)-9H-purine (23)

Yield 190 mg (49%), mp 237–239 °C. ¹H NMR (CDCl₃) δ 7.51 (d, *J* = 8.4 Hz, 2H, H-3',5' in phenyl), 7.87 (d, *J* = 8.8 Hz, 2H, H-3,5 in phenyl), 8.49 (d, *J* = 8.8 Hz, 2H, H-2',6' in phenyl), 8.70 (d, *J* = 8.8 Hz, 2H, H-2,6 in phenyl), 9.11 (s, 1H, H-8 in purine), 9.19 (s, 1H, H-2 in purine). ¹³C NMR (DMSO-*d*₆) δ 126.75, 129.08, 129.40, 131.21, 133.02, 136.84, 138.21 (C in phenyl), 140.10 (C-5), 140.94 (C-8), 151.07 (C-6), 154.04 (C-2), 155.10 (C-4). MS (ESI+) *m/z*: 231.6 (100%) [M+H-(4-F-Ph-SO₂)]. Anal. Calcd for: C₁₇H₁₀ClFN₄O₂S · 0.4 CH₂Cl₂: C, 49.43; H, 2.57; N, 13.25; S, 7.58. Found C, 49.11; H, 2.46; N, 12.85; S 7.38.

9-(4-Fluorophenylsulfonyl)-6-(4-bromophenyl)-9H-purine (24)

Yield 110 mg (25%), mp 243–245 °C. ¹H NMR (CDCl₃) δ 7.21 (t, *J* = 8.8 Hz, 2H, H-3',5' in phenyl), 7.61 (d, *J* = 8.4 Hz, 2H, H-3,5 in phenyl), 8.32 (dd, *J*₁ = 5.2 Hz, *J*₂ = 7.2 Hz, 2H, H-2',6' in phenyl), 8.50 (s, 1H, H-8 in purine), 8.56 (d, *J* = 8.4 Hz, 2H, H-2,6 in phenyl), 9.01 (s, 1H, H-2 in purine). MS (ESI+) *m/z*: 433.7 (100%) (M), 435.8 (M+2) (60%). Anal. Calcd for: C₁₇H₁₀BrFN₄O₂S: C, 47.13; H, 2.33; N, 12.93; S, 7.40. Found C, 47.39; H, 2.27; N, 12.89; S 7.62.

9-(4-Fluorophenylsulfonyl)-6-(4-trifluoromethylphenyl)-9H-purine (25)

Yield 110 mg (26%), mp 240–242 °C. ¹H NMR (CDCl₃) δ 7.28 (t, *J* = 8.8 Hz, 2H, H-3',5' in phenyl), 7.79 (d, *J* = 8.4 Hz, 2H, H-2,6 in phenyl), 8.39 (dd, *J*₁ = 5.2 Hz, *J*₂ = 9.2 Hz, 2H, H-2',6' in phenyl), 8.59 (s, 1H, H-8 in purine), 8.85 (d, *J* = 8 Hz, 2H, H-3,5 in phenyl), 9.13 (s, 1H, H-2 in purine). MS (ESI+) *m/z*: 423.8 (80%) (M+H). Anal. Calcd for: C₁₈H₁₀F₄N₄O₂S: C, 51.19; H, 2.39; N, 13.27; S, 7.59. Found C, 51.37; H, 2.26; N, 13.54; S 7.60.

9-(4-Trifluoromethylphenylsulfonyl)-6-(4-trifluoromethylphenyl)-9H-purine (26)

Yield 140 mg (31%) mp 240–241 °C. ¹H NMR (CDCl₃) δ 7.79 (d, *J* = 8.4 Hz, 2H, H-2,6 in phenyl), 7.88 (d, *J* = 8.4 Hz, 2H, H-3,5 in phenyl), 8.50 (d, *J* = 8 Hz, 2H, H-2',6' in phenyl), 8.60 (s, 1H, H-8 in purine), 8.84 (d, *J* = 8 Hz, 2H, H-3',5' in phenyl), 9.14 (s, 1H, H-2 in purine). MS (ESI+) *m/z*: 265.6 (100%) [M+H-(4-F-Ph-SO₂)]. Anal. Calcd for: C₁₉H₁₀F₆N₄O₂S · 0.6CH₂Cl₂: C, 44.98; H, 2.16; N, 10.70; S, 6.13. Found C, 45.26; H, 2.28; N, 11.10; S 6.38.

9-(4-tert-Butylphenylsulfonyl)-6-(4-trifluoromethylphenyl)-9H-purine (27)

Yield 100 mg (22%), mp 193–195 °C. ¹H NMR (DMSO-*d*₆) δ 1.30 (s, 9H, CH₃), 7.61 (d, *J* = 9.2 Hz, 2H, H-3',5' in phenyl), 7.79 (d, *J* = 8.4 Hz, 2H, H-2,6 in phenyl), 8.25 (d, *J* = 9.2 Hz, 2H, H-2',6' in phenyl), 8.61 (s, 1H, H-8 in purine), 8.86 (d, *J* = 8.4 Hz, 2H, H-3,5 in phenyl), 9.16 (s, 1H, H-2 in purine). ¹³C NMR (DMSO-*d*₆) δ 30.88 (CH₃), 35.53 (C in *tert*-butyl), 125.61 (q) (CF₃), 126.75, 128.60, 130.14, 130.86, 131.66, 132.73, 133.49, 138.04 (C in phenyl), 141.97 (C-5), 151.34 (C-8), 153.96 (C-6), 154.25 (C-2), 160.04 (C-4). MS (ESI+) *m/z*: 461.8 (100%) (M+H). Anal. Calcd for: C₂₂H₁₉F₃N₄O₂S · 0.1Hexane: C, 57.87; H, 4.38; N, 11.94; S, 6.84. Found C, 58.31; H, 4.55; N, 11.62; S 6.52.

9-(4-Fluorophenylsulfonyl)-6-(4-tert-butylphenyl)-9H-purine (28)

Yield 180 mg (44%), mp: 240–242 °C. ¹H NMR (CDCl₃) δ 1.35 (s, 9H, CH₃), 7.27 (t, *J* = 8.8 Hz, 2H, H-3',5' in phenyl), 7.56 (d, *J* = 8.8 Hz, 2H, H-3,5 in phenyl), 8.38 (dd, *J*₁ = 4.8 Hz, *J*₂ = 8.8 Hz, 2H, H-2',6' in phenyl), 8.55 (s, 1H, H-8 in purine), 8.59 (d, *J* = 8.4 Hz, 2H, H-2,6 in phenyl), 9.10 (s, 1H, H-2 in purine). ¹³C NMR (DMSO-*d*₆) δ 31.13 (CH₃), 35.01 (C in *tert*-butyl), 115.32, 117.20, 125.82, 127.06, 128.38, 129.68, 131.13, 131.87 (C in phenyl), 140.83 (C-5), 150.85 (C-8), 153.96 (C-6), 155.30 (C-2), 156.38 (C-4). MS (ESI+) *m/z*: 411.8 (100%) (M+H). Anal. Calcd for: C₂₁H₁₉FN₄O₂S: C, 61.45; H, 4.67; N, 13.65; S, 7.81. Found C, 61.09; H, 4.89; N, 13.22; S 7.69.

9-(4-Trifluoromethylphenylsulfonyl)-6-(4-*tert*-butylphenyl)-9H-purine (29)

Yield 120 mg (26%), mp 199–201 °C. ^1H NMR (CDCl_3) δ 1.38 (s, 9H, CH_3), 7.57 (d, $J = 8.8$ Hz, 2H, H-3,5 in phenyl), 7.87 (d, $J = 8.4$ Hz, 2H, H-2',6' in phenyl), 8.50 (d, $J = 8$ Hz, 2H, H-2,6 in phenyl), 8.55 (s, 1H, H-8 in purine), 8.61 (d, $J = 8.4$ Hz, 2H, H-3',5' in phenyl), 9.08 (s, 1H, H-2 in purine). ^{13}C NMR ($\text{DMSO-}d_6$) δ 31.12 (CH_3), 35.03 (C in *tert*-butyl), 124.89, 125.84, 126.78 (q) (CF_3), 129.38, 129.70, 131.12, 131.78, 135.38, 137.07 (C in phenyl), 140.61 (C-5), 150.87 (C-8), 154.12 (C-6), 155.40 (C-2), 156.60 (C-4). MS (ESI+) m/z : 461.9 (100%) (M+H). Anal. Calcd for: $\text{C}_{22}\text{H}_{19}\text{F}_3\text{N}_4\text{O}_2\text{S} \cdot 0.3\text{Hexane}$: C, 58.77; H, 4.80; N, 11.52; S, 6.59. Found C, 58.84; H, 4.55; N, 11.21; S 6.24.

9-(4-Fluorophenylsulfonyl)-6-(4-phenoxyphenyl)-9H-purine (30)

Yield 300 mg (66%), mp 178–180 °C. ^1H NMR (CDCl_3) δ 7.04–7.13 (m, 4H, H-3,5 in phenyl, H-2,6 in O-phenyl), 7.17 (t, $J = 8.4$ Hz, 1H, H-4 in O-phenyl), 7.27 (t, $J = 8.4$ Hz, 2H, H-3,5 in O-phenyl), 7.38 (t, $J = 8.4$ Hz, 2H, H-3',5' in phenyl), 8.38 (dd, $J_1 = 4.8$ Hz, $J_2 = 9.2$ Hz, 2H, H-2',6' in phenyl), 8.54 (s, 1H, H-8 in purine), 8.71 (d, $J = 8.8$ Hz, 2H, H-2,6 in phenyl), 9.06 (s, 1H, H-2 in purine). ^{13}C NMR ($\text{DMSO-}d_6$) δ 115.33, 117.21, 118.05, 119.95, 124.31, 127.10, 128.47, 129.02, 129.96, 130.83, 131.87, 132.62 (C in phenyl), 140.83 (C-5), 150.88 (C-8), 153.85 (C-6), 155.84 (C-2), 160.91 (C-4). MS (ESI+) m/z : 447.7 (100%) (M+H). Anal. Calcd for: $\text{C}_{23}\text{H}_{15}\text{FN}_4\text{O}_3\text{S} \cdot 0.5\text{H}_2\text{O}$: C, 60.65; H, 3.54; N, 12.30; S, 7.04. Found C, 60.89; H, 3.45; N, 11.90; S 7.42.

9-(4-Trifluoromethylphenylsulfonyl)-6-(4-phenoxyphenyl)-9H-purine (31)

Yield 110 mg (23%), mp 184–186 °C. ^1H NMR (CDCl_3) δ 7.07–7.12 (m, 4H, H-3,5 in phenyl, H-2,6 in O-phenyl), 7.17 (t, 1H, H-4 O-phenyl), 7.38 (t, $J = 8.4$ Hz, 2H, H-3,5 in O-phenyl), 7.87 (d, $J = 8.8$ Hz, 2H, H-2',6' in phenyl), 8.49 (d, $J = 9.2$ Hz, 2H, H-3',5' in phenyl), 8.53 (s, 1H, H-8 in purine), 8.71 (d, $J = 8.8$ Hz, 2H, H-2,6 in phenyl), 9.04 (s, 1H, H-2 in purine). MS (ESI+) m/z : 497.8 (100%) (M+H). Anal. Calcd for: $\text{C}_{24}\text{H}_{15}\text{F}_3\text{N}_4\text{O}_3\text{S} \cdot 0.35\text{Hexane}$: C, 59.53; H, 3.80; N, 10.64; S, 6.09. Found C, 59.66; H, 3.41; N, 10.36; S 5.94.

9-(4-*tert*-Butylphenylsulfonyl)-6-(4-phenoxyphenyl)-9H-purine (32)

Yield 210 mg (43%), mp 157–159 °C. ^1H NMR (CDCl_3) δ 1.33 (s, 9H, CH_3), 7.07–7.12 (m, 3H, H-2,4,6 in O-phenyl), 7.37 (t, $J = 8.8$ Hz, 2H, H-3,5 in O-phenyl), 7.54 (d, $J = 8.8$ Hz, 2H, H-3,5 in phenyl), 7.82 (d, $J = 8.8$ Hz, 2H, H-3',5' in phenyl), 8.22 (d, $J = 8.8$ Hz, 2H, H-2',6' in phenyl), 8.53 (s, 1H, H-8 in purine), 8.71 (d, $J = 8.8$ Hz, 2H, H-2,6 in phenyl), 9.07 (s, 1H, H-2 in purine). ^{13}C NMR ($\text{DMSO-}d_6$) δ 30.89 (CH_3), 35.50 (C in *tert*-

butyl), 118.07, 119.89, 124.22, 126.19, 126.68, 127.69, 128.52, 129.38, 129.93, 130.91, 131.77, 133.69 (C in phenyl), 141.12 (C-5), 151.02 (C-8), 153.93 (C-6), 155.38 (C-2), 160.70 (C-4). MS (ESI+) m/z : 485.9 (100%) (M+H). Anal. Calcd for: $\text{C}_{27}\text{H}_{24}\text{N}_4\text{O}_3\text{S}$: C, 66.92; H, 4.99; N, 11.56; S, 6.62. Found C, 66.63; H, 4.78; N, 11.84; S 6.29.

2. 2. Cytotoxic Activity**2. 2. 1. Cells and Culture**

The human primary liver cancer cell lines (Huh7, HepG2, Mahlavu and FOCUS) were grown in Dulbecco's Modified Eagle's Medium (DMEM) (Invitrogen GIBCO), with 10% fetal bovine serum (FBS) (Invitrogen GIBCO), nonessential amino acids, and 1% penicillin (Biochrome). It was incubated in 37 °C with 5% CO_2 . DMSO (Sigma) was used as the solvent for the compounds. The concentration of DMSO was always less than 1% in the cell culture medium. The cytotoxic drugs (5-FU, Fludarabine and Cladribine) used as positive controls were from Calbiochem.

2. 2. 2. Sulforhodamine B (SRB) Assay for Cytotoxicity Screening

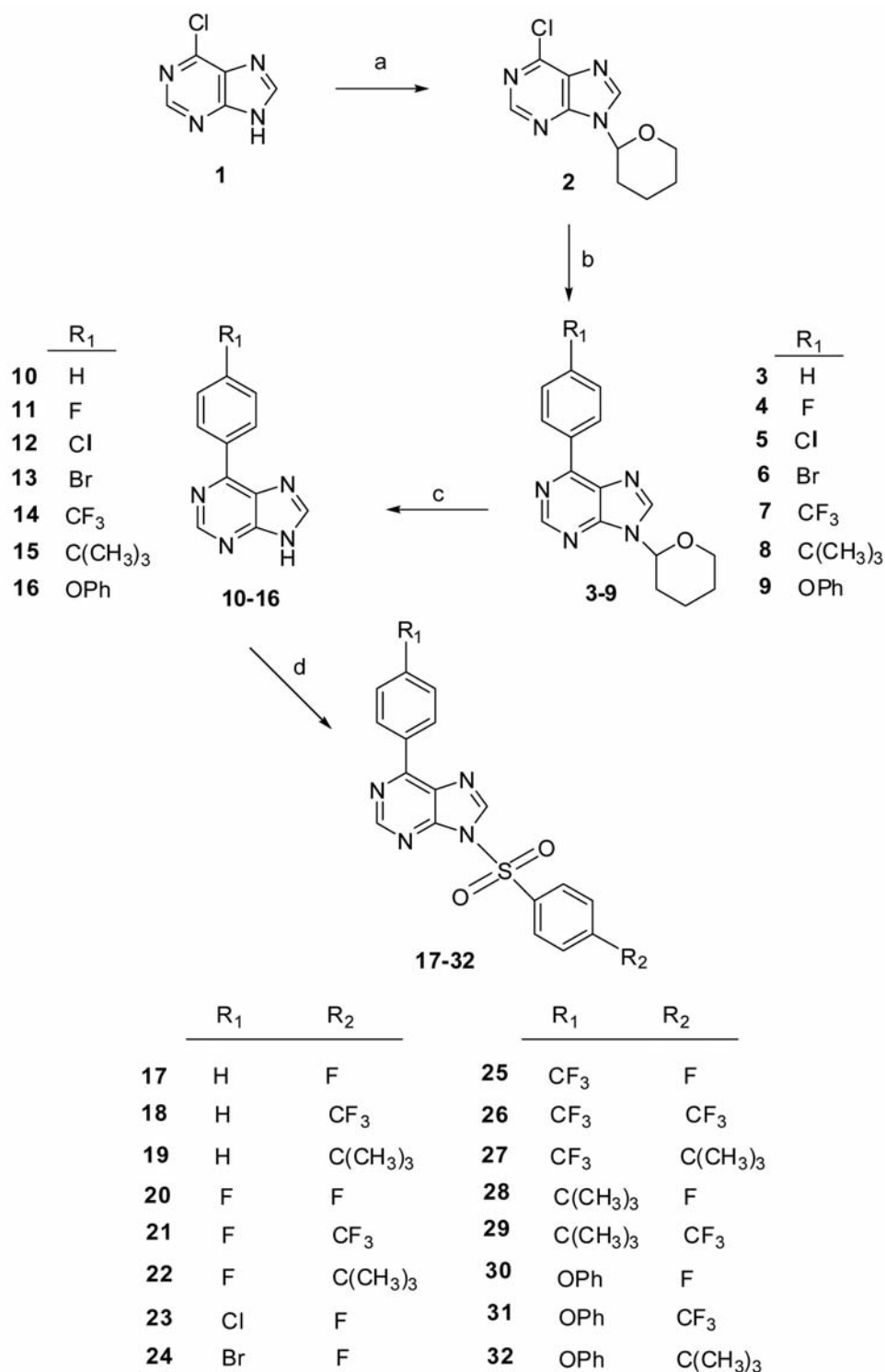
Huh7, HCT116, MCF7, HepG2, Mahlavu, and FOCUS cells were inoculated (2000–10000 cells/well in 200 μL) in 96-well plates. The next day, the media were refreshed and the compounds dissolved in DMSO were applied in concentrations between 1 and 40 μM in parallel with DMSO-only treated cells as negative controls. At the 72nd hour of treatment with compounds **3–32** and the other drugs, the cancer cells were fixed with 100 μL of 10% (w/v) trichloroacetic acid (TCA) and kept at +4 °C in the dark for one hour. TCA fixation was terminated by washing the wells with ddH_2O five times. Air-dried plates were stained with 0.4% sulphorhodamine B (SRB) dissolved in 1% acetic acid solution for 10 min in the dark and at room temperature. The protein-bound and dried SRB dye was then solubilized with 10 mM Tris-Base pH 8. The absorbance values were obtained at 515 nm in a microplate reader. The data were normalized against DMSO only treated wells, which were used as controls in serial dilutions. In all experiments, a linear response was observed, with serial dilutions of the compounds and the drugs.

3. Results and Discussion**3. 1. Chemistry**

The 6-(4-substituted phenyl)-9-[(4-substituted phenyl)sulfonyl]purine derivatives **17–32** were prepared as shown in Scheme 1. The *N*-9 position in the starting compound 6-chloropurine (**1**) was protected as the tetrahydropyran-2-yl (THP) derivative **2**³⁰ by reacting **1** with

the carbocation formed *in situ* from 3,4-dihydro-2*H*-pyran and catalytic amount of *p*-TSA in refluxing THF. We prepared the 6-(substituted phenyl)purines **3–9** by Suzuki coupling reaction. This coupling with 4-substituted phenyl boronic acids in toluene catalyzed by Pd(PPh₃)₄

gave compounds **3–9**. The THP derivatives **3–9** were de-protected using wet Dowex 50 × 8 (H+) in methanol to obtain 6-(4-substituted phenyl)purines **10–16**. Compounds **10–16** were *N*-sulfonylated with complete regioselectivity applying the same set of reaction conditions as



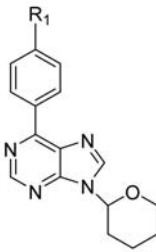
Scheme 1. (a) 3,4-dihydro-2*H*-pyran, *p*-TSA, THF; (b) R₁PhB(OH)₂, Pd(PPh₃)₄, K₂CO₃, toluene; (c) Dowex 50 × 8 (H+), MeOH, H₂O; (d) (4-substituted benzene)sulfonyl chloride, pyridine, CH₂Cl₂

reported for the sulfonylation of adenine. This reaction took place only at the *N*-9 atom, without the simultaneous *N*-7 sulfonylation.^{29,32} Treatment of 6-(4-substituted phenyl)-9*H*-purines **10–16** with (4-substituted phenyl)sulfonyl chlorides in CH₂Cl₂ and pyridine on an ice bath gave the corresponding *N*⁹-sulfonylated purines **17–32**.

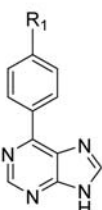
3. 2. Cytotoxic Activity and Structure-Activity Relationship (SAR)

The *in vitro* cytotoxicity of the compounds **3–32** were initially analyzed on human cancer cells (liver Huh7, colon HCT116, breast MCF7), using a sulforhodamine B (SRB) assay. The IC₅₀ values for each compound were also calculated in comparison with the known cell growth

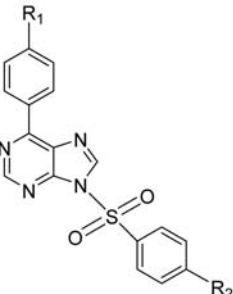
Table 1. *In vitro* cytotoxicity of the compounds **3–32** on different human cancer cell lines (Huh7, HCT116, MCF7)



3–9



10–16



17–32

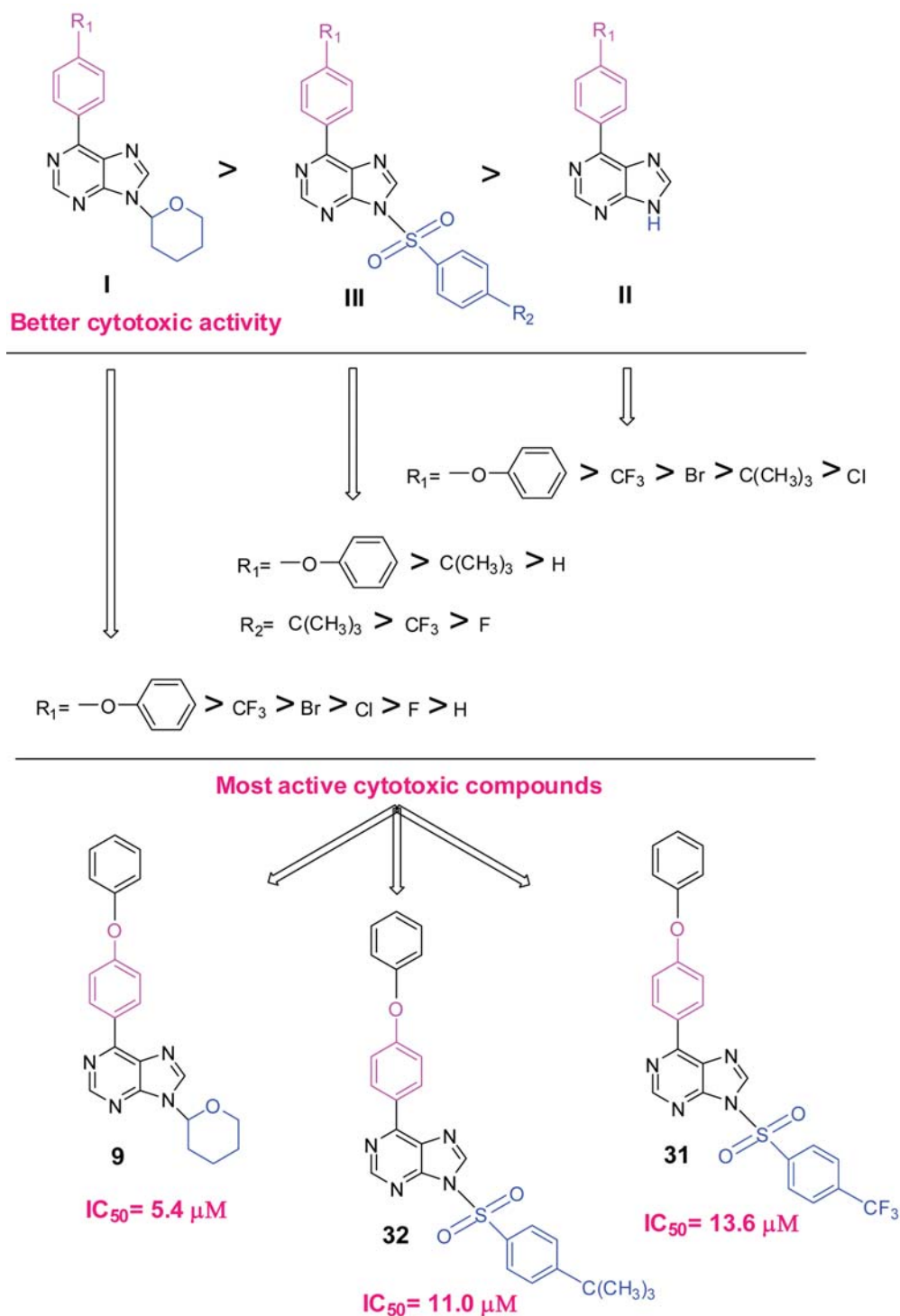
Compound	R ₁	R ₂	Cancer cell lines, IC ₅₀ (μM) ^a		
			Huh7	HCT116	MCF7
3	H	–	69.8 ± 12.1	NI	NI
4	F	–	49.6 ± 1.9	NI	NI
5	Cl	–	29.2 ± 7.2	NI	NI
6	Br	–	27.3 ± 12.6	NI	NI
7	CF ₃	–	22.2 ± 6.9	NI	NI
8	C(CH ₃) ₃	–	NI	NI	NI
9	OPh	–	5.4 ± 0.7	15.9 ± 9.3	7.4 ± 1.3
10	H	–	NI	NI	NI
11	F	–	NI	NI	NI
12	Cl	–	>100	78.8 ± 21.1	NI
13	Br	–	56.4 ± 16.7	NI	NI
14	CF ₃	–	44.1 ± 17.5	NI	NI
15	C(CH ₃) ₃	–	>100	NI	NI
16	OPh	–	16.0 ± 1.2	44.8 ± 1.1	24.0 ± 0.1
17	H	F	NI	>100	NI
18	H	CF ₃	42.1 ± 5.5	NI	54.9 ± 5.7
19	H	C(CH ₃) ₃	NI	NI	NI
20	F	F	NI	65.2 ± 25.8	NI
21	F	CF ₃	NI	53.1 ± 41.6	NI
22	F	C(CH ₃) ₃	NI	NI	NI
23	Cl	F	NI	78.2 ± 59.9	NI
24	Br	F	NI	NI	NI
25	CF ₃	F	NI	NI	NI
26	CF ₃	CF ₃	NI	NI	NI
27	CF ₃	C(CH ₃) ₃	NI	NI	NI
28	C(CH ₃) ₃	F	NI	NI	NI
29	C(CH ₃) ₃	CF ₃	16.0 ± 1.2	30.2 ± 4.9	27.1 ± 0.3
30	OPh	F	14.3 ± 1.6	14.5 ± 2.1	22.7 ± 0.5
31	OPh	CF ₃	13.6 ± 0.9	13.1 ± 4.6	17.0 ± 0.7
32	OPh	C(CH ₃) ₃	11.0 ± 0.8	18.2 ± 3.3	21.1 ± 1.6
5-FU			30.6 ± 1.8	4.1 ± 0.3	3.5 ± 0.7
Fludarabine			28.4 ± 19.2	8.0 ± 3.4	15.2 ± 0.1
Cladribine			0.9 ± 0.7	<0.1	2.4 ± 2.4

^a IC₅₀ values were calculated from the cell growth inhibition percentages obtained with 5 different concentrations (40, 20, 10, 5, and 2.5 μM) of each molecule incubated for 72 h. NI: No inhibition

inhibitors 5-fluorouracil (5-FU), fludarabine and cladribine and the results are summarized in Table 1.

Among the molecules synthesized in this study, analogues accommodate substituted tetrahydropyran moiety at their *N*-9 position **3–9**, and the one with a promising IC_{50} value against Huh7 (5.4 μ M) is 6-(4-phenoxyphenyl)-9-(tetrahydropyran-2-yl)-9*H*-purine (**9**).

Analyzing the data presented in Table 1, highlights the 4-phenoxyphenyl substitution as the group at C-6 as the most responsible for the anti-cancer activity against Huh7. When we compared their IC_{50} values with the nucleobase analogue 5-FU and nucleoside analogue Fludarabine, we observed that our compounds **9**, **16**, **30**, **31** and **32** had showed lower values in micromolar concen-



Scheme 2. Structure-activity relationship (SAR) of substituted purines against Huh7 (**3–32**)

trations and these molecules had a better cytotoxic activity on Huh7 cells (5.4, 16.0, 14.3, 13.6 and 11.0 vs 30.6 μ M and 28.4 for 5-FU and Fludarabine). Compound **29**,

bearing a 4-*tert*-butylphenyl substituent at C-6 position of the purine, was active derivative with greater potency against Huh7 cell line than 5-FU and Fludarabine. The

Table 2. IC₅₀ values of **5–9**, **14**, **16**, **18**, **28–32** against hepatocellular carcinoma (HCC) cell lines: Huh7, HepG2, MAHLAVU, FOCUS.

Compound	HCC Cancer cell lines, IC ₅₀ (μ M) ^a			
	Huh7	HepG2	Mahlavu	FOCUS
5	29.2 \pm 7.2	39.7 \pm 17.7	NI	NI
6	27.3 \pm 12.6	38.4 \pm 13.9	NI	82.6 \pm 43.3
7	22.2 \pm 6.9	NI	NI	NI
8	NI	NI	NI	NI
9	5.4 \pm 0.7	NI	54.9 \pm 69.4	6.2 \pm 1.6
14	44.1 \pm 17.5	44.9 \pm 23.6	54.1 \pm 4.9	45.0 \pm 14.6
16	16.0 \pm 1.2	23.4 \pm 0.6	30.2 \pm 1.7	25.4 \pm 4.8
18	42.1 \pm 5.5	NI	NI	90.0 \pm 39.8
28	NI	NI	NI	NI
29	16.0 \pm 1.2	47.1 \pm 19.5	17.4 \pm 0.9	NI
30	14.3 \pm 1.6	34.4 \pm 9.5	16.6 \pm 2.1	17.3 \pm 1.5
31	13.6 \pm 0.9	23.4 \pm 1.5	21.0 \pm 0.3	27.0 \pm 5.4
32	11.0 \pm 0.8	14.5 \pm 0.9	23.5 \pm 0.4	22.2 \pm 3.0
5-FU	30.6 \pm 1.8	5.1 \pm 0.8	10.0 \pm 1.8	3.7 \pm 0.5
Fludarabine	28.4 \pm 19.2	17.0 \pm 5.9	13.5 \pm 4.9	13.7 \pm 1.2
Cladribine	0.9 \pm 0.7	0.4 \pm 0.1	<0.1	<0.1

^a IC₅₀ values were calculated from the cell growth inhibition percentages obtained with 5 different concentrations (40, 20, 10, 5, and 2.5 μ M) of each molecule incubated for 72 h. NI: No inhibition

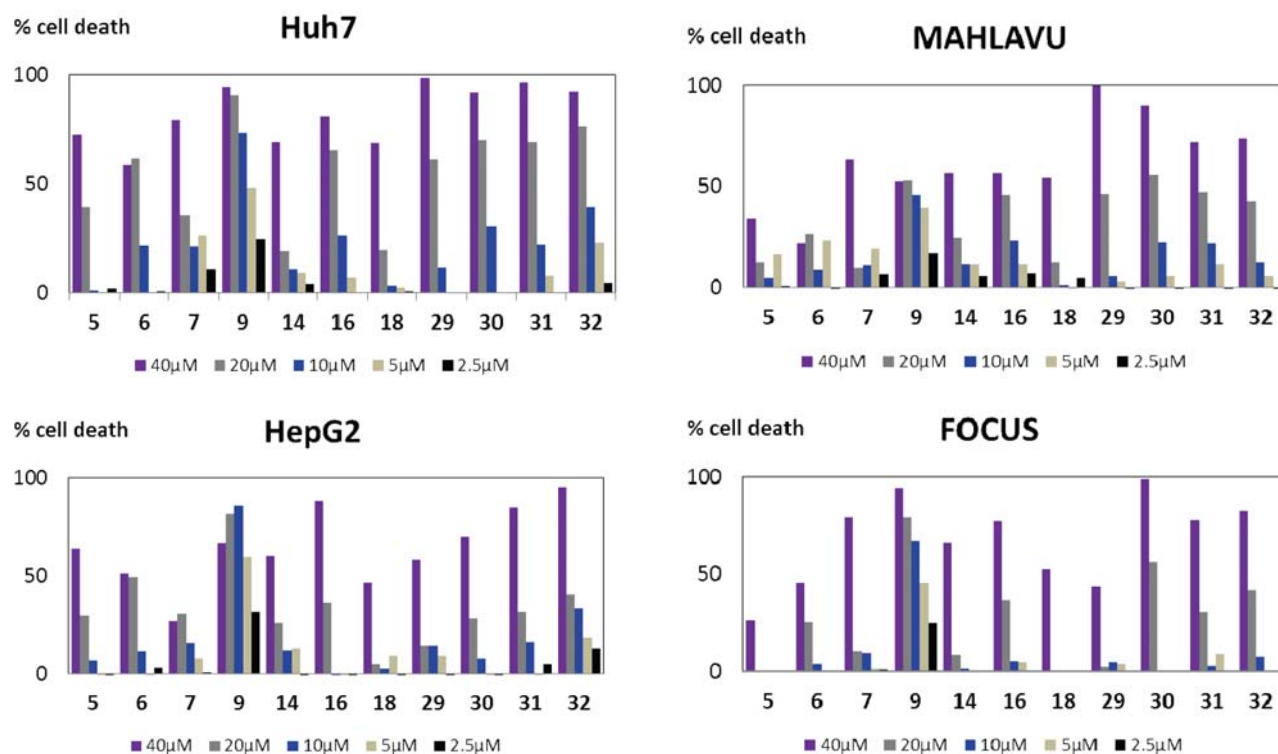


Figure 4. Percent cell death in the presence of the most active compounds. Huh7, HepG2, Mahlavu and FOCUS cells were inoculated in 96-well plates. All molecules and their DMSO controls were administered to the cells in triplicate with five different concentrations: 40, 20, 10, 5, and 2.5 μ M. After 72 h of incubation, SRB assays were generated and the cell death percentages were calculated in comparison with DMSO-treated wells.

structure-activity relationship (SAR) results are summarized in Scheme 2.

Notably 6,9-disubstituted derivative **9** showed superior cytotoxic activity (IC_{50} 7.4 μ M) compared with Fludarabine (IC_{50} 15.2 μ M) against MCF7 tumor cell line. Within the tested purine analogues on HCT116 cell, compounds **9** and **31** with 4-phenoxyphenyl group at *N*-9 position, showed good cytotoxic activity (IC_{50} 15.9 and 13.1 μ M, respectively).

We then screened the cytotoxic activity of the most potent purine derivatives (**5–9**, **14**, **16**, **18**, **28–32**) against further hepatocellular cancer (HCC) cells: HepG2, Mahlavu, and FOCUS (Table 2, Fig. 4). We found out that the most important cell growth inhibition was observed in the presence of 6-(4-phenoxyphenyl)-9-(tetrahydropyran-2-yl)purine derivative **9**, with IC_{50} values of 5.4–6.2 μ M against Huh7 and FOCUS cell lines. Furthermore, **9** had a better cytotoxic activity than the cytotoxic drugs 5-FU and Fludarabine on Huh7 cells (Table 2). The 9-(4-(*tert*-butyl)phenylsulfonyl) analogue **32** was also very active (IC_{50} values in range of 11.0–14.5 μ M) against Huh7 and HepG2 cell lines.

4. Conclusion

A series of 6-(4-substituted phenyl)-9-(tetrahydropyran-2-yl)purines **3–9**, 6-(4-substituted phenyl)purines **10–16**, and 9-(4-substituted phenylsulfonyl)-6-(4-substituted phenyl)purine analogues **17–32** were prepared and their cytotoxic activities identified. 6-(4-Phenoxyphenyl)purine derivatives **9**, **16**, **30**, **31**, **32** showed potent anticancer activity at low concentrations against Huh7 cell line when compared to 5-FU and Fludarabine as potent cytotoxic drugs. Among the 30 compounds investigated, the most potent purine derivatives **5–9**, **14**, **16**, **18**, **28–32** were further analysed for their activity on HCC cells (Huh7, HepG2, Mahlavu, FOCUS). The molecule **9** exhibited promising cytotoxic activity with IC_{50} value of 5.4 μ M on Huh7 cell line.

5. Acknowledgements

This work was supported by the Scientific and Technological Research Council of Turkey-TUBITAK (TBAG-109T987), the KANILTEK Project from the State Planning Organization of Turkey (DPT) and Bilkent University Funds.

6. References

1. P. Karran, *Br. Med. Bull.* **2006**, *79–80*, 153–170.
<https://doi.org/10.1093/bmb/ldl020>
2. A. K. Fotoohi, S. A. Coulthard, F. Albertionii, *Biochem. Pharmacol.* **2010**, *79*, 1211–1222.
<https://doi.org/10.1016/j.bcp.2010.01.006>
3. G. Escherich, S. Richards, L. C. Stork, A. J. Vora, *Leukemia*, **2011**, *25*, 953–959.
<https://doi.org/10.1038/leu.2011.37>
4. M. Hoffmann, M. Chrzanowska, T. Hermann, J. Rychlewski, *J. Med. Chem.* **2005**, *48*, 4482–4486.
<https://doi.org/10.1021/jm0495273>
5. J. L. Haesslein, N. Jullian, *Curr. Topics Med. Chem.* **2002**, *2*, 1037–1050.
6. W. F. De Azevedo, S. Leclerc, L. Meijer, L. Havlicek, M. Strnad, S. H. Kim, *Eur. J. Biochem.* **1997**, *243*, 518–526.
<https://doi.org/10.1111/j.1432-1033.1997.0518a.x>
7. Y. T. Chang, N. S. Gray, G. R. Rosania, D. P. Sutherland, S. Kwon, T. C. Norman, R. Sarohia, M. Leost, L. Meijer, P. G. Schultz, *Chem. and Biol.* **1999**, *6*, 361–375.
[https://doi.org/10.1016/S1074-5521\(99\)80048-9](https://doi.org/10.1016/S1074-5521(99)80048-9)
8. K. Zurbonsen, A. Michel, P. A. Bonnet, L. Gannoun-Zaki, M. N. Mathieu, C. Chevillard, *Eur. J. Pharmacol.* **1997**, *320*, 215–221. [https://doi.org/10.1016/S0014-2999\(96\)00890-4](https://doi.org/10.1016/S0014-2999(96)00890-4)
9. M. F. Brana, M. Cacho, M. L. Garcya, E. P. Mayoral, B. Lopez, B. De Pascual-Teresa, A. Ramos, N. Acero, F. Llinares, D. Munoz-Mingarro, O. Lozach, L. Meijer, *J. Med. Chem.* **2005**, *48*, 6843–6854.
<https://doi.org/10.1021/jm058013g>
10. C. Jaramillo, J. E. Diego, C. Hamdouchi, E. Collins, H. Keyser, C. Sanchez-Martinez, M. Prado, B. Norman, H. B. Brooks, S. A. Watkins, C. D. Spencer, J. A. Dempsey, B. D. Anderson, R. M. Campbell, T. Leggett, B. Patel, R. M. Schultz, J. Espinosa, M. Vieth, F. M. Zhang D. E. Timm, *Bioorg. Med. Chem. Lett.* **2004**, *14*, 6095–6099.
<https://doi.org/10.1016/j.bmcl.2004.09.053>
11. R. M. Mohareb, A. A. Mohamed, A. E. M. Abdallah, *Acta Chim. Slov.* **2016**, *63*, 227–240.
<https://doi.org/10.17344/acsi.2015.1668>
12. R. M. Mohareb, N. Y. M. Abdo, F. O. Al-Farouk, *Acta Chim. Slov.* **2017**, *64*, 117–128.
<https://doi.org/10.17344/acsi.2016.2920>
13. A. Gaagjee, X. Lin, R. L. Kisliuk, J. J. McGuire, *J. Med. Chem.* **2005**, *48*, 7215–7222.
<https://doi.org/10.1021/jm058234m>
14. S. Schenone, O. Bruno, A. Ranise, F. Bondavalli, C. Brullo, P. Fossa, L. Mosti, G. Menozzi, F. Carraro, A. Naldini, C. Bernini, F. Manetti, M. Botta, *Bioorg. Med. Chem. Lett.* **2004**, *14*, 2511–2517.
<https://doi.org/10.1016/j.bmcl.2004.03.013>
15. J. A. Markwalder, M. R. Arnone, P. A. Benfield, M. Biosdir, M. Boisclair, C. R. Burton, C. H. Chang, S. S. Cox, P. M. Czerniak, C. L. Dean, D. Doleniak, R. Grafstrom, B. A. Harrison, R. F. Kaltenbach, D. A. Nugiel, K. A. Rossi, S. R. Sherk, L. M. Sisk, P. Stouten, G. L. Trainor, P. Worland, S. P. Seitz, *J. Med. Chem.* **2004**, *47*, 5894–5911.
<https://doi.org/10.1021/jm020455u>
16. L. Havlicek, K. Fuksova, V. Krystof, M. Orsag, B. Vojtesek, M. Strnad, *Bioorg. Med. Chem.* **2005**, *13*, 5399–5407.
<https://doi.org/10.1016/j.bmc.2005.06.007>

17. S. Botros, O. M. Khalil, M. M. Kamel, Y. S. El-Dash, *Acta Chim. Slov.* **2017**, *64*, 102–116.
<https://doi.org/10.17344/acsi.2016.2901>
18. E. Lech-Maranda, A. Korycka, T. Robak, *Mini Rev. Med. Chem.* **2006**, *6*, 575–581.
<https://doi.org/10.2174/138955706776876212>
19. T. Robak, E. Lech-Maranda, A. Korycka, *Curr. Med. Chem.* **2006**, *13*, 3165–3189.
<https://doi.org/10.2174/092986706778742918>
20. A. Lonardo, P. Loria, *J. Gastroenterol. Hepatol.* **2012**, *27*, 1654–1664.
<https://doi.org/10.1111/j.1440-1746.2012.07232.x>
21. D. L. Corte, A. Aghemo, M. Colombo, *World J. Gastroenterol.* **2013**, *19*, 1359–1371.
<https://doi.org/10.3748/wjg.v19.i9.1359>
22. A. Subramaniam, M. K. Shanmugam, E. Perumal, F. Li, A. Nachiyappan, X. Dai, S. N. Swamy, K. S. Ahn, A. P. Kumar, B. K. H. Tan, K. M. Hui, G. Sethi, *Biochim. Biophys. Acta*, **2013**, *1835*, 46–60.
23. M. B. Irmak, G. Ince, M. Ozturk, R. Cetin-Atalay, *Cancer Res.* **2003**, *63*, 6707–6715.
24. R. S. Finn, *J. Hepatol.* **2012**, *56*, 723–725.
<https://doi.org/10.1016/j.jhep.2011.08.023>
25. C. Berasain, *Gut*, **2013**, *62*, 1674–1675.
<https://doi.org/10.1136/gutjnl-2013-304564>
26. K. Sugimoto, F. Moriyasu, K. Saito, N. Rognin, N. Kamiyama, Y. Furuichi, Y. Imai, *Liver International*, **2013**, *33*, 605–615. <https://doi.org/10.1111/liv.12098>
27. A. Gauthier, M. Ho, *Hepatology Research*, **2013**, *43*, 147–154. <https://doi.org/10.1111/j.1872-034X.2012.01113.x>
28. M. Tuncbilek, E. Bilget Guven, T. Onder, R. Cetin Atalay, *J. Med. Chem.* **2012**, *55*, 3058–3065.
<https://doi.org/10.1021/jm3001532>
29. Z. Demir, E. Bilget Guven, S. Ozbey, C. Kazak, R. Cetin Atalay, M. Tuncbilek, *Eur. J. Med. Chem.* **2015**, *89*, 701–720. <https://doi.org/10.1016/j.ejmech.2014.10.080>
30. R. K. Robins, E. F. Godefroi, E. C. Taylor, L. R. Lewis, A. Jackson, *J. Chem. Soc.* **1961**, *83*, 2574–2579.
<https://doi.org/10.1021/ja01472a034>
31. M. Hocek, A. Holy, I. Votruba, H. Dvorakova, *J. Med. Chem.* **2000**, *43*, 1817–1825.
<https://doi.org/10.1021/jm991167+>
32. J. L. García-Giménez, G. Alzuet, M. Gonzalez-Alvarez, A. Castiñeiras, M. Liu-Gonzalez, J. A. Borrás, *Inorg. Chem.* **2007**, *46*, 7178–7188.
<https://doi.org/10.1021/ic700751j>

Povzetek

Pripravili smo serijo 6-(4-substituiranih fenil)-9-(tetrahidropiran-2-il)purinov **3–9**, 6-(4-substituiranih fenil)purinov **10–16** in 9-((4-substituiranih fenil)sulfonil)-6-(4-substituiranih fenil)purinov **17–32**. Pripravljenim spojinam smo določili njihovo *in vitro* aktivnost proti izbranim človeških rakastim celicam (jeter Huh7, debelega črevesja HCT116, dojk MCF7). 6-(4-fenoksifenil)purinski analogi **9**, **16**, **30–32** so izkazali visoke citotoksične aktivnosti. Za najbolj aktivne purinske derivate **5–9**, **14**, **16**, **18**, **28–32** smo nadalje določili citotoksično aktivnost za hepatocelične rakaste celice. Izkazalo se je, da ima 6-(4-fenoksifenil)-9-(tetrahidropiran-2-il)-9*H*-purin (**9**) večjo citotoksično aktivnost (IC₅₀ 5.4 μM) na Huh7 celice kot pa dobro znani analog nukleinskih baz 5-FU in tudi večjo kot nukleozidna učinkovina fludarabin. Iz študij odvisnosti aktivnosti od strukture lahko zaključimo, da so za delovanje proti raku pomembni zlasti substituenti na položaju C-6 purinskega jedra; 4-fenoksifenilna skupina pa se je izkazala kot najbolj učinkovita izbira.

Scientific paper

Synthesis and Properties of two Cu^I Complexes Involving Tetrathia-fulvalene-Fused Phenanthroline Ligand

Zhi-Gang Niu,^{1,2,†} Xue-You Wang,^{1,†} Hao-Hua Chen,¹ Xun Wang¹ Sun Wei,¹
Dong-Min Wu,¹ Guang-Ying Chen,² Jie Qin^{3,*} and Gao-Nan Li^{1,*}

¹ College of Chemistry and Chemical Engineering, Hainan Normal University, Haikou 571158, PR China

² Key Laboratory of Tropical Medicinal Plant Chemistry of Ministry of Education, Hainan Normal University, Haikou 571158, PR China

³ School of Life Sciences, Shandong University of Technology, Zibo 255049, PR China

* Corresponding author: E-mail: mailto:ligaonan2008@63.com

Received: 08-04-2017

† These authors made equal contributions.

Abstract

Two Cu^I complexes based on the π -conjugated tetrathiafulvalene-annulated phenanthroline ligands (TTF-Phen, **L**₁ and **L**₂), [Cu^I(Xantphos)(**L**₁)]BF₄ (**1**, Xantphos = 9,9-dimethyl-4,5-bis(diphenylphosphino)xanthene) and [Cu^I(Binap)(**L**₂)]BF₄ (**2**, Binap = 2,2'-bis(diphenylphosphino)-1,1'-binaphthyl), have been synthesized. They have been fully characterized, and their photophysical and electrochemical properties are reported together with those of **L**₁ and **L**₂ for comparison. Both Cu^I complexes show metal-to-ligand charge transfer (MLCT) absorption bands, whereas the ³MLCT luminescence is strongly quenched.

Keywords: Copper(I) complexes; Tetrathiafulvalene ligands; Photoluminescence; Cyclic voltammetry

1. Introduction

In the recent study of TTF chemistry, multifunctional molecular material involving interplay and synergy between multiple physical properties have received considerable attention.^{1–3} An established strategy for the preparation of such molecular materials is the combination of functional groups and electro-active TTF moieties.^{4–7} Indeed, in the past years this strategy has led to materials exhibiting novel photofunctional properties, such as fluorescence switches, metal ion sensors, photovoltaic cells, and nonlinear optics.^{8–11} Following this strategy, we recently reported two TTF-based Cu^I complexes, [Cu^I(Binap)(TTF-TzPy)]BF₄ and [Cu^I(Xantphos)(TTF-TzPy)]BF₄, which exhibit interesting electrochemical and photophysical properties.¹³

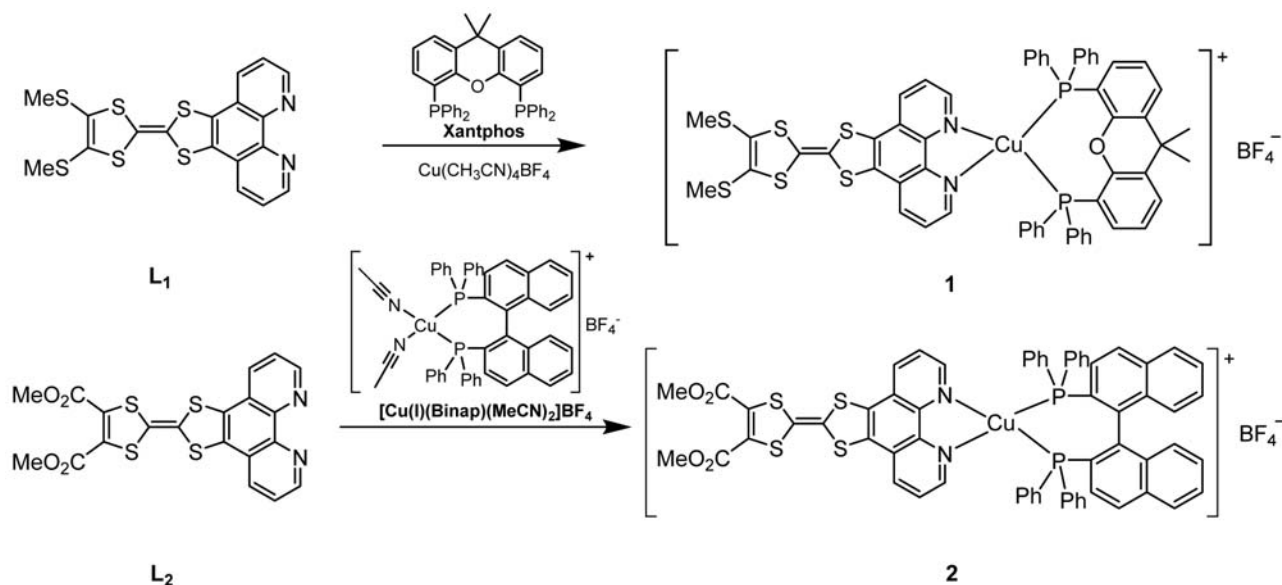
However, TTF-TzPy is a non-conjugated system with σ -bonded molecular bridge. Thus, in this paper, we

use more π -conjugated TTF-Phen ligand instead of TTF-TzPy ligand to form two Cu^I complexes, [Cu^I(Xantphos)(**L**₁)]BF₄ (**1**, Xantphos = 9,9-dimethyl-4,5-bis(diphenylphosphino)xanthene) and [Cu^I(Binap)(**L**₂)]BF₄ (**2**, Binap = 2,2'-bis(diphenylphosphino)-1,1'-binaphthyl). The photophysical and electrochemical properties of these complexes are investigated.

2. Experimental

2.1. Materials and Measurements

All air-sensitive and/or water-sensitive reactions were carried out under a dry nitrogen atmosphere. All commercial chemicals were used without further purification unless otherwise stated. Solvents were dried and degassed following standard procedures. Column chromatography was carried out using 200–300 μ m mesh silica.



Scheme 1. Synthetic routes of Cu^{I} complexes 1–2.

4',5'-dimethyldithiotetrathiafulvenyl[4,5-f][1,10]phenanthroline (L_1) and 4',5'-bis(methoxycarbonyl)dithiotetrathiafulvenyl[4,5-f][1,10]phenanthroline (L_2) were synthesized according to the literature.¹⁴

^1H NMR spectra were recorded on a Bruker AM 400 MHz instrument. Chemical shifts were reported in ppm relative to Me_4Si as internal standard. ESIMS spectra were recorded on an Esquire HCT-Agilent 1200 LC/MS spectrometer. FT-IR spectra were taken on a Nicolet 6700 FTIR spectrometer ($400\text{--}4000\text{ cm}^{-1}$) with KBr pellets. The thermoanalytical analysis (TG) was performed with a simultaneous NETZSCH STA 449C thermal analyzer. The elemental analyses were performed on a Vario EL Cube Analyzer system. UV-Vis spectra were recorded on a Hitachi U3900/3900H spectrophotometer. Fluorescence spectra were carried out on a Hitachi F-7000 spectrophotometer.

2. 2. Synthesis

2. 2. 1. Preparation of $[\text{Cu}^{\text{I}}(\text{Xantphos})(\text{L}_1)]\text{BF}_4$ (1)

To a solution of L_1 (30 mg, 0.067 mmol) in degassed, dry DCM (5 mL) and MeOH (5 mL), was added $[\text{Cu}^{\text{I}}(\text{MeCN})_4]\text{BF}_4$ (25 mg, 0.080 mmol) and Xantphos (42 mg, 0.074 mmol). Then the mixture was degassed by vacuum and charged with N_2 (three times). The mixture was stirred at room temperature for 5 h under nitrogen atmosphere. The resulting solution was concentrated and Et_2O was added to precipitate the product **1** (42 mg, yield: 53%) as a red solid. ^1H NMR (400 MHz, CDCl_3) δ 8.50 (d, $J = 4.4$ Hz, 2H), 8.15 (d, $J = 8.0$ Hz, 2H), 7.85 (dd, $J_1 = 4.8$ Hz, $J_2 = 8.0$ Hz, 2H), 7.69 (d, $J = 7.6$ Hz, 2H), 7.11–7.25 (m, 8H), 7.04–7.08 (m, 8H), 6.86–6.91 (m, 8H), 2.49 (s, 6H), 1.78 (s, 6H). FT-IR (KBr, cm^{-1}):

3056(w), 2922(w), 1578(w), 1405(s), 1228(m), 1058(s), 746(m), 696(m). MS (EI): m/z 1089.1 (M-BF_4). Anal. Calcd for $\text{C}_{57}\text{H}_{44}\text{BCuF}_4\text{N}_2\text{OP}_2\text{S}_6$ (%): C 58.14, H 3.77, N 2.38; Found: C 57.87, H 3.53, N 2.42.

2. 2. 2. Preparation of $[\text{Cu}^{\text{I}}(\text{Binap})(\text{L}_2)]\text{BF}_4$ (2)

$[\text{Cu}^{\text{I}}(\text{Binap})(\text{MeCN})_2]\text{BF}_4$ (60 mg, 0.070 mmol) and L_2 (30 mg mg, 0.063 mmol) were stirred in degassed, dry DCM (5 mL) and MeOH (5 mL) for 5 h under nitrogen atmosphere. The resulting solution was concentrated and Et_2O was added to precipitate the product **2** (38 mg, yield: 48%) as a red solid. ^1H NMR (400 MHz, CDCl_3) δ 8.74 (s, 2H), 8.12 (d, $J = 6.8$ Hz, 2H), 7.92 (s, 2H), 7.31–7.34 (m, 6H), 7.07–7.18 (m, 26H), 3.89 (s, 6H). FT-IR (KBr, cm^{-1}): 3056(w), 2925(w), 1727(s), 1576(m), 1433(s), 1269(s), 1060(s), 749(m), 697(m). MS (EI): m/z 1157.1 (M-BF_4). Anal. Calcd for $\text{C}_{64}\text{H}_{44}\text{BCuF}_4\text{N}_2\text{O}_4\text{P}_2\text{S}_4$ (%): C 61.71, H 3.56, N 2.25; Found: C 61.45, H 3.58, N 2.12.

2. 3. Cyclic Voltammetry

Cyclic voltammetry (CV) was performed on a CHI 1210B electrochemical workstation, with a glassy carbon electrode as the working electrode, a platinum wire as the counter electrode, an aqueous saturated calomel electrode (SCE) as the reference electrode, and 0.1 M $n\text{-Bu}_4\text{NClO}_4$ as the supporting electrolyte.

3. Results and Discussion

The synthetic routes to complexes **1–2** are shown in Scheme 1. The TTF-fused ligands, copper(I) salt and PCP

ligands were added in dry DCM and MeOH, and coordinated to afford corresponding Cu^{I} complexes **1–2**. The crude product was recrystallized from dichloromethane and diethyl ether. Complexes **1–2** were characterized by IR, ESI-MS, elemental analysis, ^1H NMR, UV-vis, FL spectra and cyclic voltammetry.

3. 1. IR and ESI Spectra

In the IR spectrum of complexes **1** and **2** (Fig. S1 and Fig. S2), their spectra have almost the same tendency. The peaks at 3056, 2922, 1405 cm^{-1} for **1** and 3056, 2925, 1433 cm^{-1} for **2** are $\nu_{\text{C-H}}$ of CH_3 group and $\nu_{\text{Ar-H}}$, and the strong absorption peak at 1058 cm^{-1} for **1** and 1060 cm^{-1} for **2** are attributed to B–F stretches of BF_4^- group. Moreover, the strong absorption peaks at 746 and 696 cm^{-1} for **1** and 746, 696 cm^{-1} for **2** are $\delta_{\text{C-CH}}$. Particularly, the strong absorption peaks at 1727 cm^{-1} for **2** are attributed to C=O stretches of CO_2Me group.

The structure of complexes **1** and **2** was also studied by electrospray ionization mass spectrometry (ESI-MS). A positive ion ESI-MS of complexes **1** and **2** (Fig. S3 and Fig. S4) were measured in methanol solution. The main peak at m/z 1089.1 of **1** is $[\text{Cu}^{\text{I}}(\text{Xantphos})(\text{L}_1)]^+$ ion and m/z 1157.1 of **2** is $[\text{Cu}^{\text{I}}(\text{Binap})(\text{L}_2)]^+$ ion, respectively.

3. 2. Photophysical Properties

3. 2. 1. Absorption Properties

The absorption spectra of the ligands L_1 – L_2 and complexes **1–2** were measured in dichloromethane solution at room temperature (Fig. 1), and the data are provided in Table 1. For complexes **1–2**, absorption spectra are similar to that of the free ligand L_1 – L_2 . Intense absorption bands from 250 to 350 nm at high energy are observed, which is attributed to spin-allowed intraligand (π – π^*) transitions. Compared with L_1 – L_2 , the absorption bands at

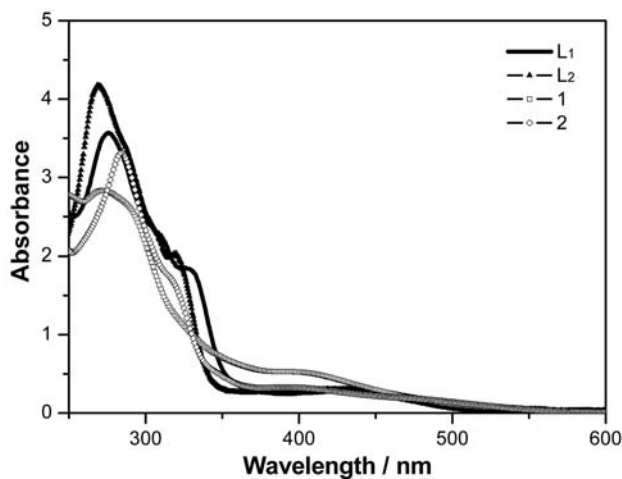


Fig. 1. Electronic absorption spectra of ligands L_1 – L_2 and complexes **1–2** in CH_2Cl_2 at room temperature.

Table 1. Photophysical data for compounds L_1 – L_2 and **1–2**

Complex	Absorption λ_{abs} (nm) ^a	Emission λ_{em} (nm) ^a
L_1 ^b	275, 308, 326, 435	382, 400
L_2 ^b	268, 318, 436	381, 400
1	271, 288, 406	383, 406
2	284, 317, 406	381, 434

^a Measured in degassed CH_2Cl_2 solution at room temperature. ^b Data from ref. 13.

low energy ($\lambda > 350$ nm) of complexes **1–2** are slightly blue shifted, and the intensities are increased around 400–410 nm, which may be related to metalation of the ligand.¹⁵

3. 2. 2. Emission Properties

The normalized emission spectra of the ligands L_1 – L_2 and complexes **1–2** in CH_2Cl_2 solution are presented in Fig. 2. The emission data are also included in Table 1. In comparison to the related ligands, the emission spectra of complexes **1–2** exhibit similar emission. The emission maxima at 381–383 nm and a shoulder peak at 406–434 nm are observed resulting from the ligand-centered (LC) π – π^* relaxations. However, no obvious emissions with $^3\text{MLCT}$ character are found. Similar observations are also found in other metal complex systems.^{16–17}

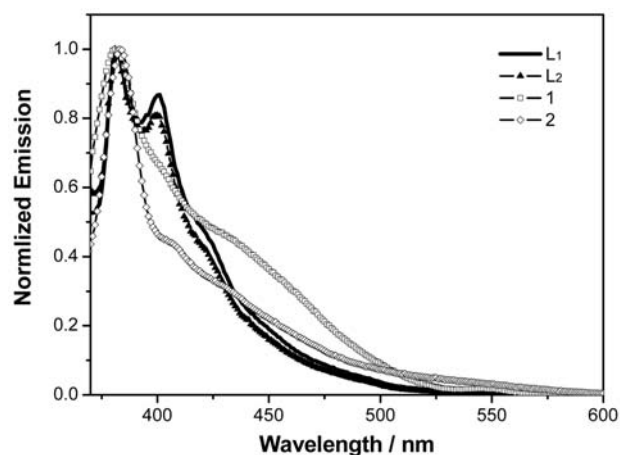


Fig. 2. Normalized emission spectra of ligands L_1 – L_2 and complexes **1–2** in CH_2Cl_2 at room temperature.

3. 3. Electrochemical Properties

Electrochemical properties of the complexes **1–2** were investigated by cyclic voltammetry in $\text{CH}_3\text{CN}/\text{CH}_2\text{Cl}_2$ as illustrated in Fig. 3, and their electrochemical data are collected in Table 2. All compounds (L_1 – L_2 , **1–2**) exhibit two one-electron oxidation processes, which are associated with the successive oxidation of the

TTF unit to TTF^+ and TTF^{2+} . The redox potentials $E_{1/2}^1$ and $E_{1/2}^2$ for **1** are 0.79 and 0.98 V, and those for **2** are 0.93 and 1.15 V, respectively. Upon coordination, the two oxidation processes of TTF subunits for **1–2** are shifted to more positive potentials in comparison with the respective ligands (Table 2). This is attributed to the electron-withdrawing inductive effect of Cu^I core.¹² For the previously synthesized Cu^I complexes based on TTF-TzPy, redox potentials for the ligand and Cu^I complexes have no obvious change.¹³ These differences result is that we use different types of ligands. TTF-TzPy is a non-conjugated system with σ -bonded molecular bridge, which is unfavorable to the transmission of electrons. However, we use more π -conjugated TTF-Phen ligand and the phen unit is grafted on the TTF core through a conjugated spacer group, which is advantageous to intramolecular electron transfer and communications. Consequently, Cu^I complexes **1–2** possess better electron-withdrawing abilities than the free ligands.

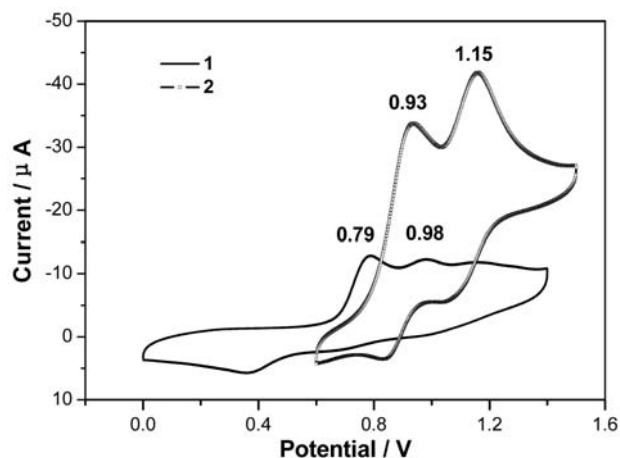


Fig. 3. Cyclic voltammogram of **1–2** measured in $\text{CH}_3\text{CN}/\text{CH}_2\text{Cl}_2$ (1:1) solution containing $n\text{-Bu}_4\text{NClO}_4$ (0.1 M), at a scan rate of 100 mV/s.

3. 4. Thermal Stability

The TG analyses were carried out from 30 °C to 700 °C in N_2 atmosphere with a heating rate of 10 °C min^{-1} . As shown in Fig.4, complex **1** began to lose weight at approximately 295 °C and continuous decomposition is observed during 295 to 650 °C with the increase of temperature. The residue weight of 6.94% is due to CuO and is in agreement

with the calculated value of 6.76%. For complex **2**, no weight loss was observed up to 250 °C, indicating that it is stable below 250 °C. With the increase of temperature, the organic fragments start to decompose gradually in range of 250 to 640 °C. The residue weight of 6.68% is due to CuO and is in agreement with the calculated value of 6.38%.

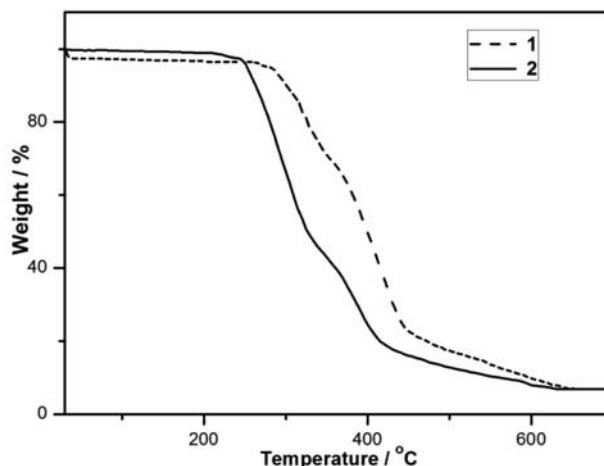


Fig. 4. TG curves of complexes **1** and **2**

4. Conclusions

In summary, we have synthesized two new Cu^I complexes with TTF-Phen as the ligands, $[\text{Cu}^I(\text{Xantphos})(\text{L}_1)]\text{BF}_4$ (**1**) and $[\text{Cu}^I(\text{Binap})(\text{L}_2)]\text{BF}_4$ (**2**). Their thermal stability, photophysical properties and electrochemical behaviors have been investigated. The two new Cu^I complexes are stable below 250 °C. The emission of complexes **1–2** is no longer of $^3\text{MLCT}$ but rather of ligand-centered (LC) nature. The interesting redox-active properties for complexes **1** and **2** have been evidenced by electrochemical studies. The association of the redox-active bridging TTF ligand to a variety of mixed-ligand transition-metal complexes may pave the way to obtain multifunctional materials, which are currently under investigation in our laboratory.

5. Acknowledgements

This work was supported by the National Natural Science Foundation of China (No. 21501037), the Natural

Table 2. Electrochemical data for compounds $\text{L}_1\text{–L}_2$ and **1–2**

Complex	$E_{1/2}^1$ (V) ^a	$E_{1/2}^2$ (V) ^a	Complex	$E_{1/2}^1$ (V) ^a	$E_{1/2}^2$ (V) ^a
L_1^b	0.48	0.75	1	0.79	0.98
L_2^b	0.64	0.94	2	0.93	1.15

^a Measured in $\text{CH}_2\text{Cl}_2/\text{CH}_3\text{CN}$ solution (1/1, v/v) containing 0.1 M $n\text{-Bu}_4\text{NClO}_4$ and the scan rate was 100 mV/s. ^b Data from ref. 13.

Science Foundation of Hainan Province (No. 20152031), the 2016 Hainan Provincial Innovation Experiment Program for University Students, Hainan Province Natural Science Foundation of Innovative Research Team Project (No. 2017CXTD007) and Program for Innovative Research Team in University (No. IRT-16R19).

6. References

- H. Y. Wang, L. Cui, J. Z. Xie, C. F. Leong, D. M. D'Alessandro, J. L. Zuo, *Coord. Chem. Rev.* **2017**, *345*, 342–361.
<http://www.sciencedirect.com/science/article/pii/S0010854516303563>
- L. Cui, J. Y. Ge, C. F. Leong, D. M. D'Alessandro, J. L. Zuo, *Dalton Trans.* **2017**, *46*, 3980–3988.
<http://pubs.rsc.org/en/content/articlepdf/2017/dt/c6dt04903f>
- J. L. Segura, N. Martín, *Angew. Chem. Int. Ed.* **2001**, *40*, 1372–1409.
[http://onlinelibrary.wiley.com/doi/10.1002/1521-3773\(20010417\)40:8%3C1372::AID-ANIE1372%3E3.0.CO;2-I/pdf](http://onlinelibrary.wiley.com/doi/10.1002/1521-3773(20010417)40:8%3C1372::AID-ANIE1372%3E3.0.CO;2-I/pdf)
- (a) Z. G. Niu, H. Xie, L. R. He, K. X. Li, Q. Xia, D. M. Wu, G. N. Li, *Acta. Chim. Slov.* **2016**, *62*, 323–326.
<https://journals.matheo.si/index.php/ACSi/article/download/2246/951>
(b) Z. G. Niu, L. R. He, L. Li, W. F. Cheng, X. Y. Li, H. H. Chen, G. N. Li, *Acta. Chim. Slov.* **2014**, *61*, 786–791.
<https://journals.matheo.si/index.php/ACSi/article/view/473>
- I. N. Avarvari, K. Kiracki, R. Llusar, V. Polo, I. Sorribes, C. Vicent, *Inorg. Chem.* **2010**, *49*, 1894–1904.
<http://pubs.acs.org/doi/pdf/10.1021/ic902244m>
- F. Riobé, N. Avarvari, *Coord. Chem. Rev.* **2010**, *254*, 1523–1533.
<http://www.sciencedirect.com/science/article/pii/S0010854509003324>
- A. Kobayashi, E. Fujiwara, H. Kobayashi, *Chem. Rev.* **2004**, *104*, 5243–5264.
<http://pubs.acs.org/doi/pdf/10.1021/cr0306561>
- S. Wenger, P.-A. Bouit, Q. Chen, J. Teuscher, D. D. Censo, R. Humphry-Baker, J.-E. Moser, J. L. Delgado, N. Martín, S. M. Zakeeruddin, M. Grätzel, *J. Am. Chem. Soc.* **2010**, *132*, 5164–5169.
<http://pubs.acs.org/doi/pdf/10.1021/ja909291h>
- F. G. Brunetti, J. L. López, C. Atienza, N. Martín, *J. Mater. Chem.* **2012**, *22*, 4188–4205.
<http://pubs.rsc.org/en/content/articlelanding/2012/jm/c2jm15710a>
- D. Canevet, M. Sallé, G. X. Zhang, D. Q. Zhang, D. B. Zhu, *Chem. Commun.* **2009**, 2245–2269.
<http://pubs.rsc.org/en/content/articlelanding/2009/cc/b818607n>
- G. X. Zhang, D. Q. Zhang, X. F. Guo, D. B. Zhu, *Org. Lett.* **2004**, *6*, 1209–1212.
<http://pubs.acs.org/doi/pdf/10.1021/ol036511i>
- J. Qin, S. Y. Deng, C. X. Qian, T. Y. Li, H. X. Ju, J. L. Zuo, *J. Organomet. Chem.* **2014**, *750*, 7–12.
<http://www.sciencedirect.com/science/article/pii/S0022328X1300781X>
- G. N. Li, L. R. He, D. Xia, L. Li, W. F. Cheng, K. X. Li, F. Cui, Z. G. Niu, *J. Chin. Chem. Soc.* **2015**, *62*, 889–897.
<http://onlinelibrary.wiley.com/doi/10.1002/jccs.201500251/pdf>
- J. Qin, L. Hu, G. N. Li, X. S. Wang, Y. Xu, J. L. Zuo, X. Z. You, *Organometallics*, **2011**, *30*, 2173–2179.
<http://pubs.acs.org/doi/pdf/10.1021/om101141h>
- J.-C. Wu, S.-X. Liu, T. D. Keene, A. Neels, V. Mereacre, A. K. Powell, S. Decurtins, *Inorg. Chem.* **2008**, *47*, 3452–3459.
<http://pubs.acs.org/doi/pdf/10.1021/ic800138x>
- R. Saha, D.P. Rillema, R. Shaver, S. V. Wallendaal, D. C. Jackman, M. Boldaji, *Inorg. Chem.* **1989**, *28*, 1022–1028.
<http://pubs.acs.org/doi/pdf/10.1021/ic00305a008>
- A. Vorler, J. Kisslinger, *Inorg. Chim. Acta.* **1986**, *115*, 193–196.
<http://www.sciencedirect.com/science/article/pii/S0020169300844138>

Povzetek

Sintetizirali smo dva Cu^I kompleksa s π-konjugiranim tetratriafulvalen vsebujočim fenantrolinskim ligandom (TTF-Phen, **L**₁ in **L**₂) [Cu^I(Xantphos)(**L**₁)]BF₄ (**1**, Xantphos = 9,9-dimetil-4,5-bis(difenilfosfino)ksanten) in [Cu^I(Binap)(**L**₂)]BF₄ (**2**, Binap = 2,2'-bis(difenilfosfino)-1,1'-binaftil) ter ju okarakterizirali in določili fotofizikalne in elektrokemijske lastnosti v primerjavi z ligandoma **L**₁ in **L**₂. Oba Cu^I kompleksa izkazujeta absorpcijski vrh za prenos naboja s kovine na ligand (MLCT), medtem ko je ³MLCT luminescenca preprečena.

Scientific paper

A Dansyl-Rhodamine Based Fluorescent Probe for Detection of Hg²⁺ and Cu²⁺

Shizhuang Yuan,¹ Wei Su¹ and Enju Wang^{1,*}¹ Key Laboratory of Tropical Medicinal Plant Chemistry of Ministry of Education, College of Chemistry and Chemical Engineering, Hainan Normal University, Haikou, 571158, China

* Corresponding author: E-mail: enjuwang@163.com

Received: 13-04-2017

Abstract

A novel fluorescent probe based on dansyl-appended rhodamine B was developed. The probe can selectively recognize and sense Hg²⁺ and Cu²⁺ from other common metal ions by showing unique fluorescence and absorption characteristics. In MeCN/HEPES buffer solution, the probe gives a ratiometric fluorescent response to Hg²⁺, which was ascribed to the fluorescence resonance energy transfer from dansyl moiety to the ring-opened rhodamine B moiety, while the presence of Cu²⁺ causes fluorescence quenching. Beside the fluorescence change, the presence of Cu²⁺ and Hg²⁺ can induce intensive absorption at about 555 nm, which resulted in a color change from colorless to pink.

Keywords: Rhodamine; Fluorescent probe; Copper ion; Mercury ion

1. Introduction

Copper and mercury are among the most ubiquitous of toxic heavy and transition metals in our environment due to their widespread use in industrial production and daily life. Copper overload is linked to brain damage and oxidative stress although it is an essential trace element.¹ Additionally, copper is highly toxic to aquatic organisms and ecosystems. Mercury is a highly toxic element. All humans are exposed to some level of mercury because it diffuses globally through atmospheric circulation. In freshwater and marine food webs, the bioaccumulation of mercury is so efficient that the mercury levels in top predators, for example shark, may be thousands of times higher than in the surrounding water.² Therefore, the development of fluorometric or colorimetric probes for the fast and convenient detection of Cu²⁺ and Hg²⁺ in organisms and environment has attracted considerable attention.^{3–11} In recent years, considerable efforts have been made to take advantage of rhodamine dyes in constructing fluorometric probes for metal ions,^{12–16} and a number of excellent fluorescent probes for Cu²⁺ or Hg²⁺ have been reported.^{17–18} However, the probes that can sense two or more metal ions separately were rarely reported.^{19–21}

In the present work, a novel fluorescent probe (**RD**) based on dansyl-appended rhodamine B was designed and

synthesized for detection of Hg²⁺ and Cu²⁺ (Scheme 1). In MeCN/HEPES buffer solution, it can give a ratiometric fluorescent response to Hg²⁺ and a fluorescent quenching response to Cu²⁺. Meanwhile, the probe can give colorimetric responses to Cu²⁺ and Hg²⁺.

2. Experimental

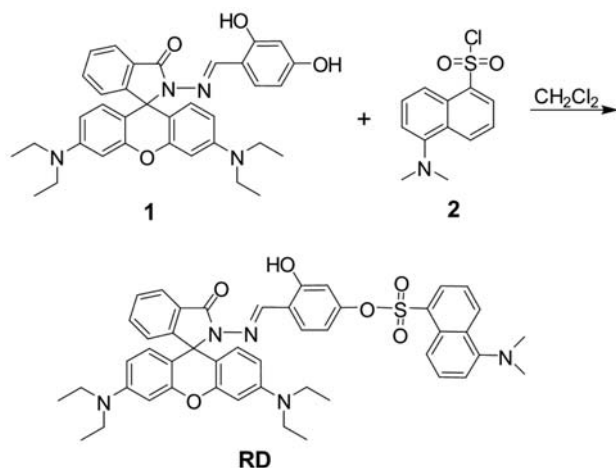
2.1. Reagents and Apparatus

All chemicals were purchased from commercial suppliers and used as received without further purification. Rhodamine B derivative (compound **1** in Scheme 1) were prepared according to the published procedure.²² Analytical grade acetonitrile and deionised water were used in all spectral measurements. The samples of metal ions were prepared by dissolving the corresponding metal nitrates in water except the sample of Hg²⁺, which was obtained by dissolving mercuric sulfate in dilute nitric acid (0.1 mol/L).

¹H and ¹³C NMR spectra were recorded on a Bruker-400 spectrometer. ESI-MS spectra were performed on a Bruker Esquire HCT mass spectrometer. Fluorescence spectra were taken on a Hitachi F-7000 fluorescence spectrometer. UV-vis absorption spectra were measured on a TU-1901 spectrophotometer. The pH values were determined on a PHS-3C digital pH meter.

2. 2. Synthesis of the Probe RD

Under $-25\text{ }^{\circ}\text{C}$, rhodamine B derivative **1** (0.69 g, 1.2 mmol), dansyl chloride (0.35 g, 1.3 mmol) and triethylamine (0.2 ml, 1.4 mmol) were combined in dichloromethane (20 mL) and then stirred for 6 h. After the solvent was evaporated under reduced pressure, the crude product was purified by column chromatography (petroleum ether/ethyl acetate, 1:1, *v:v*) to give **RD** as a red solid (0.59 g, 61%). ^1H NMR (400 MHz, CDCl_3) δ (ppm): 11.00 (s, 1H), 9.10 (s, 1H), 8.57 (d, 1H, $J = 8.0$ Hz), 8.39 (d, 1H, $J = 8.0$ Hz), 8.04 (t, 1H, $J = 7.2$ Hz), 7.94 (d, 1H, $J = 7.2$ Hz), 7.64 (t, 1H, $J = 8.0$ Hz), 7.52 (m, 2H), 7.41 (t, 1H, $J = 8.0$ Hz), 7.23 (d, 1H, $J = 8.0$ Hz), 7.15 (d, 1H, $J = 7.2$ Hz), 6.92 (d, 1H, $J = 8.0$ Hz), 6.42 (m, 5H), 6.36 (s, 1H), 6.23 (d, 2H, $J = 8.0$ Hz), 3.31 (q, 8H, $J = 6.8$ Hz), 2.90 (s, 6H), 1.14 (t, 12H, $J = 6.8$ Hz). ^{13}C NMR (100 MHz, CDCl_3) δ (ppm): 164.2, 159.6, 153.5, 151.9, 151.4, 151.3, 150.6, 149.1, 133.6, 132.1, 132.0, 131.2, 131.0, 129.95, 129.86, 129.8, 129.0, 128.6, 128.0, 124.2, 123.3, 123.0, 119.4, 117.7, 115.7, 112.8, 110.6, 108.1, 105.2, 97.9, 66.5, 45.4, 44.3, 12.6. ESI-MS *m/z*: 810.4 $[\text{M}+\text{H}]^+$; calcd for $\text{C}_{47}\text{H}_{48}\text{N}_5\text{O}_6\text{S}$, 810.3 (Fig.S1-3).



Scheme 1. Synthesis of **RD**

3. Results and Discussion

3. 1. Fluorescence Responses to Hg^{2+} and Cu^{2+}

The fluorescence changes of **RD** were investigated in $\text{MeCN}/\text{H}_2\text{O}$ solution (9/1, 10 mM HEPES buffer, pH 7.2) upon addition of a wide range of metal ions including Na^+ , K^+ , Ca^{2+} , Mg^{2+} , Al^{3+} , Mn^{2+} , Co^{2+} , Ni^{2+} , Cu^{2+} , Cr^{3+} , Ag^+ , Pb^{2+} , Zn^{2+} , Cd^{2+} , Hg^{2+} , Fe^{2+} , and Fe^{3+} . As shown in Fig. 1, **RD** alone displayed the emission of the dansyl moiety around 545 nm when excited at 370 nm. Upon addition of Hg^{2+} , the emission at 545 nm decreased, and in the meantime the fluorescence of the rhodamine moiety near 580 nm was observed. Besides Hg^{2+} , the presence of

Cu^{2+} has a great impact on the **RD** fluorescence, which was quenched by the addition of Cu^{2+} . The fluorescence changes were visible to the naked eye: the addition of Hg^{2+} causes a fluorescence color change from green to orange, while the addition of Cu^{2+} leads to fluorescence disappearance (Fig. 1 inset). Except Hg^{2+} and Cu^{2+} , no tested metal ions show any significant effect on the fluorescence spectrum of **RD**.

The fluorescence titrations of **RD** with Hg^{2+} and Cu^{2+} were carried out by the addition of increasing amount of Hg^{2+} or Cu^{2+} , respectively, to **RD** solution. As shown in Fig. 2, upon gradual addition of Hg^{2+} the significant fluorescence enhancement at 580 nm, and mean-

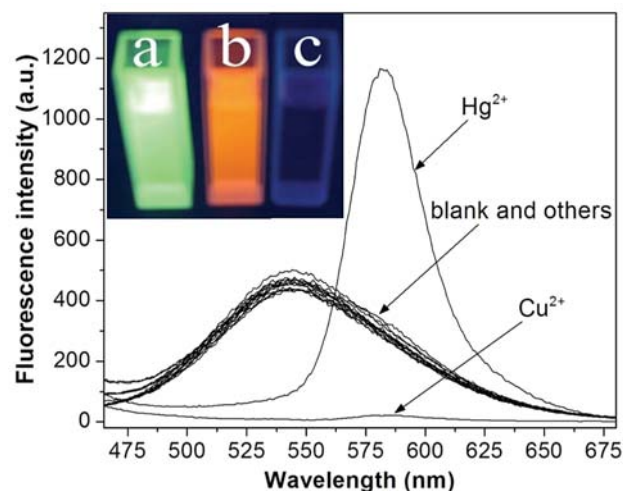


Figure 1. Fluorescence spectra of **RD** (10 μM) upon addition of various cations (10 μM) in $\text{MeCN}-\text{H}_2\text{O}$ solution (9/1, 10 mM HEPES buffer, pH 7.2) when excited at 370 nm. Inset: the fluorescence photographs of **RD** in the absence (a) and presence of Hg^{2+} (b) and Cu^{2+} (c) in dark-box ultraviolet analyzer when excited at 365 nm.

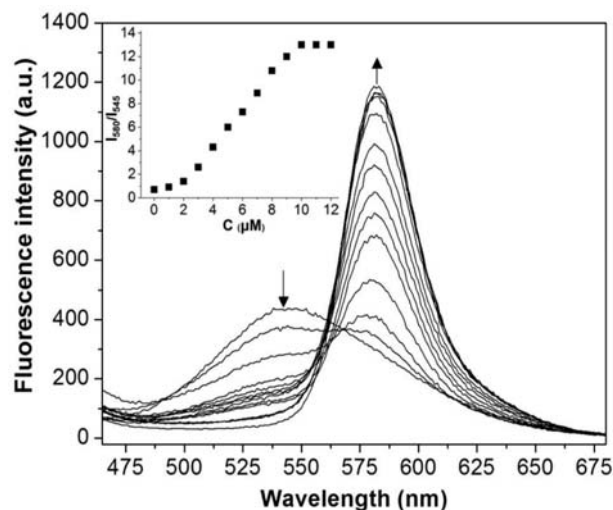


Figure 2. Fluorescence titration spectra of **RD** (10 μM) with Hg^{2+} (0–12 μM). Inset: the fluorescent intensity ratio (I_{580}/I_{545}) as a function of Hg^{2+} concentration.

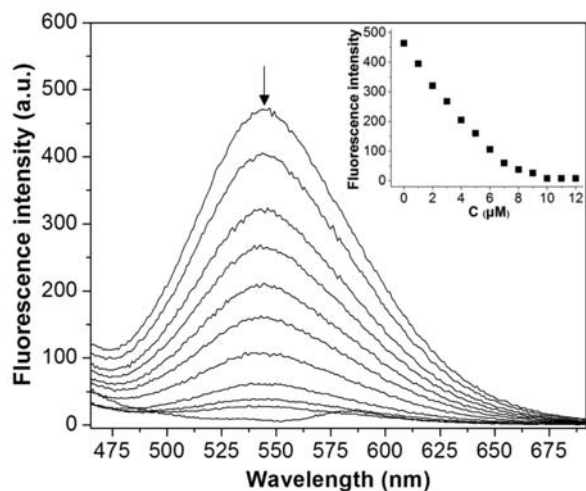


Figure 3. Fluorescence titration spectra of **RD** (10 μM) with Cu^{2+} (0–12 μM). Inset: the fluorescent intensity at 545 nm as a function of Cu^{2+} concentration.

while, the gradual fluorescence disappearance at 540 nm were observed, which should be ascribed to the fluorescence resonance energy transfer (FRET) from dansyl moiety to the ring-opened rhodamine moiety.^{23–26} Therefore, **RD** as a ratiometric fluorescent probe for Hg^{2+} was established. Fig. 3 shows the gradual fluorescence quenching along with the increase of Cu^{2+} concentration. Consequently, **RD** can serve only as a fluorescence-quenching probe for Cu^{2+} . The detection limits of **RD** for Hg^{2+} and Cu^{2+} were calculated to be 2.22×10^{-8} mol/L and 4.35×10^{-8} mol/L, respectively, with the equation $\text{DL} = 3\delta/S$ (δ : the standard deviation of the blank solution; S : the slope of the calibration plot, Fig. S4–5).

3. 2. Colorimetric Signaling of Hg^{2+} and Cu^{2+}

RD alone shows no absorption in the visible light region, so it is colorless. Upon addition of Cu^{2+} and Hg^{2+} separately, strong absorption appeared at 552 nm and 558 nm, respectively, along with a color change from colorless to pink. Obviously, the addition of Cu^{2+} induced a stronger absorption and thicker pink color than that of Hg^{2+} . Excluding Cu^{2+} or Hg^{2+} , all the other metal ions have no effect on the UV/vis spectrum of **RD** (Fig. 4). UV/vis absorption titration with Cu^{2+} and Hg^{2+} were recorded respectively in Fig. 5 and 6. The absorbance of **RD** was found to increase gradually with the increasing concentration of metal ions. In addition, a linear relationship between the absorbance and metal ions concentration was observed (Fig. 5 and 6, inset). This implies the possibility of quantitative determination of $\text{Cu}^{2+}/\text{Hg}^{2+}$ by spectrophotometry. The colorimetric detection limits of **RD** for Hg^{2+} and Cu^{2+} were calculated to be 4.17×10^{-7} mol/L and 1.36×10^{-7} mol/L, respectively, with the equation $\text{DL} = 3\delta/S$ (δ : the standard deviation of the blank solution; S : the slope of the calibration plot Fig. S6–7).

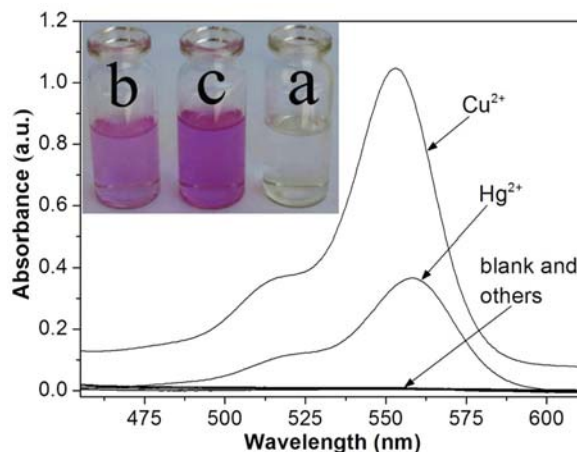


Figure 4. UV-vis spectra of **RD** (10 μM) upon addition of various cations (10 μM) in MeCN- H_2O buffer solution. Inset: Colors of **RD** solution before (a) and after the addition of Hg^{2+} (b) or Cu^{2+} (c) under natural light.

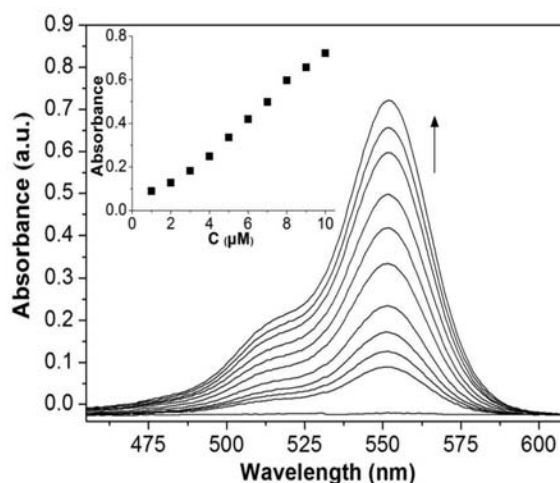


Figure 5. UV-vis spectra of **RD** (10 μM) in the presence of different concentrations of Cu^{2+} (0–10 μM) in MeCN- H_2O buffer solution. Inset: absorbance as a function of Cu^{2+} concentration.

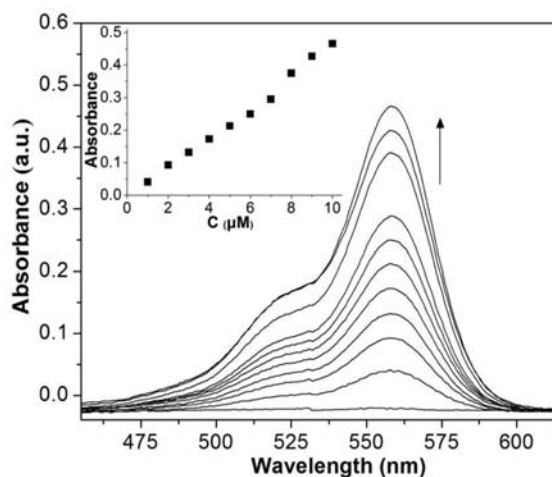


Figure 6. UV-vis spectra of **RD** (10 μM) in the presence of different concentrations of Hg^{2+} (0–10 μM) in MeCN- H_2O buffer solution. Inset: absorbance as a function of Hg^{2+} concentration.

3.3. Effect of pH and Selectivities for Hg²⁺ and Cu²⁺

It is well known that the spiroring-opening of rhodamines can be induced by H⁺ besides metal ions, so it is necessary to investigate the pH effect on the fluorescence change of **RD**. The fluorescence intensity ratios (I_{580}/I_{545}) of **RD** in the absence and presence of Hg²⁺ at different pH values were shown in Fig. 7. When pH > 6.0, the fluorescence of **RD** without any interference was observed. When Hg²⁺ was added, the fluorescence intensity ratios were maintained at maximum value under pH < 8.0. When pH > 8.0, the ratiometric fluorescent responses rapidly disappeared. Therefore, the probe can be used in the pH range from 6.0 to 8.0. The pH value of 7.2 was chosen for all the spectral measurements in this work.

For evaluating the effects of common metal ions on the selectivity of **RD** for Hg²⁺/Cu²⁺, competition experi-

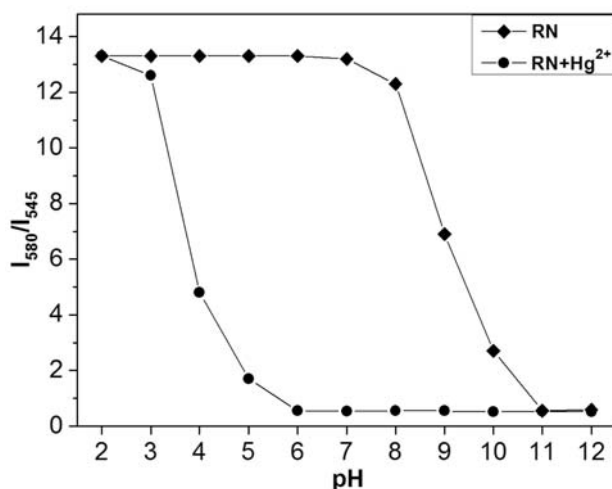


Figure 7. pH-dependent fluorescence intensity ratios of probe **RD** (10 μ M) in the absence and presence of Hg²⁺ (10 μ M).

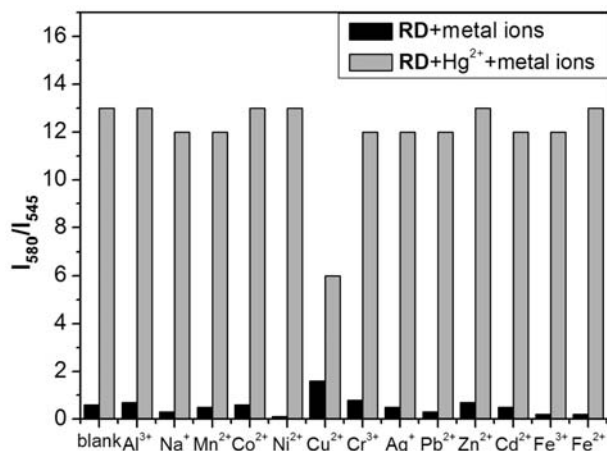


Figure 8. Selective responses of **RD** (10 μ M) to 10 μ M Hg²⁺ in the presence of 10 μ M various other ions.

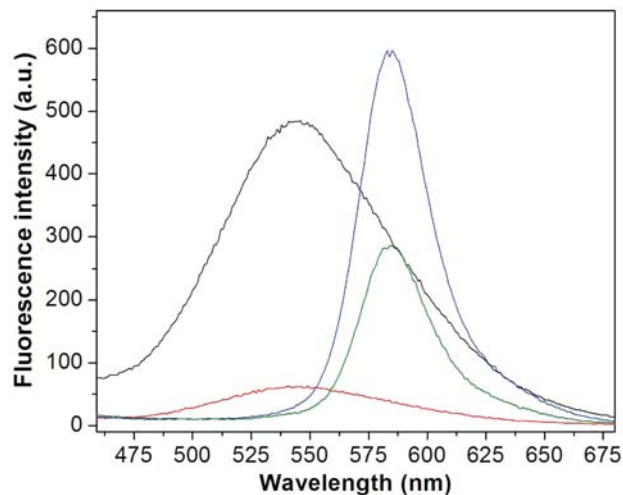


Figure 9. Fluorescence spectra of 10 μ M **RD** (black) upon successive addition of 8 μ M Cu²⁺ (red), 8 μ M Hg²⁺ (blue) and then 8 μ M Cu²⁺ (green).

ments were carried out by measuring the fluorescence spectra of **RD** in the presence of testing ions and various interfering metal ions. As can be seen from Fig. 8, the highly selective response of **RD** to Hg²⁺ was observed in the presence of various interfering metal ions except Cu²⁺ which can partially quench the Hg²⁺-induced fluorescence. The interactive effect between Hg²⁺ and Cu²⁺ was examined by measuring fluorescence of **RD** upon successive addition of Cu²⁺, Hg²⁺ and then Cu²⁺. As shown in Fig. 9, the presence of Cu²⁺ induces a fluorescence quenching at 545 nm. The subsequent addition of Hg²⁺ causes a new fluorescence enhancement at 580 nm, which decreases following the addition of Cu²⁺.

3.4. Binding Mode and Signaling Mechanism

As is well known, the rhodamine-based probes give turn-on fluorescence responses to specific metal ions by way of coordination between them and the subsequent spirolactam ring-opening. To determine the stoichiometry between Hg²⁺/Cu²⁺ and **RD**, Job's plots were employed by using the absorbance as functions of molar fraction of Hg²⁺/Cu²⁺. For both metal ions, the maximum absorbance appeared when molar fractions are 0.5, indicating 1:1 stoichiometry for **RD**-Hg²⁺ and **RD**-Cu²⁺ complexes (Fig. S8). The binding mode of **RD**-Cu²⁺ complex was further illuminated by ESI-MS testing of **RD** in the presence of 1.2 equiv of Cu(NO₃)₂. As seen in Fig. 10, a peak with m/z 871.3 was observed, which was assigned to [RD-H+Cu]⁺ (calcd. 871.2). The observed and calculated isotopic patterns agree well with each other (Fig. 10, inset). The presence of [RD-H+Cu]⁺ suggests the deprotonation of the phenolic hydroxyl upon the coordination of **RD** with Cu²⁺. Based on above discussion, the coordination structure of **RD**-Cu²⁺ complex was proposed as shown in Fig. 10 inset. It is regrettable that the peak corresponding to

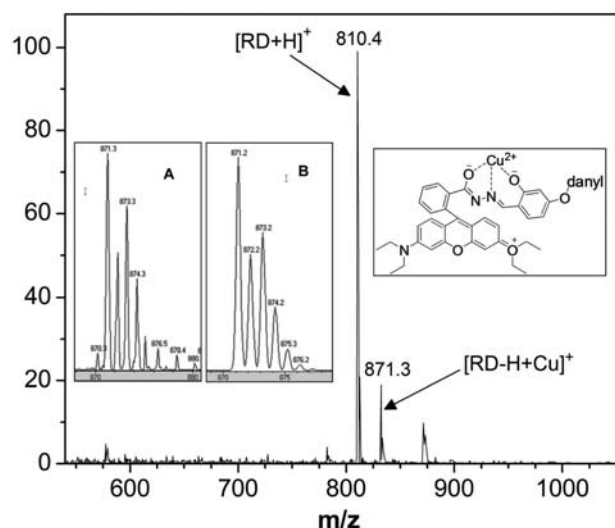


Figure 10. ESI-MS spectrum of **RD** in the presence of $\text{Cu}(\text{NO}_3)_2$. Inset: observed (A) and calculated (B) isotopic patterns for $[\text{RD-H}+\text{Cu}]^+$, and the proposed coordination pattern of **RD**- Cu^{2+} complex.

RD- Hg^{2+} complex was not observed, but it can be inferred that Hg^{2+} should coordinate with **RD** just like Cu^{2+} . The Cu^{2+} -induced fluorescence quenching should be ascribed to the fact that paramagnetic Cu^{2+} is the most notorious fluorescence quencher.^{27–30}

4. Conclusion

In summary, a new probe based on dansyl-appended rhodamine B, which is capable of detecting Cu^{2+} and Hg^{2+} , has been developed. Free **RD** emits green fluorescence. The presence of Cu^{2+} can cause the green fluorescence quenching. Upon addition of Hg^{2+} , an orange fluorescence enhancement and meanwhile the disappearance of the green emission were observed, which was ascribed to the fluorescence resonance energy transfer from dansyl moiety to the ring-opened rhodamine B moiety. Additionally, the probe can give colorimetric responses to Cu^{2+} and Hg^{2+} by producing intense absorptions at 552 nm and 558 nm, respectively, which resulted in a color change from colorless to pink. Other common metal ions including heavy and transition metal ions have no effect on the fluorometric and colorimetric responses to Hg^{2+} and Cu^{2+} .

5. Acknowledgements

This work is supported by the Natural Science Foundation of Hainan Province (No. 20162028), the National Natural Science Foundation of China (21162010) and Program for Innovative Research Team in University (IRT-16R19)

6. References

- H. Tapiero, D. M. Townsend and K. D. Tew, *Biomed. Pharmacother.*, **2003**, *57*, 386–398. doi:10.1016/S0753-3322(03)00012-X
- P. M. Bolger and B. A. Schwetz, *N. Engl. J. Med.*, **2002**, *347*, 1735–1736. doi:10.1056/NEJMp020139
- X. Chen, J. Wang, J. Cui, Z. Xu and X. Peng, *Tetrahedron*, **2001**, *67*, 4869–4873. http://dx.doi.org/10.1016/j.tet.2011.05.001
- C. X. Yin, L. J. Qu and F. J. Huo, *Chin. Chem. Lett.*, **2014**, *25*, 1230–1234. http://dx.doi.org/10.1016/j.ccllet.2014.06.017
- X. B. Li, Z. G. Niu, L. L. Chang, M. X. Chen and E. J. Wang, *Chin. Chem. Lett.*, **2014**, *25*, 80–82. http://dx.doi.org/10.1016/j.ccllet.2013.08.002
- J. Huang, X. Ma, B. Liu, L. Cai, Q. Li, Y. Zhang, K. Jiang and S. Yin, *J. Lumin.*, **2013**, *141*, 130–136. http://dx.doi.org/10.1016/j.jlumin.2013.03.038
- T. He, C. Lin, Z. Gu, L. Xu, A. Yang, Y. Liu, H. Fang, H. Qiu, J. Zhang and S. Yin, *Spectrochim. Acta A*, **2016**, *167*, 66–71. https://doi.org/10.1016/j.saa.2016.05.032
- X. He, J. Zhang, X. Liu, L. Dong, D. Li, H. Qiu and S. Yin, *Sensor. Actuat. B-Chem.*, **2014**, *192*, 29–35. https://doi.org/10.1016/j.snb.2013.10.093
- S. Yin, V. Leen, S. Van Snick, N. Boens and W. Dehaen, *Chem. Commun.* **2010**, *46*, 6329–6331. Doi:10.1039/C0CC01772H
- J. Chen, W. Shu and E. Wang, *Chem. Res. Chinese Universities*, **2016**, *32*(5), 742–745. doi:10.1007/s40242-016-6001-1
- C. Wang, D. Zhang, X. Huang, P. Ding, Z. Wang, Y. Zhao and Y. Ye, *Sensor. Actuat. B-Chem.*, **2014**, *198*, 33–40. http://dx.doi.org/10.1016/j.snb.2014.03.032
- X. Chen, T. Pradhan, F. Wang, J. S. Kim and J. Yoon, *Chem. Rev.*, **2012**, *112*, 1910–1956. doi:10.1021/cr200201z
- H. N. Kim, M. H. Lee, H. J. Kim, J. S. Kim and J. Yoon, *Chem. Soc. Rev.*, **2008**, *37*, 1465–1472. doi:10.1039/B802497A
- S. Ji, X. Meng, W. Ye, Y. Feng, H. Sheng, Y. Cai, J. Liu, X. Zhu and Q. Guo, *Dalton Trans.*, **2014**, *43*, 1583–1588. doi:10.1039/C3DT52422A
- J. Piao, J. Lv, X. Zhou, T. Zhao and X. Wu, *Spectrochim. Acta A*, **2014**, *128*, 475–480. http://dx.doi.org/10.1016/j.saa.2014.03.002
- S. Ma, Z. Yang, M. She, W. Sun, B. Yin, P. Liu, S. Zhang and J. Li, *Dyes Pigments*, **2015**, *115*, 120–126. http://dx.doi.org/10.1016/j.dyepig.2014.12.014
- Z. Yang, M. She, J. Zhang, X. Chen, Y. Huang, H. Zhu, P. Liu, J. Li and Z. Shi, *Sensor. Actuat. B-Chem.*, **2013**, *176*, 482–487. http://dx.doi.org/10.1016/j.snb.2012.07.035
- X. Chen, X. Meng, S. Wang, Y. Cai, Y. Wu, Y. Feng, M. Zhu and Q. Guo, *Dalton Trans.*, **2013**, *42*, 14819–14825. doi: 10.1039/C3DT51279G
- L. Xu, Y. Xu, W. Zhu, X. Sun, Z. Xu and X. Qian, *RSC Adv.*, **2012**, *2*, 6323–6328.

- doi: 10.1039/C2RA20840G
20. M. Wang, F. Yan, Y. Zou, L. Chen, N. Yang and X. Zhou, *Sensor. Actuat. B-Chem.*, **2014**, *192*, 512–521.
<http://dx.doi.org/10.1016/j.snb.2013.11.031>
21. Y. Hu, Q. Li, H. Li, Q. Guo, Y. Lu and Z. Li, *Dalton Trans.*, **2010**, *39*, 11344–11352. doi:10.1039/C0DT00737D
22. Y. Xiang, A. Tong, P. Jin and Y. Ju. *Org. Lett.*, **2006**, *8*, 2863–2866. doi: 10.1021/ol0610340
23. Z. Hu, J. Hu, Y. Cui, G. Wang, X. Zhang, K. Uvdal and H. W. Gao, *J. Mater. Chem. B*, **2014**, *2*, 4467–4472.
doi: 10.1039/C4TB00441H
24. H. J. Kim, S. Yoon, N. Park, J. S. Kim and M. H. Lee, *Org. Lett.*, **2008**, *10*, 213–216. doi: 10.1021/ol702558p
25. P. Xie, F. Guo, R. Xia, Y. Wang, D. Yao, G. Yang and L. Xie, *J. Lumin.*, **2014**, *145*, 849–854.
<http://dx.doi.org/10.1016/j.jlumin.2013.09.003>
26. P. Xie, F. Guo, L. Wang, S. Yang, D. Yao and G. Yang, *J. Fluoresc.*, **2015**, *25*, 319–325.
doi:10.1007/s10895-015-1511-7
27. J. H. Ding, L. D. Yuan, L. Gao and J. W. Chen, *J. Lumin.*, **2012**, *132*, 1987–1993.
<http://dx.doi.org/10.1016/j.jlumin.2012.03.039>
28. S. He, Q. Liu, Y. Li, F. Wei, S. Ci, Y. Lu and X. Zeng, *Chem. Res. Chinese Universities*, **2014**, *30*, 32–36.
doi:10.1007/s40242-014-3364-z
29. A. Sikdar, W. Roy, K. Haldar, S. Sarkar and S. S. Panja, *J. Fluoresc.*, **2013**, *23*, 495–501.
doi:10.1007/s10895-013-1169-y
30. Y. Yang, C. Gao, B. Li, L. Xu and L. Duan. *Sensor. Actuat. B-Chem.*, **2014**, *199*, 121–126.
<http://dx.doi.org/10.1016/j.snb.2014.03.064>

Povzetek

Razvili smo novo fluorescenčno senzorsko probo, osnovano na rodaminu B s pripeto danzilno skupino. Proba lahko selektivno prepozna in zazna Hg^{2+} in Cu^{2+} ione preko edinstvenih fluorescenčnih in absorpcijskih lastnosti, ne pa tudi ostalih običajnih kovinskih ionov. V pufrski raztopini MeCN/HEPES daje proba ratiometrični fluorescenčni odgovor na Hg^{2+} , ki ga pripisujemo fluorescenčnemu resonančnemu prenosu energije z danzilne skupine na odprti obroč rodamina B, medtem ko prisotnost Cu^{2+} povzroči dušenje fluorescence. Poleg sprememb v fluorescenci prisotnost Cu^{2+} in Hg^{2+} povzroči tudi intenzivno absorpcijo pri približno 555 nm, zaradi česar se barva spremeni iz brezbarvne v rožnato.

Scientific paper

Surface Modification of Alumina Nanoparticles: A Dispersion Study in Organic Media

Esmail Soleimani* and Narges Zamani

Inorganic Chemistry Research Laboratory, Faculty of Chemistry, Shahrood University of Technology, Shahrood, IRAN

* Corresponding author: E-mail: essoleimani@shshroodut.ac.ir; ssoleimani64@gmail.com
Tel-fax: 98 23 32395441

Received: 19-04-2017

Abstract

The alumina nanoparticles (NPs) have been synthesized from reaction between alum with ammonia and then calcined the precipitate at 1200 °C for 4 h. Its surface was modified by oleic acid (OA) and trimethoxyvinylsilane (TMVS) in *o*-xylene at 50 °C. The alumina NPs and its modified were characterized by XRD, FT-IR, SEM, EDX and TGA. The TGA analysis indicated that the grafting amount of OA and TMVS were 10.5 and 8.0% respectively. The dispersion of modified NPs was determined in monomers such as methyl methacrylate (MMA), butyl acrylate (BuA) and styrene (St) and in solvents such as ethanol, hexane and acetone. The experimental results showed that the highest dispersion was happened NPs modified by oleic acid in n-hexane, while the highest dispersion was observed NPs modified by TMVS in acetone. The results indicate that NPs modified by oleic acid formed a stable dispersion in MMA and BuA. The highest amount of dispersion happened NPs modified by oleic acid in MMA and BuA in initial weight of 5 and 2.5% respectively, while stable dispersion is formed in styrene when TMVS is used as modifier. The highest amount of dispersion was happened NPs modified by TMVS in styrene in initial weight of 2.5%.

Keywords: Surface modification; alumina nanoparticles; oleic acid; trimethoxyvinylsilane; dispersibility; lipophilic degree

1. Introduction

In recent decades, the superfine particles in the nano-scale were of great interest due to their high surface area.^{1,2} Nano-sized ceramic powders, because of their excellent properties such as structural, optical and electrical behavior are effective in many fields.^{3–5}

Alumina is an important component of ceramic oxides. Alumina is used in the chemical industry, metallurgy, pharmaceutical and food industries due to the cheapness and having good mechanical and optical properties.^{6,7} Al₂O₃ has been widely used as catalyst and catalyst support, and also it has extensive applications in ceramic industry and structural composites.⁸

The Surface of mostly ceramic NPs such as alumina is polar and hydrophilic nature. That's why they do not disperse in organic environments. This feature prevents their use in the industry. This limitation can be overcome by modifying their surface by appropriate modifiers.

Fatty acids are used as modifiers for surface NPs,^{9–11} such as the surface of SiO₂ NPs was modified by oleic

acid. Oleic acid was connected through an ester bond to the surface of nano-SiO₂. Results showed the modified NPs dispersion capabilities in non-polar solvents such as petroleum or mineral oils.¹² The surface modified ZnO NPs increases dispersibility NPs in organic solvents and reduces photo-catalyst behavior. To do this, the surface of ZnO NPs was modified through using plasticizers silane (γ -methacryloxypropyltrimethoxysilan) and modified by polystyrene. Experimental results showed good dispersion of NPs in non-polar solvents such as acetone after surface modification.¹³ The surface HfO₂ NPs was modified by oleic acid. The presence of organic groups on the surface of the hafnium oxide NPs was proved by FT-IR spectra, and it indicated that oleic acid is attached to the carboxylate form on the surface of the HfO₂ NPs. The surface of NPs changed from hydrophilic to hydrophobic by surface modification, so they were dispersed well in hexane.¹⁴

The nanocomposites (NCs) containing non-aggregated NPs were functionalized by two coupling agents (citric and ascorbic acids). Surface morphology indicated a picturesque network structure due to the existence of

hydrogen bonds in the modified Al_2O_3 . It also proved good dispersion of modified NPs in the polymer matrix.¹⁵ The surface of alumina NPs was modified using epoxy-containing alkoxy-silanes. Coupling of organic groups onto the surface of oxides using alkoxy-silanes occurs via the formation of Si-O-M or metallasiloxane bonds. The surface modification decreased the thermal stability of alumina, in comparison with pristine alumina NPs.¹⁶

The surface of Al_2O_3 NPs was modified using vinyltrimethoxysilane (VTMS) layer. Analyses revealed that the silane coupling successfully adsorbed on the surface of nano Al_2O_3 via chemical interaction. Results show that NPs with 3% VTMS was in good agreement with the storage modulus and glass transition temperature values revealed by DMTA analysis.¹⁷

High performance polysulfone/alumina biocompatible NCs are reported and the effects of alumina surface modification are explored by Anaya and co-workers.¹⁸ They show that some fatty acids (palmitic, stearic, oleic and erucic acids) chemisorb over the surface of alumina forming nano-sized self-assembled structures. These structures present thermal transitions at high temperatures, 100 °C higher than the melting point of the pure acids, and are further shifted about 50 °C in the presence of polysulfone.¹⁸

Llorente and co-workers have investigated the wear and mechanical behavior, along with the thermal stability, of polysulfone/modified alumina. Alumina NPs have been modified with polysulfone (PSU) chains of two different molecular weights. The modification leads to an enhanced homogeneous dispersion and enhanced mechanical and wear behavior.¹⁹ Nano-indentation measurements confirmed that the elastic modulus values were enhanced when modified NPs were used to prepare NCs. The PSU chains grafted to alumina promoted enhanced particle dispersion, which at the same time induced protection in the polysulfone matrix against wearing off. The results showed a clear tendency for increased strength and wear resistance, without sacrificing transparency.¹⁹

Alumina NPs have been modified with polysulfone (PSU) chains *via* 1,3-dipolar cyclo-addition reaction between functionalized alumina with vinyl groups and terminal azide polysulfone chains of two different molecular weights.²⁰ Homo-polymer NCs have been prepared by extrusion and microinjection. The effectiveness of the grafts on the dispersibility has been analyzed in terms of the parameters that govern the wettability between grafted and matrix chains. The dispersion state and interfacial adhesion of PSU grafted NPs have been evaluated. Results show that the incorporation of the modified alumina improves the dispersion state in comparison with bare alumina NPs. These results can be explained by enthalpic compatibility between polysulfone grafted layer and host polysulfone matrix.²⁰

The application of non-fouling thin films such as poly(ethylene glycol) (PEG) to alumina membranes is

useful in drug delivery applications to prevent membrane fouling in long-term usage. Popat and co-workers have covalently attached PEG to nano-porous alumina surfaces to improve their non-fouling properties.²¹ A PEG-silane coupling technique was used to modify the surface.

The modification of nanometric aluminum oxides particles by bis-phosphonic acid-based oligomers of aromatic polyester, polyether, or polydimethylsiloxane (PDMS) was achieved with the formation of covalent bonds between the oxide and the oligomers.²² The melt blending of the unmodified as well as the modified particles with PMMA led to well-dispersed NCs structures. Thermal stability and fire behavior of PMMA were improved due to physical and physico-chemical processes involving the presence of the nanometric alumina. Significant improvements for these properties in relation to the grafting of the mineral were only noticed for the PDMS phosphonic acid-based formulation, despite the very low amount of oligomer present in PMMA. It is suggested that this compound could act in the condensed phase due to its important thermal stability and could also promote modifications of the degradation pathway of PMMA in the interphase region surrounding the alumina particles.²²

Chemical surface modification of aluminum oxide (AO) NPs with graft copolymer of AO and poly (isobutyl vinyl ether) (PIBVE) (AO-graft-PIBVE) was carried out by ball milling of AO NPs with IBVE in vacuum at low temperature. The surface modified AO NPs with monodispersed particle diameter exhibited structural blue color which was evidenced by photograph, optical spectroscopy (UV-Vis) and SEM image.²³

Several protocols reported for the surface modification of Al_2O_3 NPs. In this regard, different surfactants and organic compounds such as a silane coupling agent, isocyanate group, stearic acid, dimethyl sulfoxide, and acetic acid have been used as modifying agents.^{24–27} To the best of our knowledge, there is no report on the comparison of the effectiveness of different modifiers for Al_2O_3 NPs and their compatibility in various organic solvents. In this study, the surface of alumina NPs was modified by two modifiers such as oleic acid (OA), trimethoxyvinylsilane (TMVS), as well as a mixture of two modified in three ratio (3:1), (1:1) and (1:3). Then the dispersibility of modified NPs was investigated in monomers such as methyl methacrylate (MMA), butyl acrylate (BuA) and styrene (St) and also in solvents including acetone, n-hexane and ethanol with different levels of hydrophobicity.

2. Experimental

2.1. Material and Methods

In this work, the chemicals such as trimethoxyvinylsilane (TMVS), oleic acid (OA), ethanol, n-hexane, *o*-xylene, ammonia (25%) and acetone were used as purchased by the chemical company (Merck) without any purifi-

cation. Alum was prepared in our laboratory according to literature.

2. 2. Preparation of Al₂O₃ NPs

The alumina NPs precursors were synthesized by the precipitation method and then calcination sediment. Firstly, 25 mL of 3.0 M ammonia solution was dropped gradually and slowly into 25 mL of ammonium alum [(NH₄Al(SO₄)₂ · 12H₂O) 1.0 M with vigorous stirring for 45 minutes. After a vigorous stirring for an hour, the reaction mixture was heated to 95 °C and then kept at that temperature for 3 h for precipitation. The precipitate obtained was first washed three times with distilled water and then washed three times with anhydrous alcohol and then dried in an oven at 60 °C for 10 h. Finally, the dried precipitate was then calcined at 1200 °C for 4 h with a heating rate of 5 °C min⁻¹. After cooling in the room temperature, the samples were milled and collected for characterization.

2. 3. Surface Modification of Al₂O₃ NPs

The experimental method of surface modification of alumina NPs using both modifiers oleic acid (OA) and trimethoxyvinylsilanes (TMVS) is the same as follows:

1.5 g of oleic acid (or TMVS) was dissolved in 50 ml of *o*-xylene and then 3.0 g of alumina NPs were added to it. The resulting suspension is heated at 50 °C within an hour along with magnetic stirring. The precipitate was centrifuged, and washed three times with 5 ml toluene. Precipitate was dried in the oven at 60 °C for 24 h.

2. 4. Effect of Modifiers Concentration

Using the above method, various amount of oleic or TMVS (0.025, 0.05, 0.15, 0.25, 0.35 and 0.45, 0.50 g) were dissolved in 10 mL *o*-xylene, and each solution was used in turn for modifying 1.0 g samples of Al₂O₃ NPs, and was stirred at 50 °C for an hour. The sediments were separated, washed three times with 5 mL toluene and dried in the oven at 60 °C for 24 h. Lipophilicity of modified alumina NPs were carried out as below:

First 0.1 g of modified alumina NPs is added to 10 mL water. Then methanol is added drop wise through a burette to these dispersed NPs until no more sediment are formed. The volume of methanol is used to calculate the degree of lipophilicity of the surface of NPs.

2. 5. Measurement of Lipophilic Degree

One way to measure the lipophilic degree (LD) of the surface of NPs is disperse a certain amount of modified NPs in water, and then to carry out titration with an organic solvent such as methanol.²⁸

When unmodified alumina NPs is added to water, sedimentation takes place promptly, whereas the alumina

NPs modified by oleic acid (or TMVS) will dispersed in water. Drop wise addition of methanol from a burette to a solution of modified NPs (0.1 g in 10 mL water) causes the modified NPs to sediment gradually. The degree of lipophilicity can be calculated using Eq. (1) by knowing the volume of the methanol used:

$$LD = \frac{v}{v+10} \times 100 \quad (1)$$

In this equation, V is the volume of methanol (mL) used. Measuring the degree of lipophilicity is used as a guide for surface modification.

2. 6. Dispersibility Modified Alumina NPs

0.05 g of modified alumina NPs were dispersed in 10 mL of solvents such as n-hexane, ethanol and acetone, and was then ultrasound within 30 min. Then, the samples were allowed to stand without shaking for 72 h in the lab, the particles were deposited. The precipitate then was centrifuged and dried in the oven at 60 °C for 24 h. The amount of stable particles in dispersion was determined gravimetrically (%). The initial weight percent of the modified alumina NPs varied from 2.5 to 30%.

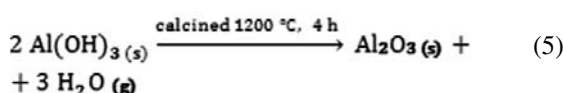
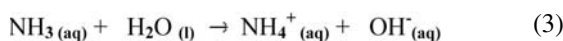
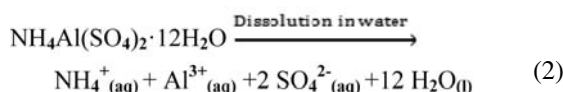
2. 7. Characterization of the Modified Alumina

The X-ray diffraction patterns (XRD) of powder samples were recorded by XRD system BRUKER-XS for characterizing the crystalline structure of the NPs. The XRD diffractometer is operated at a voltage of 40 kV and Cu K α radiation over Bragg angles ranging from 10 to 80° with the scanning rate of 0.05 °C min⁻¹. The surface morphology of samples was recorded using SEM, Hitachi Japan, and TESCAN model. The instrument was equipped with EDX analysis for the determination of elemental analysis. The EDX model and its detector type were S4800 (I) and 7747/17-ME, respectively. The FT-IR spectra of the samples were recorded on FT-IR Rayleigh WQF-510 a spectrophotometer. The spectra of solids were obtained using KBr pellets. Ultrasonic irradiation was carried out with an ultrasonic equipped with a probe which was immersed directly in the mixture solution system with frequency of 2.25 × 10⁴ Hz and power of 100 W. Thermo-gravimetric analysis (TGA) was carried out on a TG-209 thermo-analyzer (Netzsch, Germany), oxygen atmosphere, heating rate 10 °C min⁻¹. An electric furnace of Raypa with HM-9 model was used for calcimining samples.

3. Results and Discussion

The Al₂O₃ NPs have been synthesized through chemical precipitation method from reaction between ammo-

nium alum $[\text{NH}_4\text{Al}(\text{SO}_4)_2 \cdot 12\text{H}_2\text{O}]$ with ammonia solution and then calcined the precipitate at $1200\text{ }^\circ\text{C}$ for 4 h. The reaction equations are as follows:



Preparation method of Al_2O_3 NPs is of unique advantages. Nanoparticles are obtained from inexpensive and easily available precursors, and without needing surfactants (surface active). The surface of alumina NPs was modified by two modifiers such as oleic acid (OA), trimethoxyvinylsilane (TMVS), as well as a mixture of two modified in three ratio (3:1), (1:1) and (1:3).

In order to confirm that the surface of alumina NPs is covered by the modifiers, the surface was studied by the usual methods of identification and morphology consideration.

3. 1. X-ray Diffraction Patterns

The X-ray diffraction pattern of alumina NPs before and after modification by oleic acid and TMVS were recorded, and results are presented in **Fig. 1**. The eight characteristic angles viz 2θ equal to 18.8 , 20.5 , 32.9 , 36.9 , 39.4 , 45.6 , 61.2 and 67.2 ° , which correspond well to the standard JCPDS card with number 29-1486, confirms that the crystal structure of Al_2O_3 is tetragonal.^{29,30} These peaks are corresponded to crystal planes of [111], [200], [220], [311], [222], [400], [511] and [440] respectively. **Figs. 1b** and **1c** show that the characteristics of peaks after surface modification have not changed, and are the same as those of unmodified nano-alumina with tetragonal crystal structure. The average size of Al_2O_3 NPs modified by oleic acid and TMVS calculated from XRD diffraction pattern according to Debye-Scherrer formula are 29.08 and 30.04 nm respectively.

3. 2. FT-IR Spectra

In order to study the bonds formed, FT-IR spectra of NPs were recorded before and after surface modification by oleic acid and TMVS. These spectra are shown in **Fig. 2**. The observed band at 672 cm^{-1} in FT-IR of unmodified NPs (**Fig. 2a**) is due to stretching frequency of Al-O in

Al_2O_3 .³¹ The broad peaks at around 3442 and 1630 cm^{-1} are attributed to the stretching and bending bands of O–H groups on the surface of alumina, respectively.^{32,33}

In the FT-IR spectra of nano-alumina modified with oleic acid (OA) and trimethoxy-vinylsilane (TMVS) in **Figs. 2b** and **2c**, in addition to the absorption bands of vibration frequencies Al-O and -OH groups, new bands were observed. Two absorption bands at 2854 and 2924 cm^{-1} (**Fig. 2b**) are due to the vibrational frequencies of CH_2 and CH_3 groups of oleic acid covering the surface of nanoparticles.³⁴ An absorption band at 1625 cm^{-1} (**Fig. 2c**) is related to the presence of vinyl double bonds ($\text{C}=\text{C}$) of trimethoxyvinylsilane coated on the surface of alumina NPs.³⁵ The observed band at 1016 cm^{-1} is due to the stretching frequency of Si-O in silane.³⁶ These observations in FT-IR spectra confirm that the surface of Al_2O_3 NPs is modified by oleic acid and TMVS.

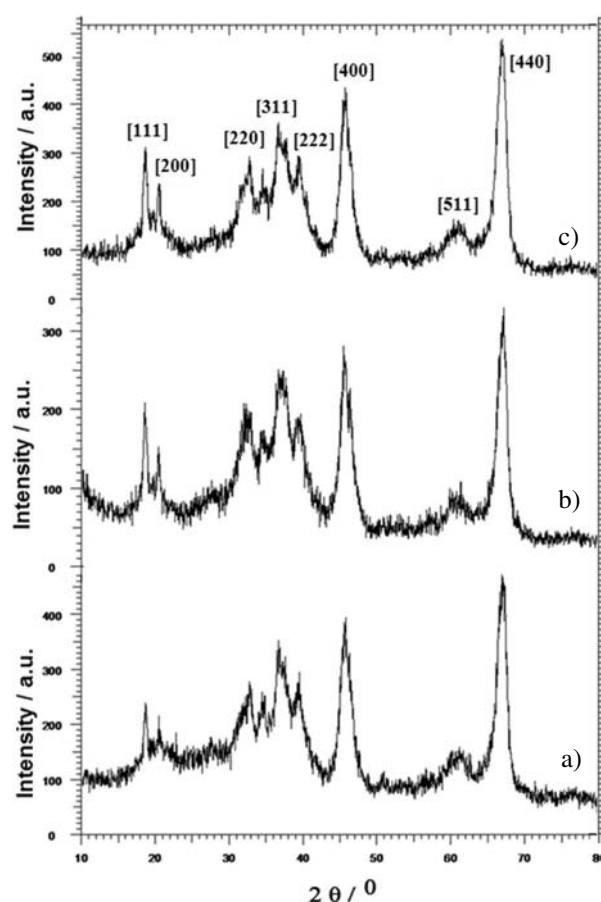


Fig. 1: XRD diffraction patterns of: (a) Al_2O_3 NPs; (b) Al_2O_3 NPs modified by oleic acid; (c) Al_2O_3 NPs modified by TMVS.

3. 3. SEM Images & EDX Analysis

Nanoparticles have a tendency to aggregate because of high surface energy. Therefore, surface modification is expected to decrease aggregation and improve dispersibi-

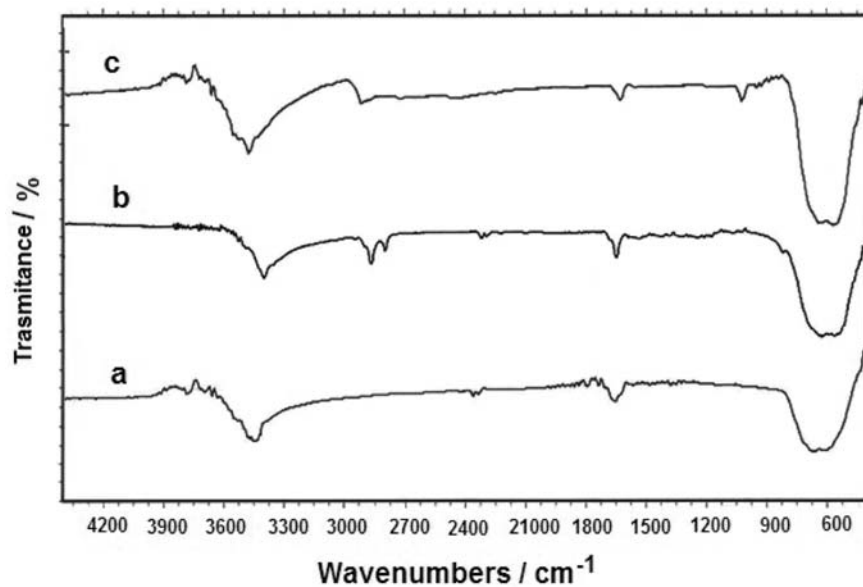


Fig. 2: FT-IR spectra of: (a) bare Al₂O₃ NPs; (b) Al₂O₃ NPs modified by oleic acid; (c) Al₂O₃ NPs modified by TMVS.

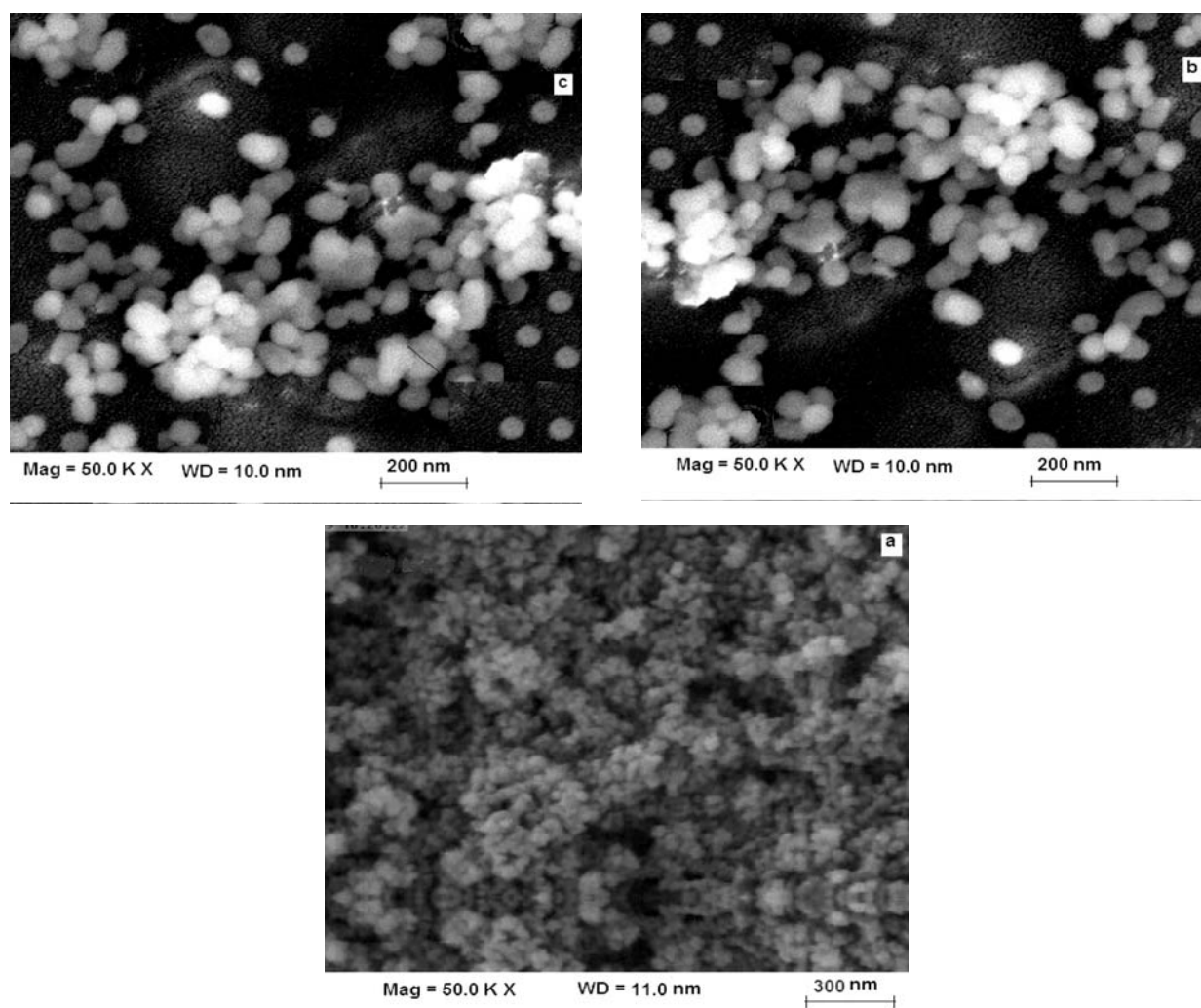


Fig. 3: SEM images of: (a) Al₂O₃ NPs; (b) Al₂O₃ NPs modified by oleic acid; (c) Al₂O₃ NPs modified by TMVS.

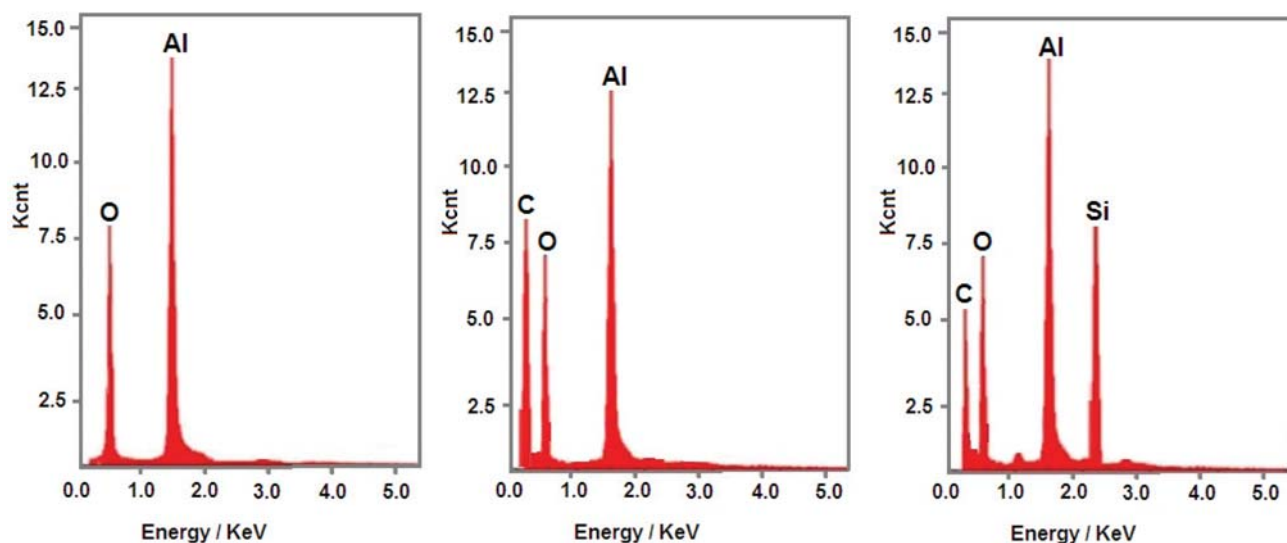


Fig. 4: EDX spectra of: (a) Al_2O_3 NPs; (b) Al_2O_3 NPs modified by oleic acid; (c) Al_2O_3 NPs modified by TMVS.

lity.^{37–39} Thus, to studying dispersibility, SEM images of alumina nanoparticles before and after modification by oleic acid and TMVS have been recorded which are shown in Fig. 3. As it can be seen in Fig. 3a, alumina unmodified NPs are highly aggregated which is due to large surface area to volume ratio and high energy of the surface of nanoparticles. Whereas in Figs. 3b and 3c good dispersibility can be seen which are due to modification of NPs by oleic acid and TMVS respectively? This improvement in dispersibility of NPs certainly confirms the surface modification of NPs by oleic acid and TMVS. The size of the modified alumina NPs appeared to be higher (50 nm) in comparison to bare alumina NPs from the XRD results (30 nm).

The EDX spectra of Al_2O_3 NPs and its modified by oleic acid and TMVS are shown in Fig. 4. The EDX spectrum given in Fig. 4a shows the presence of Al and O as the only elementary components of Al_2O_3 NPs. The presence of carbon and oxygen in alumina NPs modified by

oleic acid (Fig. 4b), and presence of carbon, oxygen and silicon in alumina NPs modified by TMVS (Fig. 4c) are the proof for surface modification of Al_2O_3 NPs respectively, and which were absent in bare alumina NPs.

3. 4. TGA Analysis

TGA analysis is taken to prove that how many of modifier is grafted on the surface of nanoparticles. TGA curves alumina NPs and its modified by oleic acid and TMVS are given in Fig. 5. The alumina NPs modified by oleic acid has a total weight loss of 10.5%, when the temperature changes from 255 to 560 °C, which is due to the burning of oleic acid on the surface of modified alumina NPs (Fig. 5b). The similar behavior was observed in alumina NPs modified by TMVS, with a total weight loss of 8%, which may be attributed the burning of silane compound on surface of modified alumina NPs (Fig. 5c).

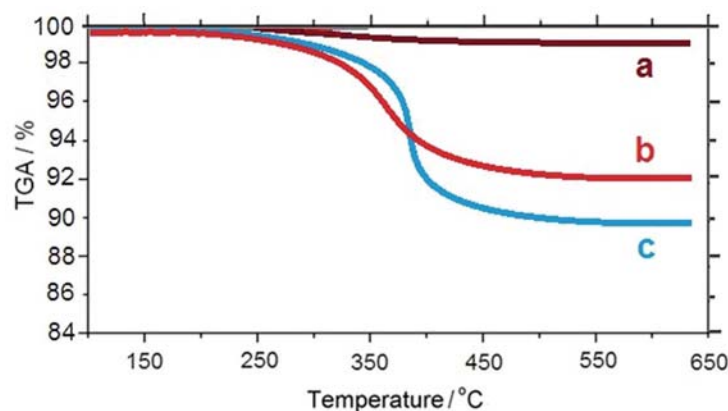


Fig. 5: TGA thermo-gram of: (a) un-modified alumina NPs; (b) alumina NPs modified by TMVS; (c) alumina NPs modified by oleic acid.

3. 5. The amount of Surface Modifier

Different amount of oleic acid and TMVS (2.5, 5.0, 7.5, 10.0, 12.5, 15.0 and 20%) as surface modifier were applied on alumina NPs, and the lipophilic degree (LD) of the modified NPs was measured. The results obtained are presented in **Table 1** as the variation of lipophilic degree versus amount of modifier. It can be seen from data that lipophilicity increases with the rise of amount of modifier up to 12.5% for oleic acid, and 10.0% for TMVS. However, if the amount of modifier is increased above this amount the lipophilicity starts to decrease. It may be due to enlarging of chain hydrocarbon of the modifier which can stop the carboxylic group (-COOH) of oleic acid or methoxy moiety (-OCH₃) of TMVS to react with the hydroxyl group on the surface of alumina NPs.¹⁴

3. 6. Dispersibility of the Modified Alumina NPs

Knowing that the incorporation of NPs into polymers can leads to improved mechanical behavior and thermal stability of polymers. Uniform and stable dispersion of NPs in the monomer is an important factor in the preparation of polymeric NCs. Therefore, effect of type and amount of modifiers were investigated on the dispersion of NPs in the monomers such as methylmethacrylate (MMA), butylacrylat (BuA) and styrene (St). To do this, certain amount of modified alumina NPs was dispersed in each monomer under stirring for one hour at room temperature. The percent of the initial weight of the modified alumina NPs varied from 2.5 to 30%. Then, modified alumina NPs loaded monomers were allowed to stand at room temperature for 72 h. The precipitated part of the NPs was separated and the amount of the stable particles

in dispersion was determined gravimetrically. The results are shown in **Table 2**.

As it can be seen in the above table, the results indicate that the majority of modified Al₂O₃ NPs by oleic acid (OA) precipitate in styrene; While OA-Al₂O₃ NPs formed a stable dispersion in MMA and BuA monomers. The highest amount of dispersion of OA-Al₂O₃ NPs in methyl methacrylate monomer happened in initial weight of 5 and 10%. Similarly, the highest amount of dispersibility of OA-Al₂O₃ NPs in butyl acrylate monomer occurred in initial weight of 2.5 and 10%. The results also represent that when TMVS is used as modifier, TMVS-Al₂O₃ NPs are stable in Styrene, however they were settled down in MMA and BuA monomers. The highest amount of dispersion of TMVS-Al₂O₃ NPs in styrene monomer happened in initial weight of 2.5, 10 and 5%.

Moreover, when a mixture of modifiers was used and the ratio of oleic acid to trimethoxyvinylsilane (OA: TMVS) was varied from 3:1 to 1:3 dispersibility behavior of modified Al₂O₃ NPs was changed, solid content of final stable dispersions are shown in **Table 3**. The amount of dispersibility of NPs was increased in all three monomers when the amount of oleic acid was high in the mixture modifiers (OA: TMVS, 3:1). On the other hand, the amount of dispersibility of alumina NPs increased in styrene monomer in all three cases including: the mixture of oleic acid (OA) and trimethylvinylsilane (TMVS) modifiers (3:1, 1:1 and 1:3).

These findings illustrated that the surface modification of Al₂O₃ NPs with oleic acid, trimethoxyvinylsilane and mixture of modifiers OA-TMVS would increase the compatibility between NPs with MMA and styrene, respectively. Either this contributes to a better dispersibility of NPs in MMA or Styrene. One can justify this fact by comparing the polarity of monomer and relevant modifier.

Table 1: The LD of alumina NPs modified by oleic acid (OA) and TMVS (%) in different amount of modifiers.

Amount of modifiers (%)	2.5	5.0	7.5	10.0	12.5	15.0	20.0
LD NPs modified by OA (%)	15.22	15.85	18.47	22.15	24.71	18.95	14.27
LD NPs modified by TMVS (%)	11.11	16.13	18.75	23.45	18.25	14.75	13.07

Reaction conditions: Amount of alumina NPs 1.0 g, o-xylene as solvent 10 mL, temperature 50 °C and reaction time 1 h.

Table 2: Dispersion of alumina NPs modified with oleic acid (OA) and trimethoxy-vinylsilan (TMVS) in some organic media (%).

Initial weight percent percent alumina NPs (%)	Dispersion in MMA		Dispersion in BuA		Dispersion in St	
	OA	TMVS	OA	TMVS	OA	TMVS
2.5	2.12	1.73	1.93	1.54	1.52	2.04
5	4.15	3.64	3.47	2.74	3.12	3.75
10	8.24	6.14	7.54	6.85	6.44	7.88
15	12.04	9.45	10.51	9.22	9.12	10.49
20	15.25	11.42	14.12	11.95	11.27	14.17
25	18.63	13.94	15.84	14.01	13.94	17.81
30	22.74	17.22	20.46	16.04	17.01	21.48

Table 3: Dispersion of alumina NPs modified with different ratios of mixtures of OA: TMVS (3:1, 1:1 and 1:3) in some organic media (%).

Initial weight percent alumina NPs (%)	Dispersion in MMA (%) (OA:TMVS)			Dispersion in BuA (%) (OA:TMVS)			Dispersion in St (%) (OA:TMVS)		
	(3:1)	(1:1)	(1:3)	(3:1)	(1:1)	(1:3)	(3:1)	(1:1)	(1:3)
2.5	1.11	0.98	0.75	1.35	1.12	0.95	2.25	1.87	1.32
5	2.15	1.75	1.25	2.78	2.05	1.84	3.87	3.42	3.11
10	6.04	5.24	3.73	7.13	5.88	5.28	8.09	7.04	6.45
15	13.21	9.08	8.22	13.56	9.86	8.94	13.91	10.23	10.04
20	14.75	13.15	12.28	15.25	14.55	13.09	17.44	15.85	14.93
25	17.73	17.22	15.63	18.84	16.34	14.83	20.03	18.44	17.05
30	20.34	18.35	15.11	22.47	19.74	17.56	24.79	21.58	21.17

Table 4: Dispersion of alumina NPs modified with oleic acid (OA) and trimethoxy-vinylsilan (TMVS) in some organic solvents (%).

Initial weight percent alumina NPs (%)	Dispersion in n-hexane (%)		Dispersion in acetone (%)		Dispersion in ethanol (%)	
	OA	TMVS	OA	TMVS	OA	TMVS
2.5	2.01	1.62	1.71	1.95	1.25	1.41
5	4.12	3.25	3.15	3.85	2.12	1.94
10	7.24	4.93	5.45	6.04	3.74	4.15
15	10.46	6.16	7.37	8.82	4.92	4.31
20	13.48	10.72	11.29	11.25	7.15	7.08
25	15.94	11.07	12.83	13.91	9.29	9.48
30	20.42	13.97	14.12	17.42	10.87	9.95

The dispersion percentage of the modified alumina NPs by oleic acid and TMVS also were investigated in solvents such as n-hexane, acetone and ethanol and the results are shown in **Table 4**. The highest dispersion of alumina NPs modified with oleic acid happened in n-hexane and the lowest occurred in ethanol. While the highest dispersion of alumina NPs modified by TMVS can be seen in acetone and lowest dispersion occur in ethanol.

The dispersibility of the alumina NPs modified by oleic acid (OA) and trimethoxyvinylsilane (TMVS) in monomers of styrene (St), poly(methyl methacrylate) (PMMA) and butylacrylate (BuA) was compared with the previous work of modified ZnO NPs and the results are shown in **Table 5**.

As it can be seen in **Table 5**, the results indicate that the majority of modified Al₂O₃ NPs by oleic acid precipitate in styrene and formed a stable dispersion in MMA and BuA monomers. While contrary to this behavior was observed in ZnO NPs modified by oleic acid.⁴⁰ The majority of modified Al₂O₃ NPs by TMVS precipitate in MMA and

BuA monomers and formed a stable dispersion in styrene. While the majority of modified ZnO NPs by TMVS precipitate in styrene and BuA monomers and formed a stable dispersion in MMA monomer.⁴⁰ On the other hand, the stability time of dispersion of modified nanoparticles in our work (72 h) is longer than the previous work (24 h).⁴⁰

4. Conclusions

The alumina NPs have been synthesized from reaction between ammonium alum with ammonia solution and then calcined the precipitate at 1200 °C. The surface of alumina NPs was changed to the hydrophobic nature due to surface modified by oleic acid (OA) and trimethoxyvinylsilane (TMVS). TGA analysis for alumina NPs indicates that the grafting amount of oleic acid and TMVS are 10.5 and 8% respectively. The presence of organic groups on the surface of NPs was proved by FT-IR spectra, and shown that oleic acid is attached to the carboxylate form

Table 5: Stable time and dispersion of modified nanoparticles.

	Stable time/ h	Stable dispersion	Majority precipitation	References
Al ₂ O ₃ -OA	72	MMA, BuA	St	This work
Al ₂ O ₃ -TMVS	72	St	MMA, BuA	This work
ZnO-OA	24	St	MMA, BuA	40
ZnO-TMVS	24	MMA	St, BuA	40

and TMVS connected via the formation of Si-O-M bond on the surface of alumina NPs. The change of behavior of hydrophobic surfaces of modified alumina NPs was confirmed through lipophilic degree (LD) experiments. The results obtained are presented that lipophilic degree increased with the rise of amount of modifier up to 12.5% for oleic acid, and 10.0% for TMVS. Experimental results showed that the highest dispersion was happened alumina NPs modified by oleic acid in n-hexane and the lowest in ethanol, while the highest dispersion was observed alumina NPs modified by TMVS in acetone and lowest dispersion in ethanol. The results indicate that modified Al₂O₃ NPs by oleic acid (OA) formed a stable dispersion in MMA and BuA monomers. The highest amount of dispersion was happened OA-Al₂O₃ NPs in MMA and BuA monomers in initial weight of 5 and 2.5% respectively, while stable dispersion are formed in styrene when TMVS is used as modifier. The highest amount of dispersion was happened TMVS-Al₂O₃ NPs in styrene monomer in initial weight of 2.5%.

5. Acknowledgements

The authors would like to appreciate the Research Council of Shahrood University of Technology for supporting this project financially.

6. References

1. Y. Xia, P. Yang, Y. Sun, Y. Wu, B. Mayers, B. Gates, Y. Yin, F. Kim, H. Yan, *Adv. Mater.* **2003**, *15*, 353–389. <https://doi.org/10.1002/adma.200390087>
2. N. A. M. Barakat, K. A. Khalil, I. H. Mahmoud, M. A. Kanjwal, F. A. Sheikh, H. Y. Kim, *J. Phys. Chem. C* **2010**, *114*, 15589–15593. <https://doi.org/10.1021/jp1041074>
3. D. Gal, G. Hodes, D. Lincot, H. W. Schock, *Thin Solid Films* **2000**, *361–362*, 79–83. [https://doi.org/10.1016/S0040-6090\(99\)00772-5](https://doi.org/10.1016/S0040-6090(99)00772-5)
4. K. Hara, T. Horiguchi, T. Kinoshita, K. Sayama, H. Sugihara, H. Arakawa, *Sol. Energy Mater. Sol. Cells* **2000**, *64*, 115–134. [https://doi.org/10.1016/S0927-0248\(00\)00065-9](https://doi.org/10.1016/S0927-0248(00)00065-9)
5. T. Pauporte, D. Lincot, *Electrochim. Acta* **2000**, *45*, 3345–3353. [https://doi.org/10.1016/S0013-4686\(00\)00405-9](https://doi.org/10.1016/S0013-4686(00)00405-9)
6. S. Guobin, Z. Huaiying, C. Weiquan, X. Jianmin, L. Huizhou, *Biophys. J.* **2005**, *89*, L58–L60. <https://doi.org/10.1529/biophysj.105.073718>
7. S. Chibowski, M. Paszkiewicz, M. Krupa, *Powder Technol.* **2000**, *107*, 251–225. [https://doi.org/10.1016/S0032-5910\(99\)00194-1](https://doi.org/10.1016/S0032-5910(99)00194-1)
8. H. Y. Zhang, G. B. Shan, H. Z. Liu, J. M. Xing, *Surf. Coat. Tech.* **2007**, *201*, 6917–6921. <https://doi.org/10.1016/j.surfcoat.2006.11.043>
9. C. Wang, Y. Sheng, H. Bala, X. Zhao, J. Zhao, X. Ma, Z. Wang, *Mater. Sci. Eng. C* **2007**, *27*, 42–45. <https://doi.org/10.1016/j.msec.2006.01.003>
10. C. Wang, X. Zhao, J. Zhao, Y. Liu, Y. Sheng, Z. Wang, *Appl. Surf. Sci.* **2007**, *253*, 4768–4772. <https://doi.org/10.1016/j.apsusc.2006.10.048>
11. X. Ma, Y. Liu, Y. Yu, H. Lei, X. Lv, L. Zhao, S. Ren, Z. Wang, *J. Appl. Polym. Sci.* **2008**, *108*, 1421–1425. <https://doi.org/10.1002/app.27812>
12. Z. Li, Y. Zhu, *Appl. Surf. Sci.* **2003**, *211*, 315–320. [https://doi.org/10.1016/S0169-4332\(03\)00259-9](https://doi.org/10.1016/S0169-4332(03)00259-9)
13. R. Y. Hong, J. H. Li, L. L. Chen, D. Q. Liu, H. Z. Li, Y. Zheng, J. Ding, *Powder Technol.* **2009**, *189*, 426–432. <https://doi.org/10.1016/j.powtec.2008.07.004>
14. R. Ramos-González, L. A. García-Cerda, M. A. Quevedo-López, *Appl. Surf. Sci.* **2012**, *258*, 6034–6039. <https://doi.org/10.1016/j.apsusc.2012.02.122>
15. S. Mallakpour, R. Sadeghzadeh, *Adv. Polym. Technol.*, doi:10.1002/adv.21622
16. L. A. S. A. Prado, M. Sriyai, M. Ghislandi, A. Barros-Timmons, K. Schulte, *J. Braz. Chem. Soc.* **2010**, *21*, 2238–2245. <https://doi.org/10.1590/S0103-50532010001200010>
17. M. Rostam, *J. Nanomed. Nanotechnol.* **2016**, *7*, 365.
18. S. Anaya, B. Serrano, B. Herrero, A. Cervera, J. Baselga, *ACS Appl. Mater. Interfaces* **2014**, *6*, 14460–14468. <https://doi.org/10.1021/am503744z>
19. A. Llorente, B. Serrano, J. Baselga, G. Gedler, R. Ozisik, *RSC Adv.* **2016**, *6*, 100239-100247.
20. A. Llorente, B. Serrano, J. Baselga, *Macromolecular Research* **2017**, *25*, 11–20. <https://doi.org/10.1007/s13233-016-4150-1>
21. K. C. Papat, G. Mor, C. A. Grimes, T. A. Desai, *Langmuir* **2004**, *20*, 8035-8041. <https://doi.org/10.1021/la049075x>
22. N. Cinausero, N. Azema, M. Cochez, M. Ferriol, M. Essahli, F. Ganachaud, J.-M. Lopez-Cuesta, *Polym. Adv. Technol.* **2008**, *19*, 701–709. <https://doi.org/10.1002/pat.1157>
23. T. Motokawa, M. Makino, K. Yamamoto, H. Takase, S. Naganano, Y. Enomoto-Rogers, T. Iwata, T. Kawaguchi, M. Sakaguchi, *Adv. Powder Technol.* **2017**, *28*, 266–279. <https://doi.org/10.1016/j.apt.2016.09.031>
24. S. Mallakpour, E. Khadem, *J. Mol. Struct.* **2014**, *1075*, 196–203. <https://doi.org/10.1016/j.molstruc.2014.06.081>
25. S. Mallakpour, P. Sirous, *Polym. Plast. Technol. Eng.* **2015**, *54*, 532–540. <https://doi.org/10.1080/03602559.2014.961083>
26. S. Mallakpour, E. Khadem, *Synth. React. Inorg. Met.-Org. Nano-Met. Chem.* **2015**, *45*, 1773–1779. <https://doi.org/10.1080/15533174.2013.872130>
27. Y. P. Zheng, J. X. Zhang, Q. Li, W. Chen, X. Zhang, *Polym. Plast. Technol. Eng.* **2009**, *48*, 384–388. <https://doi.org/10.1080/0360255902725381>
28. R. Y. Hong, L. L. Chen, J. H. Li, H. Z. Li, Y. Zheng, J. Ding, *Polym. Adv. Technol.* **2007**, *18*, 901–909. <https://doi.org/10.1002/pat.926>
29. Z. Ghezelbash, D. Ashouri, S. Mousavian, A. M. Ghandi, Y. Rahnama, *Bull. Mater. Sci.* **2012**, *35*, 925–931. <https://doi.org/10.1007/s12034-012-0385-4>

30. R. Y. Hong, J. Z. Qian, J. X. Cao, *Powder Technol.* **2006**, *163*, 160–168.
<https://doi.org/10.1016/j.powtec.2006.01.015>
31. Y. Sui, Y. Cui, Y. Nie, G. M. Xia, G. X. Sun, J. T. Han, *Colloids Surfaces B* **2012**, *93*, 24–28.
<https://doi.org/10.1016/j.colsurfb.2011.11.054>
32. Y. Wang, W. Eli, L. Zhang, H. Gao, Y. Liu, P. Li, *Adv. Powder Technol.* **2010**, *21*, 203–205.
<https://doi.org/10.1016/j.appt.2009.12.006>
33. T. F. Gan, B. Q. Shentu, Z. X. Weng, *Chin. J. Polym. Sci.* **2008**, *26*, 489–494.
<https://doi.org/10.1142/S0256767908003163>
34. J. Zhao, M. Milanova, M. M. C. G. Warmoeskerken, V. Dutschk, *Colloids Surfaces A* **2012**, *413*, 273–279.
<https://doi.org/10.1016/j.colsurfa.2011.11.033>
35. M.-E. Becerra, N.-P. Arias, O.-H. Giraldo, F.-E. López-Suárez, M.-J. Illán-Gómez, A. Bueno-López, *Catalysts* **2012**, *2*, 352–367.
<https://doi.org/10.3390/catal2030352>
36. F. Klose, T. Wolff, H. Lorenz, A. Seidel-Morgenstern, Y. Suchorski, M. Piórkowska, H. Weiss, *J. Catal.* **2007**, *247*, 176–193. <https://doi.org/10.1016/j.jcat.2007.01.013>
37. B. Faure, G. Salazar-Alvarez, A. Ahniyaz, I. Villaluenga, G. Berriozabal, Y. R. De Miguel, L. Bergström, *Sci. Technol. Adv. Mater.* **2013**, *14*, 023001.
<https://doi.org/10.1088/1468-6996/14/2/023001>
38. A. A. Keller, H. Wang, D. Zhou, H. S. Lenihan, G. Cherr, B. J. Cardinale, R. Miller, Z. Ji, *Environ. Sci. Technol.* **2010**, *44*, 1962–1967. <https://doi.org/10.1021/es902987d>
39. S. Mallakpour, M. Madani, *Prog. Org. Coat.* **2015**, *86*, 194–207. <https://doi.org/10.1016/j.porgcoat.2015.05.023>
40. G. A. Farzi, R. Tayebbe, S. Naghibinasab, *Int. J. Nano Dimens.* **2015**, *6*, 67–75.

Povzetek

Nanodelce aluminijevega(III) oksida (Al_2O_3) smo pripravili z metodo obarjanja pri reakciji med raztopino amonijaka in $[(\text{NH}_4)\text{Al}(\text{SO}_4)_2 \cdot 12\text{H}_2\text{O}]$ ter nadaljnjo kalcinacijo sedimenta pri $1200\text{ }^\circ\text{C}$. Površino nanodelcev smo modificirali z oleinsko kislino (OA) in trimetoksivinilsilanom (TMVS) v o-ksilenu pri $50\text{ }^\circ\text{C}$. Nanodelce Al_2O_3 in modificirane nanodelce smo karakterizirali z naslednjimi metodami: rentgensko praškovo difrakcijo (XRD), infrardečo spektroskopijo (FT-IR), vrstično elektronsko mikroskopijo (SEM), energijsko disperzivno rentgensko spektroskopijo (EDX) in termogravimetrično analizo (TGA). S TGA smo določali množino na površino nanodelcev vezane OA (10.5%) in TMVS (8.0%). Disperzijo modificiranih nanodelcev smo raziskovali v metil metakrilatu (MMA), butilakrilatu (BuA) in stirenu (St) ter topilih kot so etanol, heksan in aceton. Najboljša disperzija nanodelcev modificiranih z OA je bila v n-heksanu, v primeru delcev modificiranih s TMVS pa v acetonu. Rezultati kažejo, da dobimo stabilno disperzijo nanodelcev modificiranih z OA v MMA in BuA (začetni odstotki nanodelcev: 5% in 2,5%). V primeru nanodelcev modificiranih s TMVS pa lahko pripravimo stabilno disperzijo v stirenu (začetni odstotek nanodelcev: 2,5%)

Scientific paper

Adsorption of Cr(III) from Aqueous Solution using Borax Sludge

Fatma Tugce Senberber,¹ Meral Yildirim,² Nevin Karamahmut Mermer²
and Emek Moroydor Derun^{2,*}

¹ Programme of Occupational Health and Safety, Atasehir Adiguzel Vocational School, Turkey

² Department of Chemical Engineering, Yildiz Technical University, Turkey

* Corresponding author: E-mail: moroydor@gmail.com, moroydor@yildiz.edu.tr,
telephone number: +90-212 3834776, fax number: +90-212 3834725

Received: 04-05-2017

Abstract

Borax sludge is the waste produced by a trommel sieve in the borax production process and is used as an adsorbent for Cr(III) removal. The effects of various parameters, including pH, initial Cr(III) concentration and contact time were investigated for batch adsorption of Cr(III). The experimental results obtained were applied to different adsorption isotherms and kinetic models.

The results indicated that the Temkin isotherm ($R^2 = 0.9749$) was most suitable to explain the adsorption characteristics of borax sludge, and the removal of Cr(III) was achieved by a physisorption process. The overall kinetic data fitted the pseudo-second order rate model ($R^2 = 0.9990$).

According to thermodynamic studies, which were carried out at different temperatures, changes in enthalpy (ΔH) and entropy (ΔS) values for Cr(III) adsorption by borax sludge were determined to be 69.395 kJ/mol and 0.276 kJ/mol K, respectively. The study implied that borax sludge could be used as an alternative adsorbent in the adsorption of Cr(III) from aqueous solutions.

Keywords: Adsorption kinetic, borax sludge, Cr (III), thermodynamic

1. Introduction

The main types of pollution, according to environmental factors, are classified as water pollution, air pollution, soil pollution, radioactive contamination and microbiological contamination.¹ Water pollution, which can be caused by sewage, solid wastes, radiation, toxic chemicals and pesticides etc., is a natural imbalance in the water environment and one of the major environmental hazards of the entire world.² Heavy metal contamination is a permanent toxic chemical pollution and has adverse effects for human health and the environment.³

Being a water-contaminating metal, chromium is ubiquitous in nature, existing as approximately 0.1 mg/m³ in the air and at 1 mg/L in unpolluted water.⁴ Therefore, exposure to chromium in high concentrations has a negative effect on fertility, the respiratory system and can also cause cancer.^{5–7} Removing chromium ions from aqueous mediums is significant for both human health and the en-

vironment. Thus, many researchers have applied various methods, including ion exchange, osmosis, foam flotation, electrolysis and surface adsorption to reduce chromium concentration under the Minimal National Standards (MINAS) upper limit for industrial wastewater, which is 0.1 mg/L.^{8,9} Adsorption is a process for removal of heavy metals that receives attention due to its ease, and its economic and efficiency advantages.

In published literature, various adsorbents have been used for the removal of the two main types of chromium ions: Cr(VI) and Cr(III), by changing adsorption parameters such as chromium concentration, adsorbent dose, pH, temperature and agitation time. Various research has been reported for chromium removal from aqueous medium using chemical, biological and industrial waste materials as adsorbents. During biosorption processes, the performances of different biological adsorbents such as chitosan, *thuja orientalis*, activated rice husk carbon, neem leaves, activated red mud, hazelnut shell activated carbon, agave

lechuguilla biomass and soya cake have been investigated for chromium adsorption.^{10–17} In many adsorption processes, layered double hydroxide, Turkish brown coals, ozonised activated carbon, acrylate-based magnetic beads and bentonite clay have been studied as chemical adsorbents.^{18–23} In addition to these studies, some industrial wastes such as fly ash and saw dust, and also Indian Rosewood timber have been preferred because of their economical usage.^{24,25}

The evaluation of borax sludge is highly important, due to the emerging amount of boron waste in Turkey, which is 600000 tons per year.^{26,27} It is envisaged that this amount will increase in future years depending on the consumption of boron sources and use of waste boron in different production processes. Storage problems and storage costs will be reduced and the polluting elements will be minimized by using boron wastes in industrial applications such as adsorption techniques.

The use of waste materials as low-cost adsorbents is attractive due to their contribution to the reduction of costs for waste disposal. Even though there have been a variety of adsorption studies performed on boron waste, chromium adsorption using boron waste has not yet been investigated.²⁸ In published literature, boron waste has been used as an adsorbent in adsorption studies for dye, cadmium (II) and zinc (II).^{29,30}

The purpose of this study is to investigate the possibility of using borax sludge as a low cost adsorbent for chromium adsorption. The adsorption performance of borax sludge was studied by varying parameters such as the contact time and the initial Cr(III) concentration. In this study, the adsorption of Cr(III) from aqueous solutions under different kinetic and equilibrium conditions was investigated in detail.

2. Experimental

2.1. Raw Material Preparation

Borax sludge, which was used as an adsorbent for removing Cr(III) ions from aqueous medium, was supplied by the Eti Mine Bandirma Boron Works (Balıkesir, Turkey). Before using the sludge in experimental studies, the adsorbent was dried in an incubator (Ecocell 111, Germany) at 105 °C for 2 hours to eliminate its moisture content. The dried adsorbent was ground with an agate mortar and sieved with a vibrating sieve-shaker (Fritsch, Germany) to produce a particle size below 90 µm. Following this preparation step, identification studies were carried out using a PANalytical Xpert Pro (PANalytical B.V., The Netherlands) X-ray diffractometer (XRD) with a Cu-K α tube and parameters of 45 kV and 40 mA. The composition of adsorbents was determined by a PANalytical Mini- μ X-ray fluorescence (XRF) spectrometer (PANalytical B.V., The Netherlands). The BET surface areas of adsorbents were measured on a Micromeritics ASAP 2020 in-

strument using N₂ adsorption after degassing the adsorbent at 300 °C for 8 hours.

A stock solution of Cr (III) was prepared by dilution of a standard chromium solution (from Cr(NO₃)₃ – supplied by Merck KGaA, Darmstadt, Germany – with double distilled water.

2.2. Adsorption Experiments

With the aim of determining the effect of pH on the removal of Cr(III), batch adsorption studies were carried out by varying the pH of the solution from 3 to 11; the contact time and initial Cr(III) concentration were set to 180 minutes and 40 mg/L, respectively. The pH of the solutions was adjusted by using 1 M NH₃ and HCl as required.

For the isotherm studies and kinetic investigations, 0.05 g of borax sludge was added to 50 mL of Cr(III) solution with varying initial Cr(III) concentrations (10–40 mg/L), and mixing was carried out for different contact times (15–180 min) at a speed of 200 rpm. The adsorption temperature was set to 20 °C. At the end of each adsorption period, the adsorbents were filtered through filter paper (Blue ribbon, Chmlab) and the residual Cr(III) concentration was analyzed by an Inductively Coupled Plasma–Optical Emission Spectrometer (ICP-OES) (Optima DV 2100, Perkin Elmer, USA). The amount of adsorbed Cr(III) after a pre-determined contact time was calculated by using the expression in Eq. (1):

$$q = \frac{C_i - C_f}{m} \times V \quad (1)$$

where q is the removal capacity of the adsorbent at equilibrium (mg/g), V is the volume of the suspension (mL), m is the weight of adsorbents (in gms), C_i and C_f are the initial and final concentrations of Cr (III) (in mg/L), respectively.³¹

For thermodynamic studies, experiments were carried out at various adsorption temperatures (20 °C, 30 °C, 40 °C and 50 °C) and equilibrium adsorption parameters.

2.3. Isothermal Analysis and Kinetic Studies

The equilibrium data were fitted to the adsorption isotherms models of Langmuir, Freundlich, Temkin, Dubinin-Radushkevich and Harkins-Jura – which give information about the adsorption process and explain the equilibrium relationship between the amount of adsorbed sample uptake and the concentration at a constant temperature – were applied to find out the effects of different initial concentrations and related times for the use of borax sludge.^{32–34}

The Langmuir isotherm, which neglects lateral interactions, was fitted to obtain the experimental quantities (Eq. (2)):

$$q_e = \frac{q_{\max} K_L C_e}{1 + K_L C_e} \times V \quad (2)$$

where q_e (mg/g) is the amount of Cr(III) adsorbed per unit mass of adsorbent, q_{max} is the maximum adsorption capacity of adsorbent (mg/g), C_e is the concentration of Cr(III) in suspension at equilibrium (mg/L) and K_L is the Langmuir constant related to the affinity of the binding sites.^{24,34} When a linear plot of $1/q_e$ versus $1/C_e$ is drawn, the values of K_L and q_{max} can be obtained from the slope and the intercept of the plot, respectively (Table 1). In Langmuir isotherms, the separation factor, R_L , is used to indicate the essential features of the isotherm. When R_L is between 0 and 1, it indicates that adsorption is favorable Eq. (3):³⁵

$$R_L = \frac{1}{1 + K_L C_i} \quad (3)$$

The Freundlich isotherm is expressed by Eq. (4):

$$q_e = K_F C_e^{1/n} \quad (4)$$

where K_F is an approximate indicator of adsorption capacity and n is a constant for the intensity of adsorption. The values of K_F and n can be determined from the plot of $\ln q_e$ versus $\ln C_e$ which are obtained by linear approximations of Eq. (4).^{31,36}

The Temkin isotherm takes into consideration the influences of some indirect interactions between adsorbent and adsorbate. The model assumes that the relationship between the decrease in adsorption heat and temperature is linear rather than logarithmic, and is affected by the surface coverage.^{37–39} The Temkin isotherm model is represented by Eq. (5) and Eq. (6):

$$q_e = B_T \ln A_T + B_T \ln C_e \quad (5)$$

$$B_T = \frac{RT}{b_i} \quad (6)$$

where B_T is the Temkin constant related to the heat of adsorption (kJ/mol), A_T is the equilibrium binding constant, R is the gas constant (8.314 J/mol K), T is the temperature (K). The values for A_T , B_T and b_i are calculated from the plot of q_e versus $\ln C_e$.

The equilibrium data were also applied to the Dubinin-Radushkevich isotherm model, which is claimed to be an empirical adaptation of the Polanyi adsorption potential theory. This isotherm model is used to estimate the porous apparent free energy and the characteristics of adsorption (physical or chemical).^{37–39} The Dubinin-Radushkevich isotherm model is represented by Eq. (7) and Eq. (8):

$$q_e = (q_m) \exp(-B\varepsilon^2) \quad (7)$$

$$\varepsilon = RT \ln\left(1 + \frac{1}{C_e}\right) \quad (8)$$

where B is the Dubinin–Radushkevich isotherm constant (mol^2/KJ^2), which gives an idea about the mean free ener-

gy E (kJ/mol) of adsorption per molecule of adsorbate during transfer of the solid to the surface from the solution (Eq. (9):

$$E = \frac{1}{\sqrt{2B}} \quad (9)$$

The values of B , q_m and E can be calculated from the slope and intercept of the plot between $\ln q_e$ versus ε^2 .

The Harkins-Jura isotherm model explains the possibility of multilayer adsorption with the existence of heterogeneous pore distribution. The Harkins-Jura isotherm model can be expressed by Eq. (10). The adsorption constants of A_H and B_H are calculated from the plot of $1/q_e^2$ versus $\log C_e$.^{37–39}

$$q_e = \sqrt{\frac{A_H}{B_H + \log C_e}} \quad (10)$$

The Lagergren pseudo-first order kinetic model, pseudo-second order kinetic model, intraparticle diffusion, and Natarajan and Khalaf models were fitted to experimental data for investigation of the kinetic parameters and mechanism of Cr(III) adsorption. The Lagergren pseudo-first order kinetic model can be expressed by Eq. (11):

$$\frac{dq_t}{dt} = k_1(q_e - q_t) \quad (11)$$

where k_1 is the pseudo-first order rate constant (min^{-1}), q_t and q_e are the amounts of adsorbed Cr(III) per unit mass of adsorbent at time t and equilibrium time (mg/g), respectively.

The pseudo-second order kinetic model is given by Eq. (12):

$$\frac{dq_t}{dt} = k_2(q_e - q_t)^2 \quad (12)$$

and k_2 is the pseudo-second order rate constant (g/mg min).

The intraparticle diffusion kinetic model, which gives information about the adsorption mechanism is described by Eq. (13):

$$dq_t = k_{id} t^{0.5} + A \quad (13)$$

In Eq. (13), q_t is the amount of adsorbed Cr(III) per unit mass of adsorbent at time t (mg/g), t is the contact time (min), k_{id} is the intraparticle diffusion rate constant ($\text{mg/g min}^{1/2}$) and A is a constant.

Natarajan and Khalaf explained the relationship between the initial concentration (C_o) and the concentration at time t (C_t). The linear approximations for the equations the Natarajan and Khalaf first order model is given by Eq. (14):⁴⁰

$$\log \frac{C_o}{C_t} = \frac{k_n}{2.303} t \quad (14)$$

The appropriate kinetic model which explains kinetics and mechanisms of Cr(III) adsorption can be determined by drawing linear plots for each kinetic model and calculation the correlation coefficient for R^2 for each model.

2. 4. Thermodynamic Studies

Different adsorption temperatures (20 °C, 30 °C, 40 °C and 50 °C) were used to predict thermodynamic parameters such as the Gibbs free energy (ΔG), enthalpy (ΔH) and entropy (ΔS) by using the following equations:

$$\Delta G = -RT \ln K_d \quad (15)$$

$$\Delta G = \Delta H - T\Delta S \quad (16)$$

$$\ln K_d = -\frac{\Delta H}{RT} + \frac{\Delta S}{R} \quad (17)$$

In the equations, K_d is the distribution coefficient of adsorbent (C_e/q_e), R is the gas constant (8.314 J/mol K), T is the adsorption temperature (K). From the plot between $\ln K_d$ and $1/T$, ΔH and ΔS can then be calculated.^{40–41}

3. Results and Discussion

3. 1. Characterization Results of Adsorbent

The XRD pattern for borax sludge is given in Fig. 1. According to the XRD results, borax sludge was identified as a mixture of dolomite (pdf. no: 00-005-0622; $\text{CaMg}(\text{CO}_3)_2$) and tinalconite (pdf. no: 00-008-0049; $\text{Na}_2\text{B}_4\text{O}_7 \cdot 5\text{H}_2\text{O}$) phases.

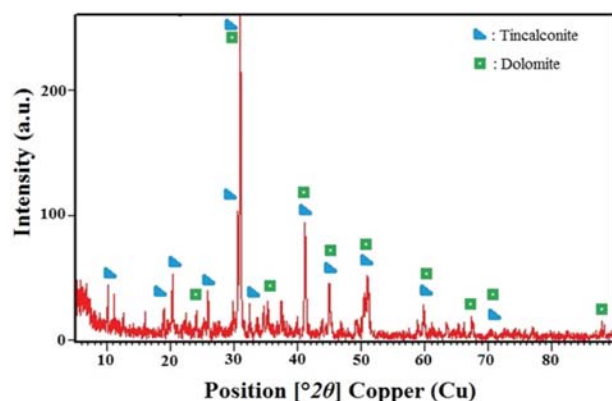


Fig. 1: XRD pattern of borax sludge

According to the XRF results, the composition of borax sludge was CaO 57.3%, MgO 22%, SiO_2 20% and K_2O 0.95%. Although having boron compounds in its composition, XRF showed an inability to measure the boron amount because of its low molecular weight.

The BET surface area for the borax sludge was determined to be 5.54 m^2/g . From the characterization re-

sults of the adsorbents, it can be seen that borax sludge has a similar chemical composition and features to pure dolomite.⁴²

3. 2. Adsorption Results

The adsorbed Cr(III) percentage is presented in Fig. 2 for various pH values. The pH of the original solution was 2, and the removal efficiency of Cr(III) showed an increase as the pH increased to 9. The increase in the adsorbed amount of Cr(III) in an alkaline environment indicated that pH values had a major effect on the adsorption mechanism.

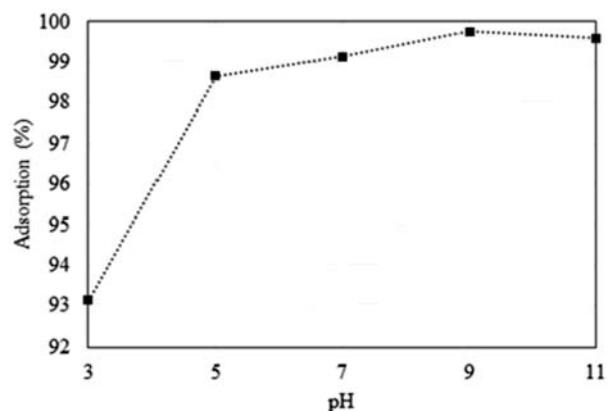


Fig. 2: Adsorption of Cr(III) produced by various pH values

The increase in removal percentage at a higher pH value can be explained by the precipitation of $\text{Cr}(\text{OH})_3$ on the borax sludge by surface adsorption.⁹ The probable removal mechanism of Cr(III) by borax sludge can be explained in three steps: (1) the dissolution of dolomite and tinalconite in the borax sludge and the formation of Ca^{2+} , Mg^{2+} and Na^+ cations; (2) the formation of $\text{Cr}(\text{OH})_3$ precipitate; (3) the cations on the adsorbent (Ca^{2+} , Mg^{2+} and Na^+) are exchanged with Cr^{3+} . According to the adsorption results, the steps of waste dissolution and $\text{Cr}(\text{OH})_3$ precipitation progress successfully in the experiments by increasing the pH values. This indicates that the adsorption mechanism proceeds well in an alkaline environment.

The results of the adsorption experiments are given in Fig. 3 by the plot of q values against t . The removal of Cr(III) increased with increasing time. In the adsorption experiments, there was a strong increase in the amount of adsorbed Cr(III) ions between 15 and 60 minutes. Maximum adsorption amounts were obtained at 120 minutes and only minor changes were observed for longer contact times. Hence, 180 minutes was assumed to be the required contact time for the equilibrium state. The changes in q values for the experiments on borax sludge adsorption can be explained by the minor differences in chemical composition of the borax sludge. The highest q value was found to be 15.986 mg/g .

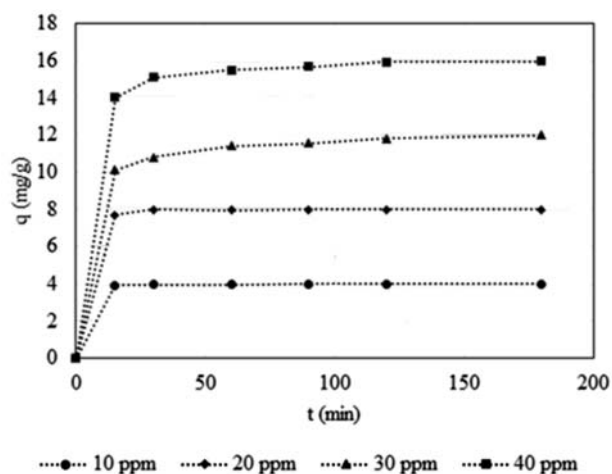


Fig. 3: Removal of Cr(III) depending on contact time

3. 3. Results of Isothermal Analyses and Kinetics

Table 1. Isotherm parameters for the adsorption of borax waste

Isotherms	Plot	Parameters	Results
Langmuir	$1/q_e$ vs $1/C_e$	q_m	24.096
		K_L	41.5
		R_L	0.0006
		R^2	0.8320
Freundlich	$\log q_e$ vs $\log C_e$	K_F	41.459
		n	2.545
		R^2	0.7876
Temkin	q_e vs $\ln C_e$	B_T	3.670
		A_T	784.631
		b_t	0.675
		R^2	0.9749
Dubinin-Radushkevich	$\ln q_e$ vs ε^2	q_m	14.756
		B	9.10^{-9}
		E	7.450
		R^2	0.8488
Harkins-Jura	$1/q_e^2$ vs $\log C_e$	A_H	30.300
		B_H	1.039
		R^2	0.5014

The adsorption results for the equilibrium state (contact time of 180 minutes and a pH value of 9) for each initial concentration were applied to various isothermal models. The results for the isothermal analysis are given in Table 1. Comparing the isotherm results, the best fitting adsorption isotherms – considering the correlation coefficient obtained for the isotherms – were in the following order: Temkin > Dubinin-Radushkevich > Langmuir > Freundlich > Harkins-Jura isotherms. The highest correlation coefficient was obtained for the Temkin isotherm model ($R^2 = 0.9749$), which shows that the Temkin isotherm was the most suitable model to explain the adsorption of Cr(III) onto borax sludge. According to the Temkin isotherm model, when the adsorbed Cr(III) amount on the sludge surface increased, the heat of adsorption decreased linearly. The Temkin isotherm assumes a low b_T (0.675) value pointing to weak interactions between the adsorbent and adsorbate, which indicates the adsorption mechanism is physical.^{37–39}

The adsorption kinetics were investigated to examine the controlling mechanism for this adsorption process. The results of the applied kinetic models are given in Table 2. The highest correlations factors were determined in the pseudo-second order kinetic model. According to the pseudo-second order kinetic equation, this adsorption is mainly controlled by the surface. K and q_e values were

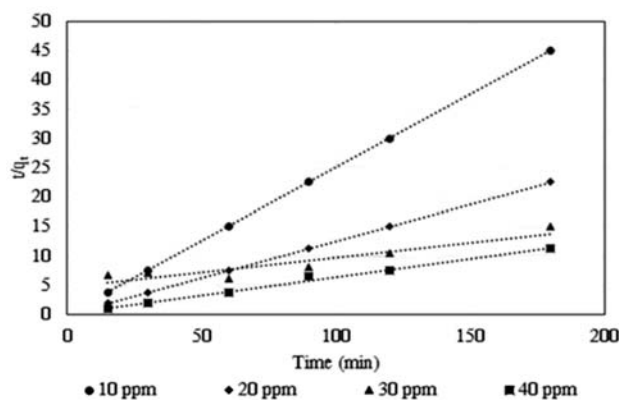


Fig. 4: Pseudo – second order kinetic plots

Table 2. Kinetic results for the adsorption process

Kinetic Model	C_0 (ppm)	10	20	30	40
		Lagergren Pseudo first order	q_e	0.1002	0.1814
	K	0.0405	0.0244	0.0302	0.0368
	R^2	0.8383	0.5940	0.9848	0.9506
Pseudo-second order	q_e	4.0012	8.0192	11.7239	16.0000
	K	4.0700	2.1353	0.0107	0.2902
	R^2	0.9990	0.9998	0.8606	0.9903
Intraparticle diffusion	K_{id}	0.0054	0.0322	1.0218	0.0961
	A	3.9317	7.6236	0.0328	14.7630
	R^2	0.8839	0.7958	0.8232	0.8877
Natarajan and Khalaf	K_n	0.0387	0.0514	0.0926	0.0454
	R^2	0.8216	0.7816	0.9563	0.9398

calculated from the relationship of t/qt versus time, and are presented in Fig. 4. K constants were found to be in the range from 4.0700 to 0.2902 for borax sludge. The q_e values obtained for borax sludge (16.000–4.001 mg/g) were compatible with previous studies which calculated the q_{\max} value of dolomite for Cr(III) removal as 10.0 mg/g (20 °C).³⁶

3. 4. Results of the Thermodynamic Studies

The thermodynamic studies were conducted on the equilibrium state (contact time of 180 minutes and a pH value of 9). The results of thermodynamic experiments for Cr(III) adsorption are presented in the plot of $\ln K_d$ versus $1/T$ (Fig. 5) and the thermodynamic parameters calculated for the adsorption process are given in Table 3.

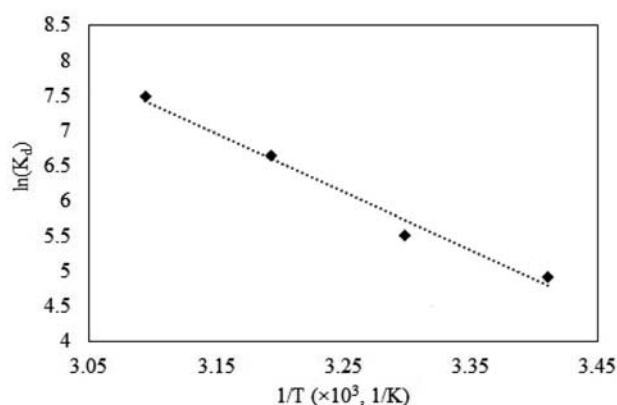


Fig. 5: Plot of $\ln K_d$ versus $1/T$ for Cr(III) adsorption by borax sludge

Table 3. Thermodynamic parameters for the adsorption process

T (K)	ΔH (kJ/mol)	ΔS (kJ/molK)	ΔG (kJ/mol)
293	69.395	0.276	-11.619
303			-14.384
313			-17.149
323			-19.914

According to Table 3, the Gibbs free energy change (ΔG) showed similarity to the experimental range of temperatures. The negative values of ΔG at different temperatures showed that adsorption of Cr(III) onto borax sludge is spontaneous, and the degree of spontaneity increases with increasing adsorption temperature. The ΔG values also confirmed that the adsorption of Cr(III) onto borax sludge is a physical process with the physical adsorption values ranging from -20 to 0 kJ/mol (while values from -80 to -400 kJ/mol describes chemical absorption).³⁰ Based on equations (15) to (17), the enthalpy (ΔH) value was determined to be 69.395 kJ/mol for borax sludge, indicating the endothermic behavior of the adsorption process.

The entropy (ΔS) value of borax sludge was found to be 0.276 kJ/mol K. The positive value of ΔS suggests the increased randomness at the solid/solution interface during the adsorption of Cr(III) onto borax sludge.^{37–39}

4. Conclusion

In this study borax sludge was used as an adsorbent for the removal of Cr(III) from waste water. To investigate the potential use of borax sludge, varying parameters, such as the contact time, the initial Cr(III) concentration, the pH and the adsorption temperature were used. Various adsorption isotherms were used to describe the observed adsorption phenomena. The Lagergren pseudo-first order kinetic model, pseudo-second order kinetic model, intra-particle diffusion and Natarajan and Khalaf models were used for investigation of the kinetic parameters and mechanism of the Cr(III) adsorption. Gibbs free energy (ΔG), enthalpy (ΔH) and entropy (ΔS) values were calculated by using the kinetic data.

This study showed that the borax sludge has been evaluated as a possible adsorbent for the removal of Cr(III) from waste water. An initial pH of 9 – where pH has a major effect on the adsorption mechanism – was found to be optimum for maximizing the Cr(III) adsorption. The adsorption is best described by the Temkin isotherm model while the adsorption mechanisms were best explained by the pseudo-second order kinetic model. ΔH and ΔS values were calculated to be 69.40 kJ/mol and 0.276 kJ/mol K for borax sludge, respectively. The negative ΔG values obtained from thermodynamic calculations confirm the feasibility of adsorption. In conclusion, borax sludge, which is readily available in Turkey, can be used as a potential adsorbent for the removal of Cr(III) from waste water.

5. References

1. M. W. Holdgate, *Cambridge University Press*, 1979.
2. S. Kolemen, N. B. Acarali, N. Tugrul, E. M. Derun and S. Piskin, *Water, Air, Soil Pollut.*, **2013**, 224, 1367. <https://doi.org/10.1007/s11270-012-1367-2>
3. C. Bolognesi, E. Landini, P. Roggeri, R. Fabbri and A. Viarengo, *Environ. Mol. Mutagen.*, **1999**, 33, 287–292. [https://doi.org/10.1002/\(SICI\)1098-2280\(1999\)33:4<287::AID-EM5>3.0.CO;2-G](https://doi.org/10.1002/(SICI)1098-2280(1999)33:4<287::AID-EM5>3.0.CO;2-G)
4. O. Kahvecioglu, G. Kartal, A. Guven and S. Timur, *Metalurgy*, **2004**, 136, 47–53.
5. A. H. Smith and C. M. Steinmaus, *Annu. Rev. Publ. Health*, **2009**, 29, 107–122. <https://doi.org/10.1146/annurev.publhealth.031308.100143>
6. A. Elbetieha and M.H. Al-Hamood, *Toxicology*, **1997**, 116, 39–47. [https://doi.org/10.1016/S0300-483X\(96\)03516-0](https://doi.org/10.1016/S0300-483X(96)03516-0)
7. W. Mertz, *J. Nutr.*, **1993**, 123, 626–633.

8. S. Rengaraj, K. H. Yeon and S. H. Moon, *J. Hazard. Mater.*, **2001**, 87, 273–287.
[https://doi.org/10.1016/S0304-3894\(01\)00291-6](https://doi.org/10.1016/S0304-3894(01)00291-6)
9. S. Debnath and U. C. Ghosh, *J. Chem. Thermodyn.*, **2008**, 40, 67–77. <https://doi.org/10.1016/j.jct.2007.05.014>
10. S. P. Ramnani and S. Sabharwal, *React. Funct. Polym.*, **2006**, 66, 902–909.
<https://doi.org/10.1016/j.reactfunctpolym.2005.11.017>
11. E. Oguz, *Colloids Surf., A*, **2005**, 252, 121–128.
<https://doi.org/10.1016/j.colsurfa.2004.10.004>
12. N. R. Bishnoi, M. Bajaj, N. Sharma and A. Gupta, *Bioresour. Technol.*, **2004**, 91, 305–307.
[https://doi.org/10.1016/S0960-8524\(03\)00204-9](https://doi.org/10.1016/S0960-8524(03)00204-9)
13. B. V. Babu and S. Gupta, *Adsorption*, **2008**, 14, 85–92.
<https://doi.org/10.1007/s10450-007-9057-x>
14. J. Pradhan, S. N. Das and R. S. Thakur, *J. Colloid Interface Sci.*, **1999**, 217, 137–141.
<https://doi.org/10.1006/jcis.1999.6288>
15. M. Kobya, *Adsorpt. Sci. Technol.*, **2004**, 22, 52–64.
16. J. R. Gonzalez, J. R. P. Videia, E. Rodriguez, S. L. Ramirez and J. L. G. Torresdey, *J. Chem. Thermodyn.*, **2005**, 37, 343–347. <https://doi.org/10.1016/j.jct.2004.09.013>
17. N. Daneshvar, D. Salari and S. Aber, *J. Hazard. Mater.*, **2002**, B94, 49–61.
[https://doi.org/10.1016/S0304-3894\(02\)00054-7](https://doi.org/10.1016/S0304-3894(02)00054-7)
18. R. L. Goswamee, P. Sengupta, K. G. Bhattacharyya and D. K. Dutta, *Appl Clay Sci.*, **1998**, 13, 21–34.
[https://doi.org/10.1016/S0169-1317\(98\)00010-6](https://doi.org/10.1016/S0169-1317(98)00010-6)
19. N. N. Das, J. Konar, M. K. Mohanta and S. C. Srivastava, *J. Colloid Interface Sci.*, **2004**, 270, 1–8.
[https://doi.org/10.1016/S0021-9797\(03\)00400-4](https://doi.org/10.1016/S0021-9797(03)00400-4)
20. F. Gode and E. Pehlivan, *Fuel Process. Technol.*, **2005**, 86, 875–884. <https://doi.org/10.1016/j.fuproc.2004.10.006>
21. J. R. Utrilla and M. S. Polo, *Water Res.*, **2003**, 37, 3335–3340. [https://doi.org/10.1016/S0043-1354\(03\)00177-5](https://doi.org/10.1016/S0043-1354(03)00177-5)
22. G. Bayramoglu and M. Y. Arica, *Chem. Eng. J.*, **2008**, 139, 20–28. <https://doi.org/10.1016/j.cej.2007.07.068>
23. S. S. Tahir and R. Naseem, *Sep. Purif. Technol.*, **2007**, 53, 312–321. <https://doi.org/10.1016/j.seppur.2006.08.008>
24. A. K. Bhattacharya, T. K. Naiya, S.N. Mandal, S. K. Das, *Chem. Eng. J.*, **2008**, 137, 529–541.
25. V. K. Garg, R. Gupta, R. Kumar and R. K. Gupta, *Bioresour. Technol.*, **2004**, 92, 79–81.
<https://doi.org/10.1016/j.biortech.2003.07.004>
26. F. Oruc, E. Sabah and Z. M. Erkan, *2nd International Boron Symposium*, **2004**.
27. Y. Erdogan and T. A. Baydır, *Journal of Science and Technology of Dumlupinar University*, **2013**, 31, 39–46.
28. A. Bhatnagar and M. Sillanpaa *Chem. Eng. J.*, **2010**, 157, 277–296. <https://doi.org/10.1016/j.cej.2010.01.007>
29. A. Olgun and N. Atar, *J. Hazard. Mater.*, **2009**, 161, 148–156. <https://doi.org/10.1016/j.jhazmat.2008.03.064>
30. N. Atar, A. Olgun and S. Wang, *Chem. Eng. J.*, **2012**, 192, 1–7. <https://doi.org/10.1016/j.cej.2012.03.067>
31. G. Qiu, Q. Xie, H. Liu, T. Chen, J. Xie and H. Li, *Appl Clay Sci.*, **2015**, 118, 107–115.
<https://doi.org/10.1016/j.clay.2015.09.008>
32. R. I. Masel, *first ed. John Wiley and Sons*, **1996**.
33. A. Dabrowski, *Adv. Colloid Interface Sci.*, **2001**, 93, 135–224. [https://doi.org/10.1016/S0001-8686\(00\)00082-8](https://doi.org/10.1016/S0001-8686(00)00082-8)
34. A. V. Tvardovskiy, *first ed. Elsevier*, **2007**.
35. A. Ghaemi, M. Torab-Mostaedi and M. Ghannadi-Maragheh, *J. Hazard. Mater.*, **2011**, 190, 916–921.
<https://doi.org/10.1016/j.jhazmat.2011.04.006>
36. V. S. Munagapati, D. Kim, *Ecotoxicol. Environ. Saf.*, **2017**, 141, 226–234.
37. R. Slimani, I. Ouahabi, A. Elmchaouri, B. Cagnon, S. Antri, S. Lazar, *Chemical Data Collections*, **2017**, 9, 184–196.
38. A. B. Albadarin, C. Mangwand, A. H. Al-Muhtaseb, G. M. Walker, S. J. Allen and M. N. M. Ahmad, *Chem. Eng. J.*, **2012**, 179, 193–202.
<https://doi.org/10.1016/j.cej.2011.10.080>
39. V. Srihari and A. Das, *Desalination*, **2008**, 225, 220–234.
<https://doi.org/10.1016/j.desal.2007.07.008>
40. M. S. Yilmaz, O. D. Ozdemir, S. Kasap and S. Pişkin, *Res. Chem. Intermed.*, **2015**, 41, 1499–1515.
41. M. S. Yilmaz, O. D. Ozdemir, and S. Pişkin, *Res. Chem. Intermed.*, **2015**, 41, 199–211.
42. I. Y. Elbeyli, *Turkish Journal of Engineering and Environmental Sciences*, **2004**, 28, 281–287.

Povzetek

Adsorpcija Cr(III) iz vodne raztopine je bila proučevana v odpadni boraksovi gošči. V šaržnem procesu so bili raziskani vplivi pH-ja, začetne koncentracije Cr(III) in kontaktnega časa. Eksperimentalni rezultati so bili obdelani z različnimi adsorpcijskimi izotermami in kinetičnimi modeli. Adsorpcijske karakteristike se da najbolje razložiti s Temkinovo izotermo ($R^2 = 0.9749$); odstranjevanje Cr(III) poteka s fizisorpcijo. Kinetični podatki pa se najbolje prilegajo hitrostnemu modelu pseudo-drugega reda ($R^2 = 0.9990$). Termodinamika procesa je bila proučevana pri različnih temperaturah. Spremembi vrednosti entalpije (ΔH) in entropije (ΔS) sta 69,40 kJ/mol in 0,276 kJ/mol K. Rezultati kažejo, da se lahko odpadna boraksova gošča uporablja kot alternativni adsorbent za odstranjevanje Cr(III) iz vodne raztopine.

Scientific paper

Effectiveness of Student Learning during Experimental Work in Primary School

Ana Logar,¹ Cirila Peklaj² and Vesna Ferik Savec³

¹ Primary school Metlika, Šolska ulica 7, 8330 Metlika, Slovenia

² Faculty of Arts, Aškerčeva 2, 1000 Ljubljana, Slovenia

³ Faculty of Education, Kardeljeva ploščad 16, 1000 Ljubljana, Slovenia

* Corresponding author: E-mail: vesna.ferik@pef.uni-lj.si

Received: 06-05-2017

Abstract

The aim of the research was to optimize the effectiveness of student learning based on experimental work in chemistry classes in Slovenian primary schools. To obtain evidence about how experimental work is implemented during regular chemistry classes, experimental work was videotaped during 19 units of chemistry lessons at 12 Slovenian primary schools from the pool of randomly selected schools. Altogether 332 eight-grade students were involved in the investigation, with an average age of 14.2 years. Students were videotaped during chemistry lessons, and their worksheets were collected afterward. The 12 chemistry teachers, who conducted lessons in these schools, were interviewed before the lessons; their teaching plans were also collected. The collected data was analyzed using qualitative methods. The results indicate that many teachers in Slovenian primary schools are not fully aware of the potential of experimental work integrated into chemistry lessons for the development of students' experimental competence. Further research of the value of different kinds of training to support teachers for the use of experimental work in chemistry teaching is needed.

Keywords: chemistry education, demonstration-based experimental work, experimental work, students' hands-on experimental work,

1. Introduction

Experimental work in chemistry curricula has an important role because it is a cornerstone of scientific literacy.^{1–5} Experimental work is essential in the teaching and learning of chemistry as it brings together several activities with different objectives, but its implementation is also a cost burden for the school. Therefore, the planning of its implementation needs to be based upon the effectiveness of the envisaged performance for achieving the learning objectives.^{6,7} This article focuses on a study of the integration of experimental work in the teaching and learning of chemistry in Slovenia from the perspective of the chemistry teachers' awareness of the potential of specific experiments integrated into chemistry lesson for the development of students' experimental competence, as well as teachers' ability to set learning objectives relevant to the teaching plan and use of learning materials related to experimental work in the classroom.

1. 1. The Role of Experimental Work in the Teaching and Learning of Chemistry

Experimental work is generally considered the main method of teaching in science education;³ therefore, it is an important building block of science education.^{8,9} Unfortunately, the teachers often use the experimental work in teaching chemistry mainly because it is required in the (national) chemistry curriculum.^{10,11} Hofstein, Kipnis, and Abrahams⁴ indicate that teachers sometimes interpret the purposes and aims for learning with experimental work differently than specified in the chemistry curriculum. Because experimental work combines experimental activities with different objectives,⁶ in the planning of such work, it is necessary to think about the effectiveness of students' foreseen activities for achieving the learning objectives.⁷

One of the main objectives of the experimental work is that students recognise a connection between observa-

tion and thinking about the observed phenomena, i.e. between the real world and the thought depicting the world. Tobin¹² stated that learning with experimental work is possible when the students can manipulate equipment and materials, and thereby simultaneously they build their knowledge of chemical concepts and related science content. Students should take advantage of experimental work to more easily understand the link between theory and the experimental activity.¹³

Unfortunately, teachers often do not think about experimental activities as a primary main asset, which provides pupils with a sensible knowledge about science. Also many teachers do not involve pupils in the experimental work in a way that would encourage the development of science concepts and do not believe that they should help pupils to develop understanding between observation and science facts.¹⁴ Abrahams and Millar⁷ found in the implementation of the experimental work that teachers are often aware only of learning of the new knowledge of chemical concepts, but not the purpose of the use of experimental work to develop understanding of scientific knowledge in general as well as the development of experimental skills.

1. 2. Effectiveness of School Experimental Work

Millar et al.⁶ proposed a four-step model for measuring the effectiveness of experimental work.

The starting point of this model is *the teacher's learning objectives (A)* or what he/she wants students to learn. This can be a specific part of the substantial subject knowledge or a specific viewpoint on the process of natural science research (e.g. collection, analysis, or interpretation of empirical evidence). Once a teacher decides on the learning objectives, the next step is *the design or the selection of experimental tasks for the learners (B)* to enable their achievement. The next stage of the model includes *consideration about what students actually do (C)* when they pursue the task. The last stage deals with *what the students actually learn (D)* during the experimental task.⁶

In this way, Millar's model distinguishes two meanings of effectiveness: (1) *effectiveness level 1* - what the teacher wanted the students to do and what students were actually able to do (comparison of steps B and C), and (2) *effectiveness level 2* - what the teacher wanted students to learn and what students actually learned (comparison of steps A and D).⁶

The important purpose of experimental work in science at school is to help students to make connections between real objects, materials, and events, and the abstract world of thoughts and ideas.⁶ According to Tiberg-hien¹⁵ experimental work intended to help students is defined as a connection between the two levels of knowledge: the level of objects and observations (o) and the level of ideas (i). Abrahams and Millar⁷ found that experimental work is appropriate for students to learn how to deal with

laboratory equipment but is less efficient in facilitating students' learning based on the collected data for the development of scientific ideas.

Properly integrated experiments in the interpretation of the new concepts facilitate the linking and understanding of three basic levels of the perception of chemical concepts: macroscopic, submicroscopic or particulate, and the symbolic level.¹⁶ Therefore, the experiment (conducted either as a demonstration or an individual or group work of students) needs to be an integral part of any interpretation of chemical content in the class.^{16,17} To support students in meaningfully connecting the results of the experimental work with the discussed chemical concepts and in learning how to present them on the symbolic and particulate level, the teachers should strive for the integration of knowledge and experimental work.¹⁸ Furthermore, Solomon¹⁹ stated that the observation of changes during the experimental work alone does not ensure students' understanding of presented concepts. Solomon¹⁹ believes that learning with experimental work is effective if students' thinking is facilitated by connecting the visual perception of phenomena with the already known science concepts.

Mancy and Reid²⁰ found that experimental work can cause an overload of information for students, accompanied by very little the actual learning (in the sense of understanding). Johnstone and Wham²¹ associated students' overload during the experimental work with the need to remember theoretical facts, names of apparatus and materials, written and oral instructions about the procedure and new skills. It is, therefore, reasonable that teachers plan experimental work in such a way that students focus on what is truly important, that they enable students to become familiar with the objectives of the experimental tasks prior to the experimental work, and that they provide students' the opportunity to discuss steps of the experimental tasks.²²

In an attempt to reduce the cognitive load of learners and simplify the experimental work, teachers began to use the written instructions according to the step-by-step principle.²³ Furthermore, in Hofstein and Lunetta's¹⁴ opinion, the role of learning tools, such as instructions (workbook or worksheet) is important in the teaching of experimental work. In their opinion, teaching materials help learners in focusing attention. Well-prepared instructions provide information about exactly how something should be done and what students need to observe, which measurements must be carried out, and what information they need to collect in order to be able to answer the questions and form the conclusions of the experimental tasks.

To recall the most important information before the experimental work, it is sometimes suggested to use pre-experimental activity,²⁴ which is perceived both as a means for reducing the workload with the information and also to interest the students in experimental work. The primary purpose of the pre-experimental activity is to focus

and prepare students for learning.²⁴ Reid and Shah²⁴ define the importance of the pre-experimental activity as encouragement for students to think during the experimental work; preparation of students for the experimental work; the guidance of students during their consideration of the procedures or chemical concepts; encouragement of students to connect the experimental work with the new concepts and previous knowledge, etc. Investigation of the effectiveness of pre-experimental activity confirmed its effectiveness and indicated that the students also form a more positive attitude towards experimental work in this way.²⁵

Abrahams and Millar⁷ propose discussing the experimental activities also in the follow-up lesson, which is defined as a post-experimental activity. Reid and Shah²⁴ propose that in the context of the post-experimental activity it is necessary to facilitate meaningful reflection on the experimental work, which can result in many benefits for the development of chemical concepts and processes. However, Abrahams and Millar⁷ note that in the case that there is a pause between the experimental activity and the discussion about the experimental work, the efficiency of the understanding of tasks decreases, so it is best to carry it out directly after the completion of the experimental work.

2. The Context and the Purpose of the Study

Experimental work has a central role in chemistry curricula at all educational levels;^{1–5} consequently, the planning and implementation of experimental work in the teaching process need to facilitate achieving the stated learning objectives. It was found that teachers sometimes interpret the purposes and aims for learning with experimental work differently than specified in the chemistry curriculum.⁴ With regard to experimental work Slovenian chemistry curriculum² indicates the objectives that are related to: (1) students' acquiring of content knowledge, (2) development of students' experimental skills and abilities, and broader (3) students' development of natural science competences. Because experimental work combines experimental activities with different objectives, it is necessary to think about the effectiveness of students' foreseen activities for achieving the learning objectives in its planning, as well the use of written materials.^{6,7}

In the present article we use the term *demonstration-based experimental work* when experimental activity is based on a frontal presentation of the experiment by the teacher or the individual student, while the remaining students observe its implementation. We use the term *students' hands-on experimental work* to denote experimental activities in which students conduct all experimental activities by themselves. In order to address the holistic potential of experimental work in supporting students' de-

velopment with regard to curriculum objectives,² the term *students' experimental competencies* is used.

The case study presented in the paper is part of a major multiple-case study,²⁶ aimed at examining teachers' concepts of learning and teaching. In particular, we focused on studying the authentic information from the school practice in Slovenia related to the implementation of experimental work in regular chemistry lessons at the primary level of education. Data collection, analysis and interpretations have been carried out within an interpretative constructivist approach.²⁷

With regard to the research aim, the following research questions (RQ) were defined:

- RQ1: Are the chemistry teachers in primary schools aware of the potential of specific experiments integrated into chemistry lesson for the development of students' experimental competences?
- RQ2: How are the worksheets used during the experimental work in chemistry lessons?
- RQ3: Is teachers' awareness of the objectives of experimental work related to students' understanding of the experimental work?

3. Method

3. 1. Sample

In September–December 2011 we invited 52 schools, based on a stratified random selection from 452 primary schools across 12 statistical regions in Slovenia (list of schools available at the homepage of Ministry of Education, Science and Sport²⁸), to collaborate in the research. Fifteen schools from different statistical regions gave a positive response to the invitation. After discussing and coordinating the terms of the research with teachers, 12 schools from five statistical regions (Osrednjeslovenska, Gorenjska, Obalno-kraška, Notranjsko-kraška, and Jugovzhodna) decided to collaborate in the research. The research collaboration included 12 chemistry teachers and a total of 332 eight-grade students, with an average age of 14.2 years; 191 students took part in lessons involving students' hands-on experimental work, while the remaining 141 students took part in lessons involving demonstration-based experimental work. To ensure anonymity, teachers' and students' data was collected by the use of code-names. In this article, the collaborating teachers are code-named by using the first 19 letters of the English alphabet from teacher A to teacher T (the letter Q is skipped), based on the nineteen recorded lessons.

3. 2. Instruments

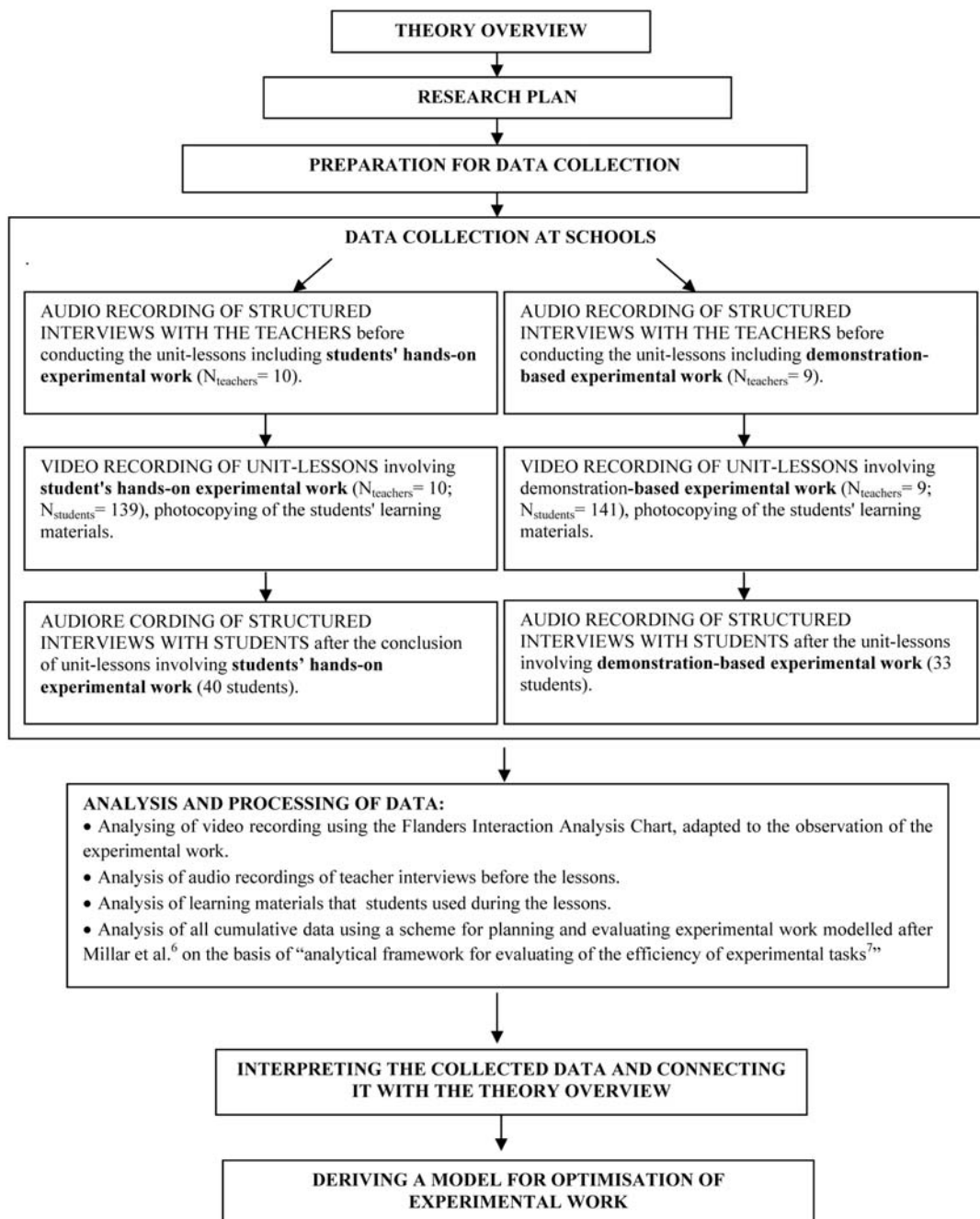
The following instruments were used for gathering the data in the interviews, which were audio recorded:

- **The Questionnaire for Teachers** is a list of four open-ended questions used in structured interviews with the

collaborating teachers before they conducted their unit-lessons with experimental work. It consists of questions about three themes: (I) *Teachers' opinion on the general objectives of experimental work in chemistry teaching*; (II) *Teachers' use of written instructions (workbook or worksheet) for students during the experimental work*; (III) *Teachers' opinion on the specific objectives of experimental work in particular chemistry lesson and students' learning during experimental work*.

• **The Questionnaire for Students** used for conducting structured interviews with the participating students after the unit-lesson including experimental work includes nine open-ended questions, to check their practical and theoretical understanding of the experimental task, and were structured into the following sections: (I) *Students' understanding of the content knowledge related to the experimental work*; (II) *Students' procedural knowledge related to the experimental work*, and (III) *Students' un-*

Research design is presented in the Scheme 1.



Scheme 1: Research design of the investigation

derstanding of the usefulness of the obtained knowledge in everyday life. In each of the sections, students were asked three questions. The questions for students varied from one unit-lesson to another as different contents were used, in particular regular unit-lessons at their school.

During video recording of the unit-lessons in chemistry classrooms four cameras were used simultaneously, thereby one camera has been placed in each of the corners of the classroom.

The full texts of the instruments can be obtained by request from the authors.

3. 3. Data Collection

In this study, we used multiple sources of data collection (individual interviews, classroom observation, and other documents) because: (a) each source provided data from a particular point of view; (b) the sources generated questions and suggestions for each other; (c) the various sources gave a variety of perspectives on particular beliefs and positions; and (d) the information obtained through one source could be cross-checked with the others.²⁹ The research proceeded through several phases; an outline of the main phases of the investigation is presented in Advance Organiser (Scheme 1).

Before starting the research, the consent of the Commission for Ethics, Faculty of Arts, University of Ljubljana was obtained. Students', teachers', and parents' consent of free and conscious decision for the participation in the survey was obtained from all participants.

We video-recorded the unit lessons at Slovenian schools during the spring of 2012. The recording took place during regular chemistry lessons, and four cameras were used simultaneously. We recorded and observed ten unit-lessons involving *students' hands-on experimental work* and nine lessons involving *demonstration-based experimental work* for a total of nineteen lessons, comprised of twenty-one classroom hours. In addition to the video recordings of 19 unit lessons, we also collected the teach-

ers' written lesson plans for the experimental work and audio-recorded interviews with teachers before conducting the unit lesson. We recorded unit lessons which lasted for one or two classroom hours, depending on the decisions of the collaborating teachers. After the recording, we randomly selected four students from each class, who were invited to take part in the interview (altogether 73 students were interviewed out of 332 participating eight-grade students – see details in Scheme 1). The interview was conducted without the presence of the teacher (only the student and the 1st author were present). We also photocopied the learning materials (the worksheet, workbook, and notebook), which these students used during the unit lesson.

The teachers could address different contents in their lessons and experiments, as the specific learning contents of the experimental work were not the object of the study. In the studied lessons, the following contents of the curriculum for chemistry in primary school² were covered: (1) particulate nature of matter ($N = 4$), chemical reactions ($N = 6$) and acids, bases and salts ($N = 9$).

3. 4. Data Analysis

The data collected was analysed in order to answer to the particular research questions as indicated in the Table 1.

Ten percent of particular data sources were independently analysed by two researchers (1st author, 3rd author) to ensure coding reliability and validity of the data.^{30,31} Their consistency in determining the categories was 91 to 95 percent. The inconsistencies between researchers were simultaneously synchronised through discussion. Eventually, the coding schemes were applied to all data.

In the analysis of the videotapes of the chemistry lesson were examined in time sequences of five seconds. For the purpose of this study, the Flanders Interaction Analysis Chart (Slovenian version by Marentič-Požarnik)³² was elaborated for observations of the students and

Table 1: Research questions and data sources analysed

	Research questions	Data sources
RQ1	Are the chemistry teachers in primary schools aware of the potential of any specific experiments integrated into chemistry lesson for the development of students' experimental competences?	<ul style="list-style-type: none"> • Audio recordings of the interviews with teachers before chemistry lessons • The teachers' unit lesson plans
RQ2	How are the worksheets used during the experimental work in chemistry lessons?	<ul style="list-style-type: none"> • Audio recordings of the interviews with teachers before chemistry lessons • Students' worksheets • Video recordings from the chemistry lessons
RQ3	Is teachers' awareness of the objectives of experimental work related to students' understanding of the experimental work?	<ul style="list-style-type: none"> • Audio recordings of the interviews with teachers before chemistry lessons • Audio recordings of the interviews with students after chemistry lessons

the teacher when conducting experimental work, in particular the teacher talk and student silence or confusion sections were adapted to the events taking place throughout the experimental work (e.g. asking questions: about the theoretical basis of the experimental work, on how to execute the experimental work tasks, about laboratory utensils, reagents, work safety, correlations between observed results of the work and already known facts, designating constants and variables in order to set a hypothesis, about the result of the work, using the results in other situations, etc.).

To determine the effectiveness of particular lessons, consequently various sources were analysed with the scheme for planning and evaluating of experimental work modelled after Millar et al.⁶ on the basis of the analytical framework for evaluating of the efficiency of experimental tasks⁷. The theoretical framework of Millar's model⁶ is in detail explained in the introductory part of the paper, accordingly the analysis was based on four steps (A – the teacher's learning objectives, B – the design or the selection of experimental tasks for the learners, C – consideration about what students actually do, D – what the students actually learn), that eventually determine the effectiveness of experimental work on level 1 (comparison of steps B and C) and the effectiveness of experimental work on level 2 (comparison of steps A and D). The rubrics developed for the purpose of the analysis can be found in the Appendices.

4. Results and Discussion

4. 1. Chemistry Teachers' Awareness of the Potential of Specific Experiments Integrated Into Chemistry Lessons for the Development of Students' Experimental Competences

Based on the interviews conducted with chemistry teachers, we determined that few teachers ($N = 3/19$) in Slovenian schools are aware of all the foreseen curriculum objectives² they could achieve using experimental work, i.e. objectives related to students' acquiring of content knowledge, development of students' experimental skills and abilities, and students' development of natural science competences.

Similarly, to what Abrahams and Millar⁷ found, also in Slovenia most teachers ($N = 9/19$) are aware of content objectives while planning the experimental work.

A typical teacher comment (Teacher D):

“During experimental work students learn to understand, where some substances dissolve and where they don't dissolve, they learn why substances dissolve based on their structure.”

Some teachers ($N = 6/19$) are in addition to content objectives also aware of the objectives related to the deve-

lopment of students' experimental skills and abilities.

A typical teacher comment (Teacher K):

“When students use hands-on experimental work, they learn to measure the temperature changes in chemical reactions and also how to correlate the changes of temperature with energy changes in chemical reactions.”

Only a few teachers ($N = 3/19$) are aware of content objectives, objectives related to the development of students' experimental skills and abilities, and objectives related to broader nature science competence, as foreseen in the curriculum.²

A typical teacher comment (Teacher R):

“I believe that the purpose of experimental work is to enable the development of students in many ways, e.g. students should learn to establish a hypothesis; create a plan for the experiment; be able to recognize and write down the utensils and chemicals needed to carry out the experiment; designate the constants and variables; carry out the experiment; observe the changes during the experiment and write down their observations. They should also develop their experimental skills and abilities, take care of safety, analyse the results, and through all of this learn new chemistry concepts and understand the processes.”

Based on the results, it seems that many teachers in Slovenian primary schools plan the integration of experimental work into lessons primarily intuitively and that many teachers are not fully aware of the potential of specific experiments integrated into chemistry lesson for the development of students' experimental competences, which agrees with the findings of other researchers.^{4, 7}

4. 2. The Use of Worksheets for Students During the Experimental Work

From the interviews with chemistry teachers, we found that for students' hands-on experimental work teachers prepare worksheets ($N = 19/19$), however, while planning demonstration-based experimental work the majority develops worksheets ($N = 17/19$). When comparing the results of the interviews with chemistry teachers and the analysis of the students' worksheets used during experimental work, we found that only a few teachers ($N = 3/19$) prepare worksheets for experimental work in accordance with their stated unit-lesson objectives in the interview.

Based on the analysis of video recordings from the chemistry lessons including experimental work and the accompanying worksheets, we see that students working with demonstration-based experimental work (Table 2) solve their worksheets better and with fewer mistakes in comparison with students doing students' hands-on experimental work (Table 3). Students taking part in demonstration-based experimental work finished 75.0–100.0% (Table 2) of all tasks on their worksheets, whereas students taking part in students' hands-on experimental work

finished 18.8–100.0% of their worksheets (Table 3). Additionally, the number of correctly solved worksheets of the students taking part in demonstration-based experimental work is 94.8% (Table 2), while for students taking part in students' hands-on experimental work, only 81.0% of them solved it entirely correctly (Table 3). Therefore, the results show an advantage of the demonstration-based experimental work, which is based on the teacher having an active role, as he leads and directs the students towards observing and efficiently recording their results.⁴

Despite the majority of teachers preparing worksheets for the students when using demonstration-based experimental work, they rarely give their students feedback after the work is finished ($N = 2/7$); when that happens, the tasks are solved with an accuracy of 95.7–100.0% ($M = 97.9%$). When the teachers do not check the worksheets, these are solved with an accuracy of 71.8–100.0% ($M = 93.5%$) (Table 2).

All teachers prepare worksheets for the students when using students' hands-on experimental work in chemistry teaching ($N = 10/10$). The high percentage of correctly solved worksheets is seen when the teacher gives students feedback about the answers on the worksheet after the work is finished. In these cases, the work percentage of worksheets solved correctly varies 75.8–100.0% ($M = 89.5%$). When the teacher does not give students feedback after the work is finished, the percentage drops down to a range of 43.9–95.1% ($M = 75.3%$) (Table 3).

On the basis of the results, we can conclude that the students follow the instructions of the teacher well and accomplish the predicted assignments required to be followed during experimental work. However, all teachers are not aware of all the objectives of experimental work (as found in RQ1); therefore, they do not include these objectives into their worksheets, and, in these cases, the students also do not achieve all the objectives that they could.

Table 2: Analysis of collected data when evaluating the worksheets, the students used during demonstration-based experimental work.

Students solving worksheets while taking part in demonstration-based experimental work			
Teachers	Solved worksheets [%]	Correctly solved worksheets*[%]	Teacher checks the worksheet at the end of the experimental work.
Teacher A	97.2	100.0	yes
Teacher B	100.0	100.0	no
Teacher C	93.6	71.8	no
Teacher H	96.3	95.7	yes
Teacher I	75.0	100.0	no
Teacher J	83.3	100.0	no
Teacher O	88.2	95.8	no
Teacher S	No worksheet	/	/
Teacher T	No worksheet	/	/
Average value	90.5	94.8	

*Percentage of correctly solved worksheet among solved worksheets.

Table 3: Analysis of collected data when evaluating the worksheets, the students used during students' hands-on experimental work.

Students solving worksheets while taking part in demonstration-based experimental work			
Teachers	Solved worksheets [%]	Correctly solved worksheets*[%]	Teacher checks the worksheet at the end of the experimental work.
Teacher D	100.0	75.8	yes
Teacher E	18.8	87.9	no
Teacher F	100.0	82.1	yes
Teacher G	68.3	43.9	no
Teacher K	97.5	100.0	yes
Teacher L	65.0	90.4	no
Teacher M	100.0	100.0	yes
Teacher N	40.0	61.4	no
Teacher P	100.0	72.9	no
Teacher R	98.1	95.1	no
Average value	78.8	81.0	

*Percentage of correctly solved worksheets among all the solved worksheets.

4. 3. Relation Between Teachers' Awareness of the Objectives of Experimental Work and the Students Understanding of the Experimental Work

Based on the analysis of interviews with the teachers and students in accordance with the scheme modelled after Millar et al.,⁶ we can summarise that the teachers' awareness of the objectives of experimental work affects the students understanding of the experimental work (effectiveness of experimental work level 2). This is the most noticeable for the teachers who are fully aware of all the objectives of experimental work as stated in the curriculum.²

When planning demonstration-based experimental work (Table 4), we found out the teacher ($N = 1/9$) who is fully aware of all the objectives of experimental work has students who understand experimental work in 100.0% of their cases have appropriate skills and abilities in 89% of their cases. We found that teachers ($N = 8/9$) who are not fully aware of all the objectives of experimental work have students who understand experimental work in 0.0–50.0% ($M = 29.6%$) of the cases and have appropriate experimental skills and abilities in 16.7–70.8% of the cases ($M = 47.7%$).

Regarding *students' hands-on experimental work*, we can see in Table 5 that teachers ($N = 2/10$) who are fully aware of all of the objectives of experimental work have students, who understand experimental work in 50.0–75.0% ($M = 62.5%$) of the cases and have appropriate experimental skills and abilities in 62.5–79.2% ($M = 70.9%$) of the cases. However, when planning students' hands-on experimental

work, we found that teachers ($N = 8/10$) who are not fully aware of all the objectives of experimental work have students who understand experimental work in 12.5–75.0% ($M = 31.3%$) of the cases and have appropriate experimental skills and abilities in 50–66.7% ($M = 59.1%$) of the cases.

It can be concluded that the teacher's holistic awareness of the objectives of experimental work is connected with the knowledge of the students both in demonstration-based experimental work and in students' hands-on experimental work. Therefore, it is essential that during experimental work teachers help their students understand the connection between the practical activity, which represents the macro level and the theory, which represents the particulate/symbolic level. This causes the students many problems, as it is difficult for them to connect their observations and nature science concepts and apply them to experimental data and the experiment's conclusion.

5. Conclusions and Implications for School Practice

The research has indicated that many teachers in Slovenian primary schools plan the integration of experimental work into lessons primarily intuitively and that many teachers are not fully aware of the potential of specific experiments integrated into chemistry lessons for the development of students' experimental competences, which is a novel research finding for Slovenian school practice, but has been found also in other countries.^{4,7,33} It was found, that in Slovenia about a half chemistry teach-

Table 4: Analysis of collected data when evaluating the knowledge of students when the teacher is/is not aware of all the objectives of demonstration-based experimental work.

Teachers' answers in the interview before the unit-lesson about the objectives of experimental work:		Correct student answers in the interview after the unit lesson about:		
		Understanding of the content knowledge related to the experimental work [%]	Understanding of the procedural knowledge related to the experimental work [%]	Understanding of the usefulness of the obtained knowledge in everyday life [%]
The teacher is aware of: (1) achieving content objectives.	Teacher A	50.0	70.8	25.0
	Teacher B	37.5	58.3	50.0
	Teacher C	20.0	40.0	20.0
	Teacher S	12.5	16.7	0.0
	Teacher T	33.3	38.9	16.7
The teacher is aware of: (1) achieving content objectives and (2) objectives related to experimental skills and abilities.	Teacher H	0.0	50.0	0.0
	Teacher I	50.0	62.5	25.0
	Teacher J	33.3	44.4	0.0
The teacher is aware of: (1) achieving content objectives, (2) objectives related to experimental skills and abilities, and (3) objectives related to broader nature science competence.	Teacher O	100.0	89.0	75.0

Table 5: Analysis of collected data when evaluating the knowledge of students, when the teacher is/is not aware of all the objectives of students' hands-on experimental work.

Teachers' answers in the interview before the unit lesson about the objectives of experimental work:		Correct student answers in the interview after the unit lesson about:		
		Understanding of the content knowledge related to the experimental work [%]	Understanding of the procedural knowledge related to the experimental work [%]	Understanding of the usefulness of the obtained knowledge in everyday life [%]
The teacher is aware of: (1) achieving content objectives.	Teacher D	25.0	52.2	0.0
	Teacher E	25.5	66.7	25.0
	Teacher F	37.5	62.3	25.0
	Teacher G	12.5	54.2	0.0
The teacher is aware of: (1) achieving content objectives and (2) objectives related to experimental skills and abilities.	Teacher K	37.5	50.0	0.0
	Teacher L	25.0	66.7	0.0
	Teacher M	75.0	66.7	25.0
The teacher is aware of: (1) achieving content objectives and (3) objectives related to broader nature science competence.	Teacher N	12.5	54.2	37.5
The teacher is aware of: (1) achieving content objectives, (2) objectives related to experimental skills and abilities, and (3) objectives related to broader nature science competence.	Teacher P	50.0	62.5	0.0
	Teacher R	75.0	79.2	25.0

hers are aware of the content objectives while planning the experimental work, but only about one third is also aware of the objectives related to the development of students' experimental skills and abilities. Surprisingly, only few teachers (about one sixth of the teachers in our sample) is aware also of the objectives related to broader nature science competence, as foreseen in the chemistry curriculum.² Additionally, in defining objectives of experimental work, it is sensible to keep in mind the potential of using experimental work to motivate students;^{4,8,13,16,35–37} to popularize the natural sciences;^{4,13,38} and to facilitate students' ability to communicate.^{13,35,38} When selecting the content of the experimental work in accordance with the objectives of experimental work, the teachers should strive for the tasks to be based on either the students' experiences or everyday life^{38,40–43} and select an appropriate form of experimental work based on its objectives (demonstration-based experimental work/students' hands-on experimental work).^{4,13,24,46}

A novel finding for Slovenian school environment derived from the presented research is also, that the majority of students can follow the instructions of the chemistry teacher well and accomplish the predicted assignments required to be followed during experimental work (effectiveness level 1). Therefore, it is essential that teachers understand how important it is, that they develop adequate written instructions for students' chemical experimental work both in demonstration-based work and in students' hands-on work. Namely, it was found, that in ca-

ses, where the teachers are not aware of all the possible objectives of experimental work and consequently that they neglect including these objectives into their worksheets, the students also cannot achieve all of the possible objectives that they could (effectiveness level 2). The importance of thoughtful preparation of learning materials for students in accordance with the selected objectives for experimental work has been pointed out also by other researchers, who indicate, that it is important, e.g. to list and name the accessories/laboratory utensils in the learning materials (names, symbolic notation, warning pictograms);^{17,35,45} that the materials include tasks to check the understanding of the experimental work using all three levels (macroscopic, particulate, symbol level);^{13,14,16,44} and to take into consideration the appropriate amount of tasks based on the different levels of Bloom's taxonomy.^{17,45,49–51}

For the improvement of the quality of experimental work in Slovenian primary school practice, it seems important, that in the future more attention is devoted to the development of pre-service and in-service teachers' understanding of the holistic perspective of the objectives for particular experimental work integrated into chemistry lesson. Although in last decades substantial efforts have been devoted to chemistry teachers' development of an understanding about students' development through implementation of the curriculum framework^{1,2,34,47} and the use of experimental work in chemistry teaching,^{16,17,48,52–53} further research of the value of different

kinds of training to support pre- and in-service teachers in their development for the use of experimental work in chemistry teaching is necessary.

6. References

1. A. Bačnik, A., Bukovec, N., Poberžnik, A., Požek Novak, T., Keuc, Z., Popič, H., Vrtačnik, M., in: N. Purkat (Ed.): Učni načrt. Program gimnazija. Kemija, Ministrstvo za šolstvo in šport, Zavod RS za šolstvo, Ljubljana, **2008**, 59p.
2. A. Bačnik, N. Bukovec, M. Vrtačnik, A. Poberžnik, M. Križaj, V. Stefanovik, K. Sotlar, S. Dražumerič: in S. Preskar (Ed.): Učni načrt. Program osnovna šola. Kemija, Ministrstvo za šolstvo in šport, Zavod Republike Slovenije za šolstvo, Ljubljana, **2011**, 31p.
3. I. Abrahams, M. J. Reiss, *J. Res. Sci. Teach.* **2012**, *49*, 1035–1055. <https://doi.org/10.1002/tea.21036>
4. A. Hofstein, M. Kipnis, I. Abrahams, in: I. Eilks, A. Hofstein (Eds.): Teaching chemistry – A studybook, Sense Publishers, Rotterdam, **2013**, pp. 153–182. https://doi.org/10.1007/978-94-6209-140-5_6
5. L. Brian, *Chem. Educ. Res. Pract.* **2014**, *15*, 35–46. <https://doi.org/10.1039/C3RP00122A>
6. R. Millar, J-F. Le Maréchal, A. Tiberghien, in: J. Leach, A. Paulsen (Eds.): Practical work in science education, Roskilde University Press/Kluwer, Roskilde/Dordrecht, The Netherlands, 1999, pp. 33–59.
7. I. Abrahams, R. Millar, *Int. J. Sci. Educ.* **2008**, *30*, 1945–1969. <https://doi.org/10.1080/09500690701749305>
8. D. Lowe, P. Newcombe, B. Stumpers, *Res. Sci. Educ.* **2013**, *43*, 1197–1219. <https://doi.org/10.1007/s11165-012-9304-3>
9. R. Millar, in: J. Osborne, J. Dillon (Eds.): Good practice in science teaching: What research has to say, Open University Press, Maidenhead, **2011**, pp. 108–134.
10. J. Wellington, in: J. Wellington (Ed.): Practical work in science: Which way now?, Routledge, London, **1998**, pp. 3–15. <https://doi.org/10.4324/9780203267059>
11. I. Abrahams, M. J. Reiss, R. Sharpe, *Res. Sci. Technol. Educ.* **2014**, *32*, 263–280. <https://doi.org/10.1080/02635143.2014.931841>
12. K. Tobin, *Sch. Sci. Math.* **1990**, *90*, 403–418. <https://doi.org/10.1111/j.1949-8594.1990.tb17229.x>
13. R. Millar, The role of practical work in the teaching and learning of science, Commissioned paper-Committee on High School Science Laboratories: Role and Vision. National Academy of Sciences, Washington DC, **2004**, 22p.
14. A. Hofstein, V. N. Lunetta, *Sci. Educ.* **2004**, *88*, 28–54. <https://doi.org/10.1002/scs.10106>
15. A. Tiberghien, in: R. Millar, J. Leach, J. Osborne (Eds.): Improving science education: The contribution of research, Open University Press, Buckingham, UK, **2000**, pp. 27–47.
16. M. Vrtačnik, S. A. Glažar, V. Ferk Savec, V. Pahor, Z. Keuc, in: V. Sodja, (Eds.): Kako uspešneje poučevati in se učiti kemijo?: monografija za učitelje kemije – mentorje, Faculty and Schools Partnership, Faculty of Chemistry and Chemical Technology, Department of Chemistry, Ljubljana, **2005**, 74p.
17. A. Logar, V. Ferk Savec, in: M. Orel (Ed.): Sodobni pristopi poučevanja prihajajočih generacij, Eduvision, Polhov Gradec, **2014**, pp. 235–244.
18. D. Denby, Practical work: a new opportunity, <http://www.rsc.org/eic/2015/09/practical-lab-work-skillsdevelopment>, (assessed: March 25, 2016).
19. J. Solomon, in: J. Leach, A. Paulsen (Eds.): Practical work in science education-Recent research studies, Roskilde University Press/Kluwer, Roskilde/Dordrecht, The Netherlands, **1999**, pp. 60–74.
20. R. Mancy, N. Reid, Aspects of Cognitive Style and Programming, 16th Workshop of the Psychology of Programming Interest Group, Carlow, Ireland, **2004**, pp. 1–9.
21. A. H. Johnstone, A. J. B. Wham, *Educ. Chem.* **1982**, *19*, 71–73.
22. F-J. Scharfenberg, F. X. Bogner, *Int. J. Sci. Educ.* **2010**, *32*, 829–844. <https://doi.org/10.1080/09500690902948862>
23. J. Carnduff, N. Reid, Enhancing undergraduate chemistry laboratories. Pre-laboratory and post-laboratory exercises, Royal Society of Chemistry, London, **2003**.
24. N. Reid, I. Shah, *Chem. Educ. Res. Pract.* **2007**, *8*, 172–185. <https://doi.org/10.1039/B5RP90026C>
25. G. M. McKelvy, *Univ. Chem. Educ.* **2000**, *4*, 46–49.
26. R. K. Yin, Case study research: Design and methods, Sage, London, **2013**, 312p.
27. E. G. Guba, Y. Lincoln, in: N. Denzin, Y. Lincoln (Eds.): Handbook of qualitative research, Sage, Newbury Park, **1994**, pp. 105–117.
28. Ministry of Education, Science and Sport, Seznam osnovnih šol, <https://krka1.mss.edus.si/registriweb/Seznam1.aspx?Seznam=2010> (assessed: July 19, 2016).
29. E. Zimmermann, J. K. Gilbert, *Educ. Res. Eval.* **1998**, *4*, 213–234. <https://doi.org/10.1076/edre.4.3.213.6955>
30. R. Popping, *Qual. Quant.* **2010**, *44*, 1067–1078. <https://doi.org/10.1007/s11135-009-9258-3>
31. J. M. Morse, M. Barrett, M. Mayan, K. Olson, J. Spiers, *Int. J. Qual. Methods* **2002**, *1*, 13–22. <https://doi.org/10.1177/160940690200100202>
32. B. Marentič-Požarnik, Nova pota v izobraževanju učiteljev, Državna založba Slovenije, Ljubljana, **1987**, pp 39.
33. D. Hodson, Research on practical work in school and university: in pursuit of better questions and better methods (pp. 25-26), Proceedings of the 6th European Conference on 571 Research in Chemical Education, Portugal: University of Aveiro, **2001**.
34. RIC – Državni izpitni center, http://www.ric.si/preverjanje_znanja/statisticni_podatki/, (assessed: July 19, 2016).
35. D. W. Johnson, R. T. Johnson, Learning together and alone: Cooperative, competitive and individualistic learning. New Jersey: Englewood Cliffs, **1987**, 242p.
36. A. H. Johnstone, A. Al-Shuaili, *Univ. Chem. Educ.* **2001**, *5*, 42–51.
37. J. Bennett, Teaching and learning science: A guide to recent research and its applications. London: Continuum Studies in

- Research in Education, **2003**, 316p.
38. D. Hodson, *Sch. Sci. Rev.* **1990**, *71*, 33–40.
39. G. Kidman, *Eurasia* **2012**, *8*, 35–47.
40. R. Artdej, *Procedia Soc. Behav. Sci.* **2012**, *46*, 5058–5062.
<https://doi.org/10.1016/j.sbspro.2012.06.385>
41. V. Albe, *Res Sci Educ.* **2008**, *38*, 67–90.
<https://doi.org/10.1007/s11165-007-9040-2>
42. R. Marks, I. Eilks, *Int. J. Env. Sci. Ed.* **2009**, *4*, 231–245.
43. R. Marks, I. Eilks, *Chem. Educ. Res. Pract.* **2010**, *11*, 129–141.
<https://doi.org/10.1039/C005357K>
44. V. Ferk Savec, Š. Hrast, I. Devetak, G. Torkar, *Acta Chim. Slov.* **2016**, *63*, 864–873.
<https://doi.org/10.17344/acsi.2016.2835>
45. B. Šket, S. A. Glažar, J. Vogrinc, *Acta Chim. Slov.* **2015**, *62*, 462–472. <https://doi.org/10.17344/acsi.2014.1148>
46. E. Kaya, P. S. Cetin, *IJONTE* **2012**, *3*, 90–98.
47. M. Vrtačnik, Smisel kurikularne prenove kemije, Zavod Republike Slovenije za šolstvo, Maribor, **1998**, pp. 11–13.
48. A. Logar, V. Ferk Savec, in: M. Orel (Ed.): Sodobni pristopi poučevanja prihajajočih generacij, Eduvision, Polhov Gradec, **2013**, pp. 190–198.
49. V. N. Lunetta, A. Hofstein, M. P. Clough, in: S. K. Abell, N. G. Lederman (Eds.): Handbook of research on science education, Erlbaum, Mahwah, **2005**, pp. 339–442.
50. A. Tiberghien, in: J. Leach, A. C. Paulsen (Eds.): Practical Work in Science Research - Recent Research Studies, Roskilde University Press, Frederiksberg, **1999**, pp. 176–194.
51. J. K. Gilbert, D. F. Treagust, in: J. K. Gilbert, D. F. Treagust (Eds.): Multiple Representations in Chemical Education, Models and Modeling in Science Education 4, Springer Netherlands, **2009**, pp. 1–8.
<https://doi.org/10.1007/978-1-4020-8872-8>
52. A. Logar, V. Ferk Savec, in: M. Orel (Ed.): Sodobni pristopi poučevanja prihajajočih generacij, Eduvision, Polhov Gradec, **2012**, pp. 216–226.
53. A. Logar, V. Ferk Savec, *Acta Chim. Slov.* **2011**, *58*, 866–875.

Povzetek

Namen predstavljene raziskave je bil izboljšati učinkovitost učenja ob uporabi eksperimentalnega dela pri pouku kemije v slovenskih osnovnih šolah. Preučevali smo, kako se eksperimentalno delo izvaja pri rednem pouku kemije, in sicer je bilo posnetih 19 učnih enot rednega pouka kemije na 12 slovenskih osnovnih šolah, ki so bile naključno izbrane iz seznama šol iz celotne države. Skupno je bilo vključenih 332 osmošolcev, s povprečno starostjo 14,2 let. Učenci so bili posneti med poukom kemije, zbrani pa so bili tudi njihovi delovni listi, ki so jih reševali med eksperimentalnim delom. Z učitelji kemije, ki so izvedli pouk v teh šolah, so bili opravljeni intervjuji, prav tako so bili zbrane njihove učne priprave. Pridobljeni podatki so bili analizirani z uporabo kvalitativnih metod. Rezultati kažejo, da se mnogi učitelji v slovenskih osnovnih šolah v celoti ne zavedajo potenciala eksperimentalnega dela pri poučevanju kemije. Potrebne so nadaljnjše študije, s katerimi bo preučena vrednost različnih oblik izobraževanja v podporo učiteljem pri nadaljnjem razvoju na področju uporabe eksperimentalnega dela pri pouku kemije.

Scientific paper

Bismuth(III) Complexes with Bis(dimethylphenyl) Dithiophosphates: Synthesis, Characterization and Crystal Structure of $[\{(3,5\text{-CH}_3)_2\text{C}_6\text{H}_3\text{O}\}_2\text{PS}_2]_3\text{Bi}$

Ruchi Khajuria,¹ Sandeep Kumar,¹ Mandeep Kour,¹ Atiya Syed,¹
Geeta Hundal² and Sushil K. Pandey^{1,*}

¹ Department of Chemistry, University of Jammu, Baba Saheb Ambedkar Road,
Jammu–180006 (J & K), India

² Department of Chemistry, Guru Nanak Dev University, Amritsar-143005, India

* Corresponding author: E-mail: kpsushil@rediffmail.com

Received: 16-05-2017

Abstract

This work presents four complexes with general formula $[(\text{ArO})_2\text{PS}_2]_3\text{Bi}$ (**1–4**), where Ar = 2,4-(CH₃)₂C₆H₃, 2,5-(CH₃)₂C₆H₃, 3,4-(CH₃)₂C₆H₃ and 3,5-(CH₃)₂C₆H₃, respectively. Reaction of $[(\text{ArO})_2\text{PS}_2\text{Na}]$ with $\text{Bi}(\text{NO}_3)_3 \cdot 5\text{H}_2\text{O}$ in toluene in 3:1 molar stoichiometry afforded the complexes $[(\text{ArO})_2\text{PS}_2]_3\text{Bi}$. These newly synthesized complexes have been characterized by elemental analysis, FT-IR and multinuclear NMR (¹H, ¹³C and ³¹P) NMR. The crystal structure of $[\{(3,5\text{-CH}_3)_2\text{C}_6\text{H}_3\text{O}\}_2\text{PS}_2]_3\text{Bi}$ (**4**) has been determined by X-ray crystallography. The compound crystallizes in monoclinic *P2₁/c* space group and Bi(III) centre is surrounded by six sulfur atoms from three symmetrically chelating bidentate diphenyl dithiophosphate ligands in a distorted octahedron environment. Screening these complexes for their antifungal activity against *Penicillium chrysogenum* gave positive results.

Keywords: Bi(III) Complexes; X-ray; Dithiophosphate; Fungicidal

1. Introduction

Dithiolates of bismuth have attracted much interest due to their diverse structural features ranging from discrete monomer to polymeric supramolecular assemblies.^{1–8} Low lability⁹ and greater thermodynamic stability^{10,11} of Bi–S compounds as compared to Bi–O compounds has resulted into their wide applicability in medicine and biology.^{12,13} Due to its non-toxic and non-carcinogenic nature, the use of bismuth compounds in medicine can be traced back to the middle ages,¹⁴ although less consideration has been paid to bismuth chemistry in comparison with that of rest of the members of group 15 elements. In addition, chemistry of bismuth compounds has advanced considerably due to its potential in applications as precursors in material sciences,^{15–27} as X-ray imaging agents²⁸ and as catalysts.²⁹ Further interest in the study of these compounds lies in their significance in medicinal chemistry. The major medicinal applications of bismuth compounds are associated with the treatment of gastrointestinal disorders, antitumor,

antimicrobial and antibacterial activity.^{30–36} Recently, with increasing environmental concerns and the need for ‘green reagents’, the interest in environmentally acceptable heavy metal and its compounds has increased tremendously in the last decade. The synthesis of coordination compounds with dithiophosphate ligand has been in the center of interest in chemical research for many years.^{37–43} Some Bi(III) complexes containing dithiophosphate ligand, such as $[\text{Bi}\{\text{S}_2\text{P}(\text{OC}_6\text{H}_4\text{Me-m})_2\}_3]$,⁴⁴ $[\text{Bi}\{\text{S}_2\text{P}(\text{i-C}_3\text{H}_7\text{O})_2\}_3]$,⁴⁵ have been reported previously. In addition to the above, there are myriad of bismuth compounds with short bite sulfur ligands for which X-ray structures are known e.g. $[\text{Bi}\{\text{S}_2\text{P}(\text{C}_6\text{H}_5)_2\}_3]$,⁴⁶ $[\text{Bi}(\text{S}_2\text{PET}_2)_3 \cdot \text{C}_6\text{H}_6]$,⁴⁷ $[\text{Bi}(\text{S}_2\text{PMe}_2)_3]$,⁴⁸ $[\text{Bi}(\text{S}_2\text{PET}_2)_3]$,⁴⁹ $[\text{Bi}(\text{S}_2\text{COPr}^t)_3]$,⁵⁰ and $[\text{Bi}(\text{S}_2\text{CNET}_2)_3]$.⁵¹

Bismuth, because of its large size, and the phosphorodithioate ligand, because it incorporates tetrahedral S_2PO_2 rather than planar S_2CN or S_2CO , were considered as logical candidates suitable for study. In the above perceptible it was considered worthwhile to prepare similar new dithiophosphate complexes and to study their structure

ral features with an aim of identifying new structural motifs. In the present communication, we describe the syntheses of a new mononuclear bismuth(III) complexes containing the disubstituted diphenyl dithiophosphate ligand. In addition, the structure of the complex **4** has been determined by X-ray diffraction. In addition to the physico-chemical studies, the compounds **1–4** have also been tested *in vitro* to assess their antifungal activities against common reference fungi, and the results were compared with similar doses of commercial antibiotic, namely ciprofloxacin.

2. Experimental

2.1. Reagents, Materials and Measurements

Owing to extremely hydrolysable nature of the starting materials as well as the newly synthesized compounds, stringent precautions were taken to exclude atmospheric moisture throughout all the experimental manipulations. All chemicals were procured from Aldrich. Solvents were freshly distilled according to standard procedures. The characterization of the novel bismuth complexes has been done by elemental analyses, FTIR and NMR spectroscopy. C, H and S microanalysis were obtained with a CHNS/O Vario EL-III full-automatic Elemental Analyser (Indian Institute of Integrative Medicine, Jammu). Bismuth was estimated gravimetrically as BiOI.⁵² The infrared spectra were recorded on a Perkin Elmer spectrum RX1 FT-IR spectrophotometer (Sophisticated Analytical Instrumentation Facility, Panjab University, Chandigarh) using KBr discs. ¹H and ¹³C{¹H} NMR in solution were recorded on a Bruker Avance III 400 MHz. ¹H and ¹³C NMR spectra of the complexes were measured in CDCl₃ solution with reference to an internal TMS. All chemical shifts are reported in δ units downfield from Me₄Si. ³¹P{¹H} NMR spectra were run, relative to external H₃PO₄ (85%), with a Bruker Avance III 400 MHz. NMR Spectral was carried out at the Department of Chemistry, University of Jammu, Jammu. The sodium salts of disubstituted *O,O'*-diphenyldithiophosphates *i.e.* {(2,4-CH₃)₂C₆H₃O}₂PS₂Na (**L1**), {(2,5-CH₃)₂C₆H₃O}₂PS₂Na (**L2**), {(3,4-CH₃)₂C₆H₃O}₂PS₂Na (**L3**) and {(3,5-CH₃)₂C₆H₃O}₂PS₂Na (**L4**) were synthesized following a previously reported procedure.³⁷

2.2. Synthesis of [(2,4-CH₃)₂C₆H₃O]₂PS₂]₃Bi (1)

The bismuth complex was prepared by adding toluene suspension (25 mL) of the ligand **L1** (1.00 g, 2.77 mmol) to the weighed amount of Bi(NO₃)₃ · 5H₂O (0.44 g, 0.90 mmol) in toluene (25 mL) while stirring continuously at room temperature for 4 hours during which the solution color changes to yellow. Excess of solvent was removed by filtration using an alkoxy funnel fitted with a

G-4 disc under reduced pressure, which resulted in the complex **1** as a yellow crystalline solid. Yield: 0.99 g (90%). FTIR (KBr, cm⁻¹): 1117 s [ν (P)–O–C], 870 s [ν P–O–(C)], 673 s [ν P–S]_{asym}, 580 m [ν P–S]_{sym}, 256 w [ν Bi–S]. ¹H NMR (CDCl₃, ppm): 2.30 (s, 18H, 2–CH₃), 2.39 (s, 18H, 4–CH₃), 6.89 (d, $J_{\text{HH}} = 8$ Hz, 6H, H₆), 7.02 (d, $J_{\text{HH}} = 8$ Hz, 6H, H₅), 7.22 (s, 6H, H₃); ¹³C NMR (CDCl₃, ppm): 17.27 (s, 2–CH₃), 21.49 (s, 4–CH₃), 121.05 (C₆), 127.28 (C₂–CH₃), 128.25 (C₅), 129.06 (C₄–CH₃), 130.22 (C₃), 147.20 (C₁–O); ³¹P NMR (CDCl₃, ppm): 94.15 (s). Anal. Calcd. for C₄₈H₅₄P₃S₆O₆Bi: C, 47.21; H, 4.46; S, 15.75; Bi, 17.11%. Found: C, 47.19; H, 4.43; S, 15.70; Bi, 16.97%.

2.3. Synthesis of [(2,5-CH₃)₂C₆H₃O]₂PS₂]₃Bi (2)

The same synthetic procedure as for complex **1** was used for complex **2**, except that ligand **L2** (1.00 g, 2.77 mmol) was used instead of **L1**. Yield: 1.01 g (92%). FTIR (KBr, cm⁻¹): 1024 s [ν (P)–O–C], 855 s [ν P–O–(C)], 682 s [ν P–S]_{asym}, 562 m [ν P–S]_{sym}, 255 w [ν Bi–S]. ¹H NMR (CDCl₃, ppm): 2.31 (s, 18H, 2–CH₃), 2.34 (s, 18H, 5–CH₃), 7.23 (d, $J_{\text{HH}} = 7.6$ Hz, 6H, H₃), 7.16 (d, $J_{\text{HH}} = 7.6$ Hz, 6H, H₄), 6.49 (s, 6 H, H₆); ¹³C NMR (CDCl₃, ppm): 15.03 (s, 2–CH₃), 21.21 (s, 5–CH₃), 120.38 (C₆), 120.98 (C₄), 128.04 (C₂–CH₃), 130.74 (C₃), 134.75 (C₅–CH₃), 155.93 (C₁–O); ³¹P NMR (CDCl₃, ppm): 94.36 (s). Anal. Calcd. for C₄₈H₅₄P₃S₆O₆Bi: C, 47.21; H, 4.46; S, 15.75; Bi, 17.11%. Found: C, 47.17; H, 4.39; S, 15.72; Bi, 16.95%.

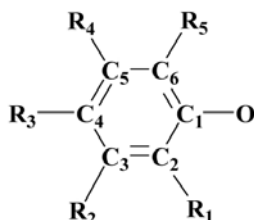
2.4. Synthesis of [(3,4-CH₃)₂C₆H₃O]₂PS₂]₃Bi (3)

The same synthetic procedure as for complex **1** was used for complex **3**, except that ligand **L3** (1.00 g, 2.77 mmol) was used instead of **L1**. Yield: 1.03 g (94%). FTIR (KBr, cm⁻¹): 1141 s [ν (P)–O–C], 843 s [ν P–O–(C)], 683 s [ν P–S]_{asym}, 578 m [ν P–S]_{sym}, 246 w [ν Bi–S]. ¹H NMR (CDCl₃, ppm): 2.49 (s, 18H, 4–CH₃), 2.65 (s, 18H, 3–CH₃), 7.35 (d, $J_{\text{HH}} = 7.6$ Hz, 6H, H₆), 7.48 (s, 6H, H₂), 7.55 (d, $J_{\text{HH}} = 8$ Hz, 6H, H₅); ¹³C NMR (CDCl₃, ppm): 19.45 (s, 4–CH₃), 21.79 (s, 3–CH₃), 150.46 (C₆), 122.88 (C₂), 130.67 (C₄–CH₃), 134.27 (C₅), 138.31 (C₃–CH₃), 148.96 (C₁–O); ³¹P NMR (CDCl₃, ppm): 95.03 (s). Anal. Calcd. for C₄₈H₅₄P₃S₆O₆Bi: C, 47.21; H, 4.46; S, 15.75; Bi, 17.11%. Found: C, 47.19; H, 4.40; S, 15.72; Bi, 16.94%.

2.5. Synthesis of [(3,5-CH₃)₂C₆H₃O]₂PS₂]₃Bi (4)

The same synthetic procedure as for complex **1** was used for complex **4**, except that ligand **L4** (1.00 g, 2.77 mmol) was used instead of **L1**. Yield: 1.04 g (95%). FTIR (KBr, cm⁻¹): 1128 s [ν (P)–O–C], 834 s [ν P–O–(C)], 682 s

[$\nu\text{P-S}$] $_{\text{asym}}$, 564 m [$\nu\text{P-S}$] $_{\text{sym}}$, 256 w [$\nu\text{Bi-S}$]. ^1H NMR (CDCl_3 , ppm): 2.35 (s, 36H, 3,5-(CH_3) $_2$), 6.84 (s, 12H, $\text{H}_{2,6}$), 6.92 (s, 6H, H_4); ^{13}C NMR (CDCl_3 , ppm): 21.26 (s, 3,5-(CH_3) $_2$), 119.16 ($\text{C}_{2,6}$), 127.49 (C_4), 139.41 ($\text{C}_{3,5}$ - CH_3), 150.50 (C_1 -O); ^{31}P NMR (CDCl_3 , ppm): 93.30 (s). Anal. Calcd. for $\text{C}_{48}\text{H}_{54}\text{P}_3\text{S}_6\text{O}_6\text{Bi}$: C, 47.21; H, 4.46; S, 15.75; Bi, 17.11%. Found: C, 47.20; H, 4.42; S, 15.74; Bi, 17.05%.



1. $\text{R}_1 = \text{CH}_3$, $\text{R}_2 = \text{H}$, $\text{R}_3 = \text{CH}_3$, $\text{R}_4 = \text{H}_5$, $\text{R}_5 = \text{H}_6$
2. $\text{R}_1 = \text{CH}_3$, $\text{R}_2 = \text{H}$, $\text{R}_3 = \text{H}_4$, $\text{R}_4 = \text{CH}_3$, $\text{R}_5 = \text{H}_6$
3. $\text{R}_1 = \text{H}_2$, $\text{R}_2 = \text{CH}_3$, $\text{R}_3 = \text{CH}_3$, $\text{R}_4 = \text{H}_5$, $\text{R}_5 = \text{H}_6$
4. $\text{R}_1 = \text{H}_2$, $\text{R}_2 = \text{CH}_3$, $\text{R}_3 = \text{H}_4$, $\text{R}_4 = \text{CH}_3$, $\text{R}_5 = \text{H}_6$

Scheme 1. Ring labelling for NMR spectroscopic assignments of complexes 1–4.

2. 6. Antifungal Activity

Agar well diffusion method⁵³ was used for screening the *in vitro* antifungal studies of these complexes. The compounds were dissolved in dimethyl sulfoxide (DMSO). Further progressive dilutions were performed to obtain the required concentrations 100 ppm, 500 ppm and 1000 ppm. Using a sterile cork borer (6 mm in diameter), three holes were made in each dish and then 0.1 mL of the tested compound dissolved in DMSO (100 ppm, 500 ppm, 1000 ppm) was added into these holes. Finally, the petri dishes were incubated at 27° C for 48 h. Distinct or light inhibition zones were observed, around each hole, which were measured in millimetres as the diameter of inhibition zones and solvent DMSO exhibited (zone of inhibition) on the organism tested.

2. 7. Crystallography Data Collection and Refinement

Suitable yellow colored and prism shaped single-crystals of complex **4** for X-ray analysis were obtained by keeping its saturated solution in toluene at low temperature for some hours. For X-ray diffraction studies suitable

single-crystal of complex **4** was mounted on a Bruker Apex-II CCD diffractometer (Department of Chemistry, Guru Nanak Dev University, Amritsar) equipped with graphite monochromated Mo $\text{K}\alpha$ ($\lambda = 0.71069$ Å) at room temperature. The data collected at room temperature were processed and corrected for absorption using SIR-92 software and refined by full-matrix least-squares refinement methods based on F^2 , using the program SHELXL97. The reflection data were collected and processed by SAINT

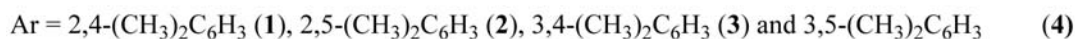
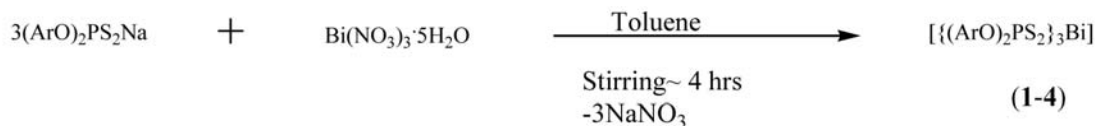
Table 1. Crystal data and structure refinements for $[\{(3,5\text{-CH}_3)_2\text{C}_6\text{H}_3\text{O}\}_2\text{PS}_2]_3\text{Bi}$ (**4**).

Chemical formula	$\text{C}_{48}\text{H}_{54}\text{BiO}_6\text{P}_3\text{S}_6$
CCDC	1547047
M_r	1221.23
Crystal system, space group	Monoclinic, $P2_1/c$
T (K)	296
a, b, c (Å)	13.076 (1), 21.6280 (14), 19.3220 (13)
β (°)	96.302 (3)
V (Å ³)	5431.4 (7)
Z	4
μ (mm ⁻¹)	3.61
No. of reflections	10867
No. of observed [$I > 2\sigma(I)$] reflections	7639
No. of parameters	589
R_{int}	0.069
$R[F^2 > 2\sigma(F^2)]$, $wR(F^2)$, S	0.038, 0.080, 0.98
$\Delta\rho_{\text{max}}$, $\Delta\rho_{\text{min}}$ (e Å ⁻³)	0.50, -0.55

correcting for Lorentz and polarization effects. An empirical absorption correction was applied using SADABS from Bruker. All non-hydrogen atoms were refined anisotropically. All calculations were performed using Wingx package. Molecular drawings were obtained using DIAMOND version 2.1. Crystallographic data and refinement details for the compound **4** are summarized in Table 1.

3. Results and Discussion

The complexes were obtained as stable compounds at room temperature by the reaction of bismuth nitrate pentahydrate with *O, O'*-bis(disubstitutedphenyl)phosphorodithioate in a 1:3 stoichiometric ratio in toluene at room



Scheme 2. Preparation of the complexes 1–4.

temperature. In order to confirm the chemical composition of the synthesized complexes, X-ray, FT-IR, and ^1H , ^{13}C and ^{31}P NMR analyses were carried out with results are presented in the experimental section. The scheme for the formation of the complexes is as follows:

3. 1. Spectroscopic Analysis

The main infrared vibration bands are reported in the experimental section. The FTIR spectra of the complexes and the ligand were compared and assigned on careful comparison. One important band which confirms the bismuth to sulfur bonding $\nu(\text{Bi-S})$ has been observed as a weak signal at $246\text{--}256\text{ cm}^{-1}$. In addition, the spectrum of the complexes shows a strong band at $1141\text{--}1024\text{ cm}^{-1}$ and $870\text{--}834\text{ cm}^{-1}$ due to the $[\nu(\text{P-O-C})]$ and $[\nu\text{P-O-(C)}]$ stretching vibrations. The most identifiable IR absorptions for complexes **1–4** are $683\text{--}673\text{ cm}^{-1}$ and $580\text{--}562\text{ cm}^{-1}$, assigned to $[\nu\text{P-S}]_{\text{asym}}$ and $[\nu\text{P-S}]_{\text{sym}}$ respectively. These bands are shifted to lower frequency as compared to the free ligand. It is found that the coordination mode of the dithiophosphate ligand is bidentate by the sulfur atoms. This is also consistent with the crystal structure of the complex.

The ^1H NMR spectra of bismuth(III) dithiophosphate complexes were recorded in CDCl_3 with tetramethylsilane as an internal standard and are reported in experimental section. The spectra show the characteristic resonance for methyl and aromatic protons. In the complexes **1–4**, chemical shift for $-\text{CH}_3$ protons attached to aryl appears at $2.30\text{--}2.65\text{ ppm}$ as a singlet. The chemical shifts for the aryl ring protons were observed in the region $6.49\text{--}7.55\text{ ppm}$ with their usual splitting pattern.^{37,38}

In the $^{13}\text{C}\{^1\text{H}\}$ NMR spectra of these complexes, the chemical shift for methyl carbon ($-\text{CH}_3$) attached to the aryl ring was observed in the region $15.03\text{--}21.79\text{ ppm}$. The carbon nuclei of the phenyl group have displayed their resonance in the region $119.16\text{--}155.93\text{ ppm}$.

$^{31}\text{P}\{^1\text{H}\}$ NMR spectra showed only one sharp resonance signal at $93.30\text{--}95.03\text{ ppm}$ in the upfield region compared to that of the free ligand ($106.5\text{--}107.4\text{ ppm}$) with a difference of 13 ppm , which indicates a considerable drift of electron density from the phosphorus to the metal atom through both sulfur atoms and thus confirms the formation of a chelated structure with a bidentate O,O' -diphenyl dithiophosphate. This range observed for ^{31}P NMR in these complexes may be correlated with bidentate behavior of the dithiophosphate moiety.⁵⁴

3. 2. Molecular and Crystal Structure of 4

In order to understand the structural details, single crystal X-ray diffraction study of compound **4** was performed. Complex **4** crystallizes in the monoclinic $P2_1/c$ space group. ORTEP view of the molecular structure of **4** with atom numbering scheme is given in Figure 1.

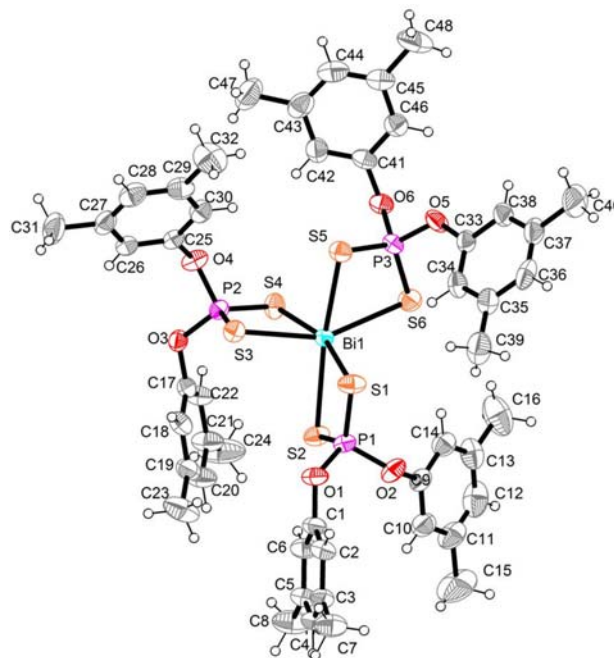


Fig. 1: ORTEP view of $[\{(3,5\text{-CH}_3)_2\text{C}_6\text{H}_3\text{O}\}_2\text{PS}_2]_3\text{Bi}$ (**4**).

The molecule consists of neutral well separated monomeric units. The ligands are bidentate but the attachment of each dithiophosphato moiety to bismuth is slightly unsymmetrical with one short ($2.6926(12)$ to $2.7884(12)\text{ \AA}$) and one long ($2.7794(12)$ to $2.9162(13)\text{ \AA}$) Bi-S bond forming distorted octahedral geometry. Due to three short and three long Bi-S bond, the configuration is approximately C_{3v} . These ranges are consistent with typical values reported for the short and long ligand bond in $[\text{Bi}\{\text{S}_2\text{P}(\text{OC}_6\text{H}_4\text{Me-m})_2\}_3]$ ($2.678(2)$ to $2.953(2)\text{ \AA}$)⁴⁴, $[\text{Bi}\{\text{S}_2\text{P}(\text{OEt})_2\}_3]$ ($2.747(14)$ to $2.795(12)\text{ \AA}$)⁵⁵ and $[\text{Bi}\{\text{S}_2\text{P}\{\text{O}(i\text{-Pr})\}_2\}_3]$ ($2.702(6)$ to $2.8784(6)\text{ \AA}$)⁴⁵.

Asymmetrical coordination necessarily leads to an inverse relationship between the Bi-S and related P-S bond lengths. $\text{P}_1\text{-S}_1$ and $\text{P}_2\text{-S}_2$ bond length in **4** [$\text{P}_1\text{-S}_1 = 1.9807(17)$ and $\text{P}_1\text{-S}_2 = 1.9727(17)\text{ \AA}$] are intermediate between single (2.14 \AA) and double (1.94 \AA) P-S bonds, suggesting the negative charge is delocalized over the S-P-S fragment. The shorter P-S ($1.9727(17)\text{ \AA}$) is associated with sulfur atoms forming the longer Bi-S interaction ($2.8457(13)\text{ \AA}$) while the longer P-S bond ($1.9807(17)\text{ \AA}$) is allied with the sulfur atoms forming the shorter bonds to the bismuth ($2.7884(12)\text{ \AA}$).

The S-Bi-S bite angle in **4** cover a wide range of $88.6(4)$ to $92.73(4)^\circ$. The interligand angles involving the longer Bi-S bonds are considerably larger ranging from $88.86(4)$ to $110.64(4)^\circ$.

3. 3. Antifungal Activity

Antifungal activities of free ligands, metal salt $\text{Bi}(\text{NO}_3)_3 \cdot 5\text{H}_2\text{O}$ and synthesized compounds have been

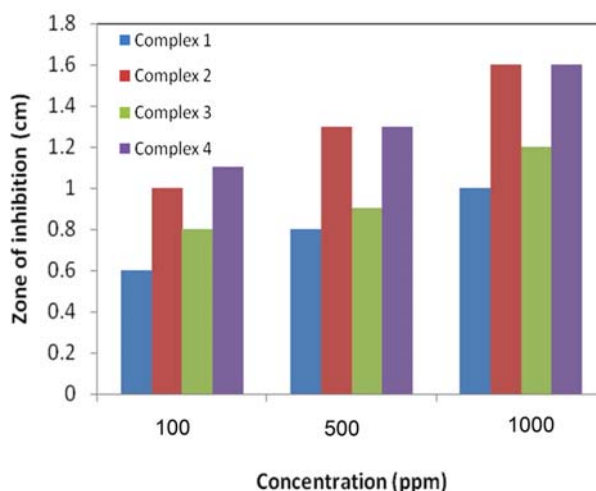
Table 2. Selected bond lengths (Å) and angles (°) for $[(3,5\text{-CH}_3)_2\text{C}_6\text{H}_3\text{O}_2\text{PS}_2]_3\text{Bi}$ (**4**)

O1–P1	1.584 (3)	P2–S3	1.9967 (16)
O2–P1	1.592 (3)	P3–S6	1.9562 (18)
O3–P2	1.586 (3)	P3–S5	1.9931 (17)
O4–P2	1.566 (3)	S1–Bi1	2.7884 (12)
O5–P3	1.582 (3)	S2–Bi1	2.8457 (13)
O6–P3	1.579 (3)	S3–Bi1	2.6926 (12)
P1–S2	1.9727 (17)	S4–Bi1	2.7794 (12)
P1–S1	1.9807 (17)	S5–Bi1	2.7347 (12)
P2–S4	1.9755 (17)	S6–Bi1	2.9162 (13)
O1–P1–O2	101.13 (17)	P2–S3–Bi1	86.97 (5)
O1–P1–S2	113.19 (14)	P2–S4–Bi1	84.99 (5)
O2–P1–S2	112.00 (14)	P3–S5–Bi1	87.76 (6)
O1–P1–S1	104.89 (14)	P3–S6–Bi1	83.43 (6)
O2–P1–S1	110.14 (15)	S3–Bi1–S5	88.68 (4)
S2–P1–S1	114.49 (8)	S3–Bi1–S4	74.67 (4)
O4–P2–O3	100.22 (17)	S5–Bi1–S4	97.02 (4)
O4–P2–S4	108.09 (14)	S3–Bi1–S1	92.82 (4)
O3–P2–S4	112.56 (13)	S5–Bi1–S1	92.17 (4)
O4–P2–S3	111.82 (13)	S4–Bi1–S1	164.23 (4)
O3–P2–S3	110.04 (13)	S3–Bi1–S2	92.73 (4)
S4–P2–S3	113.37 (7)	S5–Bi1–S2	164.47 (4)
O6–P3–O5	99.74 (16)	S4–Bi1–S2	98.27 (4)
O6–P3–S6	107.88 (14)	S1–Bi1–S2	72.32 (4)
O5–P3–S6	112.63 (15)	S3–Bi1–S6	153.29 (4)
O6–P3–S5	110.40 (13)	S5–Bi1–S6	72.33 (4)
O5–P3–S5	109.66 (15)	S4–Bi1–S6	88.86 (4)
S6–P3–S5	115.38 (8)	S1–Bi1–S6	106.19 (4)
P1–S1–Bi1	87.01 (5)	S2–Bi1–S6	110.64 (4)
P1–S2–Bi1	85.57 (5)		

examined at four different concentrations 100 ppm, 500 ppm and 1000 ppm against fungus *Penicillium chrysogenum*. Obtained results have been compared with the standard drug. We conclude that sulfur donor bismuth complexes inhibit the growth of fungi to a greater extent, as concentration is increased. All the results are summarized in Table 3. The results have been obtained as follows:

1. The ligands **L1**, **L2**, **L3** and **L4** showed a negligible inhibitory effect compared to the complexes.
2. Complexes exhibit higher antifungal activities than the corresponding free ligands due to the chelation of the ligand with bismuth.
3. On increasing the concentration of the complex, antifungal activity increases.
4. The increase in antifungal activity might be due to faster diffusion of the complexes as a whole through the cell membrane, or due to a combined activity effect of the metal and the ligand. The polarity of the metal ion will be reduced to a greater extent due to the overlap of the ligand orbitals.

The illustrated comparative results of antifungal analysis are given graphically in Figure 2.

**Fig. 2:** Comparative results of antifungal screening data.**Table 3.** Antifungal activity of diphenyl dithiophosphate ligands and bismuth(III) complexes against the fungus *Penicillium chrysogenum*.

S.No.	Concentration (ppm)	Zone of inhibition (cm)
	100	0.0
	500	0.0
	1000	0.0
<hr/>		
	100	0.0
	500	0.0
	1000	0.0
<hr/>		
	100	0.0
	500	0.0
	1000	0.0
<hr/>		
	100	0.0
	500	0.0
	1000	0.0
<hr/>		
	100	0.6
	500	0.8
	1000	1.0
<hr/>		
	100	1.1
	500	1.3
	1000	1.6
<hr/>		
	100	0.8
	500	0.9
	1000	1.2
<hr/>		
	100	1.1
	500	1.3
	1000	1.6

5. Conclusion

Four new complexes of Bi(III) with disubstituted diphenyl dithiophosphate ligands have been isolated and characterized by IR and NMR (^1H , ^{13}C and ^{31}P) spectroscopy. The molecular structure of complex **4** was determi-

ned by single-crystal X-ray diffraction study and depicted that the diphenyldithiophosphate ions act as bidentate ligands coordinating to the bismuth atom through their two S atoms. Each forms a four-membered chelate ring in the equatorial plane having [BiS₂] unit. The structural analysis reveals that these monomeric complexes possess a distorted octahedral about the bismuth center. The bismuth complexes proved to be a potent antifungal agent as compared to the free dithiophosphate ligand.

6. Supplementary Information

CCDC 1547047 contains the supplementary crystallographic data for compound **4**. The data can be obtained free of charge via <http://www.ccdc.cam.ac.uk/conts/retrieving.html>, or from the Cambridge Crystallographic Data Centre, 12 Union Road, Cambridge CB2 1EZ, UK; fax: (+44) 1223-336-033; or e-mail: deposit@ccdc.cam.ac.uk.

7. Acknowledgements

The authors are grateful to the NMR laboratory Department of Chemistry, University of Jammu, Jammu, for providing the spectral facilities. The authors are grateful to Professor Geeta Hundal, Department of Chemistry, Guru Nanak Dev University, Amritsar, India, for her valuable suggestions.

8. References

- O. C. Monteri, T. Trindade, J. H. Park, P. O'Brien, *Chem. Vap. Dep.* **2000**, *6*, 230–232.
- Y. W. Koh, C. S. Lai, A. Y. Du, E. R. T. Tiekink, K. P. Loh, *Chem. Mater.* **2003**, *15*, 4544–4554. <https://doi.org/10.1021/cm021813k>
- A. Gupta, R. K. Sharma, R. Bohra, V. K. Jain, J. E. Drake, M. B. Hursthouse, M. E. Light, *J. Organomet. Chem.* **2003**, *678*, 122–127. [https://doi.org/10.1016/S0022-328X\(03\)00435-2](https://doi.org/10.1016/S0022-328X(03)00435-2)
- M. Kimura, A. Iwata, M. Itoh, K. Yamada, T. Kimura, N. Sugiura, M. Ishida, S. Kato, *Helv. Chim. Acta* **2006**, *89*, 747–783. <https://doi.org/10.1002/hlca.200690070>
- W. Lou, M. Chen, X. Wang, W. Liu, *Chem. Mater.* **2007**, *19*, 872–878. <https://doi.org/10.1021/cm062549o>
- K. R. Chaudhari, A. Wadawale, S. Ghoshal, S. M. Chopade, V. S. Sagoria, V. K. Jain, *Inorg. Chim. Acta* **2009**, *362*, 1819–1824. <https://doi.org/10.1016/j.ica.2008.08.022>
- D. W. Zhang, W. T. Chen, Y. F. Wang, *Luminescence* **2017**, *32*, 201–205. <https://doi.org/10.1002/bio.3168>
- W. T. Chen, J. G. Huang, X. G. Yi, *Acta Chim. Slov.* **2016**, *63*, 899–904. <https://doi.org/10.17344/acsi.2016.2897>
- N. Yang, H. Sun, *Coord. Chem. Rev.* **2007**, *251*, 2354–2366. <https://doi.org/10.1016/j.ccr.2007.03.003>
- A. Luqman, V. L. Blair, R. Brammanan, P. K. Crellin, R. L. Coppel, P. C. Andrews, *Chem. Eur. J.* **2014**, *20*, 14362–14377. <https://doi.org/10.1002/chem.201404109>
- L. Agoes, G. G. Briand, N. Burford, M. D. Eelman, N. Aumeerally, D. MacKay, K. N. Robertson, T. S. Cameron, *Can. J. Chem.* **2003**, *81*, 632–637. <https://doi.org/10.1139/v03-054>
- R. Mohan, *Nat. Chem.* **2010**, *2*, 336–336. <https://doi.org/10.1038/nchem.609>
- O. Rohr, *Ind. Lubr. Tribol.* **2002**, *54*, 153–164. <https://doi.org/10.1108/00368790210431709>
- G. G. Briand, N. Burford, *Chem. Rev.* **1999**, *99*, 2601–2657. <https://doi.org/10.1021/cr980425s>
- H. Maeda, Y. Tamaka, M. Fukutomi, T. Asano, *Jpn. J. Appl. Phys.* **1988**, *27*, L209–L210. <https://doi.org/10.1143/JJAP.27.L209>
- T. Asaka, Y. Okazawa, T. Hirayama, K. Tachikawa, *Jpn. J. Appl. Phys.* **1990**, *29*, L280–L283. <https://doi.org/10.1143/JJAP.29.L280>
- S. Katayama, M. Sekine, *J. Mater. Res.* **1991**, *6*, 36–41. <https://doi.org/10.1557/JMR.1991.0036>
- B. A. Vaarstra, J. C. Huffman, W. E. Streib, K. G. Caulton, *Inorg. Chem.* **1991**, *30*, 3068–3072. <https://doi.org/10.1021/ic00015a024>
- R. D. Rogers, A. H. Bond, S. Aguinaga, *J. Am. Chem. Soc.* **1992**, *114*, 2960–2967. <https://doi.org/10.1021/ja00034a031>
- R. D. Rogers, A. H. Bond, S. Aguinaga, A. Reyes, *J. Am. Chem. Soc.* **1992**, *114*, 2967–2977. <https://doi.org/10.1021/ja00034a032>
- S. R. Breeze, S. Wang, L. K. Thompson, *Inorg. Chim. Acta* **1996**, *250*, 163–171. [https://doi.org/10.1016/S0020-1693\(96\)05223-1](https://doi.org/10.1016/S0020-1693(96)05223-1)
- E. Moya, L. Contreras, C. Zaldo, *J. Opt. Soc. Am.* **1988**, *B5*, 1737–1742. <https://doi.org/10.1364/JOSAB.5.001737>
- S. Wang, D. B. Mitzi, G. A. Landrum, H. Genin, R. Hoffmann, *J. Am. Chem. Soc.* **1997**, *119*, 724–732. <https://doi.org/10.1021/ja961753h>
- P. Majewski, *Adv. Mater.* **1994**, *6*, 460–469. <https://doi.org/10.1002/adma.19940060604>
- J. F. Scott, F. M. Ross, C. A. Paz de Araujo, M. C. Scott, M. Huffman, *Mater. Res. Soc. Bull.* **1996**, *21*, 33–39. <https://doi.org/10.1557/S0883769400035892>
- A. Ekstrand, M. Nygren, G. Westin, *J. Sol-Gel Sci. Technol.* **1997**, *8*, 697–701.
- F. Soares-Carvalho, P. Thomas, J. P. Mercurio, B. Frit, S. Parola, *J. Sol-Gel Sci. Technol.* **1997**, *8*, 759–763.
- L. O. Rosik, *U. S. Patent, Mallinckrodt Medical. Inc.* **1995**, A61B 005/055.
- C. Coin, T. Zevaco, E. Dunach, M. Postel, *Bull. Soc. Chim. Fr.* **1996**, *133*, 913–918.
- J. L. Lambert, P. Midolo, *Aliment Pharmacol. Ther.* **1997**, *11*, 27–33. <https://doi.org/10.1046/j.1365-2036.11.s1.13.x>
- P. J. Sadler, H. Sun, *J. Chem. Soc., Dalton Trans.* **1995**,

- 1395–1401. <https://doi.org/10.1039/dt9950001395>
32. E. Asato, K. Katsura, M. Mikuriya, U. Turpeinen, I. Mutikainen, J. Reedijk, *Inorg. Chem.* **1995**, *34*, 2447–2454. <https://doi.org/10.1021/ic00113a028>
33. S. L. Gorbach, *Gastroenterology* **1990**, *99*, 863–875. [https://doi.org/10.1016/0016-5085\(90\)90983-8](https://doi.org/10.1016/0016-5085(90)90983-8)
34. X. Wang, X. Zhang, J. Lin, J. Chen, Q. Xu, Z. Guo, *J. Chem. Soc., Dalton Trans.* **2003**, 2379–2380. <https://doi.org/10.1039/b305290g>
35. P. Köpf-Maier, T. Klapötke, *Inorg. Chim. Acta* **1988**, *152*, 49–52. [https://doi.org/10.1016/S0020-1693\(00\)90730-8](https://doi.org/10.1016/S0020-1693(00)90730-8)
36. D. E. Mahony, S. Lim-Morrison, L. Bryden, G. Faulkner, P. S. Hoffman, L. Agocs, G. G. Briand, N. Burford, H. Maguire, *Antimicrob. Agents Chemother.* **1999**, *43*, 582–588.
37. R. Khajuria, S. Kumar, A. Syed, G. Kour, S. Anthal, V. K. Gupta, R. Kant, S. K. Pandey, *J. Coord. Chem.* **2014**, *67*, 2925–2941. <https://doi.org/10.1080/00958972.2014.958473>
38. S. Kumar, R. Khajuria, V. K. Gupta, R. Kant, S. K. Pandey, *Polyhedron* **2014**, *72*, 140–146. <https://doi.org/10.1016/j.poly.2014.01.036>
39. A. Syed, R. Khajuria, S. Kumar, A. K. Jassal, M. S. Hundal, S. K. Pandey, *Acta Chim. Slov.* **2014**, *61*, 866–874.
40. S. Kumar, R. Khajuria, A. K. Jassal, G. Hundal, M. S. Hundal, S. K. Pandey, *Acta Cryst.* **2014**, *B70*, 761–767. <http://dx.doi.org/10.1107/S2052520614014966>
41. S. Kumar, R. Khajuria, A. Syed, A. K. Jassal, L. K. Rana, G. Hundal, S. K. Pandey, *Monatsh. Chem.* **2016**, *147*, 1037–1043. <https://doi.org/10.1007/s00706-015-1569-6>
42. S. Kumar, R. Khajuria, A. Syed, V. K. Gupta, R. Kant, S. K. Pandey, *Transit. Met. Chem.* **2015**, *40*, 519–523.
43. S. Kumar, S. Andotra, M. Kour, V. K. Gupta, R. Kant, S. K. Pandey, *Crystallogr. Rep.* **2016**, *61*, 810–814. <https://doi.org/10.1134/S1063774516050126>
44. S. Maheshwari, J. E. Drake, K. Kori, M. E. Light, R. Ratna, *Polyhedron* **2009**, *28*, 689–694. <https://doi.org/10.1016/j.poly.2008.12.017>
45. S. L. Lawton, C. J. Fuhrmeister, R. G. Haas, C. S. Jarman, F. G. Lohmeyer, *Inorg. Chem.* **1974**, *13*, 135–143. <https://doi.org/10.1021/ic50131a026>
46. M. J. Begley, D. B. Sowerby, I. Haiduc, *J. Chem. Soc. Dalton Trans.* **1987**, 145–150. <https://doi.org/10.1039/dt9870000145>
47. D. Bryan Sowerby, I. Haiduc, *J. Chem. Soc. Dalton Trans.* **1987**, 1257–1259. <https://doi.org/10.1039/DT9870001257>
48. F. T. Edelmann, M. Noltmeyer, I. Haiduc, C. Silvestru, R. Cea-Olivares, *Polyhedron* **1994**, *13*, 547–552. [https://doi.org/10.1016/S0277-5387\(00\)84730-0](https://doi.org/10.1016/S0277-5387(00)84730-0)
49. G. Svensson, J. Albertsson, *Acta Chem. Scand.* **1989**, *43*, 511–517. <https://doi.org/10.3891/acta.chem.scand.43-0511>
50. B. F. Hoskins, E. R. T. Tiekink, G. Winter, *Inorg. Chim. Acta* **1984**, *81*, L33–34. [https://doi.org/10.1016/S0020-1693\(00\)88725-3](https://doi.org/10.1016/S0020-1693(00)88725-3)
51. C. L. Raston, A. H. White, *J. Chem. Soc. Dalton Trans.* **1976**, 791–794. <https://doi.org/10.1039/dt9760000791>
52. A. I. Vogel Quantitative, *Inorganic Analysis*, 3rd Edn, Longmans, London, **1961**.
53. M. A. Neelakantan, M. Esakkiammal, S. S. Mariappan, J. Dharmaraja, T. Jeyakumar, *Indian J. Pharm. Sci.* **2010**, *72*, 216–222. <https://doi.org/10.4103/0250-474X.65015>
54. C. Glidewell, *Inorg. Chim. Acta* **1977**, *25*, 159–163. [https://doi.org/10.1016/S0020-1693\(00\)95706-2](https://doi.org/10.1016/S0020-1693(00)95706-2)
55. M. Iglesias, C. D. Pino, S. M. Carrera, *Polyhedron* **1989**, *8*, 483–489. [https://doi.org/10.1016/S0277-5387\(00\)80746-9](https://doi.org/10.1016/S0277-5387(00)80746-9)

Povzetek

Predstavljeni so štiri kompleksi s splošno formulo $[(ArO)_2PS_2]_3Bi$ (**1–4**), kjer je Ar = 2,4-(CH₃)₂C₆H₃, 2,5-(CH₃)₂C₆H₃, 3,4-(CH₃)₂C₆H₃ in 3,5-(CH₃)₂C₆H₃. Reakcija $[(ArO)_2PS_2Na]$ z $Bi(NO_3)_3 \cdot 5H_2O$ v molskem razmerju 3:1 v toluenu vodi do nastanka kompleksov $[(ArO)_2PS_2]_3Bi$. Navedeni sintetizirani kompleksi so bili okarakterizirani z elementno analizo, FT-IR in NMR spektroskopijo (¹H, ¹³C in ³¹P NMR). Kristalna struktura $[(3,5-CH_3)_2C_6H_3O]_2PS_2]_3Bi$ (**4**) je bila določena s pomočjo rentgenske difrakcije. Spojina kristalizira v monoklinski $P2_1/c$ prostorski skupini, Bi(III) center je obdan s šestimi žveplovimi atomi treh kelatnih difenil ditiofosfatnih ligandov v obliki popačenega oktaedra. Testiranje teh kompleksov proti *Penicillium chrysogenum* je dalo pozitivne rezultate.

Scientific paper

Electrospun Nanofibrous Polyacrylonitrile/calixarene Mats: an Excellent Adsorbent for the Removal of Chromate Ions from Aqueous Solutions

Mevlut Bayrakci,^{1,*} Fatih Ozcan,² Bahar Yilmaz¹ and Seref Ertul²¹ Department of Bioengineering, Faculty of Engineering, Karamanoglu Mehmetbey University, Karaman, Turkey² Department of Chemistry, Faculty of Science, Selcuk University, Konya, Turkey

* Corresponding author: E-mail: mevlutbayrakci@gmail.com

Tel.: +90 388 2252106 fax: +90 388 2250180;

Received: 18-05-2017

Abstract

Herein, calixarene molecules containing piperidine units at lower rim or upper rim of calix skeleton was turned into a water resistant composite nanofiber adsorbent using polyacrylonitrile (PAN) polymeric support via electrospinning process. The PAN based calixarene nanofibrous adsorbents showed an excellent adsorption capacity toward the toxic chromate anions in aqueous solution. Furthermore, this new nanofiber mats would be promising filter materials for drinking water purification.

Keywords: Calixarene, Nanofiber, Membrane, Chromate, Electrospinning

1. Introduction

Chromium is a naturally occurring element and found in rocks, animals, plants, soil, and in volcanic dust and gases.¹ Chromium can exist in four different oxidation states such as metallic chromium Cr, chromous Cr²⁺, chromic Cr³⁺ and chromates Cr⁶⁺.² In natural waters, Cr exists mainly in two different oxidation states, Cr⁶⁺ and Cr³⁺. Chromium (VI) and chromium (III) enter the body through inhalation, ingestion and dermal contact. The trivalent and hexavalent forms are believed to be the biologically active species; but, their health impacts are not identical. Chromium (VI) readily penetrates biological membranes while chromium (III) generally does not. Cr (VI) is considered to be toxic because of its adverse effects on the health.³ On the other hand, Cr (III) is virtually both less toxic than Cr (VI) and required nutrient for living organisms.⁴ The most commonly reported chronic effects of chromium (VI) exposure include contact dermatitis, skin ulcers, irritation and ulceration of the nasal mucosa and perforation of the nasal septum. Less common are reports of hepatic and renal damage and pulmonary effects (bronchitis, asthma, and bronchospasm).⁵ Therefore, it is important to remove Chromium (VI) from polluted wa-

ters, especially those belonging to the electroplating industry. In the drinking water, chromium contaminations are probably due to the industrial using of them such as mining, leather tanning, dye, cement and electroplating applications.⁶ The removal of Cr(VI) from wastewater is important before disposal of industrial waste into the water reservoirs such as river and lake.⁷ For the removal of the Cr(VI) from drinking water sources, different techniques such as chemical precipitation, electrokinetic remediation, membrane separation, bioremediation photocatalysis and adsorption are used.⁸ Among these techniques, adsorption of Cr(VI) can be effective and versatile method for chromium removal particularly owing to the more economically viable, especially if low cost adsorbents are used. But in practice its advantages are largely related to the performance of the adsorbents. Compared to conventional adsorbents, nanomaterials have been counted as very promising candidates for high-performance adsorbents in the most adsorbents, due to their higher surface-to-volume ratio.⁹ Up to now, some adsorbents, such as carbon nanospheres and/or nanotubes, graphene derivatives, metal oxide nanoparticles, and other nano adsorbents have been widely researched for Cr (VI) removal.^{9–12} Considering that oxyanions are the main form of

chromate existing in water, the adsorption capacity of chromate can be expected to improve by introducing cationic units onto the adsorbent surface, because of the static electrical interaction between oxyanions and positive component on the adsorbent surface.^{13,14} Presence of the amino groups on the surface of adsorbents with various amino compounds is very effective route to prepare cationic adsorbents for the removing of the chromate ions. For instance, the chromate adsorption capacity of bare magnetic Fe₃O₄ nanoparticles from the aqueous phase was effectively improved after they were coated with piperidine units containing protonable amino groups at lower pH values.^{15,16} However, the large-scale treatment of magnetite nanoparticles in plants or water sources are still insufficient because of the challenges such as demagnetization, large-scale synthesis and recycling process of magnetic nano adsorbent. Recently, nanofiber adsorbents have been attracting much attention due to the both high adsorption properties and packing and durability advantages of conventional fiber materials.¹⁷ From this point of view functionalized nano-fibers will be most important topic and used as affinity membranes for filtering heavy metals and toxic anions that are difficult to purify by conventional purification methods. Keeping the above aspects in view, we designed and synthesized a new kind of calixarene and polyacrylonitrile (PAN) nanofiber adsorbent for chromate removal via an electrospinning technique (Figure 1 and Figure 2). Furthermore, the extraction capacity of this newly developed nanomaterial for dichromate anions was also explored and studied at different pH values by solid-phase extraction process. While PAN provides the flexibility, high surface area and porosity for good chromium adsorption, calixarene molecules containing protonable amino groups as piperidine on the surface of adsorbent sup-

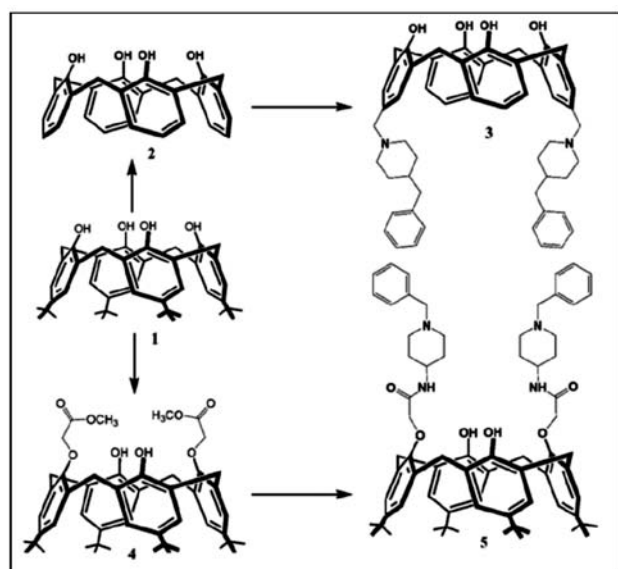


Figure 1. Synthetic route for the preparation of the lower rim or upper rim modified piperidine calixarene (3) and (5).

port the possible interaction between surface and chromate anions with high affinity by electrostatic attraction.

2. Experimental

2. 1. General

¹H and ¹³C NMR spectra were obtained using a Varian 400 MHz spectrometer operating at 400 MHz. The prepared nanofiber mats were characterized by using a Bruker Vertex 70 ATR-FTIR instrument. Thermogravimetric analysis (TGA) data were obtained with a Setaram SETSYS thermal analyzer. SEM images were received using a Zeiss LS-10 field emission SEM instrument. UV–Visible spectra were recorded on Shimadzu 1800 UV–Visible. Millipore Milli-Q Plus water purification system is used for the distilled water. For the pH measurements, An Orion 410A_p pH meter was used. All of the reagents used in this study were obtained from analytical grade and used without further purification.

2. 2. Synthesis

p-*tert*-butylcalix[4]arene (1), calix[4]arene (2), 5,17-Bis-[(4-benzylpiperidine)methyl]-calix[4]arene (3), *p*-*tert*-butylcalix[4]arene diester (4) and *p*-*tert*-butylcalix[4]arene diamide (5) compounds were synthesized according to the literature procedures.^{15–18}

2. 3. Electrospinning

Fibers were electrospun as reported in literatures.^{17–20} The polymer solution were prepared by dissolving calixarene compounds in DMF which is containing 15% (w/v) PAN. The concentration of calixarenes was 50 wt% with respect to the PAN concentration in DMF. The polymer solution was held in a horizontally plastic syringe fitted with a metallic needle of 0.7 mm inner diameter. A stainless steel electrode was immersed in the solution and connected to a high voltage power supply. A metal plate coated with aluminum foil placed opposite served as a counter electrode. The applied voltages between the needle tip and collector were set at around 15–20 kV with a tip-to-collector distance of 15 cm. The electrospinning temperature and the relative humidity were 25 °C and 50%, respectively.

2. 4. Adsorption Experiments

The sorption capacities of the prepared nanofibers were determined by the following technique. Aqueous solution (10 mL) of Na₂Cr₂O₇ with 1.0 × 10⁻⁴ M concentration and 25 mg of the sorbent were pipetted in a stoppered flask that was shaken at 175 rpm and 25 °C for 1 h. The sorbent was separated before measurements. The residual dichromate concentration of aqueous solute was determi-

ned by UV–Vis analyses at 346 nm. The effect of pH was studied by adjusting the pH of aqueous solutions using diluted HCl and KOH solutions at 25 °C. The experiments were performed three times. From the blank experiments data it was observed that no dichromate extraction occurred in the absence of the fiber mats. The percent extraction (E %) was calculated through the absorbance of the aqueous phase measured using the following expression:

$$\text{Extraction } E\% = (A_0 - A) / A_0 \times 100 \quad (1)$$

where A_0 and A are the initial and final concentrations of the dichromate ion before and after the extraction, respectively (Eq. 1).

3. Results and Discussion

3.1. Synthesis and Characterization

The synthesis of desired calix[4]arene derivatives containing piperidine units at upper rim or lower rim is depicted in the Figure 1. For this purpose, the required starting materials, *p*-tert-butylcalix[4]arene (1), calix[4]arene (2) and diester derivative (4) were synthesized by following the procedure available in the literature.¹⁸ In case, compounds (3) and (5) were prepared according to previous reports as follow.^{15,16} For the lower rim modified calixarene derivative, starting material (4) and 4-amino-1-benzylpiperidine were reacted in refluxing toluene-methanol solvent mixture. After 10 days, crude product was purified by column chromatography (SiO_2 , EtOAc/n-hexan; 2:1) and lower rim modified calixarene based piperidine was obtained as a pale yellow

solid with 54% yields. As for upper rim functionalized calixare derivative (3), calix[4]arene (2) were interacted with 4-benzylpiperidine in presence of formaldehyde and acetic acid in THF at room temperature and upper rim functionalized compound (3) was obtained as a white solid product with 53% yields after 24 hours via Mannich type reaction. After synthesis of the calix[4]arene compounds containing piperidine units, polyacrylonitrile (PAN) nanofibers containing calixarene piperidine derivatives were electrospun from the dimethylformamide solution mixture of PAN and calixarene molecules (3) and (5). For the comparison study, pure PAN nanofibers without calixarene molecules were also electrospun.

Fracture morphologies of pure PAN, PAN-CLX3 and PAN-CLX4 nanofibers can be seen in Figure 3. The SEM images of nanofibers showed that there was no phase separation in the cross sectional morphology and they were comparable. In the case of PAN with and without calixarene units, while the nanofibers were mostly uniform, in the fiber matrix, aggregates of calixarene crystals were also distributed. Mostly, the fiber diameters were between 285 and 330 nm for all the samples. But, compared the samples, small variations were observed. For PAN-calixarene systems, slightly thicker fibers were obtained when compared to pure PAN system owing to the higher solution viscosity by the presence of calixarene molecules. In the case of pure PAN system, thinner fibers were observed because of the absence of calixarene molecules caused the lower viscosity of pure PAN in DMF solution. As clearly seen from SEM images, the surface morphologies of all PAN-CLX3 and PAN-CLX5 nanofibers were obviously different from the pure PAN nanofibers.

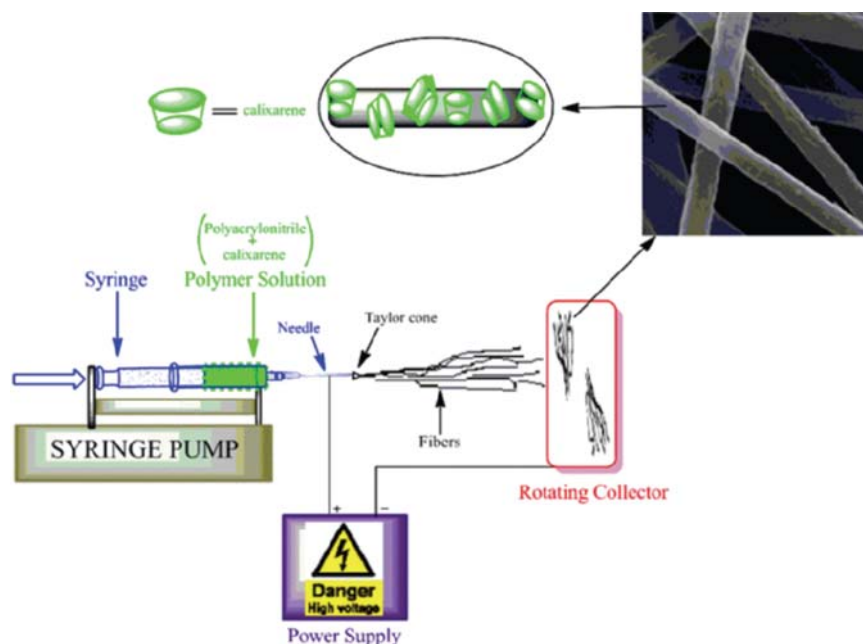


Figure 2. A setup for the electrospinning process of calixarene compounds (3),(5) and polyacrylonitrile solutions.

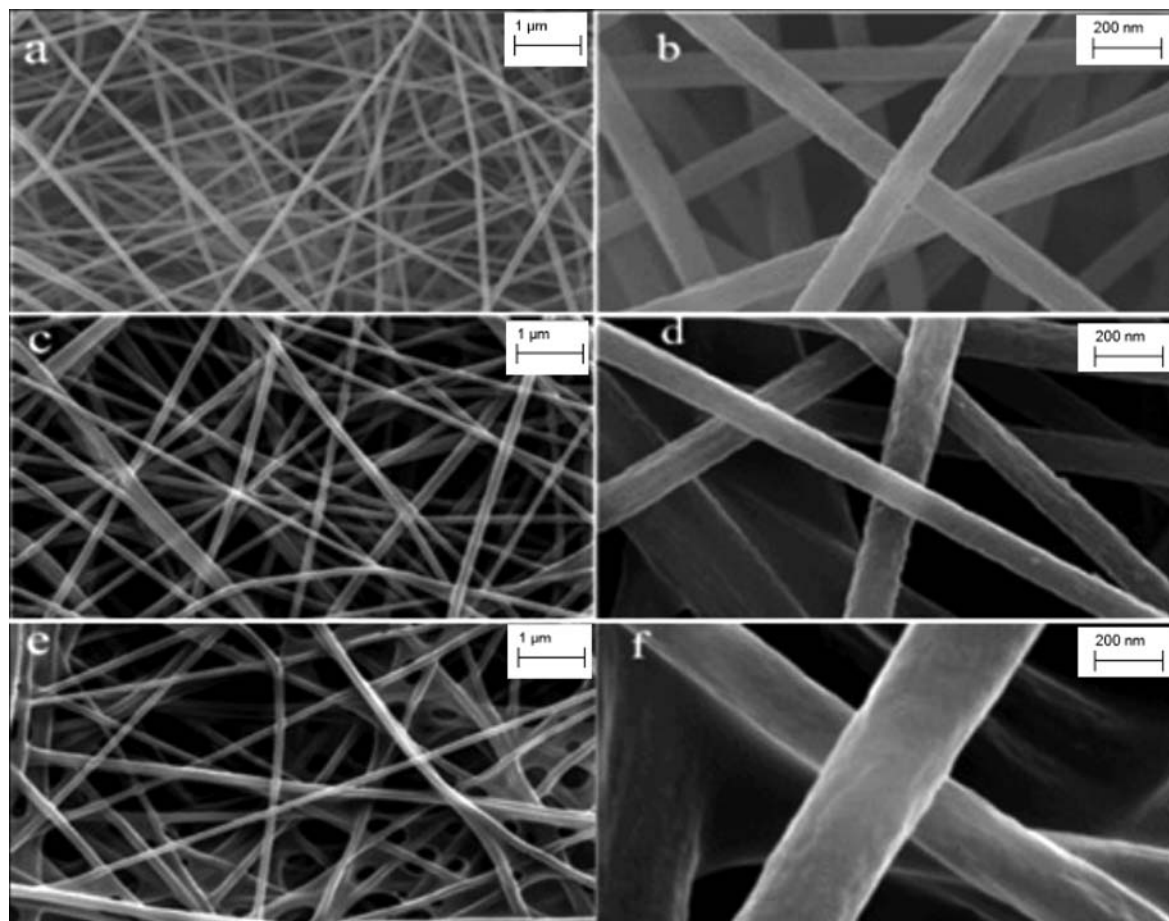


Figure 3. SEM images of prepared nanofibers: a. and b. pure PAN; c. and d. PAN-CLX5; e. and f. PAN-CLX3.

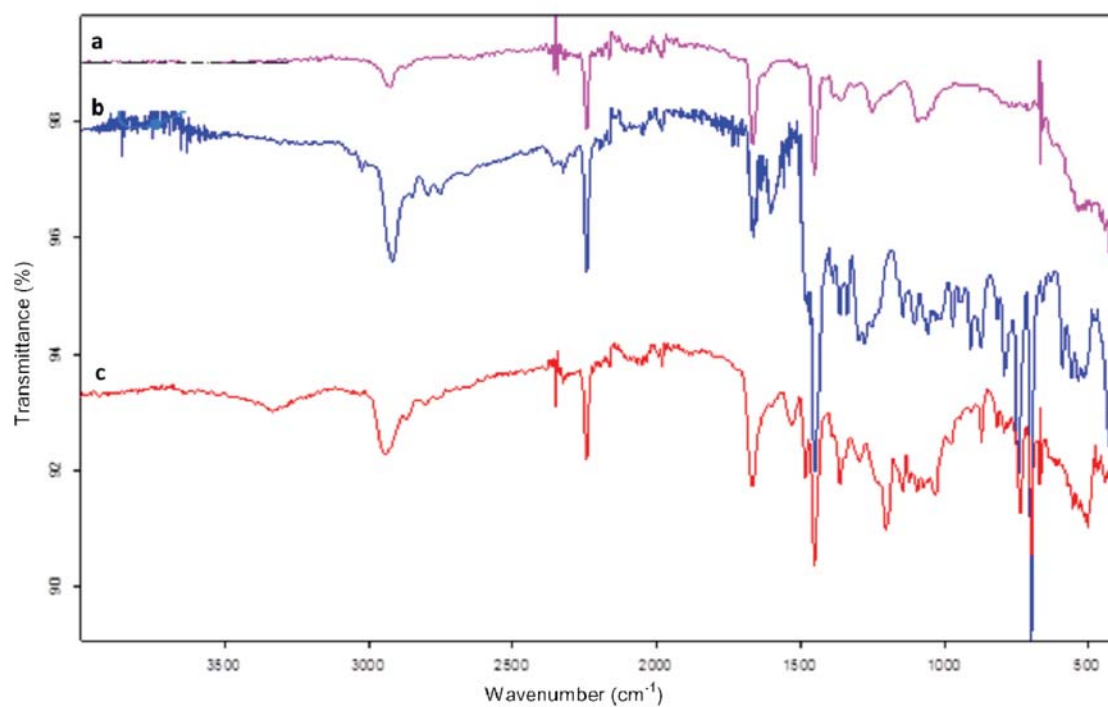


Figure 4. FTIR (ATR) spectra of prepared nanofibers. (a: pure PAN, and b: PAN-CLX3 and c: PAN-CLX5)

To confirm the presence of calixarene molecules on the surface of fiber webs, PAN-CLX3, PAN-CLX5 and pure PAN analyzed by a surface sensitive technique, attenuated total reflection Fourier transform infrared (ATR-FTIR) spectroscopy. The ATR-FTIR spectra of (a) pure PAN, (b) PAN-CLX3 and (c) PAN-CLX5 nanofibers are presented in Figure 4. Typical bands include stretching vibrations of CH and CH₂ groups at 2800–3000 cm⁻¹, intense stretching vibration of CN at 2240 cm⁻¹ and CH/CH₂ deformation vibrations at 1250–1500 cm⁻¹ were observed in the all FTIR spectrum.^{19,20} On the other hand, the absorption bands at around 3462 and 1667 cm⁻¹ attributable stretching vibration of phenolic hydroxyl groups and the phenyl plane bending vibration observed for PAN-CLX3 and PAN-CLX5 nanofibers were also observed, respectively. These new bands confirmed that calixarene molecules were present on the surface of the nanofibers. In addition, the absorption bands corresponding to stretching vibration of amide band I and amide band II for PAN-CLX3 nanofibers were observed at around 1650 and 1530 cm⁻¹, respectively. Moreover, the frequency of the mentioned typical bands ascribed to the structure of calixarene skeleton was found to be unaffected by the electrospinning process. For this reason, no covalent bond formation between calixarene molecules and PAN was evidenced from the FTIR analysis. Therefore, incorporation of calixarene molecules containing piperidine units into nanofiber scaffold was evaluated as a process which is governed by strong physical interactions.

The thermal behaviors of the prepared nanofibers was determined by thermo gravimetric analysis in a temperature range of 25–600 °C. TG curves of (a) PAN, (b) PAN-CLX3 and (c) PAN-CLX5 were presented Figure 5. The first and rapid weight loss of PAN nanofibers was observed between 275 and 330 °C due to the side chain degradation of the polymer backbone. Decomposition of the carbon-carbon main chains caused the weight loss was seen around 360–465 °C in TGA curves for all nanofibers. Compared with PAN nanofibers, it is clearly seen from the inset of Figure 5 that PAN-CLX3 and PAN-CLX5 nanofibers begin to lose weight at slightly shorter temperatures demonstrating a stabilizing effect of calixarene molecules into the polymer chain. The thermal decomposition behaviors of the PAN nanofibers with calixarene molecules are slightly higher than pure PAN. Furthermore, DSC curves displayed an exothermic for all samples and endothermic peaks only for calix nanofibers, which indicated thermal stabilizing, cyclization of nitrile group and melting process of PAN nanofibers. The exothermic peak of pure PAN displayed at 290 °C due to multiple complex chemical reactions, such as dehydrogenation, instantaneous cyclization and crosslinking reactions associated with the oxidative stabilization of PAN.^{21,22} In addition, the weak endothermic peaks attributable the melting of the pure calixarene compounds for PAN-CLX3 and PAN-5 during the heating stage, which are centered around 200 °C, were also observed.

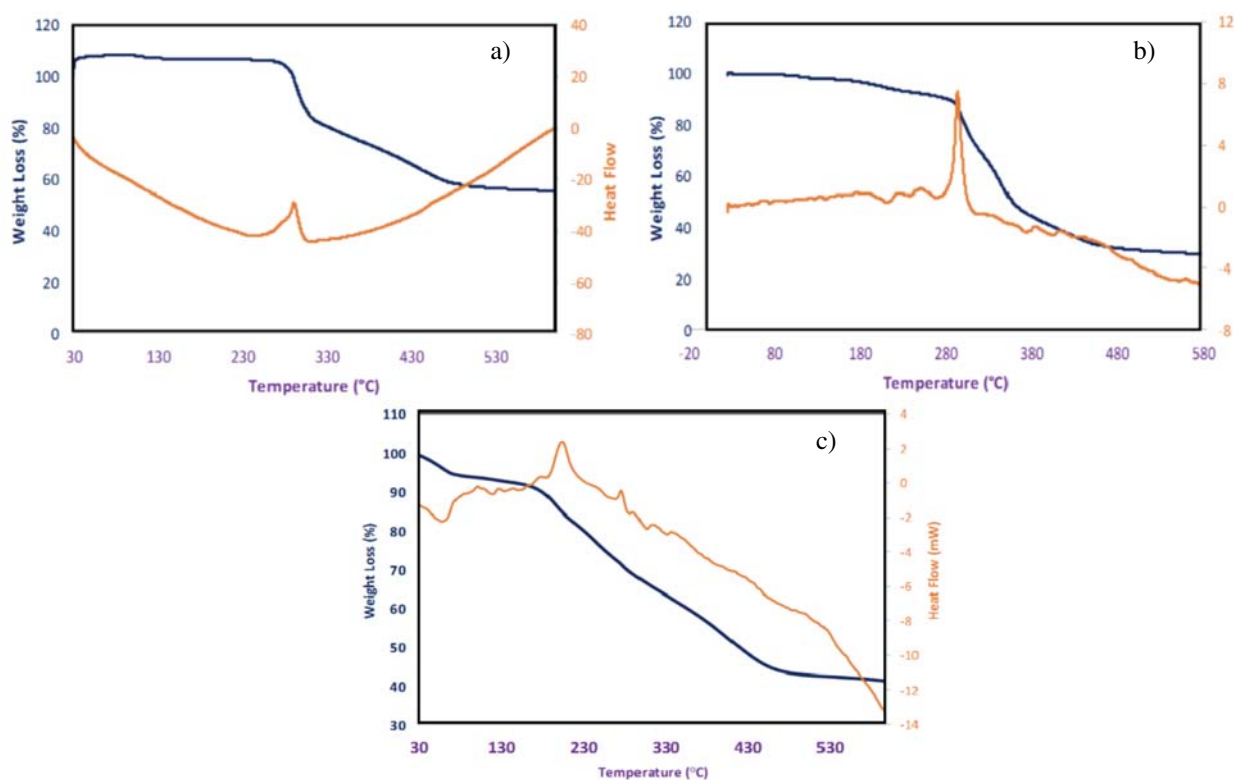


Figure 5. TG and DSC curves of nanofibers (a) PAN, (b) PAN-CLX3 and (c) PAN-CLX5.

3. 2. Chromate Extraction Studies

From the spectroscopic data, it can be seen that the obtained fibers are porous and amine modified calixarene molecules were immobilized on the surface. This distinct morphology of the resultant nanofiber mats would be very favorable to the adsorption of anionic chromate ions. The synthesis of supports and hosts for specific anions as dichromate is an important goal. Because Cr (VI) has well known effects on environment and living organism, it is necessarily to remove Cr (VI) from wastewater. Therefore, a series of experiments were carried out to evaluate the binding capability of nanofibers mats towards chromate ions in aqueous solution. The effect of pH on the chromate adsorption abilities of the prepared nanofibers pure PAN, PAN-CLX3 and PAN-CLX5 at room temperature was presented at Figure 6. From the adsorption experiments, it was found that the chromate uptake ability of the nanofibers PAN-CLX3 and PAN-CLX5 reached a maximum at pH 1.5. When the pH of studied solutions gradually decreased, the adsorption performance for PAN-CLX3 and PAN-CLX5 sharply increased. From Figure 6, it is clear that maximum extraction 90% for PAN-CLX3 and 85% for PAN-CLX5 occur in aqueous solution at pH 1.5; which shows that best interaction between fibers PAN-CLX3, PAN-CLX5 and the chromate ions occurs at this pH. On the other hand, pure PAN nanofibers have almost no adsorption capacity for chromate anions, whereas calixarene-modified nanofiber exhibited increased adsorption percentage at different pH values. The following reasons should be accountable for these findings. Firstly, the amino groups of calixarene piperidine molecules on the surface of fiber mats are prone to protonation in acid solution which enhances the electrostatic interaction between protonated calix piperidine units and anionic chromate ions as well hydrogen bonding. The next reason is that PAN nanofibers based calixarene containing piperidine units have a more stable skeleton and functionalized groups due to presence of calixarene molecules. With increasing pH values, the possible interaction between chromate ions and fiber webs

at aqueous solutions decreased and the extraction percentage became less for all studied nanofibers. The slight increase in anion binding efficiency of all nanofibers at increased pH values (from 5.5 to 8.5) may be explained by the location of the sodium cation coming from dichromate so-called ion-pairs. Cr (VI) is unstable and shows very oxidizing behaviors in the presence of the electron donor in acidic medium. HCrO_4^- is the dominant form of the chromium at pH 1 and 6 and only CrO_4^{2-} ions exist above pH 7. With the increase of pH, the proportion of HCrO_4^- decreased and the content of CrO_4^{2-} increased until it was the predominant species at pH values over 7.5.

Apparently, the CrO_4^{2-} oxyanion needs one more adsorption site than the HCrO_4^- oxyanion. It is understandable that the adsorption capacity decreased with the pH increasing from 1.5 to 8.5. Compared the published literature results about dichromate extraction by solid materials as magnetite nanoparticle with piperidine units, fiber version of calixarene piperidine molecules showed excellent extraction results.^{15,16} These results are probably due to the special and large surface area, high porosity, microporosity and high flexibility properties of the fiber structures of calixarene piperidine nanofiber mats. At the lower pH values both the formation of $\text{HCr}_2\text{O}_7^- \text{Na}^+$ and the protonation of the amine nitrogens of piperidine units of calixarene molecules favor extraction. Additionally, both the competing ion and temperature effect on chromate anion extraction of PAN-CLX3 and PAN-CLX4 was explored by using the mixture of Cl^- , SO_4^{2-} , NO_3^- and chromate anions at the different temperatures such as 25, 30 and 35 °C. From the obtained results, it was clearly observed that both the presence of the competing ions such as Cl^- , SO_4^{2-} , NO_3^- and different temperature values did not have any considerably effect onto the extraction percentage of chromate ions with PAN-CLX3 and PAN-CLX4. In the light of these results, PAN-CLX3 and PAN-CLX4 nanofibers could be used as selective ionophore based nanofibers for chromate anions in the presence of foreign anions at different temperatures.

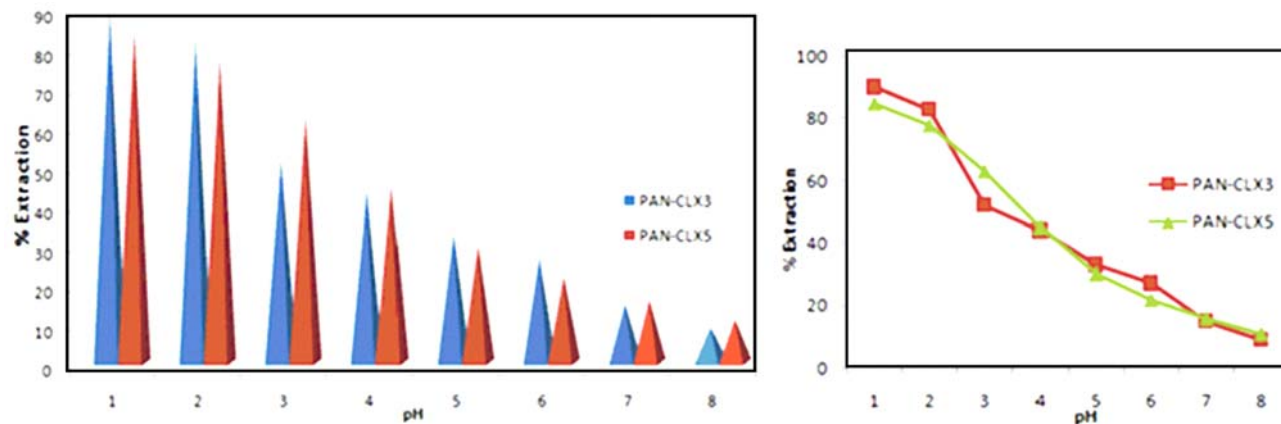


Figure 6. Extraction percentages (%E) versus pH following the solid phase extraction of dichromate anions with nanofibers PAN-CLX3 and PAN-CLX5.

4. Conclusion

As a summary in this study, the preparation and anion binding properties of PAN nanofibers based calixarene containing piperidine units with amide and/or amine functionality were successfully carried out. In the fabrication process, PAN nanofibers based calixarene piperidine units were first produced with the aim to develop functional nanofibers. Owing to the presence of calixarene piperidine molecules onto the nanofiber scaffold, PAN-CLX3 and PAN-CLX5 exhibited higher affinity toward chromate anions. This situation is probably due to the very high surface area, porosity, flexibility and microporosity of PAN nanofibers and surface associated with calixarene molecules. Calixarenes are already being used in variety areas such as pharmaceuticals, catalyst, filtrations and controlled drug delivery systems, therefore, having nanofiber structures might hopefully extend the use of calixarenes in these fields or in other functional systems. Hence, a new inexpensive material is proposed via electrospinning as a useful membrane type adsorbent for removal of chromate anions in aqueous solution. Moreover, our findings may contribute to the fabrication of new functional nanofibers from other types of calixarene and/or other supramolecular systems via electrospinning.

5. Acknowledgments

The authors gratefully would like to thank Karamanoglu Mehmetbey University Research Foundation (Project number 25-M-15) for financial support.

6. References

1. A. E. P. Del Real, J. M. Silvan, S. de Pascual-Teresa, A. Guerrero, P. García-Gonzalo, M. C. Lobo, A. Pérez-Sanz, *Environ. Sci. and Pol. Res.* **2017**, 1–11. <https://doi.org/10.1007/s11356-016-8218-4>
2. J. S. Chin, A. I. Gopalan, N. Muthuchamy, K. P. Lee, *Polymers* **2016**, 8, 445. <https://doi.org/10.3390/polym8120445>
3. L. C. Hsu, S. L. Wang, Y. C. Lin, M. K. Wang, P. N. Chiang, J. C. Liu, Y. M. Tzou, *Enviro. sci. & tech.* **2010**, 44, 6202–6208. <https://doi.org/10.1021/es1017015>
4. M. Gheju, *Water. Air Soil Pol.* **2011**, 222, 103–148. <https://doi.org/10.1007/s11270-011-0812-y>
5. T. Burks, *PhD Thesis. KTH Royal Institute of Technology* 2016.
6. D. K. Harijan, V. Chandra, *J. Environ. Chem. Eng.* **2016**, 3006–3012. <https://doi.org/10.1016/j.jece.2016.06.014>
7. R. Bhatia, D. Jain, *Sustain Water Resour. Manag.* **2016**, 2, 161–173. <https://doi.org/10.1007/s40899-015-0014-7>
8. S. Kuppusamy, T. Palanisami, M. Megharaj, K. Venkateswarlu, R. Naidu, *I Rev. Environ. Contam. and Toxic.* **2016**, 236, 117–192. <https://doi.org/10.1039/C5RA26973C>
9. Y. Ma, B. Zhang, H. Ma, M. Yu, L. Li, J. Li, *RSC Adv.* **2016**, 6, 30739–30746. <https://doi.org/10.1007/978-3-319-20013-2>
10. M. Li, C. Wang, M. J. O'Connell, C. K. Chan, *Environ. Science: Nano* **2015**, 2, 245–250. <https://doi.org/10.1039/C4EN00204K>
11. L. Yu, Y. Ma, C. N. Ong, J. Xie, Y. Liu, *Rsc. Adv.* **2015**, 5, 80, 64983–64990. <https://doi.org/10.1039/C5RA08922K>
12. L. Zhang, W. Xia, X. Liu, W. Zhang, *J. Mater. Chem. A* **2015**, 3, 331–340. <https://doi.org/10.1039/C4TA05194G>
13. A. Benhamou, J. P. Basly, M. Baudu, Z. Derriche, R. Hamacha, *J. Colloid Interface Sci.* **2013**, 404, 135–139. <https://doi.org/10.1016/j.jcis.2013.04.026>
14. T. Wang, L. Zhang, C. Li, W. Yang, T. Song, C. Tang, J. Luo, *Environ. Sci. Tech.* **2015**, 49, 5654–5662. <https://doi.org/10.1021/es5061275>
15. S. Sayin, M. Yilmaz, M. Tavasli, *Tetrahedron* **2011**, 67, 3743–3753. <https://doi.org/10.1016/j.tet.2011.03.012>
16. S. Sayin, F. Ozcan, M. Yilmaz, A. Tor, S. Memon, Y. Cengeloglu, *CLEAN–Soil. Air. Wat.* **2010**, 38, 639–648. <https://doi.org/10.1002/clen.201000039>
17. F. Ozcan, M. Bayrakci, S. Ertul, *J. Incl Phenom. Macrocycl. Chem.* **2016**, 85, 49–58. <https://doi.org/10.1007/s10847-016-0604-5>
18. C. D. Gutsche, K. C. Nam, *J. Am. Chem. Soc.* **1988**, 110, 6153–6162. <https://doi.org/10.1021/ja00226a034>
19. Y. Liu, G. Jiang, L. Li, H. Chen, Q. Huang, T. Jiang, X. Du, W. Chen, *J. Mater. Sci.* **2015**, 50, 8120–8127. <https://doi.org/10.1007/s10853-015-9385-2>
20. H. Chen, G. Jiang, W. Yu, D. Liu, Y. Liu, L. Li, Q. Huang, Z. Tong, W. Chen, *Powder Technol.* **2016**, 298, 1–8. <https://doi.org/10.1016/j.powtec.2016.05.017>
21. L. Ji, Z. Lin, M. Alcoutlabi, O. Toprakci, Y. Yao, G. Xu, X. Zhang, *Rsc. Adv.* **2012**, 2, 192–198. <https://doi.org/10.1039/C1RA00676B>
22. M. Bayrakci, F. Ozcan, S. Ertul, *Tetrahedron* **2015**, 71, 3404–3410. <https://doi.org/10.1016/j.tet.2015.03.090>

Povzetek

Molekule kaliksarena s piperidinskimi enotami v zgornjem ali spodnjem obroču skeleta smo uporabili za pripravo voodoo-pornega komposita nanovlaken. V procesu elektropredenja smo uporabili polimeren nosilec poliakrilnitril (PAN). Tako pripravljen adsorbent na osnovi PAN kaliksaren nanovlaken je pokazal odlično adsorpcijsko kapaciteto napram toksičnim anionom kroma (VI) v vodnih raztopinah. Nova nanovlakna predstavljajo obetajoč material za pripravo filtrov za čiščenje pitne vode.

Scientific paper

Synthesis of Hetero- and Homo-multinuclear Complexes with a Tetracyanonickelate Anion: Structural Characterization $[\text{Cu}(\text{bcen})\text{Ni}(\text{CN})_4]_2$

Rasoul Vafazadeh,^{1,*} Amin Deghani-Firouzabadi¹ and Anthony C. Willis²

¹ Department of Chemistry, Yazd University, Yazd, Iran.

² Research School of Chemistry, Australian National University, Canberra, ACT 2601, Australia.

* Corresponding author: E-mail: rvafazadeh@yazd.ac.ir

Tel: +98 351 8214778; Fax: +98 351 7250110

Received: 23-05-2017

Abstract

Two new complexes $[\text{Cu}(\text{bcen})\text{Ni}(\text{CN})_4]_2$ (**1**) and $[\text{Ni}(\text{bcen})\text{Ni}(\text{CN})_4]$ (**2**) where bcen is 4,7-diazadecanediamide, were synthesized by reaction of equimolar amounts of $\text{M}(\text{NO}_3)_2$ ($\text{M} = \text{Cu}$ and Ni), bcen ligand and $\text{K}_2[\text{Ni}(\text{CN})_4]$. Single-crystal X-ray diffraction analysis of compound **1**, shows that the bcen ligand acts as a tridentate chelate, coordinating to the Cu(II) ion via the two nitrogen atoms of the amine groups and one oxygen atom of one amide group, and the other amide unit is left uncoordinated. The coordination geometry around the Cu(II) ions is five coordinate with a distorted square pyramid geometry, comprising two nitrogen atoms and one oxygen atom belonging to the bcen ligand and two nitrogen atoms of the cyano groups of two $\text{Ni}(\text{CN})_4^{2-}$ units. The distance between the copper ion and the amide oxygen of the dangling arm of an adjacent tetranuclear species is within the expected range for an axial Cu–O bond, and hence suggests that the amide oxygen of an adjacent tetranuclear complex may weakly coordinate to the copper ion in an axial position. These contacts link the tetranuclear species into infinite chain polymers.

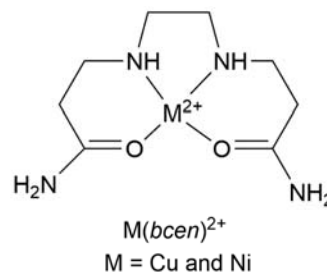
Keyword: Cyano bridged; Multinuclear; diamine-diamide; Crystal structure; Tetracyanonickelate

1. Introduction

In recent years a great effort has been focused on the design, synthesis and study of multinuclear transition metal complexes. These complexes not only have played an important role in the development of modern coordination chemistry, but also can be utilized as model compounds for the active sites of multimetallo enzymes.^{1,2} Among them, investigations of hetero-nuclear complexes tend to be more informative than the homo-nuclear complexes, due to interesting properties which can arise from the presence of two different metal ions.^{3–5}

There are variety of strategies for synthesizing homo and hetero-multinuclear complexes. A general approach is to use bridging ligands such as halides, pseudo-halides, oxalate, sulfate, etc.^{6–10} Self-assembly is the most efficient approach for the construction of such molecular systems.^{11–13} Another popular and successful approach for the preparation of multinuclear complexes with unusual

and interesting properties is to employ cyano complexes (metalloligand) such as $\text{Ag}(\text{CN})_2^-$, $\text{Ni}(\text{CN})_4^{2-}$, $\text{Cr}(\text{CN})_6^{3-}$, $\text{Pd}(\text{CN})_4^{2-}$, $\text{Pt}(\text{CN})_4^{2-}$, etc.^{14–17} The cyano anion is able to act either as a terminal or as a bridging ligand. Tetracyanometallic complex anions, $\text{M}(\text{CN})_4^{2-}$ ($\text{M} = \text{Ni}$, Pd and Pt) can act in the bridging mode by using either one, two, three or all four cyano groups. It usually leads to formation of one-(1D), two-(2D) or three-dimensional (3D) structures.^{17–19}



Scheme 1. Structure of diamine-diamide complexes

Herein, we report the synthesis, spectroscopic characterization and structural aspects of two new homo and hetero-nuclear complexes derived from the metalloligand complexes $\text{Ni}(\text{CN})_4^{2-}$, and coordinatively unsaturated $\text{Cu}(\text{bcen})^{2+}$ and $\text{Ni}(\text{bcen})^{2+}$ complexes (bcen = 4,7-diaza-decanediamide, also known as *N,N'*-bis(β -carbamoylethyl)ethylenediamine) (Scheme 1).

2. Experimental

2.1. Materials and Measurements

All chemicals were of analytical reagent grade and were used without further purification. The complex $\text{K}_2[\text{Ni}(\text{CN})_4] \cdot \text{H}_2\text{O}$ was prepared according to the literature procedure by mixing stoichiometric amounts of nickel(II) chloride hexahydrate (2.00 mmol, 0.475 g) in H_2O (10 mL) with potassium cyanide (8.00 mmol, 0.521 g) in 10 mL of water.²³ The diamine-diamide ligand 4,7-diaza-decanediamide (bcen) was prepared as previously reported from ethylenediamine and acrylamide in acetonitrile by heating the mixture under reflux.^{24–26} The white powder was re-crystallized from CHCl_3 . Infrared spectra were taken with an Equinox 55 Bruker FT-IR spectrometer using KBr pellets in the 400–4000 cm^{-1} range. Elemental analyses (C, H, N) were performed by using a CHNS-O 2400II PERKIN-ELMER elemental analyzer.

2.2. X-ray Crystallography

Diffraction images were measured at 150 K on SuperNova diffractometer using $\text{Cu K}\alpha$ ($\lambda = 1.54180 \text{ \AA}$) radiation. Data were extracted using the CrysAlis PRO package.²⁰ The structures were solved by direct methods with the use of SIR92.²¹ The structures were refined on F^2 by full matrix least-squares techniques using the CRYSTALS program package.²² The H atoms were initially refined with soft restraints on the bond lengths and angles to regularise their geometry (C–H in the range 0.93–0.98, N–H = 0.87, O–H = 0.83 Å) and with $U_{\text{iso}}(\text{H})$ in the range 1.2–1.5 times U_{eq} of the parent atom, after which the positions of the H atoms were refined without constraints. Atomic coordinates, bond lengths and angles and displacement parameters have been deposited at the Cambridge Crystallographic Data Centre. Crystallographic data and refinement details for the complex is given in Table 1.

2.3. Syntheses

2.3.1 $[\text{Cu}(\text{bcen})\text{Ni}(\text{CN})_4]_2 \cdot 2\text{CH}_3\text{OH}$, **1**

To a solution of bcen (1.00 mmol, 0.198 g) in methanol (40 mL) was added $\text{Cu}(\text{NO}_3)_2 \cdot 3\text{H}_2\text{O}$ (1.00 mmol, 0.242 g) with stirring for 10 min. Then, to this blue solution of $[\text{Cu}(\text{bcen})]^{2+}$, $[\text{Ni}(\text{CN})_4]^{2-}$ (1.00 mmol, 0.260 g) dissolved in a minimum volume of water was added drop-

Table 1. Crystallographic data of $[\text{Cu}(\text{bcen})\text{Ni}(\text{CN})_4]_2$ complex

Compound	1
Chemical formula	$\text{C}_{26}\text{H}_{44}\text{Cu}_2\text{N}_{16}\text{Ni}_2\text{O}_6$
Formula weight	921.25
<i>T</i> (K)	150
Space group	Triclinic, $\bar{P}1$
<i>Z</i>	1
<i>a</i> (Å)	9.1232(6)
<i>b</i> (Å)	10.2600(6)
<i>c</i> (Å)	10.4739(6)
α (°)	78.683(5)
β (°)	78.604(5)
γ (°)	79.671(5)
<i>V</i> (Å ³)	932.26(10)
<i>F</i> (000)	474
<i>D</i> _{calc} (g cm ⁻³)	1.641
μ (mm ⁻¹)	2.94
Measured reflections	14724
Independent reflections	3685
<i>R</i> _{int}	0.023
Observed reflections	3555
$R[F^2 > 2\sigma(F^2)]$	0.025
$wR(F^2)$ (all data)	0.069*

$$*w = 1/[\sigma^2(F^2) + (0.04P)^2 + 0.53P], \text{ where } P = (\max(F_o^2, 0) + 2F_c^2)/3$$

wise with stirring for 5 min. The precipitate that was initially obtained was filtered off and the filtrate was left aside for crystallization. Blue cube-shaped crystals suitable for X-ray diffraction appeared at the bottom of the vessel upon slow evaporation of the solvents at room temperature, and were collected by filtration, washed with methanol and dried in the air. The yield was 87%. Anal. Calc. for $\text{C}_{26}\text{H}_{44}\text{Cu}_2\text{N}_{16}\text{Ni}_2\text{O}_6$: C, 33.90; H, 4.81; N, 24.33. Found: C, 34.06; H, 4.83; N, 24.27. IR (KBr, cm^{-1}): $\nu_{\text{C=N}}$ = 2126 and 2172.

2.3.2. $\{[\text{Ni}(\text{bcen})\text{Ni}(\text{CN})_4] \cdot 2\text{H}_2\text{O}\}_n$, **2**

The complex **2** was synthesized in a similar manner as described for **1** by using $\text{Ni}(\text{NO}_3)_2 \cdot 6\text{H}_2\text{O}$ (1.00 mmol, 0.291 g) instead of $\text{Cu}(\text{NO}_3)_2 \cdot 3\text{H}_2\text{O}$. The pale blue precipitate was filtered off and the filtrate left aside. Upon slow evaporation of the solvents at room temperature, a pale blue precipitate was obtained. The precipitate is insoluble in most common organic solvents such as methanol, ethanol, acetone, acetonitrile and dichloromethane and also is only very slightly soluble in water and DMF. We attempted to grow single crystals of the complex but had no success due to its insolubility. The complex was purified by washing with methanol-water (1:1 v/v) solution to remove unreacted materials from the crude solid. The yield was 71%. Anal. Calc. for $\text{C}_{12}\text{H}_{22}\text{N}_8\text{Ni}_2\text{O}_4$: C, 31.35; H, 4.82; N, 24.37. Found: C, 30.90; H, 4.74; N, 23.88. IR (KBr, cm^{-1}): $\nu_{\text{C=N}}$ = 2122 and 2152.

3. Results and Discussion

3.1. Syntheses and Characterization of the Complexes

The $M(\text{bcen})^{2+}$ complexes ($M = \text{Cu}$ and Ni) were obtained by the *in-situ* reaction of metal nitrate and bcen ligand in methanol at room temperature. The $M(\text{bcen})^{2+}$ complexes upon the addition of an equimolar ratio of $\text{Ni}(\text{CN})_4^{2-}$ form of complexes **1** and **2**. Both complexes are stable in air and insoluble in common organic solvents and very slightly soluble in water and DMF. The insolubility of the complexes suggests that they are polymeric compounds.²⁷

Besides elemental analysis, the complexes were initially characterized by infrared spectral techniques which were useful in identifying the bonding mode (terminal or bridging) of the cyano groups in $\text{Ni}(\text{CN})_4^{2-}$ to the metal(II) ion. The absorption bands due to the cyano groups are the most important aspects of the infrared spectra in these types of complexes. In the IR spectrum of the free CN^- , the cyanide stretching vibration band appears at 2077 cm^{-1} .²⁸ In the IR spectrum of $\text{K}_2[\text{Ni}(\text{CN})_4]$ complex this band appears at 2128 cm^{-1} .^{28–30} In the IR spectra of **1** and **2**, there are two peaks for cyano stretching vibrations arising from the presence of both bridged and non-bridged cyano groups. For **1** these are at 2126 (non-bridged) and 2172 cm^{-1} (bridged) and for **2** they are at 2120 (non-bridged) and 2151 cm^{-1} (bridged) (Fig. 1). The increase of cyano stretching vibration band with the formation of cyano bridge, $M-\text{N}\equiv\text{C}-\text{Ni}$ ($M = \text{Cu}$ and Ni) in the complexes in comparison with the cyano non-bridge are due to the kinematic effect, i.e. the impediment of the C–N vibration due to the attachment of the second metal unit Ni and M.³⁰

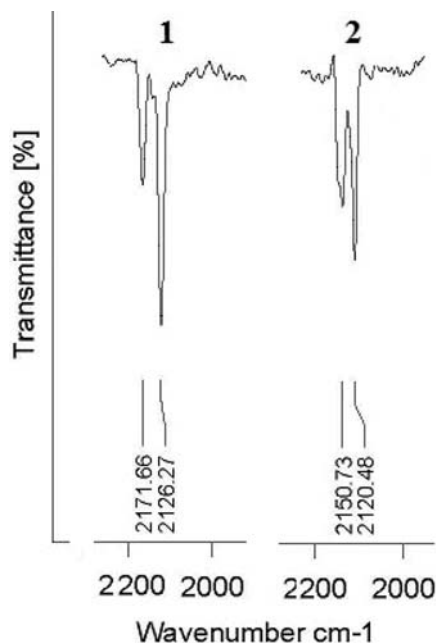


Fig. 1. The infrared spectra of complexes **1** and **2**

3.2. Description of Crystal Structure the Complex, 1

The molecular structure of hetero-tetranuclear **1** is shown in Fig. 2. Selected bond lengths and angles as well as interatomic distances are summarized in Table 2.

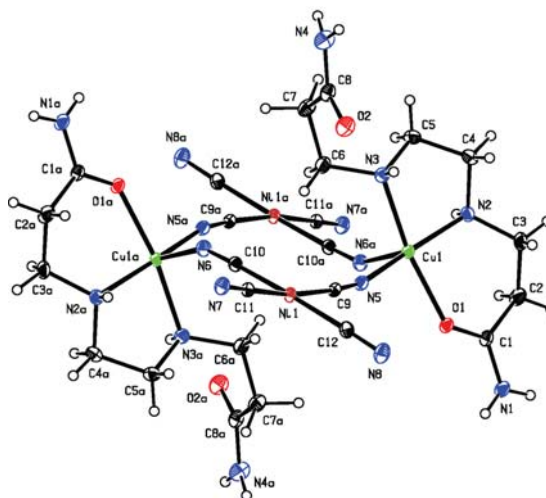


Fig. 2. The structure of the $[\text{Cu}(\text{bcen})\text{Ni}(\text{CN})_4]_2$ complex, **1**, with labelling of selected atoms. Anisotropic displacement ellipsoids exhibit 30% probability levels. Hydrogen atoms are drawn as circles with small radii.

Complex **1** consists of discrete tetranuclear mixed metal species with two copper and two nickel centers which are connected *via* cyano bridging ligands.

Table 2. Selected bond lengths (Å) and angles (°) in $[\text{Cu}(\text{bcen})\text{Ni}(\text{CN})_4]_2$ complex

Cu1O1	2.0486 (11)	Ni1–C9	1.8553 (16)
Cu1N2	1.9989 (14)	Ni1–C10	1.8728 (17)
Cu1N3	2.0417 (14)	Ni1–C11	1.8767 (16)
Cu1N5	1.9628 (14)	Ni1–C12	1.8721 (17)
Cu1N6 ^a	2.2182 (14)	N5–C9	1.146 (2)
C1–O1	1.2617 (19)	N6–C10	1.152 (2)
C8–O2	1.2250 (20)	N7–C11	1.149 (2)
Cu1...O2 ^b	2.9070 (15)	N8–C12	1.153 (2)
O1–Cu1–N2	93.10 (6)	C9–Ni1–C10	86.88 (7)
N6 ^a –Cu1–O1	96.04 (5)	C9–Ni1–C11	171.96 (7)
N6 ^a –Cu1–N2	91.60 (6)	C10–Ni1–C11	92.14 (7)
N6 ^a –Cu1–N3	97.80 (6)	C9–Ni1–C12	89.11 (7)
N2–Cu1–N3	84.94 (6)	C10–Ni1–C12	174.55 (7)
N3–Cu1–N5	91.40 (6)	C11–Ni1–C12	92.34 (7)
O1–Cu1–N3	166.06 (5)	N5–C9–Ni1	175.34 (16)
N2–Cu1–N3	84.94 (6)	N6–C10–Ni1	172.85 (14)
O1–Cu1–N5	86.90 (5)	N7–C11–Ni1	179.28 (14)
N6 ^a –Cu1–N5	103.55 (6)	N8–C12–Ni1	175.69 (15)
Cu1–N5–C9	164.64 (13)		
Cu1 ^a –N6–C10	150.09 (13)		

Symmetry codes: a = $-x + 1, -y + 1, -z + 1$; b = $-x + 2, -y + 1, -z + 1$

Previous studies on the diamine-diamide ligands and copper(II) have shown complexes where the ligand is tetradentate and coordinates to the metal center through the two amine nitrogen atoms and the two amide oxygen atoms.^{31,32} However, in complex **1** the crystallographic analyses reveals that the bcen ligand is tridentate chelate, coordinating to the metal ion *via* the two nitrogen atoms of the amine groups and the oxygen atom of one amide group, and other amide unit does not bond to that Cu atom. There have been a few studies on the formation and dissociation of the Cu(bcen)²⁺ complex and also on the kinetics of metal exchange complexes with the bcen ligand, and they reported that the Cu(II)–O bond to the amide is

substitutionally labile.^{25,26,33} The X-ray characterization of complex **1** shows that the bond between Cu(II) and a labile amide oxygen of bcen ligand has broken under these experimental conditions, followed by coordination of Cu(II) to cyanide nitrogen atoms of Ni(CN)₄²⁻ moieties.

The distance between copper ion (Cu1) and the amide oxygen of the dangling arm of an adjacent tetranuclear species (O2a, symmetry code: $-x + 1, -y + 1, -z + 1$) is 2.9070(15) Å which is significantly longer than the typical Cu–O covalent bond (1.98 Å), but it is slightly shorter than the sum of the van der Waals radii (2.92 Å).³⁴ This distance is within the range of 2.2–2.9 Å, known for axial Cu–O bonds,³⁵ and hence suggests that the amide oxygen

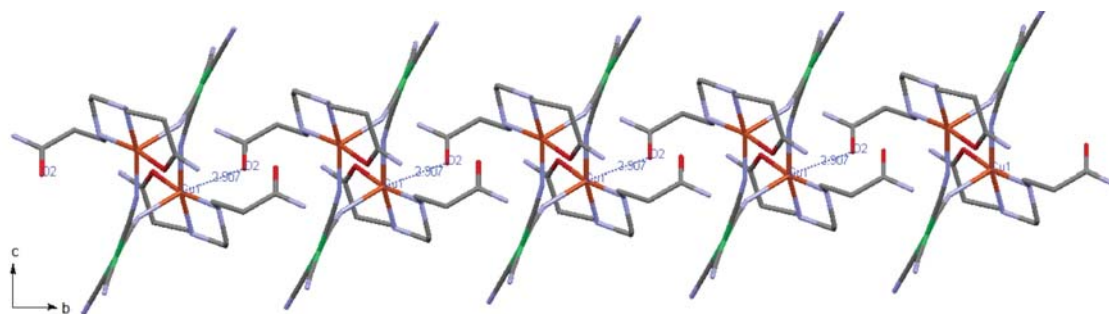


Fig. 3. The contacts between copper ion and the amide oxygen of dangling arm in adjacent tetranuclear species in complex **1**.

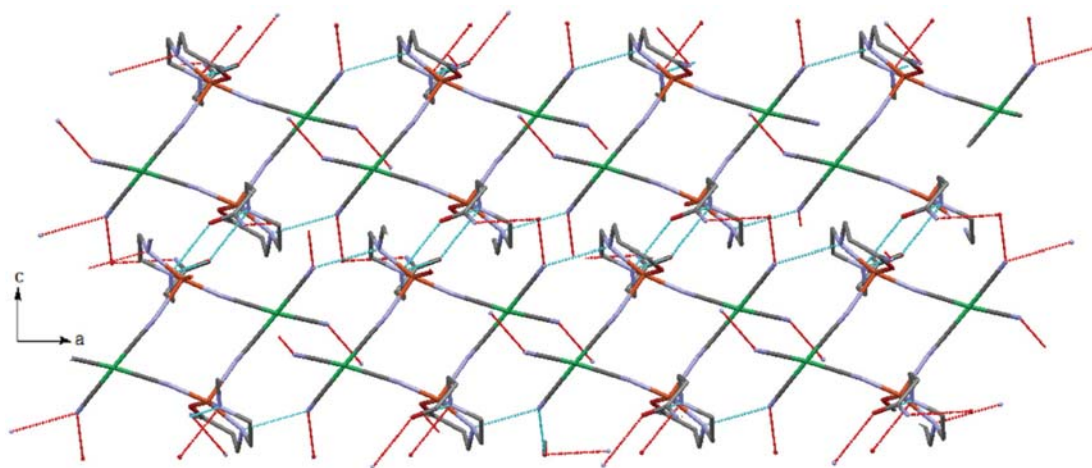


Fig. 4. Various hydrogen bonding interactions in complex **1** along *ac* plane.

Table 3. Hydrogen bonding (Å) and angles (°) for [Cu(bcen)Ni(CN)₄]₂ complex

D–H...A	D–H	H...A	D...A	D–H...A	Symmetry code
N1–H1... O1	0.83(3)	2.37(3)	3.199(3)	173(2)	$-x + 1, -y + 1, -z + 2$
N1–H2... N7	0.83(3)	2.19(3)	3.006(3)	168(2)	$x, y - 1, z + 1$
N2–H3... N8	0.89(3)	2.25(3)	3.023(3)	145(2)	$x, y - 1, z$
N3–H4... O2	0.86(2)	2.45(2)	3.026(3)	125(2)	x, y, z
N3–H4... O2	0.86(2)	2.37(2)	2.996(3)	130(2)	$-x + 2, -y + 1, -z + 1$
N4–H5... O1	0.91(2)	2.22(2)	3.123(3)	171(2)	$-x + 2, -y + 1, -z + 1$
N4–H6... O3	0.96(2)	1.97(2)	2.911(3)	165(2)	$-x + 2, -y + 1, -z + 1$
O3–H7... N8	0.89(2)	1.96(2)	2.834(3)	170(3)	x, y, z

of adjacent tetranuclear complex may weakly coordinate to the copper ion in an axial position. These contacts link the tetranuclear species into infinite chains along the *b* axis (Fig. 3).

Adjacent 1D chains are connected by C≡N(terminal)⋯H₂N(amide ligand) contacts to form a 2D layer structure (Fig. 4). The 2D layers are extended into 3D supramolecular networks by C≡N(terminal)⋯HN(amine) hydrogen bonds interactions. Full details of the hydrogen bonding are given in Table 3. Insolubility of the complex in different solvents is consistent with its polymeric nature.²⁷

The copper(II) centers are five-coordinate with a N₄O donor set from the bcn ligand (N₂O) and two bridging cyanides. Coordination geometry about each copper ion is essentially a square pyramid with one oxygen and two nitrogen atoms from the bcn ligand and two nitrogen atoms, one from each of two of [Ni(CN)₄]²⁻ units. According to the bond lengths between the copper ions and the coordinating atoms, the square base consists of the N₂O donors from the bcn ligand and the closer of the bridging cyanide nitrogen atoms (Cu–N = 1.9628(14) Å), and the apical position is occupied by the longer Cu–N from the bridging cyanide (2.2182(14) Å). The copper is displaced from the basal plane of N₃O by 0.254 Å towards the apical nitrogen atom. The Addison parameter τ value is 0.022. The τ parameter is defined as $\tau = (\alpha - \beta)/60$, $\alpha > \beta$, where α and β are the largest angles; $\tau = 1$ for a regular trigonal bipyramid and $\tau = 0$ for a regular square pyramid.³⁶

The Ni(II) ions are coordinated by the C atoms of four cyanide ligands in a square planar geometry. The bond distances for Ni–C and C≡N in the Ni(CN)₄²⁻ moiety are in range of 1.8553(16)–1.8767(16) Å and 1.146(2)–1.153(2) Å, respectively, which is in accordance with the reported values for similar complexes.^{14–16,18,37} Although Ni–C and C≡N bond lengths can vary depending on whether they are in bridging and terminal modes, here there are no significant variations. The Cu–N≡C bond angles (164.64(13) and 150.09(13)°) are significantly bent, whereas the Ni–C≡N bond angles are essentially linear and range from 172.85(14) to 179.28(14)°.

The nickel core has a τ_4 index of 0.096. The τ_4 parameter is $[360^\circ - (\alpha + \beta)]/141^\circ$, where α and β are the largest angles around the central metal in the complex; $\tau_4 = 1$ for a regular tetrahedron and $\tau_4 = 0$ for a regular square planar geometry.³⁸ Each [Ni(CN)₄]²⁻ group coordinates to two Cu(II) ions using two *cis*-cyanide ligands. Each Cu(bcn) unit is connected to two [Ni(CN)₄]²⁻ moieties through a basal plane and an apical position.

4. Conclusions

We have synthesized two multi-nuclear complexes by reaction of M(bcn)²⁺ (M = Cu and Ni) and K₂[Ni(CN)₄]. The IR spectra of the two complexes revealed

the presence of both bridged and non-bridged cyano groups. The crystallographic analyses revealed that complex **1** consists of discrete tetranuclear mixed metal species with two copper and two nickel centers which are connected *via* cyano bridging ligands of [Ni(CN)₄]²⁻ moieties. The bcn tetradentate ligand in complex **1** acts as a tridentate ligand and an amide unit of the bcn was left as a dangling arm. The contact between the amide of the dangling arm and copper ion of an adjacent tetranuclear unit give rise to infinite chain polymers. Insolubility of the complex in several solvents is consistent with its polymeric nature.

5. Supplementary Material

The deposition number of the studied complex is CCDC 1547091. These data can be obtained free-of-charge via www.ccdc.cam.ac.uk/data_request/cif, by emailing data-request@ccdc.cam.ac.uk, or by contacting The Cambridge Crystallographic Data Centre, 12 Union Road, Cambridge CB2 1EZ, UK; fax +44 1223 336033.

6. Acknowledgement

The authors are grateful to the Yazd University and the Australian National University for their valuable support of this work.

References

1. E. I. Solomon, D. E. Heppner, E. M. Johnston, J. W. Ginsbach, J. Cirera, M. Qayyum, M. T. Kieber-Emmons, C. H. Kjaergaard, R. G. Hadt, L. Tian, *Chem. Rev.* **2014**, *114*, 3659–3853. <https://doi.org/10.1021/cr400327t>
2. C. E. Elwell, N. L. Gagnon, B. D. Neisen, D. Dhar, A. D. Spaeth, G. M. Yee, W. B. Tolman, *Chem. Rev.* **2017**, *117*, 2059–2107. <https://doi.org/10.1021/acs.chemrev.6b00636>
3. R. Vafazadeh, B. Khaledi, A. C. Willis, *Acta Chim. Slov.* **2012**, *59*, 954–958.
4. S. Uysal, *J. Coord. Chem.* **2010**, *63*, 2370–2378. <https://doi.org/10.1080/00958972.2010.501106>
5. J. A. Garden, P. K. Saini, C. K. Williams, *J. Am. Chem. Soc.* **2015**, *137*, 15078–15081. <https://doi.org/10.1021/jacs.5b09913>
6. R. Vafazadeh, N. Hasanzade, M. M. Heidari, A. C. Willis, *Acta Chim. Slov.* **2015**, *62*, 122–129. <https://doi.org/10.17344/acsi.2014.797>
7. R. Vafazadeh, Z. Moghadas, A. C. Willis, *J. Coord. Chem.* **2015**, *68*, 4255–4271. <https://doi.org/10.1080/00958972.2015.1096349>
8. R. Vafazadeh, R. Esteghamat-Panaha, A. C. Willis, A. F. Hill, *Polyhedron* **2012**, *48*, 51–57. <https://doi.org/10.1016/j.poly.2012.08.057>

9. R. Vafazadeh, A. C. Willis, *Acta Chim. Slov.* **2016**, *63*, 186–192. <https://doi.org/10.17344/acsi.2016.2263>
10. Z. Yolcu, S. Demir, Ö. Andaç, O. Büyükgüngör, *Acta Chim. Slov.* **2016**, *63*, 646–653. <https://doi.org/10.17344/acsi.2016.2475>
11. R. Vafazadeh, F. Jafari, M. M. Heidari, A. C. Willis, *J. Coord. Chem.* **2016**, *69*, 1313–1325. <https://doi.org/10.1080/00958972.2016.1163547>
12. R. Vafazadeh, A. C. Willis, *J. Coord. Chem.* **2015**, *68*, 2240–2252. <https://doi.org/10.1080/00958972.2015.1048688>
13. D. Venegas-Yazigia, D. Aravenab, E. Spodineb, E. Ruizd, S. Alvarez, *Coord. Chem. Rev.* **2010**, *254*, 2086–2095. <https://doi.org/10.1016/j.ccr.2010.04.003>
14. D. Zhang, L. Kong, H. Zhang, *Acta Chim. Slov.* **2015**, *62*, 219–224.
15. I. Kocanová, J. Kuchár, M. Orendác, J. Cernák, *Polyhedron* **2010**, *29*, 3372–3379. <https://doi.org/10.1016/j.poly.2010.09.018>
16. I. Nemeč, R. Herchel, R. Boca, I. Svoboda, Z. Travnicek, L. Dlhán, K. Matelková, H. Fuess, *Inorg. Chim. Acta* **2011**, *366*, 366–372. <https://doi.org/10.1016/j.ica.2010.11.028>
17. I. Potocnak, M. Vavra, E. Cizmár, M. Dušek, T. Müller, D. Steinborn, *Inorg. Chim. Acta* **2009**, *362*, 4152–4157. <https://doi.org/10.1016/j.ica.2009.06.014>
18. J. Shi, C. Xue, L. Kong, D. Zhang, *Acta Chim. Slov.* **2017**, *64*, 215–220. <https://doi.org/10.17344/acsi.2016.3132>
19. G. S. Kürkcüoğlu, O. Z. Yesilel, I. Kavlak, O. Büyükgüngör, *Z. Anorg. Allg. Chem.* **2009**, *635*, 175–178. <https://doi.org/10.1002/zaac.200800337>
20. *CrysAlis PRO*, Agilent Technologies, 2014.
21. A. Altomare, G. Cascarano, G. Giacovazzo, A. Guagliardi, M. C. Burla, G. Polidori, M. Camalli, *J. Appl. Cryst.* **1994**, *27*, 435–436.
22. P. W. Betteridge, J. R. Carruthers, R. I. Cooper, K. Prout, D. J. Watkin, *J. Appl. Cryst.* **2003**, *36*, 1487–1487. <https://doi.org/10.1107/S0021889803021800>
23. G. S. Kurkcüoğlu, O. Z. Yesilel, I. Kavlak, O. Buyukgungor, *Struct. Chem.* **2008**, *19*, 879–888. <https://doi.org/10.1007/s11224-008-9354-3>
24. S. H. Liu, C. S. Chung, *Inorg. Chem.* **1986**, *25*, 3890–3896. <https://doi.org/10.1021/ic00242a013>
25. R. Vafazadeh, F. Gholami, *Acta Chim. Slov.* **2010**, *57*, 746–750.
26. R. Vafazadeh, G. Zare-Sadrabadi, *Acta Chim. Slov.* **2015**, *62*, 889–894. <https://doi.org/10.17344/acsi.2015.1611>
27. S. A. Khan, N. Nishat, S. Parveen, R. Rasool, *Spectrochim. Acta A* **2011**, *81*, 290–395. <https://doi.org/10.1016/j.saa.2011.06.012>
28. K. Nakamoto, *Infrared and Raman Spectra of Inorganic and Coordination Compounds*, 5th ed., John Wiley and Sons, New York, 1997.
29. A. Bienko, J. Klak, J. Mrozinski, S. Domagala, B. Korybut-Daszkievicz, K. Wozniak, *Polyhedron* **2007**, *26*, 5030–5038. <https://doi.org/10.1016/j.poly.2007.07.016>
30. T. Sheng, H. Vahrenkamp, *Inorg. Chim. Acta* **2004**, *357*, 1739–1747. <https://doi.org/10.1016/j.ica.2003.11.006>
31. C. Y. Hong, T. Y. Lee, T. J. Lee, M. S. Chao, C. S. Chung, *Acta Cryst.* **1987**, *C43*, 34–37.
32. T. H. Lu, H. C. Shan, M. S. Chao, C. S. Chung, *Acta Cryst.* **1987**, *C43*, 207–209.
33. S. H. Liu, C. S. Chung, *Inorg. Chem.* **1986**, *25*, 3890–3896. <https://doi.org/10.1021/ic00242a013>
34. B. Cordero, V. Gómez, A. E. Platero-Prats, M. Revés, J. Echeverría, E. Cremades, F. Arragán, S. Alvarez, *Dalton Trans.* **2008**, 2832–3838. <https://doi.org/10.1039/b801115j>
35. I. M. Procter, B. J. Hathaway, P. Nicholls, *J. Chem. Soc. A* **1968**, 1678–1684. <https://doi.org/10.1039/j19680001678>
36. A. W. Addison, N. Rao, J. Reedijk, J. V. Rijn, G. C. Verschoor, *J. Chem. Soc. Dalton Trans.* **1984**, 1349–1356. <https://doi.org/10.1039/DT9840001349>
37. A. Ray, D. Dutta, P. C. Mondal, W. S. Sheldrick, H. Mayer-Figge, M. Ali, *Polyhedron* **2007**, *26*, 1012–1022. <https://doi.org/10.1016/j.poly.2006.09.095>
38. P. Seth, S. Ghosh, A. Figuerola, A. Ghosh, *Dalton Trans.* **2014**, *43*, 990–998. <https://doi.org/10.1039/C3DT52012A>

Povzetek

Z reakcijo ekvimolarnih količin $M(\text{NO}_3)_2$ ($M = \text{Cu}$ in Ni), bcen liganda in $\text{K}_2[\text{Ni}(\text{CN})_4]$ smo sintetizirali dva nova kompleksa $[\text{Cu}(\text{bcen})\text{Ni}(\text{CN})_4]_2$ (**1**) in $[\text{Ni}(\text{bcen})\text{Ni}(\text{CN})_4]$ (**2**), kjer je bcen 4,7-diazadekandiamid. Monokristalna rentgenska analiza spojine **1** razkrije, da se bcen ligand koordinira na $\text{Cu}(\text{II})$ ion kot trovezni kelatni ligand preko dveh dušikovih atomovaminske skupine in enega kisikovega atoma ene amidne skupine, medtem ko druga amidna enota ni koordinirana. $\text{Cu}(\text{II})$ center ima koordinacijsko število pet s popačeno kvadratno piramidalno geometrijo, ki jo tvorijo en kisikov atom in dva dušikova atoma bcen liganda in dva dušikova atoma ciano skupin dveh $\text{Ni}(\text{CN})_4^{2-}$ enot. Razdalja med bakrovim ionom in amidnim kisikom na nekoordinirani skupini sosednje štirijedrne zvrsti je znotraj pričakovanega območja za aksialno $\text{Cu}-\text{O}$ vez, kar nakazuje, da je amidni kisikov atom s sosednjega štirijedrnega kompleksa šibko koordiniran na bakrov ion v aksialni legi. Ta kontakt povezuje štirijedrne zvrsti v neskončno verigo.

Scientific paper

Magnetite-Containing Sulfonated Polyacrylamide as a Nanocatalyst for the Preparation of Biscoumarins

Kaveh Parvanak Boroujeni,^{1,*} Shahla Hadizadeh,¹ Sodabeh Hasani,¹
Abdulhamid Fadavi² and Mansooreh Shahrokh¹

¹ Department of Chemistry, Shahrekord University, P.O. Box 88186-34141 Shahrekord, Iran

² Department of Chemistry, Marvdasht Branch, Islamic Azad University, Marvdasht, Iran

* Corresponding author: E-mail: parvanak-ka@asci.sku.ac.ir

Tel.: +0098-38-32324401; fax: 0098-38-32324419

Received: 12-04-2017

Abstract

Magnetite-containing sulfonated polyacrylamide was easily prepared through polymerization of the corresponding monomers followed by the reaction with Fe₃O₄ nanoparticles. The characterization of the obtained catalyst was performed by Fourier transform infrared spectroscopy (FT-IR), thermal gravimetric analysis (TGA), scanning electron microscopy (SEM), energy dispersive spectroscopy (EDS), X-ray diffraction (XRD), and vibrating sample magnetometer (VSM). The acidic SO₃H moiety was found to be 1.1 mmol per gram of the obtained polymer. The catalytic activity of the polymer was examined for the synthesis of biscoumarin derivatives by two-component one-pot domino Knoevenagel-type condensation/Michael reaction between aldehydes and 4-hydroxycoumarin. Biscoumarins were obtained in high to excellent yields in short time. The work-up procedure of this reaction was very simple. The catalyst is stable (as a bench top catalyst) with easy-handling and it can be used again.

Keywords: Nanoparticles; Radical polymerization; Magnetism and magnetic properties; Catalysts; Biscoumarins

1. Introduction

Due to the unique characteristics of magnetite Fe₃O₄ nanoparticles, they have attracted great attention in the field of biology, medicine, electronics, and catalytic processes.¹ However, Fe₃O₄ nanoparticles respond to external stimuli such as the pH value and temperature, due to the pH- and temperature-sensitive properties. Also, they are unstable in the presence of oxygen at light and coagulation of nanoparticles is usually unavoidable during their use. Therefore, there has been a considerable research effort to stabilize Fe₃O₄ nanoparticles through coating the surface of such nanoparticles with carbon, precious metals, silica, and polymers. In this regard, the use of polymers containing a functional group that binds strongly to the nanoparticles through covalent or electrostatic interactions has been the subject of great interest to researchers.² For this purpose, a variety of polymeric materials, such as poly(glycerol monoacrylate), polyaniline, polyacrylamide, poly(*N*-vinyl-2-pyrrolidone), poly(*para*-phenylenediamine), poly(vinylalcohol), poly(ether-amide), polypyr-

role, and chitosan as well as polymers containing polar pendant groups, such as carboxylate, phosphate, or sulfate groups have been used.^{3–6}

Recently, magnetic nanomaterials have emerged as a promising catalysts for various organic and inorganic reactions because of their large surface-to-volume ratio relative to bulk materials and hence the large ratio of atoms available at the surface.² These types of catalysts can be easily separated using an external magnet and their catalytic activity remains high even after several reaction cycles. Magnetite catalysts were used as efficient catalytic systems in many chemical transformations including asymmetric hydrogenation of aromatic ketones,⁷ the desymmetrization of racemic 1,2-diols through asymmetric benzylation,⁸ synthesis of 14-aryl- or alkyl-14*H*-dibenzo[*a,j*]xanthenes and 1,8-dioxocotahydroxanthene derivatives,^{9,10} Sonogashira cross-coupling reaction,¹¹ synthesis of tetrahydrobenzo[*a*]xanthene-11-ones,¹² C–N bond formation *via* aza-Michael addition,⁶ and preparation of functionalized tricarboxamide derivatives.¹³

Coumarin and its derivatives are important as anti-HIV, antibiotic, antifungal, antibacterial, antioxidant, anti-cancer, and anticoagulant agents.^{14–16} Among various derivatives of coumarin, biscoumarins have aroused considerable interest. These important compounds were usually prepared from the reaction of aldehydes with 4-hydroxycoumarin. Several types of catalysts were introduced previously for this reaction, such as piperidine,¹⁷ tetrabutylammonium bromide,¹⁸ I₂,¹⁹ sodium dodecyl sulfate,²⁰ 1-buthyl-3-methylimidazolium tetrafluoroborate,²¹ 1-ethyl-3-(3-sulfopropyl)-benzimidazolium trifluoromethanesulfonate,²² *para*-dodecylbenzenesulfonic acid/piperidine,²³ 3-methyl-1-(4-sulfonic acid)butylimidazolium hydrogen sulfate,²⁴ B(HSO₄)₃,²⁵ polyvinylpyrrolidone-supported nickel nanoparticles,²⁶ poly(4-vinylpyridine)-supported ionic liquids,^{27,28} and cellulose sulfonic acid.²⁹ Also, biscoumarin derivatives have been prepared by the condensation of 1,2-diols and 4-hydroxycoumarin using Pb(OAc)₄.³⁰ However, many of these methods have some drawbacks, such as a requirement for either a long reaction time or harsh reaction conditions, provide low yields, include laborious work-up procedures, inefficiency of method when aliphatic aldehydes are used in the reaction, and the use of unrecyclable, hazardous or difficult to handle catalysts.

In continuation of our research on the synthesis and applications of polymer-supported catalysts and nanocomposites,^{27,28,31,32} we now wish to introduce poly(2-acrylamido-2-methyl propane sulphonic acid-*co*-acrylamide) containing Fe₃O₄ nanoparticles (poly(AMPS-*co*-AA)@Fe₃O₄) as a heterogeneous catalyst for the synthesis of biscoumarin derivatives. Poly(AMPS-*co*-AA)@Fe₃O₄ was prepared by benzoyl peroxide (Bz₂O₂) initiated polymerization of 2-acrylamido-2-methylpropane sulphonic acid (AMPS) with acrylamide (AA) followed by reaction with Fe₃O₄ nanoparticles

2. Experimental

2. 1. Materials and Methods

All chemicals were either prepared in our laboratory or were purchased from Merck and Fluka. Reaction monitoring and purity determination of the products were accomplished by GLC or TLC on silica-gel polygram SILG/UV₂₅₄ plates. Gas chromatography was carried out on Shimadzu GC 14–A. IR spectra were obtained by a Shimadzu model 8300 FT-IR spectrophotometer. ¹H NMR spectra were recorded on 400 MHz spectrometer in CDCl₃. TGA was carried out on a Stanton Redcraft STA–780 with a 20 °C/min heating rate. Melting points were determined on a Fisher–Jones melting-point apparatus. XRD patterns were recorded by a Phillips X-ray diffractometer using graphite monochromatized Cu K α radiation. A morphological study of the synthesized products was carried out directly by a Hitachi S4160 field emission scanning electron microscope (FESEM). Room

temperature magnetic properties were investigated by Larkeshore device in an applied magnetic field sweeping between ± 8000 Oe.

2. 2. Preparation of Fe₃O₄ Nanoparticles

To a solution of ferrous chloride (FeCl₂, 1 M), NaOH (4 M) was added dropwise with vigorous stirring to produce a black solid product (magnetite Fe₃O₄ nanoparticles) when the reaction media reaches pH 12. The resulting nanoparticles were carefully decanted and washed repeatedly with doubly distilled water and absolute ethanol and then dried under vacuum at room temperature.

2. 3. Synthesis of (Poly(AMPS-*co*-AA)@Fe₃O₄)

First, in a round bottomed flask (50 mL) equipped with a reflux condenser, 0.051 g (0.214 mmol) of Bz₂O₂ was added to a solution of acrylamide (15 mmol, 1.066 g), AMPS (6.42 mmol, 1.330 g), and ethanol (25 mL) and the mixture was refluxed for 5 h. Afterwards, Fe₃O₄ nanoparticles (12 mmol, 2.78 g) were added to the mixture and refluxed for 1 h. Then, the obtained solid was easily separated from the reaction mixture by an external magnet and washed with deionized water and ethanol three times and dried overnight in vacuum at 80 °C.

The same procedure applied for the preparation of poly(AMPS-*co*-AA)@Fe₃O₄ was also repeated for the preparation of poly(AMPS-*co*-AA) without addition of Fe₃O₄ nanoparticles. In this case, the polymer formed in the first step was collected by filtration, washed three times with ethanol, and dried overnight in vacuum at 60 °C.

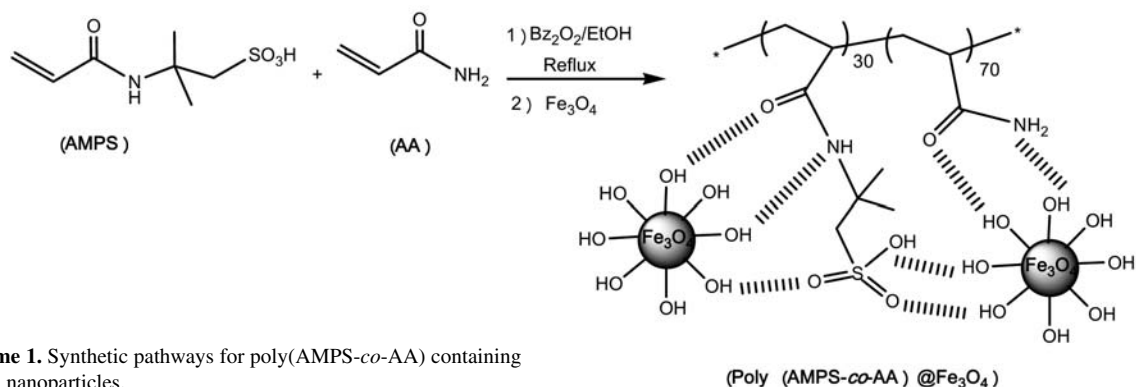
2. 4. Preparation of 3,3'-(4-Nitrobenzylidene)-bis-(4-hydroxycoumarin) as a Typical Procedure for the Synthesis of Biscoumarines

A mixture of 1 mmol of 4-nitrobenzaldehyde, 2 mmol of 4-hydroxycoumarin, 0.04 mmol of poly(AMPS-*co*-AA)@Fe₃O₄, and 3 mL of toluene was heated at 90 °C. After the completion of the reaction (monitored by TLC), the catalyst was removed by an external magnet and washed with toluene (2 \times 5 mL) and the filtrate was concentrated on a rotary evaporator under reduced pressure. The crude product was recrystallized from ethanol to give the pure 3,3'-(4-nitrobenzylidene)-bis-(4-hydroxycoumarin).

3. Results and Discussion

3. 1. Synthesis of Poly(AMPS-*co*-AA)@Fe₃O₄

Poly(AMPS-*co*-AA)@Fe₃O₄ was synthesized by free radical polymerization of AA and AMPS monomers



Scheme 1. Synthetic pathways for poly(AMPS-*co*-AA) containing Fe₃O₄ nanoparticles.

in the presence of Bz₂O₂ initiator followed by the reaction with Fe₃O₄ nanoparticles (Scheme 1). The acidic sites loading in poly(AMPS-*co*-AA)@Fe₃O₄ obtained by means of acid–base titration was found to be 1.1 mmol/g.^{27,28} For comparison purposes, poly(AMPS-*co*-AA) was also prepared *via* the same procedure applied for the preparation of poly(AMPS-*co*-AA)@Fe₃O₄ without addition of Fe₃O₄.

3. 2. Characterization of Poly (AMPS-*co*-AA)@Fe₃O₄

Figure 1 shows the FT-IR spectra of Fe₃O₄, poly(AMPS-*co*-AA), and poly(AMPS-*co*-AA)@Fe₃O₄. The IR spectral data of Fe₃O₄ show two characteristic peaks at 425 and 567 cm⁻¹, which are due to Fe–O stretching vibrations (Figure 3a).³¹ As shown in Figure 3b, the IR spectrum of poly(AMPS-*co*-AA) exhibits peaks at 3346 and 3428 cm⁻¹ (N–H vibrations of amide groups), 1663 cm⁻¹ (C=O vibrations of carbonyl groups), and 1208 cm⁻¹ (S=O vibrations of sulfonic groups).^{27,28} Also, the IR spectrum of poly(AMPS-*co*-AA)@Fe₃O₄ displayed peaks at 3422, 1658, and 1185 cm⁻¹ which are assigned to stretch-

ing vibrations of NH and NH₂, C=O, and S=O, respectively (Figure 3b). In IR spectrum of poly(AMPS-*co*-AA)@Fe₃O₄ the appearance of peaks at 429 and 574 cm⁻¹, attributed to Fe–O stretching vibrations, indicates that Fe₃O₄ nanoparticles were attached to the polymer chains.

Thermal data obtained from TGA analysis are presented in Figure 2. In TGA curves of Fe₃O₄ and poly(AMPS-*co*-AA)@Fe₃O₄ a slow mass loss observed between room temperature and 150 °C could be related to the removal of surface adsorbed water, the remaining solvent, and residual monomers. The second step weight loss starting from 180 °C in TGA curve of Fe₃O₄ could be attributed to thermal crystal phase transformations of Fe₃O₄ to Fe₂O₃. In the case of poly(AMPS-*co*-AA)@Fe₃O₄ the second step weight loss starting from 180 °C could be related to thermal oxidation of Fe₃O₄ and also the decomposition of amide and 2-methylpropane sulphonic acid pendant groups. The last weight losses in TGA curves of poly(AMPS-*co*-AA)@Fe₃O₄ at about 360 °C was likely due to the degradation of the polymer backbone. Based on the char yield of poly(AMPS-*co*-AA)@Fe₃O₄ at 800 °C and assuming that the final residues are mainly Fe₃O₄ and

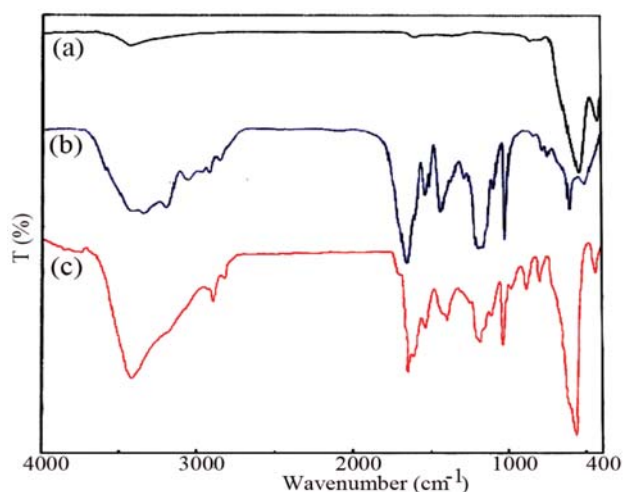


Figure 1. FT-IR spectra of Fe₃O₄ (a), poly(AMPS-*co*-AA) (b), and poly(AMPS-*co*-AA)@Fe₃O₄ (c).

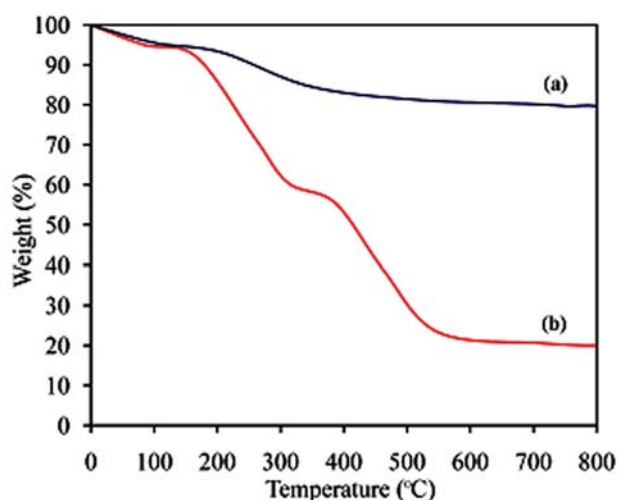


Figure 2. TGA curves of Fe₃O₄ (a) and poly(AMPS-*co*-AA)@Fe₃O₄ (b).

Fe_2O_3 , the anchoring amount of Fe_3O_4 in poly(AMPS-*co*-AA)@ Fe_3O_4 is about 20 wt.%. The relatively high char yield of poly(AMPS-*co*-AA)@ Fe_3O_4 also indicates that the incorporation of Fe_3O_4 into the polymer chains im-

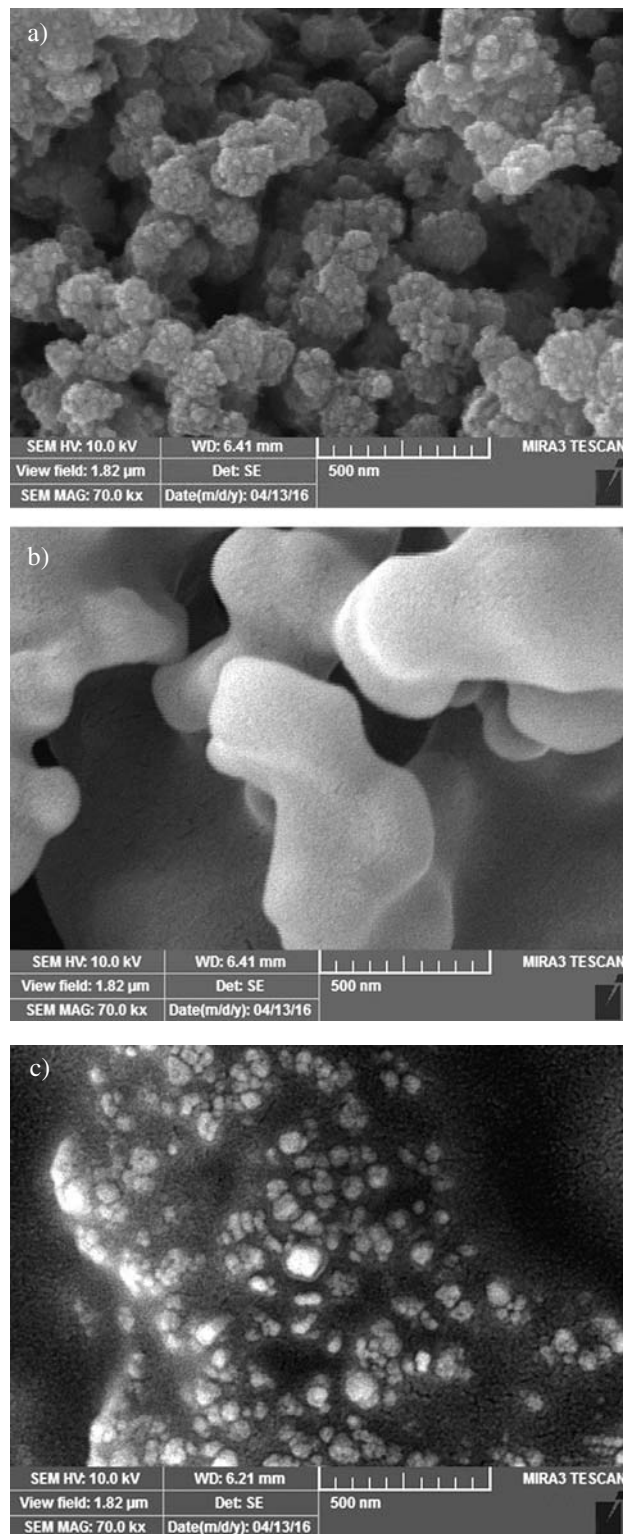


Figure 3. SEM photographs of Fe_3O_4 (a), poly(AMPS-*co*-AA) (b), and poly(AMPS-*co*-AA)@ Fe_3O_4 (c).

parts significant thermal stability to the resulting poly(AMPS-*co*-AA)@ Fe_3O_4 .

Figure 3 shows the SEM images of synthesized samples. Figure 3a indicates that the most of Fe_3O_4 nanoparticles are monodisperse and have a spherical crystal morphology with a diameter range between 40–50 nm. With comparison of SEM micrographs of the magnetic poly(AMPS-*co*-AA) (Figure 3c) with poly(AMPS-*co*-AA) (Figure 3b), it can be deduced that the polymer chains clearly loaded on Fe_3O_4 nanoparticles.

EDS analyses of poly(AMPS-*co*-AA) and poly(AMPS-*co*-AA)@ Fe_3O_4 are shown in Figure 4. EDS of poly(AMPS-*co*-AA)@ Fe_3O_4 shows that there are no impurities in this catalyst and confirms the presence of S and Fe elements (Figure 4b).

Figure 5 shows the XRD patterns of Fe_3O_4 nanoparticles and poly(AMPS-*co*-AA)@ Fe_3O_4 . The XRD pattern of Fe_3O_4 nanoparticles (Figure 5a) exhibited the peaks at $2\theta = 30.21, 35.52, 43.32, 53.61, 57.09, 62.63, 71.19,$ and 74.20° that could be assigned to 220, 111, 311, 400, 422, 511, 440, and 442 planes of Fe_3O_4 , respectively. Due to

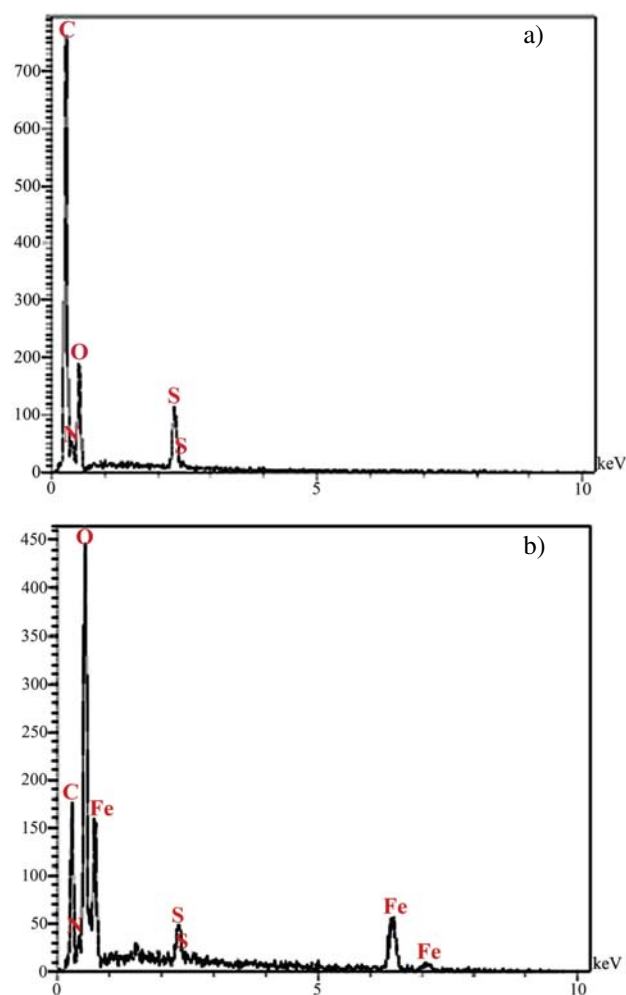


Figure 4. EDS spectra of poly(AMPS-*co*-AA) (a) and poly(AMPS-*co*-AA)@ Fe_3O_4 (b).

the agreement with the card no. 88-0315, it seems the resultant particles are pure magnetite. The crystal size of the particles was calculated by line broadening from the XRD pattern using the Debye–Scherrer formula and they were estimated to be between 20–25 nm. The weaker diffraction lines of poly(AMPS-*co*-AA)@Fe₃O₄ (Figure 5b) compared with Fe₃O₄ nanoparticles indicate that the Fe₃O₄ nanoparticles were covered by amorphous polymer.

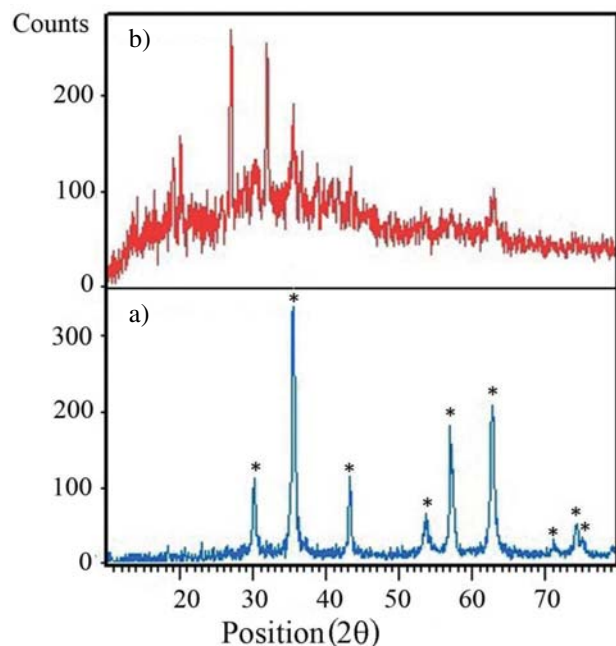


Figure 5. The XRD patterns of Fe₃O₄ nanoparticles (a) and poly(AMPS-*co*-AA)@Fe₃O₄ (b).

Magnetic properties of the samples were also studied. Hysteresis loops of Fe₃O₄ nanoparticles and poly(AMPS-*co*-AA)@Fe₃O₄ are depicted in Figure 6. The Fe₃O₄ nanoparticles exhibited ferromagnetic behavior in saturation magnetization of 63.53 emu/g and a coactivity of 1.76 Oe at room temperature (Figure 6a).

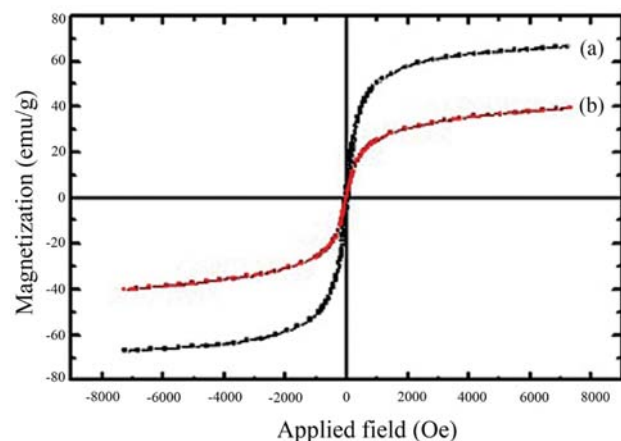


Figure 6. Magnetization curves for Fe₃O₄ nanoparticles (a) and poly(AMPS-*co*-AA)@Fe₃O₄ (b).

The results showed that the saturation magnetization value of poly(AMPS-*co*-AA)@Fe₃O₄ (Figure 6b, 48 emu/g) was lower than Fe₃O₄ nanoparticles due to the interaction of polymer and Fe₃O₄ nanoparticles.

3. 3. Catalytic Application of Poly(AMPS-*co*-AA)@Fe₃O₄ in the Synthesis of Biscoumarins

After synthesis of poly(AMPS-*co*-AA)@Fe₃O₄ we tried to convert aldehydes to the corresponding biscoumarins in the presence of this catalyst. To optimize the reaction conditions, initially, the condensation reactions of benzaldehyde (1 mmol) with 4-hydroxycoumarin (2 mmol) in the presence of different molar ratios of poly(AMPS-*co*-AA)@Fe₃O₄ in various solvents and also under solvent free conditions were studied. The results indicate that this reaction goes well in toluene and the product was obtained in excellent yield in the presence of 0.04 mmol of the catalyst at 90 °C. After establishing the optimal conditions, in order to prove the generality of this method, a variety of aromatic aldehydes bearing electron-deficient or electron-rich substituents on the aromatic ring (Table 1, entries 1–7), heteroaromatic aldehydes such as 2-thienyl and 2-furanyl carbaldehyde (entries 8, 9), and aliphatic aldehydes (entries 10–12) reacted with 4-hydroxycoumarin to give the corresponding biscoumarin products in excellent yields. ¹H NMR spectrum of the product 3,3'-(4-nitrobenzylidene)-bis-(4-hydroxycoumarin) is shown in Figure 7.

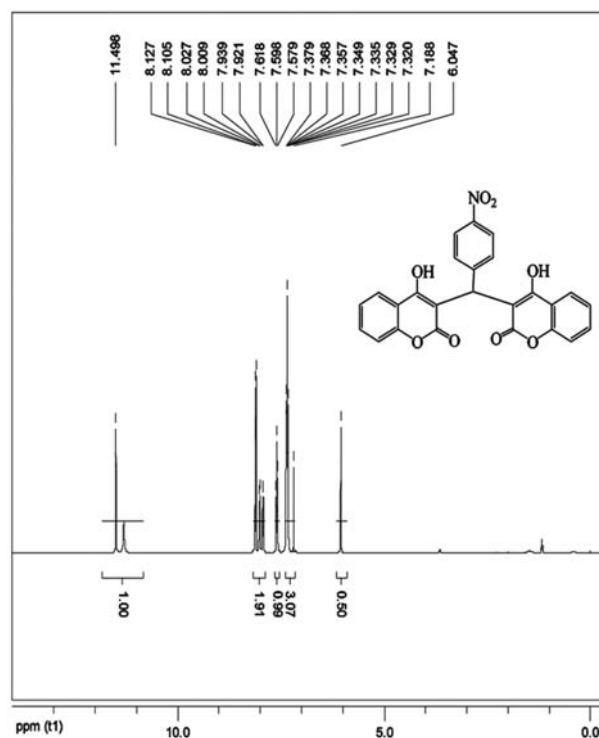
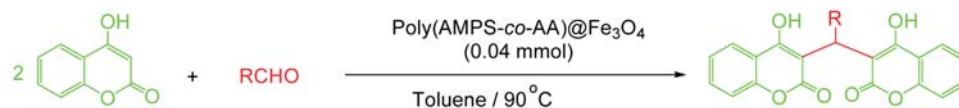


Figure 7. ¹H NMR spectrum of the 3,3'-(4-nitrobenzylidene)-bis-(4-hydroxycoumarin).

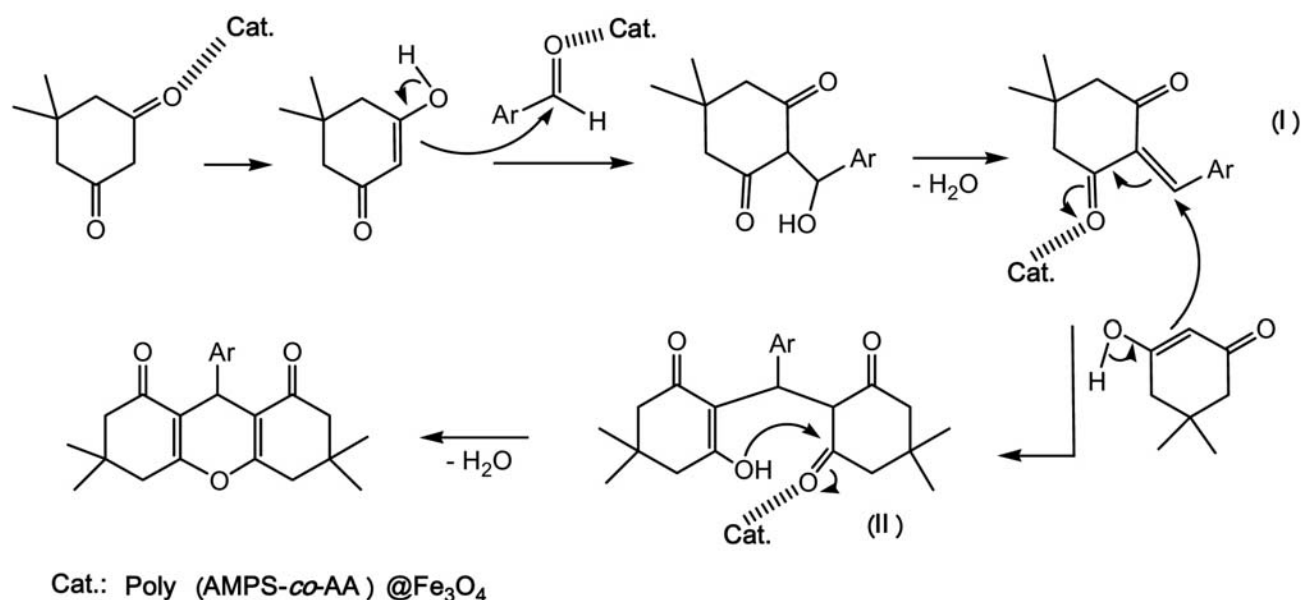
Table 1: Synthesis of biscoumarin derivatives catalyzed by poly(AMPS-co-AA)@Fe₃O₄.

Entry	Aldehyde	Time (min.)	Yield (%) ^{a,b}	M.P. (°C)	
				Obs.	Lit.
1	Benzaldehyde	15	97	226–230	230–232 ²⁰
2	4-Methylbenzaldehyde	19	94	263–267	266–268 ²⁰
3	4-Methoxybenzaldehyde	20	96	238–240	242–244 ¹⁹
4	4-Bromobenzaldehyde	19	96	266–268	265–267 ²⁰
5	4-Hydroxybenzaldehyde	22	95	224–226	222–224 ¹⁹
6	4-Nitrobenzaldehyde	10	97	227–230	232–234 ¹⁹
7	3-Nitrobenzaldehyde	10	97	236–239	236–238 ¹⁹
8	2-Thienyl carbaldehyde	20	96	211–213	210 ¹⁹
9	2-Furanyl carbaldehyde	21	95	205–207	202 ¹⁹
10	Cinnamaldehyde	27	94	275–279	279–281 ²⁸
11	3-Phenylpropionaldehyde	30	94	188–191	190 ¹⁷
12	Butyraldehyde	33	94	121–125	123 ¹⁷

^a Isolated yields. ^b All products are known compounds and were identified by comparison of their physical and spectral data with those of the authentic samples.

To determine the extent of sulfuric acid groups leaching from poly(AMPS-co-AA)@Fe₃O₄ one test was performed. Poly(AMPS-co-AA)@Fe₃O₄ was added to toluene and the mixture was stirred for 2 h at 90 °C. Then, the catalyst was removed by using magnetic field and the filtrate was analyzed for its acid content, which showed a negligible release of the acidic sites. The filtrate was found to be inactive in the reaction of aldehydes with 4-hydroxycoumarin. Thus, this leaching test suggested that the poly(AMPS-co-AA)@Fe₃O₄ catalyst was a true heterogeneous catalyst without significant acid moieties leaching.

Scheme 2 shows a possible mechanism for the preparation of biscoumarins using poly(AMPS-co-AA)@Fe₃O₄. First, the acidic nature of catalyst may facilitate the enolization step of 4-hydroxycoumarin. Second, nucleophilic addition of 4-hydroxycoumarin to the activated aldehyde followed by loss of H₂O generates intermediate I, which is further activated by poly(AMPS-co-AA)@Fe₃O₄. Then, the 1,4-nucleophilic addition of a second molecule of 4-hydroxycoumarin on the activated intermediate I, in the Michael addition fashion, affords the biscoumarin product. Based on this mechanism, it is clear

**Scheme 2.** Suggested mechanism for the preparation of biscoumarins catalyzed by poly(AMPS-co-AA)@Fe₃O₄.

that in the cases of electron withdrawing groups present on the aromatic aldehyde (Table 1, entries 6, 7), the 1,4-nucleophilic addition of a second molecule of 4-hydroxycoumarin on the activated intermediate I is more favored which can finally cause the decrease of reaction time for these types of aldehydes when reacting with 4-hydroxycoumarin.^{27,33} We believe that the catalytic efficiency of poly(AMPS-*co*-AA)@Fe₃O₄ may be attributed to the acidic hydrogen (SO₃H) as well as Lewis acid properties of Fe₃O₄ nanoparticles.

Very recently, we have introduced carbon nanotube-supported butyl 1-sulfonic acid groups as a heterogeneous catalyst for the synthesis of 1,8-dioxo-octahydroxanthenes.³² Along this line and based on the above encouraging results, we tried to examine the applicability of poly(AMPS-*co*-AA)@Fe₃O₄ for the synthesis of 1,8-dioxo-octahydroxanthenes and 12-aryl-9,9-dimethyl-

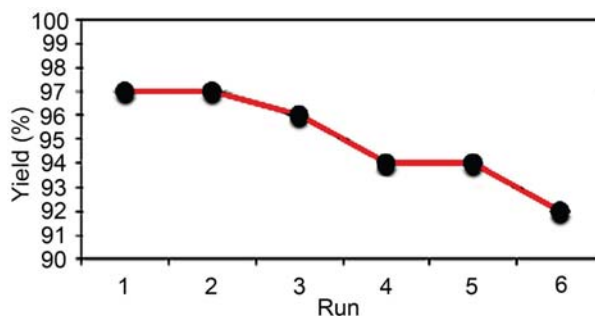


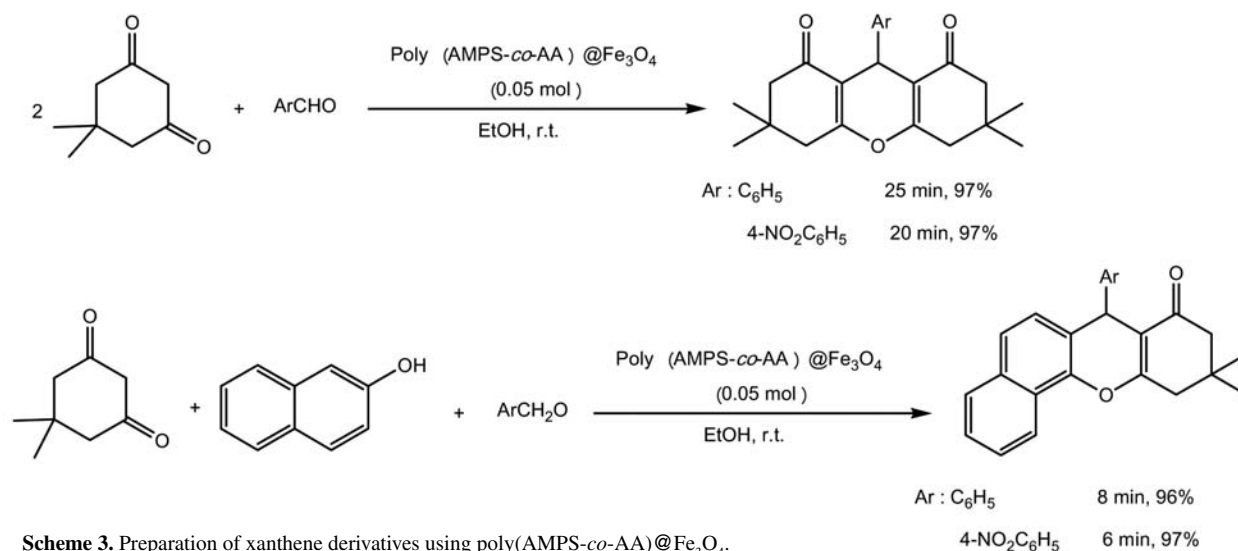
Figure 8. Recyclability of poly(AMPS-*co*-AA)@Fe₃O₄ (0.04 mmol) in the reaction of benzaldehyde (1 mmol) with 4-hydroxycoumarin (2 mmol) in toluene at 90 °C after 15 min.

8,9,10,12-tetrahydrobenzo[*a*]xanthene-11-ones through condensation of aromatic aldehydes with dimedone and β-naphthol. We observed that 1,8-dioxo-octahydroxanthene-

Table 2: Comparison results of poly(AMPS-*co*-AA)@Fe₃O₄ with other catalysts reported in the literature in the condensation of benzaldehyde with two equivalents of 4-hydroxycoumarin.

Entry	Reaction conditions	Time (min.)	Yield (%) ^a
1	Piperidine, EtOH, r.t.	240	92 ¹⁷
2	Tetrabutylammonium bromide, H ₂ O, 100 °C	25	92 ¹⁸
3	I ₂ , H ₂ O, 100 °C	25	97 ¹⁹
4	Sodium dodecyl sulfate, H ₂ O, 60 °C	138	90 ²⁰
5	1-Buthyl-3-methylimidazolium tetrafluoroborate, 70 °C	120	84 ²¹
6	1-Ethyl-3-(3-sulfopropyl)-benzimidazolium trifluoromethanesulfonate, 70 °C	120	95 ²²
7	<i>p</i> -Dodecylbenzenesulfonic acid/piperidine, H ₂ O, r.t.	360	89 ²³
8	3-Methyl-1-(4-sulfonic acid)butylimidazolium hydrogen sulfate, 70 °C	30	92 ²⁴
9	B(HSO ₄) ₃ , EtOH/H ₂ O, 70 °C	6	86 ²⁵
10	Polyvinyl pyrrolidone-nickel nanoparticles, ethylene glycol, r.t. ^b	15	93 ²⁶
11	[Poly(4-vinylpyridine)-BuSO ₃ H]Cl-xAlCl ₃ , toluene, 90 °C	36	95 ²⁷
12	[Poly(4-vinylpyridine)-BuSO ₃ H]HSO ₄ , toluene, 90 °C	48	93 ²⁸
13	Cellulose sulfonic acid, H ₂ O, reflux	120	90 ²⁹
14	Poly(AMPS- <i>co</i> -AA)@Fe ₃ O ₄ , toluene, 90 °C	15	97

^a Isolated yields. ^b With 4-nitrobenzaldehyde.



Scheme 3. Preparation of xanthene derivatives using poly(AMPS-*co*-AA)@Fe₃O₄.

nes and 12-aryl-9,9-dimethyl-8,9,10,12-tetrahydrobenzo[*a*]xanthene-11-ones were obtained in high yields in ethanol at room temperature in the presence of 0.05 mmol of poly(AMPS-*co*-AA)@Fe₃O₄ (Scheme 3). It is worth noting that, to the best of our knowledge, relatively few examples were reported on the synthesis of xanthene derivatives at room temperature. Usually, these reactions need high temperatures, long time or an additional source of energy (ultrasound or microwave irradiation).^{34–36}

Finally, we investigated the reusability of the poly(AMPS-*co*-AA)@Fe₃O₄ catalyst, and it was found that the catalyst could be completely recovered and used again at least six times without any noticeable loss of catalytic activity (Figure 8).

In comparison with selected previously known protocols employed for the synthesis of biscoumarins, poly(AMPS-*co*-AA)@Fe₃O₄ showed that in addition to having the general advantages attributed to the solid catalysts it has a much higher activity evident in the terms of high yields reached after short reaction times and at mild reaction conditions (Table 2).

4. Conclusion

In this study the coating of Fe₃O₄ nanoparticles with sulfonated polyacrylamide has been described. Magnetization measurements showed that the obtained poly(AMPS-*co*-AA)@Fe₃O₄ particles have paramagnetic properties. Poly(AMPS-*co*-AA)@Fe₃O₄ showed good catalytic activity in a one-pot domino Knoevenagel-type condensation/Michael reaction between aldehydes and 4-hydroxycoumarin, aromatic aldehydes with dimedone, and aromatic aldehydes with dimedone and β-naphthol. Work-up of these reactions is a “green” process because the catalyst was easily separated from the reaction media by the application of an external magnetic source. The high thermal and chemical stabilities of the catalyst, easy preparation, handling, and recycling of the catalyst, high yields achieved, and short reaction times needed are the other obvious advantages of the present method.

5. Acknowledgement

The authors are thankful to the Research Council of Shahrekord University and Marvdasht Branch Islamic Azad University for their partial support of this work.

6. References

1. R. M. Cornell, U. Schwartzmann, *The Iron Oxide: Structure, Properties, Reactions, Currencies and Uses*, Wiley-VCH, Weinheim, 2003.
<https://doi.org/10.1002/3527602097>
2. V. Polshettiwar, R. Luque, A. Fihri, H. Zhu, M. Bouhrara, J. M. Basset, *Chem. Rev.* **2011**, *111*, 3036–3075.
<https://doi.org/10.1021/cr100230z>
3. S. Shylesh, V. Schmemann, W. R. Thiel, *Angew. Chem. Int. Ed.* **2010**, *49*, 3428–3459.
<https://doi.org/10.1002/anie.200905684>
4. K. R. Reddy, K. P. Lee, A. I. Gopalan, A. M. Showkat, *Polym. Adv. Technol.* **2007**, *18*, 38–43.
<https://doi.org/10.1002/pat.735>
5. M. M. Lakouraj, E. Nazarzadeh Zare, P. Najafi Moghadam, *Adv. Poly. Tech.* **2014**, *33*, 21385 (1–7).
6. V. Panwar, S. S. Ray, S. L. Jain, *Tetrahedron Lett.* **2016**, *57*, 5026–5032.
<https://doi.org/10.1016/j.tetlet.2016.09.093>
7. A. Hu, G. T. Yee, W. Lin, *J. Am. Chem. Soc.* **2005**, *127*, 12486–12487.
<https://doi.org/10.1021/ja053881o>
8. A. Schätz, M. Hager, O. Reiser, *Adv. Funct. Mater.* **2009**, *19*, 2109–2115.
<https://doi.org/10.1002/adfm.200801861>
9. M. A. Ghasemzadeh, J. Safaei-Ghomi, S. Zahedi, *J. Serb. Chem. Soc.* **2013**, *78*, 769–779.
10. A. Gharib, L. Vojdani Fard, N. Noroozi Pesyan, M. Roshani, *Chem. J.* **2015**, *1*, 58–67.
11. K. Karami, S. Dehghani Najvani, N. Haghghat Naeini, P. Hervés, *Chin. J. Catal.* **2015**, *36*, 1047–1053.
[https://doi.org/10.1016/S1872-2067\(15\)60837-3](https://doi.org/10.1016/S1872-2067(15)60837-3)
12. M. A. Ghasemzadeh, *Acta Chim. Slov.* **2015**, *62*, 977–985.
<https://doi.org/10.17344/acsi.2015.1501>
13. M. A. Ghasemzadeh *Quim. Nova*, **2017**, *40*, 47–53.
14. A. Maresca, A. Scozzafava, C. T. Supuran, *Bioorg. Med. Chem. Lett.* **2010**, *20*, 7255–7258.
<https://doi.org/10.1016/j.bmcl.2010.10.094>
15. N. Vukovic, S. Sukdolak, S. Solujic, N. Niciforovic, *Food Chem.* **2010**, *120*, 1011–1018.
<https://doi.org/10.1016/j.foodchem.2009.11.040>
16. F. Carta, A. Maresca, A. Scozzafava, C. T. Supuran, *Bioorg. Med. Chem.* **2012**, *20*, 2266–2273.
<https://doi.org/10.1016/j.bmc.2012.02.014>
17. K. M. Khan, S. Iqbal, M. A. Lodhi, G. M. Maharvi, Z. Ullah, M. I. Choudhary, A. U. Rahmana, S. Perveen, *Bioorg. Med. Chem.* **2004**, *12*, 1963–1968.
<https://doi.org/10.1016/j.bmc.2004.01.010>
18. J. Khurana, M. S. Kumar, *Tetrahedron Lett.* **2009**, *50*, 4125–4127.
<https://doi.org/10.1016/j.tetlet.2009.04.125>
19. M. Kidwai, V. Bansal, P. Mothra, S. Saxena, R. K. Somvanshi, S. Dey, T. P. Singh, *J. Mol. Catal. A Chem.* **2007**, *268*, 76–81.
<https://doi.org/10.1016/j.molcata.2006.11.054>
20. H. Mehrabi, H. Abusaidi, *J. Iran. Chem. Soc.* **2010**, *7*, 890–894. <https://doi.org/10.1007/BF03246084>
21. J. M. Khurana, S. Kumar, *Monatsh. Chem.* **2010**, *141*, 561–564. <https://doi.org/10.1007/s00706-010-0306-4>
22. W. Li, Y. Wang, Z. Wang, L. Dai, Y. Wang, *Catal. Lett.* **2011**, *141*, 1651–1658.

- <https://doi.org/10.1007/s10562-011-0689-9>
23. A. Kumar, M. K. Gupta, M. Kumar, *Tetrahedron Lett.* **2011**, 52, 4521–4525. <https://doi.org/10.1016/j.tetlet.2011.06.040>
24. N. Tavakoli-Hoseini, M. M. Heravi, F. F. Bamoharram, A. Davoodnia, M. Ghassemzadeh, *J. Mol. Liq.* **2011**, 163, 122–127. <https://doi.org/10.1016/j.molliq.2011.08.007>
25. Z. Karimi-Jaberi, M. R. Nazarifar, B. Pooladian, *Chin. Chem. Lett.* **2012**, 23, 781–784. <https://doi.org/10.1016/j.ccllet.2012.05.003>
26. J. M. Khurana, K. Vij, *J. Chem. Sci.* **2012**, 124, 907–912. <https://doi.org/10.1007/s12039-012-0275-8>
27. K. Parvanak Boroujeni, P. Ghasemi, *Catal. Commun.* **2013**, 37, 50–54. <https://doi.org/10.1016/j.catcom.2013.03.025>
28. K. Parvanak Boroujeni, P. Ghasemi, Z. Rafienia, *Monatsh. Chem.* **2014**, 145, 1023–1026. <https://doi.org/10.1007/s00706-014-1156-2>
29. M. Sedighi, N. Montazeri, *Adv. Stud. Biol.* **2015**, 7, 89–95. <https://doi.org/10.12988/asb.2015.41160>
30. N. Jagadishbabu, K. Shivashankar, *J. Heterocycl. Chem.* **2017**, 54, 1543–1549. <https://doi.org/10.1002/jhet.2742>
31. F. Gholamian, M. Shabaniyan, M. Shahrokh, *J. Clust. Sci.* **2013**, 24, 177–188.
32. K. Parvanak Boroujeni, Z. Heidari, R. Khalifeh, *Acta Chim. Slov.* **2016**, 63, 602–608. <https://doi.org/10.17344/acsi.2016.2291>
33. E. V. Anslyn, D. A. Dougherty, *Modern Physical Organic Chemistry*, University Science Books, California, **2006**.
34. T.-S. Jin, J.-S. Zhang, J.-C. Xiao, A.-Q. Wang, T.-S. Li, *Ultrason. Sonochem.* **2006**, 13, 220–224. <https://doi.org/10.1016/j.ultsonch.2005.04.002>
35. K. Venkatesan, S. S. Pujari, R. J. Lahoti, K. V. Srinivasan, *Ultrason. Sonochem.* **2008**, 15, 548–553. <https://doi.org/10.1016/j.ultsonch.2007.06.001>
36. C. S. Sundar, K. U. M. Rao, N. B. Reddy, M. V. N. Reddy, S. S. Prasad, C. S. Reddy, *Catal. Sci. Technol.* **2012**, 2, 1382–1385. <https://doi.org/10.1039/c2cy20041d>

Povzetek

S polimerizacijo ustreznih monomerov in z nadaljnjo reakcijo s Fe_3O_4 nanodelci smo pripravili magnetitne delce s sulfoniranim poliakrilamidnim ovojem. Karakterizacijo dobljenega katalitskega materiala smo izvedli s Fourierjevo transformacijsko infrardečo spektroskopijo (FT-IR), termično gravimetrijo (TGA), vrstično elektronsko mikroskopijo (SEM), energijsko disperzijsko spektroskopijo (EDS), rentgensko difrakcijo (XRD) in vibracijsko magnetometrijo (VSM). Ugotovili smo, da pripravljeni polimer vsebuje 1.1 mmol na gram kislil SO_3H ostankov. Katalitsko učinkovitost polimera smo raziskali na primeru sinteze biskumarinskih derivatov, ki smo jih pripravili z dvokomponentno enolončno domino Knoevenaglovo kondenzacijo s sledečo Michaelovo reakcijo med aldehidi in 4-hidroksikumarinom. Biskumarine smo pripravili z visokimi izkoristki in s kratkimi reakcijskim časi. Izolacije so bile zelo enostavne. Katalizatorji so stabilni (pri sobnih pogojih), z njimi je enostavno ravnati in jih je moč ponovno uporabiti.

Short communication

Synthesis of 2,4,5-Trisubstituted Phenanthroimidazole Derivatives using SBA-Pr-SO₃H as a Nanocatalyst

Ghodsii Mohammadi Ziarani,^{1*} Elham Tavaf,¹ Vaezeh Fathi Vavsari¹
and Alireza Badiei²

¹ Department of Chemistry, Alzahra University, PO Box 1993893973, Tehran, Iran

² School of Chemistry, College of Science, University of Tehran, PO Box 14155-6455, Tehran, Iran

* Corresponding author: E-mail: gmziarani@hotmail.com, gmohammadi@alzahra.ac.ir
Tel-fax: +98 2188041344

Received: 26-11-2016

Abstract

An efficient one-pot approach for the preparation of 2,4,5-trisubstituted phenanthroimidazole derivatives is described. The three-component reaction between 9,10-phenanthraquinone, benzaldehyde derivatives, and ammonium acetate proceeds in the presence of SBA-Pr-SO₃H as a nanoporous solid acid catalyst in short reaction times and good to excellent yields.

Keywords: Trisubstituted phenanthroimidazole; 9,10-Phenanthraquinone; SBA-Pr-SO₃H; Nanocatalyst; Heterogeneous catalysis

1. Introduction

Application of imidazole and their derivatives is unavoidable in the field of medicinal chemistry due to their biologically active properties as biocides,¹ platelet aggregation inhibitors,² analgetics,³ antibacterial,^{4,5} antitumor,^{6,7} and anti-inflammatory activity.^{8,9} Additionally, derivatives of imidazole conjugated with aromatic rings have been widely used as fluorescent dyes.¹⁰

In recent years, several methods have been reported for the preparation of three-substituted imidazole derivatives from 9,10-phenanthraquinones, benzaldehyde derivatives and ammonium acetate using different catalysts such as I₂,¹¹ mercaptopropylsilica,¹² zirconium Schiff base,¹³ iron(III) triflate,¹⁴ sulfamic acid,¹⁵ and ionic liquid modified surface.¹⁶

Recently, mesoporous ordered silica materials such as SBA-15 have received more attention in the field of catalysis.^{17,18} As a well ordered hexagonal mesoporous silica, SBA-15 has relevant characteristics such as large uniform pore size, high surface area, thick walls, and high thermal stability which makes it a good candidate for preparing organic-inorganic hybrid materials and using as catalyst in different reactions.¹⁹ Furthermore, the propyl sulfonic acid modified SBA-15 can behave as an efficient

Brønsted acid in organic synthesis. Due to our interest in the field of nano-heterogeneous acidic catalysts,^{20–23} and based on different studies on applying SBA-Pr-SO₃H in organic synthesis,^{24–30} we have discovered a green and efficient method for the synthesis of 2,4,5-trisubstituted phenanthroimidazoles **4a-i** using SBA-Pr-SO₃H. In our previous studies, we have already reported the efficient synthesis of benzimidazoquinazolinones³¹ and 1,2,4,5-tetrasubstituted imidazoles³² in the presence of SBA-Pr-SO₃H.

2. Experimental

2.1. Materials and Instrumentations

All chemicals were obtained commercially and used without further purification. The IR spectra were recorded on KBr disks using a FT-IR Bruker Tensor 27 instrument. Melting points were measured using the capillary tube method with an Electrothermal 9200 apparatus. ¹H NMR and ¹³C NMR spectra were obtained by a Bruker 400 MHz and 100 MHz spectrometer, respectively, in either DMSO-*d*₆ or CDCl₃ solution. Mass spectra data were obtained by using a Network mass selective detector 5973 (Agilent). Scanning electron microscope (SEM) analysis

was performed on a Philips XL-30 field-emission SEM operated at 16 kV, while TEM was carried out on a Tecnai G² F30 apparatus at 300 kV. Weight change curve in nitrogen was measured on a BHR Thermo analyser STA 503 with the maximum heating rate of 20 °C/min.

2. 2. General Procedure for the Synthesis of 2,4,5-trisubstituted phenanthroimidazoles (4a–i)

The mixture of 9,10-phenanthraquinone (0.20 g, 1 mmol), benzaldehyde derivatives (1 mmol), and ammonium acetate (0.31 g, 4 mmol) was stirred in refluxing acetic acid (3 mL) for about 30 min using SBA-Pr-SO₃H (0.02 g) as the catalyst. The completion of the reaction was monitored by TLC technique (ethyl acetate/petroleum ether, 2:1). The precipitated product was filtered and dissolved in hot ethanol and DMF to remove the catalyst, and the solvent evaporated to obtain the pure product. The catalyst was subsequently washed with a diluted hydrochloric acid solution, distilled water, acetone and dried under reduced pressure, and reused for several times without significant loss of catalytic activity.³³ Physical and spectroscopic data of two new compounds are given below.

2. 3. Spectral Data of New Products

2-(2,4-Dimethoxyphenyl)-1*H*-phenanthro[9,10-*d*]imidazole (4h)

IR (KBr, ν_{\max}): 3523, 3430, 3048, 2987, 2942, 2833, 1935, 1603, 1462, 1371, 1311, 1266, 1204, 1161, 1083, 1022, 923, 835, 747, 714, 564, 434 cm⁻¹. ¹H NMR (400 MHz, DMSO-*d*₆) δ : 3.87 (s, 3H, CH₃), 4.03 (s, 3H, CH₃), 6.76 (dd, 1H, *J*=11.5 Hz, *J*=3 Hz, ArH), 6.80 (d, 1H, *J*=2.8 Hz, ArH), 7.58–7.74 (m, 4H, ArH), 8.20 (d, 1H, *J*=11.4 Hz, ArH), 8.62 (d, 1H, *J*=10.4 Hz, ArH), 8.70 (d, 1H, *J*=10.5 Hz, ArH), 8.82 (t, 2H, *J*=10.8 Hz, ArH), 12.57 (s, 1H, NH) ppm. ¹³C NMR (100 MHz, DMSO-*d*₆) δ : 55.5, 55.9, 98.5, 105.9, 111.8, 111.9, 121.9, 122.4, 122.5, 123.7, 123.9, 125, 126.6, 126.8, 126.9, 127, 127.3, 127.4, 131.1, 136.2, 147.3, 157.8, 161.6 ppm. MS (*m/z*, %): 354 (M⁺, 100), 336(33), 321(47), 309(23), 267(24), 190(20), 177(28), 163(13), 137(22).

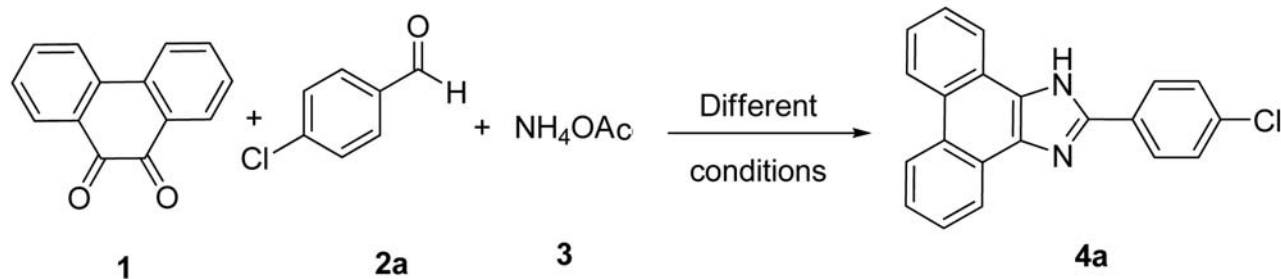
2-(2,6-Dichlorophenyl)-1*H*-phenanthro[9,10-*d*]imidazole (4i)

IR (KBr, ν_{\max}): 3063, 2973, 2904, 2845, 2737, 1948, 1702, 1602, 1548, 1481, 1437, 1327, 1191, 1153, 1041, 954, 880, 784, 740, 617, 531, 432 cm⁻¹. ¹H NMR (400 MHz, DMSO-*d*₆) δ : 7.60–7.75 (m, 7H, ArH), 8.36 (d, 1H, *J*=10.4 Hz, ArH), 8.56 (d, 1H, *J*=10.3 Hz, ArH), 8.81–8.88 (m, 2H, ArH), 13.82 (s, 1H, NH) ppm. ¹³C NMR (100 MHz, DMSO-*d*₆) δ : 121.7, 122, 122.4, 123.8, 124.2, 125.3, 125.6, 127.1, 127.14, 127.3, 127.5, 127.8, 128.4, 130.7, 132.5, 135.7, 136.5, 144.2 ppm. MS (*m/z*, %): 362 (M⁺, 100), 336(9), 190(86), 171(18), 163(53), 136(18).

3. Results and Discussion

The reaction of 9,10-phenanthraquinone (**1**), 4-chlorobenzaldehyde (**2a**), and ammonium acetate (**3**) was selected for optimizing conditions and investigating the role of nanocatalyst, SBA-Pr-SO₃H (Scheme 1). In order to study the solvent effect, different solvents were tested including solvent-free system at ambient temperature and at 120 °C, refluxing in water, ethanol and/or acetic acid as green solvents. As shown in Table 1, the best yield was obtained under refluxing in acetic acid in the presence of SBA-Pr-SO₃H (0.02 g). On the other hand, to indicate the catalyst effect, the results of different catalysts were compared with SBA-Pr-SO₃H under modified conditions (Figure 1). Clearly, SBA-Pr-SO₃H led to both, shorter reaction times and higher yields. After optimizing the reaction conditions, several aromatic aldehydes were used for the synthesis of 2,4,5-trisubstituted phenanthroimidazoles (Figure 2), which are listed in Table 2.

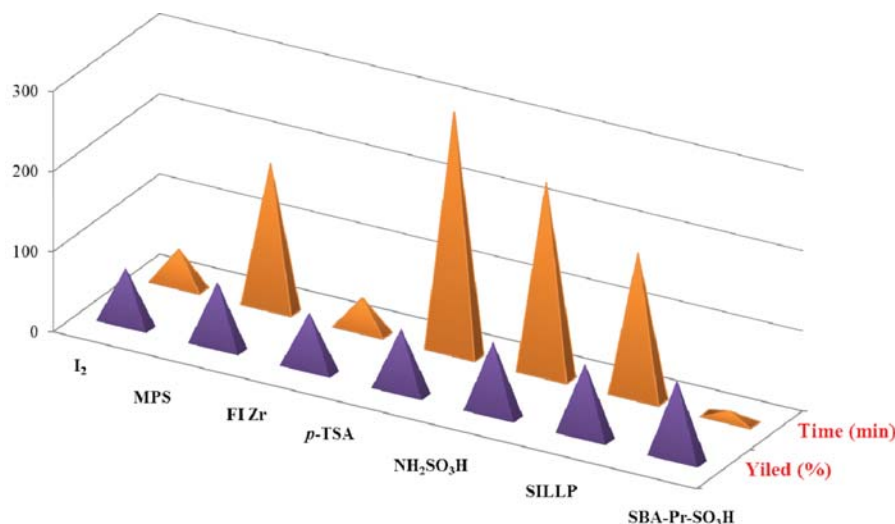
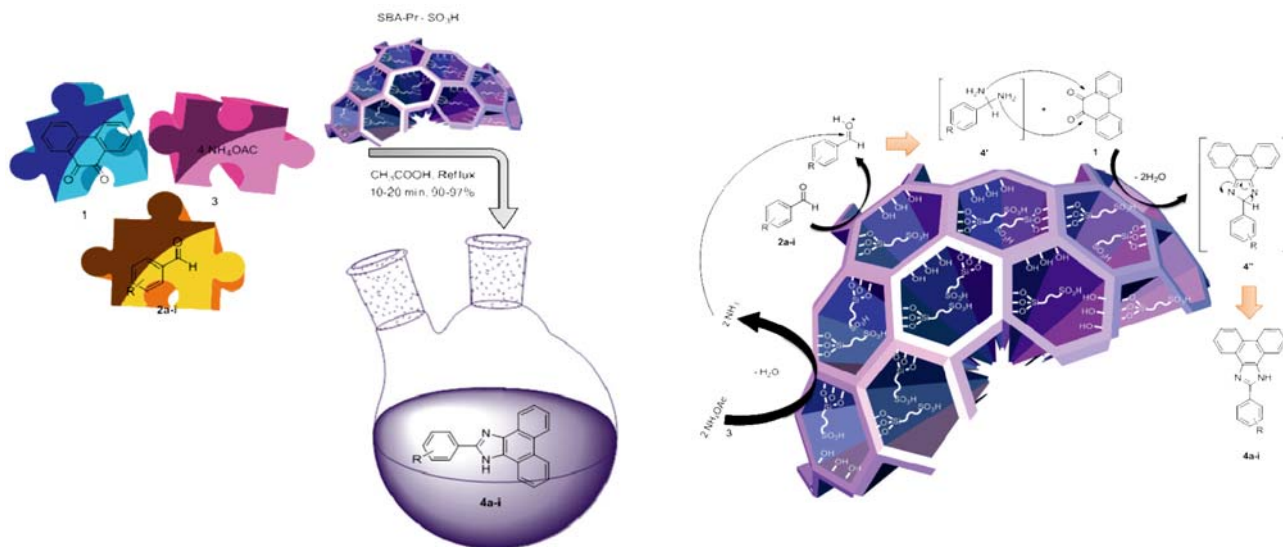
The proposed mechanism is shown in Scheme 2. In the first step, aldehyde carbonyl group is protonated on the SBA-Pr-SO₃H surface acidic sites. The activated carbonyl group is susceptible to the nucleophilic attack of ammonia, produced from the ammonium acetate (**3**), and gives the intermediate (**4'**). Condensation of 9,10-phenanthraquinone (**1**) with intermediate **4'** through an imination process and proton replacement in intermediate **4''**, produces the desired products **4a-i**.



Scheme 1. Model reaction of 9,10-phenanthraquinone **1**, 4-chlorobenzaldehyde **2a**, and ammonium acetate **3** for the synthesis of **4a**.

Table 1: Optimizing the reaction conditions for the synthesis of **4a**.

Entry	Catalyst	Solvent	Condition	Time (min)	Yield (%)
1	SBA-Pr-SO ₃ H	–	r.t.	24 h	Trace
2	SBA-Pr-SO ₃ H	–	120 °C	N. R.	80
3	SBA-Pr-SO ₃ H	H ₂ O	Reflux	>5 h	–
4	SBA-Pr-SO ₃ H	EtOH	Reflux	>5 h	73
5	SBA-Pr-SO ₃ H	CH ₃ COOH	Reflux	5	95
6	–	CH ₃ COOH	Reflux	10	90

**Figure 1.** Comparison of reaction times and product yields for the synthesis of **4** using different catalysts including I₂,¹¹ mercaptopropylsilica (MPS),¹² *p*-toluenesulfonic acid (*p*-TSA),¹³ NH₂SO₃H,¹⁵ supported ionic liquid-like phase (SILLP),¹⁶ and SBA-Pr-SO₃H.**Figure 2.** Schematic synthesis of 2,4,5-trisubstituted phenanthroimidazoles (**4**).**Scheme 2.** The proposed mechanism for the synthesis of 2,4,5-trisubstituted phenanthroimidazoles (**4**).

SBA-15 was synthesized according to the reported method.³³ Then, its internal surface was modified by using (3-mercaptopropyl)trimethoxysilane, and further oxidation with H₂O₂ in methanol, producing SBA-Pr-SO₃H, which was characterized *via* different techniques, including TGA, SEM and TEM analysis. The

weight reduction in TGA analysis (Figure 3) in the temperature range of 200–600 °C, indicates that propyl sulfonic acid groups were grafted onto the pores of silica material and that the average amount is 1.2 mmol/g. The mass loss before 200 °C is due the adsorbed water onto the pores of SBA-Pr-SO₃H. SEM image of SBA-

Table 2: Synthesis of 2,4,5-trisubstituted phenanthroimidazoles (**4**) in the presence of SBA-Pr-SO₃H under reflux conditions in acetic acid.^a

Entry	R	Product	Time (min)	Yield (%)	mp (°C)	mp (Lit.)
1	4-Cl		10	95	263–265	275–276 ¹⁴
2	4-F		20	96	205–208	–
3	4-OMe		10	95	265–267	265–257 ³⁴
4	4-Me		10	97	292–295	290–292 ³⁵
5	4-OH		20	97	>300	350–352 ¹⁴
6	3-NO ₂		20	90	278–280	271–272 ³⁶
7	2,4-(Cl) ₂		10	94	242–244	245–246 ¹⁵
8	2,4-(OMe) ₂		20	93	203–205	New
9	2,6-(Cl) ₂		20	90	230–232	New

^a Typical reaction conditions: 9,10-phenanthraquinone (1 mmol), benzaldehyde (1 mmol), and ammonium acetate (4 mmol) in the presence of SBA-Pr-SO₃H (0.02 g) were stirred in refluxing acetic acid (3 mL).

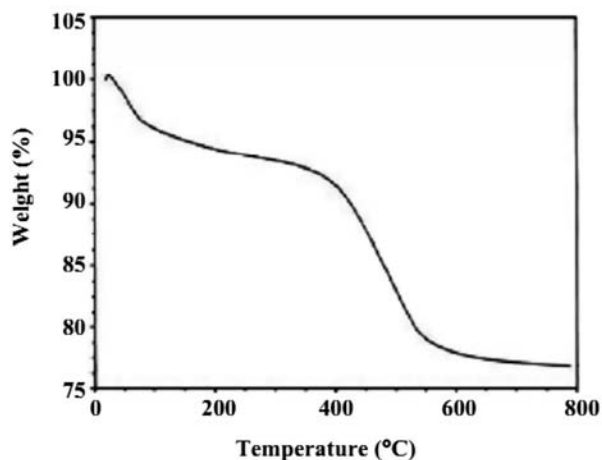


Figure 3. TGA curve of SBA-Pr-SO₃H.

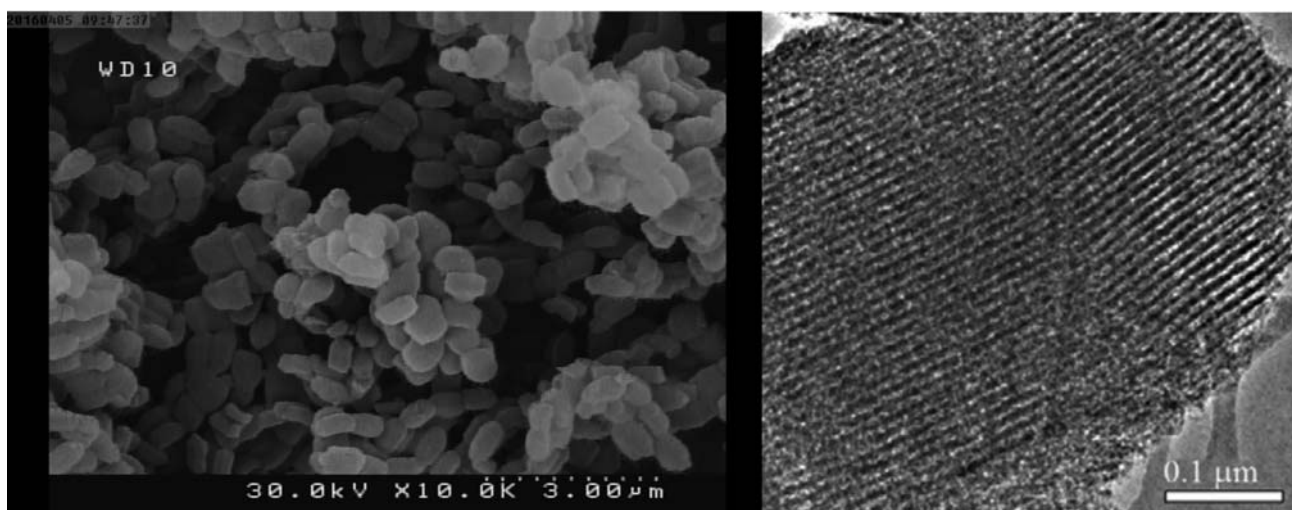


Figure 4. The SEM (left) and TEM (right) images of SBA-Pr-SO₃H.

Pr-SO₃H showed same morphology as obtained for SBA-15, proving this process didn't change the structure of SBA-15 itself (Figure 4). TEM image also demonstrated the presence of channels onto the SBA-Pr-SO₃H structure which were not collapsed after modification.

4. Conclusion

In conclusion, we have developed a novel three-component reaction to prepare 2,4,5-trisubstituted phenanthroimidazoles (**4**) from 9,10-phenanthraquinones, benzaldehyde derivatives and ammonium acetate. High yields, mild reaction conditions, simple purification, and the ability to recycle the heterogenous nanocatalyst, SBA-Pr-SO₃H, make this method an ecologically friendly for the synthesis of **4**. This protocol expands the new pathways for employing green catalysts to design other similar multicomponent reactions.

5. Acknowledgements

We gratefully acknowledge the financial support from the Research Council of Alzahra University and University of Tehran.

This research did not receive any specific grant from funding agencies in the public, commercial, or not-for-profit sectors.

6. References

1. T. Maier, R. Schmierer, K. Bauer, H. Bieringer, H. Burstell, B. Sachse, 1-Substituted imidazole-5-carboxylic acid derivatives, their preparation and their use as biocides, US Patent Number 4820335 A, **1989**.
2. P. Needleman, A. Raz, J. A. Ferrendelli, M. Minkes, *Proc. Natl. Acad. Sci.* **1977**, *74*, 1716–1720.
<http://dx.doi.org/10.1073/pnas.74.4.1716>
3. Ü. Uçucu, N. G. Karaburun, İ. Işıklıdağ, *Il Farmaco* **2001**, *56*, 285–290.
[http://dx.doi.org/10.1016/S0014-827X\(01\)01076-X](http://dx.doi.org/10.1016/S0014-827X(01)01076-X)
4. M. Antolini, A. Bozzoli, C. Ghiron, G. Kennedy, T. Rossi, A. Ursini, *Bioorg. Med. Chem. Lett.* **1999**, *9*, 1023–1028.
[http://dx.doi.org/10.1016/S0960-894X\(99\)00112-2](http://dx.doi.org/10.1016/S0960-894X(99)00112-2)
5. L. H. Jawaharmal, S. Narwal, G. Singh, D. Saini, A. Kaur, S. Narwal, *Indo Global J. Pharm. Sci.* **2012**, *2*, 147–156.
6. L. Wang, K. W. Woods, Q. Li, K. J. Barr, R. W. McCroskey, S. M. Hannick, L. Gherke, R. B. Credo, Y.-H. Hui, K. Marsh, R. Warner, J. Y. Lee, N. Zielinski-Mozng, D. Frost, S. H. Rosenberg, H. L. Sham, *J. Med. Chem.* **2002**, *45*, 1697–1711.
<http://dx.doi.org/10.1021/jm010523x>
7. J. C. Lee, J. T. Laydon, P. C. McDonnell, T. F. Gallagher, S. Kumar, D. Green, D. McNulty, M. J. Blumenthal, J. R. Keys, S. W. Land vatter, J. E. Strickler, M. M. McLaughlin, I. R. Siemens, S. M. Fisher, G. P. Livi, J. R. White, J. L. Adams, P. R. Young, *Nature* **1994**, *372*, 739–746.

- <http://dx.doi.org/10.1038/372739a0>
8. T. Corell, G. Hasselmann, *Acta Pharmacol. Toxicol.* **1983**, 53, 288–296.
<http://dx.doi.org/10.1111/j.1600-0773.1983.tb03425.x>
 9. I. K. Khanna, R. M. Weier, Y. Yu, X. D. Xu, F. J. Koszyk, P. W. Collins, C. M. Koboldt, A. W. Veenhuizen, W. E. Perkins, J. J. Casler, J. L. Masferrer, Y. Y. Zhang, S. A. Gregory, K. Seibert, P. C. Isakson, *J. Med. Chem.* **1997**, 40, 1634–1647.
<http://dx.doi.org/10.1021/jm9700225>
 10. K. Skonieczny, A. I. Ciuciu, E. M. Nichols, V. Hugues, M. Blanchard-Desce, L. Flamigni, D. T. Gryko, *J. Mater. Chem.* **2012**, 22, 20649–20664.
<http://dx.doi.org/10.1039/C2JM33891B>
 11. H. Behmadi, M. Roshani, S. M. Saadati, *Chin. Chem. Lett.* **2009**, 20, 5–8.
<http://dx.doi.org/10.1016/j.ccllet.2008.09.047>
 12. C. Mukhopadhyay, P. K. Tapaswi, M. G. B. Drew, *Tetrahedron Lett.* **2010**, 51, 3944–3950.
<http://dx.doi.org/10.1016/j.tetlet.2010.05.102>
 13. S. Damavandi, *Synth. React. Inorg., Met.-Org., Nano-Met. Chem.* **2011**, 41, 1274–1277.
<http://dx.doi.org/10.1080/15533174.2011.594839>
 14. S. Damavandi, R. Sandaroos, *Heterocycl. Communi* **2011**, 17, 121–124.
<http://dx.doi.org/10.1515/hc.2011.028>
 15. H.-N. Peng, X.-M. Peng, D.-G. Zheng, F. Yu, M. Rao, *Heterocycl. Communi* **2011**, 17, 223–226.
<http://dx.doi.org/10.1515/HC.2011.040>
 16. M. Saffari Jourshari, M. Mamaghani, F. Shirini, K. Tabatabaieian, M. Rassa, H. Langari, *Chin. Chem. Lett.* **2013**, 24, 993–996.
<http://dx.doi.org/10.1016/j.ccllet.2013.06.005>
 17. G. Mohammadi Ziarani, N. Lashgari, A. Badiei, *J. Mol. Catal. A: Chem.* **2015**, 397, 166–191.
<http://dx.doi.org/10.1016/j.molcata.2014.10.009>
 18. G. Mohammadi Ziarani, N. Lashgari, A. Badiei, *Curr. Org. Chem.* **2017**, 21, 674–687.
<http://dx.doi.org/10.2174/1385272820666160525123600>
 19. F. Hoffmann, M. Cornelius, J. Morell, M. Fröba, *Angew. Chem. Int. Ed.* **2006**, 45, 3216–3251.
<http://dx.doi.org/10.1002/anie.200503075>
 20. V. Fathi Vavsari, G. Mohammadi Ziarani, S. Balalaie, A. Latifi, M. Karimi, A. Badiei, *Tetrahedron* **2016**, 72, 5420–5426.
<http://dx.doi.org/10.1016/j.tet.2016.07.034>
 21. M. Rahimifard, G. Mohammadi Ziarani, A. Badiei, *Res. Chem. Intermed.* **2016**, 42, 6327–6336.
<http://dx.doi.org/10.1007/s11164-016-2465-3>
 22. G. Mohammadi Ziarani, L. Seyedakbari, S. Asadi, A. Badiei, M. Yadavi, *Res. Chem. Intermed.* **2016**, 42, 499–509.
<http://dx.doi.org/10.1007/s11164-015-2036-z>
 23. G. Mohammadi Ziarani, M. Shakiba Nahad, N. Lashgari, A. Badiei, *Acta Chim. Slov.* **2015**, 62, 709–715.
<http://dx.doi.org/10.17344/acsi.2014.972>
 24. V. Fathi Vavsari, G. Mohammadi Ziarani, A. Badiei, S. Balalaie, *J. Iran. Chem. Soc.* **2016**, 13, 1037–1043.
<http://dx.doi.org/10.1007/s13738-016-0817-y>
 25. P. Gholamzadeh, G. Mohammadi Ziarani, A. Badiei, A. Abolhassani Soorki, N. Lashgari, *Res. Chem. Intermed.* **2013**, 39, 3925–3936.
<http://dx.doi.org/10.1007/s11164-012-0909-y>
 26. P. Gholamzadeh, G. Mohammadi Ziarani, A. Badiei, Z. Bahrami, *Eur. J. Chem.* **2012**, 3, 279–282.
<http://dx.doi.org/10.5155/eurjchem.3.3.279-282.630>
 27. N. Lashgari, G. Mohammadi Ziarani, A. Badiei, M. Zarezadeh-Mehrzi, *J. Heterocycl. Chem.* **2014**, 51, 1628–1633.
<http://dx.doi.org/10.1002/jhet.1746>
 28. G. Mohammadi Ziarani, A. Badiei, M. Azizi, N. Lashgari, *J. Chin. Chem. Soc.* **2013**, 60, 499–502.
<http://dx.doi.org/10.1002/jccs.201200530>
 29. G. Mohammadi Ziarani, N. H. Mohtasham, A. Badiei, N. Lashgari, *J. Chin. Chem. Soc.* **2014**, 61, 990–994.
<http://dx.doi.org/10.1002/jccs.201300538>
 30. G. Mohammadi Ziarani, N. Lashgari, S. Faramarzi, A. Badiei, *Acta Chim. Slov.* **2014**, 61, 574–579.
 31. G. Mohammadi Ziarani, A. Badiei, Z. Aslani, N. Lashgari, *Arabian J. Chem.* **2015**, 8, 54–61.
<http://dx.doi.org/10.1016/j.arabjc.2011.06.020>
 32. G. Mohammadi Ziarani, A. Badiei, N. Lashgari, Z. Farahani, *J. Saudi Chem. Soc.* **2016**, 20, 419–427.
<http://dx.doi.org/10.1016/j.jscs.2013.01.005>
 33. G. Mohammadi Ziarani, S. Ghorbi, P. Gholamzadeh, A. Badiei, *Iran. J. Catal.* **2016**, 6, 229–235.
 34. E. K. Dora, B. Dash, C. S. Panda, *J. Indian Chem. Soc.* **1979**, 56, 620–624.
 35. L. Weiyang, L. Lingliang, Y. Lin, C. Zengmei, C. Bingbing, T. Wen, *Org. Lett.* **2008**, 10, 5577–5580.
<http://dx.doi.org/10.1021/ol802436j>
 36. Y. Sakaino, H. Kakisawa, K. Arita, M. Kouno, H. Morishima, *Tetrahedron* **1973**, 29, 1185–1191.
[http://dx.doi.org/10.1016/0040-4020\(73\)80099-7](http://dx.doi.org/10.1016/0040-4020(73)80099-7)

Povzetek

V prispevku je predstavljena učinkovita enostopenjska reakcija priprave 2,4,5-trisubstituiranih fenantroimidazolnih derivatov. Trikomponentna reakcija med 9,10-fenantrokinonom, različnimi derivati benzaldehda in amonijevim acetatom, v prisotnosti SBA-Pr-SO₃H kot trnega, nanoporoznega kislega katalizatorja, poteka hitro, s kratkimi reakcijskimi časi in odličnimi izkoristki.

Short communication

Design, Preparation and Characterization of MoO₃H-functionalized Fe₃O₄@SiO₂ Magnetic Nanocatalyst and Application for the One-pot Multicomponent Reactions

Mahtab Kiani,^{1,4*} Mehrnoosh Hendijani,² Mohammad Mohammadipour³ and Ali Zamanian⁴

¹ Young Researchers and Elite Club, Karaj Branch, Islamic Azad University, Karaj, Iran

² Department of Chemistry, Kharazmi University, Tehran 15719-14911, Iran

³ Department of Chemistry, Semnan University, Semnan 35131-19111, Iran

⁴ Department of Nanotechnology and Advance Materials, Materials and Energy Research Center, Karaj, Alborz, Iran

* Corresponding author: E-mail: mahtabkiani47@yahoo.com

Tel: 00989372059283; fax: 00987412242167

Received: 05-01-2017

Abstract

Molybdenic acid-functionalized silica-based Fe₃O₄ nanoparticles (Fe₃O₄@SiO₂-MoO₃H) are found to be a powerful and magnetically recyclable nanocatalyst. The morphology and structure of this nanocatalyst were investigated by Fourier transform infrared spectroscopy (FT-IR), energy dispersive X-ray spectroscopy (EDX), transmission electron microscopy (TEM), field emission scanning electron microscopy (FE-SEM), thermo gravimetric analyses (TGA), X-ray diffraction (XRD) and vibrating sample magnetometer (VSM) techniques. The high catalytic activity of this catalyst was investigated in the synthesis of pyrano[2,3-*c*]chromenes, representing potent biologically active compounds. The catalyst can be readily separated by applying an external magnet device and recycled up to 8 times without significant decrease in its catalytic activity, which makes it highly beneficial to address the industrial needs and environmental concerns. Fe₃O₄@SiO₂-MoO₃H has many advantages, such as low cost, low toxicity, ease of preparation, good stability, high reusability and operational simplicity.

Keywords: Fe₃O₄@SiO₂-MoO₃H, Magnetically recyclable nanocatalyst, Pyrano[2,3-*c*]chromenes, Biological activity

1. Introduction

Nowadays, the design and synthesis of efficient, reusable, easily separable, low toxicity, low cost, and insoluble acidic nanocatalysts have become an important area of research in chemistry.¹ The use of nanoparticles as heterogeneous catalysts has attracted considerable attention because of the interesting structural features and high levels of catalytic activity associated with these materials.²

Magnetic nanoparticles (MNP) are widely applied in various fields, such as magnetic resonance imaging (MRI) contrast agents, biomedical science, bioseparation

and hyperthermia.³⁻⁶ Transition metal nanoparticles are used as efficient catalysts for various synthetic organic transformations due to their high surface area-to-volume ratio and coordination sites which are mainly responsible for their catalytic activity.⁷ Because the Fe₃O₄ nanoparticles will aggregate quickly into large bunches and therefore lose their unique properties, various surface modification methods have been developed to modify the surface of naked Fe₃O₄ nanoparticles to improve the dispersibility, stability, biocompatibility and biodegradability for specific purposes. The resulting modified Fe₃O₄ nanoparticles have been extensively used for various applications.⁸ Among them, the silica coating is a very good surface modifier,

because of its excellent stability, biocompatibility, nontoxicity and ease of furthered conjugation with various functional groups, thus enabling the coupling and labeling of biotargets with high selectivity and specificity.^{9–11}

Development of MCRs can lead to new efficient synthetic methodologies to afford many small organic compounds in the field of modern organic, bioorganic, and medicinal chemistry.¹⁰ Hence, MCRs are considered as a pivotal theme in the synthesis of many important heterocyclic compounds, such as pyranocoumarin derivatives nowadays.¹²

In continuation of our research on the introduction of recoverable catalysts in organic synthesis,^{13–16} recently, we disclosed that $\text{Fe}_3\text{O}_4@\text{SiO}_2\text{-MoO}_3\text{H}$ can be used as a novel magnetic nanocatalyst for the synthesis of 1,8-dioxodecahydroacridine derivatives.¹⁷ In this work, we demonstrate high catalytic activity of this new catalyst in the synthesis of pyrano[2,3-*c*]chromenes as potent biologically active compounds.

It is also interesting to note that the catalyst can be recovered and reused several times.

2. Experimental

2.1. General

The chemicals were purchased from Merck and Aldrich chemical companies. The reactions were monitored by TLC (silica gel 60 F 254, hexane : EtOAc). Fourier transform infrared (FT-IR) spectroscopy spectra were recorded on a Shimadzu-470 spectrometer, using KBr pellets and the melting points were determined on a KRUSS model instrument. ¹H NMR spectra were recorded on a Bruker Avance II 400 NMR spectrometer at 400 MHz, with DMSO-*d*₆ used as the solvent and TMS as the internal standard. X-Ray diffraction (XRD) pattern was obtained by Philips X Pert Pro X diffractometer operated with a Ni filtered Cu K α radiation source. Transmission electron microscopy (TEM) images of the electrocatalyst were recorded using a Philips CM-10 TEM microscope operated at 100 kV. Field emission scanning electron microscopy (SEM) and X-ray energy dispersive spectroscopy (EDS) analyses were carried out on a Philips XL30, operated at a 20 kV accelerating voltage. Thermogravimetric analyses (TGA) were conducted on a Rheometric Scientific Inc. 1998 thermal analysis apparatus under a N₂ atmosphere at a heating rate of 10 °C/min. The magnetic measurement was carried out in a vibrating sample magnetometer (Model 7407 VSM system, Lake Shore Cryotronic, Inc., Westerville, OH, USA) at room temperature.

2.2. General Procedure for the Preparation of nano-Fe₃O₄ (1)

FeCl₃ · 6H₂O (20 mmol) and FeCl₂ · 4H₂O (10 mmol) were dissolved in distilled water (100 mL) in a

three-necked round-bottom flask (250 mL). The resulting transparent solution was heated at 90 °C with rapid mechanical stirring under N₂ atmosphere for 1 h. A solution of concentrated aqueous ammonia (10 mL, 25 wt%) was then added to the solution in a drop-wise manner over a 30 min period using a dropping funnel. The reaction mixture was then cooled to room temperature and the resulting magnetic particles collected with a magnet and rinsed thoroughly with distilled water.

2.3. General Procedure for the Preparation of nano-Fe₃O₄@SiO₂ (2)

Nano-Fe₃O₄@SiO₂ (2) was synthesized according to a previously published literature method. Magnetic nano particles (1.0 g) were initially diluted via the sequential addition of water (20 mL), ethanol (60 mL) and concentrated aqueous ammonia (1.5 mL, 28 wt%). The resulting dispersion was then homogenized by ultrasonic vibration in a water bath. A solution of TEOS (0.45 mL) in ethanol (10 mL) was then added to the dispersion in a drop-wise manner under continuous mechanical stirring. Following a 12 h period of stirring, the resulting product was collected by magnetic separation and washed three times with ethanol.

2.4. General Procedure for the Preparation of nano-Fe₃O₄@SiO₂-OMoO₃H (3)

To an oven-dried (125 °C, vacuum) sample of nano-Fe₃O₄@SiO₂ (2 g) in a round bottomed flask (50 mL) equipped with a condenser and a drying tube, thionyl chloride (8 mL) was added and the mixture in the presence of CaCl₂ as a drying agent was refluxed for 48 h. The resulting dark powder was filtered and stored in a tightly capped bottle. To a mixture of Fe₃O₄@SiO₂-Cl (1 g) and sodium molybdate (0.84 g) *n*-hexane (5 mL) was added. The reaction mixture was stirred under refluxing conditions (70 °C) for 4 h. After completion of the reaction, the reaction mixture was filtered and washed with distilled water, and dried and then stirred in the presence of 0.1 N HCl (20 mL) for an hour. Finally, the mixture was filtered, washed with distilled water, and dried to afford nano-Fe₃O₄@SiO₂-OMoO₃H.

2.5. General Procedure for the Preparation of Pyrano[2,3-*c*]coumarin Derivatives 7

Malononitrile **4** (1.1 mmol), aromatic aldehyde **5** (1 mmol), 4-hydroxycoumarin **6** (1 mmol), and nano-Fe₃O₄@SiO₂-OMoO₃H (0.02 g) were added to a 10 mL mixture EtOH/H₂O (50/50) in a 25-mL pyrex flask and refluxed for an appropriate time (Table 3). The reaction progress was controlled by thin layer chromatography (TLC) using hexane/EtOAc (1:1). After completion of the reaction, the solvent was removed under vacuum, the cru-

de products **7** were obtained after recrystallization from EtOH.

3. Results and Discussion

3.1. Characterization of $\text{Fe}_3\text{O}_4@ \text{SiO}_2\text{-OMoO}_3\text{H}$

As can be seen in Scheme 1, from the reaction $\text{Fe}_3\text{O}_4@ \text{SiO}_2$ nanoparticles **2** with thionyl chloride, the $\text{Fe}_3\text{O}_4@ \text{SiO}_2\text{-Cl}$ has been prepared. The $\text{Fe}_3\text{O}_4@ \text{SiO}_2\text{-OMoO}_3\text{H}$ **3** was prepared from nucleophilic substitution of $\text{Fe}_3\text{O}_4@ \text{SiO}_2\text{-Cl}$ with anhydrous sodium molybdate in *n*-hexane (Scheme 1).

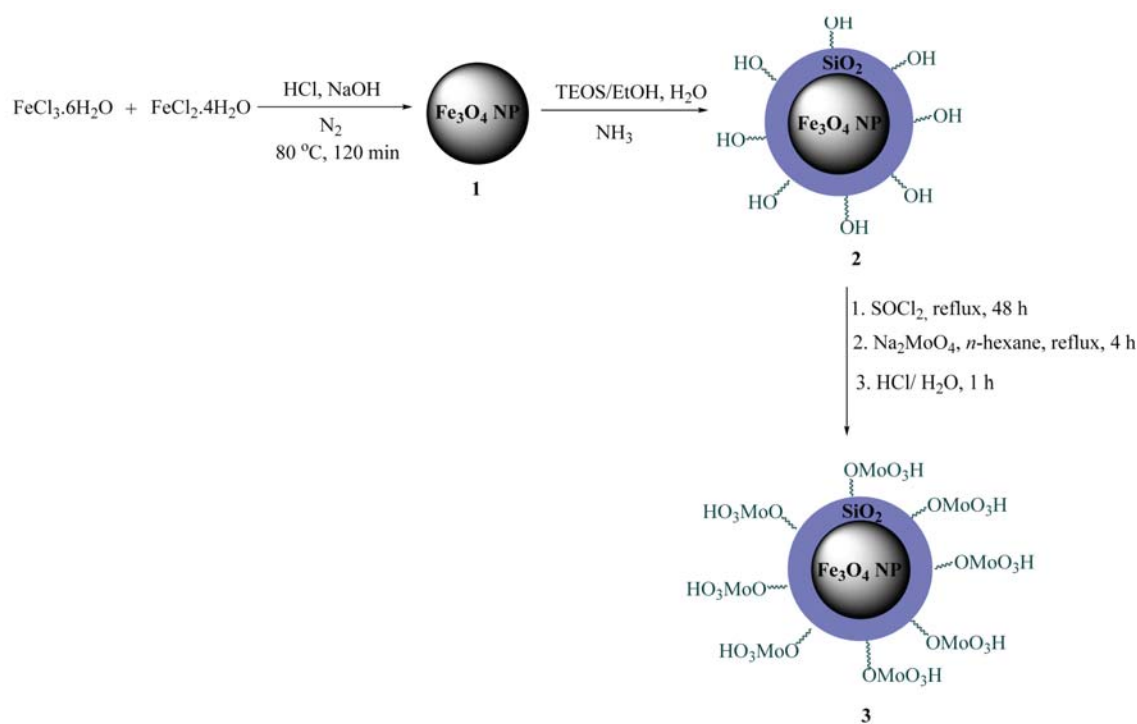
The resulting MNP acid catalyst was characterized by XRD, FT-IR, TEM, SEM, TGA and EDX.¹⁷

The transmission electron microscopy (TEM) image of $\text{Fe}_3\text{O}_4@ \text{SiO}_2\text{-MoO}_3\text{H}$ powder reveals the spherical $\text{Fe}_3\text{O}_4@ \text{SiO}_2\text{-MoO}_3\text{H}$ powder with an average particle sizes of about 10–30 nm (Fig. 1a).

Surface morphology, particle shape and size distribution features of $\text{Fe}_3\text{O}_4@ \text{SiO}_2\text{-MoO}_3\text{H}$ nanoparticles were examined by FE-SEM (Fig. 1b).

The successful incorporation of molybdate groups was also confirmed by EDAX analysis (Fig. 1c), which showed the presence of Fe, Si, Mo and O elements.

Fig. 2a shows the XRD patterns of Fe_3O_4 particles powder before modification. The following peak signals at $2\theta = 30.1^\circ$, 35.4° , 43.1° , 53.6° , 57° , and 62.8° corres-



Scheme 1. Schematic procedure for the preparation of $\text{Fe}_3\text{O}_4@ \text{SiO}_2\text{-MoO}_3\text{H}$.

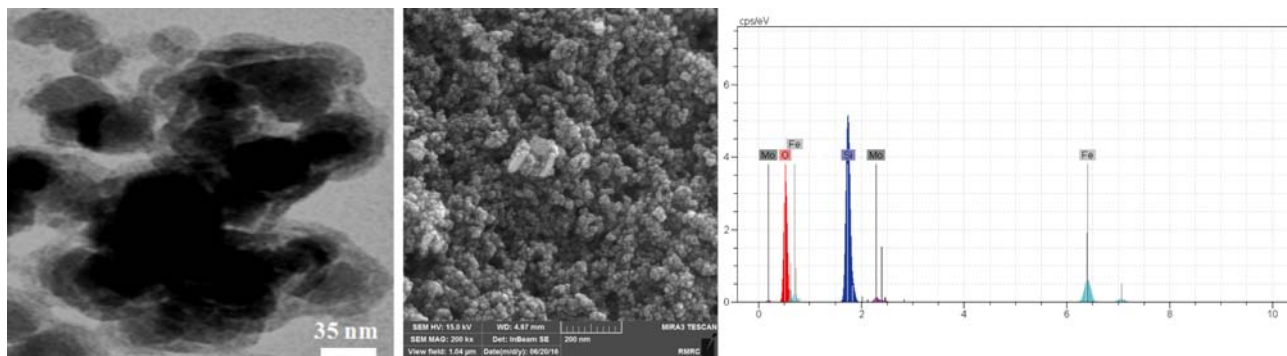


Figure 1. TEM image of $\text{Fe}_3\text{O}_4@ \text{SiO}_2\text{-MoO}_3\text{H}$ (a), Histogram of particle size distribution (b), SEM image of $\text{Fe}_3\text{O}_4@ \text{SiO}_2\text{-MoO}_3\text{H}$ (c) and EDAX spectrum of $\text{Fe}_3\text{O}_4@ \text{SiO}_2\text{-MoO}_3\text{H}$ (d)

pond to the spinel structure of Fe_3O_4 , which can be assigned to the diffraction of the (220), (311), (400), (422), (511), and (440) planes of the crystals, respectively.¹⁸ Fig. 2b shows the XRD pattern of $\text{Fe}_3\text{O}_4@ \text{SiO}_2\text{-OMoO}_3\text{H}$ demonstrating that the crystalline structure of the Fe_3O_4 particles was retained after the deposition of SiO_2 layers. The broad peak at around $2\theta = 20^\circ$ to 27° indicates the presence of amorphous silica in $\text{Fe}_3\text{O}_4@ \text{SiO}_2\text{-OMoO}_3\text{H}$. The intensity of this peak increased with the introduction of molybdate on the silica-coated magnetic nanoparticles, which can be attributed to the amorphous molybdate supported on the composite. The XRD results showed that the $\text{Fe}_3\text{O}_4@ \text{SiO}_2$ particles have been successfully coated with molybdate.

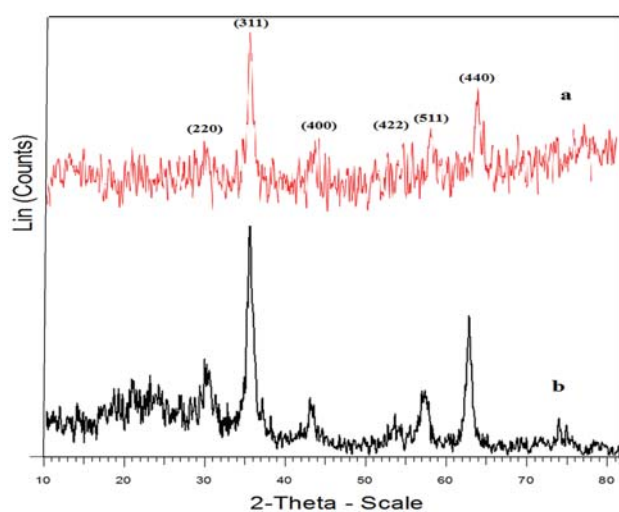


Figure 2. X-ray powder diffraction patterns of (a) Fe_3O_4 NPs, (b) $\text{Fe}_3\text{O}_4@ \text{SiO}_2\text{-OMoO}_3\text{H}$.

The thermogravimetric analysis (TGA) was used to study the thermal stability of the acid catalyst (Fig. 3). The first weight loss which occurred below 150°C , displayed a mass loss that was attributable to the loss of adsorbed solvent or trapped water from the catalyst. A weight loss of approximately 5% weight occurred between 300 and 500°C which can be attributed to the loss of molybdate groups covalently bound to silica surface. Thus, it can be concluded that the catalyst is stable up to 300°C .

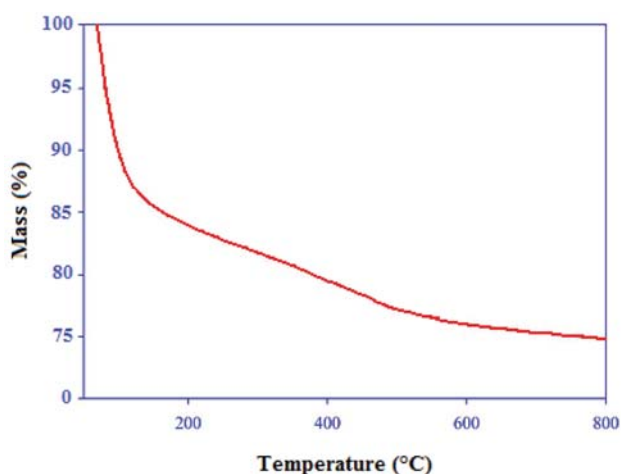


Figure 3. TGA curve of $\text{Fe}_3\text{O}_4@ \text{SiO}_2\text{-MoO}_3\text{H}$.

Typical magnetization curves for Fe_3O_4 nanoparticles and $\text{Fe}_3\text{O}_4@ \text{SiO}_2\text{-MoO}_3\text{H}$ are shown in Fig. 4. Room temperature specific magnetization (M) versus applied magnetic field (H) curve measurements of the sample indicate a saturation magnetization value (M_s) of 20.30 emu g^{-1} , lo-

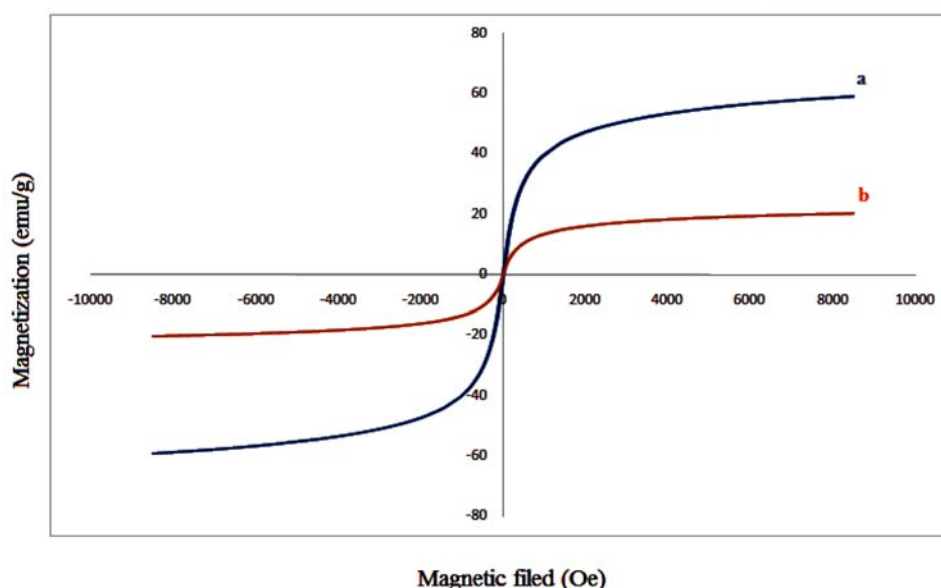
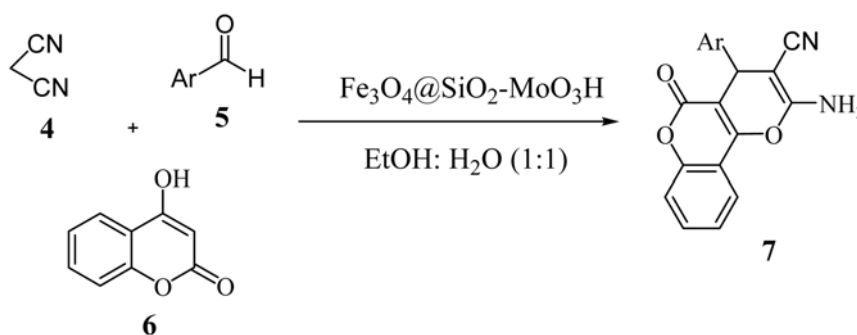


Figure 4. Magnetization curves for the prepared Fe_3O_4 MNPs (a) and $\text{Fe}_3\text{O}_4@ \text{SiO}_2\text{-MoO}_3\text{H}$ (b)

wer than that of bare MNPs (59.14 emu g⁻¹) due to the presence of coated shell.

3. 2. Application of Fe₃O₄@SiO₂-MoO₃H for the Synthesis of Pyrano[2,3-*c*]chromenes

In continuation of our studies on developing novel, efficient, and green procedures for the synthesis of organic compounds using safe catalysts,^{19–21} we decided to prepare pyrano[2,3-*c*]chromenes **7** via the synthesis by condensation between malononitrile **4**, aromatic aldehydes **5**, and 4-hydroxycoumarin **6** in the presence of catalytic amounts of Fe₃O₄@SiO₂-MoO₃H (Scheme 2).



Scheme 2. Synthesis of 1,8-dioxo-octahydroxanthene derivatives **7** by Fe₃O₄@SiO₂-MoO₃H.

In order to explore the catalytic efficiency of Fe₃O₄@SiO₂-MoO₃H, the model reaction was carried out under the catalyst-free conditions and compared with the one carried out in the presence of Fe₃O₄@SiO₂-MoO₃H and nano-Fe₃O₄. The obtained results showed higher yields for the reaction with the addition of Fe₃O₄@SiO₂-MoO₃H (94% yield) compared to the catalyst-free reaction (13% yield) and with the reaction with the addition of nano-Fe₃O₄ (86% yield).

The influence of the solvent was studied when the model reaction was performed using Fe₃O₄@SiO₂-Mo-

Table 1. Optimization of the model reaction by using various solvents and amount of Fe₃O₄@SiO₂-MoO₃H

Entry	Catalyst (mol%)	Solvent	Yield (%)
1	5	CH ₂ Cl ₂	60
2	5	CH ₃ Cl	65
3	5	EtOH	90
4	5	MeOH	80
5	5	H ₂ O	70
6	–	H ₂ O/EtOH	Trace
7	1	H ₂ O/EtOH	94
8	3	H ₂ O/EtOH	88
9	5	H ₂ O/EtOH	86
10	10	H ₂ O/EtOH	85

O₃H nanoparticles, a mixture of H₂O/EtOH (1:1) was opted as the reaction medium. It should be noted that the reaction progress in pure water and/or absolute ethanol was considerable, however it was not better than in the mixture of these two solvents. From different ratios of H₂O/EtOH mixtures, equal mixture H₂O/EtOH (1:1) was considered as the most effective ratio.

After optimization of the reaction conditions, in order to extend the scope of this reaction, a wide range of aromatic aldehydes was used with **3** and **5** (Table 2). All the products were characterized by comparison of their spectra and physical data with those reported in the literature.^{22–25}

As shown in Table 2, the new catalyst fortunately also works very well for the preparation of a vast variety of

Table 2. Synthesis of pyrano[2,3-*c*]coumarin derivatives **7** using Fe₃O₄@SiO₂-MoO₃H

Product	Ar	Time (min)	Yield ^a (%)	Mp (°C)
7a	C ₆ H ₅	30	96	262–264
7b	4-MeO-C ₆ H ₄	18	92	240–242
7c	2-Cl-C ₆ H ₄	25	78	260–262
7d	3-NO ₂ -C ₆ H ₄	35	81	255–257
7e	4-NO ₂ -C ₆ H ₄	75	73	248–250
7f	4-Me-C ₆ H ₄	70	87	250–252
7g	4-Cl-C ₆ H ₄	50	90	258–260
7h	thiophene-2-yl	75	70	234–236
7i	3-Br-C ₆ H ₄	20	91	272–274
7j	2-Cl-6-F-C ₆ H ₃	30	95	288–290
7k	4-benzyloxy-C ₆ H ₄	450	84	275–277
7l	1-naphthyl	90	90	260–262
7m	4-isopropyl-C ₆ H ₄	40	92	239–241
7n	cyclohexyl	25	86	265–267

^a Isolated yields.

pyrano[2,3-*c*]coumarin derivatives **7a–n**. The present method not only affords the products **7** in excellent yields, but also avoids the problems associated with catalyst cost, handling, safety and pollution.

3. 3. Reusability of the $\text{Fe}_3\text{O}_4@\text{SiO}_2\text{-MoO}_3\text{H}$

The main disadvantage for many of the reported methods is that the catalysts are destroyed in the work-up procedure and cannot be recovered or reused. In this process, as outlined in Fig. 5., the recycled catalyst can be used in up to eight cycles, during which there are negligible losses in the catalytic activity.

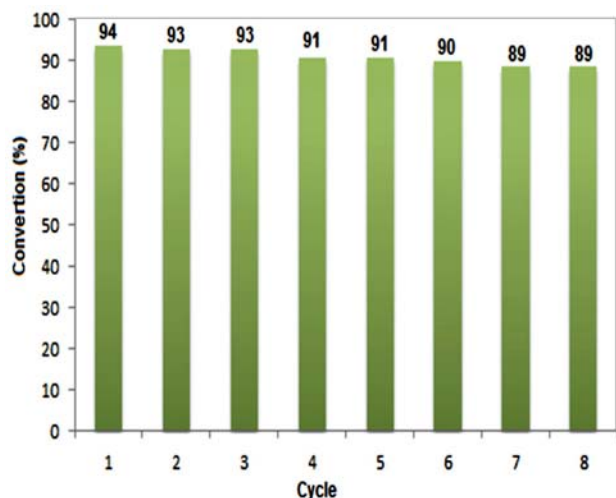


Figure 5. Reusability of $\text{Fe}_3\text{O}_4@\text{SiO}_2\text{-MoO}_3\text{H}$ for the synthesis of 7a.

4. Conclusions

In summary, we found $\text{Fe}_3\text{O}_4@\text{SiO}_2\text{-OMoO}_3\text{H}$ to be an effective acidic magnetic nanocatalyst which successfully catalyzed the reaction between 4-hydroxycoumarin, various aromatic aldehydes and malononitrile to produce new and known pyrano[2,3-*c*]chromens of potential synthetic and pharmaceutical interest. High catalytic activity under solvent free conditions, high yields, a clean process, reusable several times without loss of activity or selectivity simple catalyst preparation, easy separation after the reaction by a magnet and green conditions are the advantages of these protocols.

5. Acknowledgement

We acknowledge the research council of Yasouj University.

6. References

1. R. B. Nasir Baig, R. S. Varma, *Green Chem.* **2012**, *14*, 625–632. <https://doi.org/10.1039/c2gc16301b>
2. N. Koukabi, E. Kolvari, M. A. Zolfigol, A. Khazaei, B. S.

- Shaghasemi, B. Fasahati, *Adv. Synth. Catal.* **2012**, *354*, 2001–2008. <https://doi.org/10.1002/adsc.201100352>
3. C. Sanjai, S. Kothan, P. Gonil, S. Saesoo, W. Sajomsang, *Carbohydr. Polym.* **2014**, *104*, 231–237. <https://doi.org/10.1016/j.carbpol.2014.01.012>
4. J. M. Montenegro, V. Grazu, A. Sukhanova, S. Agarwal, J. M. dela Fuente, I. Nabiev, A. Greiner, W. J. Parak, *Adv. Drug. Deliv. Rev.* **2013**, *65*, 677–688. <https://doi.org/10.1016/j.addr.2012.12.003>
5. Y. H. Hou, X. Y. Han, J. Chen, Z. L. Li, X. C. Chen, L. G. Gai, *Sep. Purif. Technol.* **2013**, *116*, 101–106. <https://doi.org/10.1016/j.seppur.2013.05.033>
6. J. Liu, Z. W. Zhao, P. H. Shao, F. Y. Cui, *Chem. Eng. J.* **2015**, *262*, 854–861. <https://doi.org/10.1016/j.cej.2014.10.043>
7. E. Rafiee, A. Ataei, Sh. Nadri, M. Joshaghani, S. Eavani, *Inorg. Chim. Acta.* **2014**, *409*, 302–309. <https://doi.org/10.1016/j.ica.2013.09.042>
8. J. Liu, R. Che, H. Chen, F. Zhang, F. Xia, Q. Wu, M. Wang, *Small*, **2012**, *18*, 1214–1221.
9. Y. Piao, A. Burns, J. Kim, U. Wiesner, T. Hyeon, *Adv. Funct. Mater.* **2008**, *18*, 3745–3758. <https://doi.org/10.1002/adfm.200800731>
10. M. A. Ghasemzadeh, B. Molaei, M. H. Abdollahi-Basir, F. Zamani, *Acta. Chim. Slov.* **2017**, *64*, 73–82. <https://doi.org/10.17344/acsi.2016.2823>
11. M. A. Ghasemzadeh, M. H. Abdollahi-Basir, *Acta. Chim. Slov.* **2016**, *63*, 627–637. <https://doi.org/10.17344/acsi.2016.2386>
12. M. N. Elinson, A. I. Ilovaisky, V. M. Merkulova, P. A. Belyakov, A. O. Chizhov, *Tetrahedron*, **2010**, *661*, 4043–4048. <https://doi.org/10.1016/j.tet.2010.04.024>
13. J. M. Khurana, B. Nand, P. Saluja, *Tetrahedron*, **2010**, *66*, 5637–5641. <https://doi.org/10.1016/j.tet.2010.05.082>
14. B. Karami, M. Kiani, S. J. Hosseini, M. Bahrami, *New. J. Chem.* **2015**, *39*, 8576–8581. <https://doi.org/10.1039/C5NJ01302J>
15. B. Karami, M. Kiani, *Res. Chem. Intermed.* **2016**, *42*, 3373–3383. <https://doi.org/10.1007/s11164-015-2218-8>
16. B. Karami, M. Kiani, *Catal. Commun.* **2011**, *14*, 62–67. <https://doi.org/10.1016/j.catcom.2011.07.002>
17. M. Kiani, M. Mohammadipour, *RSC Adv.* **2017**, *7*, 997–1007.
18. L. Cabrera, S. Gutierrez, M. P. Morales, N. Menendez, P. Herrasti, *Magn. Magn. Mater.* **2009**, *321*, 2115–2120. <https://doi.org/10.1016/j.jmmm.2009.01.021>
19. B. Karami, M. Kiani, *J. Chin. Chem. Soc.* **2015**, *62*, 756–760. <https://doi.org/10.1002/jccs.201500135>
20. B. Karami, M. Kiani, *J. Iran. Chem. Soc.* **2016**, *13*, 111–116. <https://doi.org/10.1007/s13738-015-0718-5>
21. B. Karami, M. Kiani, M. A. Hoseini, *Chin. J. Catal.* **2014**, *35*, 1206–1211. [https://doi.org/10.1016/S1872-2067\(14\)60090-5](https://doi.org/10.1016/S1872-2067(14)60090-5)
22. H. J. Wang, J. Lu, Z. H. Zhang, *Monatsh. Chem.* **2010**, *141*, 1107–1112. <https://doi.org/10.1007/s00706-010-0383-4>
23. Patra, T. Mahapatra, *J. Indian. Chem. Soc.* **2012**, *89*, 925–932.

24. J. M. Khurana, S. Kumar *Tetrahedron Lett.* **2009**, *50*, 4125–4127. <https://doi.org/10.1016/j.tetlet.2009.04.125>
25. B. Karami, S. Khodabakhshi, F. Hashemi, *Tetrahedron Lett.* **2013**, *54*, 3583–3585. <https://doi.org/10.1016/j.tetlet.2013.03.124>

Povzetek

Z molibdenovo kislino funkcionalizirani Fe_3O_4 nanodelci, ki temeljijo na silicijevem dioksidu ($\text{Fe}_3\text{O}_4 @ \text{SiO}_2\text{-MoO}_3\text{H}$), so se izkazali kot učinkoviti nanokatalizatorji, ki se jih lahko reciklira z magnetom. Morfologijo in strukturo tega nanokatalizatorja smo raziskali s Fourierjevo transformacijsko infrardečo spektroskopijo (FT-IR), energijsko disperzivno rentgensko spektroskopijo (EDX), transmisivno elektronsko mikroskopijo (TEM), »field emission« vrstično elektronsko mikroskopijo (FE-SEM), termogravimetrično analizo (TGA), rentgensko difrakcijo (XRD) in vibracijsko magnetometrično tehniko (VSM). Veliko katalitsko aktivnost teh katalizatorjev smo preverili na primeru sinteze pirano[2,3-*c*] kromenov, ki predstavljajo biološko zelo aktivne spojine. Katalizator je možno enostavno ločiti iz reakcijske zmesi z uporabo zunanega vira magnetnega polja in reciklirati vsaj osemkrat brez opazne izgube katalitske aktivnosti; to bi lahko bil razlog za njegovo uporabo v industrijskih procesih, kar bi zmanjšalo okoljske obremenitve. $\text{Fe}_3\text{O}_4 @ \text{SiO}_2\text{-MoO}_3\text{H}$ ima torej mnoge prednosti, med drugim nizko ceno, majhno strupenost, enostavnost ločevanja iz reakcijskih zmesi, dobro stabilnost, veliko možnost ponovne uporabe in enostavnost izvedbe reakcij.

DRUŠTVENE VESTI IN DRUGE AKTIVNOSTI
SOCIETY NEWS, ANNOUNCEMENTS, ACTIVITIES

Vsebina

49. Mednarodna kemijska olimpijada v Bangkoku, Tajska	S101
Koledar znanstvenih in strokovnih srečanj	S107
Navodila za avtorje	S112

Contents

49 th Chemical Olympiad in Bangkok, Thailand	S101
Scientific meetings – chemistry, chemical technology and chemical engineering ...	S107
Instructions for authors	S112

49. Mednarodna kemijska olimpijada v Bangkoku, Tajska

Tekst in foto:

Andrej Godec

Letošnja mednarodna kemijska olimpijada je potekala od 6. do 15. julija v Bangkoku na Tajskem. Na olimpijadi je sodelovalo 297 dijakov iz 76 držav, dve državi pa sta bili opazovalki.

Po pravilih olimpijade lahko vsako državo zastopa ekipa, sestavljena iz največ štirih dijakov in dveh mentorjev. Slovenijo so letos zastopali Vid Kermelj in Martin Rihtaršič (oba gimnazija Škofja Loka), ter Jože Gašperlin (gimnazija Kranj) in Anže Hubman (gimnazija Ravne na Koroškem). Vid in Martin sta osvojila srebrni medalji, Jože bronasto, Anže pa je dobil častno priznanje organizatorja olimpijade. To je odličen rezultat, zato vsem štirim iskrene čestitke!

Mentorja ekipe sva bila dr. Helena Prosen in dr. Andrej Godec, oba UL FKKT.

Običajno se organizatorji olimpijade izmenjujejo geografsko na dve leti: dvakrat je na vrsti Vzhod, in potem dvakrat Zahod. Letošnja olimpijada je potekala na Tajskem, na Univerzi Mahidol v mestu Nakhon Pathon streljaj od Bangkoka. Prebivali smo sicer v Bangkoku. V tem delu Tajske je sedaj sezona dežja, na kar so nas organizatorji že vnaprej opozorili. Vendar smo imeli srečo z vremenom, deževalo je večinoma ponoči, čez dan pa je bilo vroče, preko 30 °C, in dokaj vlažno, z relativno vlažnostjo čez 70 %.

Kraljevina Tajska (do leta 1939 Siam) obsega danes ogromno področje z velikimi kmetijskimi površinami v centralnem delu ter med turisti zelo priljubljenimi plažami na jugu med Andamanskim morjem ter Tajskim zalivom. Ima skoraj 70 milijonov prebivalcev, ki govorijo različne dialekte.

Bangkok ima v originalnem jeziku najdaljše ime na svetu, ki se v transkripciji glasi: Krung Thep Mahanakhon Amon Rattanakosin Mahinthara Ayuthaya Mahadilok Phop Nopparat Ratchathani Burirom Udomratchaniwet Mahasathan Amon Piman Awatan Sathit Sakkathattiya Witsanukam Prasit. Domačini ga imenujejo Krung Thep, kar pomeni mesto angelov, krajše pa ga pišejo กรุงเทพมหานคร. Mesto je kot glavno mesto takratnega Siam pred več kot 200 leti ustanovil kralj Rama. Trenutno je na Tajskem obdobje enoletnega žalovanja za kraljem Ramo IX, ki je bil vladar z najdaljšim stažem na svetu; prestol je zasedel leta 1946, umrl pa je lani.

V ožjem delu mesta živi preko 8 milijonov ljudi, zato so ulice vedno živahne. Mesto se hitro modernizira, nastajajo novi odseki podzemne železnice in nove avtoceste. Tudi sicer je promet v Bangkoku zelo gost; za turiste so poleg javnega prometa najudobnejše prometno sredstvo taksiji. Najhitreje pa se pripeljete, če uporabite tuk tuk ali pa prevoz na navadnem motorju, kjer sedite zadaj. Seveda



Slovenska ekipa na kemijski olimpijadi 2017: z leve strani Martin, Vid, Anže, Jože, Helena Prosen in Andrej Godec.



Tuk tuk.

pa za to potrebujete tudi precej poguma, saj tak prevoz pomeni vrtoglavo vijuganje v zelo gostem prometu.

Za Tajsko je sicer značilna eksplozija barv, in to vsepovsod, čeprav trenutno malo manj zaradi žalovanja. Sladokusci bodo uživali v pestrem tropskem sadju in odlični hrani, ki obsega mesno in tudi brezmesno varianto. 93 % Tajcev je namreč teravada budistov, ki pa jedo meso; ostali so muslimani, kristjani, hinduisti in konfucijanci. Tajska je danes tudi največja izvoznica duriana, zelo okusnega sadeža, ki pa ima neprijeten vonj, in ga je naprimer prepovedano nesti na letalo.

Bangkok je z zgodovino bogato mesto. Če ste tukaj, si morate ogledati vsaj Veliko palačo na bregovih reke Chao Praya. Palača, administrativni in verski center, je bila dokončana leta 1782; postala je sedež siamskih kraljev, in se še danes uporablja za protokolarne namene. Velik del je odprt za javnost, v njej pa najdete tempelj smaragdne Bude (Wat Phra Kaew), več zgradb, pa tudi krasne paviljone in vrtove.

V Bangkoku so tudi ogromne tržnice, kjer lahko kupite vse od hrane pa do oblačil in živali. Posebnost je plavajoča tržnica, kjer trgovci ponujajo blago na čolnih.



Zmajev sadež.



Tradicionalno in moderno.

Vožnjo s hitrimi čolni si lahko tudi sicer omislite, je pa potrebno držati zaprta usta, saj lahko sicer pogoltnete precej neprav čiste vode, ki pljuska od drugih čolnov. Bangkok zaradi obilice kanalov imenujejo tudi Vzhodne Benetke.

Na olimpijadi organizator takoj po otvoritvi loči dijake od mentorjev. Dijaki imajo dva tekmovalna dneva, ostalih sedem pa so polno zasedeni z raznimi aktivnostmi in izleti, kar vse si lahko pogledate tukaj: <https://ic-ho2017.sc.mahidol.ac.th/#>. Urnik mentorjev pa je nasprotje tega; večino časa porabimo za usklajevanje tekstov, nalog, prevajanje in na koncu ocenjevanje.

Kljub temu smo si en dan ogledali Ayutthayo, staro prestolnico Tajske, ustanovljeno leta 1350. Mesto je tudi zaradi lokacije cvetelo vse do leta 1767, ko ga je napadla in uničila burmanska vojska. Kljub vsemu je zelo očarljivo, in absolutno vredno ogleda. Še danes so tukaj impozantne ruševine; precej je velikih stup, in budističnih samostanov.

V bližini Ayutthaye smo si ogledali tudi farmo, kjer dobro skrbijo za slone. Na Tajskem jih je samo še nekaj čez 3000, tako da so oblasti začele s projekti ohranjanja teh čudovitih, a ogroženih živali. Tajski sloni spadajo v



Odrpta kuhinja.

skupino azijskih slonov; so sicer nižji od indijskih, vendar pa so obilnejši.

Otvoritev letošnje olimpijade je bila 7. julija 2017 na Univerzi Mahidol. Posebnost letošnje otvoritve je bila, da se je udeležila tudi princesa njena visokost Maha Chakri Sirindhorn in precejšen diplomatski zbor, zato so bili varnostni ukrepi na prireditvi izjemno strogi, fotografiranje pa prepovedano. Smo pa zato kasneje imeli na vseh transferjih prisotna tudi policijska vozila, ki so nam utirala pot skozi gost mestni promet.

Takoj po otvoritvi smo mentorji odšli na ogled laboratorijev, kjer bodo dijaki opravili praktični del tekmovanja. Letos je tekmovanje gostila Univerza Mahidol, laboratoriji pa so bili popolnoma novi. Nasploh je bil eksperimentalni del letos precej drag, saj sta si med drugim dva dijaka delila en spektrofotometer.

Ogledu sledi usklajevanje nalog na dolgi seji, in naslednji dan prevajanje. Na tem mestu sledi kratek opis nalog, ki pa si jih sicer lahko ogledate v spletni učilnici Kemljud (<http://skupnost.sio.si/login/index.php>), ali pa na spletni strani letošnje olimpijade.

Eksperimentalni del je bil sestavljen iz treh nalog, za katere so imeli dijaki na voljo 5 ur časa. Prva naloga je bila na temo indikatorjev. Dijaki so morali določati položaj ravnotežja $\text{HIn} \rightleftharpoons \text{H}^+ + \text{In}^-$, kar so okarakterizirali s spektrofotometričnimi meritvami v metiloranžu in bromotimol modrem. Iz podatkov so morali izračunati konstanto disociacije indikatorja. Nato pa so z indikatorjem metil rdečim določili še pH neznanе raztopine.

Druga naloga je bila proučevanje ravnotežja $\text{Ca}(\text{IO}_3)_2(\text{s}) \rightleftharpoons \text{Ca}^{2+}(\text{aq}) + \text{IO}_3^-(\text{aq})$. S titracijami so določili koncentracijo jodatnih ionov v nasičeni raztopini, in izračunali topnostni produkt. Titracija je potekala s standardno raztopino $\text{Na}_2\text{S}_2\text{O}_3$ v prisotnosti KI in s škrobom kot indikatorjem. Nato so $\text{Ca}(\text{IO}_3)_2$ raztopili v razredčeni raztopini KIO_3 z neznanо koncentracijo, in določili s titracijami njeno koncentracijo.

Tretja praktična naloga je bila preparativa: iz komercialnih p-klorobenzaldehida in 3-pentanona so sintetizirali nove spojine. Pri tem so uporabili vročo kopel, nučiranje, in izvedli prekrystalizacijo iz etanola. Produkt je organizator okarakteriziral z NMR.

Čez dva dni je sledil teoretični test. Letos je vseboval 11 nalog, čas pa je tudi tukaj omejen na 5 ur.

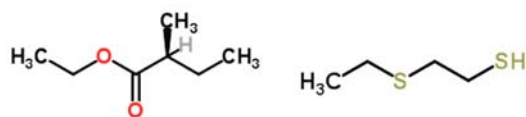
Prva naloga je bila na temo proizvodnje propena iz propana s heterogeno katalizo. Dijaki so morali s pomočjo veznih entalpij termodinamsko okarakterizirati to reakcijo. Določiti so morali tudi parametre v hitrostnem zakonu za oksidativno dehidrogenacijo, ki poteka na trdnih katalizatorjih v prisotnosti kisika:

$$r_{\text{C}_3\text{H}_6} = \frac{I}{\left(\frac{p^\circ}{k_{\text{red}} P_{\text{C}_3\text{H}_8}} + \frac{p^\circ}{k_{\text{ox}} P_{\text{O}_2}} \right)}$$

Oceniti pa so morali tudi dogajanje na površini katalizatorja.



Durian.



Za karakterističen neprijeten vonj duriana sta »krivca«
etil(2S)-2-metilbutanoat in 1-(etilsulfanil)etan-1-tiol. sadež.



Ayutthaya.



V objemu korenin.



Laboratorijski pult dijaka.



Prevajanje nalog traja cel dan.

Druga naloga je bila kinetični izotopski efekt (KIE) in ničelna vibracijska energija (ZPE). Dijaki so uporabili model harmoničnega oscilatorja, da so ugotovili razliko med hitrostima aktivacije vezi med C-H in C-D (kjer je D = devterij). Za oba so morali izračunati reducirano maso, vibracijsko frekvenco in ZPE. Nato pa so iz znanih podatkov za reakcijo prvega reda določili konstante reakcijske hitrosti in najpočasnejšo reakcijo v reakciji oksidacije ne-devteriranega in devteriranega difenilmetanola z uporabo presežka kromove kisline.

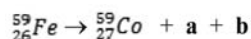
Tretja naloga je bila termodinamika reakcije pridobivanja metanola $\text{CO(g)} + 2\text{H}_2\text{(g)} \rightarrow \text{CH}_3\text{OH(g)}$. Dijaki so morali izračunati ΔH° , ΔS° , Δ° , in K_p za reakcijo pri 298 K, ter vrednost K_p pri temperature 600K, če sta ΔH° in ΔS° neodvisna od temperature. Poleg tega so izračunali še spremembo proste entalpije ΔG pri 300 K za process mešanja dveh plinov.

Četrta naloga je bila na temo elektrokemije. Galvanski člen je bil sestavljen iz vodikovega polčlena $[\text{Pt(s)} | \text{H}_2\text{(g)} | \text{H}^+(\text{aq})]$, ki je povezan z drugim polčlenom, v katerem je kovinski trak potopljen v raztopino iona iste kovine $\text{M}^{2+}(\text{aq})$ z neznan koncentracijo. Iz napetosti člena so

morali izračunati standardni elektroodni potencial kovinskega polčlena, pa koncentracijo kovinskih ionov iz podatkov za jodometrično titracijo, za katero so morali tudi napisati urejene enačbe reakcij.

Peta naloga je obravnavala fosfate in silikate v zemlji. Najprej so določili celotni fosfat (PO_4^{3-}) in silikat (SiO_4^{4-}) pri postopku ekstrakcije iz zemlje; fosfat so analizirali v kislinskem ekstraktu s postopkom z metilenskim modrim in z uporabo spektrofotometrije, nato pa še oba pri reakciji z molibdatom v bazični raztopini. Pri tej nalogi je bilo kar precej računanja.

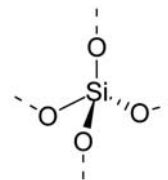
Šesta naloga je bila posvečena železu in njegovi kristalni strukturi. Razen ugotavljanja strukture so predvideli produkte pri reakciji Fe^{2+} s KMnO_4 v bazični raztopini, in nato še obnašanje izotopa. ^{59}Fe je radiofarmacevtski izotop, ki se uporablja za preučevanje metabolizma železa v vranici. Ta izotop razpada do ^{59}Co po naslednji reakciji:



Ugotoviti so morali, kaj sta a in b, ter izračunati razpolovni čas ^{59}Fe .

Sedma naloga je bila na temo sinteze in karakterizacije nekaterih titanovih kompleksov, ki nastanejo pri reakciji z različnimi ligandi. Iz spektrofotometričnih, NMR v CDCl_3 in IR podatkov so morali narisati strukturo kompleksa titana. Naloga je bila precej zahtevna.

Osma naloga je bila povezana s silicijevim dioksidom in njegovo površino. Silicijev dioksid obstaja v različnih oblikah, npr. v amorfni in kristalinični. Silicijevi atomi so tetraedrsko vezani na štiri atome kisika, kar daje tridimenzionalno trdno mrežo.

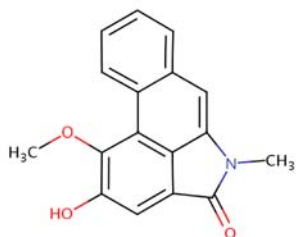


Pri tej nalogi so morali dijaki predvideti možne prostorske strukture te spojine, in njenih kompleksov s Cu^{2+} , saj se lahko uporablja kot učinkovit adsorbent kovin v vodi. Narisati so morali tudi diagrame razcepa, in strukture kompleksov z Hg^{2+} , ki povečajo selektivnost tega adsorbenta.

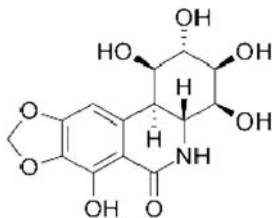
Deveta naloga je bila organska. Dijaki so morali uganiti spojino, ki je kiralna, ki vsebuje samo tri elemente, ter ima relativno molekularno maso (M_r) 149 (zaokroženo na celo število). Drugi podatki so bili, da ^1H NMR spekter te spojine med ostalimi signali kaže tudi tri tipe aromatskih protonov, medtem ko ^{13}C NMR spekter kaže osem signalov, pri čemer so štirje signali v območju 120–140 ppm. To spojino lahko pripravimo tako, da karbonilno spojino obdelamo z metilaminom, nato pa še z NaBH_3CN . Dijaki so morali napisati vse možne strukturne formule te spojine, ter formule spojin, ki nastopajo v reakcijski shemi njene sinteze iz dveh neznan diolov.

Tudi deseta naloga je bila iz organske kemije. Šlo je za totalno sintezo alkaloidov, in sicer dveh značilnih predstavnikov – sauristolaktama in pankratistatina, ki kažeta potencialno biološko aktivnost. Pankratistatin naprimer so

izolirali iz havajske rastline pajkove lilije, kaže pa inhibitorsko aktivnost proti rasti rakavih celic. Dijaki so morali urediti sintezno sekvenco obeh alkaloidov, pri čemer so si lahko pomagali s podatki $^1\text{H-NMR}$ v CDCl_3 pri 300 MHz.



Sauristolaktam.



Pankratistatin.

Zadnja, enajsta naloga, je bila na temo *trans*-ciklooktena. Leta 2011 so Fox in sodelavci razvili fotokemijsko sintezo raznih derivatov *trans*-ciklooktena. Dijaki so morali pri tej nalogi predvideti stereoizomerijo vmesnih snovi pri tej sintezi; ta naloga je bila krajša.

Nasplošno so bile naloge težke, vendar pa časovno ne preveč obsežne. 30 % nalog je bilo iz fizikalne kemije;

27 % iz anorganske, 25 % iz organske, in 18 % iz analizne kemije.

Najboljši dosežek na letošnji olimpijadi je bil okrog 98 % (dijak iz Rusije), sledil je dijak iz Tajvana, tretji pa je bil dijak iz Irana. Naš najboljši Vid Kermelj pa je dosegel malo nad 82 %, kar je pomenilo odličen rezultat, ki mu je prinesel srebrno medaljo. Veseli pa smo predvsem, da naši dijaki tudi v praktičnem delu dosegajo vedno boljše rezultate.

Priprave na olimpijado potekajo na Fakulteti za kemijo in kemijsko tehnologijo v Ljubljani. Letos so pri pripravah sodelovale naslednje sodelavke in sodelavci: dr. Helena Prosen, dr. Alojz Demšar, dr. Darko Dolenc, dr. Črtomir Podlipnik in dr. Andrej Godec. Vsem se najlepše zahvaljujemo.

Pri organizaciji udeležbe na olimpijadi sodelujemo z Zvezo za tehnično kulturo Slovenije, ki se ji prav tako iskreno zahvaljujemo, kot tudi Slovensku kemijskemu društvu, kjer je sedež Odbora za pripravo kemijske olimpijade.

Prihodnja, jubilejna 50. Olimpijada, pa bo tam, kjer se je leta 1968 vse skupaj začelo: skupaj jo bosta gostili Češka in Slovaška, ki sta vmes postali samostojni državi, ki pa očitno zelo dobro sodelujeta. Vabljeni!

KOLENDAR VAŽNEJŠIH ZNANSTVENIH SREČANJ S PODROČJA KEMIJE IN KEMIJSKE TEHNOLOGIJE

SCIENTIFIC MEETINGS – CHEMISTRY AND CHEMICAL ENGINEERING

2017

October 2017

- 1 – 5 EPIC 2017 – 6TH EUROPEAN PROCESS INTENSIFICATION CONFERENCE 2017
Barcelona, Spain
Information: <http://www.wcce10.org/index.php/en/>
- 1 – 5 WCCE10 – 10TH WORLD CONGRESS OF CHEMICAL ENGINEERING
INCORPORATING THE 11TH EUROPEAN CONGRESS OF CHEMICAL ENGINEERING
(ECCE11)
Barcelona, Spain
Information: <http://www.wcce10.org/index.php/en/>
- 1 – 5 4TH EUROPEAN CONGRESS OF APPLIED BIOTECHNOLOGY – ECAB3
Barcelona, Spain
Information: <http://www.wcce10.org/index.php/en/>
- 2 – 5 7TH IUPAC INTERNATIONAL CONFERENCE ON GREEN CHEMISTRY
Moscow, Russian Federation
Information: <http://greeniupac2017.muctr.ru>
- 2 – 5 SMMAP2017
Chessy, France
Information: <https://smmap2017.sciencesconf.org/>
- 4 – 6 XIXTH EUROFOODCHEM CONFERENCE
Budapest, Hungary
Information: <http://www.eurofoodchem2017.mke.org.hu/index.php>
- 9 – 11 THE 3RD INTERNATIONAL CONFERENCE ON NANOMATERIALS: FUNDAMENTALS
AND APPLICATIONS
Vysoké Tatry, Slovakia
Information: <https://nfa2017.science.upjs.sk/index.php>
- 9 – 12 9TH WORKSHOP ON PROFICIENCY TESTING IN ANALYTICAL CHEMISTRY,
MICROBIOLOGY AND LABORATORY MEDICINE
Portorož, Slovenia
Information: <http://eurachempt2017.eu/>
- 9 – 13 POLYCHAR 25 – 25TH ANNUAL WORLD FORUM ON ADVANCED MATERIALS
Kuala Lumpur, Malaysia
Information: <http://www.25POLYCHAR.org.my>
- 11 – 13 IUPAC-FAPS 2017 POLYMER CONGRESS ON SMART MATERIALS FOR EMERGING
TECHNOLOGY
Jeju Island, Republic of Korea
Information: <http://www.faps2017.org>

- 11 – 13 5TH MS FOOD DAY
Bologna, Italy
Information: <http://www.spettrometriadimassa.it/Congressi/5MS-FoodDay/>
- 11 – 15 YoungChem 2017
Lublin, Poland
Information: <http://www.youngchem.com/?lang=en>
- 12 – 14 EWCC 2017 – EAST-WEST CHEMISTRY CONFERENCE 2017
Skopje, Macedonia
Information: <http://ewcc2017.org/>
- 16 – 18 5TH INTERNATIONAL CONFERENCE ON NANOTECHNOLOGY AND MATERIALS SCIENCE
Dubai, United Arab Emirates
Information: <http://www.worldnanoconference.com/dubai/index.php>
- 23 – 25 THE 3RD INTERNATIONAL SYMPOSIUM ON APPLIED CHEMISTRY (ISAC) 2017
Jakarta, Indonesia
Information: <http://situs.opi.lipi.go.id/isac2017/>
- November 2017**
-
- 2 – 4 INTERNATIONAL CONFERENCE ON POTENTIAL IMPACT OF PESTICIDES ON ENVIRONMENT AND HUMAN HEALTH
Bengaluru, India
Information: <http://www.dsu.edu.in/index.php/international-conference-on-icpipehh-2017-by-chemistry-department-DSU-SOE>
- 2 – 4 III INTERNATIONAL CONFERENCE ON FOOD CHEMISTRY AND TECHNOLOGY (FCT-2017)
Baltimore, United States
Information: <https://unitedscientificgroup.com/conferences/food-chemistry-and-technology/>
- 5 – 9 HPLC 2017 – THE 46TH INTERNATIONAL SYMPOSIUM ON HIGH PERFORMANCE LIQUID PHASE SEPARATIONS AND RELATED TECHNIQUES
Jeju Island, Republic Of Korea
Information: <http://www.hplc2017-jeju.org>
- 6 – 9 2ND INTERNATIONAL CAPARICA CONFERENCE ON POLLUTANT TOXIC IONS AND MOLECULES
Lisbon, Portugal
Information: <http://www.ptim2017.com/>
- 13 – 14 5TH INTERNATIONAL CONFERENCE ON PLASMA CHEMISTRY AND PLASMA PROCESSING
Paris, France
Information: <http://plasmachemistry.alliedacademies.com/>
- 25 – 28 2ND INTERNATIONAL CONFERENCE ON APPLIED CHEMISTRY
Hurgada, Egypt
Information: <http://isac-chem.sohag-univ.edu.eg/index.html>
- 26 – 29 EMEC 18 – 18TH EUROPEAN MEETING ON ENVIRONMENTAL CHEMISTRY
Porto, Portugal
Information: <http://emec18.eventos.chemistry.pt/>
- December 2017**
-
- 11 – 15 4TH INTERNATIONAL CONGRESS ON CATALYSIS FOR BIOREFINERIES (CATBIOR 2017)
Lyon, France
Information: <http://catbior2017.univ-lyon1.fr/en/pages/catbior-2017-home>

2018

February 2018

21 – 23 ChemCYS 2018 – 14TH CHEMISTRY CONFERENCE FOR YOUNG SCIENTISTS
Blankenberge, Belgium
Information: <http://chemcys.be/>

March 2018

13 – 15 FILTECH 2018 – INTERNATIONAL CONFERENCE AND EXHIBITION FOR
FILTRATION AND SEPARATION TECHNOLOGIES
Cologne, Germany
Information: <http://www.filtech.de/conference/call-for-papers>

19 – 21 WORLD CONGRESS ON CHEMISTRY
Valencia, Spain
Information: <http://worldchemicalsciences.com/cs/home>

April 2018

15 – 18 PETROMASS 2018 – XI. INTERNATIONAL MASS SPECTROMETRY CONFERENCE
ON PETROCHEMISTRY, ENVIRONMENTAL AND FOOD CHEMISTRY
Bled, Slovenia
Information: <http://www.petromass2018.com/>

June 2018

4 – 7 IIS PRAGUE 2018 – 13TH INTERNATIONAL SYMPOSIUM ON THE SYNTHESIS AND
APPLICATIONS OF ISOTOPES AND ISOTOPICALLY LABELLED COMPOUNDS
Prague, Czech Republic
Information: <http://www.iis-prague2018.cz/>

4 – 7 POLYMERS AND ORGANIC CHEMISTRY 2018 (POC 2018)
Montpellier, France
Information: <https://iupac.org/event/polymers-organic-chemistry-2018-poc-2018/>

July 2018

8 – 13 27TH IUPAC INTERNATIONAL SYMPOSIUM ON PHOTOCHEMISTRY
Dublin, Ireland
Information: <https://iupac.org/event/27th-iupac-international-symposium-photochemistry/>

15 – 20 THE 18TH INTERNATIONAL SYMPOSIUM ON SOLUBILITY PHENOMENA AND
RELATED EQUILIBRIUM PROCESSES (ISSP)
Tours, France
Information: <http://issp18.org/>

August 2018

26 – 30 ECC7 – 7TH EuCheMS CHEMISTRY CONGRESS
Liverpool, UK
Information: <https://www.euchems2018.org/>

September 2018

2 – 7 ECIS 2018 – 32nd Conference of The European Colloid and Interface Society
Ljubljana, Slovenia
Information: <http://ecis2018.fkkt.uni-lj.si/>

16 – 19 DISTILLATION & ABSORPTION CONFERENCE 2018
Firenze, Italy
Information: <http://www.aidic.it/da2018/>

October 2018

4 – 7 N-LIGANDS2018 – 7TH EuCheMS CONFERENCE ON NITROGEN-LIGANDS
Lisbon, Portugal
Information: <http://www.n-ligands2018.com/>

16 – 21 22ND INTERNATIONAL CONFERENCE ON ORGANIC SYNTHESIS (22-ICOS)
Florence, Italy
Information: <http://www.22-icos-florence.it>

2019

May 2019

19 – 24 14TH IUPAC INTERNATIONAL CONGRESS OF CROP PROTECTION CHEMISTRY
Ghent, Belgium
Information: <https://www.iupac2019.be>

June 2019

26 – 30 6TH EUROPEAN CONFERENCE ON ENVIRONMENTAL APPLICATIONS OF
ADVANCED OXIDATION PROCESSES (EAAOP-6)
Portorož, Slovenia
Information: <http://eaaop6.ki.si/>

July 2019

5 – 12 IUPAC 2019
Paris, France
Information: <https://www.iupac2019.org/>

21 – 26 THE 18TH INTERNATIONAL SYMPOSIUM ON NOVEL AROMATIC COMPOUNDS
(ISNA-18)
Sapporo City, Japan
Information: <https://iupac.org/event/18th-international-symposium-novel-aromatic-compounds-isna-18/>

Acta Chimica Slovenica

Author Guidelines

Submissions

Submission to ACSi is made with the implicit understanding that neither the manuscript nor the essence of its content has been published in whole or in part and that it is not being considered for publication elsewhere. All the listed authors should have agreed on the content and the corresponding (submitting) author is responsible for having ensured that this agreement has been reached. The acceptance of an article is based entirely on its scientific merit, as judged by peer review. There are no page charges for publishing articles in ACSi.

Submission material

Typical submission consists of:

- full manuscript (Word file, with title, authors, abstract, keywords, figures and tables embedded, and references);
- supplementary files:
 - **Statement of novelty** (Word file),
 - **List of suggested reviewers** (Word file),
 - ZIP file containing **graphics** (figures, illustrations, images, photographs),
 - **Graphical abstract** (single graphics file),
 - **Proposed cover picture** (optional, single graphics file),
 - **Appendices** (optional, Word files, graphics files).

Submission process

Submission process consists of 5 steps. Before submission, authors should go through the checklist at the bottom of these guidelines page and prepare for submission:

Step 1: Starting the submission

- Choose one of the journal sections.
- Confirm all the requirements of the **checklist**.
- Additional plain text comments for the editor can be provided in the relevant text field.

Step 2: Upload submission

- Upload full manuscript in the form of a Word file (with title, authors, abstract, keywords, figures and tables embedded, and references).

Step 3: Enter metadata

- First name, last name, contact email and affiliation for all authors, in relevant order, must be provided. Corresponding author has to be selected. Full postal address and phone number of the corresponding author has to be provided.
- **Title and abstract** must be provided in plain text.
- Keywords must be provided (max. 6, separated by semicolons).

- Data about contributors and supporting agencies may be entered.
- **References** in plain text must be provided in the relevant text filed.

Step 4: Upload supplementary files

- **Statement of novelty** in a Word file must be uploaded
- **List of suggested reviewers** with at least three reviewers must be uploaded as a Word file.
- All **graphics** have to be uploaded in a single ZIP file. Graphics should be named Figure 1.jpg, Figure 2.eps, etc.
- **Graphical abstract image** must be uploaded separately.
- **Proposed cover picture** (optional) should be uploaded separately.
- Any additional **appendices** (optional) to the paper may be uploaded. Appendices may be published as a supplementary material to the paper, if accepted.
- For each uploaded file the author is asked for additional metadata which may be provided. Depending of the type of the file please provide the relevant title (Statement of novelty, List of suggested reviewers, Figures, Graphical abstract, Proposed cover picture, Appendix).

Step 5: Confirmation

- Final confirmation is required.

Article Types

Review articles are welcome in any area of chemistry and may cover a wider or a more specialized area, if a high impact is expected. Manuscripts normally should not exceed 40 pages of one column format (letter size 12, 33 lines per page). Authors should consult the ACSi editor prior to preparation of a review article.

Scientific articles should have the following structure:

1. Title (max. 150 characters),
2. Authors and affiliations,
3. Abstract (max. 1000 characters),
4. Keywords (max. 6),
5. Introduction,
6. Experimental (Results and Discussion),
7. Results and Discussion (Experimental),
8. Conclusions,
9. Acknowledgements (if any),
10. References.

The sections should be arranged in the sequence generally accepted for publications in the respective fields. Scientific articles should report significant

and innovative achievements and exhibit a high level of originality.

Short communications generally follow the same order of sections, but should be short (max. 2500 words) and report a significant aspect of research work meriting separate publication.

Technical articles report applications of an already described innovation. Typically, technical articles are not based on new experiments.

Preparation of Submissions

Text of the submitted articles must be prepared with Word for Windows. Normal style set to single column, 1.5 line spacing, and 12 pt Times New Roman font is recommended. Line numbering (continuous, for the whole document) must be enabled to simplify the reviewing process. For any other format, please consult the editor. Articles should be written preferably in English. Correct spelling and grammar are the sole responsibility of the author(s). Papers should be written in a concise and succinct manner. The authors shall respect the ISO 80000 standard, and IUPAC Green Book rules on the names and symbols of quantities and units. The Syst me International d'Unit s (SI) must be used for all dimensional quantities.

Graphics (figures, graphs, illustrations, digital images, photographs) should be inserted in the text where appropriate. The captions should be self-explanatory. Lettering should be readable (suggested 8 point Arial font) with equal size in all figures. Use common programs such as Word Excel to prepare figures (graphs) and ChemDraw to prepare structures in their final size (8 cm for single column width or 17 cm for double column width) so that neither reduction nor enlargement is required. In **graphs**, only the graph area determined by both axes should be in the frame, while a frame around the whole graph should be omitted. The graph area should be white. The legend should be inside the graph area. The style of all graphs should be the same. **Figures and illustrations** should be of sufficient quality for the printed version, i.e. 300 dpi minimum. **Digital images and photographs** should be of high quality (minimum 250 dpi resolution). On submission, figures should be of good enough resolution to be assessed by the referees, ideally as JPEGs. High-resolution figures (in JPEG, TIFF, or EPS format) might be required if the paper is accepted for publication.

Tables should be prepared in the Word file of the paper as usual Word tables. The captions should be above the table and self-explanatory.

References should be numbered and ordered sequentially as they appear in the text, likewise methods, tables, figure captions. When cited in the text, reference numbers should be superscripted, following punctuation marks. It is the sole respon-

sibility of authors to cite articles that have been submitted to a journal or were in print at the time of submission to ACSi. Formatting of references to published work should follow the journal style; please also consult a recent issue:

1. J. W. Smith, A. G. White, *Acta Chim. Slov.* **2008**, *55*, 1055–1059.
2. M. F. Kemmere, T. F. Keurentjes, in: S. P. Nunes, K. V. Peinemann (Ed.): *Membrane Technology in the Chemical Industry*, Wiley-VCH, Weinheim, Germany, **2008**, pp. 229–255.
3. J. Levec, Arrangement and process for oxidizing an aqueous medium, US Patent Number 5,928,521, date of patent July 27, **1999**.
4. L. A. Bursill, J. M. Thomas, in: R. Sersale, C. Collela, R. Aiello (Eds.), *Recent Progress Report and Discussions: 5th International Zeolite Conference*, Naples, Italy, 1980, Gianini, Naples, **1981**, pp. 25–30.
5. J. Segezdi, F. Csizmadia, Prediction of dissociation constant using microconstants, http://www.chemaxon.com/conf/Prediction_of_dissociation_constant_using_microconstants.pdf, (assessed: March 31, 2008)

Titles of journals should be abbreviated according to Chemical Abstracts Service Source Index (CASSI).

Special Notes

- Complete characterization, **including crystal structure**, should be given when the synthesis of new compounds in crystal form is reported.
- Numerical **data should be reported with the number of significant digits corresponding to the magnitude** of experimental uncertainty.
- **The SI system of units and IUPAC recommendations** for nomenclature, symbols and abbreviations should be followed closely. Additionally, the authors should follow the general guidelines when citing spectral and analytical data, and depositing crystallographic data.
- **Characters** should be correctly represented throughout the manuscript: for example, 1 (one) and l (ell), 0 (zero) and O (oh), x (ex), D7 (times sign), B0 (degree sign). Use Symbol font for all Greek letters and mathematical symbols.
- The rules and recommendations of the **IUBMB** and the **International Union of Pure and Applied Chemistry (IUPAC)** should be used for abbreviation of chemical names, nomenclature of chemical compounds, enzyme nomenclature, isotopic compounds, optically active isomers, and spectroscopic data.
- **A conflict of interest** occurs when an individual (author, reviewer, editor) or its organization is involved in multiple interests, one of which could possibly corrupt the motivation for an act in the other. Financial relationships are the most easily identifiable conflicts of interest, while conflicts can occur also as personal relationships, academic competition, etc. **The Edi-**

tors will make effort to ensure that conflicts of interest will not compromise the evaluation process; potential editors and reviewers will be asked to exempt themselves from review process when such conflict of interest exists. When the manuscript is submitted for publication, **the authors** are expected to disclose any relationships that might pose potential conflict of interest with respect to results reported in that manuscript. In the Acknowledgement section the source of funding support should be mentioned. The statement of disclosure must be provided as Comments to Editor during the submission process.

- **Published statement of Informed Consent.** Research described in papers submitted to ACSi must adhere to the principles of the Declaration of Helsinki (<http://www.wma.net/e/policy/b3.htm>). These studies must be approved by an appropriate institutional review board or committee, and informed consent must be obtained from subjects. The Methods section of the paper must include: 1) a statement of protocol approval from an institutional review board or committee and 2), a statement that informed consent was obtained from the human subjects or their representatives.
- **Published Statement of Human and Animal Rights.** When reporting experiments on human subjects, authors should indicate whether the procedures followed were in accordance with the ethical standards of the responsible committee on human experimentation (institutional and national) and with the Helsinki Declaration of 1975, as revised in 2008. If doubt exists whether the research was conducted in accordance with the Helsinki Declaration, the authors must explain the rationale for their approach and demonstrate that the institutional review body explicitly approved the doubtful aspects of the study. When reporting experiments on animals, authors should indicate whether the institutional and national guide for the care and use of laboratory animals was followed.
- Contributions authored by **Slovenian scientists** are evaluated by non-Slovenian referees.
- Papers describing **microwave-assisted reactions** performed in domestic microwave ovens are not considered for publication in *Acta Chimica Slovenica*.
- *Manuscripts that are **not prepared and submitted** in accord with the instructions for authors are not considered for publication.*

Appendices

Authors are encouraged to make use of supporting information for publication, which is supplementary material (appendices) that is submitted at the same time as the manuscript. It is made available on

the Journal's web site and is linked to the article in the Journal's Web edition. The use of supporting information is particularly appropriate for presenting additional graphs, spectra, tables and discussion and is more likely to be of interest to specialists than to general readers. When preparing supporting information, authors should keep in mind that the supporting information files will not be edited by the editorial staff. In addition, the files should be not too large (upper limit 10 MB) and should be provided in common widely known file formats so as to be accessible to readers without difficulty. All files of supplementary materials are loaded separately during the submission process as supplementary files.

Proposed Cover Picture and Graphical Abstract Image

Authors are encouraged to submit illustrations as candidates for the journal Cover Picture as well as graphical abstracts. Graphical abstract contains an image that appears as a part of the entry in the table of contents in both online and printed edition. The pictures may be the same. The illustrations must be related to the subject matter of the paper. Usually both proposed cover picture and picture for graphical abstract are the same, but authors may provide different pictures as well.

Graphical content: an ideally full-colour illustration of resolution 300 dpi from the manuscript must be proposed with the submission. Graphical abstract pictures are printed in size 6.5 × 4 cm (hence minimal resolution of 770 × 470 pixels). Cover picture is printed in size 11 × 9.5 cm (hence minimal resolution of 1300 × 1130 pixels).

Statement of novelty

Statement of novelty is provided in a Word file and submitted as a supplementary file in step 4 of submission process. Authors should in no more than 100 words emphasize the scientific novelty of the presented research. Do not repeat for this purpose the content of your abstract.

List of suggested reviewers

List of suggested reviewers is a Word file submitted as a supplementary file in step 4 of submission process. Authors should propose the names, full affiliation (department, institution, city and country) and e-mail addresses of three potential referees. For each reviewer at least one reference relevant to the scientific field should be provided as well. Appropriate referees should be knowledgeable about the subject but have no close connection with any of the authors. In addition, referees should be from institutions other than (and preferably countries other than) those of any of the authors.

How to Submit

Users registered in the role of author can start submission by choosing USER HOME link on the top of

the page, then choosing the role of the Author and follow the relevant link for start of submission. Prior to submission we strongly recommend that you familiarize yourself with ACSi style by browsing the journal, either in print or online, particularly if you have not submitted to the ACSi before or recently.

Correspondence

All correspondence with the ACSi editor regarding the paper goes through this web site and emails. Emails are sent and recorded in the web site database. All emails you receive from the system contain relevant links. **Please do not answer the emails directly but use the embedded links in the emails for carrying out relevant actions.** Alternatively, you can carry out all the actions and correspondence through the online system by logging in and selecting relevant options.

Proofs

Proofs will be dispatched via e-mail and corrections should be returned to the editor by e-mail as quickly as possible, normally within 48 hours of receipt. Typing errors should be corrected; other changes of contents will be treated as new submissions.

Submission Preparation Checklist

As part of the submission process, authors are required to check off their submission's compliance with all of the following items, and submissions may be returned to authors that do not adhere to these guidelines.

1. The submission has not been previously published, nor is it under consideration for publication in any other journal (or an explanation has been provided in Comments to the Editor).
2. All the listed authors have agreed on the content and the corresponding (submitting) author is responsible for having ensured that this agreement has been reached.
3. The submission files are in the correct format: manuscript in MS Word; diagrams and graphs are created in Excel and saved in one of the file formats: TIFF, EPS or JPG; illustrations are also saved in one of these formats (See **Author guidelines** for details).
4. The manuscript has been examined for spelling and grammar (spell checked).
5. The **title** (maximum 150 characters) briefly explains the contents of the manuscript.
6. Full names (first and last) of all authors together with the affiliation address are provided. Name of author(s) denoted as the corresponding author(s), together with their e-mail address, full postal address and telephone/fax numbers are given.

7. The **abstract** states the objective and conclusions of the research concisely in no more than 150 words.
8. Keywords (maximum six) are provided.
9. **Statement of novelty** is prepared as a Word file.
10. The text adheres to the stylistic and bibliographic requirements outlined in the **Author guidelines**.
11. Text in normal style is set to single column, 1.5 line spacing, and 12 pt. Times New Roman font is recommended. All tables, figures and illustrations have appropriate captions and are placed within the text at the appropriate points.
12. Mathematical and chemical equations are provided in separate lines and numbered (Arabic numbers) consecutively in parenthesis at the end of the line. All equation numbers are (if necessary) appropriately included in the text. Corresponding numbers are checked.
13. Tables, Figures, illustrations, are prepared in correct format and resolution (see **Author guidelines**).
14. The lettering used in the figures and graphs do not vary greatly in size. The recommended lettering size is 8 point Arial.
15. Separate files for each figure and illustration are prepared. The names (numbers) of the separate files are the same as they appear in the text. All the figure files are packed for uploading in a single ZIP file.
16. Authors have read **special notes** and have accordingly prepared their manuscript (if necessary).
17. References in the text and in the References are correctly cited. (see **Author guidelines**). All references mentioned in the Reference list are cited in the text, and *vice versa*.
18. Permission has been obtained for use of copyrighted material from other sources (including the Web).
19. The names, full affiliation (department, institution, city and country), e-mail addresses and references of three potential referees from institutions other than (and preferably countries other than) those of any of the authors are prepared in the word file.
20. Full-colour illustration or graph from the manuscript is proposed for graphical abstract.
21. **Appendices** (if appropriate) as supplementary material are prepared and will be submitted at the same time as the manuscript.

Privacy Statement

The names and email addresses entered in this journal site will be used exclusively for the stated purposes of this journal and will not be made available for any other purpose or to any other party.

ISSN: 1580-3155

Koristni naslovi

Slovensko kemijsko društvo
Slovenian Chemical Society



Slovensko kemijsko društvo

www.chem-soc.si

e-mail: chem.soc@ki.si



Wessex Institute of Technology

www.wessex.ac.uk



SETAC

www.setac.org



European Water Association

<http://www.ewa-online.eu/>



European Science Foundation

www.esf.org



European Federation of Chemical Engineering

<https://efce.info/>



IUPAC

INTERNATIONAL UNION OF
PURE AND APPLIED CHEMISTRY

International Union of Pure and Applied Chemistry

<https://iupac.org/>

Novice evropske zveze kemijskih društev (EuCheMS) najdete na:



EuCheMS: Brussels News Updates

<http://www.euchems.eu/newsletters/>



Izdajo pripravili
Neil G. Connolly, Ture Dambus
Richard M. Hartshorn, Alan T. Hutton

PRIPOROČILA IUPAC 2005
**NOMENKLATURA
ANORGANSKE
KEMIJE**

ISBN 978-961-90731-8-6
Obseg: 367 str.

Kemijska nomenklatura oz. poimenovanje kemijskih elementov in spojin je potrebno zato, da se vsi, ki jih uporabljajo, med seboj lahko sporazumevajo. Najpomembnejše pri tem je, da je poimenovanje spojin enotno in enoznačno, saj mora biti zagotovljeno, da si pod določenim imenom vsi predstavljajo isto kemijsko spojino.

Z razvojem kemije in celotne splošne znanosti je bilo v preteklosti odkritih ali sintetiziranih ogromno število kemijskih spojin, kar se bo v prihodnosti brez dvoma nadaljevalo s še večjo intenziteto. Vzporedno z odkritji in raziskavami pa se je razvijalo in prilagajalo tudi poimenovanje kemijskih spojin. IUPAC (Mednarodna unija za čisto in uporabno kemijo) skrbi za vsklajeno delovanje na tem področju. V predgovoru k originalu knjige, ki sledi le-temu, je zato natančno opisano, kako je Mednarodna unija poimenovanje kemijskih spojin spremljala, zasledovala in

spreminjala, kadar je bilo to potrebno zaradi jasnosti ali možnosti različnih razumevanj.

Pred nami je tako v letu 2008 prevod »Nomenclature of Inorganic Chemistry, IUPAC Recommendations 2005« v slovenskem jeziku, le tri leta po izidu izvirnika. Zadnja slovenska nomenklatura anorganske kemije je bila izdana leta 1986, njen obseg pa je bil 86 strani (brez preglednic). Nova izdaja prevoda obsega skoraj 400 strani strokovno izjemno zahtevnega teksta. Slovenski prevod je pripravil Andrej Šmalc, z recenzijo in z nekaterimi dodatnimi dejavnostmi v zvezi s pripravo za tisk pa mu je pomagal Primož Šegedin. Za obsežno in strokovno korektno opravljeno delo se obema iskreno zahvaljujem.

Venčeslav Kaučič
Predsednik Slovensko kemijsko društvo



Publikacijo lahko kupite v Slovenskem kemijskem društvu,
Hajdrihova 19, 1000 Ljubljana
Naročilo oddate preko društvene spletne strani:
<http://www.chem-soc.si/publikacije/nomenklatura-anorganske-kemije>
Cena: 17,50 EUR

Sistemi za čisto in ultračisto vodo

Kvaliteta vode 1 do 3*

*v skladu s standardom ISO 3696 in ustreznimi ASTM ter CLSI



DONAU LAB Ljubljana
Member of LPPgroup

Donau Lab d.o.o., Ljubljana
Tbilisijska 85
SI-1000 Ljubljana
www.donaulab.si
office-si@donaulab.com

adrona

Že od
3.214€ +DDV
(B30 Trače s 25 L. Pro rezerv.
Slika je simbolična.)



KEMIJSKI PRIROČNIK

Opisi posameznih kemikalij so opremljeni tudi s CAS in s številkami carinske tarife, ki je usklajena s kombinirano nomenklaturou EU.

Vsebina knjige je prilagojena dosežkom mednarodnih organizacij (Organizacija za hrano in kmetijstvo – FAO, Organizacija za ekonomsko sodelovanje in razvoj OECD, Svetovna zdravstvena organizacija WHO...), ki so v osemdesetih letih prejšnjega stoletja postavljale temelje nove svetovne politike pri obravnavi kemijskih snovi in njihovega vpliva na človekovo okolje.

Priročnik je rezultat dela strokovnjakov Fakultete za farmacijo in Fakultete za kemijo in kemijsko tehnologijo. Podatki so zbrani iz različnih virov, ki so bili dosegljivi v strokovni literaturi, na spletnih straneh, v uradnih listih in drugih sprejemljivih publikacijah.

Ker je takšen način obravnave nevarnih kemikalij pripravljen v slovenščini, je knjiga pomemben prispevek uresničevanju nacionalnega programa o kemijski varnosti.

Avtorji knjige so Prof. Dr. Aleš Krbavčič, Prof. Dr. Aleš Obreza, Prof. Dr. Marija Sollner-Dolenc, Prof. Dr. Branko Stanovnik in Mag. Milan Škrlič.

Vsebinsko priročnik zajema opise blizu 800 kemikalij, IUPAC kemijski nomenklturni sistem za organske in neorganske spojine, opis svetovnega usklajenega sistema za razvrščanje in označevanje kemikalij (GHS), mednarodni sistem merskih enot, pregled aktivnih snovi in preparatov za zaščito rastlin registriranih v RS in osnovne farmakološko toksikološke lastnosti nekaterih kemijskih funkcionalnih skupin.

Priročnik predstavlja monografije nevarnih kemikalij, opisuje njihove kemijske in fizikalne lastnosti, praktično uporabo ter njihov vpliv na žive organizme in okolje. Namenjena je strokovnjakom, ki delujejo na področju kemije, farmacije, veterine, agronomije pa tudi poslovnim osebam, ki se ukvarjajo s proizvodnjo in prometom z nevarnimi kemikalijami ter nadzirajo njihov promet.

Priročnik nudi veliko koristih podatkov osebam, ki so pogosto v stiku z naravnim okoljem (lovci, čebelarji, ribiči, ekologi), ki skrbijo za zaščito rastlin (gozdarstvo, poljedelstvo, sadjarstvo) in živali (veterina). V tem pogledu so posebno predstavljene kemikalije, katerih uporaba je dovoljena v Sloveniji na področju kmetijstva, sadjarstva in gozdarstva.

Publikacija je izredno primerena kot učbenik za študente kemije, kemijske tehnologije, farmacije in drugih sorodnih znanosti.

V publikaciji so zajete zakonske določbe glede razvrščanja in označevanja kemikalij v prometu, obnem z uredbo Evropskega parlamenta in Sveta o razvrščanju, označevanju in pakiranju snovi ter zmesi, ki se začne izvajati za snovi s 1. decembrom 2010, za zmesi pa s 1. junijem 2015.



Cena knjige v elektronski obliki (CD-ROM) znaša 15 EUR



Strast do pametnih premazov

Visoki **standardi, znanje**, strast do **inovacij** ter želja po nenehnih izboljšavah – to je okolje v katerem že več kot 150 let nastajajo Heliovi **pametni premazi**.

Rešitve, ki zadostijo široki paleti potreb ustvarjajo vez, zaradi katere kupci postanejo naši partnerji in tako rastemo – skupaj.

BODITE NEUSTAVLJIVI

MAGNEZIJ Krka 300



Granulat za pripravo napitka vsebuje magnezijev citrat in vitamin B₂.



Magnezij in vitamin B₂ prispevata k zmanjšanju utrujenosti in izčrpanosti ter normalnemu delovanju živčnega sistema.



Magnezij prispeva tudi k delovanju mišic.



- ✔ Okus po pomaranči in limeti. ✔ Brez konzervansov.
- ✔ Brez umetnih barvil, arom in sladil. ✔ Ena vrečka na dan.

Prehransko dopolnilo ni nadomestilo za uravnoteženo in raznovrstno prehrano. Skrbite tudi za zdrav življenjski slog.

www.krka.si



*Naša inovativnost in znanje
za učinkovite in varne
izdelke vrhunske kakovosti.*

NOVO